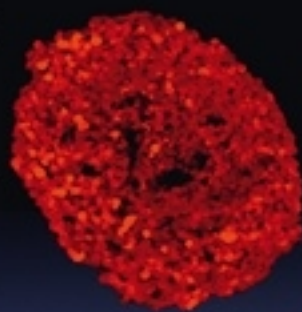


# Cancer Cell



Volume 21  
Number 2

February 14, 2012

[www.cellpress.com](http://www.cellpress.com)



## MYC-Subgroup Medulloblastoma

# Three Down and One To Go: Modeling Medulloblastoma Subgroups

Charles G. Eberhart<sup>1,\*</sup>

<sup>1</sup>Departments of Pathology, Ophthalmology and Oncology, Johns Hopkins University School of Medicine, Baltimore, MD 21205, USA

\*Correspondence: [ceberha@jhmi.edu](mailto:ceberha@jhmi.edu)

DOI 10.1016/j.ccr.2012.01.013

In this issue of *Cancer Cell*, Pei et al. and Kawauchi et al. describe murine models of an aggressive medulloblastoma subtype driven by *Myc*. These tumors have a cellular origin, microscopic appearance, and molecular profile distinct from those of three other major subgroups. Thus, the models fill a significant clinical need.

Medulloblastoma are embryonal tumors involving the cerebellum and comprised of tightly packed stem-like cells that retain the capacity to differentiate along multiple lineages. Current treatments cure only a subset of patients and result in significant long-term morbidity. Thus, improved prognostic markers and therapies are clearly needed. Recent gene expression studies have divided medulloblastoma into four major molecular subtypes, many of which also have unique clinical and histopathological features (Cho et al., 2011; Northcott et al., 2011). An international consensus panel has proposed names for the four groups (Taylor et al., 2011; Figure 1). It is hoped that our improving molecular understanding of medulloblastoma will lead to more targeted therapeutic approaches, promoting reduced morbidity in children harboring less aggressive tumors and longer survival in those with more aggressive variants.

The first two medulloblastoma subgroups are defined molecularly by WNT and Sonic Hedgehog (SHH) pathway activation, respectively, with the former associated with very good clinical behavior and the latter showing fairly good outcomes in infants and intermediate ones in older individuals. Because of their roles in Turcot and Gorlin syndromes, these pathways have long been associated with medulloblastoma formation. A transgenic mouse model of WNT-induced medulloblastoma has recently been reported, with tumors arising from progenitor cells in the embryonic dorsal brainstem and lower rhombic lip but not from granule neuron precursors (GNPs) that generate most of the cells in the cerebellum (Gibson et al., 2010). In contrast, using several transgenic medulloblastoma models driven by increased

Hedgehog signaling, it has been shown that even when SHH tumors are initiated in cerebellar stem cells in vivo, they must first commit to a GNP lineage before growing into neoplastic masses in the brain (Schüller et al., 2008; Yang et al., 2008).

What has been lacking until now is a well-validated model of Group 3 medulloblastoma. This is clinically important, as this subgroup is the most aggressive in terms of its growth, dissemination, and resistance to current therapies. Group 3 medulloblastoma are characterized by amplification and overexpression of the *c-myc* (*MYC*) oncogene, and many of them are of the large cell/anaplastic (LCA) histopathological subtype (Taylor et al., 2011). It has been shown that *Mycn* can drive medulloblastoma formation in mice, but only a subset of these show an LCA phenotype, and most Group 3 tumors are not associated with elevated *MYCN* levels (Swartling et al., 2010). In human medulloblastoma cell lines, the introduction of *MYC* can promote aggressive xenograft growth and an LCA appearance (Stearns et al., 2006). However, it has not been clear if *MYC* plays a role in the initiation of medulloblastoma, or what cells might be susceptible to transformation by this oncogene. The models described in this issue of *Cancer Cell* significantly improve our understanding of how Group 3 medulloblastoma form, and will be critical for testing potential therapies for the group of children with highly aggressive medulloblastoma, which needs them most.

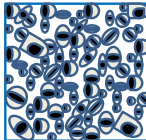
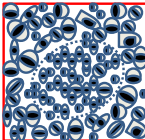
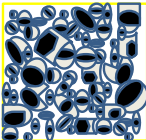
Pei et al. (2012 [in this issue of *Cancer Cell*]) isolated cells from postnatal murine cerebellum based on expression of the stem cell marker Prominin1 (Prom1) and lack of lineage marker expression that defines GNPs. They have previously

shown that this population has functional stem cell properties and resides predominantly in the cerebellar white matter. The introduction of a mutant, stabilized *Myc* construct was sufficient to promote proliferation and self-renewal in vitro; however, when injected into the cerebella of immunocompromised mice, cells proliferated for a few weeks but also showed significant apoptosis and did not form tumors. By introducing both stabilized *Myc* and dominant negative p53 (DNp53), the investigators were able to block this apoptotic induction and tumors formed in vivo within three months of injection. Wild-type *Myc* could also induce tumors in conjunction with DNp53, but with reduced penetrance and increased latency.

Importantly, the murine tumors recapitulated many features of human Group 3 medulloblastoma. The cells were larger than those in SHH-driven models and showed other morphological similarities to LCA tumors, including nuclear molding and prominent cell death. Gene expression analysis revealed that they were distinct from SHH-induced murine medulloblastomas and, among human medulloblastomas, were most similar to the subgroups defined by elevated *MYC* (Cho et al., 2011; Northcott et al., 2011). Both immunohistochemical analysis and RNA profiling suggested that the tumors were largely undifferentiated.

Kawauchi et al. (2012 [in this issue of *Cancer Cell*]) also introduced *Myc* into cerebellar cells ex vivo, but they used *Trp53* null GNPs sorted using the neuronal lineage marker Atoh1. Injection of these cells into immunocompromised mice resulted in tumors with LCA features distinct from the WNT or SHH-induced medulloblastoma previously analyzed by this group, both of which have a more

	WNT	SHH	Group 3	Group 4
<b>Subgroup Prevalence</b>	7-8%	28-32%	26-27%	34-38%
<b>Common Histology</b>	Classic	Desmoplastic/ Nodular	Large Cell/ Anaplastic	Classic
<b>Clinical Outcome</b>	Very Good	Good to Intermediate	Poor	Intermediate
<b>Gene Expression</b>	WNT	SHH	MYC	Neuronal/ Glutamatergic
<b>Cellular Origin/ Phenotype</b>	Dorsal Brainstem Progenitor	Cerebellar GNP	Cerebellar Stem Cell	?

Classic
Nodular
LCA

**Figure 1. Medulloblastoma Subgroups**

Transcriptional profiling supports the existence of four main medulloblastoma subgroups that differ with respect to their common microscopic appearance and clinical associations. The cartoons below depict a classic medulloblastoma comprised of heterogeneous embryonal cells, a desmoplastic/nodular tumor with a central region of neuronal differentiation, and a large cell anaplastic medulloblastoma with increased nuclear size and pronounced cellular molding/engulfment.

classic histopathological appearance. Analysis of the *Myc*-driven tumor transcriptome also supported the notion that they were similar to human Group 3 medulloblastoma and distinct from prior murine models induced by WNT, SHH, or *Mycn*. *Mycn* is a target of the SHH pathway in the developing cerebellum, and medulloblastoma previously generated using *Mycn* by this group had a gene expression profile more similar to SHH tumors than those promoted by *Myc*.

Kawauchi et al. (2012) also detected increased expression of *Prom1* and other stem cell factors in their *Myc*-driven tumors despite the fact that they were initiated in sorted populations of GNPs largely negative for these markers. Indeed, *Atoh1* expression was lost in tumors, suggesting that either they had arisen from rare *Atoh1* negative cells in the highly enriched starting material or that sorted GNPs were de-differentiating or otherwise silencing expression of lineage markers as part of their transformation. Pei et al. (2012) also could induce tumors from sorted GNP populations and found that the resulting medulloblastoma had lost expression of neuronal lineage markers. Moreover, both groups found that expression profiles of the *Myc*-driven

medulloblastoma showed significant overlap with those of neural stem cells, induced pluripotent stem cells, and embryonic stem cells. Together, these suggest that Group 3 medulloblastoma either arise from neural stem cells or de-differentiate and take on a stem-like phenotype as part of their *Myc*-induced transformation.

Both groups also began to use their new models to evaluate potential therapies for these clinically aggressive tumors. Kawauchi et al. (2012) showed that the tumors are resistant to SHH pathway inhibitors, a significant finding as these compounds have begun to enter clinical trials, and it had been suggested that their efficacy might not be limited to the SHH medulloblastoma subgroup. Pei et al. (2012) similarly found that their tumors were insensitive to SHH pathway blockade but demonstrated that ongoing *Myc* expression is required to maintain tumor growth. They also used gene expression profiling to identify PI3K and mTOR signaling as potential novel therapeutic targets in *Myc*-driven medulloblastoma, demonstrated that small molecule inhibitors of PI3K and mTOR could slow tumor cell growth in vitro, and then validated the pro-survival effects of one compound in vivo.

To improve our treatment of cancer, we must embrace and seek to understand its complexity. Over the last two decades, analysis of the pediatric brain tumor medulloblastoma has generated numerous insights into how cancer can be meaningfully subgrouped and how oncogenic stimuli associated with developmentally important signaling pathways interact with specific populations of stem and progenitor cells to induce tumors. The two studies discussed above represent the next link in this chain, providing important new tools for preclinical testing and yielding insights into the origin and nature of an aggressive medulloblastoma subgroup associated with *Myc*. The new models will also be useful in addressing unexpected recent findings, such as the discovery of a strong photoreceptor expression signature in Group 3 medulloblastoma.

## REFERENCES

- Cho, Y.J., Tsherniak, A., Tamayo, P., Santagata, S., Ligon, A., Greulich, H., Berhoukim, R., Amani, V., Goumnerova, L., Eberhart, C.G., et al. (2011). *J. Clin. Oncol.* 29, 1424–1430.
- Gibson, P., Tong, Y., Robinson, G., Thompson, M.C., Currie, D.S., Eden, C., Kranenburg, T.A., Hogg, T., Poppleton, H., Martin, J., et al. (2010). *Nature* 468, 1095–1099.
- Kawauchi, D., Robinson, G., Uziel, T., Gibson, P., Rehg, J.E., Gao, C., Finkelstein, D., Qu, C., and Pounds, S. (2012). *Cancer Cell* 21, this issue, 168–180.
- Northcott, P.A., Korshunov, A., Witt, H., Hielscher, T., Eberhart, C.G., Mack, S., Bouffet, E., Clifford, S.C., Hawkins, C.E., French, P., et al. (2011). *J. Clin. Oncol.* 29, 1408–1414.
- Pei, Y., Moore, C.E., Wang, J., Tewari, A.K., Eroshkin, A., Cho, Y.J., Witt, H., Korshunov, A., Read, T.A., and Sun, J.L. (2012). *Cancer Cell* 21, this issue, 155–167.
- Schüller, U., Heine, V.M., Mao, J., Kho, A.T., Dillon, A.K., Han, Y.G., Huillard, E., Sun, T., Ligon, A.H., Qian, Y., et al. (2008). *Cancer Cell* 14, 123–134.
- Stearns, D., Chaudhry, A., Abel, T.W., Burger, P.C., Dang, C.V., and Eberhart, C.G. (2006). *Cancer Res.* 66, 673–681.
- Swartling, F.J., Grimmer, M.R., Hackett, C.S., Northcott, P.A., Fan, Q.W., Goldenberg, D.D., Lau, J., Masic, S., Nguyen, K., Yakovenko, S., et al. (2010). *Genes Dev.* 24, 1059–1072.
- Taylor, M.D., Northcott, P.A., Korshunov, A., Remke, M., Cho, Y.J., Clifford, S.C., Eberhart, C.G., Parsons, D.W., Rutkowski, S., Gajjar, A., et al. (2011). *Acta Neuropathol.*
- Yang, Z.J., Ellis, T., Markant, S.L., Read, T.A., Kessler, J.D., Bourboulas, M., Schüller, U., Mac-hold, R., Fishell, G., Rowitch, D.H., et al. (2008). *Cancer Cell* 14, 135–145.

# VEGF-D(ilated) Lymphatics as Gateways to Metastasis

Janusz Rak<sup>1,\*</sup>

<sup>1</sup>Montreal Children's Hospital The Research Institute – McGill University Health Centre, 4060 Ste Catherine West, Montreal, QC, H3Z 3Z2, Canada

\*Correspondence: [janusz.rak@mcgill.ca](mailto:janusz.rak@mcgill.ca)

DOI 10.1016/j.ccr.2012.01.012

**VEGF-C and VEGF-D have been implicated in lymphatic metastasis, mainly as inducers of new intra/peritumoral capillary lymphatics. In this issue of *Cancer Cell*, Karnezis and colleagues challenge this notion and demonstrate that tumor-derived VEGF-D promotes metastasis by causing prostaglandin-dependent dilation of collecting lymphatics outside of the tumor mass.**

Metastasis defines the progressive, systemic, and intractable nature of late-stage human cancers. Implicitly, this process involves trafficking of cancer cells within blood and lymphatic compartments to sites of their secondary growth in distant organs and regional lymph nodes, respectively (Fidler, 2003). By extension, the corresponding processes of tumor-induced formation of new blood vessels (angiogenesis) and lymphatics (lymphangiogenesis) are often viewed as prerequisites for the onset of hematogenous and lymphatic dissemination. Either of the resulting microvascular networks may constitute a point of entry for cancer cells into the vascular system and a rate limiting step in disease spreading (Folkman, 2007; Alitalo, 2011). In spite of some controversy as to the causal role of lymph node metastases as “launch pads” of systemic dissemination (Sleeman and Thiele, 2009), the inherent appeal of this possibility has contributed to a growing interest in targeting lymphangiogenesis as an early pro-metastatic switch in cancer (Alitalo, 2011).

Much of the effort in this area has centered around obliteration of major lymphangiogenic growth factor pathways triggered by members of the vascular endothelial growth factor (VEGF) family, especially VEGF-C, VEGF-D, and to some extent VEGF-A, all of which may be expressed by metastatic cancer cells. The respective receptors for these factors, VEGFR3 and VEGFR2, are present on lymphatic endothelial cells (LECs), which can be distinguished from their vascular counterparts by patterns of gene expression and distinct molecular markers (LYVE-1, Prox1, and podoplanin) (Alitalo, 2011). LECs line both the terminal, thin walled lymphatics, devoid of supporting mural cells, and their draining

contractile ducts, collecting lymphatic vessels (CLVs), which contain mural cells and pass the interstitial fluid (and cancer cells) to the regional lymph nodes.

Several specific monoclonal antibodies, soluble receptors, and small molecule inhibitors have been developed to block VEGF/VEGF receptor (VEGFR) pathways and impede lymphangiogenesis. In addition, the expression of VEGFs by cancer cells can be inhibited using non-steroidal anti-inflammatory drugs (NSAIDs) and other agents. The intuitively obvious way to observe whether these drugs actually work in cancer would be to follow the expected decline in density of capillary lymphatics within, and adjacent to, the tumor mass, using LEC markers such as LYVE-1. Indeed, such effects have been observed and may, at least in some cases, be rate-limiting for lymphatic and systemic metastasis.

As it turns out, clues as to the role of VEGFs in lymph node metastasis may also be found outside of the proverbial “box,” i.e., away from the tumor masses, and within their draining CLVs. A compelling example of this scenario is described by Karnezis et al., (2012) in this issue of *Cancer Cell*. These authors set out to explore processes by which tumors expressing VEGF-D trigger lymph node metastasis. Although such tumors do contain rich networks of capillary lymphatics, these investigators noticed that what separated them from their non-metastatic counterparts was a startling (macroscopic) enlargement of CLVs draining the tumor basin to sentinel lymph nodes. The striking images of this CLV dilation suggest that the lymphatic influence of a growing cancer is not confined to its physical boundaries, but extends far beyond. What

might be the mechanism by which VEGF-D-expressing tumor cells exert such a long distance influence (over tens of millimeters), and what are the consequences?

In search for answers Karnezis et al., (2012) first documented that CLV dilation is, indeed, directly VEGF-D-dependent. For example, this effect was absent in the case of non-metastatic and VEGF-D non-expressing tumors or when VEGF-D was replaced with VEGF-A. Likewise, treatment with neutralizing antibodies against VEGF-D (VD1), VEGFR3 (mF4-31C1), or VEGFR2 (DC101) abolished CLV dilation. These observations suggest that VEGF-D causes dilation through cooperative activation of VEGFR3 and VEGFR2 in LECs that are located in the extra-tumoral CLV segments. To determine the nature of these responses, CLVs were isolated, and their LEC populations were purified and profiled for gene expression. This revealed a distinct molecular signature of these cells, including their ability to markedly downregulate prostaglandin dehydrogenase (PGDH) in the presence of VEGF-D. PGDH breaks down prostaglandins (e.g., PGE<sub>2</sub>), thereby opposing the action of the prostaglandin synthesis pathway driven by cyclooxygenase 2. Thus, downregulation of PGDH in LECs exposed to VEGF-D raises the levels of circulating prostaglandins, which in turn act on mural cells within tumor-related CLVs, causing their dilation.

These events have profound consequences for metastasis. Karnezis et al., (2012) demonstrated that essentially all treatments that counteracted CLV dilation also diminished the metastatic load in draining lymph nodes. Interestingly, Etodolac, an NSAID, triggers these effects essentially without changing the lymphatic or blood vessel density within

the primary tumor, which suggests that CLV dilation may have a far more central role in the metastatic process than hitherto appreciated. Interestingly, Etodolac also diminished metastatic burden in the lung. These results suggest that a level of control over the lymphatic and systemic dissemination could potentially be achieved by administration of relatively safe anti-inflammatory agents.

This provocative study adds an important dimension to the process that might be viewed as vascular system “conditioning” for cancer metastasis. While the focus of the present study is on CLV dilation, others observed lymphangiogenesis within lymph nodes prior to their metastatic colonization (Tobler and Detmar, 2006), a process that may be attributed to remote influences of growth factors or exosomes (Hood et al., 2011). Analogous pre-metastatic niches were also described at sites of blood borne metastases (Kaplan et al., 2005).

The enlargement of macroscopic vessels located outside of a growing tumor is not restricted to CLVs. Similar increases in diameter are often observed in the case of blood vessels that supply tumor microcirculation (feeding arteries and collecting veins), which is also apparent from some of the images included in the study by Karnezis et al., (2012). Although this is a commonly observed phenomenon, the underlying biological process has thus far attracted minimal attention (Yu and Rak, 2003). In contrast to angiogenesis, which occurs at the level of microscopic capillaries (Carmeliet and Jain, 2011), formation of larger tumor-feeding blood vessels may involve such mechanisms as dilation, similar to that occurring in CLVs, or circumferential growth (“tumor arteriogenesis”) (Yu and Rak, 2003). Whether such macroscopic changes control tumor microenvironment, growth, or hematogenous metastasis (by analogy to CLVs) remains to be studied.

The novel and fascinating link between CLV dilation and lymphatic metastasis described by these authors raises several important questions. For example, how does CLV dilation promote metastasis? Is this merely a wider conduit (“plumbing”) effect, or does it involve more subtle regulatory mechanisms (e.g., tumor-LEC interactions)? Since the VEGF-D-induced increase in prostaglandin levels is detected in peripheral blood, could such a change be indicative of impending lymphatic metastasis in the clinic? How early in progression of human cancers would increase in prostaglandins occur, and how discrete, how detectable, would this event be? What systemic consequences may be associated with VEGF-D-induced increase in prostaglandins in blood, e.g., for the vascular system? What turns on lymphangiogenic growth factors in metastatic cancers, and is there a link between oncogenic pathways and CLV dilation?

It is fascinating to think that a pharmacological blockade of the pathological CLV dilation and metastasis could be achieved with already available agents (VEGF/VEGFR3/2 inhibitors and NSAIDs). However, one wonders whether such treatment could interfere with the lymph outflow from the primary tumor mass leading to a build up of interstitial fluid pressure (IFP)? Increase in IFP has been linked to impaired drug delivery and could result in vascular compression, hypoxia, and perhaps in hematogenous metastasis. It is unclear if any of these effects might accompany therapeutic interference with CLV dilation. Indeed, the work of Karnezis et al., (2012) opens up several new lines of inquiry and a new domain in the field of lymphangiogenesis and cancer progression.

REFERENCES

#### REFERENCES

- Fidler, I.J. (2003). *Nat. Rev. Cancer* 3, 453–458.
- Folkman, J. (2007). *Nat. Rev. Drug Discov.* 6, 273–286.
- Alitalo, K. (2011). *Nat. Med.* 17, 1371–1380.
- Sleeman, J.P., and Thiele, W. (2009). *Int. J. Cancer* 125, 2747–2756.
- Karnezis, T., Shayan, R., Ceasar, C., Roufail, S., Harris, N.C., Ardipradja, K., Zhang, Y.F., Williams, S.P., Farnsworth, R.H., Chai, M.G., et al. (2012). *Cancer Cell* 21, this issue, 181–195.
- Tobler, N.E., and Detmar, M. (2006). *J. Leukoc. Biol.* 80, 691–696.
- Hood, J.L., San, R.S., and Wickline, S.A. (2011). *Cancer Res.* 71, 3792–3801.
- Kaplan, R.N., Riba, R.D., Zacharoulis, S., Bramley, A.H., Vincent, L., Costa, C., MacDonald, D.D., Jin, D.K., Shido, K., Kerns, S.A., et al. (2005). *Nature* 438, 820–827.
- Yu, J.L., and Rak, J.W. (2003). *Breast Cancer Res.* 5, 83–88.
- Carmeliet, P., and Jain, R.K. (2011). *Nature* 473, 298–307.

## aSIRTING Control over Cancer Stem Cells

Takahiro Ito,<sup>1</sup> Bryan Zimdahl,<sup>1,2</sup> and Tannishtha Reya<sup>1,\*</sup>

<sup>1</sup>Department of Pharmacology, University of California San Diego School of Medicine, La Jolla, CA 92093, USA

<sup>2</sup>Department of Pharmacology and Cancer Biology, Duke University Medical Center, Durham, NC 27710, USA

\*Correspondence: treya@ucsd.edu

DOI 10.1016/j.ccr.2012.01.014

Cancer stem cells lie at the root of chronic myelogenous leukemia (CML) and mediate its continued growth. Their resistance to current therapies results in an inability to eradicate the disease. In this issue of *Cancer Cell*, Li et al. identify SIRT1 as a new target for eliminating CML cancer stem cells.

Chronic myelogenous leukemia (CML) is a cancer that begins in hematopoietic

stem cells. Triggered by the BCR-ABL translocation (Melo and Barnes, 2007),

additional mutations can induce its progression from a slow-growing chronic

the primary tumor, which suggests that CLV dilation may have a far more central role in the metastatic process than hitherto appreciated. Interestingly, Etodolac also diminished metastatic burden in the lung. These results suggest that a level of control over the lymphatic and systemic dissemination could potentially be achieved by administration of relatively safe anti-inflammatory agents.

This provocative study adds an important dimension to the process that might be viewed as vascular system “conditioning” for cancer metastasis. While the focus of the present study is on CLV dilation, others observed lymphangiogenesis within lymph nodes prior to their metastatic colonization (Tobler and Detmar, 2006), a process that may be attributed to remote influences of growth factors or exosomes (Hood et al., 2011). Analogous pre-metastatic niches were also described at sites of blood borne metastases (Kaplan et al., 2005).

The enlargement of macroscopic vessels located outside of a growing tumor is not restricted to CLVs. Similar increases in diameter are often observed in the case of blood vessels that supply tumor microcirculation (feeding arteries and collecting veins), which is also apparent from some of the images included in the study by Karnezis et al., (2012). Although this is a commonly observed phenomenon, the underlying biological process has thus far attracted minimal attention (Yu and Rak, 2003). In contrast to angiogenesis, which occurs at the level of microscopic capillaries (Carmeliet and Jain, 2011), formation of larger tumor-feeding blood vessels may involve such mechanisms as dilation, similar to that occurring in CLVs, or circumferential growth (“tumor arteriogenesis”) (Yu and Rak, 2003). Whether such macroscopic changes control tumor microenvironment, growth, or hematogenous metastasis (by analogy to CLVs) remains to be studied.

The novel and fascinating link between CLV dilation and lymphatic metastasis described by these authors raises several important questions. For example, how does CLV dilation promote metastasis? Is this merely a wider conduit (“plumbing”) effect, or does it involve more subtle regulatory mechanisms (e.g., tumor-LEC interactions)? Since the VEGF-D-induced increase in prostaglandin levels is detected in peripheral blood, could such a change be indicative of impending lymphatic metastasis in the clinic? How early in progression of human cancers would increase in prostaglandins occur, and how discrete, how detectable, would this event be? What systemic consequences may be associated with VEGF-D-induced increase in prostaglandins in blood, e.g., for the vascular system? What turns on lymphangiogenic growth factors in metastatic cancers, and is there a link between oncogenic pathways and CLV dilation?

It is fascinating to think that a pharmacological blockade of the pathological CLV dilation and metastasis could be achieved with already available agents (VEGF/VEGFR3/2 inhibitors and NSAIDs). However, one wonders whether such treatment could interfere with the lymph outflow from the primary tumor mass leading to a build up of interstitial fluid pressure (IFP)? Increase in IFP has been linked to impaired drug delivery and could result in vascular compression, hypoxia, and perhaps in hematogenous metastasis. It is unclear if any of these effects might accompany therapeutic interference with CLV dilation. Indeed, the work of Karnezis et al., (2012) opens up several new lines of inquiry and a new domain in the field of lymphangiogenesis and cancer progression.

REFERENCES

#### REFERENCES

- Fidler, I.J. (2003). *Nat. Rev. Cancer* 3, 453–458.
- Folkman, J. (2007). *Nat. Rev. Drug Discov.* 6, 273–286.
- Alitalo, K. (2011). *Nat. Med.* 17, 1371–1380.
- Sleeman, J.P., and Thiele, W. (2009). *Int. J. Cancer* 125, 2747–2756.
- Karnezis, T., Shayan, R., Ceasar, C., Roufail, S., Harris, N.C., Ardipradja, K., Zhang, Y.F., Williams, S.P., Farnsworth, R.H., Chai, M.G., et al. (2012). *Cancer Cell* 21, this issue, 181–195.
- Tobler, N.E., and Detmar, M. (2006). *J. Leukoc. Biol.* 80, 691–696.
- Hood, J.L., San, R.S., and Wickline, S.A. (2011). *Cancer Res.* 71, 3792–3801.
- Kaplan, R.N., Riba, R.D., Zacharoulis, S., Bramley, A.H., Vincent, L., Costa, C., MacDonald, D.D., Jin, D.K., Shido, K., Kerns, S.A., et al. (2005). *Nature* 438, 820–827.
- Yu, J.L., and Rak, J.W. (2003). *Breast Cancer Res.* 5, 83–88.
- Carmeliet, P., and Jain, R.K. (2011). *Nature* 473, 298–307.

## aSIRTING Control over Cancer Stem Cells

Takahiro Ito,<sup>1</sup> Bryan Zimdahl,<sup>1,2</sup> and Tannishtha Reya<sup>1,\*</sup>

<sup>1</sup>Department of Pharmacology, University of California San Diego School of Medicine, La Jolla, CA 92093, USA

<sup>2</sup>Department of Pharmacology and Cancer Biology, Duke University Medical Center, Durham, NC 27710, USA

\*Correspondence: treya@ucsd.edu

DOI 10.1016/j.ccr.2012.01.014

Cancer stem cells lie at the root of chronic myelogenous leukemia (CML) and mediate its continued growth. Their resistance to current therapies results in an inability to eradicate the disease. In this issue of *Cancer Cell*, Li et al. identify SIRT1 as a new target for eliminating CML cancer stem cells.

Chronic myelogenous leukemia (CML) is a cancer that begins in hematopoietic

stem cells. Triggered by the BCR-ABL translocation (Melo and Barnes, 2007),

additional mutations can induce its progression from a slow-growing chronic

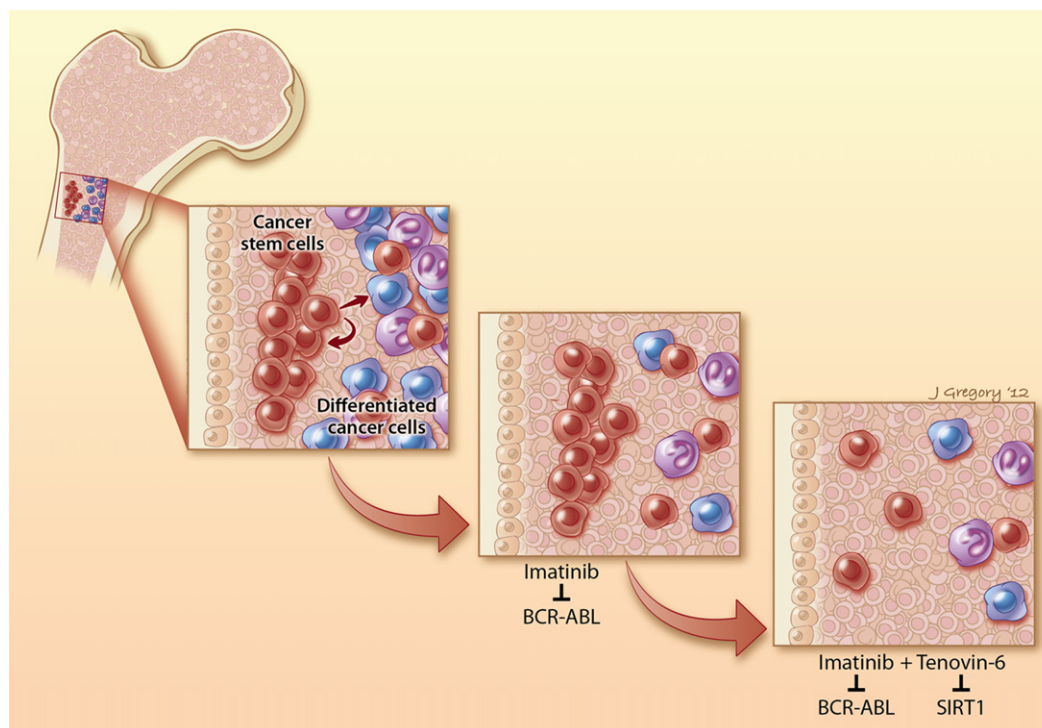


**Figure 1. SIRT1 Inhibition Effectively Targets CML Cancer Stem Cells**

Chronic myelogenous leukemia (CML) is composed of differentiated cells (blue and purple) as well as a more primitive pool of cancer stem cells (red) that have the capacity to propagate the disease (left). The kinase inhibitor Imatinib can eliminate differentiated CML cells but cannot effectively target cancer stem cells (middle). Though insensitive to Imatinib, cancer stem cells remain dependent on SIRT1. Thus, the combined use of the SIRT1 inhibitor Tenovin 6 and Imatinib effectively removes residual cancer stem cells and may block CML at its root (right).

phase to a more aggressive and undifferentiated blast crisis phase. The discovery of the kinase inhibitor imatinib mesylate revolutionized the treatment of CML. Over the years, however, it has become clear that while kinase inhibitors can hold CML at bay, they are unable to eradicate the disease, leading to a life-long dependence on the drug and an increased risk of relapse and progression. In addition, kinase inhibitors are ineffective against drug-resistant and advanced stage disease. Although such patients may not form a large group in developed countries, the global face of CML is very different, and many patients are not diagnosed until the disease is at an advanced stage. Insight into the limitations of targeted kinase therapy came from an understanding that CML is composed of differentiated cells as well as a more undifferentiated pool of cancer stem cells that have the capacity to propagate the disease (Wang et al., 1998). Emerging evidence suggests that differentiated CML cells are addicted to ABL and can be eliminated by kinase inhibitors, while

cancer stem cells can become ABL independent and thus persist despite therapy (Graham et al., 2002; Corbin et al., 2011). Thus, identifying regulators that are required for CML cancer stem cell growth and renewal is critical for effectively targeting the disease. In this issue of *Cancer Cell*, Li et al. (2012) identify SIRT1, the founding member of the Sirtuin family of proteins, as an exciting new target for eradicating CML cancer stem cells and thereby stopping CML growth.

Sirtuins, mammalian homologs of the yeast protein silent information regulator 2, represent a unique subclass of histone deacetylases; their substrates can include both histones and non histone proteins, and unlike other HDACs, they act in an NAD-dependent manner (Haigis and Sinclair, 2010). Sirtuins exert a powerful influence on a wide array of cellular processes including DNA repair, cell survival, metabolism, and aging in diverse organisms (Haigis and Sinclair, 2010).

In this study, the authors use a combination of genetically engineered mouse models and primary leukemia xenografts

to assess the role of SIRT1 in mouse and human CML growth. The authors first examined the expression of SIRT1 in normal and CML cells, focusing on the stem cell enriched CD34<sup>+</sup> population. SIRT1 was expressed at higher levels in human CML CD34<sup>+</sup> cells than in normal CD34<sup>+</sup> cells. Moreover, knockdown of SIRT1 in CD34<sup>+</sup> CML cells led to reduced proliferation, enhanced apoptosis, and impaired colony-forming ability. Importantly, SIRT1 knockdown had less of an effect on proliferation and apoptosis of normal CD34<sup>+</sup> cells, suggesting that CML and normal stem cells display a differential dependence on SIRT1. Further, the combined use of SIRT1 inhibition together with imatinib led to an increase in cell death, suggesting that suppression of SIRT1 could cooperate with imatinib to more effectively block CML stem cells (Figure 1).

To test if the dependence of CML on SIRT1 could be useful in a therapeutic context, the authors used the small molecule Tenovin 6 (TV-6), which blocks the activity of sirtuin family proteins (Lain

et al., 2008). In vitro treatment with TV-6, and to a greater extent with TV-6 and imatinib, reduced colony formation and in vivo engraftment more effectively than imatinib alone, highlighting the potential utility of SIRT inhibition in the context of combination therapy.

While the experiments involving ex vivo exposure suggested that pharmacologic blockade of SIRT1 was effective against CML, it was critical to assess whether the drug could affect disease in a physiological context. To test this, the group isolated leukemic cells from an inducible BCR-ABL transgenic mouse and transplanted them into irradiated recipients. These mice were subsequently treated with imatinib, TV-6, or the combination daily for 21 days. Although imatinib alone impaired leukemia growth, it failed to target CML stem cells. In contrast, TV-6 alone, and to a greater extent TV-6 and imatinib, led to a very significant loss of CML stem cells. Consistent with this, mice treated with the combination showed improved survival, with reduced numbers of residual leukemic cells in the bone marrow after discontinuation of treatment. Although the changes in survival were perhaps not as dramatic as the drop in cancer stem cell content may have predicted, it is important to note that the drug was discontinued after 3 weeks; thus, continued treatment, modified dosing or the use of alternate inhibitors might show further benefits in vivo. In a key experiment, the authors also tested the effect of TV-6 on mice xenografted with an imatinib-resistant blast crisis CML patient sample and found that it led to a significant reduction in engraftment at multiple sites of leukemia growth. This suggests that targeting SIRT1 may be effective against both chronic phase and in imatinib-resistant advanced stage disease. More broadly, this work identifies Sirtuins as an impor-

tant control point for cancer stem cells and provides a strong rationale for considering SIRT1 inhibitors for treatment of myeloid leukemias and perhaps other malignancies that display activation of this pathway.

How does SIRT1 inhibition eliminate CML cancer stem cells? SIRT1 has previously been shown to deacetylate p53 and thereby regulate its transcriptional activity (Haigis and Sinclair, 2010). In support of this notion, SIRT1 inhibition elevated acetylated and total p53 levels in both chronic and blast crisis phase CML CD34<sup>+</sup> cells, triggering a rise in p53 target genes. Loss of function studies indicated that TV-6 depends on p53 to affect CML, consistent with the fact that p53 activation can effectively target CML. This suggests that consideration of SIRT1 as a target should take into account a patient's p53 status, since the 30% of blast crisis patients whose disease display p53 mutations are unlikely to respond to this strategy (Melo and Barnes, 2007).

In the last few years, basic and translational work has identified several pathways that are critical for CML stem cell function and renewal, including promyelocytic leukemia protein (PML),  $\beta$ -catenin, Alox5, and Smoothened (reviewed in Chen et al., 2010). These studies shed light on the molecular mechanisms that protect and sustain CML cancer stem cells, allowing them to evade imatinib. Some have been of immediate translational interest because they can be readily targeted; this is true in particular for PML and Smoothened, which can be inhibited by arsenic trioxide and by Hedgehog pathway antagonists (Dierks et al., 2008; Ito et al., 2008; Zhao et al., 2009). Both strategies are currently being tested in trials of myeloid leukemia, and it will be of great interest to see how effective and durable they turn out to be. But considering the fact that kinase inhibitors can

hold CML at bay in many patients, the bar for a new therapeutic in this disease may be high. At this stage, it is not unreasonable to hope for eradication of residual cancer stem cells and an ability to discontinue therapy without relapse. Perhaps the blockade of SIRT1 will allow us to finally assert control over CML cancer stem cells and accelerate progress toward this goal.

## REFERENCES

- Chen, Y., Peng, C., Sullivan, C., Li, D., and Li, S. (2010). *Leukemia* 24, 1545–1554.
- Corbin, A.S., Agarwal, A., Loriaux, M., Cortes, J., Deininger, M.W., and Druker, B.J. (2011). *J. Clin. Invest.* 121, 396–409.
- Dierks, C., Beigi, R., Guo, G.R., Zirlik, K., Stegert, M.R., Manley, P., Trussell, C., Schmitt-Graeff, A., Landwerlin, K., Veelken, H., and Warmuth, M. (2008). *Cancer Cell* 14, 238–249.
- Graham, S.M., Jørgensen, H.G., Allan, E., Pearson, C., Alcorn, M.J., Richmond, L., and Holyoake, T.L. (2002). *Blood* 99, 319–325.
- Haigis, M.C., and Sinclair, D.A. (2010). *Annu. Rev. Pathol.* 5, 253–295.
- Ito, K., Bernardi, R., Morotti, A., Matsuoka, S., Sglio, G., Ikeda, Y., Rosenblatt, J., Avigan, D.E., Teruya-Feldstein, J., and Pandolfi, P.P. (2008). *Nature* 453, 1072–1078.
- Lain, S., Hollick, J.J., Campbell, J., Staples, O.D., Higgins, M., Aoubala, M., McCarthy, A., Appleyard, V., Murray, K.E., Baker, L., et al. (2008). *Cancer Cell* 13, 454–463.
- Li, L., Wang, L., Liang, L., Wang, Z., Ho, Y., McDonald, T., Holyoake, T.L., Chen, W., and Bhatia, R. (2012). *Cancer Cell* 21, this issue, 266–281.
- Melo, J.V., and Barnes, D.J. (2007). *Nat. Rev. Cancer* 7, 441–453.
- Wang, J.C., Lapidot, T., Cashman, J.D., Doedens, M., Addy, L., Sutherland, D.R., Nayar, R., Laraya, P., Minden, M., Keating, A., et al. (1998). *Blood* 91, 2406–2414.
- Zhao, C., Chen, A., Jamieson, C.H., Fereshteh, M., Abrahamsson, A., Blum, J., Kwon, H.Y., Kim, J., Chute, J.P., Rizzieri, D., et al. (2009). *Nature* 458, 776–779.

# Glycine Decarboxylase Cleaves a “Malignant” Metabolic Path to Promote Tumor Initiation

John E. Dominy,<sup>1,3</sup> Francisca Vazquez,<sup>2,4</sup> and Pere Puigserver<sup>1,3,\*</sup>

<sup>1</sup>Department of Cancer Biology

<sup>2</sup>Department of Medical Oncology, Dana-Farber Cancer Institute

<sup>3</sup>Department of Cell Biology

Harvard Medical School, Boston, MA 02115, USA

<sup>4</sup>Broad Institute of Harvard and MIT, Cambridge, MA 02142, USA

\*Correspondence: [pere\\_puigserver@dfci.harvard.edu](mailto:pere_puigserver@dfci.harvard.edu)

DOI 10.1016/j.ccr.2012.01.019

**Tumor-initiating cells (TICs) are thought to be critical for promoting tumorigenesis. In a recent *Cell* article, Zhang and colleagues found that non-small cell lung cancer TICs overexpress the metabolic enzyme glycine decarboxylase, which leads to increases in pyrimidine synthesis and is critical for proliferation and tumor initiation.**

Tumors are frequently composed of a heterogeneous population of cancer cells, and accumulating evidence suggests that, in many tumor types, only a subpopulation of these cells, named cancer stem cells or tumor-initiating cells (TICs) (Nguyen et al., 2012), are responsible for tumor maintenance and progression. There is also evidence that TICs are more resistant to many conventional chemotherapies and radiotherapies and, as such, are suspected to be responsible for tumor recurrence after treatment (Singh and Settleman, 2010). Hence, understanding the vulnerabilities of TICs could enable more effective cancer therapies.

Within this context, Zhang et al., (2012) describe the isolation of TICs from non-small cell lung cancer (NSCLC) and characterization of some of the TICs' unique phenotypic features in a recent *Cell* article. Remarkably, NSCLC TICs have robust increases in glycolysis as well as in glycine/serine metabolism, most notably at the level of the glycine cleavage system enzyme, leading to increased pyrimidine synthesis and proliferation. This study supports a large body of work indicating that cancer cells differ from non-transformed cells in their programming for nutrient metabolism (Ferreira et al., 2012).

In a very deft series of experiments, Zhang et al., (2012) report that within the otherwise heterogeneous NSCLCs, there exists a subpopulation of CD166<sup>+</sup> cells that are extremely potent in their ability

to induce tumor formation in immunocompromised NOD/SCID *Il2r $\gamma$ <sup>-/-</sup>* mice and form tumor spheres in vitro. As such, they can be considered TICs. Yet another remarkable feature of the TICs is their metabolic profile. Concomitant with an upregulation of glycolytic genes, there is also a strong upregulation of genes involved in serine, glycine, and one-carbon metabolism. Intracellular metabolite levels from TICs accord well with the gene expression profiles, as there is a relative increase in glycolytic intermediates as well as intermediates associated with glycine/serine and nucleotide metabolism. Among all of the gene expression changes observed in TICs, the most striking one is a powerful increase in glycine decarboxylase (GLDC), a member of the protein complex that catabolizes glycine into carbon dioxide, ammonia, and 5,10-methylene-tetrahydrofolate.

Convincingly, Zhang et al., (2012) showed that GLDC overexpression promotes glycolysis, serine/glycine metabolism, and the accumulation of pyrimidine nucleotides. Consistent with the idea that the deviant serine/glycine metabolism of TICs facilitates their tumorigenic capacity, CD166<sup>+</sup> lung tumor cells, which are otherwise non-tumorigenic, were able to establish tumors at low frequency when made to overexpress GLDC. Furthermore, GLDC overexpression alone was able to transform NIH 3T3 cells in vitro and drive tumor formation in vivo, which required GLDC's enzymatic activity

to be intact. Knockdown of this enzyme, on the other hand, was effective in diminishing many of these parameters, including tumorigenicity, in cells that express high levels of GLDC. Together, these results suggest that GLDC could be a new NSCLC oncogene—a finding that will be strengthened if recurrent genomic alterations that increase GLDC activity are found in primary tumors. The potential clinical relevance of GLDC overexpression in NSCLC was given further salience by the revelation that high expression of GLDC in primary NSCLC tumors is significantly associated with a higher risk of patient mortality.

Although originally identified in TICs derived from primary lung tumors, Zhang et al., (2012) also show that GLDC is expressed at high levels in many other tumor types and in about 25% of cancer cell lines tested. Knockdown of GLDC in these high expressing cell lines, such as A549 lung adenocarcinoma cells and CACO2 colon cancer cells, reduces their proliferation and tumorigenic potential. Importantly, to demonstrate that this is a newly acquired vulnerability of these cancer cell lines and not an activity that is generally required for proliferation, Zhang et al., (2012) showed that GLDC knockdown did not affect the proliferation of normal human lung fibroblasts. They also hint on the possibility of exploiting this new metabolic vulnerability for therapeutic purposes by showing that cells that overexpress this enzyme are more sensitive to the antifolate drug

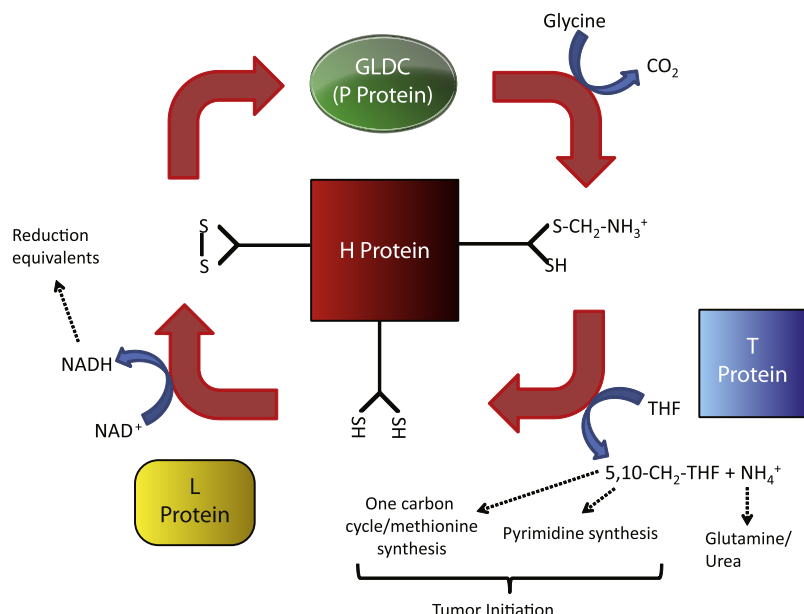


**Figure 1. A Summary of the Protein Constituents of the Glycine Cleavage Complex and the Reactions that They Catalyze**

The oxidative decarboxylation and deamination of glycine begins with glycine decarboxylase (GLDC; P protein), which removes carbon dioxide from glycine and transfers a methylamino group to the dithiolane ring of a lipoic acid molecule attached to H protein. The methylamino moiety is transferred to tetrahydrofolate (THF) by T protein, generating 5,10-methylene-tetrahydrofolate and reduced lipoate-H protein in the process. The reduced lipoate group of H protein is subsequently oxidized by L protein using  $\text{NAD}^+$ . This reaction regenerates the dithiolane ring of H protein's lipoate functional group, permitting it to participate in another catalytic cycle. Reducing equivalents in the form of NADH, one-carbon groups in the form of 5,10-methylene-THF and ammonium are important products of this reaction system. Based upon the work of Zhang et al., (2012), it is the enhanced supply of 5,10-methylene-THF available for use in the one-carbon cycle as well as for the synthesis of pyrimidines whereby upregulation of GLDC promotes tumor initiation.

methotrexane. It will be interesting to investigate if GLDC expression is a predictor of response to antifolate drugs in some cancers.

The work presented by Zhang et al., (2012) is a technical tour-de-force for its isolation of a rare subpopulation of TICs from primary NSCLC and for providing the scientific community with an explanation for what is genetically and metabolically unique about them. Although it certainly adds to our understanding about the metabolic differences between cancerous and non-cancerous cells, it also raised several fascinating questions.

The first—and most general—question concerns the nature of the recurring association between serine/glycine metabolism and tumorigenesis/cell proliferation. Other groups have also reported that many cancers have elevated levels of enzymes involved in the processing of serine/glycine (Possemato et al., 2011; Locasale et al., 2011; Vazquez et al.,

2011; Vié et al., 2008), and overexpression of some of these enzymes is sufficient to enhance the potential for cellular transformation and/or increase the rate of cellular proliferation (Locasale et al., 2011; Vié et al., 2008). How does an increase in this pathway facilitate proliferation and tumorigenesis? Does it provide extra pyrimidines for DNA replication and prevent uracil accumulation? Are there epigenetic effects on proliferative gene expression, perhaps due to changes in one-carbon metabolism and cellular methylation capacity? Or are there other explanations? The metabolic fate of the amino acids serine and glycine is complexly intertwined with pathways associated with the TCA cycle, glycolysis, protein synthesis, generation of intermediates for one-carbon metabolism, phospholipid synthesis, nucleotide synthesis, and maintenance of cellular osmolarity. Carefully dissecting the contribution of changes in the flux of these subsidiary metabolic pathways as a consequence

of a change in the rate in which a cell processes serine/glycine is an arduous task and will require more than a simple measurement of steady-state metabolite levels—an often deceptive marker of both the rate and directionality of flux (Fell, 1992; Snell and Fell, 1990). This later point is particularly important when evaluating the serine/glycine pathway, as many of the enzymes operate with only a slight displacement from equilibrium and flux determining steps are not intuitive.

The second question, as a corollary to the first, is how upregulated flux through the serine/glycine pathway is sustained in cancerous cells given all of the feedback mechanisms that are present in normal cells that prevent excess cycling through this pathway. Zhang et al., (2012) provide a tantalizing hint that, at least in the case of GLDC, oncogenes may drive the chronically high expression of serine/glycine metabolic enzymes, but how this occurs is unknown.

Finally, in regard to the biology of GLDC, it is curious that overexpression of only one component of the glycine cleavage complex is sufficient to massively perturb glycine dissimilation (Figure 1). The glycine cleavage complex is a multi-enzyme complex composed of four different subunits (P-[aka, GLDC] and H-, T-, and L-subunits) that are present in a ratio of 2P:27H:9T:1L and cooperate to channel substrates to reaction completion. Given this information, why are other subunits of the glycine cleavage complex not elevated in TICs? Is there a stoichiometric deficiency of GLDC in non-TICs that normally limits flux through the glycine cleavage complex? Is there a rearrangement of the complex ratios or modifications to the constituent subunits to handle an increase in GLDC-mediated product formation?

Overall, the paper presented by Zhang et al., (2012) makes a number of important contributions toward our understanding of the genetic and metabolic heterogeneity that is found in the cells within human tumors. It also suggests that inhibition of GLDC can be used in conjunction with existing antifolate chemotherapeutic regimens for the treatment of certain types of cancer. We shall watch with great interest as the story behind serine/glycine metabolism in cancer unfolds over the coming years.

## REFERENCES

- Fell, D.A. (1992). *Biochem. J.* 286, 313–330.
- Ferreira, L.M.R., Hebrant, A., and Dumont, J.E. (2012). *Oncogene*. Published online January 9, 2012. 10.1038/onc.2011.576.
- Locasale, J.W., Grassian, A.R., Melman, T., Lyssiotis, C.A., Mattaini, K.R., Bass, A.J., Heffron, G., Metallo, C.M., Muranen, T., Sharfi, H., et al. (2011). *Nat. Genet.* 43, 869–874.
- Nguyen, L.V., Vanner, R., Dirks, P., and Eaves, C.J. (2012). *Nat. Rev. Cancer* 12, 133–143.
- Possemato, R., Marks, K.M., Shaul, Y.D., Pacold, M.E., Kim, D., Birsoy, K., Sethumadhavan, S., Woo, H.K., Jang, H.G., Jha, A.K., et al. (2011). *Nature* 476, 346–350.
- Singh, A., and Settleman, J. (2010). *Oncogene* 29, 4741–4751.
- Snell, K., and Fell, D.A. (1990). *Adv. Enzyme Regul.* 30, 13–32.
- Vazquez, A., Markert, E.K., and Oltvai, Z.N. (2011). *PLoS ONE* 6, e25881.
- Vié, N., Copois, V., Bascoul-Molle, C., Denis, V., Bec, N., Robert, B., Fraslon, C., Conseiller, E., Molina, F., Larroque, C., et al. (2008). *Mol. Cancer* 7, 14.
- Zhang, W.C., Shyh-Chang, N., Yang, H., Rai, A., Umashankar, S., Ma, S., Soh, B.S., Sun, L.L., Tai, B.C., Nga, M.E., et al. (2012). *Cell* 148, 259–272.

# PI3King on MYCN to Improve Neuroblastoma Therapeutics

Michael D. Hogarty<sup>1,\*</sup> and John M. Maris<sup>1,\*</sup>

<sup>1</sup>Division of Oncology, Children's Hospital of Philadelphia, Perelman School of Medicine University of Pennsylvania, Philadelphia, PA 19104, USA

\*Correspondence: hogartym@email.chop.edu (M.D.H.), maris@chop.edu (J.M.M.)

DOI 10.1016/j.ccr.2012.01.018

**MYCN is an oncogenic driver of childhood neuroblastoma, a frequently lethal pediatric tumor. In a recent paper in *Science Translational Medicine*, Chantry and colleagues demonstrate that PI3K inhibition leads to the dual therapeutic benefits of enhanced MYCN degradation and loss of a paracrine angiogenic signal mediated by MYCN.**

Despite decades of ever-improving outcomes across diverse pediatric cancers, neuroblastoma has remained a frustrating clinical entity. Most children are diagnosed with tumors that harbor genetic and biological features highly correlated with a poor treatment outcome. Current therapy for such high-risk patients includes dose-intensive chemotherapy, radiotherapy, and retinoids. Though there have been recent impressive translational successes for this tumor, such as immunotherapy using an antibody targeting cell-surface GD2 given with immunostimulatory cytokines (Yu et al., 2010), 3 year relapse free survival estimates for high-risk disease remain under 50%.

Further compounding the frustration is the fact that the genome of neuroblastoma is one of the most comprehensively characterized among pediatric cancers, but it has not yet led to more effective treatment. The recent discovery that the *ALK* receptor tyrosine kinase is constitutively activated in ~10% of neuroblastomas (Mossé et al., 2008) provides one

such therapeutic opportunity, as *ALK* inhibitors have been in development due to the involvement of this kinase in a subset of non-small-cell lung cancers and anaplastic lymphomas. First generation *ALK* inhibitors such as crizotinib are already in Phase 2 trials for children with relapsed or refractory neuroblastoma and may make their way soon into upfront therapy for those patients with *ALK*-mutated tumors.

Contrast that with *MYCN*, the only other bona fide oncogene yet discovered in neuroblastoma that was initially identified almost 30 years ago (Brodeur et al., 1984). Despite this lead-time and a great deal of effort, no therapeutic has yet emerged to be able to target this clear oncogenic driver of the most aggressive subset of neuroblastomas. *MYCN*, which is a homolog of the *MYC* proto-oncogene, is somatically amplified in the tumor cells of ~20% of neuroblastoma patients (and in ~40% of those with a high-risk phenotype). *MYCN* amplification is independently correlated with advanced stage disease and poor outcome and therefore

is used worldwide in risk classification algorithms. Moreover, genetically engineered mouse models with *MYCN* expression targeted to neural crest tissue develop tumors that resemble human neuroblastoma (Weiss et al., 1997). *MYC* proteins, including *MYCN*, serve pleiotropic roles in malignancy, such as altering metabolic programs, supporting angiogenesis, promoting self-renewal and “stemness,” and driving proliferation while inhibiting differentiation.

*ALK* as a kinase is a pharmacologically tractable target, and a wealth of experience suggests that inhibition of activated kinases can lead to clinically impressive tumor responses. *MYCN*, in contrast, has long been seen as a problematic therapeutic target, as inactivating a highly abundant nuclear transcription factor that operates through a network of protein-protein interactions is pharmacologically daunting. Still, tumors are remarkably heterogeneous and cancer cells are remarkably adaptive. Resistance to targeted therapeutics can be efficiently selected for, especially when cells have

## REFERENCES

- Fell, D.A. (1992). *Biochem. J.* 286, 313–330.
- Ferreira, L.M.R., Hebrant, A., and Dumont, J.E. (2012). *Oncogene*. Published online January 9, 2012. 10.1038/onc.2011.576.
- Locasale, J.W., Grassian, A.R., Melman, T., Lyssiotis, C.A., Mattaini, K.R., Bass, A.J., Heffron, G., Metallo, C.M., Muranen, T., Sharfi, H., et al. (2011). *Nat. Genet.* 43, 869–874.
- Nguyen, L.V., Vanner, R., Dirks, P., and Eaves, C.J. (2012). *Nat. Rev. Cancer* 12, 133–143.
- Possemato, R., Marks, K.M., Shaul, Y.D., Pacold, M.E., Kim, D., Birsoy, K., Sethumadhavan, S., Woo, H.K., Jang, H.G., Jha, A.K., et al. (2011). *Nature* 476, 346–350.
- Singh, A., and Settleman, J. (2010). *Oncogene* 29, 4741–4751.
- Snell, K., and Fell, D.A. (1990). *Adv. Enzyme Regul.* 30, 13–32.
- Vazquez, A., Markert, E.K., and Oltvai, Z.N. (2011). *PLoS ONE* 6, e25881.
- Vié, N., Copois, V., Bascoul-Molle, C., Denis, V., Bec, N., Robert, B., Fraslon, C., Conseiller, E., Molina, F., Larroque, C., et al. (2008). *Mol. Cancer* 7, 14.
- Zhang, W.C., Shyh-Chang, N., Yang, H., Rai, A., Umashankar, S., Ma, S., Soh, B.S., Sun, L.L., Tai, B.C., Nga, M.E., et al. (2012). *Cell* 148, 259–272.

# PI3King on MYCN to Improve Neuroblastoma Therapeutics

Michael D. Hogarty<sup>1,\*</sup> and John M. Maris<sup>1,\*</sup>

<sup>1</sup>Division of Oncology, Children's Hospital of Philadelphia, Perelman School of Medicine University of Pennsylvania, Philadelphia, PA 19104, USA

\*Correspondence: [hogartym@email.chop.edu](mailto:hogartym@email.chop.edu) (M.D.H.), [maris@chop.edu](mailto:maris@chop.edu) (J.M.M.)

DOI 10.1016/j.ccr.2012.01.018

**MYCN is an oncogenic driver of childhood neuroblastoma, a frequently lethal pediatric tumor. In a recent paper in *Science Translational Medicine*, Chantry and colleagues demonstrate that PI3K inhibition leads to the dual therapeutic benefits of enhanced MYCN degradation and loss of a paracrine angiogenic signal mediated by MYCN.**

Despite decades of ever-improving outcomes across diverse pediatric cancers, neuroblastoma has remained a frustrating clinical entity. Most children are diagnosed with tumors that harbor genetic and biological features highly correlated with a poor treatment outcome. Current therapy for such high-risk patients includes dose-intensive chemotherapy, radiotherapy, and retinoids. Though there have been recent impressive translational successes for this tumor, such as immunotherapy using an antibody targeting cell-surface GD2 given with immunostimulatory cytokines (Yu et al., 2010), 3 year relapse free survival estimates for high-risk disease remain under 50%.

Further compounding the frustration is the fact that the genome of neuroblastoma is one of the most comprehensively characterized among pediatric cancers, but it has not yet led to more effective treatment. The recent discovery that the *ALK* receptor tyrosine kinase is constitutively activated in ~10% of neuroblastomas (Mossé et al., 2008) provides one

such therapeutic opportunity, as *ALK* inhibitors have been in development due to the involvement of this kinase in a subset of non-small-cell lung cancers and anaplastic lymphomas. First generation *ALK* inhibitors such as crizotinib are already in Phase 2 trials for children with relapsed or refractory neuroblastoma and may make their way soon into upfront therapy for those patients with *ALK*-mutated tumors.

Contrast that with *MYCN*, the only other bona fide oncogene yet discovered in neuroblastoma that was initially identified almost 30 years ago (Brodeur et al., 1984). Despite this lead-time and a great deal of effort, no therapeutic has yet emerged to be able to target this clear oncogenic driver of the most aggressive subset of neuroblastomas. *MYCN*, which is a homolog of the *MYC* proto-oncogene, is somatically amplified in the tumor cells of ~20% of neuroblastoma patients (and in ~40% of those with a high-risk phenotype). *MYCN* amplification is independently correlated with advanced stage disease and poor outcome and therefore

is used worldwide in risk classification algorithms. Moreover, genetically engineered mouse models with *MYCN* expression targeted to neural crest tissue develop tumors that resemble human neuroblastoma (Weiss et al., 1997). *MYC* proteins, including *MYCN*, serve pleiotropic roles in malignancy, such as altering metabolic programs, supporting angiogenesis, promoting self-renewal and “stemness,” and driving proliferation while inhibiting differentiation.

*ALK* as a kinase is a pharmacologically tractable target, and a wealth of experience suggests that inhibition of activated kinases can lead to clinically impressive tumor responses. *MYCN*, in contrast, has long been seen as a problematic therapeutic target, as inactivating a highly abundant nuclear transcription factor that operates through a network of protein-protein interactions is pharmacologically daunting. Still, tumors are remarkably heterogeneous and cancer cells are remarkably adaptive. Resistance to targeted therapeutics can be efficiently selected for, especially when cells have

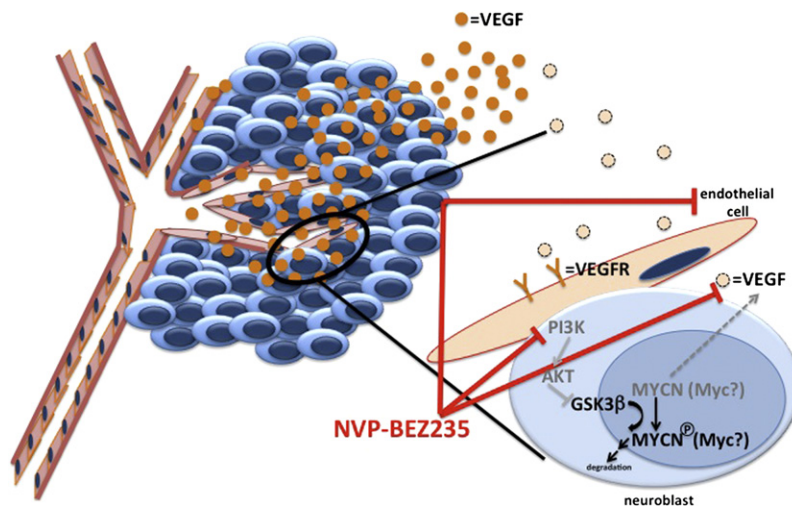


**Figure 1. Neuroblast-Intrinsic and -Extrinsic Therapeutic Effects of the Dual PI3K/mTOR Inhibitor NVP-BE2235**

MYCN (and MYC, when similarly dysregulated) induce vasculogenesis via secretion of VEGF and other angiogenic factors. Tumor-associated angiogenesis is similarly supported by paracrine signaling via VEGF downstream of MYCN. NVP-BE2235 impacts tumorigenesis through inhibition of PI3K and mTOR kinases, through PI3K inhibition-mediated degradation of MYCN, through GSK3 $\beta$ -mediated phosphodegradation pathways, and through direct anti-angiogenic effects on tumor-associated endothelial cells themselves. Not shown are effects attributable to mTOR inhibition, and pleiotropic effects realized by antagonism of MYCN activity in neuroblasts.

functionally redundant or degenerate pathways to compensate for the one being targeted, as is often the case with apical kinases such as ALK. MYC proteins, however, are unique in that their actions are largely non-redundant. In many experimental systems, the only gene products that can substitute for MYC are other MYC homologs. Emerging data using animal models also suggest that toxicity associating with MYC inhibition might not be as problematic as initially feared (Soucek et al., 2008). So MYC remains a compelling therapeutic target for neuroblastoma and many other cancers (Delmore et al., 2011).

It is therefore of great interest that a recent paper in *Science Translational Medicine* demonstrates the benefits of inhibiting PI3K and mTOR signaling with the small molecule NVP-BE2235 in complementary models of neuroblastoma (Chanthery et al., 2012). Neuroblastomas are richly vascular tumors, particularly those with MYCN amplification, and it has long been inferred that MYCN may modulate tumor angiogenesis via regulation of VEGF expression, as has been more formally demonstrated for MYC (Baudino et al., 2002). Indeed, it has been shown that PI3K/mTOR blockade leads to destabilization of MYCN and com-

surate reduction in VEGF secretion, along with inhibition of neuroblastoma progression in murine models (Chesler et al., 2006). One critical component lacking up until now had been the relative contributions of inhibiting PI3K/mTOR in the tumor cells themselves, as opposed to in other cells within the tumor microenvironment. That is, is the observed anti-tumor activity mediated by tumor cell intrinsic or extrinsic mechanisms, or both?

Chanthery et al., (2012) demonstrate that NVP-BE2235 inhibits neuroblast proliferation in vitro and that this effect is more pronounced in those cell lines with MYCN amplification and overexpression. They then corroborate an impact on tumor progression using both a neuroblastoma xenograft model (in which contributions of the immune compartment are lacking) as well as a MYCN-dependent transgenic model (recapitulating a MYCN “amplified” tumor arising at its autochthonous site). Though tumor regressions were not described, there was inhibition of tumor growth in both models, attributed to both reductions in tumor-associated vascular density and neuroblast proliferation. MYCN was markedly reduced in treated tumors, and evidence for both PI3K and mTOR inhibition was demonstrated, supporting the

notion that PI3K inhibition led to derepression of GSK3 $\beta$  with resultant Thr58 phosphorylation and destabilization of MYCN.

The authors used a series of elegant experiments to then decipher the contributions of the tumor compartment by introducing wild-type MYCN or a Thr58 mutant MYCN that is resistant to Thr58-mediated destabilization into a neuroblastoma cell line with undetectable MYCN. These models allow the investigators to attribute tumor-cell autonomous effects of NVP-BE2235 to MYCN degradation by correlating MYCN stability, VEGF secretion, and recruitment of HUVEC cells in endothelial migration assays. The impact of NVP-BE2235 on MYCN stability and proliferation was reduced in cells expressing the Thr58 mutant MYCN. Importantly, VEGF secretion and HUVEC migration also was shown to be substantially MYCN-dependent, supporting a paracrine role downstream of MYCN. Indeed, direct knock-down of MYCN or indirect upregulation via knock-down of HUWE1 (an E3-ligase that degrades phosphorylated MYCN) led to commensurate changes in MYCN stability, VEGF secretion, and HUVEC recruitment, underscoring a prominent role for MYCN in this paracrine activity. NVP-BE2235 clearly had a direct impact on endothelial cells themselves. However, this suggests the anti-angiogenic effects seen in vivo were both tumor cell intrinsic and extrinsic (Figure 1).

It should be noted that the impact of NVP-BE2235 (via PI3K/mTOR inhibition) was more modest in most of these assays than was knock-down of MYCN, suggesting that its impact on MYCN was suboptimal. Still, an agent that targets the predominant oncogenic driver in this malignancy to impact diverse MYCN-mediated functions and represses tumor-associated angiogenesis directly through effects on endothelial cells and indirectly through paracrine mediated effects of tumor cells is certainly worth exploring clinically. Chanthery et al., (2012) demonstrate compelling indirect evidence that VEGF is the intermediate in this paracrine process but do not directly demonstrate this either by VEGF knock-down or by using available VEGF antagonists in their assays. Might PI3K/mTOR inhibition synergize with VEGF antagonists to potentiate these anti-angiogenic effects? Also, it is fair to

wonder whether these effects are truly restricted to neuroblastomas with *MYCN* amplification, as surmised, or might operate similarly through *MYC* when this homolog is deregulated. In high-risk neuroblastomas that lack *MYCN* amplification, *MYC* is frequently deregulated (Westermann et al., 2008), suggesting some degree of *MYC* or *MYCN* augmentation may be essential for the high-risk phenotype. This was not directly tested because the available transgenic model for this tumor mimics *MYCN* amplification as an oncogenic driver and no *MYCN* non-amplified tumor xenografts were explored. Though elucidation of a novel *MYCN*-directed therapeutic is significant enough, the impact may be further broadened to a greater proportion of patients with high-risk neuroblastoma should *MYC* serve a similar role, which is a worthy

pursuit, and may extend the relevance of these findings to all human cancers that usurp *MYC* signaling as an essential component of sustaining the malignant phenotype.

#### REFERENCES

- Baudino, T.A., McKay, C., Pendeville-Samain, H., Nilsson, J.A., Maclean, K.H., White, E.L., Davis, A.C., Ihle, J.N., and Cleveland, J.L. (2002). *Genes Dev.* 16, 2530–2543.
- Breider, G.M., Seeger, R.C., Schwab, M., Varmus, H.E., and Bishop, J.M. (1984). *Science* 224, 1121–1124.
- Chantry, Y.H., Gustafson, W.C., Itsara, M., Persson, A., Hackett, C.S., Grimmer, M., Charron, E., Yakovenko, S., Kim, G., Matthay, K.K., and Weiss, W.A. (2012). *Sci Transl Med.* 4, 115ra113.
- Chesler, L., Schlieve, C., Goldenberg, D.D., Kenney, A., Kim, G., McMillan, A., Matthay, K.K., Rowitch, D., and Weiss, W.A. (2006). *Cancer Res.* 66, 8139–8146.

Delmore, J.E., Issa, G.C., Lemieux, M.E., Rahl, P.B., Shi, J., Jacobs, H.M., Kastiris, E., Gilpatrick, T., Paranal, R.M., Qi, J., et al. (2011). *Cell* 146, 904–917.

Mossé, Y.P., Laudenslager, M., Longo, L., Cole, K.A., Wood, A., Attiyeh, E.F., Laquaglia, M.J., Sennett, R., Lynch, J.E., Perri, P., et al. (2008). *Nature* 455, 930–935.

Soucek, L., Whitfield, J., Martins, C.P., Finch, A.J., Murphy, D.J., Sodik, N.M., Karnezis, A.N., Swigart, L.B., Nasi, S., and Evan, G.I. (2008). *Nature* 455, 679–683.

Weiss, W.A., Aldape, K., Mohapatra, G., Feuerstein, B.G., and Bishop, J.M. (1997). *EMBO J.* 16, 2985–2995.

Westermann, F., Muth, D., Benner, A., Bauer, T., Henrich, K.O., Oberthuer, A., Brors, B., Beissbarth, T., Vandesompele, J., Pattyn, F., et al. (2008). *Genome Biol.* 9, R150.

Yu, A.L., Gilman, A.L., Ozkaynak, M.F., London, W.B., Kreissman, S.G., Chen, H.X., Smith, M., Anderson, B., Villablanca, J.G., Matthay, K.K., et al; Children's Oncology Group. (2010). *N. Engl. J. Med.* 363, 1324–1334.

## The RAF Inhibitor Paradox Revisited

Adrienne D. Cox<sup>1,2,\*</sup> and Channing J. Der<sup>1,\*</sup>

<sup>1</sup>Department of Radiation Oncology

<sup>2</sup>Department of Pharmacology

Lineberger Comprehensive Cancer Center, University of North Carolina at Chapel Hill, Chapel Hill, NC 27599, USA

\*Correspondence: [adricox@med.unc.edu](mailto:adricox@med.unc.edu) (A.D.C.), [cjder@med.unc.edu](mailto:cjder@med.unc.edu) (C.J.D.)

DOI 10.1016/j.ccr.2012.01.017

**The success of the RAF protein kinase inhibitor vemurafenib for the treatment of *BRAF* mutant metastatic melanoma has produced another poster child for the promise of personalized medicine. However, the results of a recent study also reveal unexpected pitfalls in the application of signal transduction-targeted therapies.**

The era of personalized cancer medicine is upon us. The cancer patient's genome can now be interrogated for specific genetic alterations to guide the application of therapies specifically targeted to those alterations. A dramatic therapeutic advance in this area is the *BRAF*-selective inhibitor vemurafenib, which has provided a significant improvement in overall survival compared to the previous standard of care for metastatic melanoma (Chapman et al., 2011). However, recent findings with vemurafenib and other protein kinase inhibitors demonstrate that the new era of signal transduction-targeted therapies is handicapped by some of the same issues that have plagued traditional cytotoxic drugs.

One key distinction between targeted versus cytotoxic therapies is decreased normal cell toxicity. Symptoms such as the classic myelosuppression associated with many cytotoxic antineoplastics are not as limiting with targeted agents, whose therapeutic effects are typically achievable at doses lower than those conferring myelosuppression or other dose-limiting toxicities. However, rapidly acquired cancer cell resistance shortens the duration of treatment response. For example, although the initial response to vemurafenib is impressive, with a response rate of ~50% and significant survival benefit, tumor resistance usually occurs within 2–18 months of initial treatment. Multiple mechanisms of resistance

have been described, including mutational activation of *NRAS* or receptor tyrosine kinase-mediated activation of *RAS*, both leading to *CRAF*-dependent activation of *MEK*-*ERK* signaling (Figure 1) (Johannessen et al., 2010; Nazarian et al., 2010). Thus, as for cytotoxic drugs, combinations of targeted therapies will be needed, both to enhance the initial response and to reduce the subsequent onset of drug resistance. Such combinations may also have advantages in blocking the existing tumor without inducing or allowing new ones to appear.

That chemotherapy can both cure and cause cancer is not a new concept. Conventional cytotoxic chemotherapy has long been known to contribute to the

# Conflicting Roles of Molecules in Hepatocarcinogenesis: Paradigm or Paradox

Gen-Sheng Feng<sup>1,2,\*</sup>

<sup>1</sup>Department of Pathology, School of Medicine

<sup>2</sup>Molecular Biology Section, Division of Biological Sciences

University of California at San Diego, La Jolla, CA 92093-0864, USA

\*Correspondence: [gfeng@ucsd.edu](mailto:gfeng@ucsd.edu)

DOI 10.1016/j.ccr.2012.01.001

In delineating the molecular pathogenesis of hepatocellular carcinoma (HCC), recent experiments in mouse tumor models have revealed unexpected tumor-suppressing effects in genes previously identified as pro-oncogenic. This contradiction underscores the complexity of hepatocarcinogenesis and predicts uncertainty in targeting these molecules for HCC therapy. Deciphering the underlying mechanisms for these paradoxical functions will elucidate the complex molecular and cellular communications driving HCC development, and will also suggest more thoughtful therapeutic strategies for this deadly disease.

Hepatocellular carcinoma (HCC) is the third leading cause of cancer-related death worldwide. However, the molecular and cellular mechanisms underlying HCC initiation and development are poorly understood. In recent studies, a number of groups have employed cell type-specific gene knockout (KO) mouse models to dissect HCC pathogenesis. This approach has no doubt provided mechanistic insights into hepatocarcinogenesis. However, opposing roles in promoting and suppressing HCC have been reported for the same molecules in different animal models (Figure 1). These conflicting results do not necessarily obscure the understanding of molecular pathogenesis in HCC. Instead, further experiments carefully designed to decipher the opposing roles will lead to better understanding of HCC development.

## Contradictory Results from Different Animal Models

The NF- $\kappa$ B pathway that promotes cell survival and proliferation is constitutively activated in a variety of tumors. Consistently, several groups have reported tumor-promoting effects of NF- $\kappa$ B in mouse models (Haybaeck et al., 2009; Pikarsky et al., 2004). Removal of Mdr-2 P-glycoprotein triggered spontaneous development of cholestatic hepatitis and consequently HCC in mice, and inactivation of the NF- $\kappa$ B pathway in hepatocytes suppressed HCC progression initiated by Mdr-2 deletion (Pikarsky et al., 2004). By controlling the timing of shutting down the NF- $\kappa$ B pathway, the authors demonstrated that NF- $\kappa$ B was required for the later stage of HCC progression, without significant impact on transformation or the early stage of tumor development. In contrast, Karin's group reported that hepatocyte-specific ablation of Ikk $\beta$  (Ikk $\beta^{\Delta\text{hep}}$ ), a kinase required for the activation of NF- $\kappa$ B, resulted in dramatic increase in HCC development induced by the chemical carcinogen diethylnitrosamine (DEN), pointing to an antitumor effect of NF- $\kappa$ B in the liver (Maeda et al., 2005). DEN, as a procarcinogen, can be metabolically activated in hepatocytes and forms bulky DNA adducts that induce genomic instability and gene mutations (Aleksic et al., 2011; Verna et al., 1996). The carcinogenic effect of DEN can be

enhanced by other tumor promoters, such as phenobarbital, in adult mice. Consistent with the increased susceptibility of Ikk $\beta^{\Delta\text{hep}}$  mice to DEN-induced tumorigenesis, hepatocyte-specific deletion of NEMO/Ikk $\gamma$ , another component of the Ikk complex, leads to spontaneous development of HCC, following hepatic steatosis and chronic inflammation in mice (Luedde et al., 2007).

Highlighting a similar paradox, several groups have demonstrated either tumor-promoting or tumor-suppressing actions of Jnk kinases in HCC. Hui et al. detected high levels of p-Jnk1 in human HCC lesions and found that the incidence of DEN/phenobarbital-induced HCC was significantly reduced in Jnk1 $^{-/-}$  but not in Jnk2 $^{-/-}$  mice (Hui et al., 2008). Consistently, siRNA-mediated Jnk1 or Jnk1 together with Jnk2 knockdown in Huh7 human HCC cells suppressed in vitro proliferation and tumor formation as subcutaneous xenografts in nude mice, with no effect observed for Jnk2 knockdown. In contrast, Davis and colleagues presented data suggesting a tumor-suppressing effect of Jnk1 and Jnk2 in hepatocytes (Das et al., 2011). The authors generated mutant mice ( $H^{\Delta\text{Jnk}}$ ) with Jnk1 and Jnk2 deficiency in hepatocytes by deleting Jnk1 specifically in hepatocytes in the Jnk2 $^{-/-}$  background. Their results indicate that combined deficiency of Jnk1 and Jnk2 leads to increased tumor sizes in DEN-treated mice.

Stat3 clearly has a pro-oncogenic function, based on the detection of activating mutations or enhanced p-Stat3 signals in different types of cancer (Calvisi, 2011; Yu et al., 2009). However, both pro- and anti-oncogenic activities of Stat3 in HCC development were observed in hepatocyte-specific Stat3 knockouts, transgenic mice expressing dominant-active or -negative mutants of Stat3, or tumor-bearing animals treated with Stat3 inhibitors (Lin et al., 2009; Schneller et al., 2011; Wang et al., 2011b). Interestingly, hepatocyte-specific deletion of the tyrosine phosphatase Shp2 resulted in a marked increase in DEN-induced HCC incidence, which was compromised by the additional removal of Stat3 (Bard-Chapeau et al., 2011). However, deleting Stat3 alone also led to enhanced

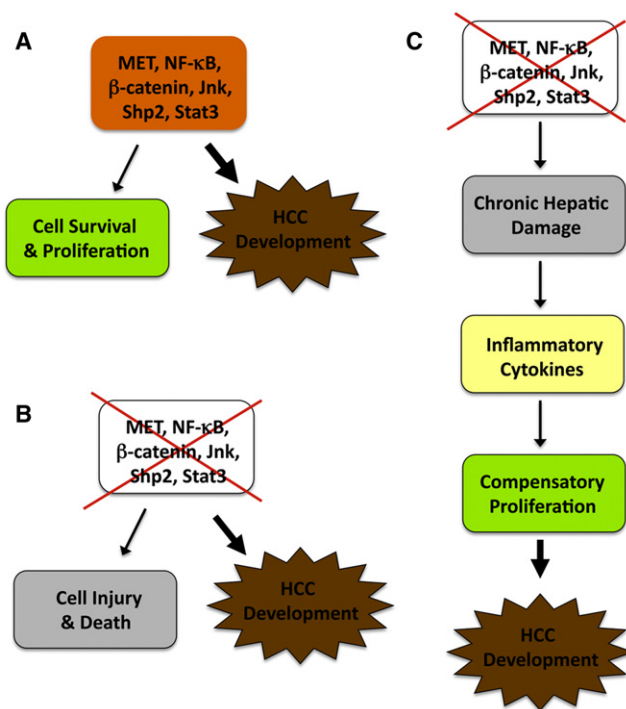


**Figure 1. A Simplified Model for the Pro- and Anti-Oncogenic Activities of the Same Molecules in Hepatocarcinogenesis**

(A) MET, NF-κB, Stat3, Jnk, Shp2, and β-catenin constitute pathways that normally promote cell survival and proliferation. Aberrant activation or overexpression of these molecules enhances cell transformation and tumorigenesis.

(B) Removal or inactivation of these protumorigenic molecules, which normally causes hepatocyte damage and death, also enhances HCC development under certain conditions.

(C) One possible explanation is that loss of a prosurvival signal enhances chronic hepatic damage, increases production of inflammatory cytokines, and triggers excessive compensatory proliferation of hepatocytes and/or progenitor cells, resulting in elevated hepatocarcinogenesis.

tumorigenesis induced by DEN (Bard-Chapeau et al., 2011) or CCl<sub>4</sub> (Wang et al., 2011b) as compared to wild-type mice.

Contrasting roles in HCC have also been observed for β-catenin, a chief effector in the Wnt pathway. Consistent with the detection of activating mutations in the β-catenin gene (*CTNNB1*) in HCCs (de La Coste et al., 1998), Monga and colleagues reported that overexpression of a dominant-active β-catenin mutant in hepatocytes accelerated DEN-induced hepatocarcinogenesis (Nejak-Bowen et al., 2010). Surprisingly, the same group found that hepatocyte-specific *Ctnnb1* KO mice also displayed higher susceptibility to DEN-induced tumorigenesis, due to excessive oxidative stress, hepatic injury, and inflammation (Zhang et al., 2010). Therefore, HCC is promoted by both gain and loss of β-catenin function in hepatocytes (Nejak-Bowen and Monga, 2011).

The opposing roles in promoting and suppressing HCC are not restricted to intracellular signaling molecules. The HGF receptor (MET) tyrosine kinase system represents a classic pro-oncogenic signaling pathway, and dominant-active mutations of MET have been found in human HCC and other tumors (Birchmeier et al., 2003). As expected, overexpression of MET in hepa-

tocytes promoted HCC development in transgenic mice (Wang et al., 2001). Turning off the transgene expression in tumor-bearing mice led to increased cell apoptosis and impaired proliferation resulting in tumor regression, suggesting that MET is required in genesis and maintenance of HCC. Surprisingly, Thorgeirsson's group showed that hepatocyte-specific *Met* KO mice exhibited higher susceptibility to DEN-induced tumorigenesis and developed larger and more tumors than control animals (Takami et al., 2007).

### Possible Explanations and Unanswered Questions

How should one interpret these conflicting findings? One can easily explain the tumor-promoting effect of these molecules based on their known pro-proliferation and anti-apoptosis functions. It is certainly more challenging to understand the unanticipated antitumor effect of these molecules. In dissecting the underlying mechanisms, several groups have shown that the outcome depends on the cell types in the liver from which a target gene is removed (Das et al., 2011; Maeda et al., 2005). Deleting *Ikkβ* or *Jnk1* and *Jnk2* in hepatocytes only by *Alb-Cre* enhanced DEN-induced HCC, whereas inactivating the same gene in both hepatocytes and nonparenchymal cells using *Mx1-Cre* suppressed tumorigenesis. Based on these and other experimental data, one emerging theory is that the loss of a prosurvival molecule triggers chronic hepatic injury, which in turn enhances compensatory proliferation through elevated production of cytokines from infiltrated inflammatory cells, including Kupffer cells. Excessive and continuous proliferation of hepatocytes or progenitor cells eventually leads to spontaneous or DEN-induced neoplastic growth in the liver (Figure 1).

In the multistage pathogenic process, elevated hepatocyte death is the first step in promoting hepatocarcinogenesis. Indeed, deletion of *Ikkβ* or β-catenin in hepatocytes caused dramatically increased accumulation of reactive oxygen species, and feeding the mice with antioxidants reduced HCC incidence (Maeda et al., 2005; Zhang et al., 2010). Additional deletion of FADD, an essential adaptor molecule downstream of death receptors, alleviated excessive apoptosis, inflammation, and steatohepatitis in *Nemo*<sup>LPC-KO</sup> mice (Luedde et al., 2007), resulting in decreased tumorigenesis in *Fadd* and *Nemo* compound mutant mice (M. Pasparakis, personal communication).

Enhanced cell death may increase compensatory proliferation of tumor-initiating cells (TICs) originating from mature hepatocytes or progenitor cells, and several lines of evidence support this notion. For example, proliferating cells were frequently located around apoptotic cells in centrilobular lesions after DEN exposure (Maeda et al., 2005). Additional deletion of *Jnk1* in *Ikkβ*<sup>Δhep</sup> mice suppressed compensatory proliferation following DEN injection and consequently reduced tumor burden (Sakurai et al., 2006). Severe steatosis induced by loss of PTEN enhanced hepatocyte death and compensatory proliferation of TICs (Galicía et al., 2010). Although loss of either Shp2 or Stat3 in hepatocytes led to increased tumorigenesis, combined deletion of both did not show an additive or synergistic effect but interestingly a neutralizing result (Bard-Chapeau et al., 2011), which is likely due to impaired compensatory proliferation in the absence of both Shp2 and Stat3 (our unpublished data). A similar compromising effect of Tak1 and NEMO ablation was observed (Bettermann et al., 2010), although it was unclear

whether removal of the two molecules suppressed hepatocyte proliferation potential.

Pro-inflammatory cytokines play important roles in these HCC animal models. Hepatic expression of  $\text{TNF}\alpha$ , IL-6, and HGF was increased in  $\text{Ikk}\beta^{\Delta\text{hep}}$  mice (Maeda et al., 2005). Higher circulating levels of IL-1 $\alpha$  and IL-6 were detected in  $\text{Ikk}\beta^{\Delta\text{hep}}$  and  $\text{p38}\alpha^{\Delta\text{hep}}$  mice following DEN injection, which were alleviated by antioxidant treatment that prevented hepatocyte death (Sakurai et al., 2008). Blocking IL-1 $\alpha$  action by injection of IL-1R antagonist or ablation of IL-1R suppressed DEN-induced IL-6 production, compensatory proliferation, and tumorigenesis. These results suggest that IL-1 $\alpha$  released from dying hepatocytes stimulates production of IL-6, which in turn induces surviving hepatocytes to proliferate (Sakurai et al., 2008). A similar mechanism involving paracrine action of cytokines was identified in mice with Jnk or Stat3 deficiency in hepatocytes only or in hepatocytes plus nonparenchymal cells (Das et al., 2011; Horiguchi et al., 2008). In aggregate, these results highlight the importance of hepatic cell communication in liver tumorigenesis.

It remains to be elucidated at which stage(s) the paracrine cytokines and the infiltrated inflammatory cells contribute to hepatocarcinogenesis. The ability to isolate TICs at early stages of HCC development following DEN exposure (He et al., 2010) will help clarify this issue. Opposite effects on tumorigenesis were observed when deleting the same gene using *Alb-Cre* and *Mx1-Cre* lines, respectively (Das et al., 2011; Maeda et al., 2005). It will be interesting to isolate and compare TICs from the two mutant mouse lines. If mutant TICs of the two origins display opposite growth properties in vitro and in allografts in recipient animals, the result would suggest that the initial transformation event is already influenced by the hepatic microenvironment. However, if the TICs of the two origins display similar phenotypes, one may conclude that the inflammatory cytokines or the hepatic microenvironment influences tumor progression without effect on TIC genesis.

One issue that could affect the interpretation of data from hepatocyte-specific KO mice is the timing and efficiency of *Cre* expression. The nature of the few surviving hepatocytes that become TICs and eventually develop into HCCs remains to be determined. It is possible that a few hepatocytes have escaped *Cre*-mediated DNA excision and thus gain survival and proliferative advantages over neighboring cells with a pro-survival gene ablated. Arguing against this theory are the data that the targeted genes were efficiently deleted in tumors (Bard-Chapeau et al., 2011; Das et al., 2011; Maeda et al., 2005; Sakurai et al., 2008). However, the possibility that a target gene was intact in TICs but was deleted later during cancer progression, which no longer requires the gene product, has not been excluded. Indeed, one report on HCC induced by *Ddb1* deletion suggests that HCC originates from hepatocytes that escaped *Alb-Cre*-mediated gene ablation (Yamaji et al., 2010). In another study, Chen and colleagues found that liver tumors developed from  $\beta$ -catenin-positive hepatic progenitor cells in *Alb-Cre*-mediated *Ctnnb1* deletion (Wang et al., 2011a). To unequivocally determine the gene deletion status during HCC initiation and progression, it is important to use inducible and tightly controlled *Cre* expression strategies that are yet to be optimized.

Thus far, most studies have largely focused on the final outcome of HCC development after a long period of DEN treatment. More rigorous analyses of the kinetics of hepatic injury and disorders associated with early stages of tumorigenesis will provide mechanistic insights into the pathogenic process. With regard to the hepatic microenvironment in tumorigenesis, relative contributions of Kupffer cells versus other infiltrating cell types will need to be clarified. Possible roles of oval cells and hepatic stellate cells in HCC development need to be carefully examined, which may help interpret the seemingly contradictory findings.

There are many open questions for the antitumor effect of protumorigenic molecules. The cell death-compensatory proliferation-transformation-hepatocarcinogenesis scheme (Figure 1) is likely an oversimplified model, and other mechanisms may also be involved in promoting HCC development. Inactivation of one protumorigenic pathway in hepatocytes may lead to aberrant activation of another. For example, overexpression of PDGFR $\alpha$  and c-Myc was detected in  $\beta$ -catenin-deficient livers (Zhang et al., 2010), and upregulated Stat3 activity was observed in the liver of  $\text{Ikk}\beta^{\Delta\text{hep}}$  or  $\text{Shp2}^{\Delta\text{hep}}$  mice (Bard-Chapeau et al., 2011; He et al., 2010). Rather than showing increased apoptosis,  $\text{Ikk}\beta$ -deficient TICs were found to exhibit higher survival and proliferative capacity in vitro, although the molecular basis is not fully understood (He et al., 2010). Thus, excessive compensatory reaction to loss of a proliferative signal may also contribute to the unexpected tumor-promoting effect observed upon removal of a protumorigenic molecule, at least in some cases.

### Implications in Human HCC Pathogenesis and Therapy

As described above, either aberrant gain or loss of function of the same molecule can lead to malignant growth, reinforcing the concept that homeostasis is critical for preventing tumorigenesis in the liver. A critical question is whether the results from these animal experiments are relevant to human HCCs. Constitutive activation of MET,  $\beta$ -catenin, NF- $\kappa$ B, and Stat3 has been detected in human HCC samples or cell lines (Birchmeier et al., 2003; Calvisi, 2011; He et al., 2010; Nejak-Bowen and Monga, 2011; Yu et al., 2009). In contrast, there has been almost no definitive report of loss-of-function mutations in these genes in human HCCs, thus the paucity of evidence to support their tumor suppressor role. Although deficient expression of *Shp2* was detected in primary human HCCs (Bard-Chapeau et al., 2011), it was unclear whether *Shp2* deficiency plays a causative role in their pathogenesis. Genome-wide sequencing of human HCC samples worldwide may identify inactivating mutations in these proto-oncogenes, most likely at low frequencies.

Despite the rare detection of corresponding mutations in humans, these mouse mutants recapitulate many aspects of pathological features in human patients, including chronic hepatocyte damage, elevated oxidative stress, inflammation, fibrosis, steatohepatitis, and cholestasis. Therefore, these animal models are useful for understanding the molecular and cellular mechanisms of liver cancer in humans. In particular, the mouse models provide access to early events in tumorigenesis, particularly the dynamic interplay of TICs with the hepatic microenvironment. Given the 100% penetrance in DEN-induced carcinogenesis and the high degree of similarity in pathogenesis, mutant mice

can serve as platforms in the search for biomarkers for early diagnosis of HCC, the significance of which cannot be overstated given the current poor prognosis of patients with late stages of HCC.

Personalized therapeutic strategies can be developed based on dominantly activating mutations detected in tumors. A potent MET inhibitor might be effective in treating a liver cancer patient with an activating MET mutation (You et al., 2011). However, the pro- and anti-oncogenic roles of signaling molecules and the cell type-specific effects of gene deletion described above bring uncertainty to using inhibitors of these molecules as anticancer drugs, as reported for Stat3 inhibitors (Yue and Turkson, 2009). One interesting idea is the development of anti-HCC therapeutics by sorting beneficial from harmful functions of a signaling molecule such as  $\beta$ -catenin (Nejak-Bowen and Monga, 2011). Due to the compensatory upregulation of one pathway in reaction to the loss of another, simultaneous blockade of several pathways by a cocktail of inhibitors may be a more effective approach. Additional removal of Stat3 reversed the tumor-promoting effect of Shp2 deletion (Bard-Chapeau et al., 2011), and inhibition of PDGFR $\alpha$  suppressed tumorigenesis induced by ablation of  $\beta$ -catenin (Zhang et al., 2010).

The debate over the relevance of mouse data to human HCCs will likely continue. However, in-depth molecular analyses in animal models cannot be replaced by examination of human HCC specimens. The opposing roles of signaling molecules revealed by these mouse models indicate a need for reassessment of current approaches in drug targeting and screening. Finally, although the discussion in this article focuses on HCC, contrasting roles of NF- $\kappa$ B have been observed in other types of cancer, such as skin cancer (van Hogerlinden et al., 2002). Therefore, it is crucial to elucidate factors that regulate various functions of each of these oncogenic pathways.

## ACKNOWLEDGMENTS

The author apologizes for not citing many other exciting papers in this short article and thanks colleagues for critical reading of the manuscript. Work in the author's laboratory has been supported by NIH grant numbers R01DK075916 and HL096125.

## REFERENCES

- Aleksic, K., Lackner, C., Geigl, J.B., Schwarz, M., Auer, M., Ulz, P., Fischer, M., Trajanoski, Z., Otte, M., and Speicher, M.R. (2011). Evolution of genomic instability in diethylnitrosamine-induced hepatocarcinogenesis in mice. *Hepatology* 53, 895–904.
- Bard-Chapeau, E.A., Li, S., Ding, J., Zhang, S.S., Zhu, H.H., Princen, F., Fang, D.D., Han, T., Bailly-Maitre, B., Poli, V., et al. (2011). Ptpn11/Shp2 acts as a tumor suppressor in hepatocellular carcinogenesis. *Cancer Cell* 19, 629–639.
- Bettermann, K., Vucur, M., Haybaeck, J., Koppe, C., Janssen, J., Heymann, F., Weber, A., Weiskirchen, R., Liedtke, C., Gassler, N., et al. (2010). TAK1 suppresses a NEMO-dependent but NF- $\kappa$ B-independent pathway to liver cancer. *Cancer Cell* 17, 481–496.
- Birchmeier, C., Birchmeier, W., Gherardi, E., and Vande Woude, G.F. (2003). Met, metastasis, motility and more. *Nat. Rev. Mol. Cell Biol.* 4, 915–925.
- Calvisi, D.F. (2011). Dr. Jekyll and Mr. Hyde: a paradoxical oncogenic and tumor suppressive role of signal transducer and activator of transcription 3 in liver cancer. *Hepatology* 54, 9–12.
- Das, M., Garlick, D.S., Greiner, D.L., and Davis, R.J. (2011). The role of JNK in the development of hepatocellular carcinoma. *Genes Dev.* 25, 634–645.
- de La Coste, A., Romagnolo, B., Billuart, P., Renard, C.A., Buendia, M.A., Soubrane, O., Fabre, M., Chelly, J., Beldjord, C., Kahn, A., and Perret, C. (1998). Somatic mutations of the  $\beta$ -catenin gene are frequent in mouse and human hepatocellular carcinomas. *Proc. Natl. Acad. Sci. USA* 95, 8847–8851.
- Galicía, V.A., He, L., Dang, H., Kanel, G., Vendryes, C., French, B.A., Zeng, N., Bayan, J.A., Ding, W., Wang, K.S., et al. (2010). Expansion of hepatic tumor progenitor cells in Pten-null mice requires liver injury and is reversed by loss of AKT2. *Gastroenterology* 139, 2170–2182.
- Haybaeck, J., Zeller, N., Wolf, M.J., Weber, A., Wagner, U., Kurrer, M.O., Bremer, J., Iezzi, G., Graf, R., Clavien, P.A., et al. (2009). A lymphotoxin-driven pathway to hepatocellular carcinoma. *Cancer Cell* 16, 295–308.
- He, G., Yu, G.Y., Temkin, V., Ogata, H., Kuntzen, C., Sakurai, T., Sieghart, W., Peck-Radosavljevic, M., Leffert, H.L., and Karin, M. (2010). Hepatocyte IKK $\beta$ /NF- $\kappa$ B inhibits tumor promotion and progression by preventing oxidative stress-driven STAT3 activation. *Cancer Cell* 17, 286–297.
- Horiguchi, N., Wang, L., Mukhopadhyay, P., Park, O., Jeong, W.I., Lafdil, F., Osei-Hyiaman, D., Moh, A., Fu, X.Y., Pacher, P., et al. (2008). Cell type-dependent pro- and anti-inflammatory role of signal transducer and activator of transcription 3 in alcoholic liver injury. *Gastroenterology* 134, 1148–1158.
- Hui, L., Zatloukal, K., Scheuch, H., Stepniak, E., and Wagner, E.F. (2008). Proliferation of human HCC cells and chemically induced mouse liver cancers requires JNK1-dependent p21 downregulation. *J. Clin. Invest.* 118, 3943–3953.
- Lin, L., Amin, R., Gallicano, G.I., Glasgow, E., Jogunoori, W., Jessup, J.M., Zaslloff, M., Marshall, J.L., Shetty, K., Johnson, L., et al. (2009). The STAT3 inhibitor NSC 74859 is effective in hepatocellular cancers with disrupted TGF- $\beta$  signaling. *Oncogene* 28, 961–972.
- Luedde, T., Beraza, N., Kotsikoris, V., van Loo, G., Nenci, A., De Vos, R., Roskams, T., Trautwein, C., and Pasparakis, M. (2007). Deletion of NEMO/IKK $\gamma$  in liver parenchymal cells causes steatohepatitis and hepatocellular carcinoma. *Cancer Cell* 11, 119–132.
- Maeda, S., Kamata, H., Luo, J.L., Leffert, H., and Karin, M. (2005). IKK $\beta$  couples hepatocyte death to cytokine-driven compensatory proliferation that promotes chemical hepatocarcinogenesis. *Cell* 121, 977–990.
- Nejak-Bowen, K.N., and Monga, S.P. (2011).  $\beta$ -catenin signaling, liver regeneration and hepatocellular cancer: sorting the good from the bad. *Semin. Cancer Biol.* 21, 44–58.
- Nejak-Bowen, K.N., Thompson, M.D., Singh, S., Bowen, W.C., Jr., Dar, M.J., Khillan, J., Dai, C., and Monga, S.P. (2010). Accelerated liver regeneration and hepatocarcinogenesis in mice overexpressing serine-45 mutant  $\beta$ -catenin. *Hepatology* 51, 1603–1613.
- Pikarsky, E., Porat, R.M., Stein, I., Abramovitch, R., Amit, S., Kasem, S., Gutskevich-Pyest, E., Urieli-Shoval, S., Galun, E., and Ben-Neriah, Y. (2004). NF- $\kappa$ B functions as a tumour promoter in inflammation-associated cancer. *Nature* 431, 461–466.
- Sakurai, T., Maeda, S., Chang, L., and Karin, M. (2006). Loss of hepatic NF- $\kappa$ B activity enhances chemical hepatocarcinogenesis through sustained c-Jun N-terminal kinase 1 activation. *Proc. Natl. Acad. Sci. USA* 103, 10544–10551.
- Sakurai, T., He, G., Matsuzawa, A., Yu, G.Y., Maeda, S., Hardiman, G., and Karin, M. (2008). Hepatocyte necrosis induced by oxidative stress and IL-1 $\alpha$  release mediate carcinogen-induced compensatory proliferation and liver tumorigenesis. *Cancer Cell* 14, 156–165.
- Schneller, D., Machat, G., Sousek, A., Proell, V., van Zijl, F., Zulehner, G., Huber, H., Mair, M., Muellner, M.K., Nijman, S.M., et al. (2011). p19(ARF)/p14(ARF) controls oncogenic functions of signal transducer and activator of transcription 3 in hepatocellular carcinoma. *Hepatology* 54, 164–172.
- Takami, T., Kaposi-Novak, P., Uchida, K., Gomez-Quiroz, L.E., Conner, E.A., Factor, V.M., and Thorgeirsson, S.S. (2007). Loss of hepatocyte growth factor/c-Met signaling pathway accelerates early stages of N-nitrosodiethylamine-induced hepatocarcinogenesis. *Cancer Res.* 67, 9844–9851.
- van Hogerlinden, M., Auer, G., and Toftgård, R. (2002). Inhibition of Rel/Nuclear Factor- $\kappa$ B signaling in skin results in defective DNA damage-induced cell cycle arrest and Ha-ras- and p53-independent tumor development. *Oncogene* 21, 4969–4977.

- Verna, L., Whysner, J., and Williams, G.M. (1996). N-nitrosodiethylamine mechanistic data and risk assessment: bioactivation, DNA-adduct formation, mutagenicity, and tumor initiation. *Pharmacol. Ther.* **71**, 57–81.
- Wang, E.Y., Yeh, S.H., Tsai, T.F., Huang, H.P., Jeng, Y.M., Lin, W.H., Chen, W.C., Yeh, K.H., Chen, P.J., and Chen, D.S. (2011a). Depletion of  $\beta$ -catenin from mature hepatocytes of mice promotes expansion of hepatic progenitor cells and tumor development. *Proc. Natl. Acad. Sci. USA* **108**, 18384–18389.
- Wang, H., Lafdil, F., Wang, L., Park, O., Yin, S., Niu, J., Miller, A.M., Sun, Z., and Gao, B. (2011b). Hepatoprotective versus oncogenic functions of STAT3 in liver tumorigenesis. *Am. J. Pathol.* **179**, 714–724.
- Wang, R., Ferrell, L.D., Faouzi, S., Maher, J.J., and Bishop, J.M. (2001). Activation of the Met receptor by cell attachment induces and sustains hepatocellular carcinomas in transgenic mice. *J. Cell Biol.* **153**, 1023–1034.
- Yamaji, S., Zhang, M., Zhang, J., Endo, Y., Bibikova, E., Goff, S.P., and Cang, Y. (2010). Hepatocyte-specific deletion of DDB1 induces liver regeneration and tumorigenesis. *Proc. Natl. Acad. Sci. USA* **107**, 22237–22242.
- You, H., Ding, W., Dang, H., Jiang, Y., and Rountree, C.B. (2011). c-Met represents a potential therapeutic target for personalized treatment in hepatocellular carcinoma. *Hepatology* **54**, 879–889.
- Yu, H., Pardoll, D., and Jove, R. (2009). STATs in cancer inflammation and immunity: a leading role for STAT3. *Nat. Rev. Cancer* **9**, 798–809.
- Yue, P., and Turkson, J. (2009). Targeting STAT3 in cancer: how successful are we? *Expert Opin. Investig. Drugs* **18**, 45–56.
- Zhang, X.F., Tan, X., Zeng, G., Misse, A., Singh, S., Kim, Y., Klaunig, J.E., and Monga, S.P. (2010). Conditional  $\beta$ -catenin loss in mice promotes chemical hepatocarcinogenesis: role of oxidative stress and platelet-derived growth factor receptor  $\alpha$ /phosphoinositide 3-kinase signaling. *Hepatology* **52**, 954–965.

# An Animal Model of MYC-Driven Medulloblastoma

Yanxin Pei,<sup>1</sup> Colin E. Moore,<sup>1</sup> Jun Wang,<sup>1</sup> Alok K. Tewari,<sup>3</sup> Alexey Eroshkin,<sup>2</sup> Yoon-Jae Cho,<sup>4</sup> Hendrik Witt,<sup>5</sup> Andrey Korshunov,<sup>5</sup> Tracy-Ann Read,<sup>6</sup> Julia L. Sun,<sup>7,8</sup> Earlene M. Schmitt,<sup>9</sup> C. Ryan Miller,<sup>11</sup> Anne F. Buckley,<sup>8</sup> Roger E. McLendon,<sup>8</sup> Thomas F. Westbrook,<sup>9,10</sup> Paul A. Northcott,<sup>12</sup> Michael D. Taylor,<sup>12</sup> Stefan M. Pfister,<sup>5</sup> Phillip G. Febbo,<sup>3</sup> and Robert J. Wechsler-Reya<sup>1,7,\*</sup>

<sup>1</sup>Tumor Development Program

<sup>2</sup>Bioinformatics Shared Resource

NCI-Designated Cancer Center, Sanford-Burnham Medical Research Institute, La Jolla, CA 92037, USA

<sup>3</sup>Department of Medicine and Helen Diller Family Comprehensive Cancer Center, University of California, San Francisco, San Francisco, CA 94158-9001, USA

<sup>4</sup>Stanford University School of Medicine, Stanford, CA 94305, USA

<sup>5</sup>German Cancer Research Center and University of Heidelberg, Heidelberg D-69120, Germany

<sup>6</sup>Department of Neurosurgery, Emory University School of Medicine, Atlanta, GA 30322, USA

<sup>7</sup>Department of Pharmacology and Cancer Biology

<sup>8</sup>Department of Pathology

Duke University Medical Center, Durham, NC 27710, USA

<sup>9</sup>Verna and Marrs McLean Department of Biochemistry and Molecular Biology, and Department of Molecular and Human Genetics Baylor College of Medicine, Houston, TX 77030, USA

<sup>10</sup>Department of Pediatrics and Dan L. Duncan Cancer Center

<sup>11</sup>Department of Pathology and Laboratory Medicine  
University of North Carolina, Chapel Hill, NC 27514, USA

<sup>12</sup>Hospital for Sick Children and University of Toronto, Toronto, M5G 1X8 Ontario, Canada

\*Correspondence: [rwreya@sanfordburnham.org](mailto:rwreya@sanfordburnham.org)

DOI 10.1016/j.ccr.2011.12.021

## SUMMARY

Medulloblastoma (MB) is the most common malignant brain tumor in children. Patients whose tumors exhibit overexpression or amplification of the *MYC* oncogene (c-*MYC*) usually have an extremely poor prognosis, but there are no animal models of this subtype of the disease. Here, we show that cerebellar stem cells expressing *Myc* and mutant *Trp53* (*p53*) generate aggressive tumors following orthotopic transplantation. These tumors consist of large, pleiomorphic cells and resemble human MYC-driven MB at a molecular level. Notably, antagonists of PI3K/mTOR signaling, but not Hedgehog signaling, inhibit growth of tumor cells. These findings suggest that cerebellar stem cells can give rise to MYC-driven MB and identify a novel model that can be used to test therapies for this devastating disease.

## INTRODUCTION

Medulloblastoma (MB) is a highly malignant tumor of the cerebellum that occurs most frequently in children between 5 and 10 years of age (Polkinghorn and Tarbell, 2007). Current treatment for MB includes resection of the tumor followed by radiation and high-dose chemotherapy. Although this has resulted in significant increases in survival, approximately one-third of

MB patients still die from their disease. Moreover, survivors often suffer severe side effects, including dramatic losses in cognitive function, endocrine disorders, and increased susceptibility to secondary tumors (Palmer et al., 2007; Stavrou et al., 2001). Thus, more effective and less toxic therapies for MB are desperately needed.

Traditionally, MB has been classified based on histological characteristics. In this context, tumors with large-cell-anaplastic

## Significance

Animal models are valuable for studying the origins and molecular mechanisms of cancer and can be used to develop and test new therapeutic strategies. Existing mouse models of MB have been extremely useful for studying MB associated with Sonic hedgehog pathway mutations. In contrast, no models have been developed to study MYC-driven MB. Here we describe a mouse model of this tumor based on transplantation of cerebellar stem cells expressing *Myc* and dominant-negative *p53*. These tumors resemble human MYC-driven MB at a histological and molecular level and can be inhibited by antagonists of the PI3K/mTOR pathway. This model represents an important tool for studying the biology and therapeutic responsiveness of MYC-driven MB.

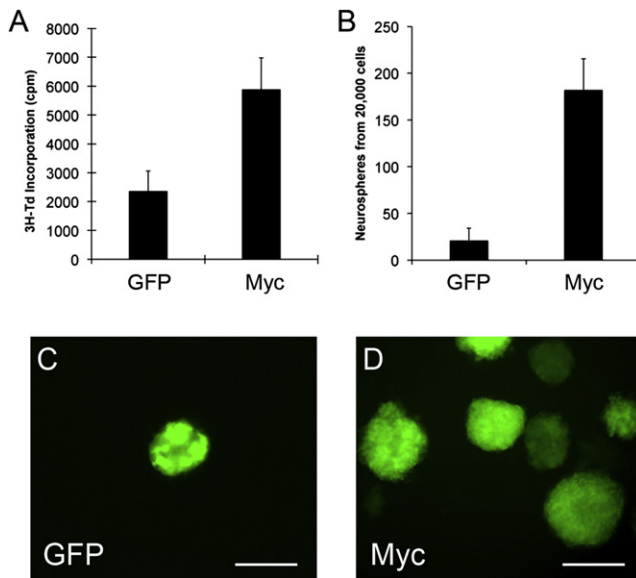


**Figure 1. Myc Promotes Proliferation of Cerebellar Stem Cells In Vitro**

(A) Prom1<sup>+</sup>Lin<sup>-</sup> cells sorted from cerebella of 5- to 7-day-old mice were infected with Myc-IRES-GFP or control (GFP only) viruses for 48 hr, pulsed with tritiated thymidine (<sup>3</sup>H-Td), and cultured overnight before being assayed for <sup>3</sup>H-Td incorporation. Data represent the mean  $\pm$  SEM of triplicate samples. (B–D) Prom1<sup>+</sup>Lin<sup>-</sup> cells infected with Myc-IRES-GFP or control viruses were cultured at low density in the presence of EGF and bFGF for 7 days. Representative fields are shown in (C) and (D) (scale bars = 100  $\mu$ m). The number of GFP<sup>+</sup> neurospheres is quantified in (B); data represent the mean  $\pm$  SEM of triplicate samples. The infection efficiency was 80% with Myc-IRES-GFP and 90% with control retrovirus. See also Figure S1.

(LCA) features are associated with a much poorer prognosis than classic or nodular/desmoplastic tumors (Eberhart and Burger, 2003; Leonard et al., 2001). Recently, several groups (Cho et al., 2011; Kool et al., 2008; Northcott et al., 2011; Remke et al., 2011; Thompson et al., 2006) have performed gene-expression profiling and DNA-copy-number analysis of MB, and have identified at least four major subtypes of the disease: WNT, Sonic hedgehog (SHH), Group C, and Group D. These molecular subtypes have distinct characteristics in terms of gene expression, mutational profiles, epidemiology, and prognosis. Among molecular subtypes, tumors associated with WNT pathway activation have the most favorable outcome, whereas those that exhibit overexpression or amplification of MYC and lack WNT pathway activation (termed Group C (Northcott et al., 2011) or Group c1 (Cho et al., 2011), herein referred to as MYC-driven MB) have the worst prognosis. Although LCA histology can be found in all molecular subtypes of the disease, it is more common in MYC-driven tumors. Patients with MYC-driven MB are also more likely to exhibit metastatic disease at the time of diagnosis, to undergo recurrence, and to die of their disease (Northcott et al., 2011). More effective treatments for MYC-driven MB depend on a deeper understanding of the biology of the disease.

The fact that ectopic expression of MYC can cause MB cell lines to adopt an anaplastic phenotype (Stearns et al., 2006)

and the fact that high MYC levels are associated with poor clinical outcome (Cho et al., 2011; Grotzer et al., 2001) suggest that MYC might play a key role in the biology of MB. But while the association between MYC and poor prognosis is well established, it remains unclear whether the gene is involved in tumor initiation, maintenance, or progression. Likewise, MYC-driven tumors frequently exhibit loss of one allele of the *TP53* tumor suppressor (in the context of isochromosome 17q) (Northcott et al., 2011; Pfister et al., 2009), and LCA tumors have been reported to express high levels of p53 protein, an indicator of dysregulation of the TP53 pathway (Eberhart et al., 2005; Frank et al., 2004). However, it is not clear whether alterations in TP53 represent causal events.

Animal models of brain tumors can be generated by targeting expression of oncogenes to neural progenitors or stem cells. Recent studies suggest that different populations of progenitors may be susceptible to transformation by distinct signaling pathways (Gilbertson and Ellison, 2008). For example, mutations in the SHH pathway promote transformation of granule neuron precursors (GNPs) in the external germinal layer of the cerebellum (Schüller et al., 2008; Yang et al., 2008), whereas dysregulation of WNT signaling causes transformation of progenitors in the lower rhombic lip and embryonic dorsal brainstem (Gibson et al., 2010). We recently identified a population of stem cells in the white matter of the postnatal cerebellum (Lee et al., 2005) and hypothesized that they might give rise to some types of MB. To test this hypothesis, and to address the functional importance of MYC and *TP53* in MB, we examined the effects of overexpressing *Myc* and disrupting *p53* function in these cells.

## RESULTS

### Myc Promotes Proliferation of Cerebellar Stem Cells In Vitro

Stem cells can be isolated from the postnatal cerebellum based on expression of Prominin1 (CD133) and lack of neuronal and glial lineage markers (Prom1<sup>+</sup>Lin<sup>-</sup>). To investigate the effects of *Myc* on these cells, we infected them with control retroviruses or viruses encoding a stabilized form of *Myc* (*Myc*<sup>T58A</sup>) (Chang et al., 2000) and measured their proliferation. As shown in Figure 1A, *Myc*-infected cells showed a 2.5-fold increase in proliferation compared to cells infected with control viruses. To examine the effects of *Myc* on self-renewal, infected Prom1<sup>+</sup>Lin<sup>-</sup> cells were cultured at low density (2000 cells/ml) in the presence of basic fibroblast growth factor (bFGF) and epidermal growth factor (EGF) to promote neurosphere formation. As shown in Figures 1B–1D, the number of neurospheres in *Myc*-infected cultures was 9-fold higher than that in control cultures. To determine whether the effects of *Myc* persisted in longer-term cultures, neurospheres were dissociated into single-cell suspensions and replated every 7 days. Over the course of 5 weeks, *Myc*-infected cultures exhibited a 1000-fold increase in cell number, compared to a 2-fold increase in control cultures (Figure S1 available online). These data indicate that overexpression of *Myc* in cerebellar stem cells promotes short-term proliferation, as well as long-term self-renewal in vitro.

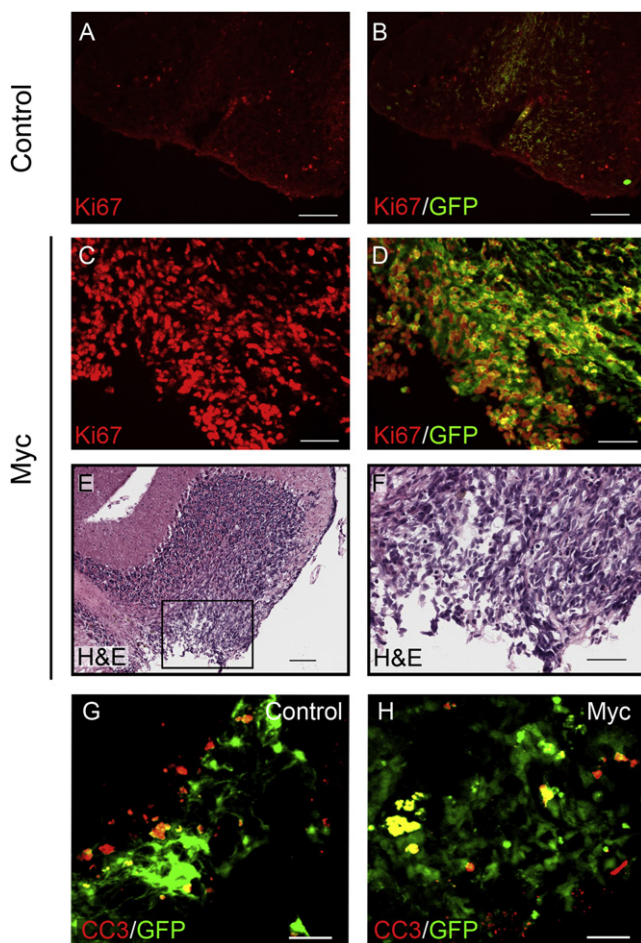


**Figure 2. Myc-Infected Stem Cells Give Rise to Transient Hyperplastic Lesions following Transplantation**

(A–F)  $\text{Prom1}^+ \text{Lin}^-$  cells were infected with Myc-IRES-GFP or control retrovirus for 20 hr and then transplanted into the cerebella of NSG mice. Hosts were sacrificed after 2.5 weeks. Frozen sections from mice that received GFP-infected (A and B) or Myc-infected (C–F) cells were stained with anti-Ki67 antibodies (A–D) or H&E (E and F). Note the large mass of proliferating (Ki67<sup>+</sup>) cells seen in animals that received Myc-infected cells (C and D). The box in (E) corresponds to the high-power field shown in (F). Scale bars = 50  $\mu\text{m}$  (A–D) and 100  $\mu\text{m}$  (E).

(G and H)  $\text{Prom1}^+$  cells were infected with Myc-IRES-GFP or control-GFP viruses for 20 hr and then transplanted into the cerebella of NSG hosts. Mice were sacrificed after 2 weeks. Frozen sections from mice that received control (G) or Myc-infected cells (H) were stained with antibodies specific for cleaved caspase-3 (CC3) to detect apoptotic cells. Scale bars = 50  $\mu\text{m}$ . See also Figure S2.

### Myc-Expressing Stem Cells Form Transient Hyperplastic Lesions In Vivo

In light of the above results, we investigated whether Myc-expressing cells could give rise to tumors in vivo. We stereotactically implanted control (GFP virus-infected) or Myc-infected stem cells into the cerebella of immunocompromised (NOD-SCID-IL2RGamma<sup>null</sup>, or NSG) mice and examined cerebella of recipients 2–3 weeks later. As shown in Figures 2A and 2B, in animals that had received control cells, few infected cells (marked by GFP) could be detected, and only a small proportion

of these were proliferating (based on Ki67 staining). In contrast, in animals transplanted with Myc-expressing cells, large masses of infected cells could be detected, and the majority of these were proliferating (Figures 2C–2F). These results suggest that Myc-infected cells can undergo persistent proliferation in vivo.

To determine whether Myc-infected cells can continue to grow and give rise to tumors, we sacrificed animals ( $n = 5$ ) four weeks after transplantation. Surprisingly, at this stage, few transplanted cells could be detected in the cerebella of mice that had received either control or Myc-infected cells. Consistent with this, we followed a cohort of mice ( $n = 6$ ) transplanted with Myc-infected cells for 6 months, and found that none of them developed symptoms during this period (data not shown). This suggested that Myc can drive proliferation of stem cells, but is not sufficient to promote tumor growth.

The fact that Myc-infected cells formed large masses 2 weeks after transplantation but were undetectable 4 weeks after transplantation raised the question of what happened to these cells. Since Myc can induce apoptosis as well as proliferation (Pelen-garis et al., 2000), we examined cerebella from recipients of control and Myc-infected cells for evidence of apoptosis by staining with anti-cleaved caspase 3 (CC3). Few control virus-infected cells were labeled with anti-CC3 (although some staining was seen around the transplant site), whereas Myc-infected cells exhibited a significant amount of CC3 staining (Figures 2G and 2H), suggesting that they were undergoing apoptosis in situ. These data suggest that Myc promotes proliferation as well as apoptosis of cerebellar stem cells.

### Mutant p53 Synergizes with Myc to Promote Tumor Formation

MYC-induced apoptosis is frequently dependent on TP53 (Her-meking and Eick, 1994). To test whether inactivation of p53 could inhibit Myc-induced cell death in cerebellar stem cells, we measured apoptosis in cells infected with control (GFP), Myc, dominant-negative p53 (DNp53) (Bowman et al., 1996), or Myc + DNp53 viruses. As shown in Figures S2A–S2D, cells infected with Myc viruses alone exhibited a marked increase in apoptosis compared to cells infected with control viruses (Figures S2A and S2B), but DNp53 completely abolished the proapoptotic effects of Myc (Figures S2C and S2D). These results suggest that Myc-mediated apoptosis of stem cells can be blocked by inhibition of p53 function.

The above findings raised the possibility that cells overexpressing Myc and DNp53 might be able to give rise to tumors. To test this, we coinfect stem cells with viruses encoding these genes and implanted them into the cerebella of NSG mice. Animals transplanted with cells coexpressing the two genes developed highly aggressive tumors and had to be sacrificed at 6–12 weeks (Figures 3A and 3B). These experiments were performed using the T58A mutant of Myc. Notably, stem cells infected with WT Myc + DNp53 also gave rise to tumors, albeit with reduced penetrance (33%) and longer latency (15–20 weeks). These studies suggest that mutant p53 can cooperate with Myc to promote transformation of cerebellar stem cells.

We characterized tumors arising from stem cells infected with Myc and DNp53 (MP tumors), using tumors from *Ptch1* mutant mice (a model for SHH-associated MB) for comparison (Figures 3C–3H). Whereas *Ptch1*<sup>+/-</sup> tumor cells were not much bigger

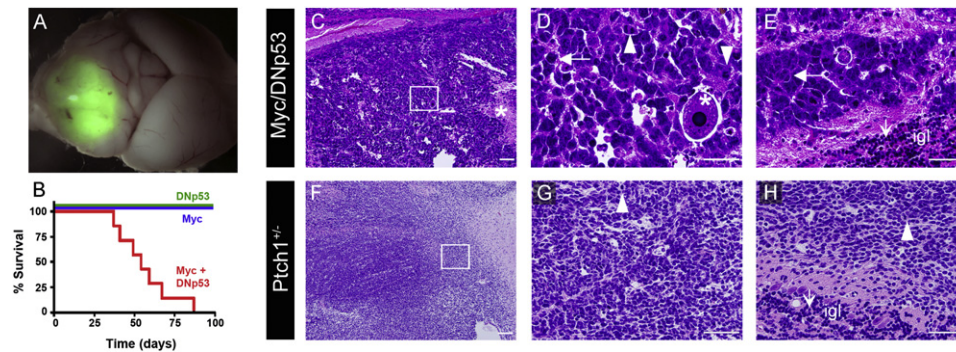


**Figure 3. Overexpression of Myc and Inactivation of p53 Transforms Cerebellar Stem Cells into Tumors**

Prom1<sup>+</sup>Lin<sup>-</sup> cells were infected with Myc + DNP53 retroviruses, Myc alone, or DNP53 alone for 20 hr, then transplanted into the cerebella of NSG mice. Animals were sacrificed when they developed symptoms.

(A) Whole-mount image of tumor, with GFP expression originating from DNP53 retrovirus.

(B) Survival curve for animals receiving  $5 \times 10^4$  cells infected with Myc viruses (blue line), DNP53 viruses (green line), or Myc + DNP53 viruses (red line) (median survival 48 days).

(C–H) Sections of tumor tissue from animals transplanted with cells expressing Myc and DNP53 (C–E) or from *Ptch1* mutant mice (F–H) were stained with hematoxylin and eosin. For (C) and (F), scale bars = 100  $\mu$ m; for (D), (E), (G), and (H), scale bars = 50  $\mu$ m. Boxes in (C) and (F) refer to (D) and (G), respectively. Asterisks in (C) and (D) show an area of necrosis and a large tumor cell with marked nuclear atypia (anaplasia), respectively. Horizontal arrows in (D) and (E) show prominent nuclear molding. Arrowheads in (D), (G), and (H) show mitotic figures. Vertical arrows in (E) and (H) show normal granule neurons in the internal granule layer (igl); the majority of tumor cells in (E) are much larger than these cells, whereas those in H are approximately the same size. See also Figure S3.

than normal granule neurons ( $\sim 5 \mu$ m, compare arrow to arrowhead in Figure 3H), cells from MP tumors were approximately 5 times bigger ( $\sim 25 \mu$ m, compare vertical and horizontal arrows in Figure 3E). In addition, MP tumors exhibited prominent necrosis (asterisk in Figure 3C) and nuclear molding (arrows in Figures 3D and 3E), whereas *Ptch1*<sup>+/-</sup> tumors rarely displayed these features (Figures 3G and 3H). Importantly, the histological features of murine MP tumors resembled those of human LCA (Group C) MB (Figure S3). Together these data suggested that MP tumors are distinct from SHH-driven tumors and histologically resemble human LCA MB.

Immunohistochemical characterization of MP tumors demonstrated that they have a high proliferative index and often express the stem cell/progenitor marker Nestin (Figures 4A–4C). Tumor cells that did exhibit differentiation predominantly expressed the early neuronal lineage marker Tuj1 (class III beta-tubulin; Figure 4D). Only rare tumor cells expressed the mature neuronal marker synaptophysin (not shown) or the astrocytic marker GFAP (Figure 4E), consistent with the notion that MP tumors are poorly differentiated. Tumors also did not express O4, NG2, PDGFR $\alpha$ , or SOX10, markers associated with oligodendrogliomas (data not shown). Finally, tumor cells expressed significant amounts of the chromatin remodeling protein BAF47 (also known as Smarcb1, Snf5, or Inr1), which is commonly lost in atypical teratoid/rhabdoid tumor (AT/RT), suggesting that we were not modeling this type of tumor (Figure 4F). Based on these observations, we concluded that MP tumors are highly proliferative and poorly differentiated, features consistent with LCA MB.

### MP Tumors Can Be Generated from Granule Neuron Precursors

Previous studies have suggested that SHH-associated MB can be initiated in GNPs or neural stem cells (Schüller et al., 2008;

Yang et al., 2008). We therefore determined whether GNPs could also be transformed by Myc and DNP53. To test this, we FACS-sorted GFP<sup>+</sup> cells (GNPs) from neonatal Math1-GFP transgenic mice (Lee et al., 2005; Lumpkin et al., 2003) (Figures S4A and S4B), infected these cells with Myc and DNP53 viruses, and then transplanted them into the cerebellum of NSG mice. We found that 7 out of 22 recipients developed tumors, with a latency of 108 days (Figures S4D–S4F). Interestingly, although the cells were GFP<sup>+</sup> prior to transplantation (Figure S4B), the tumors that developed from them were no longer GFP<sup>+</sup> when analyzed by microscopy or flow cytometry (Figures S4C and S4E), suggesting that they had lost a key marker of the granule lineage during the course of transformation. These studies demonstrate that both stem cells and GNPs can give rise to MYC-driven tumors.

### Myc Is Required to Maintain MP Tumor Growth

In many tumors driven by MYC, shutting off the expression of MYC results in tumor regression (Jain et al., 2002; Soucek et al., 2008). To determine whether MP tumors continue to depend on Myc once they are established, we infected stem cells with viruses encoding a tetracycline-inducible form of Myc along with DNP53-IRES-Luciferase, and transplanted these cells into the cerebellum of NSG mice. Mice were fed doxycycline (DOX)-containing food until they developed tumors (3–4 weeks after transplantation). Tumors were removed, dissociated, and retransplanted into cerebella of naive NSG mice. Secondary recipients were separated into three groups: Group 1 (n = 14) was maintained on DOX-containing food; Group 2 (n = 14) was fed DOX-containing food for 1 week, then switched to normal food; and Group 3 (n = 12) was fed food without DOX (Figure 5A). Animals in all groups developed bioluminescent signals (from the luciferase encoded by the DNP53 virus), indicating the presence of transplanted tumor cells. Group 1 animals

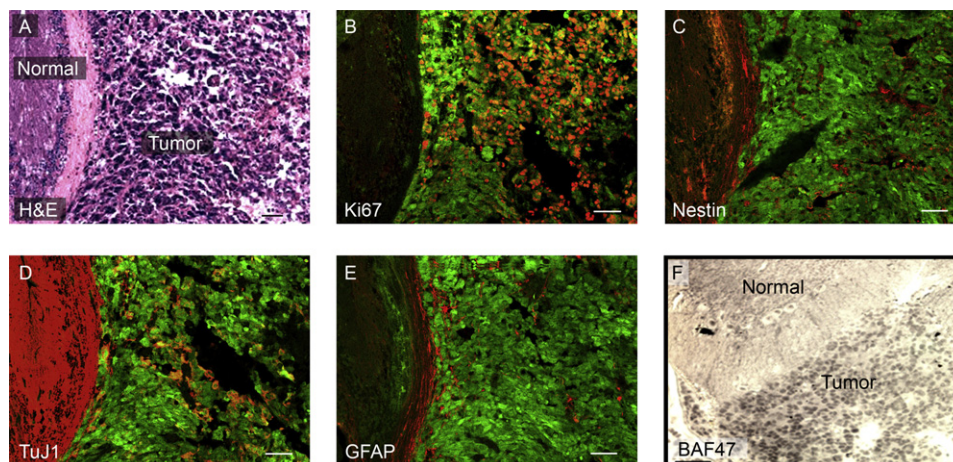


**Figure 4. MP Tumors Exhibit Characteristics of Human MB**

Cryosections from MP tumors were stained with H&E (A) or with antibodies specific for Ki67 (B), Nestin (C), Tuj1 (D), GFAP (E), or BAF47/Ini1 (F). Images in (A)–(E) represent adjacent sections. Scale bars = 50  $\mu$ m.

See also Figure S4.

showed a rapid and dramatic increase in bioluminescence (Figure 5B, top graph), and by 3–4 weeks after transplantation, all mice had developed symptoms and had to be sacrificed (Figure 5F). Analysis of brains from these mice revealed large tumors in every animal (Figure 5C). In contrast, bioluminescence in Group 2 and Group 3 mice decayed in the absence of DOX (Figure 5B, bottom two graphs). Moreover, no tumors could be detected in these animals 3 weeks after transplantation (Figures 5D and 5E), and animals remained asymptomatic at 6 weeks (Figure 5F). Together these data suggest that *Myc* is not only necessary for tumor initiation but is also required to maintain growth of MP tumors.

#### MP Tumors Resemble Human MYC-Driven MB

Our histological analysis indicated that MP tumors resemble human LCA MB. Since LCA histology is more common in MYC-driven tumors (Cho et al., 2011; Northcott et al., 2011), this supported the notion that MP tumors might represent a model for human MYC-driven MB. To test whether MP tumors resembled human MYC-driven MB at a molecular level, we performed gene expression analysis of MP tumors and compared the resulting gene expression profiles with profiles of the four subtypes of human MB (WNT, SHH, Group C, and Group D) defined by Northcott et al. (2011). In this classification scheme, Group C tumors, which are associated with the poorest prognosis, frequently exhibit amplification or overexpression of MYC (Northcott et al., 2011). Using genes differentially expressed in each subgroup and previously published methods (Bild et al., 2006), we identified four sets of genes (“subgroup signatures”) whose expression accurately predicted the subgroup of the human MB samples (see Human Tumor Analysis in the Supplemental Information).

Human MB subgroup signatures were then applied to gene expression data from murine MP and *Ptch1* mutant tumors, with each tumor receiving a subgroup signature score representing its similarity to each subgroup of human MB. As shown in Figure 6A and Table S1, murine *Ptch1* tumors most closely

resembled human SHH-associated tumors, with one exception, which possessed a profile consistent with both the WNT and SHH groups. In contrast, MP tumors were most similar to Group C/D tumors, with the exception of a tumor that resembled both the WNT and Group C/D signatures. To validate these findings, we compared data from murine tumors to expression profiles from a distinct set of human MB samples (Cho et al., 2011). Utilizing a subclass mapping algorithm (Hoshida et al., 2007), we generated a similarity metric between MP tumors and the MB subgroups defined in Cho et al. (2011). As shown in Figure S5, this analysis revealed a high degree of similarity between MP tumors and the ‘c1’ subtype of human MB, which is characterized by copy number gains of c-MYC and gene expression signatures indicative of robust MYC transcriptional activity (Cho et al., 2011).

Finally, we stained an independent set of MP and *Ptch1* tumors with antibodies that have been found to mark each of the four human MB subgroups (Northcott et al., 2011). Murine *Ptch1* mutant tumors expressed high levels of the SHH-subgroup marker SFRP1 (Figure 6B) and lacked expression of the WNT-subgroup marker nuclear CTNNB1 (not shown), the Group C marker NPR3 (Figure 6C), and the Group D marker KCNA1 (Figure 6D). In contrast, MP tumors exhibited high levels of NPR3 (Figure 6F) and lacked expression of the other markers (Figures 6E and 6G and data not shown). Together, these data suggested that MP tumors resemble human Group C (MYC-driven) MB.

#### Gene Expression Profile of MP Tumors

We compared the gene-expression profiles of MP tumors to those of freshly isolated cerebellar stem cells and tumors from *Ptch1* mutant mice. Using principal component analysis, an unsupervised approach designed to group samples based on their similarity in gene expression, we determined that MP tumors generated by infection of Prom1<sup>+</sup>Lin<sup>−</sup> stem cells and those generated by infection of Prom1<sup>+</sup> cells were indistinguishable based upon global RNA expression (Figure 7A). Both of these tumor types were distinct from normal (uninfected)

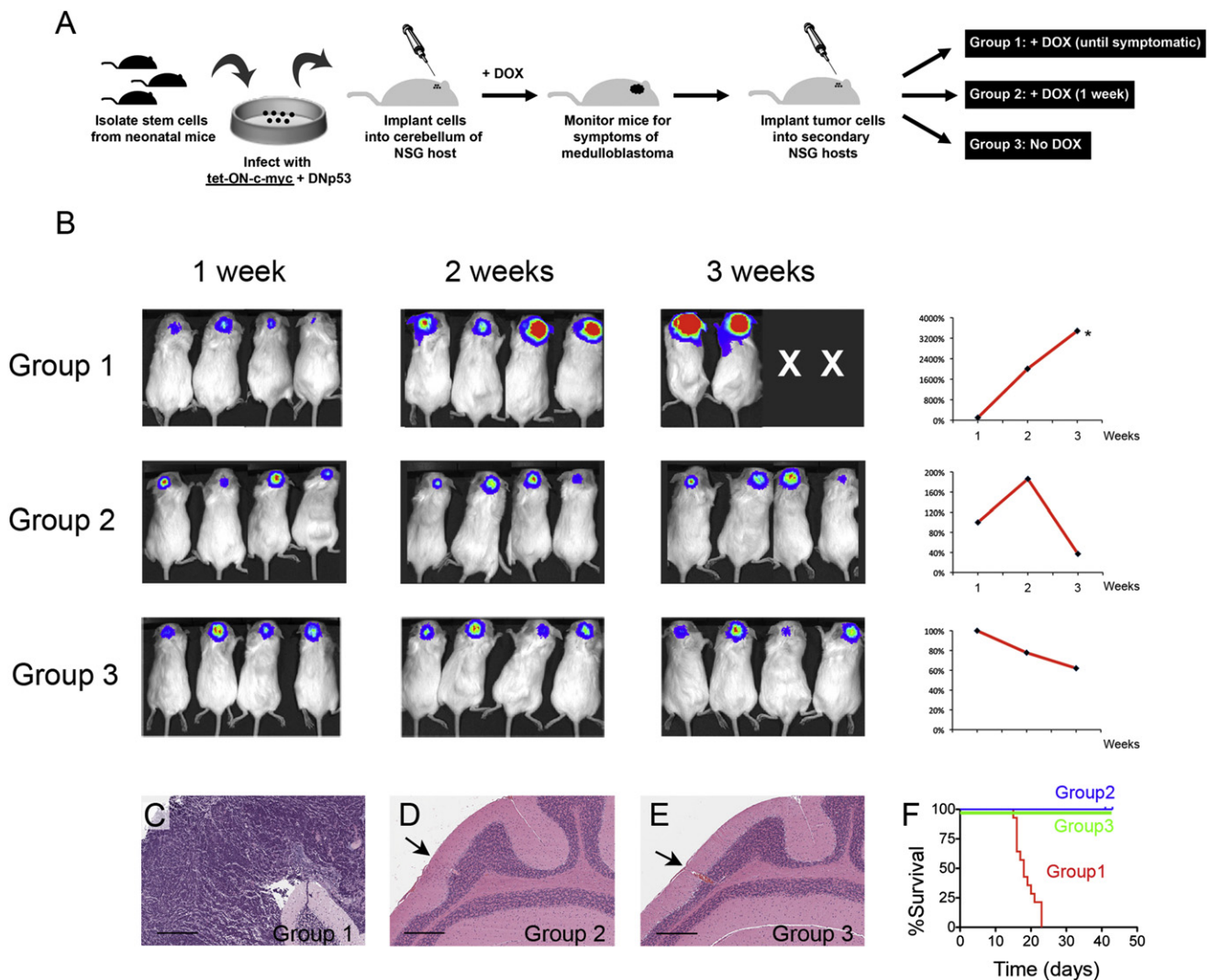


**Figure 5. Myc Is Required for Continued Growth of MP Tumors**

(A) Strategy for generating Tet-regulatable MP tumors.

(B–F) Bioluminescent imaging of animals at 1, 2, and 3 weeks after tumor cell transplantation. (B) Representative images of four animals from each group at each time point (X's denote animals that died before they could be imaged). Graphs at right show the mean percent increase in bioluminescence for all animals in the group (with the 1-week signal for each animal set at 100%). In the top graph, the 1- and 2-week time points represent the average signal intensity for all 14 animals; the 3-week time point (marked by an asterisk) represents the average for the three animals that remained alive at the time of imaging. (C–E) H&E-stained cerebellar sections from representative animals in Groups 1 (C), 2 (D), and 3 (E) 3 weeks after transplantation. Arrows in (D) and (E) point to the injection site. Scale bars = 250  $\mu$ m. (F) Survival curve (Groups 1 and 2,  $n = 14$ ; Group 3,  $n = 12$ ).

cerebellar stem cells and from *Ptch1* mutant tumors. Hierarchical clustering (Figure 7B) confirmed the similarity between MP tumors generated from *Prom1*<sup>+</sup>*Lin*<sup>−</sup> and *Prom1*<sup>+</sup> cells, as well as the differences between these tumors, *Ptch1* tumors, and normal stem cells. Focusing on changes in gene expression of 3-fold and higher (p-value with FDR correction < 0.0001), we identified 1228 genes (1465 probe sets) that were differentially expressed between MP tumors and *Ptch1* tumors (Comparison A, Table S2), and 812 genes (955 probe sets) differentially expressed between MP tumors and normal stem cells (Comparison B, Table S3).

To learn about the functional significance of these genes, we analyzed them using gene set enrichment analysis (GSEA) (Sub-

ramanian et al., 2005) and NextBio software (Kupersmidt et al., 2010) (see Figure 7 and Table S4 and Table S5). Several important correlations emerged from this analysis. First, we noted that genes expressed at high levels in MP tumors were similar to those found to be targets of MYC in other studies (Figure 7C, Table S4 and Table S5). Another set of differentially expressed genes, which exhibited decreased expression in MP tumors, were targets of forkhead transcription factors (e.g., Foxo1) (Figure 7D). This is notable, because FOXO proteins often inhibit expression of MYC targets, induce expression of MYC antagonists, and suppress MYC-induced transformation (Bouchard et al., 2004, 2007; Delpuech et al., 2007). We also noted a marked similarity between genes expressed in MP tumors and those

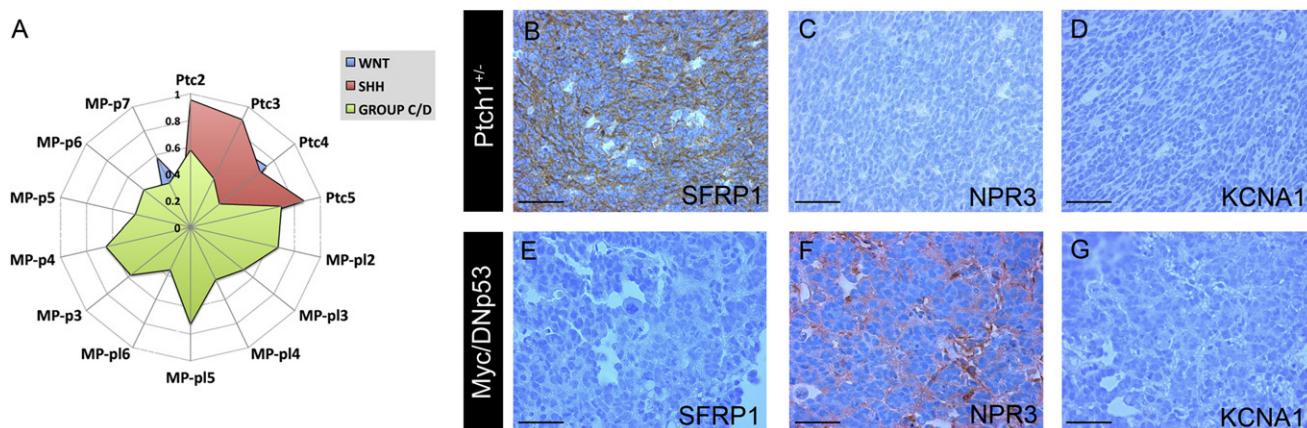


**Figure 6. MP Tumors Resemble Human MYC-Driven MB**

(A) Gene expression profiles of *Myc/DNp53* tumors from *Prom1*<sup>+</sup>/*Lin*<sup>-</sup> cells (MP-pl2-6) or from *Prom1*<sup>+</sup> cells (MP-p3-7) and *Ptch1* mutant (*Ptc1*-4) tumors were compared to signatures generated from human MB subtypes WNT (blue), SHH (red), and Group C/D (green). Each murine tumor was assigned a score denoting its similarity to each subtype of human tumor (for details, see Supplemental Experimental Procedures and Table S1).

(B–G) *Ptch1* and MP tumors were stained with antibodies specific for secreted frizzled-related protein 1 (SFRP1, a marker for SHH tumors), natriuretic peptide receptor C (NPR3, a marker for Group C tumors), or potassium voltage-gated channel, shaker-related subfamily, member 1 (KCNA1, a marker for Group D tumors). Scale bars = 100  $\mu$ m.

See also Figure S5 and Table S1.

enriched in embryonic stem (ES) cells and induced pluripotent stem (iPS) cells, including those induced by *Oct4* and *Klf4* (i.e., in the absence of exogenous *Myc*) (Figure 7F). These genes were enriched in MP tumors compared to *Ptch1* tumors, consistent with the fact that the former are derived from stem cells and the latter originate from lineage-restricted neuronal progenitors. However, they were also enriched in MP tumors compared to cerebellar stem cells, suggesting that MP tumors have adopted a more primitive differentiation state than the cells from which they were derived. In support of this notion, MP tumors showed decreased expression of genes associated with neuronal lineage commitment and differentiation (Figure 7E). Finally, our analysis revealed significant enrichment of a PI3K signaling gene set, as well as a set of genes downregulated by rapamycin in another cancer cell line (Table S4 and Table S5). Notably, analysis of human MYC-driven (Group c1) tumors using Connectivity Map (CMAP), an algorithm that screens a given gene expression signature against a compendium of drug-induced gene expression signatures (Lamb et al., 2006), suggested that genes regulated by PI3K and mTOR inhibitors are also enriched in these tumors (Table S6). These observations, and the fact that MP tumors have decreased expression of Foxo targets, which are negatively regulated by the PI3K pathway, suggested that this pathway might play an important role in tumor growth.

#### MP Tumors Are Sensitive to Inhibitors of PI3 Kinase and mTOR

To determine whether MP tumors were dependent on PI3K/mTOR signaling, we first tested the effects of PI3K/mTOR inhibitors on tumor cell growth in vitro (Figure 8A). MP tumors showed complete growth inhibition in the presence of 1–5  $\mu$ M BEZ-235 (an antagonist of both PI3K and mTOR) and 5  $\mu$ M BKM-120 (an antagonist of PI3K), and partial inhibition in the presence of lower concentrations of these compounds. The mTOR antago-

nist RAD-001 also inhibited growth, albeit incompletely, at concentrations of 0.2–5  $\mu$ M. Consistent with their continued dependency on *Myc*, tumor cells were dramatically inhibited by 10058-F4, a small molecule that interferes with *Myc*-Max dimerization (Huang et al., 2006). In contrast, we found that MP tumor cells showed no growth inhibition in response to the SHH antagonist cyclopamine.

To determine whether BEZ-235 and BKM-120 could also affect long-term tumor cell growth, we cultured MP tumor cells for 3, 7, or 14 days in the presence of these inhibitors, and counted cell number at each time point. We found that all three doses of BEZ-235 inhibited cell growth, whereas only the highest concentration of BKM-120 (5  $\mu$ M) was able to cause growth inhibition (Figure 7B). Similar results were observed when we used neurosphere assays to measure tumor cell clonogenicity (Figure S6).

To confirm that these compounds were acting on the PI3K/mTOR pathway, we performed western blotting to analyze phosphorylation of critical proteins in the pathway. As shown in Figure 8C, MP tumor cells showed substantial amounts of phospho-AKT and phospho-S6 in the absence of inhibitors (DMSO lanes). Treatment with BEZ-235 or BKM-120 inhibited phosphorylation of both AKT and S6. In contrast, RAD-001 inhibited S6 phosphorylation but did not affect phospho-AKT. The fact that BEZ-235 and BKM-120 were more potent inhibitors of tumor cell proliferation than RAD-001 (Figures 8A and 8B) suggested that blocking activity of PI3K, or both PI3K and mTOR, might be required for effective tumor inhibition.

To determine whether inhibition of PI3K/mTOR signaling could also inhibit growth of MP tumors in vivo, we isolated MP tumor cells and transplanted them into naive NSG mice. After 7 days, we began treating animals with BKM-120 once daily until clinical signs of tumor formation were observed. Animals treated with BKM-120 survived significantly longer than controls (median

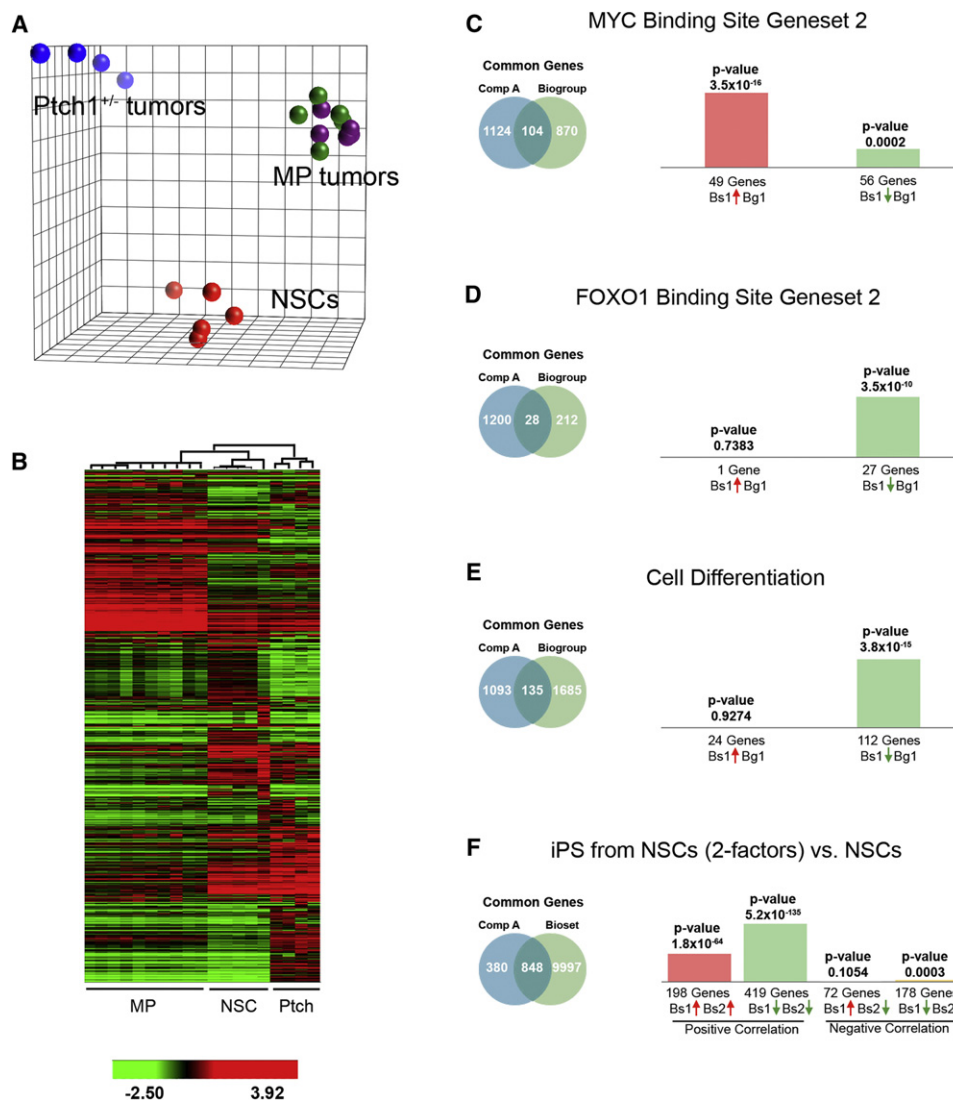


**Figure 7. MP Tumors Are Molecularly Distinct from Stem Cells and from *Ptch1* Tumors**

(A) Principal component analysis (PCA). Three PCA coordinates describe 55.2% of the total data variation (PC1, 27.2%; PC2, 19.8%; and PC3, 8.23%). Green, MP tumors derived from *Prom1*<sup>+</sup>*Lin*<sup>-</sup> cells; purple, MP tumors derived from *Prom1*<sup>+</sup> cells; blue, *Ptch1* tumors; red, normal stem cells (NSCs).

(B) Unsupervised hierarchical clustering analysis. Each column represents a distinct sample and each row represents an individual gene. The normalized (log2) and standardized (each sample to mean signal = 0 and standard deviation = 1) level of gene expression is denoted by color (green, low; dark, intermediate; red, high), as indicated in the gradient at the bottom.

(C–F) Genes differentially expressed between MP tumors and *Ptch1* tumors (Comp A) were subjected to NextBio analysis, to identify biogroups and studies (biosets) that contain similar genes. Representative biogroups (C–E) and studies (F) are shown. Venn diagrams show the number of common and unique genes in both sets. Bars at right show the significance of overlap between gene subsets (the scale of the bar is measured in  $-\log(p\text{-value})$ , so the taller the bar, the higher the significance of the gene overlap). Whereas each biogroup is represented by a single list of genes, signature genes from studies have two lists, one for upregulated and one for downregulated genes. Thus, biogroup comparisons consist of just two graphs, whereas comparisons of studies consist of four graphs. See also Tables S2–S6.

survival = 35 versus 25 days) (Figure 8D). These results suggest that inhibitors of PI3K/mTOR signaling might be useful for treatment of MYC-driven MB.

## DISCUSSION

MYC-driven MB is a highly malignant pediatric brain tumor that is often resistant to conventional radiation and chemotherapy. More effective approaches to treat this disease are critical, and

these can be facilitated by the development of robust animal models. The fact that a subset of human MBs exhibit amplification or overexpression of MYC prompted us to develop a mouse model that can be used to investigate the biology of, and test therapies for, MYC-driven MB.

## Cooperation between *Myc* and Mutant *p53*

Our observation that *Myc* induces proliferation of cerebellar stem cells is consistent with previous reports showing mitogenic

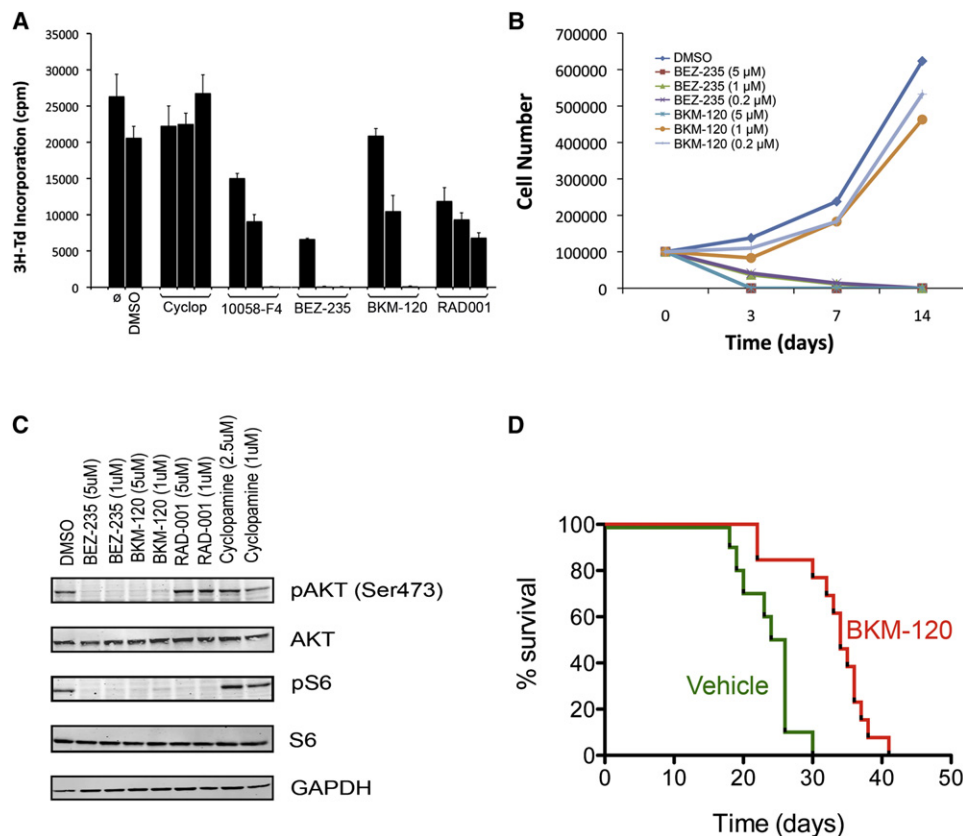


**Figure 8. Growth of MP Tumor Cells Is Inhibited by Antagonists of PI3K/mTOR Signaling**

(A) Effects of inhibitors on short-term proliferation. MP tumor cells were cultured in serum-free media containing no additive (ø), vehicle (DMSO), cyclopamine (0.1, 1, and 2.5 µM), 10058-F4 (10, 25, and 100 µM), BEZ-235 (0.2, 1, and 5 µM), BKM-120 (0.2, 1, and 5 µM), or RAD-001 (0.2, 1, and 5 µM). For each inhibitor, columns are ordered from lowest to highest concentration. After 48 hr, cells were pulsed with <sup>3</sup>H-Td and cultured overnight before being assayed for <sup>3</sup>H-Td incorporation. Data represent means of triplicate samples ± SEM.

(B) Effects on long-term growth. Tumor cells were cultured for 3, 7, or 14 days in the presence of different doses of inhibitors, and cell number was counted at the indicated time points.

(C) Effects on PI3K signaling. Tumor cells were treated with DMSO, BEZ-235 (5 µM and 1 µM), BKM-120 (5 µM and 1 µM), RAD-001 (5 µM and 1 µM) or cyclopamine (2.5 µM and 1 µM) for 3 hr. Cells were lysed and protein was analyzed for phosphorylation of AKT and S6 (pAKT and pS6) or for GAPDH by western blotting.

(D) Effects on tumor growth in vivo. Five hundred MP tumor cells were retransplanted into naive NSG mice. After 7 days, mice were imaged for luciferase activity and separated into two groups randomly. Mice in Group 1 were treated with vehicle (0.5% methyl-cellulose) and those in Group 2 were treated with BKM-120 (30mg/kg/d) by oral gavage until they developed symptoms. BKM-120 treatment significantly prolonged survival compared to vehicle (p = 0.001). See also Figure S6.

effects of *Myc* in normal and malignant stem cells (Nagao et al., 2008; Wang et al., 2008). However, while *Myc* can promote proliferation of cerebellar stem cells in vitro, it cannot, on its own, sustain long-term growth in vivo. Our studies suggest that this is due to *Myc*-induced apoptosis, but this raises the question: why are these cells more sensitive to apoptosis in vivo? One reason may be that in vitro they are maintained under conditions that favor neurosphere formation, including high levels of EGF and bFGF. In the presence of such growth factors, the proliferative response to *Myc* often dominates over the apoptotic response (Harrington et al., 1994). It is also possible that the in vivo microenvironment contains factors that actively inhibit growth or survival of transplanted stem cells. In either case, it is clear that the potent mitogenic effects of *Myc* are insufficient to drive transformation.

Whereas stem cells expressing *Myc* alone do not form tumors, cells expressing *Myc* and mutant *p53* are highly tumorigenic. Dysregulation of the *TP53* pathway, as evidenced by elevated expression of *p53* protein, is a common feature of human LCA MB (Eberhart et al., 2005; Frank et al., 2004; Tabori et al., 2010). Moreover, human MYC-driven MBs often exhibit isochromosome 17q, which is associated with monoallelic loss of *TP53* (Cho et al., 2011; Northcott et al., 2010). Thus, loss of *p53* function could synergize with MYC overexpression in human MB as well. The ability of mutant *TP53* to cooperate with MYC has been observed in many other cancers (Elson et al., 1995; Hemann et al., 2005), but the mechanisms underlying this cooperation are not fully understood. In our system, *Myc*-induced apoptosis is dependent on endogenous *p53*, and DN*p53* acts, at least in part, by blocking this function. (Hermeking and Eick,

1994). However, loss of *p53* function has also been reported to increase neural stem cell self-renewal and to promote pluripotency (Kawamura et al., 2009; Meletis et al., 2006; Zheng et al., 2008), both of which could certainly contribute to transformation. Moreover, loss of *p53* function promotes genomic instability (Hanel and Moll, 2012), which could result in additional mutations that promote tumor formation. Which of these functions of *p53* are most critical in our tumors is the subject of ongoing studies.

Our observation that stem cells can be transformed by the combination of *Myc* and *Dnp53*, but not by either gene alone, suggests that these genes are both required for tumor initiation. But whether initiating oncogenes continue to be required once tumors are formed is unclear. Previous studies have demonstrated that in many types of cancer, tumors become addicted to expression of the oncogene and undergo regression when expression is shut off (Jain et al., 2002; Soucek et al., 2008). However, there have been reports of tumors that continue to grow even when *Myc* is silenced (Boxer et al., 2004). Our results suggest that continued expression of *Myc* is required for maintenance of MP tumor growth. If similar findings hold true for human MYC-driven MB, it would suggest that targeting MYC itself might be an effective approach to therapy.

#### MP Tumors as a Model for Human MB

The tumors that are induced by *Myc* and *Dnp53* resemble human LCA and MYC-driven MB. Interestingly, two other groups have recently described animal models of LCA MB. Deletion of *Rb* and *p53* in neural progenitors results in tumors that exhibit amplification of *MycN* and resemble LCA MB (Shakhova et al., 2006). Likewise, mice in which *MycN* is overexpressed in Glt1<sup>+</sup> progenitors develop either classic or LCA MB (Swartling et al., 2010). While each of these tumors exhibits large cell-anaplastic histology, it is important to note that they may not all represent the same subtype of MB. We have previously reported that LCA histology can occur in all molecular subgroups of MB, including WNT, SHH, Group C and Group D tumors (Northcott et al., 2010). However, MBs that overexpress MYCN are largely distinct from those that overexpress MYC. Thus, the models described by these groups may correspond to human MYCN-associated MB, whereas MP tumors may represent human MYC-driven (Group C) MB. Interestingly, tumors from a recently developed MB model in which *Rb* and *p53* were deleted in post-natal cerebellar stem cells did not overexpress *MycN* and, like our tumors, expressed high levels of NSC markers (Sutter et al., 2010). It will be interesting to compare these models at a molecular level to determine the similarities and differences between them.

#### Cellular Origins of *Myc*-Associated Tumors

Previous studies have shown that activation of the SHH pathway in GNP results in MB with 100% penetrance (Schüller et al., 2008; Yang et al., 2008). Moreover, activation of the SHH pathway in stem cells within the cerebellar ventricular zone (VZ) results in expansion of the VZ, but cells do not become transformed until they commit to the granule lineage (Schüller et al., 2008; Yang et al., 2008). These studies suggest that lineage restriction is a critical determinant of susceptibility to transformation by SHH signaling. The current studies suggest that *Myc* + *Dnp53* can also cause transformation of both stem

cells and GNPs. However, once transformed, the stem cells do not appear to undergo lineage commitment; indeed, their gene expression profile suggests that *Myc/Dnp53*-transformed cells are even more immature or undifferentiated than normal neural stem cells. Moreover, when GNPs are infected with *Myc* and *Dnp53* viruses, they lose expression of GNP lineage markers during the course of transformation. These results demonstrate that stem cells and GNPs can both serve as cells of origin for MYC-driven MB, and suggest that lineage commitment is not required for (and in fact, may be incompatible with) transformation.

#### Molecular Phenotype of MP Tumors

In addition to highlighting the similarities between MP tumors and human MYC-driven MB, our gene expression analysis also revealed that genes overexpressed in MP tumors are similar to those expressed by embryonic and pluripotent stem cells. The association between pluripotency and cancer has been noted in a number of other systems. For example, in breast cancer, glioblastoma and bladder carcinoma, an ES-like signature is associated with aggressive, poorly differentiated tumors and is a predictor of poor prognosis (Ben-Porath et al., 2008). Likewise, a pluripotency signature is associated with transformation of follicular lymphoma to diffuse large B cell lymphoma (Gentles et al., 2009). There has been some debate about whether this signature reflects true acquisition of pluripotent characteristics or simply activation of a MYC-driven gene expression profile (Kim et al., 2010). In the case of MP tumors, there is no question that a *Myc*-driven transcriptional program is active and plays a significant role in driving tumor growth. However, it is worth noting that the genes identified as differentially expressed in MP tumors also resemble those associated with pluripotency induced by *Oct4* and *Klf4*, suggesting that the pluripotency program in our cells is not purely a consequence of *Myc* overexpression. It is also notable that MP tumors express lower levels of neural differentiation markers compared to not only *Ptch1* tumors (which consist of neuronal progenitor-like cells) but also normal neural stem cells, from which they were derived. These findings suggest that transformation of NSCs may involve dedifferentiation to a more pluripotent state.

Among the most important results of our analysis was the observation that MP tumors have increased expression of genes associated with PI3K/AKT/mTOR signaling and decreased expression of Foxo target genes. FOXO proteins have been shown to inhibit expression of MYC targets (Bouchard et al., 2004), and MYC-induced transformation requires inactivation of FOXO proteins (Bouchard et al., 2007). Importantly, AKT has been shown to phosphorylate FOXO proteins and thereby prevent them from entering the nucleus (Bouchard et al., 2004). Although the cause of PI3K pathway activation in MP tumors is unclear, it seems likely that this activation interferes with Foxo activity and thereby synergizes with *Myc* overexpression to promote transformation. PI3K signaling has also been shown to increase *Myc* protein stability (Kumar et al., 2006) and to enhance *Myc* function by promoting degradation of its antagonist Mad1 (Zhu et al., 2008). Thus, the PI3K pathway may be a critical regulator of transformation in MP tumors.

In light of the above findings, we hypothesized that inhibition of PI3K signaling might block growth of MP tumors. Whereas

inhibition of the SHH pathway had little effect on growth of these cells, treatment with the PI3K/mTOR inhibitors BEZ-235 and BKM-120 had a potent inhibitory effect on tumor growth both in vitro and in vivo. Several studies have documented activation of PI3K signaling in human MB (Castellino et al., 2010; Hartmann et al., 2006). In particular, genomic analysis suggests that MYC-driven MBs frequently exhibit loss of chromosome 10q (where *PTEN* is located) (Northcott et al., 2011). Consistent with this, our CMAP analysis (Table S6) suggests that MYC-driven tumors have elevated expression of genes that are regulated by PI3K and mTOR inhibitors. Together, these findings suggest that targeting the PI3K/mTOR pathway may be useful for treatment of human MB. Further studies using this model of MYC-driven MB will shed light on the biology of this disease and open up new targets for therapy.

## EXPERIMENTAL PROCEDURES

### Animals

C57BL/6J mice used as a source of stem cells and immunocompromised (NOD-scid IL2Rgamma<sup>null</sup> or NSG) mice used for transplantation were purchased from Jackson Labs (Bar Harbor, ME). Mice were maintained in the Cancer Center Isolation Facility at Duke University and in the Animal Facility at Sanford-Burnham. All experiments were performed in accordance with national guidelines and regulations, and with the approval of the animal care and use committees at each institution.

### Orthotopic Transplantation and Tumor Formation

Before transplantation, cerebellar stem cells (Prom1<sup>+</sup>Lin<sup>-</sup> cells) or GNP (GFP<sup>+</sup> cells FACS-sorted from Math1-GFP transgenic mice) were infected with *Myc* and *Dnp53* retroviruses for 20 hr. Either 1 × 10<sup>5</sup> stem cells in Neurocult medium or 1 × 10<sup>6</sup> GNPs suspended in Neurobasal medium were injected into the cerebella of NSG mice (6–8 weeks old) using a stereotaxic frame with a mouse adaptor (David Kopf Instruments), as described previously (Yang et al., 2008). Animals were monitored weekly, and sacrificed when they showed symptoms of MB.

To generate tetracycline (Tet)-regulatable tumors, stem cells were infected with Tet-inducible *Myc* lentivirus and *Dnp53* retrovirus. The Tet-inducible vector (pCUE-myc<sup>T58A</sup>) consisted of a Tet-response element (TRE2) controlling expression of turbo red fluorescent protein (tRFP) and *Myc*-T58A and a constitutive promoter controlling expression of the reverse tetracycline transactivator (rtTA3) and eGFP (Meerbrey et al., 2011). Infected cells were implanted into cerebella of NSG mice, and mice were maintained on DOX-containing food. When mice became symptomatic, they were sacrificed and tumor cells were retransplanted into secondary NSG mice. These mice were separated into three groups. Group 1 (n = 14) was continually fed DOX-containing food, Group 2 (n = 14) was fed DOX-food for one week and normal food thereafter; and Group 3 (n = 12) was not fed DOX-food at all. Mice were subjected to bioluminescent imaging at 1, 2, and 3 weeks and were sacrificed at the onset of symptoms. At the time of sacrifice, brains were removed, paraffin-embedded, sectioned, and stained with H&E.

### In Vivo Bioluminescent Imaging

Mice were given intraperitoneal injections of 150 ng/g D-Luciferin (Caliper Life Sciences, cat#12279) and anesthetized with 2.5% isoflurane. At 7–8 min after injection, animals were imaged using the Xenogen Spectrum (IVIS-200) imaging system.

### In Vivo Inhibitor Treatment

To study effects of the PI3-kinase antagonist BKM-120 on tumor growth in vivo, we retransplanted 500 MP tumor cells into the cerebella of secondary NSG mice. Seven days after transplantation, mice were randomly separated into two groups: Group 1 was given vehicle (0.5% methyl-cellulose) and Group 2 was given 30 mg/kg BKM-120 by oral gavage once daily until symptom onset. BKM-120 was dissolved in 0.5% methylcellulose and sonicated using

an ultrasonicator (Misonix) at an amplitude of 20 for 12 min. Survival was defined as the time from transplantation until symptom onset.

## ACCESSION NUMBERS

Microarray data have been deposited in the GEO public database (<http://www.ncbi.nlm.nih.gov/geo/>), with accession number GSE34126.

## SUPPLEMENTAL INFORMATION

Supplemental Information includes six figures, six tables, and Supplemental Experimental Procedures and can be found with this article online at doi:10.1016/j.ccr.2011.12.021.

## ACKNOWLEDGMENTS

We dedicate this paper to the memory of Cameron Jackson. In addition, we would like to thank Jack Dutton and Adriana Charbono for assistance with animal colony maintenance and screening; Beth Harvat, Lynn Martinek, Mike Cook, Amy Cortez, and Yoav Altman for help with flow cytometry; Zhengzheng Wei for processing and analysis of microarrays; Irina Leiss for performing immunohistochemistry; and Daisuke Kawauchi and Martine Rousset for helpful discussions. This work was supported by funds from the Alexander and Margaret Stewart Trust and the Duke Comprehensive Cancer Center (R.W.R.), the Southeastern Brain Tumor Foundation (R.W.R.), Alex's Lemonade Stand Foundation (R.W.R.), Pediatric Brain Tumor Foundation (R.E.M. and R.W.R.), NCI grants CA122759 (R.W.R.) and CA159859 (M.D.T. and R.W.R.). C.R.M. is a Damon Runyon-Genentech Clinical Investigator supported in part by a grant (CI-45-09) from the Damon Runyon Cancer Research Foundation. R.W.R. is supported by a Leadership Award (LA1-01747) from the California Institute of Regenerative Medicine.

Received: July 7, 2011

Revised: November 21, 2011

Accepted: December 22, 2011

Published: February 13, 2012

## REFERENCES

- Ben-Porath, I., Thomson, M.W., Carey, V.J., Ge, R., Bell, G.W., Regev, A., and Weinberg, R.A. (2008). An embryonic stem cell-like gene expression signature in poorly differentiated aggressive human tumors. *Nat. Genet.* 40, 499–507.
- Bild, A.H., Yao, G., Chang, J.T., Wang, Q., Potti, A., Chasse, D., Joshi, M.B., Harpole, D., Lancaster, J.M., Berchuck, A., et al. (2006). Oncogenic pathway signatures in human cancers as a guide to targeted therapies. *Nature* 439, 353–357.
- Bouchard, C., Lee, S., Paulus-Hock, V., Lodenkemper, C., Eilers, M., and Schmitt, C.A. (2007). FoxO transcription factors suppress Myc-driven lymphomagenesis via direct activation of Arf. *Genes Dev.* 21, 2775–2787.
- Bouchard, C., Marquardt, J., Brás, A., Medema, R.H., and Eilers, M. (2004). Myc-induced proliferation and transformation require Akt-mediated phosphorylation of FoxO proteins. *EMBO J.* 23, 2830–2840.
- Bowman, T., Symonds, H., Gu, L., Yin, C., Oren, M., and Van Dyke, T. (1996). Tissue-specific inactivation of p53 tumor suppression in the mouse. *Genes Dev.* 10, 826–835.
- Boxer, R.B., Jang, J.W., Sintasath, L., and Chodosh, L.A. (2004). Lack of sustained regression of c-MYC-induced mammary adenocarcinomas following brief or prolonged MYC inactivation. *Cancer Cell* 6, 577–586.
- Castellino, R.C., Barwick, B.G., Schniederjan, M., Buss, M.C., Becher, O., Hambarzumyan, D., Macdonald, T.J., Brat, D.J., and Durden, D.L. (2010). Heterozygosity for Pten promotes tumorigenesis in a mouse model of medulloblastoma. *PLoS ONE* 5, e10849.
- Chang, D.W., Claassen, G.F., Hann, S.R., and Cole, M.D. (2000). The c-Myc transactivation domain is a direct modulator of apoptotic versus proliferative signals. *Mol. Cell. Biol.* 20, 4309–4319.
- Cho, Y.J., Tsherniak, A., Tamayo, P., Santagata, S., Ligon, A., Greulich, H., Berhoukim, R., Amani, V., Goumnerova, L., Eberhart, C.G., et al. (2011).

- Integrative genomic analysis of medulloblastoma identifies a molecular subgroup that drives poor clinical outcome. *J. Clin. Oncol.* 29, 1424–1430.
- Delpuech, O., Griffiths, B., East, P., Essafi, A., Lam, E.W., Burgering, B., Downward, J., and Schulze, A. (2007). Induction of Mxi1-SR alpha by FOXO3a contributes to repression of Myc-dependent gene expression. *Mol. Cell. Biol.* 27, 4917–4930.
- Eberhart, C.G., and Burger, P.C. (2003). Anaplasia and grading in medulloblastomas. *Brain Pathol.* 13, 376–385.
- Eberhart, C.G., Chaudhry, A., Daniel, R.W., Khaki, L., Shah, K.V., and Gravitt, P.E. (2005). Increased p53 immunopositivity in anaplastic medulloblastoma and supratentorial PNET is not caused by JC virus. *BMC Cancer* 5, 19.
- Elson, A., Deng, C., Campos-Torres, J., Donehower, L.A., and Leder, P. (1995). The MMTV/c-myc transgene and p53 null alleles collaborate to induce T-cell lymphomas, but not mammary carcinomas in transgenic mice. *Oncogene* 11, 181–190.
- Frank, A.J., Hernan, R., Hollander, A., Lindsey, J.C., Lusher, M.E., Fuller, C.E., Clifford, S.C., and Gilbertson, R.J. (2004). The TP53-ARF tumor suppressor pathway is frequently disrupted in large/cell anaplastic medulloblastoma. *Brain Res. Mol. Brain Res.* 121, 137–140.
- Gentles, A.J., Alizadeh, A.A., Lee, S.I., Myklebust, J.H., Shachaf, C.M., Shahbaba, B., Levy, R., Koller, D., and Plevritis, S.K. (2009). A pluripotency signature predicts histologic transformation and influences survival in follicular lymphoma patients. *Blood* 114, 3158–3166.
- Gibson, P., Tong, Y., Robinson, G., Thompson, M.C., Currie, D.S., Eden, C., Kranenburg, T.A., Hogg, T., Poppleton, H., Martin, J., et al. (2010). Subtypes of medulloblastoma have distinct developmental origins. *Nature* 468, 1095–1099.
- Gilbertson, R.J., and Ellison, D.W. (2008). The origins of medulloblastoma subtypes. *Annu. Rev. Pathol.* 3, 341–365.
- Grotzer, M.A., Hogarty, M.D., Janss, A.J., Liu, X., Zhao, H., Eggert, A., Sutton, L.N., Rorke, L.B., Brodeur, G.M., and Phillips, P.C. (2001). MYC messenger RNA expression predicts survival outcome in childhood primitive neuroectodermal tumor/medulloblastoma. *Clin. Cancer Res.* 7, 2425–2433.
- Hanel, W., and Moll, U.M. (2012). Links between mutant p53 and genomic instability. *J. Cell. Biochem.* 113, 433–439. 10.1002/jcb.23400.
- Harrington, E.A., Bennett, M.R., Fanidi, A., and Evan, G.I. (1994). c-Myc-induced apoptosis in fibroblasts is inhibited by specific cytokines. *EMBO J.* 13, 3286–3295.
- Hartmann, W., Digon-Söntgerath, B., Koch, A., Waha, A., Endl, E., Dani, I., Denkhaus, D., Goodyer, C.G., Sörensen, N., Wiestler, O.D., and Pietsch, T. (2006). Phosphatidylinositol 3'-kinase/AKT signaling is activated in medulloblastoma cell proliferation and is associated with reduced expression of PTEN. *Clin. Cancer Res.* 12, 3019–3027.
- Hemann, M.T., Bric, A., Teruya-Feldstein, J., Herbst, A., Nilsson, J.A., Cordon-Cardo, C., Cleveland, J.L., Tansey, W.P., and Lowe, S.W. (2005). Evasion of the p53 tumour surveillance network by tumour-derived MYC mutants. *Nature* 436, 807–811.
- Hermeking, H., and Eick, D. (1994). Mediation of c-Myc-induced apoptosis by p53. *Science* 265, 2091–2093.
- Hoshida, Y., Brunet, J.P., Tamayo, P., Golub, T.R., and Mesirov, J.P. (2007). Subclass mapping: identifying common subtypes in independent disease data sets. *PLoS ONE* 2, e1195.
- Huang, M.J., Cheng, Y.C., Liu, C.R., Lin, S., and Liu, H.E. (2006). A small-molecule c-Myc inhibitor, 10058-F4, induces cell-cycle arrest, apoptosis, and myeloid differentiation of human acute myeloid leukemia. *Exp. Hematol.* 34, 1480–1489.
- Jain, M., Arvanitis, C., Chu, K., Dewey, W., Leonhardt, E., Trinh, M., Sundberg, C.D., Bishop, J.M., and Felsher, D.W. (2002). Sustained loss of a neoplastic phenotype by brief inactivation of MYC. *Science* 297, 102–104.
- Kawamura, T., Suzuki, J., Wang, Y.V., Menendez, S., Morera, L.B., Raya, A., Wahl, G.M., and Izpisua Belmonte, J.C. (2009). Linking the p53 tumour suppressor pathway to somatic cell reprogramming. *Nature* 460, 1140–1144.
- Kim, J., Woo, A.J., Chu, J., Snow, J.W., Fujiwara, Y., Kim, C.G., Cantor, A.B., and Orkin, S.H. (2010). A Myc network accounts for similarities between embryonic stem and cancer cell transcription programs. *Cell* 143, 313–324.
- Kool, M., Koster, J., Bunt, J., Hasselt, N.E., Lakeman, A., van Sluis, P., Troost, D., Meeteren, N.S., Caron, H.N., Cloos, J., et al. (2008). Integrated genomics identifies five medulloblastoma subtypes with distinct genetic profiles, pathway signatures and clinicopathological features. *PLoS ONE* 3, e3088.
- Kumar, A., Marqués, M., and Carrera, A.C. (2006). Phosphoinositide 3-kinase activation in late G1 is required for c-Myc stabilization and S phase entry. *Mol. Cell. Biol.* 26, 9116–9125.
- Kupersmidt, I., Su, Q.J., Grewal, A., Sundaresh, S., Halperin, I., Flynn, J., Shekar, M., Wang, H., Park, J., Cui, W., et al. (2010). Ontology-based meta-analysis of global collections of high-throughput public data. *PLoS ONE* 5, e13066.
- Lamb, J., Crawford, E.D., Peck, D., Modell, J.W., Blat, I.C., Wrobel, M.J., Lerner, J., Brunet, J.P., Subramanian, A., Ross, K.N., et al. (2006). The Connectivity Map: using gene-expression signatures to connect small molecules, genes, and disease. *Science* 313, 1929–1935.
- Lee, A., Kessler, J.D., Read, T.A., Kaiser, C., Corbeil, D., Huttner, W.B., Johnson, J.E., and Wechsler-Reya, R.J. (2005). Isolation of neural stem cells from the postnatal cerebellum. *Nat. Neurosci.* 8, 723–729.
- Leonard, J.R., Cai, D.X., Rivet, D.J., Kaufman, B.A., Park, T.S., Levy, B.K., and Perry, A. (2001). Large cell/anaplastic medulloblastomas and medulloblastomas: clinicopathological and genetic features. *J. Neurosurg.* 95, 82–88.
- Lumpkin, E.A., Collisson, T., Parab, P., Omer-Abdalla, A., Haeberle, H., Chen, P., Doetzlhofer, A., White, P., Groves, A., Segil, N., and Johnson, J.E. (2003). Math1-driven GFP expression in the developing nervous system of transgenic mice. *Gene Expr. Patterns* 3, 389–395.
- Meerbrey, K.L., Hu, G., Kessler, J.D., Roarty, K., Li, M.Z., Fang, J.E., Herschkowitz, J.I., Burrows, A.E., Ciccio, A., Sun, T., et al. (2011). The pINDUCER lentiviral toolkit for inducible RNA interference in vitro and in vivo. *Proc. Natl. Acad. Sci. USA* 108, 3665–3670.
- Meletis, K., Wirta, V., Hede, S.M., Nistér, M., Lundeberg, J., and Frisén, J. (2006). p53 suppresses the self-renewal of adult neural stem cells. *Development* 133, 363–369.
- Nagao, M., Campbell, K., Burns, K., Kuan, C.Y., Trumpp, A., and Nakafuku, M. (2008). Coordinated control of self-renewal and differentiation of neural stem cells by Myc and the p19ARF-p53 pathway. *J. Cell Biol.* 183, 1243–1257.
- Northcott, P.A., Korshunov, A., Witt, H., Hielscher, T., Eberhart, C.G., Mack, S., Bouffet, E., Clifford, S.C., Hawkins, C.E., French, P., et al. (2011). Medulloblastoma comprises four distinct molecular variants. *J. Clin. Oncol.* 29, 1408–1414. Published online September 7, 2010. 10.1200/JCO.2009.27.4324.
- Palmer, S.L., Reddick, W.E., and Gajjar, A. (2007). Understanding the cognitive impact on children who are treated for medulloblastoma. *J. Pediatr. Psychol.* 32, 1040–1049.
- Pelengaris, S., Rudolph, B., and Littlewood, T. (2000). Action of Myc in vivo - proliferation and apoptosis. *Curr. Opin. Genet. Dev.* 10, 100–105.
- Pfister, S., Remke, M., Benner, A., Mendrzyk, F., Toedt, G., Felsberg, J., Wittmann, A., Devens, F., Gerber, N.U., Joos, S., et al. (2009). Outcome prediction in pediatric medulloblastoma based on DNA copy-number aberrations of chromosomes 6q and 17q and the MYC and MYCN loci. *J. Clin. Oncol.* 27, 1627–1636.
- Polkinghorn, W.R., and Tarbell, N.J. (2007). Medulloblastoma: tumorigenesis, current clinical paradigm, and efforts to improve risk stratification. *Nat. Clin. Pract. Oncol.* 4, 295–304.
- Remke, M., Hielscher, T., Northcott, P.A., Witt, H., Ryzhova, M., Wittmann, A., Benner, A., von Deimling, A., Scheurle, W., Perry, A., et al. (2011). Adult medulloblastoma comprises three major molecular variants. *J. Clin. Oncol.* 29, 2717–2723.
- Schüller, U., Heine, V.M., Mao, J., Kho, A.T., Dillon, A.K., Han, Y.G., Huillard, E., Sun, T., Ligon, A.H., Qian, Y., et al. (2008). Acquisition of granule neuron precursor identity is a critical determinant of progenitor cell competence to form Shh-induced medulloblastoma. *Cancer Cell* 14, 123–134.

- Shakhova, O., Leung, C., van Montfort, E., Berns, A., and Marino, S. (2006). Lack of Rb and p53 delays cerebellar development and predisposes to large cell anaplastic medulloblastoma through amplification of N-Myc and Ptch2. *Cancer Res.* 66, 5190–5200.
- Soucek, L., Whitfield, J., Martins, C.P., Finch, A.J., Murphy, D.J., Sodik, N.M., Karnezis, A.N., Swigart, L.B., Nasi, S., and Evan, G.I. (2008). Modelling Myc inhibition as a cancer therapy. *Nature* 455, 679–683.
- Stavrou, T., Bromley, C.M., Nicholson, H.S., Byrne, J., Packer, R.J., Goldstein, A.M., and Reaman, G.H. (2001). Prognostic factors and secondary malignancies in childhood medulloblastoma. *J. Pediatr. Hematol. Oncol.* 23, 431–436.
- Stearns, D., Chaudhry, A., Abel, T.W., Burger, P.C., Dang, C.V., and Eberhart, C.G. (2006). c-myc overexpression causes anaplasia in medulloblastoma. *Cancer Res.* 66, 673–681.
- Subramanian, A., Tamayo, P., Mootha, V.K., Mukherjee, S., Ebert, B.L., Gillette, M.A., Paulovich, A., Pomeroy, S.L., Golub, T.R., Lander, E.S., and Mesirov, J.P. (2005). Gene set enrichment analysis: a knowledge-based approach for interpreting genome-wide expression profiles. *Proc. Natl. Acad. Sci. USA* 102, 15545–15550.
- Sutter, R., Shakhova, O., Bhagat, H., Behesti, H., Sutter, C., Penkar, S., Santucci, A., Bernays, R., Heppner, F.L., Schüller, U., et al. (2010). Cerebellar stem cells act as medulloblastoma-initiating cells in a mouse model and a neural stem cell signature characterizes a subset of human medulloblastomas. *Oncogene* 29, 1845–1856.
- Swartling, F.J., Grimmer, M.R., Hackett, C.S., Northcott, P.A., Fan, Q.W., Goldenberg, D.D., Lau, J., Masic, S., Nguyen, K., Yakovenko, S., et al. (2010). Pleiotropic role for MYCN in medulloblastoma. *Genes Dev.* 24, 1059–1072.
- Tabori, U., Baskin, B., Shago, M., Alon, N., Taylor, M.D., Ray, P.N., Bouffet, E., Malkin, D., and Hawkins, C. (2010). Universal poor survival in children with medulloblastoma harboring somatic TP53 mutations. *J. Clin. Oncol.* 28, 1345–1350.
- Thompson, M.C., Fuller, C., Hogg, T.L., Dalton, J., Finkelstein, D., Lau, C.C., Chintagumpala, M., Adesina, A., Ashley, D.M., Kellie, S.J., et al. (2006). Genomics identifies medulloblastoma subgroups that are enriched for specific genetic alterations. *J. Clin. Oncol.* 24, 1924–1931.
- Wang, J., Wang, H., Li, Z., Wu, Q., Lathia, J.D., McLendon, R.E., Hjelmeland, A.B., and Rich, J.N. (2008). c-Myc is required for maintenance of glioma cancer stem cells. *PLoS ONE* 3, e3769.
- Yang, Z.J., Ellis, T., Markant, S.L., Read, T.A., Kessler, J.D., Bourboulas, M., Schüller, U., Machold, R., Fishell, G., Rowitch, D.H., et al. (2008). Medulloblastoma can be initiated by deletion of Patched in lineage-restricted progenitors or stem cells. *Cancer Cell* 14, 135–145.
- Zheng, H., Ying, H., Yan, H., Kimmelman, A.C., Hiller, D.J., Chen, A.J., Perry, S.R., Tonon, G., Chu, G.C., Ding, Z., et al. (2008). p53 and Pten control neural and glioma stem/progenitor cell renewal and differentiation. *Nature* 455, 1129–1133.
- Zhu, J., Blenis, J., and Yuan, J. (2008). Activation of PI3K/Akt and MAPK pathways regulates Myc-mediated transcription by phosphorylating and promoting the degradation of Mad1. *Proc. Natl. Acad. Sci. USA* 105, 6584–6589.

# A Mouse Model of the Most Aggressive Subgroup of Human Medulloblastoma

Daisuke Kawauchi,<sup>1,7</sup> Giles Robinson,<sup>2,7</sup> Tamar Uziel,<sup>1,8</sup> Paul Gibson,<sup>5</sup> Jerold Rehg,<sup>3</sup> Cuilan Gao,<sup>4</sup> David Finkelstein,<sup>4</sup> Chunxu Qu,<sup>6</sup> Stanley Pounds,<sup>4</sup> David W. Ellison,<sup>3</sup> Richard J. Gilbertson,<sup>5,\*</sup> and Martine F. Roussel<sup>1,\*</sup>

<sup>1</sup>Department of Tumor Cell Biology

<sup>2</sup>Department of Oncology

<sup>3</sup>Department of Pathology

<sup>4</sup>Department of Biostatistics

<sup>5</sup>Department of Developmental Neurobiology

<sup>6</sup>Department of Information Sciences

St. Jude Children's Research Hospital, 262 Danny Thomas Place, Memphis, TN 38105, USA

<sup>7</sup>These authors contributed equally to this work

<sup>8</sup>Present address: Global Pharmaceutical Research and Development—Cancer Research, Abbott Laboratories, 100 Abbott Park Road, Building AP-10, Room 201, Abbott Park, IL 60064, USA

\*Correspondence: [martine.roussel@stjude.org](mailto:martine.roussel@stjude.org) (M.F.R.), [richard.gilbertson@stjude.org](mailto:richard.gilbertson@stjude.org) (R.J.G.)

DOI 10.1016/j.ccr.2011.12.023

## SUMMARY

Medulloblastomas that display a large cell/anaplastic morphology and overexpress the cellular *c-MYC* gene are highly aggressive and carry a very poor prognosis. This so-called MYC-subgroup differs in its histopathology, gene expression profile, and clinical behavior from other forms of medulloblastoma. We generated a mouse model of MYC-subgroup medulloblastoma by transducing *Trp53*-null cerebellar progenitor cells with *Myc*. The cardinal features of these mouse medulloblastomas closely mimic those of human MYC-subgroup tumors and significantly differ from mouse models of the Sonic-Hedgehog- and WNT-disease subgroups. This mouse model should significantly accelerate understanding and treatment of the most aggressive form of medulloblastoma and infers distinct roles for *MYC* and *MYCN* in tumorigenesis.

## INTRODUCTION

Medulloblastoma (MB)—the most common malignant pediatric brain tumor—includes at least four clinically and molecularly distinct subgroups (Cho et al., 2011; Kool et al., 2008; Northcott et al., 2011; Thompson et al., 2006). Sonic Hedgehog (SHH)-subgroup MB most frequently results from inactivating mutations of PTCH1 (the SHH receptor) or suppressor of fused (a downstream signal transducer). SHH signaling ultimately activates GLI family transcription factors that upregulate pro-proliferative genes, such as *MYCN*, *CCND1*, and *CCND2* (cyclins D1 and D2), and lead to the reduced expression of inhibitors of cyclin-dependent kinases (CDKs), including p27<sup>KIP1</sup> and p18<sup>INK4c</sup> (Roussel and Hatten, 2011). About 50%

of SHH-subgroup MBs exhibit a desmoplastic/nodular histology and carry an intermediate prognosis in patients who receive contemporary surgical intervention and chemotherapy (Cho et al., 2011; Ellison et al., 2011a; Lam et al., 1999; Northcott et al., 2011; Raffel et al., 1997). In contrast, the WNT-subgroup disease has an excellent prognosis, exhibits a “classic” morphology, and is frequently triggered by mutations in the WNT pathway effector CTNNB1 ( $\beta$ -catenin; Cho et al., 2011; Ellison et al., 2005; Gajjar et al., 2006; Kool et al., 2008; Northcott et al., 2011; Thompson et al., 2006). An interesting distinction between SHH- and WNT-driven MBs is their anatomic location, with SHH tumors arising laterally in the cerebellum and WNT MBs arising in the midline close to the brainstem; recent results indicate that these features reflect

### Significance

MYC-subgroup medulloblastoma (MB) is one of the most aggressive pediatric brain tumors. This disease is resistant to combination surgery, radiotherapy, and chemotherapy and kills most affected children within three years of diagnosis. Mouse models of the Sonic Hedgehog and WNT forms of MB have advanced understanding of the biology and treatment of these disease subgroups. In contrast, the absence of preclinical models of MYC-driven MB has limited understanding of this important tumor. Here, we describe the MYC-driven mouse model of MB that accurately mimics the transcriptome, histopathology, and clinical behavior of human MYC-subgroup disease. This model should significantly advance efforts to develop therapeutic modalities and determine the origin of this deadly childhood cancer.

the different cells of origin of the two MB subgroups (Gibson et al., 2010).

Modeling both the SHH- and WNT-subgroups of MB in the mouse (Wu et al., 2011) has been instrumental in providing insights into the cellular origins of these different disease forms and paving the way for therapeutic development (Romer et al., 2004). SHH-subgroup MBs arise within the cerebellum from committed, SHH-dependent granule neuron precursors (GNPs; Schüller et al., 2008; Yang et al., 2008). Very recently, we demonstrated that WNT-subgroup MBs arise outside of the cerebellum from progenitor cells in the lower rhombic lip (Gibson et al., 2010). Thus, subgroups of MB are likely to reflect intrinsically different diseases with distinct origins and driver mutations.

In contrast to the SHH- and WNT-subgroups, very little is known about the molecular aberrations that drive two other subgroups of the disease. Non-SHH/WNT tumors include the most aggressive form of the disease (MYC-subgroup) that exhibits frequent amplification and/or overexpression of *MYC*, portends a dismal prognosis, and generates a high proportion of aggressive and invasive tumors with large cell/anaplastic (LC/A) histology (Cho et al., 2011; Ellison et al., 2011a; Northcott et al., 2011; Pfister et al., 2009).

*Mycn* is a critical mediator of SHH signals in GNPs (Kenney et al., 2003) and is absolutely required for normal cerebellar development; however, much less is known about the function of *Myc* in the mouse hindbrain (Knoepfler et al., 2002; Zindy et al., 2006). *Myc* is not normally expressed in GNPs (Zindy et al., 2006), and overexpression of *MYC* and *MYCN* is mutually exclusive and associated with distinct subgroups of human MBs (Cho et al., 2011; Northcott et al., 2011). High-level expression and amplification of *MYCN* are observed across the various subgroups of human MB. Aberrant activation of *Mycn* expression in the developing mouse cerebellum initiates a variety of MBs, including both classic and LC/A tumors (Swartling et al., 2010). In contrast, the highest levels of *MYC* expression and *MYC* amplification are found almost exclusively in the aggressive MYC-subgroup disease (Cho et al., 2011; Northcott et al., 2011). Thus, whereas *MYCN* may play a role in the pathogenesis of a variety of MBs, *MYC* may drive a specific aggressive subgroup of the disease. This may seem somewhat counterintuitive, because it is widely thought that the biochemical transcriptional functions of different *MYC*-family genes are similar.

Here, we assessed the role of *MYC* and *MYCN* in medulloblastoma development in the absence of *TRP53*.

## RESULTS

### Enforced Expression of *Myc* but Not *Mycn* in *Trp53*-Deficient Cerebellar Neuronal Progenitors Induces Aggressive MB

We showed previously that GNP-enriched cell isolates from the cerebella of postnatal day (P)6–P7 *Cdkn2c*<sup>−/−</sup>, *Ptch1*<sup>+/−</sup> or *Cdkn2c*<sup>−/−</sup>, *Trp53*<sup>−/−</sup> mice, but not from *Cdkn2c*<sup>−/−</sup> or wild-type mice, generate SHH-subgroup MBs when transduced with a retroviral vector expressing *Mycn* but not a control virus (Zindy et al., 2007). To test if *Myc* might similarly transform *Cdkn2c*<sup>−/−</sup>, *Trp53*<sup>−/−</sup> GNPs, we isolated proliferating GNPs from *Cdkn2c*<sup>−/−</sup>, *Trp53*<sup>−/−</sup>, *Atoh1*-GFP mice, which are marked by co-expression of green fluorescent protein (GFP; Lumpkin

et al., 2003). Enrichment of GNPs showed that, on average, we obtained 91.9% of GFP-positive (+) GNPs and 8.1% of GFP-negative (−) progenitor cells per preparation and found that the sorted GFP-expressing population contained 1.1% of GFP<sup>−</sup> cells, and, conversely, the GFP<sup>−</sup> population contained 1.7% of GFP<sup>+</sup> cells. We transduced these cells with viruses either encoding *Myc* and co-expressing red fluorescent protein (*RFP*) or expressing *Mycn* in lieu of *Myc*. Fluorescence-activated cell sorting (FACS) of *Myc*- and *Mycn*-transduced cells confirmed comparable infection efficiencies by the two retroviral vectors (45.9 ± 11.7% of GFP<sup>+</sup>/RFP<sup>+</sup> for *Myc*-*RFP* and 51.6 ± 2.1% of GFP<sup>+</sup>/RFP<sup>+</sup> for *Mycn*-*RFP*). Cells transduced with either *Myc* or *Mycn* (2 × 10<sup>6</sup> per mouse) were injected separately into the cerebral cortices of naïve recipient CD-1 *nu/nu* mice. *Myc*-transduced cells formed aggressive tumors that killed mice significantly faster than GNPs transduced with *Mycn* (median survival = 33 days for *Myc* vs. 48 days for *Mycn*, *p* < 0.0001, Figure 1A). Immunoblotting demonstrated significant levels of ectopic *Myc* or *Mycn* protein expression within the two tumor subsets (Figures S1A and S1B available online). *Myc*-derived tumors generated from P6–P7 cerebellar cells of either *Cdkn2c*<sup>−/−</sup>, *Trp53*<sup>−/−</sup>, or *Trp53*<sup>−/−</sup> mice occurred with similar latency (median survival = 39 days for *Cdkn2c*<sup>−/−</sup>, *Trp53*<sup>−/−</sup> vs. 39 days for *Trp53*<sup>−/−</sup>, *p* = 0.7096), indicating that the loss of *Cdkn2c* was not required for *Myc* expression to induce MB in the absence of *Trp53* (Figure S1C). *Myc*-tumors displayed a consistent morphology that was strikingly similar to human MBs of the MYC-subgroup (Figure 1B). Morphometric and terminal deoxynucleotidyl transferase dUTP nick end labeling (TUNEL) assays of mouse MBs revealed a much larger cell size and apoptotic rate in *Myc*-tumors than did mouse models of the WNT- (Gibson et al., 2010) or SHH-subgroups disease (*Ptch*-tumors; Uziel et al., 2005), which typically show a classic morphology (Figures 1B and 1C). Thus, *Myc*-induced mouse MBs resemble the human LC/A MB phenotype reported previously (McManamy et al., 2003), and *Myc* and *Mycn* drive distinct tumors that appear to recapitulate aggressive LC/A and classic forms of human MB, respectively.

### *Myc*-engineered Murine MBs Have a Distinct Transcriptome that Mimics Human MYC-Subgroup Tumors

The decreased latency and LC/A morphology of *Myc*-generated tumors suggested that these were distinct from classic MBs induced by *Mycn*. We compared gene expression profiles of *Myc*-tumors with those of *Mycn*-tumors, as well as profiles generated from previously characterized mouse models of WNT- and SHH-subgroup MB (Gibson et al., 2010; Uziel et al., 2005). In addition, we compared these tumor profiles with those of FACS-sorted *Atoh1*-GFP-expressing GNPs obtained from the cerebellum of normal P6 mice lacking both *Trp53* and *p18*<sup>Ink4c</sup> protein expression [*Cdkn2c*<sup>−/−</sup>, *Trp53*<sup>−/−</sup>, *Atoh1*-GFP] mice (designated GNPs; Figure 2A). The transcriptome of *Myc*-tumors was distinct from those of the other mouse MBs (Figure 2A). Unsupervised hierarchical clustering co-segregated the gene expression profiles of mouse *Mycn*-tumors and those of mouse models of SHH-subgroup disease. In contrast, transcriptomes of *Myc*-tumors and the mouse WNT-subgroup model formed two separate clusters. The *Mycn*/SHH/GNP profiles

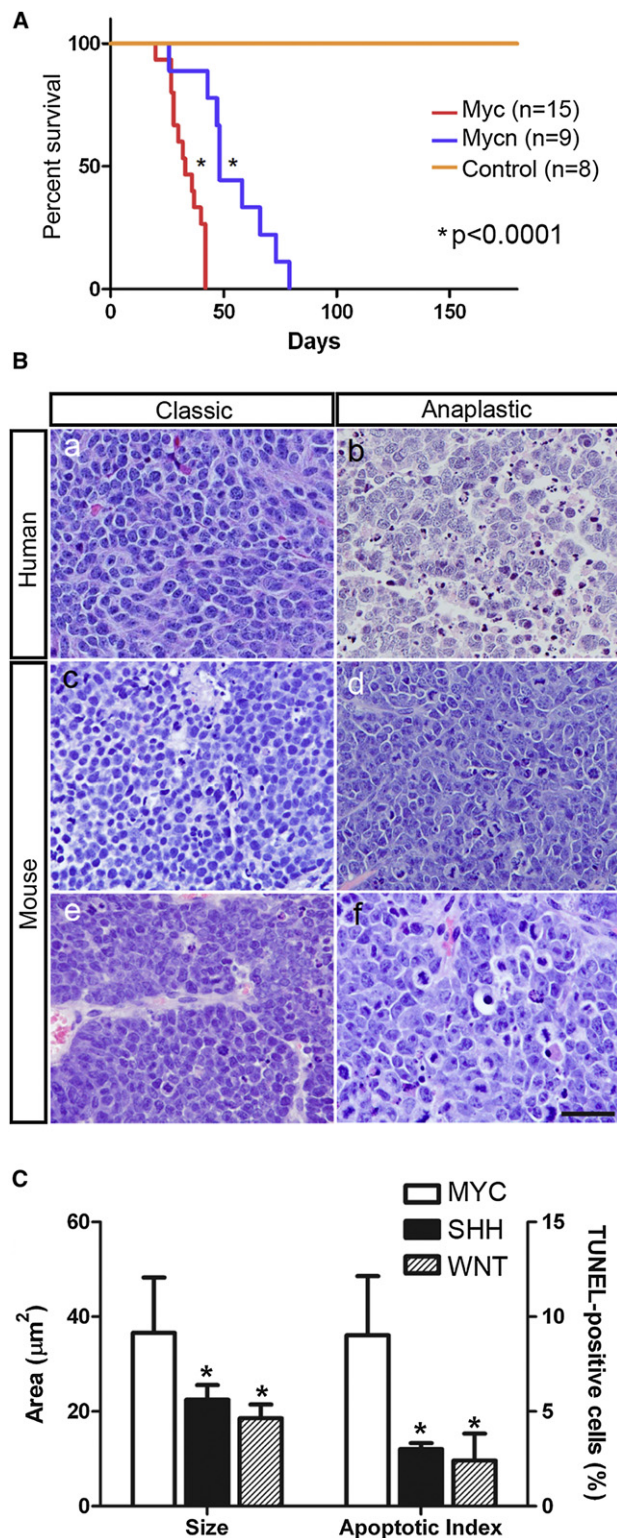


**Figure 1. MBs Derived from Orthotopic Transplants in the Cortices of Naïve Recipient Mice of Cerebellar Progenitors Overexpressing *Myc* and *Mycn***

(A) Kaplan-Meier survival curves of mice transplanted with cerebellar cells purified from [*Cdkn2c*<sup>-/-</sup>, *Trp53*<sup>-/-</sup>, *Atoh1-GFP*] mice infected with *Myc-RFP* (red line), *Mycn-RFP* (blue line), or *RFP* empty vector (orange line).

were characterized by high expression of known members of the SHH pathway and signature genes of SHH-subgroup MB (Figure 2B). This observation was confirmed by quantitative RT-PCR (qRT-PCR), including analysis of *Atoh1*, *Gli1*, *Sfrp1*, and *Boc1* (Figures 2C and 2D). In contrast, *Myc* and *Npr3*, which are specifically expressed in the human MYC-subgroup (Northcott et al., 2011), were highly expressed in the mouse *Myc*-derived MBs (Figure 2B). Immunohistochemical analysis confirmed that *Npr3* is expressed selectively in mouse MYC-subgroup MBs (Figure S2A). *Myc*-induced tumors also exhibited high levels of transcription of *Prom1* and *Lgr5* (Figure 2B), which are frequently expressed in stem-cell-like progenitor cells (Barker et al., 2007; Lee et al., 2005; Zhu et al., 2009). In addition, high expression of *Nanog* and *Oct4* proteins, considered to be canonical markers of embryonic pluripotency (Silva and Smith, 2008), was observed in mouse MYC-subgroup and SHH-subgroup MBs (Figures S2B–S2P). On the other hand, putative markers of brain tumor stem cells (Rich, 2009) exhibited various expression levels among the three distinct tumor subgroups (Figure S2Q).

As a further test of the degree to which mouse *Myc*-derived tumors resemble the MYC-subgroup of human MB, we compared the expression of mouse genes with orthologs previously shown to specifically distinguish the human WNT-, SHH-, and MYC-subgroup tumors (Cho et al., 2011; Northcott et al., 2011; Thompson et al., 2006). Thirty-one of 52 orthologs (60%) that exhibited increased expression in the human MYC-subgroup were similarly upregulated in the mouse *Myc*-tumors (Figure 3A). Forty of 54 orthologs (74%) with increased expression in the human WNT-subgroup were similarly increased in the mouse WNT-tumors (Figure 3B). Thirty-one of 53 orthologs (58%) upregulated in the human SHH-subgroup were increased in the mouse *Ptch*-tumors (Figure 3C). Thus, mouse *Myc*-induced tumors express signature genes remarkably similar to those reported for human MYC-subgroup MB, whereas the mouse *Mycn*, *Ptch*, and *Trp53* tumors resemble the human SHH-subgroup, and WNT mouse tumors recapitulate human WNT-subgroup MBs, as reported previously (Gibson et al., 2010). Furthermore, cross-species comparison of human and mouse MB transcriptomes (Johnson et al., 2010) revealed a statistically significant match between mouse and human MYC-subgroups (Figure S3A). Overall, 56% of 14,261 ortholog probe pairs showed agreement in gene expression (upregulation or downregulation) between the human MYC-subgroup and mouse *Myc*-tumors ( $p = 0.009$  and  $p = 0.079$  by permutation of the human and mouse data, respectively;

(B) Pathology of human and mouse MBs (H&E): (a) a human tumor with *MYCN* amplification and classic morphological features, and (b) a human anaplastic tumor with *MYC* amplification. Note the difference in nuclear pleomorphism between classic and anaplastic tumors. The anaplastic tumor also shows a paving stone-like pattern of cell molding and contains abundant apoptotic cells, a hallmark of this variant. *Mycn*-tumors with a classic morphology of round cells (c, e) contrast with *Myc*-tumors that show an anaplastic morphology with cell molding and abundant mitotic figures and apoptotic bodies (d, f). Scale bar = 50  $\mu\text{m}$ .

(C) *Myc*-tumor cells are significantly larger and more likely to undergo apoptosis than are their SHH- and WNT-subgroups counterparts. Error bars indicate standard deviation. \* $p < 0.05$  for SHH- and WNT-subgroup tumors compared to the MYC-subgroup. See also Figure S1.

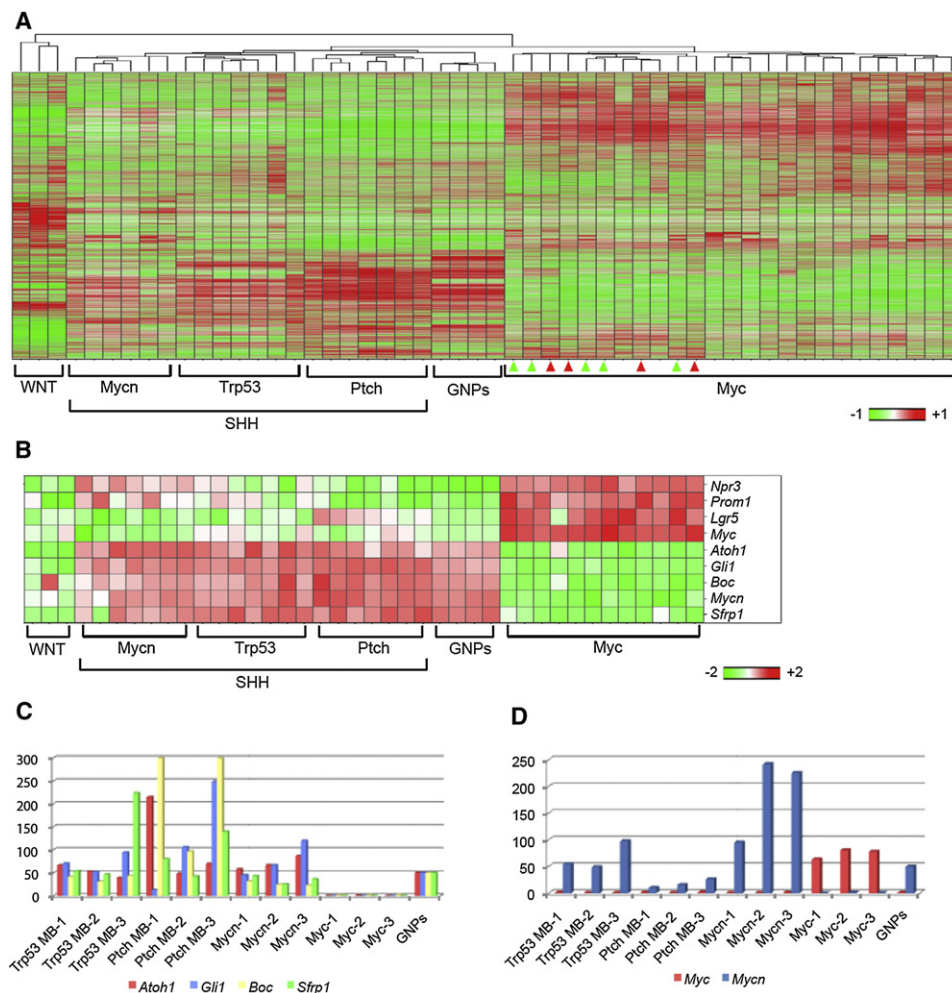


**Figure 2. Comparative Molecular Analysis of Engineered Mouse MBs and GNPs**

(A) Affymetrix gene chip analysis of mouse Myc- and Mycn-tumors, GNPs purified from the cerebellum of P6 [*Cdkn2c*<sup>-/-</sup>, *Trp53*<sup>-/-</sup>, *Atoh1*-GFP] mice, from spontaneous MBs of the SHH-subgroup from [*Cdkn2c*<sup>-/-</sup>, *Trp53*<sup>-/-</sup>, *Nestin*-cre] and [*Cdkn2c*<sup>-/-</sup>, *Ptch1*<sup>+/-</sup>] mice and from the mouse WNT-subgroup from [*Ctnnb1*<sup>+lox(ex3)</sup>, *Bilbp*-Cre; *Trp53*<sup>-/-</sup>] mice. Arrowheads indicate Myc-tumors from FACS-sorted GFP-positive (GFP<sup>+</sup>; green) and GFP-negative (GFP<sup>-</sup>; red) cerebellar cells.

(B) Heatmap of differentially regulated genes between Myc- and Mycn-mouse MBs and the SHH-subgroup MBs from the *Ptch1*<sup>-/-</sup> and *Trp53* null mice, the WNT-subgroup of tumors, and GNPs.

(C and D) Quantitative RT-PCR (QRT-PCR) analysis of *Atoh1*, *Gli1*, *Boc*, and *Sfrp1* (C) and *Myc* and *Mycn* (D) in Myc-engineered MBs (Myc-1,2,3) compared to spontaneous Trp53 and Ptch MBs, Mycn-engineered (Mycn-1,2,3) MBs, and GNPs. See also Figure S2.

Figure S3B). Together, these data confirm that the mouse Myc-tumors accurately model the transcriptome of human MYC-subgroup MB.

### Probing the Origin of Myc-Engineered MBs

All MBs generated from neuronal progenitors purified from P7 cerebella of *Cdkn2c*<sup>-/-</sup>, *Trp53*<sup>-/-</sup>, *Atoh1*-GFP mice and infected with Myc-encoding retroviruses before cortical injection expressed vector-encoded RFP (Figures 1 and S1D). Mycn tumors consisted mainly of GFP<sup>+</sup>/RFP<sup>+</sup> cells (70.0 ± 8.20%, n = 7; Figure S1E). Surprisingly, Myc-induced tumors expressed little or no GFP (17.2 ± 3.67%, n = 14; Figure S1E), suggesting that these tumors arise from a small fraction (~5%) of GFP<sup>-</sup> cells in the GNP-enriched isolates or from GFP<sup>+</sup> GNP progenitors that

subsequently silence *Atoh1*-GFP expression during tumor formation.

To more rigorously characterize the source of mouse MYC-MBs, we further profiled our cell isolates. Comparison of gene expression profiles between GFP<sup>+</sup>, GFP<sup>-</sup> populations and Myc-engineered MBs revealed that MYC-subgroup medulloblastoma most closely matched that of GFP-negative cells (Figure S4A); however, not all genes, including *Lgr5* and *Npr3*, were expressed in the GFP-negative sorted cell population (Figure S4B). As a first step in understanding which cell population might generate MYC-subgroup MBs, we FACS-sorted GFP-positive and GFP-negative progenitor cells. These separate fractions were then transduced with Myc-encoding retroviruses at an efficiency of ~30%, and 5 × 10<sup>4</sup> cells from each transduced fraction were

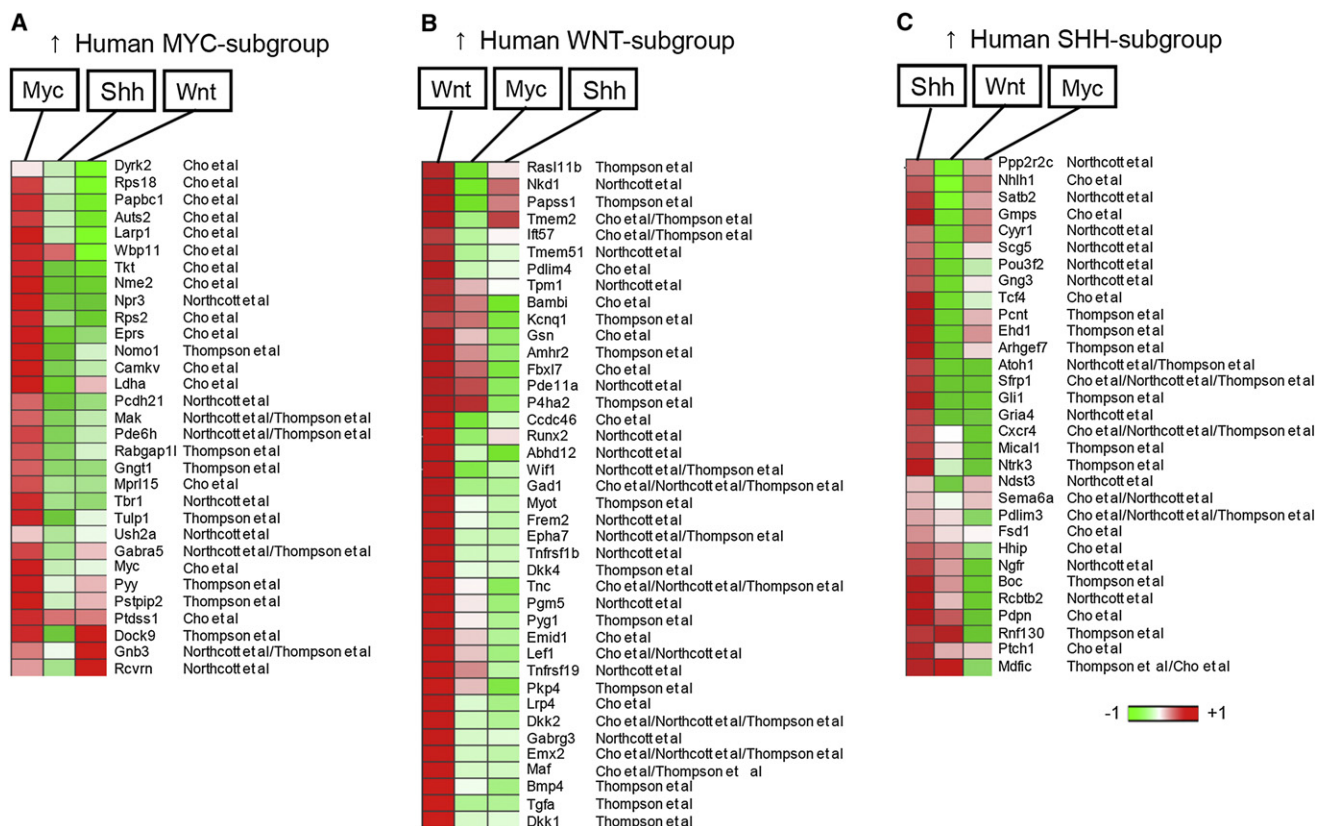


**Figure 3. Comparison of the Gene Expression Signature of Human MYC-, SHH-, and WNT-Subgroup MB with that of Mouse MBs Reveals Three Representative Murine Models of the Human Disease**

Signature genes that specifically distinguish the human WNT-, SHH-, and MYC-subgroup tumors by their broad subgroup overexpression relative to the others were compiled from three recent publications on subgroups of MB (Cho et al., 2011; Northcott et al., 2011; Thompson et al., 2006). 52 signature genes relatively overexpressed by the human MYC-subgroup, 54 by the human WNT-subgroup, and 53 by the human SHH-subgroup were found to have corresponding mouse orthologs on the Affymetrix 430v2 chip. Shown here are representative heat maps columns which compare mean average expression of the orthologs in the three mouse medulloblastoma models (Myc, Shh, and Wnt). Red indicates a log scale relative increase of expression, whereas green signifies a log scale relative decrease of expression. The ortholog name and the corresponding first author of the study from which the signature gene was described are listed in the columns immediately to the right of the heat map.

(A) Thirty-one of 52 orthologs (60%) with increased expression in the human MYC-medulloblastoma subgroup and in the mouse Myc-tumors.

(B) Forty of 54 orthologs (74%) with increased expression in the human WNT-subgroup and in the mouse WNT-tumors.

(C) Thirty-one of 53 orthologs (58%) with increased expression in the human SHH-subgroup and mouse Ptch-tumors. See also Figure S3.

then separately implanted into the cortices of recipient mice. Both *Myc*-transduced population generated tumors in the cortex of naïve recipient animals (Table 1). Histopathological analysis of tumors revealed that all medulloblastomas derived from GFP<sup>+</sup> FACS-sorted cells infected with *Myc*-encoding viruses (5/8) showed LC/A characteristics (Table 1 and Figure S4C). In contrast, tumors occurring after transplants of GFP-negative cells infected with *Myc*-expressing retroviruses included two T-cell lymphomas (2/8), as well as a range of CNS embryonal tumors—high-grade neuroepithelial tumor with dominant PNET and focal glial phenotype (3/8) and MBs with LC/A features (3/8; Table 1). All LC/A MBs expressed low levels of *Atoh1* when compared to that of normal GNPs percoll-purified from the cerebella of P7 wild-type mice (Figure S4D). Comparative gene expression analysis showed that the MYC-subgroup MBs derived from *Myc*-transduced FACS sorted GFP-positive and GFP-negative cerebellar cell populations had similar gene profiles as do *Myc*-tumors derived from unsorted cere-

bellar cells (Figure 2A). These observations suggest that both GFP<sup>+</sup> and GFP<sup>−</sup> populations contain cells that can form MYC-subgroup MBs.

### MYC-Engineered MBs Contain Numerous Tumor-Propagating Cells with High Proliferative Potential

Human MYC-type MBs are the most aggressive of all subgroups (Cho et al., 2011; Northcott et al., 2011), and consistent with clinical data, mouse *Myc*-induced tumors developed faster than did *Mycn*-MBs (Figure 1A). One possible feature of MYC tumors that could explain their aggressiveness is that MYC-subgroup MBs contain a greater fraction of tumor-propagating cells than do tumors of other subgroups. To estimate the numbers of cells capable of initiating MBs, cells were purified from mouse MBs of the SHH- and MYC-subgroups, and different numbers of tumor cells were injected into the cortices of recipient nude mice (Figure 4A). Limited dilution experiments revealed that

**Table 1. Orthotopic Transplants of FACS sorted Cerebellar Progenitor Cells before Infection with Myc-Encoding Retroviruses**

Myc-Infected FACS-Sorted Population	Transplanted Cells (Number)	Tumor Latency (Days)	Phenotype
GFP <sup>+</sup> (n = 8)	5 × 10 <sup>4</sup>	52, 55, 98, 113, 75	LC/A, MYC-subgroup
GFP <sup>-</sup> (n = 8)	5 × 10 <sup>4</sup>	34, 37	T cell lymphoma
		51, 53, 69	High-grade neuroepithelial tumor with dominant PNET and focal glial phenotype
		60, 68, 60	LC/A, MYC-subgroup

Neuronal progenitors were purified from the cerebella of postnatal day P7 *Cdkn2c*<sup>-/-</sup>; *Trp53*<sup>-/-</sup>; *Atoh1*-GFP mice and sorted for GFP-positive and GFP-negative cell populations. Sorted cells were infected with vectors co-expressing both *Myc* and *RFP*, and 5 × 10<sup>4</sup> cells were transplanted into the cortices of naïve recipient animals. Data were obtained from three independent experiments. Tumor latency represents the time at which mice become moribund (median survival = 105.5 days for GFP-positive population and 56.5 days for GFP-negative population). See also Figure S4.

equal to more than 2 × 10<sup>5</sup> purified SHH-subgroup tumor cells were required for secondary tumor formation (Figure S5), consistent with previous reports (Read et al., 2009). Unlike SHH-subgroup MB cells, only 1 × 10<sup>2</sup> Myc-induced tumor cells were required to generate secondary tumors (5/5; Figure 4A). Histological analysis confirmed that secondary tumors shared similar immunohistological characteristics with the parental primary tumor (Figures 4B–4K).

CD133/Prom1-positive tumor-propagating cells from human MBs expand in vitro to form “neurosphere” colonies when plated under conditions that prevent their attachment to the culture dish (Singh et al., 2004). Given that mouse MYC-subgroup tumors upregulated *Prom1*, we tested whether these tumor cells could similarly form neurospheres. Purified cells from Myc-tumors were plated on an ultra-low attachment dish at a density of 5 × 10<sup>4</sup> cells/ml in culture medium supplemented at 3-day intervals with basic fibroblast growth factor (FGF) and epidermal growth factor (EGF). One week later, spheres were harvested, dissociated with trypsin, and the total number of cells per plate was enumerated. Dissociated cells were replated at the same initial density, cultured under the same conditions, and sequentially passaged multiple times. Six to seven days after their first plating, single RFP-positive Myc-derived tumor cells generated macroscopic red colonies (Figure 5A), the overall numbers of which had increased more than 20-fold (Figure 5B, passage 1). Thus, on average, sphere-forming cells underwent 5–6 population doublings in the first 7-day period. More cells were recovered at passages 2 and 3, after which the doubling time of the population slowed down; however, a consistent proliferative rate approximately equal to 4 population doublings in the succeeding 7-day intervals was maintained from passages 5 to 10 (Figure 5B). In stark contrast, spheres derived from canonical SHH-subgroup MBs that arose in *Cdkn2c*<sup>-/-</sup>; *Ptch1*<sup>+/-</sup> mice could not be serially passaged at all under the same culture conditions (Figure S6). Immunohistochemical analysis (Figure 5C) and qRT-PCR (Figure 5D) revealed that neurospheres from Myc-induced MBs expressed several markers identified in stem/progenitor cells, including Nanog, Oct4, Sox2, and Lgr5, as well as Nestin and Npr3 (Figure 5C).

To examine whether tumor spheres could be transplanted and would recapitulate primary Myc-induced MBs, we injected spheres at passages 2 and 6 into the cortices of recipient mice. Interestingly, 2 × 10<sup>5</sup> cells formed tumors with a similar latency as the secondary MBs generated from cells purified

from Myc-engineered tumors (7/7, median latency = 22 days; Figure 6A). Primary and secondary tumors shared the same pathology and expressed similar immunohistochemical markers (Figure 6B). Gene profiling of primary and secondary MBs confirmed that the tumors were distinct from the SHH-subgroup tumors used as a control (Figure 6C). Thus, tumor spheres recapitulate MYC-subgroup MBs after transplantation.

### Myc-Engineered MB Cells Are Resistant to SHH Signaling Inhibitors

Smoothed inhibitors, including cyclopamine and HhAntag, inhibit the proliferation and induce the differentiation of SHH-subgroup MB in vitro and in vivo (Berman et al., 2002; Romer et al., 2004). Similarly, BMP4 antagonizes SHH signaling, induces the neuronal differentiation of GNP (Rios et al., 2004), extinguishes protein Atoh1 expression, and inhibits the proliferation of MBs of the SHH-subgroup (Zhao et al., 2008). Because human MYC-subgroup MBs lack an active SHH gene expression signature and do not contain activating mutations in SHH pathway genes, we reasoned that mouse MYC-subgroup tumors might resist smoothed antagonists. Purified GNPs from cerebella of P7 wild-type mice, from MYC-subgroup MB, and from a SHH-subgroup MB derived from *Cdkn2c*<sup>-/-</sup>; *Trp53*<sup>F/F</sup>; *Nestin-Cre* mice were cultured for 3 days, either in the presence of cyclopamine, BMP4, or a vehicle control. Cells were then labeled with BrdU and analyzed by FACS with an antibody to BrdU. Cyclopamine or BMP4 reduced the S phase fraction of *Cdkn2c*<sup>-/-</sup>; *Trp53*<sup>F/F</sup>; *Nestin-Cre* “primary” tumor cells by 35% to 85% (Figure 7A). In contrast, tumor cells isolated from 3 independently derived mouse MYC-subgroup tumors were insensitive to cyclopamine or BMP4 treatment (Figure 7A), consistent with the finding that MYC-tumors were associated with low expression of SHH signature genes (Figure 7B). Similarly, we saw no inhibition of proliferation of neurospheres from MYC-tumors plated in the constant presence of SHH signaling inhibitors in the culture medium for 2 weeks (Figure 7C).

### DISCUSSION

Enforced expression of *Myc*, but not *Mycn*, in concert with the loss of *Trp53* in GNP-enriched mouse cerebellar progenitor cells gives rise to tumors that recapitulate the most aggressive form of human MB. These tumors exhibited neither of the characteristic gene expression signatures previously ascribed to the SHH- or

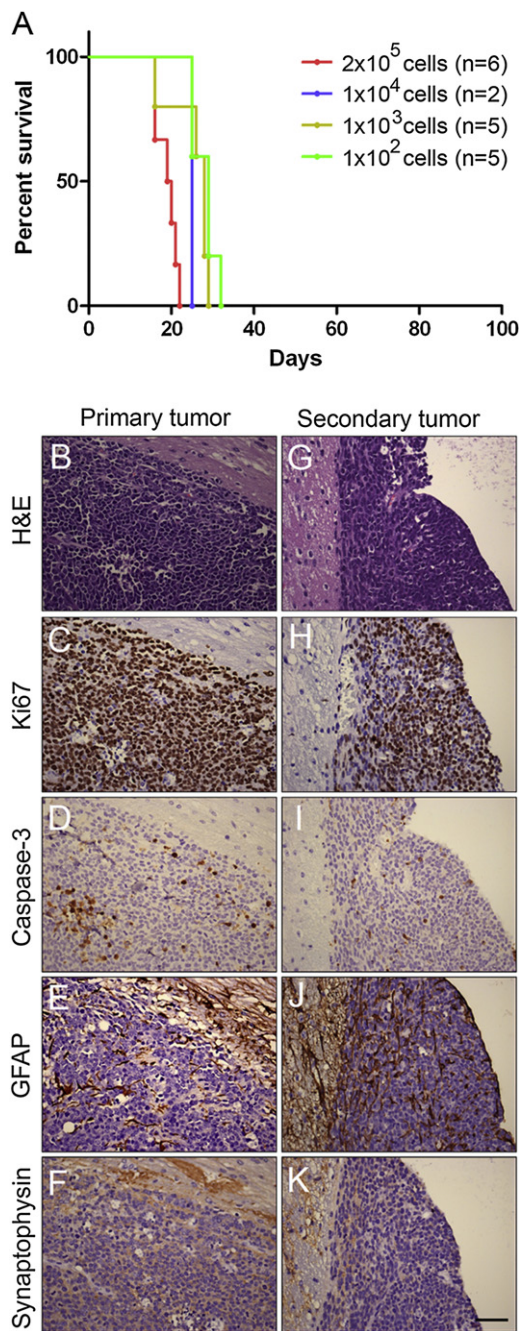


**Figure 4. Mouse MYC-Subgroup MBs before and after Orthotopic Transplants**

(A) Kaplan-Meier survival curve of mice subjected to orthotopic cranial injection of decreasing number of Myc- primary tumor cells.

(B–K) Sections of tumors were immunostained with H&E (B and G), Ki67, a marker of proliferating cells (C and H), cleaved Caspase-3, a marker of apoptosis (D and I), GFAP, that marks glial and neural progenitor cells (E and J), and synaptophysin that characterizes mature neurons (F and K). Scale bar = 50  $\mu$ m. See also Figure S5.

WNT-subgroups of the disease (Cho et al., 2011; Northcott et al., 2011; Thompson et al., 2006). Instead, multitiered analysis of data comparing the murine tumors with the human MYC-subgroup revealed convincing similarities in histology, clinical

behavior, and gene expression between the tumors of both species.

Marker proteins, including Prom1, Lgr5, Oct4 and Nanog, found either in embryonic or adult tissue stem cells, as well as in some “cancer stem cells,” were highly expressed as part of the defining gene expression signature of *Myc*-engineered tumors. Prom1 is a marker of tumor-initiating cells in many cancers (Curley et al., 2009; Reya et al., 2001; Singh et al., 2004; Todaro et al., 2010), and Lgr5 is expressed in mitotically dividing stem cells within the colon and intestinal crypts but not in their proliferating transient amplifying progeny (Barker et al., 2007; Zhu et al., 2009). Oct4 and Nanog are considered markers of pluripotency; although distinct from the “MYC expression module” (Kim et al., 2010), they can collaborate with MYC in reprogramming somatic cells to induced pluripotent stem cells (Takahashi and Yamanaka, 2006). Like those cells with stem cell characteristics, whose frequencies correlate with poor prognosis in other cancers (Ben-Porath et al., 2008), cells from mouse MYC-subgroup MBs could be sequentially and continuously propagated as cultured neurospheres through many ex vivo passages. These cells retained tumor-propagating potential after transplantation into the cortices of recipient mice and re-induced MBs with the same robust efficiency and defining cardinal features as the primary MYC-subgroup MBs from which they were derived. In contrast, tumor cells explanted from MBs of the SHH-subgroup tend to undergo spontaneous differentiation in culture, and neurospheres generated from these tumors rapidly lose their self-renewal capacity when sequentially passaged (Read et al., 2009; Figure S5). Given that standard front line therapies fail in children with MYC-subgroup MBs and such tumors in the mouse are unaffected by SHH inhibitors now being incorporated into human clinical trials, the ability to maintain tumor-propagating cells in cultures from mouse MYC-subgroup MBs may prove useful in establishing a platform for identifying therapeutic drugs.

The generation of an entirely unique subgroup of MB in the mouse after *Myc* transduction into *Trp53*-deficient GNPs (irrespective of *Cdkn2c* loss) was unexpected. In fact, upon embarking on these experiments, a reasonable hypothesis might have been that ectopically enforced overexpression of *Myc* would have had the same effect as overexpression of *Mycn*, given that *Myc*-family proteins bind to the same canonical DNA consensus sequences (Grandori and Eisenman, 1997) and interact with similar dimerization partners, co-activators, and corepressors (Blackwood and Eisenman, 1991; Grandori et al., 2000). Indeed, despite the fact that *Mycn* and *Myc* genes are differentially expressed in the hindbrain (Zindy et al., 2006) and that *Mycn*, but not *Myc*, is a target of SHH signaling (Kenney et al., 2003), genetic experiments showed that *Mycn* can functionally replace *Myc* in mouse development, proliferation, and differentiation (Malynn et al., 2000), implying many interchangeable functions.

The gene expression pattern of the human SHH-subgroup MB resembles that of GNP cells (Lee et al., 2003) and that of the WNT-subgroup MB resembles cells derived from the dorsal brainstem (Gibson et al., 2010), but the gene expression pattern of the MYC-subgroup of MB, either in mouse or humans, is quite distinct. This suggests that the latter tumors might arise from a class of MYC-responsive progenitor cells that differ from those

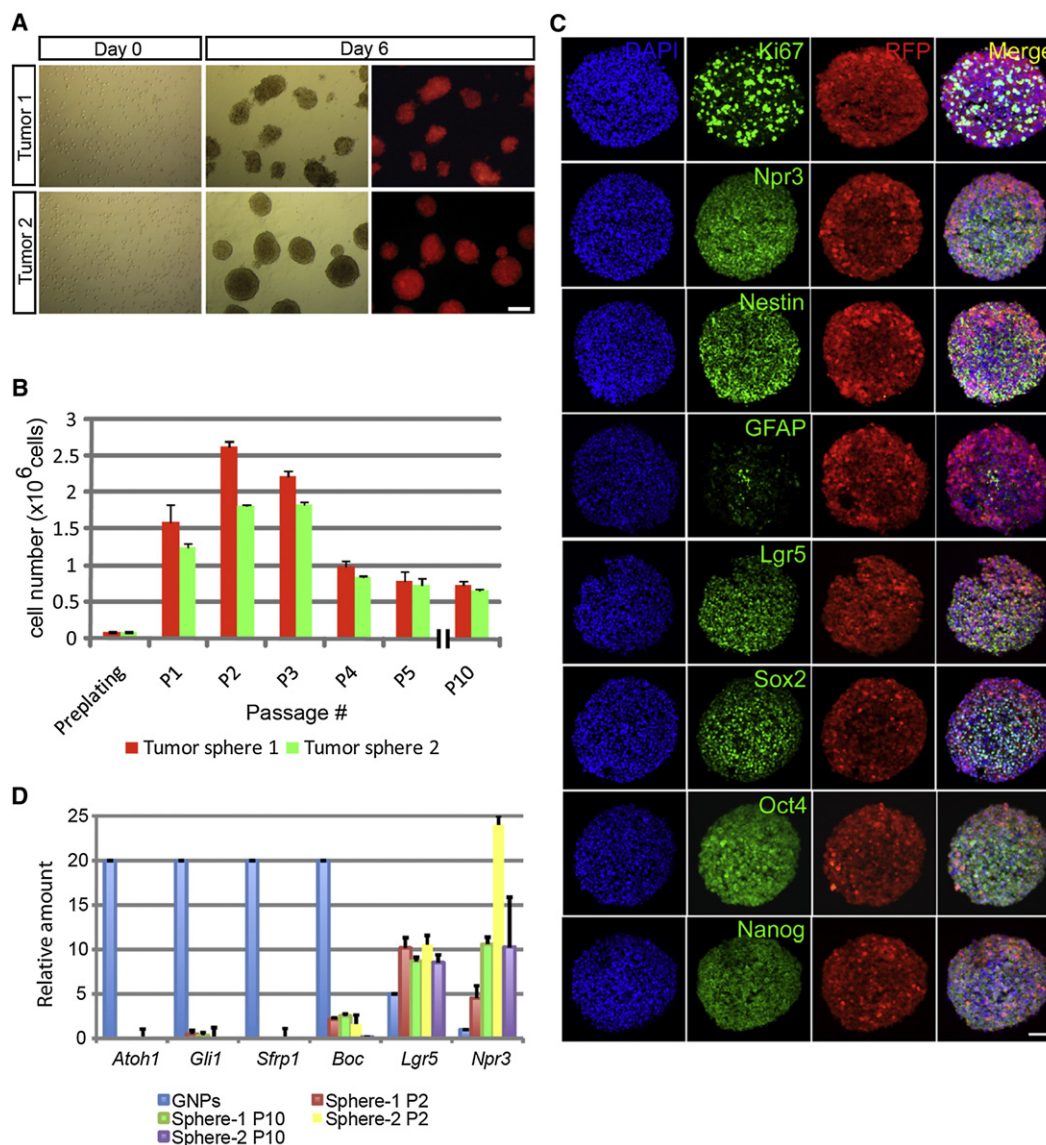


**Figure 5. Myc-Induced Tumor Cells Grow as Neurospheres In Vitro**

(A) Tumor cells from mouse MYC-subgroup MBs form red spheres by day 6 after plating. Scale bar = 200  $\mu$ m.

(B) Spheres can be passaged continuously; here shown up to passage 10 with the cell number increasing up to 25-fold.

(C) Immunostaining of tumor spheres with antibodies against Ki67, Npr3, Nestin, Sox2, Oct4, Nanog, Lgr5, and GFAP. Scale bar = 50  $\mu$ m.

(D) Spheres share a similar molecular signature (lower levels of SHH signature genes and higher levels of *Lgr5* and *Npr3*) than that of GNPs after several passages up to passage 10. Data are represented as the mean  $\pm$  SD. See also Figure S6.

that give rise to the other MB subgroups. Notably, although previous models of mouse MB generated by targeting cerebellar GNPs invariably yielded tumors of the SHH-subgroup, regardless of many different genetic perturbations used to initiate tumorigenesis (Wu et al., 2011), the more recent derivation of a WNT-subgroup mouse model stemmed from observations that a different group of progenitor cells expressed in the dorsal brain stem, and not cerebellar GNPs, were the most sensitive to constitutive activation of the WNT signaling pathway (Gibson et al., 2010). Therefore, one possibility is that target cells most sensitive to Myc overexpression had contaminated the highly purified Atoh1-GFP-expressing GNP population into which the

*Myc-RFP* vector was introduced. Alternatively, enforced *Myc* expression in the context of *Trp53* loss may have significantly altered the transcriptional program of GNPs, resulting in their transdifferentiation, loss of canonical GNP markers, and the emergence of distinctly different phenotypic features. Either scenario would account for the observation that RFP-expressing MYC-subgroup MBs no longer expressed Atoh1-GFP. By analogy to the strategy for modeling WNT-subgroup MBs (Gibson et al., 2010), the identification of the cell of origin of MYC-subgroup tumors will likely require the systematic generation of genetically engineered animals in which *Myc* expression is conditionally regulated within different cell lineages.

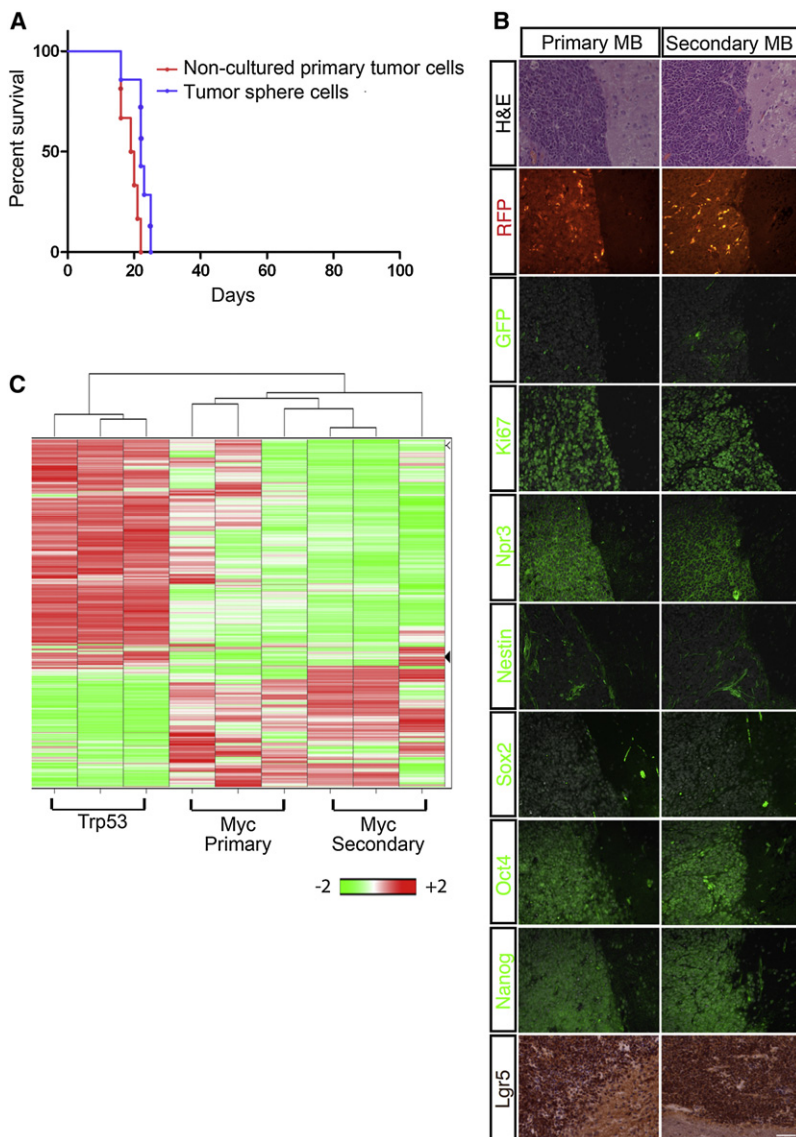


**Figure 6. Tumor Sphere Cells Contain Tumor-Propagating Cells**

(A) Myc-engineered MBs form after transplant of purified tumor cells or tumor sphere cells at passage 2 ( $2 \times 10^5$  cells) into the cortices of recipient mice.

(B) Comparison of the expression of RFP, GFP, Ki67, Npr3, Nestin, Sox2, Oct4, Nanog, and Lgr5 by immunohistochemistry between primary MB (Primary MB) and those induced after transplant of spheres (Secondary MB). Scale bar = 50  $\mu$ m.

(C) Comparison of gene signature among Trp53 tumors, Myc-primary tumors, and Myc-secondary tumors.

feel that there are distinctions in the two models that may explain this discrepancy. The Swartling model links *Mycn* to a *Glt-1* promoter. *Glt-1* is a gene that is not widely expressed by cells in the external granule layer (EGL) of the cerebellum, and it is likely that, via *Glt-1*, *Mycn* is influencing a developing cerebellar cell pool that is distinct from that of the EGL. On the contrary, in our study *Mycn* is transfected into a highly concentrated pool of GNP cells. It stands to reason that the introduction of a SHH pathway target member, like *Mycn* into GNP/EGL cells, which are particularly sensitive to SHH stimulated growth, may favor the induction of SHH-subgroup MB. On the other hand, MYC—probably because it is not a direct target of the SHH pathway—appears to have a very unique and specific effect when transduced into a similar pool of cerebellar precursor cells.

Mutations of the *TP53* gene are found in human LC/A MBs together with *MYC* amplification (Aldosari et al., 2002; Frank et al., 2004; Pfister et al., 2009). Although *TP53* is frequently disrupted in LC/A MBs, its loss of function is observed only infrequently across other subgroups (Pfaff et al., 2010; Thompson et al., 2006). Under the conditions used in our mouse

modeling experiments, concurrent deregulation of both *Myc* and *Trp53* was required to induce MYC-subgroup tumors, whereas neither was effective alone. The genetic interaction between *MYC* and *TP53* is known to be important in many different cancers. Whereas *Trp53* represses *Myc* expression transcriptionally, miss-regulation of *Myc* abrogates *Trp53*-mediated cell cycle arrest through the repression of inhibitors of CDKs (Hoffman and Liebermann, 2008). Overexpression of *Myc* also induces *Trp53*-dependent apoptosis (Hermeking and Eick, 1994; Wagner et al., 1994), but when accompanied by either *Trp53* mutation or bi-allelic *Arf* deletion, *Myc* can readily generate immortalized tumor cells (Eischen et al., 1999; Hemann et al., 2005; Zindy et al., 1998).

Sublethal ionizing irradiation of *Trp53* null mice at P5–P7 is sufficient to induce MBs of the SHH-subgroup with very high penetrance, implying that in this setting, the primary function of *Trp53* is to eliminate rapidly proliferating GNPs that have sustained DNA damage (Uziel et al., 2005). Inactivation of *Trp53*

Recent studies have more clearly identified the subgroup of human MBs that feature high *MYC* expression and/or amplification and carry a dismal prognosis (Cho et al., 2011; Ellison et al., 2011b; Northcott et al., 2011). Both amplification and overexpression of *MYC* or *MYCN* have been associated with poor prognosis in human MB (Pfister et al., 2009). However, in a large cohort of children studied in the SIOP/PNET3 clinical trial, Ellison et al. (2011b) recently concluded that amplification of *MYC*, rather than *MYCN*, is associated with the poorest outcome. In agreement with the latter findings, Myc-induced mouse MBs were more anaplastic and aggressive than were their Mycn-induced counterparts, contained a several log-fold higher fraction of tumor-propagating cells, and initiated tumors after a significantly shorter latency period.

Whereas our finding that *Mycn* overexpression results in MBs of the SHH-subgroup seems contradictory to the finding published in a recent study by Swartling et al. (2010), which ascribes *Mycn* overexpression to the production of a variety of MBs, we

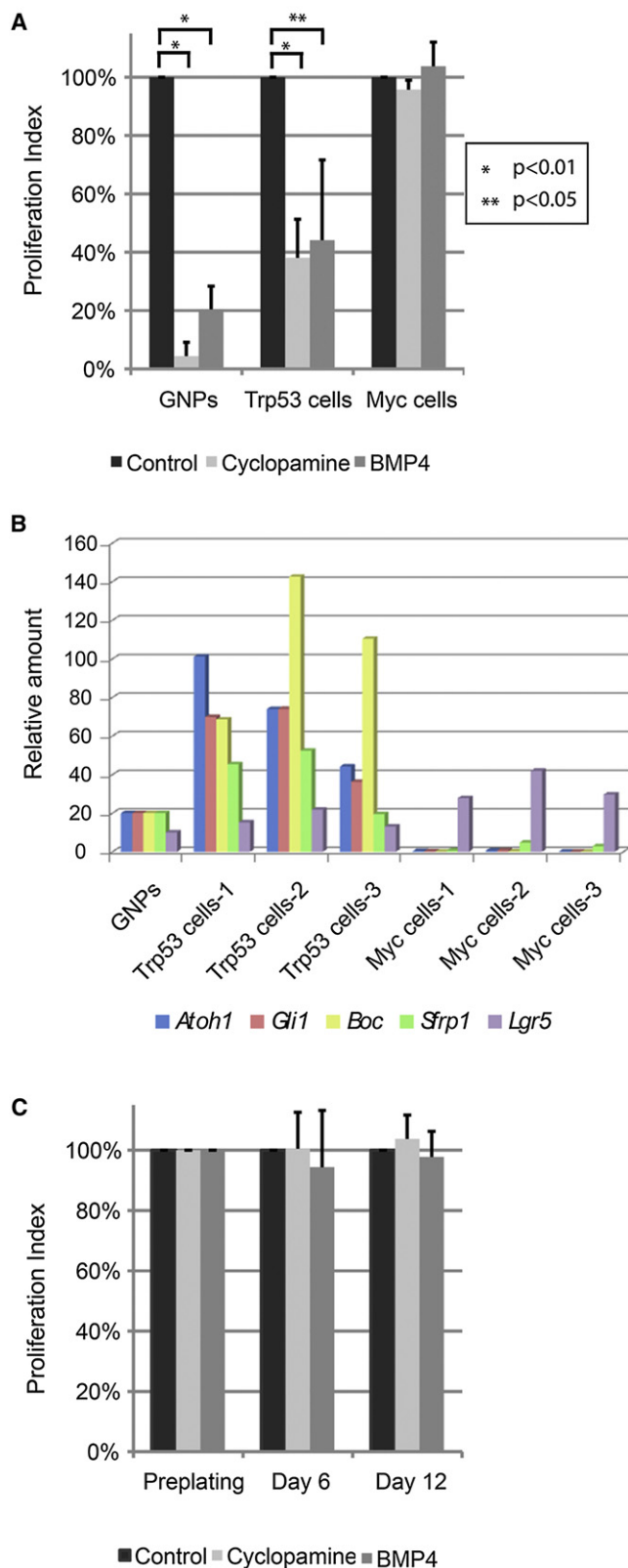


**Figure 7. Myc-Tumor Cells Are Resistant to SHH Signaling Inhibitors**  
(A) GNPs purified from the cerebellum from 7-day-old pups and purified tumor cells were grown in serum-free medium in the absence (Control, black square)

similarly accelerates MB formation in *Ptch1* heterozygous mice, a context in which *Arf* deletion has no such effect (Wetmore et al., 2001). Although *Arf* is induced by high-signaling thresholds conveyed by constitutively activated oncogenes, including *Myc* (Zindy et al., 1998), *Arf* is not induced by acute DNA damage (Kamijo et al., 1997). Moreover, *Atoh1*-expressing, proliferating GNPs normally express relatively high levels of *Bmi1*, a polycomb protein suppressor of the *Ink4a/Arf* locus (Bruggeman et al., 2005). If the cell of origin of *Myc*-induced tumors is not an *Atoh1*-expressing GNP, this begs the question of whether *Arf* null mice, like those lacking *Trp53*, might be predisposed to MYC-subgroup MB formation. Conceivably, other mutations in the *Trp53* signaling network might also substitute for inactivation of *Trp53* itself. Next-generation sequencing and comprehensive analysis of the methylome of primary MYC-subgroup human MBs should shed light on this issue.

In summary, the generation of a mouse model of MYC-subgroup MB is of particular importance, because it mimics the most aggressive subgroup of human MBs that remain the least responsive to therapy (Ellison et al., 2011b). The model provides an opportunity to further explore the identity of the progenitor cells from which these tumors arise and screen for molecules that may offer improved therapeutic impact.

## EXPERIMENTAL PROCEDURES

A detailed description of the Experimental Procedures utilized in this work can be found in the Supplemental Experimental Procedures (available online).

### Mouse Strains and Animal Husbandry

*Cdkn2c*<sup>-/-</sup>, *Trp53*<sup>-/-</sup>, *Atoh1*-GFP mice were generated by breeding *Cdkn2c*<sup>-/-</sup>; *Trp53*<sup>-/-</sup> animals (Uziel et al., 2005) with *Atoh1*-GFP transgenic mice (Lumpkin et al., 2003). Other mice used in this study were *Cdkn2c*<sup>-/-</sup>; *Ptch1*<sup>+/-</sup> (Uziel et al., 2005), *Cdkn2c*<sup>-/-</sup>; *Trp53*<sup>F/F</sup>, *Nestin*-Cre, and *CTNNB1*<sup>+/-lox(ex3)</sup>; *BLBP*-Cre; *Trp53*<sup>F/F</sup> (Gibson et al., 2010). All animal work was performed under established guidelines and supervision by the St. Jude Children's Research Hospital's Institutional Animal Care and Use Committee, as required by the United States Animal Welfare Act and the National Institutes of Health's policy to ensure proper care and use of laboratory animals for research.

### GNP Culture, Retrovirus Production, and Infection

Purification of GNPs and other progenitor populations, retrovirus production, infections, and orthotopic transplants were performed as previously described (Ayrault et al., 2010). Mouse stem cell virus (MSCV)-based retroviruses encode the red fluorescent protein (RFP) in cis expressed from an internal ribosomal entry site. These viruses either express RFP alone or co-express mouse *Myc* or *Mycn* cDNA inserted downstream of the MSCV-LTR. Infection efficiency was analyzed using FACS for RFP and GFP expression. In some experiments, 2 days after plating, infected GNPs were harvested and transplanted into the cerebella or cortices of CD-1 *nu/nu* mice (Charles River Laboratories, Wilmington, MA, USA). In other experiments, GNP-enriched cerebellar cells

or the presence of cyclopamine (light gray square) or BMP4 (dark gray square). Proliferation was assessed by FACS by calculating the percent of BrdU positive cells. Proliferation index was defined as the ratio of the percentage of BrdU-incorporated cells with SHH signaling antagonists to that of control.

(B) GNPs and tumor cells were analyzed by qRT-PCR for specific gene expression to validate the expression of genes in the SHH signaling pathway. (C) Treatment of MYC-tumor sphere cells with or without SHH signaling antagonists under neurosphere culture conditions. Proliferation index represents the ratio of cell number of cultured neurosphere cells with SHH signaling antagonists to that of control, 6 and 12 days after plating. Data in graphs A and C represent the mean  $\pm$  SD.

were sorted by FACS based on GFP expression immediately after purification. GFP<sup>+</sup> and GFP<sup>-</sup> populations were independently infected with *Myc*-carrying retroviruses, and  $5 \times 10^4$  infected cells from each population were transplanted into the cortices of mice 2 days after infection.

#### Orthotopic Transplants

Transplantation of infected GNP-enriched cerebellar cells into the cortices or cerebellum of nude recipient mice was performed essentially as described previously (Ayrault et al., 2010). After transplant of virus-infected progenitor cells, mice were examined daily for symptoms of sickness (doming of the head or ataxia or reduced activity). In some instances, purified MB cells or cultured tumor sphere cells from MYC-tumors were injected back into the cortices of naïve *nu/nu* recipient animals.

#### Tumor Cell Culture and BrdU Analysis

We analyzed progenitors purified from P7 wild-type mice and tumor cells from three independently derived *Myc*-engineered MBs and MBs arising spontaneously in *Cdkn2c*<sup>-/-</sup>; *Trp53*<sup>Fl/Fl</sup>; *Nestin-Cre* mice. Purified GNPs and tumor cells were plated at  $8 \times 10^5$  cells/well on a Matrigel-coated 24-well plate and grown as previously described (Zhao et al., 2008). GNPs were treated with SHH, whereas tumor cells were not. Both cell populations were cultured in the presence or absence of SHH signaling inhibitors, 2.5  $\mu$ M cyclopamine (LC Laboratories, Woburn, MA, USA), or 100 ng/ml BMP4 (R&D Systems). The medium was changed every 24 hr. Three days after initiation of culture, BrdU was added to the culture medium at a final concentration of 10  $\mu$ M, and cells were harvested 2.5 hr later. Cells that incorporated BrdU were stained with an anti-BrdU antibody using a BrdU-APC flow kit (BD Bioscience, San Jose, CA, USA) and analyzed by FACS.

#### Histopathology, Immunohistochemistry, and Immunoblotting

For histopathology, samples of murine MBs (three separate tumors for each genotype) were formalin-fixed, paraffin-embedded, and sectioned at 5  $\mu$ m thickness. For each sample, a section was stained using a standard hematoxylin and eosin (H&E) protocol; a second section was stained for apoptotic cells, using the ApopTag kit (Millipore, Billerica, MA, USA) with peroxidase detection of TUNEL labeling. Representative images of each sample/stain combination were captured (under oil immersion at 40 $\times$  original magnification) and analyzed using Axiovision software (Carl Zeiss Microscopy, Thornwood, NY, USA). A single observer scored each tumor for apoptotic index (percentage of positive cells following ApopTag labeling) and nuclear area as previously described (McManamy et al., 2003).

For immunoblotting, purified GNPs from the cerebellum of P7 wild-type mice or *Myc*- and *Mycn*-engineered MB cells were lysed and proteins subjected to immunoblotting as described previously (Zindy et al., 2007).

Procedures and antibodies used for immunohistochemistry and antibodies for immunoblotting are provided in the [Supplemental Experimental Procedures](#).

#### Affymetrix Microarray Analysis

RNA from GNPs or tumor cells were subjected to hybridization using Affymetrix Mouse Genechips 430 (version 2; e.g., [Figures 2 and 3](#)). For comparative gene expression analysis between primary and secondary *Myc*-engineered tumors, we used Affymetrix Mouse Genechips HT430PM (e.g., [Figure 7C](#)). Microarray results were validated by qRT-PCR using PCR primers shown in the [Supplemental Experimental Procedures](#).

#### Neurosphere Assays

Tumor cells were cultured under conditions described previously (Taylor et al., 2005). Briefly, cells from *Myc*-engineered tumors were purified and plated on an ultra-low attachment dish at  $5 \times 10^4$  cells/ml or  $1 \times 10^5$  cells/well per 6-well plate. Human recombinant basic FGF and EGF (Peprotech, Rocky Hill, NJ, USA) were added into the culture medium every 3 days. One week later, tumor spheres were harvested, pooled, and dissociated with trypsin (Invitrogen, Grand Island, NY, USA), and total cell numbers were determined. In parallel,  $1 \times 10^5$  of the dissociated cells were plated again and cultured under the same conditions. Total RNA was extracted from the remainder of the cultured cells followed by qRT-PCR analysis of selected RNAs. To test the role of

SHH-antagonists, *Myc*-engineered tumor cells were cultured in the presence of 2.5  $\mu$ M cyclopamine or 100 ng/ml BMP4.

#### ACCESSION NUMBERS

Affymetrix data for mouse MBs using 430V2 and HT430PM chips can be found in the GenBank database numbers GSE33199 and GSE33200, respectively.

#### SUPPLEMENTAL INFORMATION

Supplemental Information includes six figures and Supplemental Experimental Procedures and can be found with this article online at [doi:10.1016/j.ccr.2011.12.023](https://doi.org/10.1016/j.ccr.2011.12.023).

#### ACKNOWLEDGMENTS

We thank Dr. Robert Eisenman for helpful suggestions; Dr. Charles J. Sherr for editing of the manuscript; Dr. Frederique Zindy for mice; Shelly Wilkerson, Sarah Gayso, and Jennifer Craig for excellent technical assistance; John Morris for Affymetrix microarrays; Drs. Richard Ashmun and Ann-Marie Hamilton-Easton for FACS analysis; Dr. Chris Calabrese, John Killmar, and Melissa Johnson for orthotopic transplants; and Pamela Johnson and Dorothy Bush for immunohistochemistry of tumor tissues. This work was funded in part by the National Institutes of Health (grant CA-096832 to M.F.R. and CA-21765 to R.J.G. and M.F.R.), the American Brain Tumor Association (T.U.), the Mochida Foundation (D.K.), the Anderson fellowship (D.K.), and the American Lebanese Syrian Associated Charities of St. Jude Children's Research Hospital.

Received: July 8, 2011

Revised: November 2, 2011

Accepted: December 20, 2011

Published: February 13, 2012

#### REFERENCES

- Aldosari, N., Bigner, S.H., Burger, P.C., Becker, L., Kepner, J.L., Friedman, H.S., and McLendon, R.E. (2002). MYC and MYCN oncogene amplification in medulloblastoma. A fluorescence in situ hybridization study on paraffin sections from the Children's Oncology Group. *Arch. Pathol. Lab. Med.* 126, 540–544.
- Ayralt, O., Zhao, H., Zindy, F., Qu, C., Sherr, C.J., and Roussel, M.F. (2010). Atoh1 inhibits neuronal differentiation and collaborates with Gli1 to generate medulloblastoma-initiating cells. *Cancer Res.* 70, 5618–5627.
- Barker, N., van Es, J.H., Kuipers, J., Kujala, P., van den Born, M., Cozijnsen, M., Haegebarth, A., Korving, J., Begthel, H., Peters, P.J., and Clevers, H. (2007). Identification of stem cells in small intestine and colon by marker gene Lgr5. *Nature* 449, 1003–1007.
- Ben-Porath, I., Thomson, M.W., Carey, V.J., Ge, R., Bell, G.W., Regev, A., and Weinberg, R.A. (2008). An embryonic stem cell-like gene expression signature in poorly differentiated aggressive human tumors. *Nat. Genet.* 40, 499–507.
- Berman, D.M., Karhadkar, S.S., Hallahan, A.R., Pritchard, J.I., Eberhart, C.G., Watkins, D.N., Chen, J.K., Cooper, M.K., Taipale, J., Olson, J.M., and Beachy, P.A. (2002). Medulloblastoma growth inhibition by hedgehog pathway blockade. *Science* 297, 1559–1561.
- Blackwood, E.M., and Eisenman, R.N. (1991). Max: a helix-loop-helix zipper protein that forms a sequence-specific DNA-binding complex with Myc. *Science* 251, 1211–1217.
- Bruggeman, S.W., Valk-Lingbeek, M.E., van der Stoep, P.P., Jacobs, J.J., Kieboom, K., Tanger, E., Hulsman, D., Leung, C., Arsenijevic, Y., Marino, S., and van Lohuizen, M. (2005). Ink4a and Arf differentially affect cell proliferation and neural stem cell self-renewal in Bmi1-deficient mice. *Genes Dev.* 19, 1438–1443.
- Cho, Y.J., Tsherniak, A., Tamayo, P., Santagata, S., Ligon, A., Greulich, H., Berhoukim, R., Amani, V., Goumnerova, L., Eberhart, C.G., et al. (2011).

- Integrative genomic analysis of medulloblastoma identifies a molecular subgroup that drives poor clinical outcome. *J. Clin. Oncol.* 29, 1424–1430.
- Curley, M.D., Therrien, V.A., Cummings, C.L., Sergent, P.A., Koulouris, C.R., Friel, A.M., Roberts, D.J., Seiden, M.V., Scadden, D.T., Rueda, B.R., and Foster, R. (2009). CD133 expression defines a tumor initiating cell population in primary human ovarian cancer. *Stem Cells* 27, 2875–2883.
- Eischen, C.M., Weber, J.D., Roussel, M.F., Sherr, C.J., and Cleveland, J.L. (1999). Disruption of the ARF-Mdm2-p53 tumor suppressor pathway in Myc-induced lymphomagenesis. *Genes Dev.* 13, 2658–2669.
- Ellison, D.W., Onilude, O.E., Lindsey, J.C., Lusher, M.E., Weston, C.L., Taylor, R.E., Pearson, A.D., and Clifford, S.C.; United Kingdom Children's Cancer Study Group Brain Tumour Committee. (2005). beta-Catenin status predicts a favorable outcome in childhood medulloblastoma: the United Kingdom Children's Cancer Study Group Brain Tumour Committee. *J. Clin. Oncol.* 23, 7951–7957.
- Ellison, D.W., Dalton, J., Kocak, M., Nicholson, S.L., Fraga, C., Neale, G., Kenney, A.M., Brat, D.J., Perry, A., Yong, W.H., et al. (2011a). Medulloblastoma: clinicopathological correlates of SHH, WNT, and non-SHH/WNT molecular subgroups. *Acta Neuropathol.* 121, 381–396.
- Ellison, D.W., Kocak, M., Dalton, J., Megahed, H., Lusher, M.E., Ryan, S.L., Zhao, W., Nicholson, S.L., Taylor, R.E., Bailey, S., and Clifford, S.C. (2011b). Definition of disease-risk stratification groups in childhood medulloblastoma using combined clinical, pathologic, and molecular variables. *J. Clin. Oncol.* 29, 1400–1407.
- Frank, A.J., Hernan, R., Hollander, A., Lindsey, J.C., Lusher, M.E., Fuller, C.E., Clifford, S.C., and Gilbertson, R.J. (2004). The TP53-ARF tumor suppressor pathway is frequently disrupted in large/cell anaplastic medulloblastoma. *Brain Res. Mol. Brain Res.* 121, 137–140.
- Gajjar, A., Chintagumpala, M., Ashley, D., Kellie, S., Kun, L.E., Merchant, T.E., Woo, S., Wheeler, G., Ahern, V., Krasin, M.J., et al. (2006). Risk-adapted craniospinal radiotherapy followed by high-dose chemotherapy and stem-cell rescue in children with newly diagnosed medulloblastoma (St Jude Medulloblastoma-96): long-term results from a prospective, multicentre trial. *Lancet Oncol.* 7, 813–820.
- Gibson, P., Tong, Y., Robinson, G., Thompson, M.C., Currie, D.S., Eden, C., Kranenburg, T.A., Hogg, T., Poppleton, H., Martin, J., et al. (2010). Subtypes of medulloblastoma have distinct developmental origins. *Nature* 468, 1095–1099.
- Grandori, C., and Eisenman, R.N. (1997). Myc target genes. *Trends Biochem. Sci.* 22, 177–181.
- Grandori, C., Cowley, S.M., James, L.P., and Eisenman, R.N. (2000). The Myc/Max/Mad network and the transcriptional control of cell behavior. *Annu. Rev. Cell Dev. Biol.* 16, 653–699.
- Hemann, M.T., Bric, A., Teruya-Feldstein, J., Herbst, A., Nilsson, J.A., Cordon-Cardo, C., Cleveland, J.L., Tansey, W.P., and Lowe, S.W. (2005). Evasion of the p53 tumour surveillance network by tumour-derived MYC mutants. *Nature* 436, 807–811.
- Hermeking, H., and Eick, D. (1994). Mediation of c-Myc-induced apoptosis by p53. *Science* 265, 2091–2093.
- Hoffman, B., and Liebermann, D.A. (2008). Apoptotic signaling by c-MYC. *Oncogene* 27, 6462–6472.
- Johnson, R.A., Wright, K.D., Poppleton, H., Mohankumar, K.M., Finkelstein, D., Pounds, S.B., Rand, V., Leary, S.E., White, E., Eden, C., et al. (2010). Cross-species genomics matches driver mutations and cell compartments to model ependymoma. *Nature* 466, 632–636.
- Kamijo, T., Zindy, F., Roussel, M.F., Quelle, D.E., Downing, J.R., Ashmun, R.A., Grosveld, G., and Sherr, C.J. (1997). Tumor suppression at the mouse INK4a locus mediated by the alternative reading frame product p19ARF. *Cell* 91, 649–659.
- Kenney, A.M., Cole, M.D., and Rowitch, D.H. (2003). Nmyc upregulation by sonic hedgehog signaling promotes proliferation in developing cerebellar granule neuron precursors. *Development* 130, 15–28.
- Kim, J., Woo, A.J., Chu, J., Snow, J.W., Fujiwara, Y., Kim, C.G., Cantor, A.B., and Orkin, S.H. (2010). A Myc network accounts for similarities between embryonic stem and cancer cell transcription programs. *Cell* 143, 313–324.
- Knoepfler, P.S., Cheng, P.F., and Eisenman, R.N. (2002). N-myc is essential during neurogenesis for the rapid expansion of progenitor cell populations and the inhibition of neuronal differentiation. *Genes Dev.* 16, 2699–2712.
- Kool, M., Koster, J., Bunt, J., Hasselt, N.E., Lakeman, A., van Sluis, P., Troost, D., Meeteren, N.S., Caron, H.N., Cloos, J., et al. (2008). Integrated genomics identifies five medulloblastoma subtypes with distinct genetic profiles, pathway signatures and clinicopathological features. *PLoS ONE* 3, e3088.
- Lam, C.W., Xie, J., To, K.F., Ng, H.K., Lee, K.C., Yuen, N.W., Lim, P.L., Chan, L.Y., Tong, S.F., and McCormick, F. (1999). A frequent activated smoothed mutation in sporadic basal cell carcinomas. *Oncogene* 18, 833–836.
- Lee, A., Kessler, J.D., Read, T.A., Kaiser, C., Corbett, D., Huttner, W.B., Johnson, J.E., and Wechsler-Reya, R.J. (2005). Isolation of neural stem cells from the postnatal cerebellum. *Nat. Neurosci.* 8, 723–729.
- Lee, Y., Miller, H.L., Jensen, P., Hernan, R., Connelly, M., Wetmore, C., Zindy, F., Roussel, M.F., Curran, T., Gilbertson, R.J., and McKinnon, P.J. (2003). A molecular fingerprint for medulloblastoma. *Cancer Res.* 63, 5428–5437.
- Lumpkin, E.A., Collisson, T., Parab, P., Omer-Abdalla, A., Haeberle, H., Chen, P., Doetzelhofer, A., White, P., Groves, A., Segil, N., and Johnson, J.E. (2003). Math1-driven GFP expression in the developing nervous system of transgenic mice. *Gene Expr. Patterns* 3, 389–395.
- Malynn, B.A., de Alboran, I.M., O'Hagan, R.C., Bronson, R., Davidson, L., DePinho, R.A., and Alt, F.W. (2000). N-myc can functionally replace c-myc in murine development, cellular growth, and differentiation. *Genes Dev.* 14, 1390–1399.
- McManamy, C.S., Lamont, J.M., Taylor, R.E., Cole, M., Pearson, A.D., Clifford, S.C., and Ellison, D.W.; United Kingdom Children's Cancer Study Group. (2003). Morphophenotypic variation predicts clinical behavior in childhood non-desmoplastic medulloblastomas. *J. Neuropathol. Exp. Neurol.* 62, 627–632.
- Northcott, P.A., Korshunov, A., Witt, H., Hielscher, T., Eberhart, C.G., Mack, S., Bouffet, E., Clifford, S.C., Hawkins, C.E., French, P., et al. (2011). Medulloblastoma comprises four distinct molecular variants. *J. Clin. Oncol.* 29, 1408–1414.
- Pfaff, E., Remke, M., Sturm, D., Benner, A., Witt, H., Milde, T., von Bueren, A.O., Wittmann, A., Schöttler, A., Jorch, N., et al. (2010). TP53 mutation is frequently associated with CTNNB1 mutation or MYCN amplification and is compatible with long-term survival in medulloblastoma. *J. Clin. Oncol.* 28, 5188–5196.
- Pfister, S., Remke, M., Benner, A., Mendrzyk, F., Toedt, G., Felsberg, J., Wittmann, A., Devens, F., Gerber, N.U., Joos, S., et al. (2009). Outcome prediction in pediatric medulloblastoma based on DNA copy-number aberrations of chromosomes 6q and 17q and the MYC and MYCN loci. *J. Clin. Oncol.* 27, 1627–1636.
- Raffel, C., Jenkins, R.B., Frederick, L., Hebrink, D., Alderete, B., Fuets, D.W., and James, C.D. (1997). Sporadic medulloblastomas contain PTCH mutations. *Cancer Res.* 57, 842–845.
- Read, T.A., Fogarty, M.P., Markant, S.L., McLendon, R.E., Wei, Z., Ellison, D.W., Febbo, P.G., and Wechsler-Reya, R.J. (2009). Identification of CD15 as a marker for tumor-propagating cells in a mouse model of medulloblastoma. *Cancer Cell* 15, 135–147.
- Reya, T., Morrison, S.J., Clarke, M.F., and Weissman, I.L. (2001). Stem cells, cancer, and cancer stem cells. *Nature* 414, 105–111.
- Rich, J.N. (2009). *Brain Tumor Stem Cell Markers* (New York: Humana Press).
- Rios, I., Alvarez-Rodriguez, R., Martí, E., and Pons, S. (2004). Bmp2 antagonizes sonic hedgehog-mediated proliferation of cerebellar granule neurons through Smad5 signalling. *Development* 131, 3159–3168.
- Romer, J.T., Kimura, H., Magdaleno, S., Sasai, K., Fuller, C., Baines, H., Connelly, M., Stewart, C.F., Gould, S., Rubin, L.L., and Curran, T. (2004). Suppression of the Shh pathway using a small molecule inhibitor eliminates medulloblastoma in Ptc1(+/-)p53(-/-) mice. *Cancer Cell* 6, 229–240.

- Roussel, M.F., and Hatten, M.E. (2011). Cerebellum development and medulloblastoma. *Curr. Top. Dev. Biol.* 94, 235–282.
- Schüller, U., Heine, V.M., Mao, J., Kho, A.T., Dillon, A.K., Han, Y.G., Huillard, E., Sun, T., Ligon, A.H., Qian, Y., et al. (2008). Acquisition of granule neuron precursor identity is a critical determinant of progenitor cell competence to form Shh-induced medulloblastoma. *Cancer Cell* 14, 123–134.
- Silva, J., and Smith, A. (2008). Capturing pluripotency. *Cell* 132, 532–536.
- Singh, S.K., Hawkins, C., Clarke, I.D., Squire, J.A., Bayani, J., Hide, T., Henkelman, R.M., Cusimano, M.D., and Dirks, P.B. (2004). Identification of human brain tumour initiating cells. *Nature* 429, 396–401.
- Swartling, F.J., Grimmer, M.R., Hackett, C.S., Northcott, P.A., Fan, Q.W., Goldenberg, D.D., Lau, J., Masic, S., Nguyen, K., Yakovenko, S., et al. (2010). Pleiotropic role for MYCN in medulloblastoma. *Genes Dev.* 24, 1059–1072.
- Takahashi, K., and Yamanaka, S. (2006). Induction of pluripotent stem cells from mouse embryonic and adult fibroblast cultures by defined factors. *Cell* 126, 663–676.
- Taylor, M.D., Poppleton, H., Fuller, C., Su, X., Liu, Y., Jensen, P., Magdaleno, S., Dalton, J., Calabrese, C., Board, J., et al. (2005). Radial glia cells are candidate stem cells of ependymoma. *Cancer Cell* 8, 323–335.
- Thompson, M.C., Fuller, C., Hogg, T.L., Dalton, J., Finkelstein, D., Lau, C.C., Chintagumpala, M., Adesina, A., Ashley, D.M., Kellie, S.J., et al. (2006). Genomics identifies medulloblastoma subgroups that are enriched for specific genetic alterations. *J. Clin. Oncol.* 24, 1924–1931.
- Todaro, M., Francipane, M.G., Medema, J.P., and Stassi, G. (2010). Colon cancer stem cells: promise of targeted therapy. *Gastroenterology* 138, 2151–2162.
- Uziel, T., Zindy, F., Xie, S., Lee, Y., Forget, A., Magdaleno, S., Reh, J.E., Calabrese, C., Solecki, D., Eberhart, C.G., et al. (2005). The tumor suppressors Ink4c and p53 collaborate independently with Patched to suppress medulloblastoma formation. *Genes Dev.* 19, 2656–2667.
- Wagner, A.J., Kokontis, J.M., and Hay, N. (1994). Myc-mediated apoptosis requires wild-type p53 in a manner independent of cell cycle arrest and the ability of p53 to induce p21waf1/cip1. *Genes Dev.* 8, 2817–2830.
- Wetmore, C., Eberhart, D.E., and Curran, T. (2001). Loss of p53 but not ARF accelerates medulloblastoma in mice heterozygous for patched. *Cancer Res.* 61, 513–516.
- Wu, X., Northcott, P.A., Croul, S., and Taylor, M.D. (2011). Mouse models of medulloblastoma. *Chin J Cancer* 30, 442–449.
- Yang, Z.J., Ellis, T., Markant, S.L., Read, T.A., Kessler, J.D., Bourbonnas, M., Schüller, U., Machold, R., Fishell, G., Rowitch, D.H., et al. (2008). Medulloblastoma can be initiated by deletion of Patched in lineage-restricted progenitors or stem cells. *Cancer Cell* 14, 135–145.
- Zhao, H., Ayrault, O., Zindy, F., Kim, J.H., and Roussel, M.F. (2008). Post-transcriptional down-regulation of Atoh1/Math1 by bone morphogenic proteins suppresses medulloblastoma development. *Genes Dev.* 22, 722–727.
- Zhu, L., Gibson, P., Currie, D.S., Tong, Y., Richardson, R.J., Bayazitov, I.T., Poppleton, H., Zakharenko, S., Ellison, D.W., and Gilbertson, R.J. (2009). Prominin 1 marks intestinal stem cells that are susceptible to neoplastic transformation. *Nature* 457, 603–607.
- Zindy, F., Eischen, C.M., Randle, D.H., Kamijo, T., Cleveland, J.L., Sherr, C.J., and Roussel, M.F. (1998). Myc signaling via the ARF tumor suppressor regulates p53-dependent apoptosis and immortalization. *Genes Dev.* 12, 2424–2433.
- Zindy, F., Knoepfler, P.S., Xie, S., Sherr, C.J., Eisenman, R.N., and Roussel, M.F. (2006). N-Myc and the cyclin-dependent kinase inhibitors p18Ink4c and p27Kip1 coordinately regulate cerebellar development. *Proc. Natl. Acad. Sci. USA* 103, 11579–11583.
- Zindy, F., Uziel, T., Ayrault, O., Calabrese, C., Valentine, M., Reh, J.E., Gilbertson, R.J., Sherr, C.J., and Roussel, M.F. (2007). Genetic alterations in mouse medulloblastomas and generation of tumors de novo from primary cerebellar granule neuron precursors. *Cancer Res.* 67, 2676–2684.

# VEGF-D Promotes Tumor Metastasis by Regulating Prostaglandins Produced by the Collecting Lymphatic Endothelium

Tara Karnezis,<sup>1,2,4,10</sup> Ramin Shayan,<sup>1,2,4,5,6,10</sup> Carol Caesar,<sup>1,2,4</sup> Sally Roufail,<sup>1,2,4</sup> Nicole C. Harris,<sup>1,2,4,5</sup> Kathryn Ardipradja,<sup>1,2,4</sup> You Fang Zhang,<sup>1,2,4</sup> Steven P. Williams,<sup>1,2,4,5</sup> Rae H. Farnsworth,<sup>1,2,4</sup> Ming G. Chai,<sup>7</sup> Thusitha W.T. Rupasinghe,<sup>3</sup> Dedreia L. Tull,<sup>3</sup> Megan E. Baldwin,<sup>8</sup> Erica K. Sloan,<sup>7</sup> Stephen B. Fox,<sup>2,9</sup> Marc G. Achen,<sup>1,2,4</sup> and Steven A. Stacker<sup>1,2,4,\*</sup>

<sup>1</sup>Tumour Angiogenesis Program, Peter MacCallum Cancer Centre, East Melbourne, Victoria 3002, Australia

<sup>2</sup>Sir Peter MacCallum Department of Oncology

<sup>3</sup>Metabolomics Australia, Bio21 Institute for Molecular Science and Biotechnology  
The University of Melbourne, Parkville, Victoria 3010, Australia

<sup>4</sup>Ludwig Institute for Cancer Research, Royal Melbourne Hospital, Parkville, Victoria 3050, Australia

<sup>5</sup>Department of Surgery, Royal Melbourne Hospital

<sup>6</sup>Jack Brockhoff Reconstructive Plastic Surgery Research Unit, Royal Melbourne Hospital and Department of Anatomy and Cell Biology  
The University of Melbourne, Parkville, Victoria 3050, Australia

<sup>7</sup>Monash Institute of Pharmaceutical Sciences, Monash University, Parkville, Victoria 3052, Australia

<sup>8</sup>Circadian Technologies Limited, Vegenics Pty Ltd., Toorak, Victoria 3142, Australia

<sup>9</sup>Department of Pathology, Peter MacCallum Cancer Centre, East Melbourne, Victoria 3002, Australia

<sup>10</sup>These authors contributed equally to this work

\*Correspondence: [steven.stacker@petermac.org](mailto:steven.stacker@petermac.org)

DOI 10.1016/j.ccr.2011.12.026

## SUMMARY

Lymphatic metastasis is facilitated by lymphangiogenic growth factors VEGF-C and VEGF-D that are secreted by some primary tumors. We identified regulation of PGDH, the key enzyme in prostaglandin catabolism, in endothelial cells of collecting lymphatics, as a key molecular change during VEGF-D-driven tumor spread. The VEGF-D-dependent regulation of the prostaglandin pathway was supported by the finding that collecting lymphatic vessel dilation and subsequent metastasis were affected by nonsteroidal anti-inflammatory drugs (NSAIDs), known inhibitors of prostaglandin synthesis. Our data suggest a control point for cancer metastasis within the collecting lymphatic endothelium, which links VEGF-D/VEGFR-2/VEGFR-3 and the prostaglandin pathways. Collecting lymphatics therefore play an active and important role in metastasis and may provide a therapeutic target to restrict tumor spread.

## INTRODUCTION

The lethality of cancer is primarily associated with metastasis, the spread of cancer cells from a primary site to distant organs (Liotta, 1992). The spread of tumor cells to lymph nodes (LNs) is an important prognostic indicator for disease staging, and thus the lymphatic vasculature is considered a route of meta-

static spread (Achen and Stacker, 2008). However, it is noteworthy that systemic metastasis can occur independently of LN spread highlighting the complex nature of the process of systemic disease (Sleeman et al., 2011).

Some tumors secrete lymphangiogenic growth factors that act on the lymphatic vasculature to facilitate metastasis. These factors can induce lymphangiogenesis, that is, the formation of

## Significance

The lymphangiogenic growth factor VEGF-D promotes cancer spread via the lymphatics, a crucial step in metastasis. Elevated VEGF-D levels in human tumors correlate with lymph node metastasis and poor patient prognosis, yet mechanisms underlying lymphogenous spread to lymph nodes remain elusive. Transcriptional profiling of collecting lymphatics draining primary tumors to sentinel lymph nodes identified a link between VEGF-D-signaling and prostaglandin pathways. VEGF-D modulates prostaglandin levels to regulate collecting lymphatic vessel dilation, an effect blocked by NSAIDs. This key interaction between lymphangiogenic factors and prostaglandins reveals a mechanism for preparing collecting vessels for tumor cell dissemination, and a mechanism by which NSAIDs reduce lymphogenous metastasis. Collecting lymphatic vessels may therefore constitute a therapeutic target for prevention and treatment of metastatic disease.

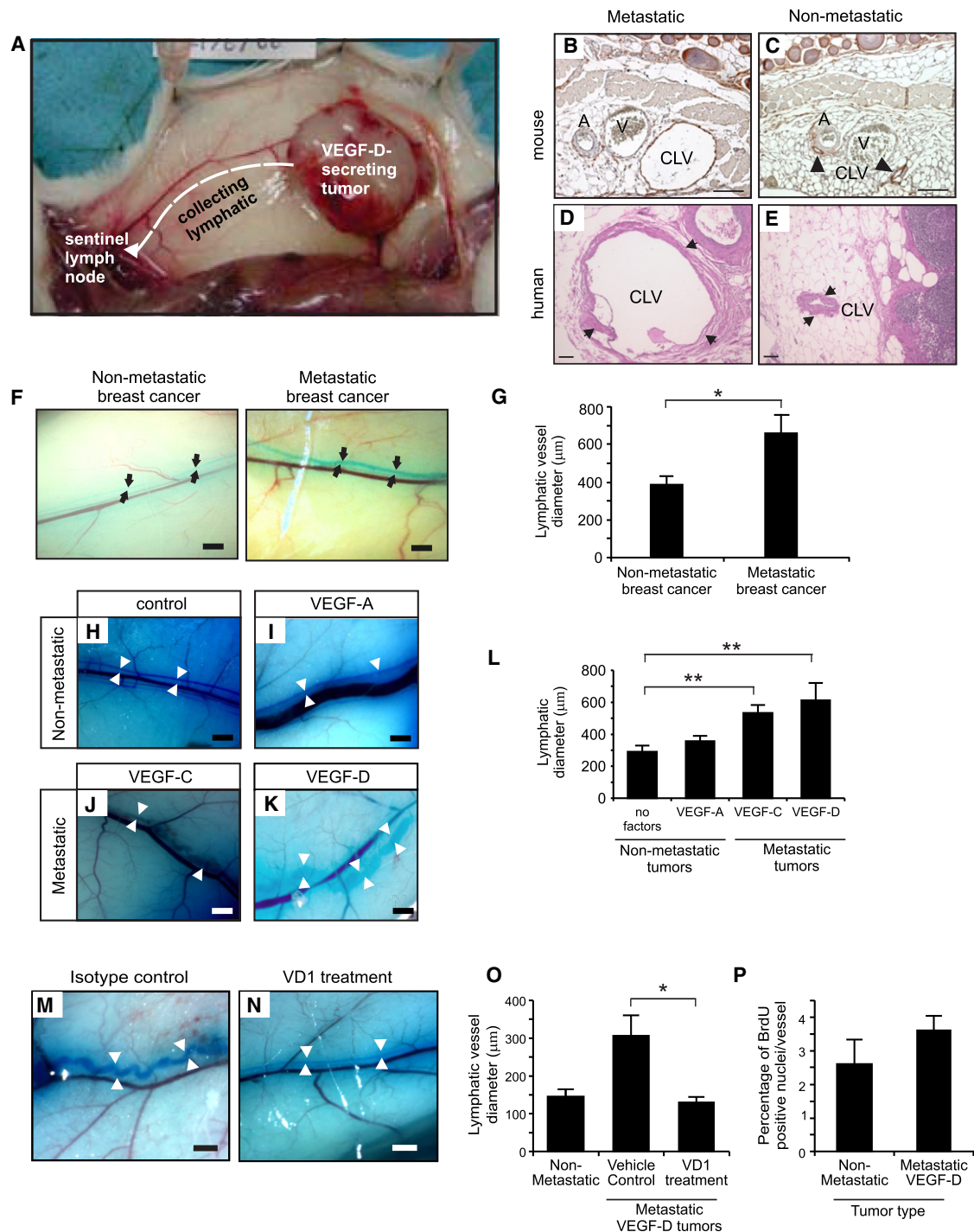


**Figure 1. Lymphangiogenic Growth Factors Induce Collecting Lymphatic Vessel Dilation**

(A) Representative image of the skin-flank 293EBNA tumor model, indicating primary tumor and the CLV (white dashed arrow) draining to the SLN. (B and C) Representative images of flank skin containing the tumor-draining CLV stained for the lymphatic marker podoplanin, from mice bearing metastatic VEGF-D-293EBNA tumors (B) and nonmetastatic 293EBNA tumors (C). A, artery; CLV, collecting lymphatic vessel (arrowheads in C); V, vein. Scale bars: 200  $\mu\text{m}$ . (D and E) Hematoxylin and eosin (H&E) staining of LNs containing afferent CLVs. A dilated afferent CLV (arrowhead) can be seen in a patient with VEGF-D-positive metastatic breast carcinoma, (D) compared to a nonmetastatic control LN, which has a nondilated afferent collecting lymphatic (arrowhead) (E). CLV, collecting lymphatic vessel. Scale bars: 100  $\mu\text{m}$ .

(F) Representative images of flank skin highlighting CLVs (black arrows) from mice bearing nonmetastatic and metastatic 66c4 mammary adenocarcinoma. Scale bars: 1 mm.

(G) Quantitative analysis of CLV diameter in mice bearing nonmetastatic and metastatic 66c4 mammary adenocarcinoma. Data are mean  $\pm$  SEM;  $n \geq 5$ . \* $p < 0.05$  by t test.

new lymphatics from preexisting vessels, in regions within or immediately adjacent to, a primary tumor (Tammela and Alitalo, 2010). They can affect vessels beyond the tumor environment, such as those within the sentinel lymph node (SLN) (Farnsworth et al., 2011) and can modulate immune responses to the tumor (Tammela and Alitalo, 2010). Despite its clinical implications, the mechanisms underpinning metastasis via the lymphatic network are not well understood.

Lymphangiogenic growth factors include two vascular endothelial growth factor (VEGF) family members, VEGF-C and VEGF-D, which act through the cell surface-localized receptor tyrosine kinases VEGFR-2 and VEGFR-3 (Joukov et al., 1996; Achen et al., 1998; Mäkinen et al., 2001). There is a strong association between elevated tumor expression of VEGF-C or VEGF-D, increased tumor lymphatic vessel density and enhanced rates of metastasis to LNs (Achen and Stacker, 2008).

The VEGF-C- or VEGF-D-signaling axes are pivotal in controlling lymphangiogenesis during cancer. Tumor models demonstrate that inhibiting this signaling may block lymphogenous cancer spread by restricting lymphatic vessel formation (Stacker et al., 2001; He et al., 2005; Hoshida et al., 2006). In addition, other VEGF-independent signaling pathways may operate in lymphatic endothelial cells (LECs) or associated cells such as mural cells or pericytes (Cao et al., 2004; Achen and Stacker, 2006).

The lymphatic network is a well-characterized hierarchy of vessels, beginning as initial lymphatics in the superficial dermis that drain into deep dermal precollecting lymphatic vessels, which, in turn, drain into subcutaneous collecting lymphatic vessels (CLVs) (Oliver and Alitalo, 2005). Individual lymphatic vessel subtypes perform distinct, specialized functions; the smaller initial lymphatics perform an absorptive role, whereas precollector vessels guide lymph down to CLVs, a conduit to the draining LN basin (Shayan et al., 2006). These features are reflected in their respective morphologies. Unlike the initial lymphatics, the CLVs have circumferential smooth muscle cells (SMCs) and regular intraluminal valves to help propel a unidirectional flow of fluid (Shayan et al., 2006).

Determining the step(s) in metastatic spread regulated by lymphangiogenic growth factors is critical for developing optimal therapeutic strategies to control metastasis. Recently, the focus of much research has been to understand the mechanisms underlying the effects of tumor-derived VEGF-C or VEGF-D on initial lymphatics within and around the primary tumor (Mandriota et al., 2001; Skobe et al., 2001; Stacker et al., 2001; Björndahl et al., 2005; Hoshida et al., 2006; Roberts et al., 2006; Kopfstein et al., 2007). However, the influence of these factors on lymphatic vessels distal to the primary tumor, for

example, the CLVs draining the primary tumor to the SLN, remains elusive. Historically, CLVs were considered passive conduits that drain defined tissue areas to LNs (Sapp, 1874). However, recent observations in tumor models of VEGF-C-driven lymphogenous spread indicate that CLVs may play an active role in metastasis by increasing lymph flow through vessel dilation (He et al., 2005; Hoshida et al., 2006).

In this study, we investigated how CLVs are altered during VEGF-D-driven metastasis and how the CLVs are prepared to facilitate tumor spread.

## RESULTS

### Lymphangiogenic Growth Factors Induce Dilation of Collecting Lymphatic Vessels

We examined the mechanism(s) by which VEGF-D could regulate CLVs that drain primary metastatic tumors using VEGF-D-expressing tumor models (Figure 1A). Our xenograft model of lymphogenous spread is based on the nonmetastatic 293EBNA cell line, which has negligible baseline expression of VEGF family members (Figures S1A–S1D available online). Lymphogenous spread occurs when lymphangiogenic growth factors are overexpressed (Stacker et al., 2001), allowing us to examine any changes to collecting lymphatic vessels exposed to tumor-secreted VEGF family members. Immunohistochemical staining of skin sections containing the CLVs draining primary VEGF-D-293EBNA metastatic tumors revealed them to be dilated compared to the same vessels from the nonmetastatic control animals (Figures 1B and 1C). The correlation between VEGF-D and dilated collecting lymphatics could also be observed in clinical specimens. The afferent CLVs were dilated in a patient with VEGF-D-positive metastatic breast cancer compared to the matched patient sample with nonmetastatic breast cancer (Figures 1D and 1E; Figures S1E and S1F).

To examine the breadth of these findings, we assessed additional tumor cell lines for endogenous levels of VEGF family members, in particular, VEGF-D. Expression analysis revealed both breast cancer cell lines 66c14 and MDA-MB-435 express endogenous levels of VEGF-D compared to other cell lines such as the prostate tumor cell line PC3 and the poorly metastatic breast cancer cell line MDA-MB-231 (Figures S1G–S1K). Therefore, in addition to our VEGF-D-overexpressing 293EBNA model, the 66c14 and MDA-MB-435 tumor cell lines were employed for subsequent manipulations.

We interrogated CLVs in our orthotopic model of breast cancer involving 66c14 mammary adenocarcinoma cells (Sloan et al., 2010). This model of metastasis is associated with an upregulation of *vegfa* and *vegfd* but not *vegfc* within the

(H–K) Representative images of flank skin containing CLVs draining 293EBNA tumors, highlighting collecting lymphatics (white arrowheads) from mice with nonmetastatic control (H) or VEGF-A-overexpressing tumors (I), or metastatic tumors overexpressing VEGF-C (J) or VEGF-D (K). Scale bars: 1 mm.

(L) Quantitative analysis of CLV diameter in mice bearing 293EBNA nonmetastatic or overexpressing VEGF-A tumors, or metastatic overexpressing VEGF-C or VEGF-D tumors. Data are mean  $\pm$  SEM;  $n \geq 10$ . \*\* $p < 0.01$  by t test.

(M and N) Representative images of flank skin highlighting collecting lymphatics (white arrowheads) from mice bearing metastatic VEGF-D-293EBNA tumors treated with an isotype control antibody (M) or VD1, a neutralizing antibody against VEGF-D (N). Scale bars: 1 mm.

(O) Quantitative analysis of CLV diameter in mice bearing nonmetastatic 293EBNA or metastatic VEGF-D-293EBNA tumors treated with an isotype control and VD1. Data are mean  $\pm$  SEM;  $n \geq 4$ . \* $p < 0.05$  by t test.

(P) Quantification of the relative percentage of BrdU-positive nuclei per CLV in mice bearing nonmetastatic 293EBNA or metastatic VEGF-D-293EBNA tumors. Data are the mean of six sections/mouse  $\pm$  SEM;  $n \geq 3$ .

See also Figure S1.

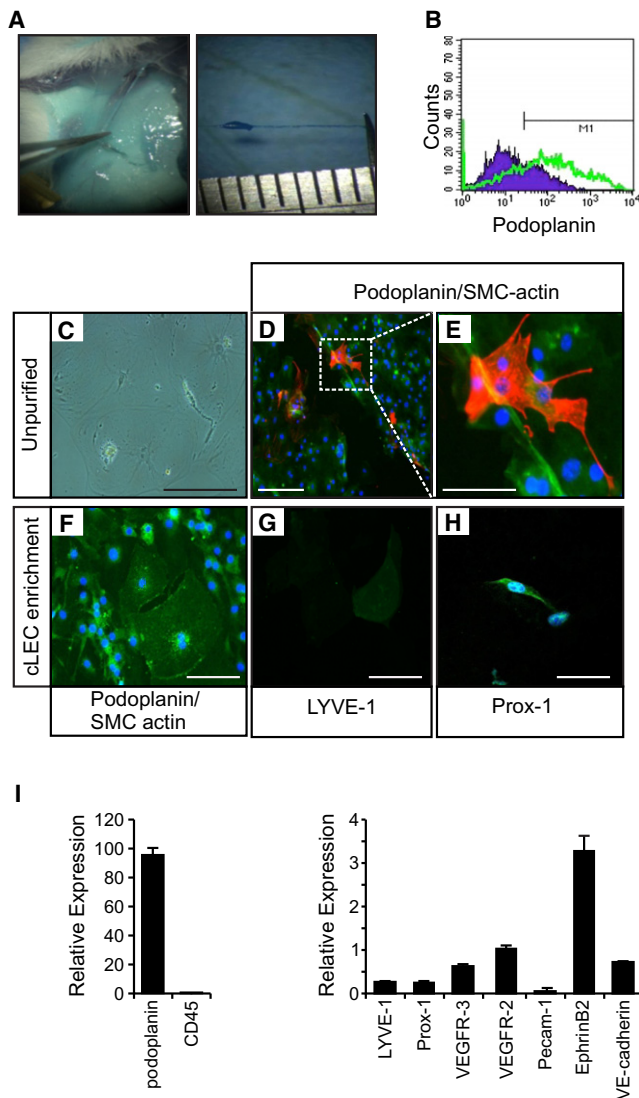


**Figure 2. Purification and Characterization of Collecting Lymphatic Endothelial Cells**

(A) Representative images of the microdissection procedure and a fully dissected CLV following identification with Patent Blue V. The ruler depicted indicates 1 mm graduation marks.

(B) Single-color flow cytometric analysis of unpurified single-cell suspension prepared from CLVs, stained with podoplanin (green) or an isotype-matched control (filled purple).

(C) Representative bright field image of unpurified cells following CLV harvest and culture. Scale bar: 10  $\mu$ m.

(D and E) Immunofluorescence of single-cell suspension culture from CLVs stained for podoplanin (green) and SMC-actin (red). Scale bar: 50  $\mu$ m. The boxed area in (D) is a magnified area from the original image to highlight the SMC-actin positive-staining cells and depicted as (E). Scale bar: 10  $\mu$ m. Nuclei were counterstained with DAPI.

(F–H) Immunofluorescence of the enriched podoplanin-positive cLEC fraction from CLVs. Cells were stained with podoplanin (green) and SMC-actin (red) (F), LYVE-1 (green) (G) and Prox-1 (green) (H). Scale bars: 10  $\mu$ m.

(I) Relative expression of lymphatic-specific genes following purification of cLECs from CLVs analyzed by qRT-PCR. Gene expression was normalized to  $\beta$ -actin. Data are mean  $\pm$  SEM;  $n \geq 5$ .

primary tumor, increased tumor-associated lymphatic vessels, and subsequent LN and distant organ metastasis (Figures S1L–S1N). Tracking of collecting lymphatics in mice bearing 66c14 breast tumors revealed that CLVs were dilated in animals bearing metastatic tumors in which VEGF-D was upregulated, compared to nonmetastatic controls (Figures 1F and 1G).

To ascertain the specific contribution of VEGF-D to collecting lymphatic dilation, we utilized variants of the 293EBNA model that overexpress VEGF-A, VEGF-C, or VEGF-D. When compared to nonmetastatic controls, mice bearing metastatic VEGF-D-expressing tumors had enlarged CLV diameters (Figures 1H, 1K, and 1L) consistent with observations made during VEGF-C-driven tumor spread (Figures 1J and 1L; He et al., 2005). This dilation was reversed when mice bearing VEGF-D tumors were treated with VD1, a neutralizing VEGF-D antibody (Figures 1M–1O). Collecting lymphatic dilation was not observed in mice bearing VEGF-A-expressing tumors (Figures 1I and 1L), suggesting that VEGF-A has little effect on collecting lymphatic dilation. Previous studies showed that lymphatic vessels have the capacity to functionally adapt by dilating in response to VEGF-C, and this was attributed to hyperplasia of the endothelium (Jeltsch et al., 1997; He et al., 2005). In contrast, we found no significant increase in the number of BrdU-positive endothelial cells in dilated collecting lymphatics from mice bearing LN metastasis in VEGF-D-secreting tumors, compared with nonmetastatic controls (Figure 1P;  $p = 0.327$ ). These data suggest that VEGF-D drives morphological changes in CLVs that correlate with metastasis, and are not due to endothelial cell proliferation.

### Isolation and Characterization of Collecting Lymphatic Endothelial Cells during Cancer Spread

To define the molecular mechanisms driving the morphological changes in collecting lymphatics during metastasis, we developed a method to isolate CLVs draining primary tumors. Large subcutaneous CLVs were visualized using Patent Blue V and separated from blood vessels and surrounding skin tissue by microdissection (Figure 2A).

LYVE-1 is strongly expressed on smaller caliber lymphatic vessels, namely, the initial and precollector lymphatics, whereas it is weakly expressed on collecting vessels (Mäkinen et al., 2005). In contrast, podoplanin is expressed strongly on all lymphatic vessel subtypes (Mäkinen et al., 2005), and podoplanin-positive selection was therefore used to isolate collecting lymphatic endothelial cells (cLECs). Flow cytometry of cell suspensions prepared from microdissected CLVs prior to purification showed that approximately 75% of cells were positive for podoplanin (Figures 2B and 2C) and immunofluorescence revealed the presence of podoplanin-positive cells interspersed with smooth muscle actin (SMA)-positive cells, a marker for mural cells (Figures 2D and 2E). The presence of SMA is consistent with in vivo observations of the association of mural cells with CLVs (Mäkinen et al., 2005). To allow molecular characterization of cLECs, podoplanin-positive cells were isolated. Immunofluorescence of the cLEC-enriched fraction revealed cells that stained weakly for the lymphatic markers, LYVE-1 and Prox-1 (Kriehuber et al., 2001), and contaminating SMC were not detected (Figures 2F–2H). The cLEC-enriched fraction was not contaminated by immune cells, as indicated by negligible levels

of the pan-immune marker CD45 (Figure 2I). Quantitative real-time (qRT)-PCR revealed expression of other lymphatic markers, such as VEGFR-3 (Podgrabska et al., 2002). In addition, VEGFR-2, recently shown to be expressed on dermal microvascular LECs (Podgrabska et al., 2002), was expressed by cLECs (Figure 2I). Other endothelial and LEC markers such as Pecam-1, VE-cadherin, and EphrinB2 (Kriehuber et al., 2001; Mäkinen et al., 2005; Baluk et al., 2007) were also detected (Figure 2I). Collectively, these data confirm the endothelial nature of the purified cLEC population that can be used to investigate the molecular pathways in collecting lymphatics necessary for tumor spread.

### Collecting Lymphatic Vessels Alter Their Gene Signature during VEGF-D-Driven Metastasis

To understand the molecular mechanisms underlying morphological changes in CLVs, we compared the molecular signature of cLECs harvested from CLVs from animals with VEGF-D-driven metastasis to that from animals with nonmetastatic disease (Figure 3A). Whole-genome profiling revealed reproducible gene expression patterns observed among replicates, and distinct and unique molecular signatures that differentiated between cLECs from animals with metastatic disease to those with nonmetastatic tumors (Figure 3B).

Several key genes that were differentially expressed between these groups could be arranged according to their cellular roles: cell surface receptors, secreted factors, transcription factors and cytoskeletal or extracellular matrix remodeling genes (Figure 3C). The cell surface genes were those important in adhesion and inflammation; many of the secreted factors were also modulators of inflammatory responses such as IL-11. Interestingly, the majority of the differentially expressed genes fell into the cytoskeletal or extracellular matrix modulatory group, which is consistent with observation of dilated collecting lymphatics. Within this gene group was *pgdh*, encoding 15-hydroxyprostaglandin dehydrogenase (PGDH), an enzyme whose key function is degradation of prostaglandins (PGs), which are small lipid-based molecules that can act as potent vasodilators. PGDH was of interest as it has been identified as a tumor suppressor in colorectal cancers (Myung et al., 2006).

### The Tumor Suppressor, PGDH, Is Downregulated in Collecting Lymphatics during VEGF-D-Driven Metastasis

To validate differential *pgdh* expression levels, qRT-PCR was employed, revealing a 20-fold reduction in the level of *pgdh* gene expression in CLVs from metastatic VEGF-D-293EBNA tumors compared to those draining nonmetastatic tumors (Figure 4A), consistent with the whole-genome profiling. To test for the specificity of VEGF-D regulation of PGDH expression, we evaluated the influence of the related lymphangiogenic factor, VEGF-C, during metastasis. Collecting lymphatics from mice bearing metastatic VEGF-C-293EBNA tumors did not reveal a statistically significant change in *pgdh* expression (Figure 4A). PGDH is a component of the catabolic arm of the PG pathway whereas the COX proteins are key biosynthetic enzymes (Gupta and Dubois, 2001). Studies have shown a correlation between VEGF-C and COX-2 expression in metastatic cancers (Di et al., 2009; Liu et al., 2010). To determine if VEGF-D could also regu-

late the biosynthetic arm of the PG pathway, we assessed VEGF-D regulation of *cox-2* expression (Figure 4A). In contrast to the VEGF-C control, VEGF-D had no effect on *cox-2* levels in collecting lymphatics (Figure 4A). To confirm the specific effect of VEGF-D and to eliminate any possible effects of tumor-secreted VEGF family members or other tumor factors on *pgdh* expression levels, cLECs harvested from nontumor bearing mice were stimulated in vitro with VEGF-A, VEGF-C, or VEGF-D (Figure 4B). qRT-PCR revealed that *pgdh* expression was not altered by VEGF-A, in keeping with the lack of collecting lymphatic dilation observed in our nonmetastatic VEGF-A-over-expressing xenograft tumors (Figure 1L). Likewise, VEGF-C stimulation in vitro had little effect on *pgdh* expression in cLECs. Conversely, *pgdh* was significantly downregulated in cells stimulated with VEGF-D compared with unstimulated control cells (Figure 4B), suggesting that VEGF-D has a specific effect on *pgdh* expression in cLECs.

We previously showed that cLECs express both VEGFR-2 and VEGFR-3 (Figure 2I). To determine which of these receptors mediates the downregulation of *pgdh*, selective blockade of VEGFR-2 or VEGFR-3 was performed. VEGF-D stimulation of cLECs following pretreatment with neutralizing antibodies against VEGFR-2 or VEGFR-3 (Figures S2A and S2B) prevented VEGF-D-induced downregulation of *pgdh* (Figure 4C).

Immunoblot analysis of cellular lysates prepared from CLVs from mice bearing metastatic VEGF-D-293EBNA tumors (Figure 4D) demonstrated that PGDH protein levels were downregulated. To assess the distribution and expression pattern of PGDH with respect to lymphatic vessel subtypes, skin sections containing major longitudinal CLVs from non-tumor-bearing mice were stained with antibodies against PGDH. These showed cytosolic protein expression in nondilated CLVs, the identity of which was confirmed by positive staining with the lymphatic marker, podoplanin (Figures 4E and 4H). In animals with VEGF-D-driven metastatic disease, however, PGDH expression in the dilated CLVs was reduced (Figures 4G and 4J) compared to the CLVs in mice bearing nonmetastatic 293EBNA tumors (Figures 4F and 4I). In combination with the microarray data, these results suggest that VEGF-D mediates the downregulation of *pgdh* expression in dilated CLVs during VEGF-D-driven lymphogenous spread, and that this process requires the actions of both VEGFR-2 and VEGFR-3.

### VEGF-D/VEGFR-2/VEGFR-3-Signaling Axes Modulate Prostaglandins Produced by Collecting Lymphatic Vessels during Metastasis

To maintain homeostasis of PGs in tissues, there is a balance between PG synthesis and degradation. We rationalized that the downregulation of the PG degrading enzyme, PGDH, may alter PG levels secreted by the collecting lymphatics, in particular PGE<sub>2</sub>, which is the main target for PGDH activity (Cha and DuBois, 2007). Since the lymphatic vasculature eventually drains into the circulatory system, we reasoned that local, continual secretion of PGs by endothelial cells may be detected in the plasma (Challis et al., 1976; Albuquerque et al., 2009). We tested the plasma of mice exposed to VEGF-D for the PGs previously shown to have vasodilatory effects (Olsson and Carlson, 1976; Whorton et al., 1978) and found that PG levels, specifically PGE<sub>2</sub>, in mice with VEGF-D-driven metastasis were elevated

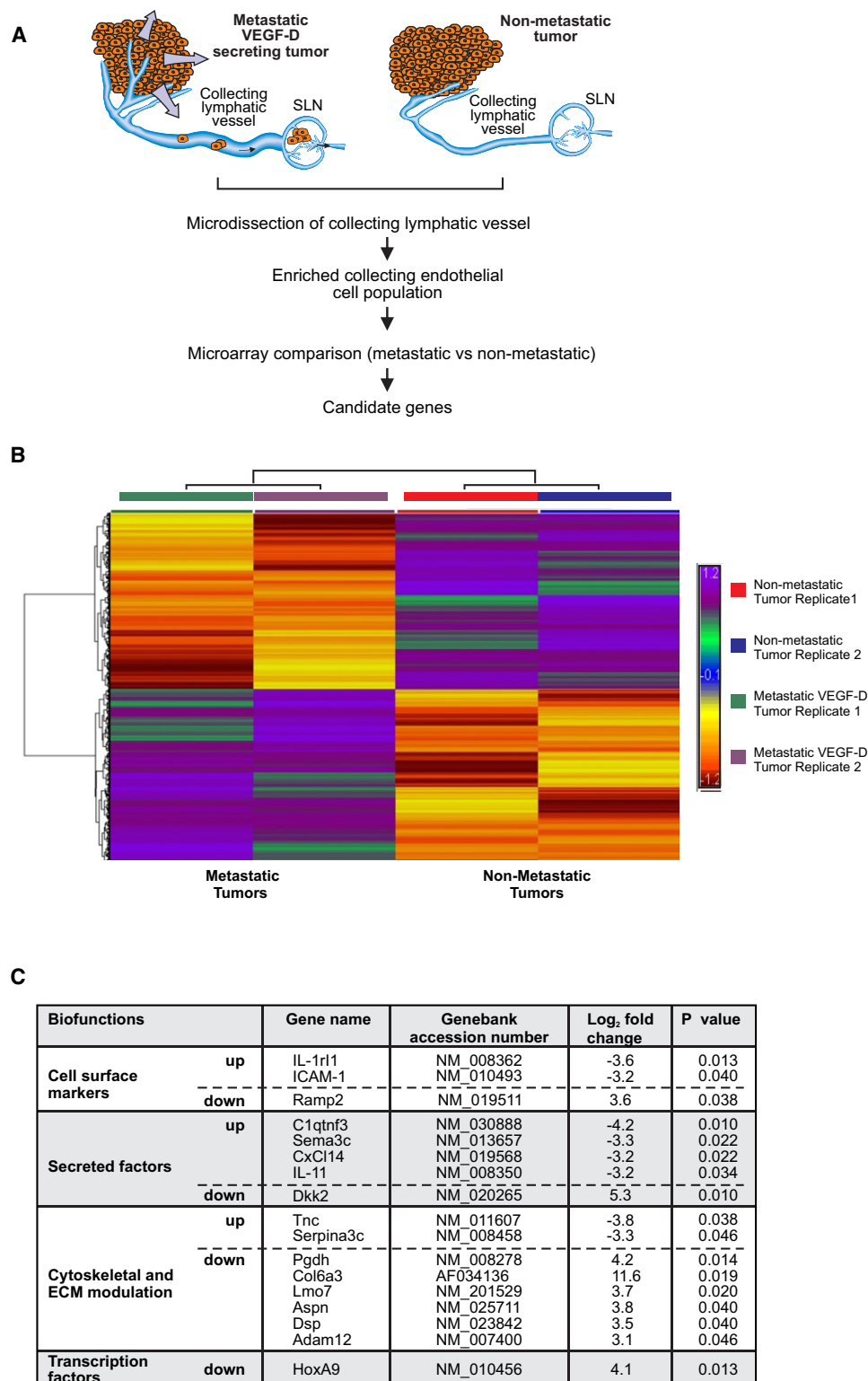


**Figure 3. Collecting Lymphatic Vessels from Metastatic VEGF-D Tumors Have Distinct Gene Signature**

(A) Schematic representation of experimental paradigm used to identify gene expression signatures in CLVs during VEGF-D-driven metastatic disease. This involved microdissection of the CLVs draining primary tumors to the SLN, purification of cLECs and microarray analysis (tumor cells: orange; collecting lymphatic vessels and SLN: blue).

(B) Microarray analysis of cLECs isolated from mice bearing metastatic VEGF-D-293EBNA or nonmetastatic 293EBNA tumors from four independent experiments. Data were visualized using Partek Genomics Suite software, by displaying a hierarchical cluster with average linkage analysis of normalized gene

compared to those with nonmetastatic control or nonmetastatic VEGF-A-secreting tumors (Figures S3A and S3B). A similar trend regarding PGE2 was also observed in collecting lymphatic tissues harvested from the same animals (Figure S3C). Next, we assessed the ability of cLECs as an isolated cell type to produce PGs in vitro and to determine whether there is a causal relationship between VEGF-D signaling and modulation of PG production by cLECs. Upon VEGF-D stimulation of cLECs, there was an increase in PG levels (Figure 5A), further supporting the notion that VEGF-D modulates tissue-specific PG production by downregulating the PG degrading enzyme, *pgdh* (Figures 4A and 4B).

We endeavored to understand the VEGFR-2/VEGFR-3-signaling mechanism necessary for VEGF-D-dependent PG modulation by CLVs. Stimulation with VEGF-D led to phosphorylation of VEGFR-2 in cLECs, which could be blocked by pretreatment with neutralizing antibodies against either VEGFR-2 or VEGFR-3 (Figure 5B). Likewise, phosphorylation of VEGFR-3 was also blocked by both neutralizing antibodies (Figure 5B), which is consistent with our observation that either anti-VEGFR-2 or anti-VEGFR-3 antibody blocked the reduction in PGDH expression induced by VEGF-D (Figure 4C). Next, we assessed whether attenuation of VEGF-D signaling by blocking VEGFR-2/VEGFR-3 activation would affect PG production by cLECs. We found a significant reduction in PGs secreted by cLECs that had been pretreated with either neutralizing anti-VEGFR-2 or anti-VEGFR-3 antibodies (Figure 5C). Finally, we investigated the effects of attenuating VEGF-D signaling in vivo by blocking VEGFR-2 and VEGFR-3 activity, and hence PG production by cLECs, on dilation of CLVs draining tumors. CLVs in animals bearing metastatic VEGF-D-293EBNA tumors treated with either VEGFR-2 or VEGFR-3 neutralizing antibodies were not dilated (Figures 5D, 5E, and 5H) in contrast to dilated collectors found in the isotype-treated and nonmetastatic controls (Figures 5F–5H). Collectively, these data suggest that VEGF-D—via the activities of both VEGFR-2 and VEGFR-3—is able to regulate the levels of vasodilatory PGs produced by collecting lymphatic vessel endothelium.

### Anti-inflammatory Drugs Reduce VEGF-D-Driven Metastasis by Reversing the Morphological Changes in Collecting Lymphatic Vessels

The discovery that the lymphangiogenic molecule VEGF-D modulates the morphology of collecting lymphatics via a tissue-specific regulation of PG activity led us to investigate whether pharmacologically manipulating this pathway would reverse the effect of VEGF-D on metastasis. NSAIDs are a class of commonly used analgesic and anti-inflammatory drugs and are prototypical inhibitors of COX enzymes. To address whether PGs contribute to “preparing” the collecting lymphatics that drain the primary tumor for spread to the SLN, we sought to shut down COX-2 and thereby ablate PG production. We reasoned that a VEGF-D-mediated increase in PG production by cLECs could be reduced concomitantly by inhibiting the

biosynthetic arm of the PG pathway by treatment with a COX-2 inhibitor, Etodolac (Glaser et al., 1995). After testing the efficacy of this drug in vitro (Figure S4A), we monitored its effects on metastasis in the VEGF-D-293EBNA model. It has been shown that NSAID treatment can reduce the levels of VEGFs in some tumor models (Iwata et al., 2007), yet we found no difference in plasma VEGF-D levels during NSAID treatment (Figure S4B).

In addition, we employed the metastatic MDA-MB-435 breast cancer model, which was shown to express endogenous VEGF-D (Figures S1H–S1K). Primary tumor growth was not significantly affected by NSAIDs in either VEGF-D-293EBNA or MDA-MB-435 models (Figure 6A), in contrast to previous studies (Greenhough et al., 2009).

The COX biosynthetic pathway has been shown to promote metastasis by stimulating tumor-associated angiogenesis and lymphangiogenesis (Iwata et al., 2007; Williams et al., 2000; Tsujii et al., 1998). We found no significant difference in the density of tumor-associated lymphatic or blood vessels between the NSAID-treated and vehicle control groups in either VEGF-D-293EBNA or MDA-MB-435 metastatic models (Figures 6B–6G; Figures S4C–S4H). When we assessed dilation of collecting lymphatics that drain the primary tumors in these models, we found a compelling reduction in vessel diameter in NSAID-treated mice in both tumor models (Figures 6I, 6L, and 6M) compared with the nonmetastatic and vehicle control groups (Figures 6H, 6J, 6K, and 6M). Cox-2-derived PGE2 promotes tumor progression and metastasis and is significantly increased in malignant tissue (Jaffe et al., 1971; Rigas et al., 1993). The chemoprotective effects of NSAIDs are mediated by reducing PGE2 levels (Hansen-Petrik et al., 2002). Treatment with Etodolac significantly reduced PGE2 levels in both the VEGF-D-293EBNA and the MDA-MB-435 breast cancer model, suggesting that the dilation observed during metastasis may, in part, be attributed to PGE2 (Figure 6N). PGs exert their biological actions, such as vasodilation, by engaging specific receptors (Amano et al., 2003). Protein expression of PGE receptors on CLVs was found at low levels (Figure S4I), with a differential expression pattern during metastasis and upregulation of EP3, the receptor commonly engaged by PGE2 (Figure S4J).

To ascertain whether NSAID-mediated reversal of CLV dilation affects metastasis, we examined the SLN (Kerjaschki et al., 2011). In both the VEGF-D-EBNA293 and MDA-MB-435 models, we found a reduction of tumor cells in LNs from NSAID-treated animals compared to the vehicle control (Figures 6O–6U). Further, in the MDA-MB-435 model which displays systemic metastasis to the lung, micrometastatic deposits in both the pleural and subpleural area of lung sections could not be detected in NSAID treated animals compared to those readily observed in the vehicle control animals (Figures 6V and 6W; Figure S4K). NSAIDs have been shown to have antiproliferative, proapoptotic, and antiangiogenesis effects (Cha and DuBois, 2007), yet we found no statistically significant differences in the proliferation/apoptosis index or blood vessel density in LNs

expression (>1.5-fold change, adjusted p values < 0.05). These data illustrate differentially upregulated (red/orange) or downregulated genes (purple/blue) in cLECs during metastatic disease compared to those from nonmetastatic tumor bearing mice. The gene expression patterns are consistent among replicates. (C) Selected genes whose expression was up- or downregulated in cLECs during VEGF-D-driven metastatic disease in the 293EBNA model. Statistical significance corresponds to p < 0.05 by HOLMS test.

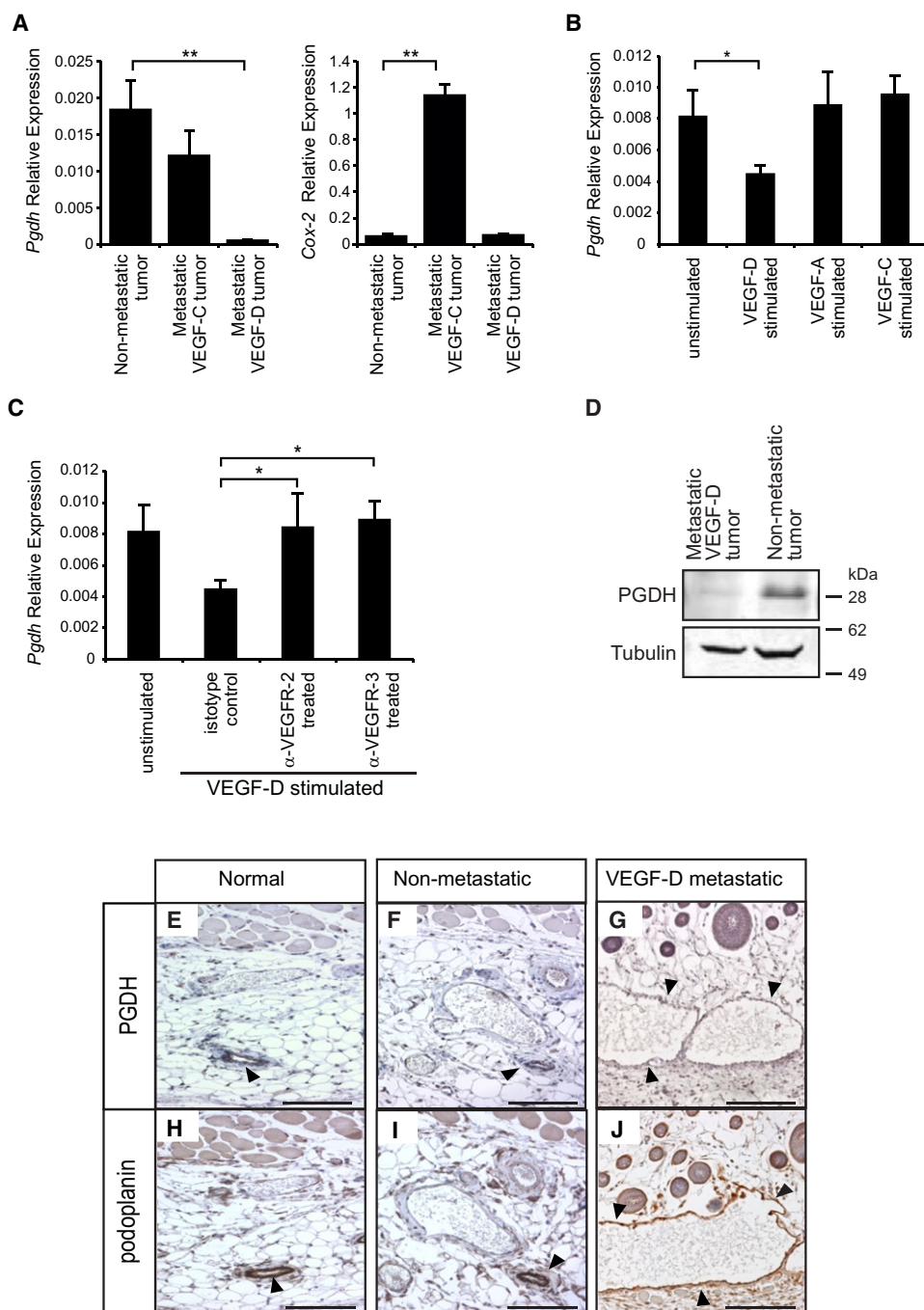


**Figure 4. VEGF-D Downregulates PGDH Expression in Collecting Lymphatic Vessels during Metastasis**

(A) Real-time qPCR analysis of *Pgdh* and *Cox-2* expression in cLECs harvested from mice bearing nonmetastatic 293EBNA or metastatic VEGF-C- or VEGF-D-293EBNA tumors. Gene expression was normalized to  $\beta$ -actin. Data are mean  $\pm$  SEM;  $n \geq 5$ . \*\* $p < 0.01$  by t test.

(B) Real-time qPCR analysis of *Pgdh* expression in cLECs stimulated for 24 hr with VEGF-A (10 ng/ml), VEGF-C (100 ng/ml), and VEGF-D (100 ng/ml). Gene expression was normalized to  $\beta$ -actin. Data are mean  $\pm$  SEM; \* $p < 0.05$  by t test.

(C) Real-time qPCR analysis of *Pgdh* expression in cLECs pretreated with neutralizing VEGFR-2 (DC101) or VEGFR-3 (mF4-31C1) antibodies before stimulation with VEGF-D (100 ng/ml) for 24 hr. Data are mean  $\pm$  SEM; \* $p < 0.05$  by t test.

(D) Immunoblots of CLV lysates harvested from pools of mice bearing VEGF-D metastatic and nonmetastatic 293EBNA tumors, probed for PGDH.  $n \geq 5$ .

(E–J) Immunohistochemical staining of serial sections of flank skin containing collecting lymphatics (arrowheads) from non-tumor-bearing mice (E and H), or mice bearing nonmetastatic 293EBNA (F and I), or metastatic VEGF-D-293EBNA tumors (G and J), stained for the cytosolic protein PGDH, or the lymphatic marker podoplanin. Representative images are shown. Scale bars: 200  $\mu$ m.

See also Figure S2.

from either NSAID or vehicle-treated groups, suggesting that the reduction of tumor cells in LNs of NSAID-treated animals was not due to changes in proliferation, apoptosis, or angiogenesis within the LN (Figures S4L and S4M) or primary tumor (data not shown). Collectively, these data suggest that NSAIDs can affect VEGF-D-regulated PG production by the collecting lymphatic endothelium. This in turn may provide an antimetastatic effect by preventing critical morphological alterations to CLVs that are necessary to facilitate tumor cell spread to the SLN (Figure 7).

## DISCUSSION

Entry of tumor cells into the lymphatic system and subsequent dissemination to LN and distant organ sites is an important event in the metastasis of many solid tumors. In contrast to our knowledge of the influence of lymphangiogenic factors on initial lymphatics within and surrounding the primary tumor (Koukourakis et al., 2000; Pepper, 2001; Stacker et al., 2004; Sleeman and Thiele, 2009), the effect of these factors on lymphatics beyond the tumor environment is only beginning to emerge.

Isolation of endothelial cells from normal and tumor samples has identified genes that are important during tumor-associated angiogenesis and lymphangiogenesis (St Croix et al., 2000; Clasper et al., 2008). We have isolated LECs from vessels beyond the tumor microenvironment and have investigated the molecular regulation that occurs in collecting lymphatics during the metastatic process. Transcriptional profiling of cLECs from CLVs draining metastatic VEGF-D-secreting tumors identified gene signatures that are implicated in tissue remodeling and inflammation. These studies found that VEGF-D regulates the structure of the tumor-draining CLVs through a PG-dependent mechanism, consistent with the elevated levels of inflammatory mediators, such as PGs (Mantovani et al., 2008). In contrast, tumor-associated initial lymphatics differentially expressed genes encoding components of endothelial junctions, subendothelial matrix, and vessel growth/patterning (Clasper et al., 2008). Such variation between gene signatures may reflect the different responses that lymphatic vessel subtypes exhibit to lymphangiogenic growth factors and the roles they perform during the course of lymphogenous spread.

As an initial step toward evaluating mechanisms of metastasis and potential therapeutic targets by which to restrict metastatic disease, we focused on *pgdh*, which catalyzes the rate-limiting step in the catabolism of PGs (Pichaud et al., 1997) and has been identified as a tumor suppressor (Myung et al., 2006). Endothelial-derived PGs are potent regulators of vasodilation, attenuating or amplifying the response of blood vessels to modulate vascular tone during normal and pathological states (Messina et al., 1974; Gupta and Dubois, 2001). We extend this finding to the CLVs, with “tissue-specific” regulation of PGs by these vessels when exposed to VEGF-D. The importance of PGDH during blood vessel dilation was initially demonstrated in PGDH null mice, which have increased tissue PGE2 levels, and as a consequence, a patent blood vessel shunt between the lungs and heart, causing them to die soon after birth (Coggins et al., 2002). It will be interesting to assess the lymphatic vasculature in PGDH heterozygous mice during normal and pathological states.

PGs are produced in tissues by COX enzymes and levels are balanced by the degrading activities of PGDH (Gupta and Dubois, 2001). Clinically, high COX-2 expression in some tumors is associated with poor patient prognosis and survival (Ristimäki et al., 1997). The protumorigenic effects of COX-2 are believed to be largely attributed to its role in synthesizing PGE2 (Pugh and Thomas, 1994). Similarly, reduced PGDH expression and a consequential rise in PGE2 levels enhance tumor growth in colon, gastrointestinal, and breast cancers (Backlund et al., 2005a; Backlund et al., 2005b; Wolf et al., 2006). Our data extend this knowledge by demonstrating that reduced PGDH expression and elevated levels of PGE2 are important in lymphatic endothelial cells beyond the tumor microenvironment, possibly “preparing” the CLVs to promote tumor spread.

It is not apparent at this stage whether lymphatic endothelium-derived PGs act in an autocrine or paracrine manner to modulate the overall tone of the CLVs during metastasis. The actions of prostaglandins such as PGE2 are mediated by engagement with their cognate receptors, EP1-4 (Greenhough et al., 2009), with EP3 signaling shown to contribute to tumor lymphangiogenesis (Kubo et al., 2010). In collecting lymphatics, cLEC-derived PGs may activate SMCs associated with the vessel walls; PG ligation of receptors on SMCs may induce vessel wall relaxation to accommodate expansions in vessel size (Tang and Vanhoutte, 2008). This effect is akin to that of nitric oxide- and PG-dependent modulation of blood vessel tone (Fukumura et al., 2006).

Lymphangiogenic growth factor modulation of PGs in CLVs is mediated by both VEGFR-2 and VEGFR-3 signaling, possibly via heterodimers. Recently published data showed that VEGF-D stimulation of endothelial cells promotes the formation of VEGFR-2/VEGFR-3 heterodimers (Nilsson et al., 2010). Consistent with these findings, anti-VEGFR-2 or anti-VEGFR-3 therapeutic agents were shown to block CLV dilation, which correlated with decreased lymph flow rates and consequently, a reduction in the number of tumor cells reaching the SLN (He et al., 2005; Hoshida et al., 2006). Based on data presented in this study, it is feasible that the mechanism of metastatic suppression by VEGFR-2 and VEGFR-3 blockade is, in part, due to attenuation of PG levels in the collecting endothelium. Since lymphatics are a conduit for immune cells, it cannot be excluded that VEGF-D-induced dilation of collecting lymphatics may contribute to metastasis by altering the traffic and behavior of immune cells in the SLN, consequently modulating metastatic burden.

NSAIDs are commonly used for the treatment of inflammatory disease and can restrict the development of colon cancer (Thun and Heath, 1995; Mantovani et al., 2008; Hirsch et al., 2010) and tumor spread in breast and prostate cancer patients (Holmes et al., 2010; Leitzmann et al., 2002), yet the precise antimetastatic mechanism is unclear. Emerging evidence suggests that COX-2 overexpression and high PGE2 levels are associated with tumor angiogenesis and lymphangiogenesis, processes crucial for metastasis (Iwata et al., 2007; Amano et al., 2003; Tsujii et al., 1998). Recently, the effect of NSAIDs on the lymphatic vasculature has been assessed within tumors, where it was shown that treatment with a COX-2 inhibitor reduced tumoral lymphangiogenesis, in turn, leading to decreased metastasis to the SLN (Iwata et al., 2007). Evidence

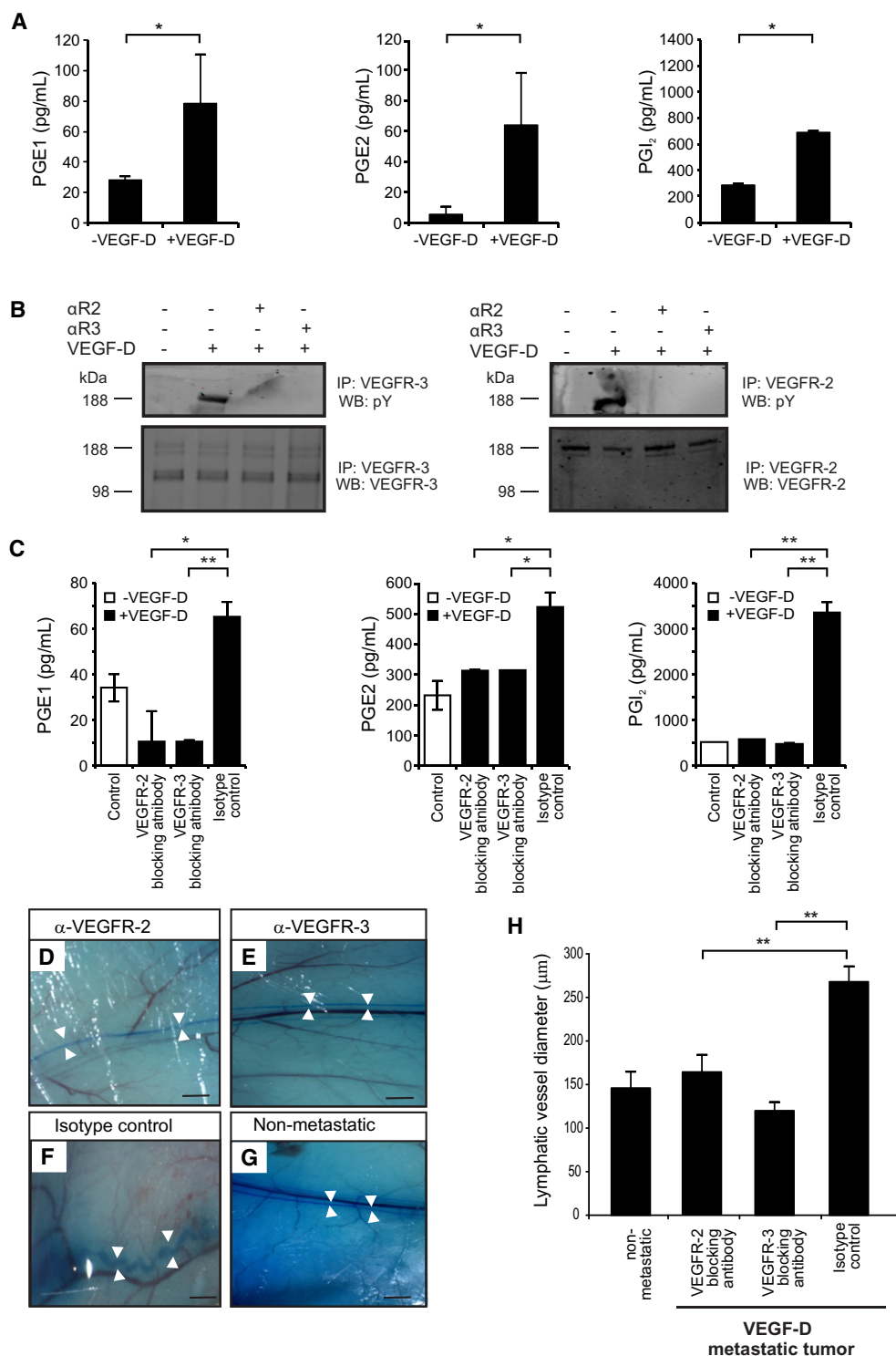


**Figure 5. VEGF-D/VEGFR-2/VEGFR-3 Signaling Regulates Prostaglandins Produced by cLECs during Metastasis**

(A) PG levels in supernatants of cLECs stimulated with VEGF-D (100 ng/ml) for up to 7 days. Assays were performed in triplicate. Data are mean  $\pm$  SEM; \* $p$  < 0.05 by t test.

(B) VEGF-D-mediated activation of VEGFR-2 and VEGFR-3 in cLECs. cLECs were pretreated for 1 hr with neutralizing VEGFR-2 (DC101) or VEGFR-3 (mF4-31C1) antibodies before stimulation with VEGF-D (100 ng/ml) for 10 min. VEGFR-2 and VEGFR-3 were immunoprecipitated from cLEC lysates and immunoblots were probed for phosphorylation of VEGFR-2 and VEGFR-3.

(C) PG levels in supernatants of cLECs were measured by ELISA. cLECs were pretreated for 1 hr with neutralizing VEGFR-2 (DC101) or VEGFR-3 (mF4-31C1) antibodies before stimulation with VEGF-D (100 ng/ml) for up to 7 days. Assays were performed in triplicate. Data are mean  $\pm$  SEM; \* $p$  < 0.05 and \*\* $p$  < 0.01 by t test.

presented in the current study indicates an additional mechanism for the antimetastatic effects of NSAID treatment beyond the tumor environment, one that involves normalizing the diameter of CLVs that facilitate tumor cell trafficking to the SLN (Figure 7B).

An emerging “subtypes-based” model for lymphogenous spread suggests that lymphangiogenic growth factors have two modalities. The first consists of proliferation or alteration of tumor-associated initial lymphatics that enables tumor cells to access to the lymphatic network (Figure 7A); the second involves dilation of the CLVs beyond the tumor, which facilitates trafficking to the SLN (Figure 7B). Understanding the functionally important effects that VEGF-C and VEGF-D have on lymphatic vessel subtypes may provide one of the missing links in the metastatic process, and further refine our knowledge of the complex nature of lymphogenous spread. These insights may assist with the design of additional therapeutic avenues for cancer patients and/or enhance current approaches to antilymphangiogenic therapies, such as blocking or neutralizing antibodies in combination with other treatments such as NSAIDs.

## EXPERIMENTAL PROCEDURES

### Mice

Female SCID/NOD (IMVS, Adelaide, Australia) or Balb/c (ARC, Perth) mice 6–8 weeks of age were used for tumor studies and/or isolation of cLECs. Ethics for approval for research using animals was obtained from the Ludwig Institute for Cancer Research, Peter MacCallum Cancer Centre and Monash University Animal Ethics Committees, in accordance with National Health and Medical Research Council of Australia guidelines.

### Human Tissue Specimens

Tissues were collected following surgical resection at the Peter MacCallum Cancer Center. Ethics approval for research using human tissue was obtained from the Peter MacCallum Cancer Centre (approval number 10/16) and includes a waiver for consent. A tissue microarray from basal-like breast carcinoma was constructed from a series of breast tumors screened for ER, PR, HER2, EGFR, and cytokeratin 5 (ck5). Those tumors that were triple negative (ER, PR, and her2) and ck5-positive and EGFR-positive were considered basal-type. 1 mm cores of tissue were punched from donor blocks. Tissue microarrays were immunostained with anti-human VEGF-D antibody (R&D Systems).

### Metastatic and Nonmetastatic Xenograft Models

Stably transfected 293EBNA-1 cell lines expressing full-length human VEGF-D (VEGF-D-293EBNA), human VEGF-C (VEGF-C-293EBNA) and mouse VEGF-A (VEGF-A-293EBNA), vector alone (293EBNA), or MDA-MB-453-expressing endogenous VEGF-D were established in SCID/NOD mice as described (Stacker et al., 2001).

### Orthotopic Metastasis Model

Six-week-old female Balb/c mice (ARC, Perth) were housed under PC2 barrier conditions. 66cl4 mammary adenocarcinoma cells were transduced with the FUhLucW lentiviral vector containing firefly luciferase under control of the ubiquitin-C promoter and were inoculated as previously described (Sloan et al., 2010). See Supplemental Experimental Procedures for full methods.

### Treatment of Tumors with Neutralizing Antibodies and NSAIDs

Mice bearing VEGF-D-expressing tumors received thrice weekly, beginning 5 days post-tumor inoculation, intraperitoneal injections of 800  $\mu$ g of neutralizing anti-VEGFR-2 antibody (DC101; ImClone) or VD1 (Achen et al., 2000); 1 mg of neutralizing anti-VEGFR-3 antibody (mF4-31C1; ImClone); or isotype matched antibody/PBS as vehicle control. For NSAID treatment, mice were treated daily by oral gavage with 5 mg/kg of Etodolac (Sigma-Aldrich) (Iwata et al., 2007) dissolved in 5% (w/v) carboxymethylcellulose, beginning 5 days post-tumor inoculation and continued daily until tumors reached a size of 1,500–2,000 mm<sup>3</sup> (typically 3–4 weeks).

Collection of tissue and isolation of cLECs used for various analyses including immunohistochemistry, flow cytometry, BrdU analysis, prostaglandin assays, RNA purification, microarray analysis, and qRT-PCR are described in detail in the Supplemental Experimental Procedures.

### Harvest of Collecting Lymphatic Vessels

0.25% (w/v) Patent Blue V dye (Sigma-Aldrich) was injected postmortem into hindlimb footpads of normal SCID/NOD mice, or intratumorally in mice bearing tumors, and massaged to promote uptake by the collecting lymphatics. Collecting lymphatics thus identified were microdissected using a Zeiss OPML MDI dissecting microscope.

### Isolation of Endothelial Cells from Collecting Lymphatic Vessels

Single-cell suspensions of cLECs were prepared by digestion of freshly dissected CLVs with a cocktail of Blendzyme III (Roche) and DNase (Sigma-Aldrich) for 1.5–2 hr at 37°C. Cells were either seeded on fibronectin (5  $\mu$ g/ml; Sigma-Aldrich)-coated dishes for in vitro expansion, or subjected to immunosolation by MACS (Miltenyi Biotec) using rabbit anti-mouse podoplanin antibody (30  $\mu$ g/ml, Sigma-Aldrich). See Supplemental Experimental Procedures for full method.

### Flow Cytometry and Immunofluorescence

See Supplemental Experimental Procedures for full method.

### Immunoprecipitation and Western Blotting

See Supplemental Experimental Procedures for full methods.

### Immunohistochemistry and BrdU Incorporation

Mouse tissues were fixed in 4% paraformaldehyde before paraffin embedding for analysis. See Supplemental Experimental Procedures for full methods.

### RNA Isolation and Microarray Analysis

RNA was isolated using the RNeasy kit as per manufacturer's instructions (QIAGEN). See Supplemental Experimental Procedures for full methods.

### Quantitative PCR

See Supplemental Experimental Procedures for a list of primers.

### Quantification and Statistical Analysis

Images were quantified using Metamorph software. Student's t test (Minitab for Windows, MiniTab Inc) and HOLMS test were used for statistical analyses where indicated.

### ACCESSION NUMBERS

Microarray data were deposited in NCBI's Gene Expression Omnibus; series accession number GSE34135. (<http://www.ncbi.nlm.nih.gov/geo/query/acc.cgi?acc=GSE34135>).

(D–G) Representative images of CLVs filled with Patent Blue V from mice bearing metastatic VEGF-D-293EBNA tumors treated with neutralizing VEGFR-2 (DC101) (D), VEGFR-3 (mF4-31C1) (E), or isotype control antibody (F) and nonmetastatic tumor control (G). Scale bars: 1 mm.

(H) Quantification of CLV diameter in mice bearing nonmetastatic and metastatic VEGF-D-293EBNA tumors treated with neutralizing VEGFR-2 (DC101), VEGFR-3 (mF4-31C1), or isotype control antibodies. Data are mean  $\pm$  SEM;  $n \geq 4$ . \*\* $p < 0.01$  by t test.

See also Figure S3.

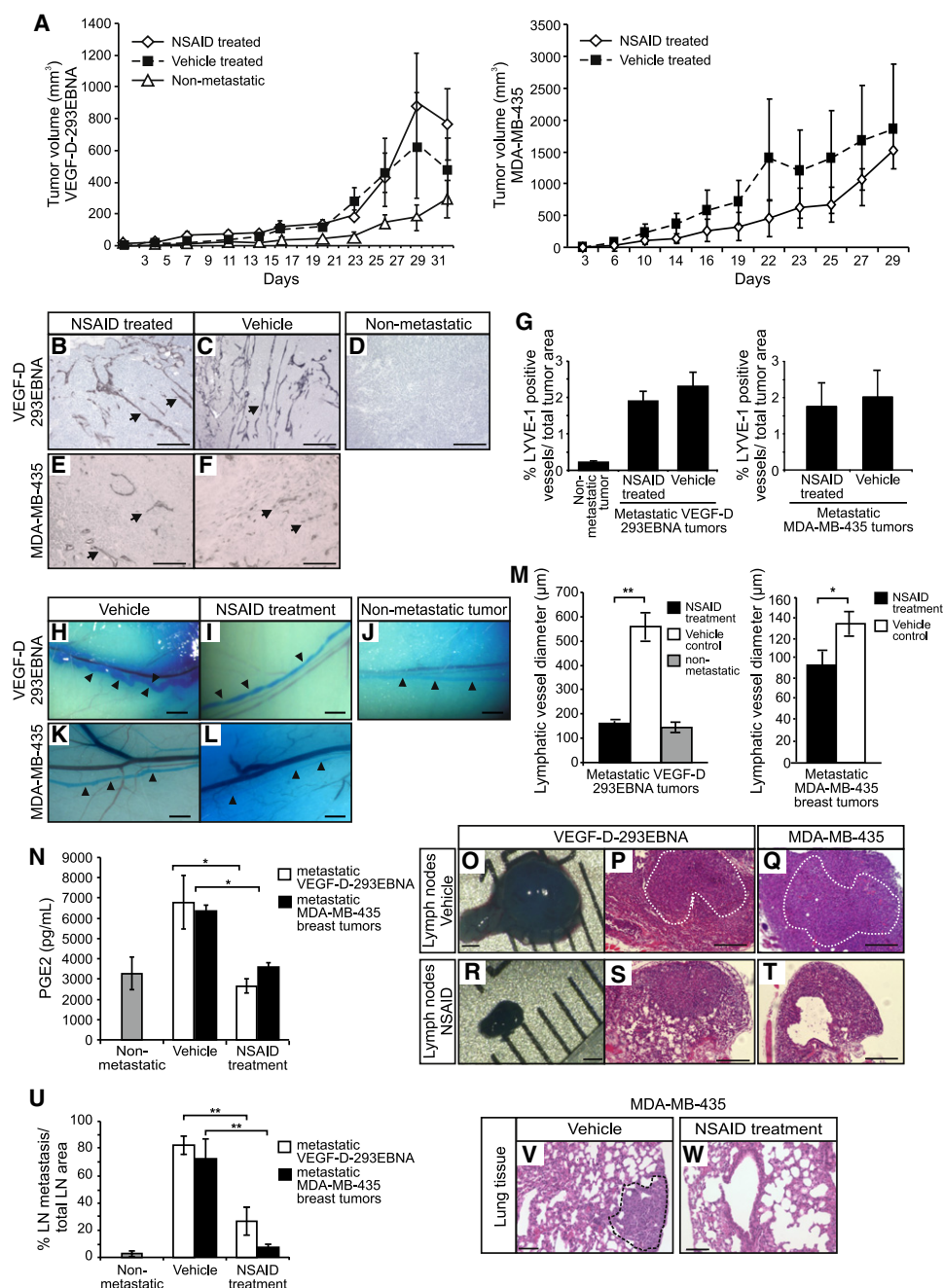


**Figure 6. NSAIDs Reverse Collecting Lymphatic Vessel Dilatation during Metastatic Disease and Suppress Tumor Spread**

(A) Measurement of subcutaneous VEGF-D-293EBNA and MDA-MB-435 tumors in mice undergoing treatment with NSAID, (Etodolac). Data are presented as mean tumor volume (mm<sup>3</sup>) ± SEM. Tumor volumes are shown as a function of time (in days); n ≥ 6.

(B–F) Immunohistochemical staining for the lymphatic marker LYVE-1 from mice bearing metastatic VEGF-D-293EBNA (B and C) and MDA-MB-435 (E and F) tumors treated with NSAID (B and E), vehicle (C and F), or nonmetastatic 293EBNA tumor control (D). Arrows indicate vessels. Representative images are depicted. Scale bars: 200 μm.

(G) Tumoral lymphatic vessel density (LYVE-1) in VEGF-D-293EBNA and MDA-MB-435 breast tumors from mice treated with either NSAID or the vehicle control. Data are the mean of three sections/mouse ± SEM; n ≥ 6.

(H–L) Macroscopic appearance of CLVs filled with Patent Blue V from mice bearing metastatic VEGF-D-293EBNA tumors (H and I) or MDA-MB-435 breast tumors (K and L) treated with either vehicle (H and K) or NSAID (I and L), compared to the nonmetastatic 293EBNA tumor control (J). Scale bars: 1 mm.

(M) Diameter of CLVs in mice bearing metastatic VEGF-D-293EBNA or MDA-MB-435 breast tumors treated with either NSAID or vehicle. Data are mean ± SEM; n ≥ 6. \*p < 0.05 and \*\*p < 0.01 by t test.

(N) PGE<sub>2</sub> levels in plasma from mice bearing metastatic VEGF-D-293EBNA or MDA-MB-435 breast tumors treated with either NSAID or vehicle. Assay was performed in triplicate. Data are mean ± SEM; n ≥ 5. \*p < 0.05 by t test.

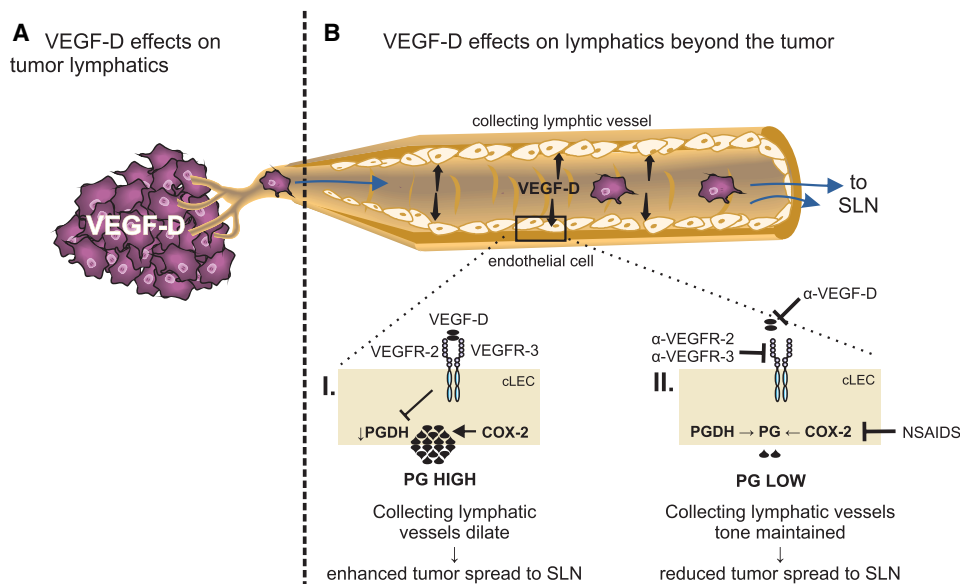


**Figure 7. Schematic Overview of VEGF-D Effects in Tumor Metastasis**

VEGF-D secreted by tumor cells promotes LN metastasis by (A) facilitating entry of tumor cells into initial lymphatics and (B) altering CLV dilation to facilitate transit of tumor cells to the SLN. This is modulated by downregulation of PGDH, resulting in high levels of PGs secreted by cLECs as depicted in (I). Inhibitors targeting the VEGF-D/VEGFR-2/VEGFR-3 or PG pathways in cLECs are likely to reduce PG levels and thereby restore vessel tone, suppressing metastasis as shown in (II).

#### SUPPLEMENTAL INFORMATION

Supplemental Information includes four figures and Supplemental Experimental Procedures and can be found with this article online at [doi:10.1016/j.ccr.2011.12.026](https://doi.org/10.1016/j.ccr.2011.12.026).

#### ACKNOWLEDGMENTS

The authors thank Dr. Maria Macheda for critically reviewing the manuscript, Ms. Janna Taylor for assistance in generating figures, Dr. Bronislaw Pytowski for providing neutralizing VEGFR-2 and VEGFR-3 antibodies, and Dr. Matthias Francois for helpful discussion. This work was funded partly by a Program Grant from the National Health and Medical Research Council of Australia (NHMRC) and by funds from the Operational Infrastructure Support Program provided by the Victorian Government, Australia. S.A.S. and M.G.A. are supported by Senior Research Fellowships from the NHMRC. S.A.S. would like to acknowledge the support of the Pfizer Australia Fellowship. R.S. is supported by the Raelene Boyle Sporting Chance Foundation and Royal Australasian College of Surgeons (RACS) Foundation Scholarship, and the RACS Surgeon Scientist Program. S.P.W. is supported by a National Breast Cancer Foundation Doctoral Research Scholarship. N.C.H. and R.H.F. are supported by a Melbourne Research Scholarship from the University of Melbourne, Australia. E.K.S. is supported by a National Breast Cancer Foundation early career award and an NHMRC grant (1008865).

Received: January 28, 2011

Revised: October 10, 2011

Accepted: December 23, 2011

Published: February 13, 2012

#### REFERENCES

- Achen, M.G., and Stacker, S.A. (2006). Tumor lymphangiogenesis and metastatic spread—new players begin to emerge. *Int. J. Cancer* 119, 1755–1760.
- Achen, M.G., and Stacker, S.A. (2008). Molecular control of lymphatic metastasis. *Ann. N.Y. Acad. Sci.* 1131, 225–234.
- Achen, M.G., Jeltsch, M., Kukk, E., Mäkinen, T., Vitale, A., Wilks, A.F., Alitalo, K., and Stacker, S.A. (1998). Vascular endothelial growth factor D (VEGF-D) is a ligand for the tyrosine kinases VEGF receptor 2 (Flk1) and VEGF receptor 3 (Flt4). *Proc. Natl. Acad. Sci. USA* 95, 548–553.
- Achen, M.G., Roufail, S., Domagala, T., Catimel, B., Nice, E.C., Geleick, D.M., Murphy, R., Scott, A.M., Caesar, C., Makinen, T., et al. (2000). Monoclonal antibodies to vascular endothelial growth factor-D block its interactions with both VEGF receptor-2 and VEGF receptor-3. *Eur. J. Biochem.* 267, 2505–2515.
- Albuquerque, R.J., Hayashi, T., Cho, W.G., Kleinman, M.E., Dridi, S., Takeda, A., Baffi, J.Z., Yamada, K., Kaneko, H., Green, M.G., et al. (2009). Alternatively spliced vascular endothelial growth factor receptor-2 is an essential endogenous inhibitor of lymphatic vessel growth. *Nat. Med.* 15, 1023–1030.

(O–T) Macroscopic appearance of LN from VEGF-D-293EBNA tumor bearing mice treated with vehicle (O) or NSAID (R). Scale bars: 1 mm. H&E staining (P, Q, S, and T) of LN sections from mice bearing VEGF-D-293EBNA (P and S) or MDA-MBA-435 tumors (Q and T), treated with either NSAID (S and T) or vehicle (P and Q). Dotted lines indicate micrometastatic foci within the LN. Scale bars: 200  $\mu$ m.

(U) Quantification of metastatic burden in LNs from mice bearing metastatic VEGF-D-293EBNA or MDA-MBA-435 tumors and treated with the NSAID or vehicle, or the nonmetastatic 293EBNA tumor control. Data are mean  $\pm$  SEM;  $n \geq 6$ . \*\* $p < 0.01$  by t test.

(V and W) H&E staining of lung tissue from mice bearing metastatic MDA-MB-435 breast tumors from animals treated with either vehicle (V) or NSAID (W). Dotted lines indicate micrometastatic foci. Scale bars: 100  $\mu$ m.

See also Figure S4.

- Amano, H., Hayashi, I., Endo, H., Kitasato, H., Yamashina, S., Maruyama, T., Kobayashi, M., Satoh, K., Narita, M., Sugimoto, Y., et al. (2003). Host prostaglandin E(2)-EP3 signaling regulates tumor-associated angiogenesis and tumor growth. *J. Exp. Med.* 197, 221–232.
- Backlund, M.G., Mann, J.R., and Dubois, R.N. (2005a). Mechanisms for the prevention of gastrointestinal cancer: the role of prostaglandin E2. *Oncology* 69 (Suppl 1), 28–32.
- Backlund, M.G., Mann, J.R., Holla, V.R., Buchanan, F.G., Tai, H.H., Musiek, E.S., Milne, G.L., Katkuri, S., and DuBois, R.N. (2005b). 15-Hydroxyprostaglandin dehydrogenase is down-regulated in colorectal cancer. *J. Biol. Chem.* 280, 3217–3223.
- Baluk, P., Fuxe, J., Hashizume, H., Romano, T., Lashnits, E., Butz, S., Vestweber, D., Corada, M., Molendini, C., Dejana, E., and McDonald, D.M. (2007). Functionally specialized junctions between endothelial cells of lymphatic vessels. *J. Exp. Med.* 204, 2349–2362.
- Björndahl, M.A., Cao, R., Burton, J.B., Brakenhielm, E., Religa, P., Galter, D., Wu, L., and Cao, Y. (2005). Vascular endothelial growth factor- $\alpha$  promotes peritumoral lymphangiogenesis and lymphatic metastasis. *Cancer Res.* 65, 9261–9268.
- Cao, R., Björndahl, M.A., Religa, P., Clasper, S., Garvin, S., Galter, D., Meister, B., Ikomi, F., Tritsaris, K., Dissing, S., et al. (2004). PDGF-BB induces intratumoral lymphangiogenesis and promotes lymphatic metastasis. *Cancer Cell* 6, 333–345.
- Cha, Y.I., and DuBois, R.N. (2007). NSAIDs and cancer prevention: targets downstream of COX-2. *Annu. Rev. Med.* 58, 239–252.
- Challis, J.R., Dilley, S.R., Robinson, J.S., and Thorburn, G.D. (1976). Prostaglandins in the circulation of the fetal lamb. *Prostaglandins* 11, 1041–1052.
- Clasper, S., Royston, D., Baban, D., Cao, Y., Ewers, S., Butz, S., Vestweber, D., and Jackson, D.G. (2008). A novel gene expression profile in lymphatics associated with tumor growth and nodal metastasis. *Cancer Res.* 68, 7293–7303.
- Coggins, K.G., Latour, A., Nguyen, M.S., Audoly, L., Coffman, T.M., and Koller, B.H. (2002). Metabolism of PGE<sub>2</sub> by prostaglandin dehydrogenase is essential for remodeling the ductus arteriosus. *Nat. Med.* 8, 91–92.
- Di, J.M., Zhou, J., Zhou, X.L., Gao, X., Shao, C.Q., Pang, J., Sun, Q.P., Zhang, Y., and Ruan, X.X. (2009). Cyclooxygenase-2 expression is associated with vascular endothelial growth factor-C and lymph node metastases in human prostate cancer. *Arch. Med. Res.* 40, 268–275.
- Farnsworth, R.H., Karnezis, T., Shayan, R., Matsumoto, M., Nowell, C.J., Achen, M.G., and Stacker, S.A. (2011). A role for bone morphogenetic protein-4 in lymph node vascular remodeling and primary tumor growth. *Cancer Res.* 71, 6547–6557.
- Fukumura, D., Kashiwagi, S., and Jain, R.K. (2006). The role of nitric oxide in tumour progression. *Nat. Rev. Cancer* 6, 521–534.
- Glaser, K., Sung, M.L., O'Neill, K., Belfast, M., Hartman, D., Carlson, R., Kreft, A., Kubrak, D., Hsiao, C.L., and Weichman, B. (1995). Etodolac selectively inhibits human prostaglandin G/H synthase 2 (PGHS-2) versus human PGHS-1. *Eur. J. Pharmacol.* 281, 107–111.
- Greenhough, A., Smartt, H.J., Moore, A.E., Roberts, H.R., Williams, A.C., Paraskeva, C., and Kaidi, A. (2009). The COX-2/PGE<sub>2</sub> pathway: key roles in the hallmarks of cancer and adaptation to the tumour microenvironment. *Carcinogenesis* 30, 377–386.
- Gupta, R.A., and Dubois, R.N. (2001). Colorectal cancer prevention and treatment by inhibition of cyclooxygenase-2. *Nat. Rev. Cancer* 1, 11–21.
- Hansen-Petrik, M.B., McEntee, M.F., Jull, B., Shi, H., Zemel, M.B., and Whelan, J. (2002). Prostaglandin E(2) protects intestinal tumors from nonsteroidal anti-inflammatory drug-induced regression in Apc(Min/+) mice. *Cancer Res.* 62, 403–408.
- He, Y., Rajantie, I., Pajusola, K., Jeltsch, M., Holopainen, T., Yla-Herttuala, S., Harding, T., Jooss, K., Takahashi, T., and Alitalo, K. (2005). Vascular endothelial cell growth factor receptor 3-mediated activation of lymphatic endothelium is crucial for tumor cell entry and spread via lymphatic vessels. *Cancer Res.* 65, 4739–4746.
- Hirsch, H.A., Iliopoulos, D., Joshi, A., Zhang, Y., Jaeger, S.A., Bulyk, M., Tschlis, P.N., Shirley Liu, X., and Struhl, K. (2010). A transcriptional signature and common gene networks link cancer with lipid metabolism and diverse human diseases. *Cancer Cell* 17, 348–361.
- Holmes, M.D., Chen, W.Y., Li, L., Hertzmark, E., Spiegelman, D., and Hankinson, S.E. (2010). Aspirin intake and survival after breast cancer. *J. Clin. Oncol.* 28, 1467–1472.
- Hoshida, T., Isaka, N., Hagendoorn, J., di Tomaso, E., Chen, Y.L., Pytowski, B., Fukumura, D., Padera, T.P., and Jain, R.K. (2006). Imaging steps of lymphatic metastasis reveals that vascular endothelial growth factor-C increases metastasis by increasing delivery of cancer cells to lymph nodes: therapeutic implications. *Cancer Res.* 66, 8065–8075.
- Iwata, C., Kano, M.R., Komuro, A., Oka, M., Kiyono, K., Johansson, E., Morishita, Y., Yashiro, M., Hirakawa, K., Kaminishi, M., and Miyazono, K. (2007). Inhibition of cyclooxygenase-2 suppresses lymph node metastasis via reduction of lymphangiogenesis. *Cancer Res.* 67, 10181–10189.
- Jaffe, B.M., Parker, C.W., and Philpott, G.W. (1971). Immunochemical measurement of prostaglandin or prostaglandin-like activity from normal and neoplastic cultured tissue. *Surg. Forum* 22, 90–92.
- Jeltsch, M., Kaipainen, A., Joukov, V., Meng, X., Lakso, M., Rauvala, H., Swartz, M., Fukumura, D., Jain, R.K., and Alitalo, K. (1997). Hyperplasia of lymphatic vessels in VEGF-C transgenic mice. *Science* 276, 1423–1425.
- Joukov, V., Pajusola, K., Kaipainen, A., Chilov, D., Lahtinen, I., Kukk, E., Saksela, O., Kalkkinen, N., and Alitalo, K. (1996). A novel vascular endothelial growth factor, VEGF-C, is a ligand for the Flt4 (VEGFR-3) and KDR (VEGFR-2) receptor tyrosine kinases. *EMBO J.* 15, 290–298.
- Kerjaschki, D., Bago-Horvath, Z., Rudas, M., Sexl, V., Schneckenleithner, C., Wolbank, S., Bartel, G., Krieger, S., Kalt, R., Hantusch, B., et al. (2011). Lipoxygenase mediates invasion of intrametastatic lymphatic vessels and propagates lymph node metastasis of human mammary carcinoma xenografts in mouse. *J. Clin. Invest.* 121, 2000–2012.
- Kopfstein, L., Veikkola, T., Djonov, V.G., Baeriswyl, V., Schomber, T., Strittmatter, K., Stacker, S.A., Achen, M.G., Alitalo, K., and Christofori, G. (2007). Distinct roles of vascular endothelial growth factor-D in lymphangiogenesis and metastasis. *Am. J. Pathol.* 170, 1348–1361.
- Koukourakis, M.I., Giatromanolaki, A., Thorpe, P.E., Brekken, R.A., Sivridis, E., Kakolyris, S., Georgoulas, V., Gatter, K.C., and Harris, A.L. (2000). Vascular endothelial growth factor/KDR activated microvessel density versus CD31 standard microvessel density in non-small cell lung cancer. *Cancer Res.* 60, 3088–3095.
- Kriehuber, E., Breiteneder-Geleff, S., Groeger, M., Soleiman, A., Schoppmann, S.F., Stingl, G., Kerjaschki, D., and Maurer, D. (2001). Isolation and characterization of dermal lymphatic and blood endothelial cells reveal stable and functionally specialized cell lineages. *J. Exp. Med.* 194, 797–808.
- Kubo, H., Hosono, K., Suzuki, T., Ogawa, Y., Kato, H., Kamata, H., Ito, Y., Amano, H., Kato, T., Sakagami, H., et al. (2010). Host prostaglandin EP3 receptor signaling relevant to tumor-associated lymphangiogenesis. *Biomed. Pharmacother.* 64, 101–106.
- Leitzmann, M.F., Stampfer, M.J., Ma, J., Chan, J.M., Colditz, G.A., Willett, W.C., and Giovannucci, E. (2002). Aspirin use in relation to risk of prostate cancer. *Cancer Epidemiol. Biomarkers Prev.* 11, 1108–1111.
- Liu, H., Yang, Y., Xiao, J., Lv, Y., Liu, Y., Yang, H., and Zhao, L. (2010). COX-2-mediated regulation of VEGF-C in association with lymphangiogenesis and lymph node metastasis in lung cancer. *Anat. Rec. (Hoboken)* 293, 1838–1846.
- Liotta, L.A. (1992). Cancer cell invasion and metastasis. *Sci. Am.* 266, 54–59, 62–63.
- Mäkinen, T., Jussila, L., Veikkola, T., Karpanen, T., Kettunen, M.I., Pulkkanen, K.J., Kauppinen, R., Jackson, D.G., Kubo, H., Nishikawa, S., et al. (2001). Inhibition of lymphangiogenesis with resulting lymphedema in transgenic mice expressing soluble VEGF receptor-3. *Nat. Med.* 7, 199–205.
- Mäkinen, T., Adams, R.H., Bailey, J., Lu, Q., Ziemiecki, A., Alitalo, K., Klein, R., and Wilkinson, G.A. (2005). PDZ interaction site in ephrinB2 is required for the remodeling of lymphatic vasculature. *Genes Dev.* 19, 397–410.

- Mandriota, S.J., Jussila, L., Jeltsch, M., Compagni, A., Baetens, D., Prevo, R., Banerji, S., Huarte, J., Montesano, R., Jackson, D.G., et al. (2001). Vascular endothelial growth factor-C-mediated lymphangiogenesis promotes tumour metastasis. *EMBO J.* 20, 672–682.
- Mantovani, A., Allavena, P., Sica, A., and Balkwill, F. (2008). Cancer-related inflammation. *Nature* 454, 436–444.
- Messina, E.J., Weiner, R., and Kaley, G. (1974). Microcirculatory effects of prostaglandins E1, E2, and A1 in the rat mesentery and cremaster muscle. *Microvasc. Res.* 8, 77–89.
- Myung, S.J., Rerko, R.M., Yan, M., Platzer, P., Guda, K., Dotson, A., Lawrence, E., Dannenberg, A.J., Lovgren, A.K., Luo, G., et al. (2006). 15-Hydroxyprostaglandin dehydrogenase is an *in vivo* suppressor of colon tumorigenesis. *Proc. Natl. Acad. Sci. USA* 103, 12098–12102.
- Nilsson, I., Bahram, F., Li, X., Gualandi, L., Koch, S., Janvius, M., Söderberg, O., Anisimov, A., Kholová, I., Pytowski, B., et al. (2010). VEGF receptor 2/3 heterodimers detected *in situ* by proximity ligation on angiogenic sprouts. *EMBO J.* 29, 1377–1388.
- Oliver, G., and Alitalo, K. (2005). The lymphatic vasculature: recent progress and paradigms. *Annu. Rev. Cell Dev. Biol.* 21, 457–483.
- Olsson, A.G., and Carlson, L.A. (1976). Clinical, hemodynamic and metabolic effects of intraarterial infusions of prostaglandin E1 in patients with peripheral vascular disease. *Adv. Prostaglandin Thromboxane Res.* 1, 429–432.
- Pepper, M.S. (2001). Lymphangiogenesis and tumor metastasis: myth or reality? *Clin. Cancer Res.* 7, 462–468.
- Pichaud, F., Roux, S., Frendo, J.L., Delage-Mourroux, R., Maclouf, J., de Vernejoul, M.C., Moukhtar, M.S., and Jullienne, A. (1997). 1,25-dihydroxyvitamin D3 induces NAD(+)-dependent 15-hydroxyprostaglandin dehydrogenase in human neonatal monocytes. *Blood* 89, 2105–2112.
- Podgrabska, S., Braun, P., Velasco, P., Kloos, B., Pepper, M.S., and Skobe, M. (2002). Molecular characterization of lymphatic endothelial cells. *Proc. Natl. Acad. Sci. USA* 99, 16069–16074.
- Pugh, S., and Thomas, G.A. (1994). Patients with adenomatous polyps and carcinomas have increased colonic mucosal prostaglandin E2. *Gut* 35, 675–678.
- Rigas, B., Goldman, I.S., and Levine, L. (1993). Altered eicosanoid levels in human colon cancer. *J. Lab. Clin. Med.* 122, 518–523.
- Ristimäki, A., Honkanen, N., Jänkäälä, H., Sipponen, P., and Härkönen, M. (1997). Expression of cyclooxygenase-2 in human gastric carcinoma. *Cancer Res.* 57, 1276–1280.
- Roberts, N., Kloos, B., Cassella, M., Podgrabska, S., Persaud, K., Wu, Y., Pytowski, B., and Skobe, M. (2006). Inhibition of VEGFR-3 activation with the antagonistic antibody more potently suppresses lymph node and distant metastases than inactivation of VEGFR-2. *Cancer Res.* 66, 2650–2657.
- Sappy, P.C. (1874). *Anatomy, Physiology and Pathology of Lymphatic Vessels in Man and Vertebrates* (Paris: DeLahaye, A).
- Shayan, R., Achen, M.G., and Stacker, S.A. (2006). Lymphatic vessels in cancer metastasis: bridging the gaps. *Carcinogenesis* 27, 1729–1738.
- Skobe, M., Hawighorst, T., Jackson, D.G., Prevo, R., Janes, L., Velasco, P., Riccardi, L., Alitalo, K., Claffey, K., and Detmar, M. (2001). Induction of tumor lymphangiogenesis by VEGF-C promotes breast cancer metastasis. *Nat. Med.* 7, 192–198.
- Sleeman, J.P., and Thiele, W. (2009). Tumor metastasis and the lymphatic vasculature. *Int. J. Cancer* 125, 2747–2756.
- Sleeman, J.P., Nazarenko, I., and Thiele, W. (2011). Do all roads lead to Rome? Routes to metastasis development. *Int. J. Cancer* 128, 2511–2526.
- Sloan, E.K., Priceman, S.J., Cox, B.F., Yu, S., Pimentel, M.A., Tangkanangkul, V., Arevalo, J.M., Morizono, K., Karanikolas, B.D., Wu, L., et al. (2010). The sympathetic nervous system induces a metastatic switch in primary breast cancer. *Cancer Res.* 70, 7042–7052.
- St Croix, B., Rago, C., Velculescu, V., Traverso, G., Romans, K.E., Montgomery, E., Lal, A., Riggins, G.J., Lengauer, C., Vogelstein, B., and Kinzler, K.W. (2000). Genes expressed in human tumor endothelium. *Science* 289, 1197–1202.
- Stacker, S.A., Caesar, C., Baldwin, M.E., Thornton, G.E., Williams, R.A., Prevo, R., Jackson, D.G., Nishikawa, S., Kubo, H., and Achen, M.G. (2001). VEGF-D promotes the metastatic spread of tumor cells via the lymphatics. *Nat. Med.* 7, 186–191.
- Stacker, S.A., Williams, R.A., and Achen, M.G. (2004). Lymphangiogenic growth factors as markers of tumor metastasis. *APMIS* 112, 539–549.
- Tang, E.H., and Vanhoutte, P.M. (2008). Gene expression changes of prostanoid synthases in endothelial cells and prostanoid receptors in vascular smooth muscle cells caused by aging and hypertension. *Physiol. Genomics* 32, 409–418.
- Tammela, T., and Alitalo, K. (2010). Lymphangiogenesis: molecular mechanisms and future promise. *Cell* 140, 460–476.
- Thun, M.J., and Heath, C.W., Jr. (1995). Aspirin use and reduced risk of gastrointestinal tract cancers in the American Cancer Society prospective studies. *Prev. Med.* 24, 116–118.
- Tsuji, M., Kawano, S., Tsuji, S., Sawaoka, H., Hori, M., and DuBois, R.N. (1998). Cyclooxygenase regulates angiogenesis induced by colon cancer cells. *Cell* 93, 705–716.
- Whorton, A.R., Smigel, M., Oates, J.A., and Frölich, J.C. (1978). Regional differences in prostacyclin formation by the kidney. Prostacyclin is a major prostaglandin of renal cortex. *Biochim. Biophys. Acta* 529, 176–180.
- Williams, C.S., Tsujii, M., Reese, J., Dey, S.K., and DuBois, R.N. (2000). Host cyclooxygenase-2 modulates carcinoma growth. *J. Clin. Invest.* 105, 1589–1594.
- Wolf, I., O'Kelly, J., Rubinek, T., Tong, M., Nguyen, A., Lin, B.T., Tai, H.H., Karlan, B.Y., and Koeffler, H.P. (2006). 15-Hydroxyprostaglandin dehydrogenase is a tumor suppressor of human breast cancer. *Cancer Res.* 66, 7818–7823.

# Aurora Kinase-A Inactivates DNA Damage-Induced Apoptosis and Spindle Assembly Checkpoint Response Functions of p73

Hiroshi Katayama,<sup>1</sup> Jin Wang,<sup>1</sup> Warapen Treekitkarnmongkol,<sup>1</sup> Hidehiko Kawai,<sup>2</sup> Kaori Sasai,<sup>1</sup> Hui Zhang,<sup>1</sup> Hua Wang,<sup>3</sup> Henry P. Adams,<sup>4</sup> Shoulei Jiang,<sup>1</sup> Sandip N. Chakraborty,<sup>1</sup> Fumio Suzuki,<sup>2</sup> Ralph B. Arlinghaus,<sup>1</sup> Jinsong Liu,<sup>3</sup> James A. Mobley,<sup>5,7</sup> William E. Grizzle,<sup>6,7</sup> Huamin Wang,<sup>3</sup> and Subrata Sen<sup>1,\*</sup>

<sup>1</sup>Department of Molecular Pathology, The University of Texas M.D. Anderson Cancer Center, Houston, TX 77054, USA

<sup>2</sup>Department of Molecular Radiobiology, Research Institute for Radiation Biology and Medicine, Hiroshima University, Hiroshima 734-8553, Japan

<sup>3</sup>Department of Pathology

<sup>4</sup>Department of Genetics

The University of Texas M.D. Anderson Cancer Center, Houston, TX 77030, USA

<sup>5</sup>Department of Surgery

<sup>6</sup>Department of Pathology

<sup>7</sup>Comprehensive Cancer Center

University of Alabama at Birmingham, Birmingham, AL 35294, USA

\*Correspondence: [ssen@mdanderson.org](mailto:ssen@mdanderson.org)

DOI 10.1016/j.ccr.2011.12.025

## SUMMARY

Elevated Aurora kinase-A expression is correlated with abrogation of DNA damage-induced apoptotic response and mitotic spindle assembly checkpoint (SAC) override in human tumor cells. We report that Aurora-A phosphorylation of p73 at serine235 abrogates its transactivation function and causes cytoplasmic sequestration in a complex with the chaperon protein mortalin. Aurora-A phosphorylated p73 also facilitates inactivation of SAC through dissociation of the MAD2-CDC20 complex in cells undergoing mitosis. Cells expressing phosphor-mimetic mutant (S235D) of p73 manifest altered growth properties, resistance to cisplatin-induced apoptosis, as well as premature dissociation of the MAD2-CDC20 complex, and accelerated mitotic exit with SAC override in the presence of spindle damage. Elevated cytoplasmic p73 in Aurora-A overexpressing primary human tumors corroborates the experimental findings.

## INTRODUCTION

Aurora kinase-A (also called STK15/BTAK; hereinafter referred to as Aurora-A), a key regulator of the mitotic cell division cycle, is overexpressed in many human tumors and is associated with abrogation of DNA damage-induced apoptotic response and spindle assembly checkpoint (SAC) override in cancer cells. Aurora-A, a cancer susceptibility gene (Ewart-Toland et al., 2003), plays essential roles in the commitment of proliferating cells to

G2/M progression, centrosome maturation-separation, bipolar spindle formation, and spindle damage recovery (Marumoto et al., 2005; Katayama et al., 2008; Macurek et al., 2008; Seki et al., 2008). We and others have previously identified functional inactivation of p53 tumor suppressor protein after Aurora-A phosphorylation at serine 315 and serine 215 residues; the former facilitates Mdm2-mediated degradation, and the latter causes loss of DNA-binding ability in human cells (Katayama et al., 2004; Liu et al., 2004). Aurora-A phosphorylation of BRCA1 at serine 308

### Significance

Resistance to DNA and spindle-damaging chemotherapeutic drugs is a major challenge to effective therapeutic interventions in human cancer. Elevated Aurora kinase-A expression is correlated with chemotherapy resistance, and p73 is a major determinant of chemosensitivity in tumor cells. Our findings demonstrate that p73 phosphorylation by Aurora-A results in inactivation of its DNA damage and spindle assembly checkpoint response functions. Aurora-A-phosphorylated p73 loses chromatin-binding affinity, is sequestered in the cytoplasm, and facilitates dissociation of the MAD2-CDC20 spindle assembly checkpoint complex. Elucidation of the molecular mechanisms underlying the development of resistance to DNA and spindle targeted therapeutic agents in Aurora-A overexpressing tumors should help us design more effective therapeutic regimens.

is correlated with silencing of DNA damage-induced G2/M checkpoint (Ouchi et al., 2004). Furthermore, overexpression of Aurora-A makes HeLa cells resistant to taxol-induced cell death due to mitotic SAC override (Anand et al., 2003). A recent study found that treatment of p53-deficient cells with Aurora-A small molecule inhibitors activates p73 transactivation function with upregulation of its downstream target genes during induction of cell death (Dar et al., 2008). However, the molecular mechanisms underlying the observed effects have not been elucidated.

The role of p73 in tumorigenesis has been debated because loss of function mutations in the gene is rare. However, recently developed transactivation-competent (TA) p73-specific gene-knockout mice have a high incidence of spontaneous and carcinogen-induced tumors (Tomasini et al., 2008). In addition, oocytes and cells lacking TAp73 exhibit abnormal spindle structure and mitotic slippage with spindle poisons, indicating participation of TAp73 in the SAC pathway (Tomasini et al., 2009). More recent studies have demonstrated that TAp73 interacts with SAC proteins Bub1, Bub3, and BubR1. TAp73-deficient or knockdown cells reveal mislocalization of Bub1 and BubR1 at the kinetochore and reduced BubR1 kinase activity, associated with aneuploidy and chromosome instability (Tomasini et al., 2009; Vernole et al., 2009). Together with proapoptotic function of TAp73 in response to genotoxic stress, these results suggest that p73 is directly involved in maintaining genomic stability and regulating SAC pathway.

In view of Aurora-A overexpression reported to induce resistance to DNA damage-mediated apoptosis response and SAC override, we investigated the possible role of Aurora-A functional interaction with p73 and the underlying molecular mechanisms involved in the development of these phenotypes.

## RESULTS

### Aurora-A Phosphorylates p73

We hypothesized that direct phosphorylation of p73 by Aurora-A negatively regulates p73 transactivation function and consequential activation of apoptosis response. Because p73 is reported to be phosphorylated in mitosis (Fulco et al., 2003), we treated nocodazole- and taxol-arrested mitotic Cos-1 cells with Aurora-A-specific inhibitor MLN8054 and proteasome inhibitor MG132 to detect Aurora-A-specific posttranslational p73 modification. p73 from inhibitor-treated mitotic cells migrated faster than that from untreated cells, whereas p73 from exponentially growing cells had intermediate mobility (Figure 1A). The slower migrating form was seen in cells with active Aurora-A, detected with anti-phospho T288 antibody. To determine whether slower mobility of p73 was due to phosphorylation and whether Aurora-A is directly involved in p73 phosphorylation, we treated cell extracts with  $\lambda$ PPase, with or without Aurora-A inhibitor. While inhibitor treatment alone resulted in minimal increase in mobility,  $\lambda$ PPase treatment, both with or without Aurora-A inhibitor, led to similar yet markedly faster migration in p73. These results indicate that slower mobility was due to multiple phosphorylations, possibly catalyzed by several kinases, including Aurora-A. Aurora-A inhibition alone resulted in a minor downward shift in gel mobility due to selective interference with Aurora-A phosphorylation, but the more rapidly migrating form was due to complete dephosphorylation

with  $\lambda$ PPase (Figure 1A). To determine direct involvement of Aurora-A in p73 phosphorylation in vivo, we performed p73 immunoprecipitation, followed by immunoblotting with the anti-phospho-PKA substrate antibody, which recognizes the Aurora-A consensus phosphorylation motif in substrate proteins (Katayama et al., 2007; Plotnikova et al., 2011). We observed clear phosphor-PKA signal in immunoprecipitated p73 from nocodazole-treated mitotic cells, which was diminished in inhibitor-treated samples. In exponentially growing cells, the phosphor-PKA signal changed little after treatment (Figure 1B). These findings further verified the involvement of Aurora-A in p73 phosphorylation in vivo (Figures 1C and 1D).

We next performed an in vitro kinase assay of p73, with or without wild-type (WT) or kinase-dead (KD) Aurora-A, with the closely related paralog Aurora-B as a control. Aurora-A-WT phosphorylated p73, but Aurora-A-KD did not (Figure 1E). Complete absence of phosphorylation signal on p73 with Aurora-B further validated Aurora-A as the bona fide kinase of p73. We next identified the specific Aurora-A phosphorylated amino acid residue in p73 using site-directed mutants in Aurora kinase consensus phosphorylation motifs and subjecting them to in vitro kinase assays. The serine 235 alanine (S235A) mutant of p73 had reduced phosphorylation than p73-WT, indicating that S235 is phosphorylated by Aurora-A (Figure 1F). We further confirmed this phosphorylation using an anti-phospho-PKA substrate-specific antibody. p73-WT phosphorylation was evident in cells coexpressing Aurora-A but not those expressing the empty vector. Phosphorylation was significantly diminished in cells expressing the S235A mutant, demonstrating that serine 235 in p73 is phosphorylated by Aurora-A (Figure 1G). It is intriguing that transactivation-defective  $\Delta$ Np73 showed minimal loss of phosphorylation in the SA mutant of the conserved motif and appeared to bind the WT and the phosphor-mimetic (S235D) mutant of p73 with similar efficiency (Figures S1A and S1B available online).

We determined in vivo interaction between Aurora-A and p73 by immunoprecipitation of 293T cells cotransfected with Flag-Aurora-A and GFP-p73. Anti-Flag antibody revealed a specific interaction between p73 and Aurora-A (Figure 1H). Anti-Flag antibody immunoprecipitations also detected enriched presence of p73-S235D mutant in the immune complex compared with S235A mutant (Figure S1C). To determine the interaction between endogenous Aurora-A and p73, we used synchronized mitotic cells for reciprocal immunoprecipitation experiments, which revealed p73 and Aurora-A in the same complex (Figure 1I) that was absent in the p73 knockdown cells (Figure 1J). This interaction was also detected in human nontumorigenic MCF-10A mammary epithelial cells and p53-deficient H1299 lung carcinoma cells (Figures S1D and S1E). Cell cycle dependence of this interaction was analyzed in synchronized cells after double thymidine block and release. Consistent with published data (Fulco et al., 2003), p73 expression was uniform through the cell cycle. The amount of Aurora-A bound to p73 progressively increased, peaking at mitosis, which was also evident in nocodazole-treated cells (Figure 1K).

### Aurora-A Phosphorylated p73 Loses DNA Binding and Transactivation Activity

Because the Aurora-A phosphorylation site is located in the DNA-binding domain, we determined the effect of Aurora-A

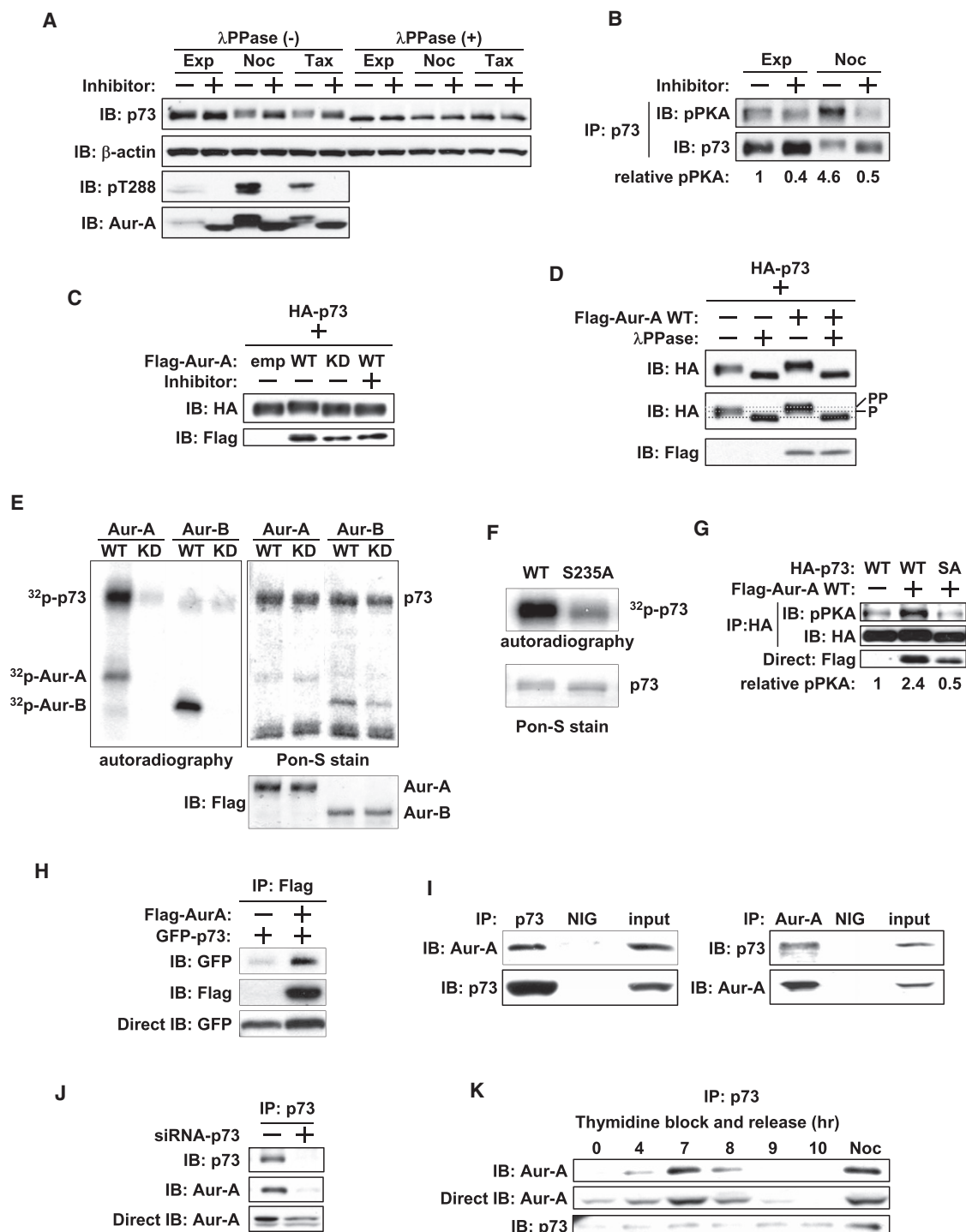


**Figure 1. Aurora A Phosphorylates and Interacts with p73**

(A) Cos-1 cells, grown with or without nocodazole or taxol for 20 hr, were cultured with or without Aurora-A inhibitor MLN8054 in the presence of MG132 for 4 hr. Whole cell extracts (WCE) were incubated with (+) or without (-)  $\lambda$ PPase for 30 min. Samples were analyzed by immunoblotting with the indicated antibodies.

(B) WCE prepared in (Figure 1A) were immunoprecipitated with anti-p73 antibody and subjected to immunoblotting with anti-pPKA substrate (top) and anti-p73 (bottom) antibodies. The pPKA signal was normalized by the amount of precipitated HA-p73, and the relative pPKA signal was quantified.

(C) HA-p73 $\alpha$  was cotransfected with empty vector, Flag-WT Aurora-A (WT), or Flag-KD Aurora-A (KD) into Cos-1 cells. Twenty-four hours later, cells were cultured with (+) or without (-) Aurora-A inhibitor for 4 hr. WCE were subjected to immunoblotting with anti-HA (top) and anti-Flag (bottom) antibodies.

(D) WCE prepared in (Figure 1C) were treated without (-) or with (+)  $\lambda$ PPase for 30 min and analyzed as in (Figure 1C). The middle shows the differential migration of HA-p73 $\alpha$ .

phosphorylation on DNA binding and transactivation activity of p73. Electrophoretic mobility shift assay (EMSA) revealed that DNA binding of S235D mutant was markedly inhibited, whereas S235A mutant had weaker DNA-binding ability compared with WT (Figure 2A). We next evaluated the transactivation function of p73 phosphor mutants using a p21 promoter-driven luciferase assay in H1299 cells. S235D mutant had minimal transactivation of the p21 promoter, whereas S235A mutant had activity similar to that of WT (Figure 2B). Endogenous p21 protein levels in cells expressing p73-WT and phosphor mutants were consistent with the p73 transcriptional activity detected by luciferase assay. p21 levels were low in S235D mutant cells, compared with WT and S235A mutant cells (Figure 2C). Similarly, p73-S235D mutant cells demonstrated diminished expression of p73 target genes Puma, Bax, and Noxa, compared with p73-WT and S235A mutant cells (Figure 2D).

We determined whether p73 activity depends on Aurora-A kinase activity and whether S235A mutant is insensitive to this activity. Luciferase assay revealed that p73-WT activity was inhibited by Aurora-A-WT but not by the KD mutant, whereas S235A mutant was not inhibited by Aurora-A (Figure 2E). Endogenous p21 expression levels in these cells were consistent with the results of luciferase assay (Figure 2F). Similar transactivation activity and endogenous target gene levels in the WT and S235A mutant cells appear to be the result of Aurora-A's inhibitory phosphorylation interfering with p73-WT's transactivation function *in vivo*. To investigate this, we transfected p73-WT and S235A mutant in MCF7 cells, which naturally express high levels of active Aurora-A (Figure 2G). The results revealed distinctly elevated p21 protein levels in cells expressing S235A mutant compared with that in cells expressing WT (Figure 2H). Aurora-A inhibitor treatment of H1299 cells transfected with empty vector revealed upregulation of p73 target PUMA mRNA, whereas S235D interfered with transactivation in a dominant-negative manner (Figure 2I). These results demonstrate that Aurora-A phosphorylation of p73 at serine 235 negatively regulates p73 transactivation.

### Aurora-A Regulates p73 Subcellular Localization

Protein fractionation experiments revealed marked accumulation of S235D mutant in the cytoplasmic fraction, whereas accumulation was predominantly nuclear in the WT and S235A

mutant cells (Figure 3A). Similar results were found on immunofluorescence microscopy (Figure 3B) and in different cell lines, such as HeLa, H1299, and MCF7 (data not shown). We next analyzed whether the cytoplasmic distribution of S235D mutant was due to its accelerated export from the nucleus or interference with its nuclear translocation by treating cells with leptomycin B, an inhibitor of nuclear export of proteins. Protein fractionations revealed cytoplasmic localization of S235D mutant, regardless of leptomycin B treatment, and more nuclear accumulation of WT (Figure 3C), indicating that phosphorylated p73 at serine 235 is tethered in the cytoplasm. Similar results were observed for S215D mutant of p53 (Figure S2A). Enrichment of the phosphor-mimetic mutant of p73 in the cytoplasmic fraction was also observed in nocadazole-arrested mitotic cells with high Aurora-A activity, possibly coinciding with nuclear envelope breakdown (Figures S2B and S2C). Because proteins with aberrant conformations are preferentially transported to the cytoplasm to be degraded, we determined whether cytoplasmic distribution of S235D mutant reflected a conformational change using a glutaraldehyde-based protein cross-linking assay. Since p73 is a tetramer in its natural state, and if S235 phosphorylation does not affect monomeric p73 structure, a slower migrating p73 tetramer would still be detectable on SDS-PAGE. High-MW S235D and S235A mutants migrated near the tetrameric form of p73-WT (Figure 3D), indicating that p73 phosphorylation status at serine 235 does not cause conformational changes.

To determine whether endogenous p73 is distributed in the cytoplasm with Aurora-A, we performed immunofluorescence microscopy with anti-p73 antibody. Cells overexpressing Aurora-A showed evenly diffused endogenous p73 staining in the cytoplasm and nucleus, which were reversed with Aurora-A inhibitor (Figures 3E and 3F). Protein fractionation experiments further confirmed these findings (Figure 3G). p73 is localized in the cytoplasm of MCF-7 breast cancer cell line and Panc-1 pancreatic cancer cell line, both express elevated Aurora-A levels (Sen et al., 1997; Li et al., 2003). Inhibitor treatment of these cell lines resulted in p73 nuclear localization (Figure 3H), confirming that cytoplasmic distribution of p73 is influenced by Aurora-A kinase activity. Protein fractionation experiments in Panc-1 cells also supported this observation (Figure 3I). Similar results were observed in Aurora-A inhibitor treated MCF-7 cells

(E) Anti-Flag M2 antibody immunoprecipitates from nocodazole-treated mitotic 293T cells transfected with Flag-Aurora-A-WT, Flag-Aurora-A-KD, Flag-Aurora-B-WT, or Flag-Aurora-B-KD were incubated with GST-p73 $\alpha$  in the presence of [ $\gamma$ -<sup>32</sup>P]ATP. GST-p73 $\alpha$  was resolved by SDS-PAGE and visualized by autoradiography (left) and Pon-S staining (right). Immunoprecipitated Aurora-A and Aurora-B were detected with anti-Flag M2 antibody (bottom right).

(F) Immunoprecipitates with anti-Aurora-A antibody from nocodazole-treated mitotic 293T cells were incubated with GST-p73 $\alpha$ -WT or GST-p73 $\alpha$ -S235A (SA) in the presence of [ $\gamma$ -<sup>32</sup>P]ATP. GST-p73 protein was resolved and visualized as in (Figure 1E).

(G) HA-p73 $\alpha$ -WT or -SA were cotransfected with either empty vector or Flag-Aurora-A-WT into Cos-1 cells. Twenty-four hours later, WCE were immunoprecipitated with anti-HA antibody, followed by immunoblotting with anti-pPKA substrate (top) and anti-HA (middle) antibodies. WCE were directly immunoblotted with anti-Flag (bottom) antibody. The pPKA signal was normalized by the amount of precipitated HA-p73, and the relative pPKA signal was quantified.

(H) GFP-p73 $\alpha$  was cotransfected with empty vector or Flag-Aurora-A in 293T cells. Twenty-four hours later, cells were immunoprecipitated with anti-Flag antibody, followed by immunoblotting with indicated antibodies (top and middle). Aliquots of the same cell lysates were directly immunoblotted with anti-GFP antibody (bottom).

(I) Cos-1 cells were immunoprecipitated with anti-p73 (right) or anti-Aurora-A (left) antibodies or normal immunoglobulin G (NIG). Immunoprecipitates were subjected to immunoblotting with anti-p73 and anti-Aurora-A antibodies. Input indicates the immunoblot of WCE.

(J) Cos-1 cells were transfected with control siRNA (–) or p73 siRNA (+) for 48 hr and subjected to immunoprecipitation with anti-p73 antibody, followed by immunoblotting with anti-p73 (top) and anti-Aurora-A (middle) antibodies, respectively. WCE were directly immunoblotted with anti-Aurora-A (bottom) antibody.

(K) Cos-1 cells synchronized by double thymidine block and release were immunoprecipitated with anti-p73 antibody followed by immunoblotting with the indicated antibodies.

See also Figure S1.

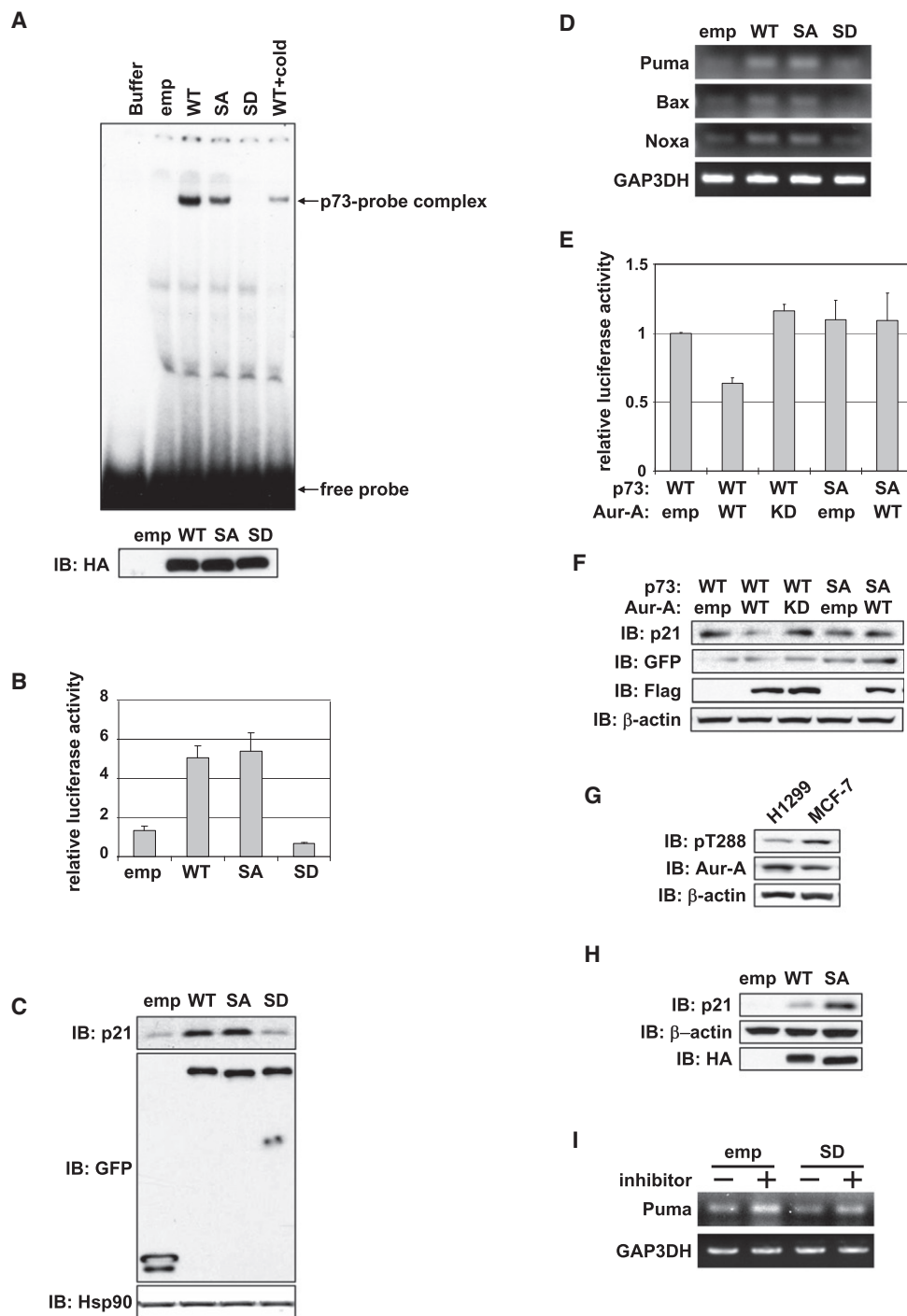


**Figure 2. Aurora-A Inhibits DNA Binding and Transactivation Activity of p73**

(A) DNA-binding activities of in vitro transcribed and translated proteins of HA-p73 $\alpha$  WT, S235A (SA), S235D (SD), and empty vector (emp) were analyzed by EMSA with a [ $\gamma$ - $^{32}$ P]ATP-labeled p53/p73 binding consensus oligonucleotide probe. A competition assay was performed with 50-fold molar excess amounts of unlabeled probe (cold). Buffer was used as a negative control. The reaction was separated by a native polyacrylamide gel (top). The amount of proteins used was analyzed by immunoblotting with anti-HA antibody (bottom).

(B) H1299 cells were cotransfected with GFP-empty or GFP-p73 $\alpha$ -WT or -mutants with luciferase reporter construct containing p21 promoter and Renilla luciferase reporter internal control plasmid. Twenty-four hours later, cells were subjected to a reporter assay. Data represent mean values  $\pm$  SD from three independent experiments.

(C) Protein expression of p21 in cells transfected with GFP-empty and GFP-p73 $\alpha$  constructs used in (Figure 2B). Proteins were detected by immunoblotting with the indicated antibodies.

(D) mRNA expression of p73 target genes in cells used in (Figure 2B), analyzed by semiquantitative RT-PCR.

(data not shown). These results validated that Aurora-A phosphorylation of p73 negatively regulates its nuclear localization.

### Mortalin Tethers Phospho-p73 in the Cytoplasm

To identify the proteins bound to phospho-p73, we immunoprecipitated protein complexes with WT and S235D mutant of p73. A protein band of approximately 80 kD MW was detected only in the immune complex of the S235D mutant but not the WT (Figure 4A). Mass spectrometry identified this protein as mortalin, a member of the hsp70 family that is implicated in immortalization and tumorigenesis (Deocaris et al., 2007). Gel filtration column chromatography revealed that p73 and mortalin existed in high-MW complexes, distributed over a wide size range. It is interesting that the S235D mutant and mortalin-containing complexes were significantly more enriched at >2-megadalton-sized fractions than were the p73-WT and mortalin complexes (Figure 4B). Enrichment of S235D mutant and mortalin in the higher molecular complex was also evident in cell extracts resolved on native gels immunoblotted with anti-p73 and mortalin antibodies (Figure S3A). We cotransfected WT or deletion mutant of mortalin (mot del-BD) lacking the p53-binding domain (aa 253–282), described earlier (Ma et al., 2006), with WT or phosphor mutants of p73 to determine whether mortalin interaction with the S235D mutant, tethered in the cytoplasm, was mediated through the same domain involved in p53 binding. WT and mutant p73 did not interact with the mortalin deletion mutant, but full-length mortalin's interaction was enhanced with S235D mutant compared with WT and S235A mutant (Figure 4C). Similar results were seen in p53 co-immunoprecipitation experiments (Figure S3B). These results demonstrate that Aurora-A phosphorylation of p73 and p53 positively regulates their interactions with mortalin, mediated through the same binding domain.

Immunoprecipitation experiments revealed enhanced interaction of p73 with mortalin in nocodazole-treated mitotic cell extracts, compared with extracts from exponentially growing cells, indicating the importance of p73 phosphorylation in mitosis for mortalin binding. The specificity of this interaction was verified by immunoprecipitating the extracts from p73 knockdown cells (Figure 4D). The interaction between Aurora-A and p73 was not affected by mortalin deletion mutant (Figure S3C).

To further validate the role of Aurora-A phosphorylation in regulating p73 binding to mortalin, coimmunoprecipitation of the two proteins was performed with or without Aurora-A inhibitor-treated cells transfected with empty vector or Aurora-A expression vector. Less mortalin bound to p73 in treated cells than in untreated cells. A similar effect was seen in empty-vector-transfected cells, reflecting the effects of endogenous Aurora-A kinase activity on the binding of p73 to mortalin (Figure 4E). This finding was corroborated in MCF-7 and Panc-1

cells (Figure 4F). Ectopic expression of Aurora-A-KD mutant demonstrated that mortalin protein stability is not affected by Aurora-A kinase activity (Figure S3D). Decreased binding of ectopically expressed and endogenous Aurora-A to p73 in inhibitor-treated cells verified that the interaction between Aurora-A and p73 is kinase activity dependent (Figures 4E and 4F).

To determine the effect of mortalin binding on subcellular localization of phosphor-mimetic p73, S235D mutant was cotransfected with the mortalin deletion mutant or an empty vector in Cos-1 cells. In cells with mutant mortalin, the p73 S235D mutant translocated into the nucleus more than in the empty-vector-transfected cells (Figures 5A and 5B). Protein fractionation experiments also revealed enhanced nuclear accumulation of S235D mutant in mortalin deletion mutant cells than in control cells (Figure 5C). To determine whether loss of mortalin expression had a similar effect on p73 localization, S235D mutant was expressed in cells transfected with control or mortalin targeting siRNAs. Protein fractionation revealed that the nuclear:cytoplasmic ratio was relatively higher in mortalin-siRNA-transfected cells than in control cells, indicating mortalin involvement in cytoplasmic sequestration of p73 (Figures 5D and 5E). We next analyzed endogenous cytoplasmic p73 in MCF7 and Panc-1 cells after ectopic expression of mortalin deletion mutant. Nuclear staining was detected in 36% of mortalin mutant MCF-7 and Panc-1 cells (n = 100) versus 2% of empty vector cells (Figure 5F). p73 was also enriched in the nuclear fraction in mortalin mutant cells, whereas it was localized in the cytoplasm in empty vector cells (Figure 5G). Aurora-A was also distributed in the nucleus in mortalin mutant cells, but its nuclear accumulation was lower than p73 (Figure S4). The microscopy and fractionation experiments demonstrated a positive correlation between nuclear p73 localization and mutant mortalin expression. Moreover, mortalin-siRNA-transfected Panc-1 cells revealed reduced cytoplasmic localization (Figures 5H and 5I) and phosphorylation of p73 along with increased p21 expression (Figure 5H and 5J), suggesting that mortalin regulates Aurora-A phosphorylation of p73 and its transactivation function. Immunoprecipitation of p73 from empty-vector-transfected cells demonstrated interaction between p73 and mortalin. This interaction was weakened in the presence of Aurora-A inhibitor, which correlated with positive nuclear p73 staining and loss of Aurora-A interaction with p73. These results point toward an important role for mortalin in cytoplasmic sequestration of p73 after phosphorylation by Aurora-A.

### Aurora-A Phosphorylation of p73 Abrogates Cell Growth Inhibition and DNA Damage-Induced Cell Death Response

We determined the physiological effects of Aurora-A phosphorylated p73 on cell growth and DNA damage-induced cell death

(E) GFP-p73 $\alpha$ -WT or -SA mutant was cotransfected with empty vector, Flag-Aurora-A-WT, and Flag-Aurora-A-KD in H1299 cells and analyzed as in (Figure 2B). Data represent mean values with  $\pm$  SD from three independent experiments.

(F) Protein expression of p21 and transfected GFP-p73 $\alpha$  and Flag-Aurora-A in cells described in (Figure 2E), analyzed by immunoblotting with the indicated antibodies.

(G) Expression analysis of active-Aurora-A (pT288) and total Aurora-A in H1299 and MCF-7 cells.

(H) MCF-7 cells transfected with empty vector, HA-p73 $\alpha$ -WT, or -SA mutant for 24 hr were analyzed by immunoblotting with the indicated antibodies.

(I) H1299 cells transfected with empty vector or HA-p73 $\alpha$ , cultured without (–) or with (+) Aurora-A inhibitor for 24 hr, and analyzed for mRNA expression of Puma by semiquantitative RT-PCR.

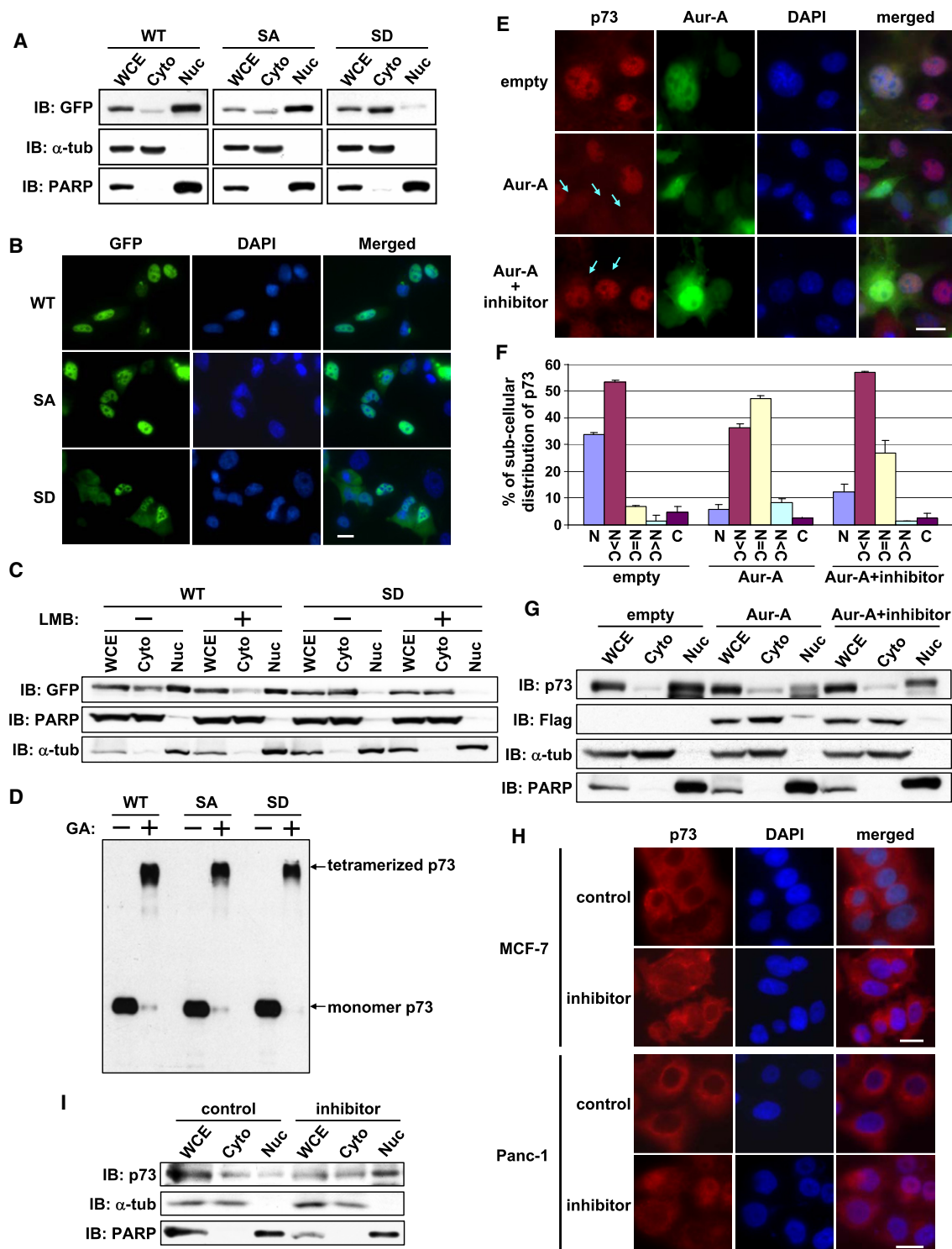


**Figure 3. Aurora-A Regulates Subcellular Localization of p73**

(A) H1299 cells transfected with GFP-p73 $\alpha$  expression plasmids for 24 hr were fractionated into cytosolic (Cyto) and nuclear (Nuc) fractions and analyzed by immunoblotting with anti-GFP antibody. The purity of Cyto and Nuc fractions was confirmed by immunoblotting with anti- $\alpha$ -tubulin and anti-PARP antibodies, respectively. WCE, whole cell extracts.

(B) H1299 cells transfected with GFP-p73 $\alpha$  expression plasmids were analyzed for subcellular localization of GFP fusion p73 by immunofluorescence microscopy and counterstained for DNA with DAPI. Scale bar corresponds to 20  $\mu$ m.

(C) GFP-p73 $\alpha$ -WT or -S235D mutant was transfected into H1299 cells. Twenty-four hours later, cells were further cultured with (+) or without (–) leptomycin B for 6 hr and subjected to subcellular fractionation as in (Figure 3A).

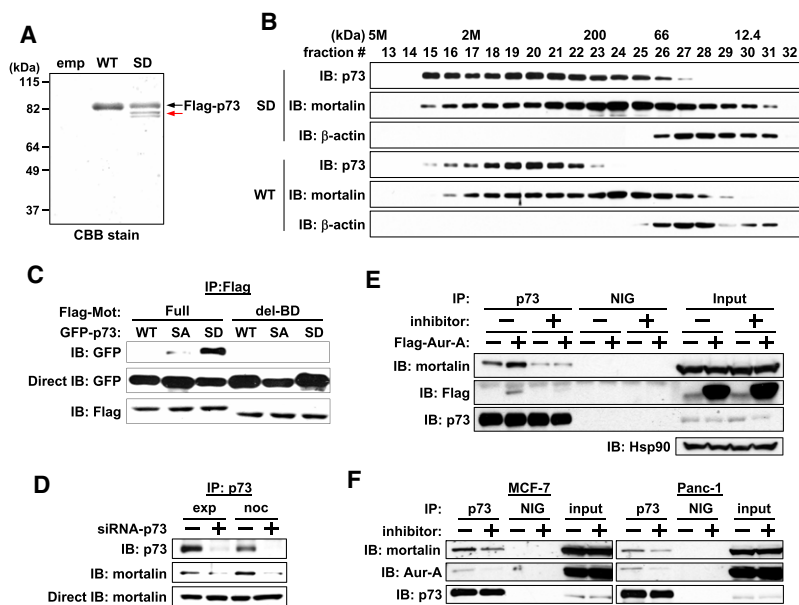


**Figure 4. Mortalin Interaction with Aurora-A Phosphorylated p73**

(A) Flag-empty vector (emp), Flag-p73 $\alpha$ -WT, or -SD mutant was transfected into HeLa cells. Twenty-four hours later, cells were immunoprecipitated with anti-Flag antibody conjugated protein-A sepharose and immunoprecipitates were eluted with Flag peptide. Eluted proteins were subjected to SDS-PAGE, and the gel was stained with Coomassie Brilliant Blue (CBB). Arrow in red shows mortalin, identified as the p73-interacting protein from this experiment.

(B) WCE, prepared as in (Figure 4A), were subjected to gel filtration column chromatography, and an equal volume of eluted proteins in each fraction was analyzed by immunoblotting with the indicated antibodies.

(C) Full-length Flag-mortalin (Full) or p53-binding domain deletion mutant of Flag-mortalin (del-BD) were co-transfected with GFP-p73 $\alpha$ -WT, -SA, or -SD in HeLa cells. Twenty-four hours later, cells were subjected to immunoprecipitation with anti-Flag antibody, followed by immunoblotting with the indicated antibodies (top and bottom). WCE were directly immunoblotted with anti-GFP antibody (middle).

(D) Cos-1 cells were transfected with control siRNA (-) or p73 siRNA (+) for 48 hr and grown with or without nocodazole for 16 hr. Cells were subjected to immunoprecipitation with anti-p73 antibody, followed by immunoblotting with the indicated antibodies (top and middle). WCE were directly immunoblotted with anti-mortalin antibody (bottom).

(E) Cos-1 cells were transfected with Flag-empty vector (-) or with Flag-Aurora-A-WT (+). Twenty-four hours later, cells were cultured for 6 hr with (+) or without (-) MLN8054. Cells were then subjected to immunoprecipitation with anti-p73 antibody or normal IgG (NIG), followed by immunoblotting with the indicated antibodies. Input shows immunoblotting of WCE.

(F) MCF-7 and Panc-1 cells were cultured for 6 hr with (+) or without (-) MLN8054, subjected to immunoprecipitation, and analyzed as in (Figure 4E).

See also Figure S3.

response in p53 null Saos-2 and H1299 cells. WT and S235A mutant significantly inhibited colony formation, compared with S235D mutant (Figure 6A). Because p73 is a critical regulator of the DNA damage-induced cell death pathway, we determined whether p73's phosphorylation status in H1299 cells influenced cisplatin-induced cell death. Consistent with the expected induction of proapoptotic genes by p73, cells expressing WT and S235A mutant showed higher apoptosis than did the vector-transfected cells, whereas S235D mutant made cells least sensitive to cisplatin-induced cell death (Figure 6B). These results demonstrate that Aurora-A phosphorylation compromises the p73-mediated DNA damage-induced cell death response. Next, we determined the plausible differential activation of Aurora-A, p73 phosphorylation, and its nuclear-cytoplasmic distribution, with or without DNA damage. DNA damage-inducing cisplatin treatment resulted in loss of Aurora-A activation and reduced p73 phosphorylation in empty-vector-

transfected cells, but in the presence of ectopic Aurora-A overexpression, minimal differences in Aurora-A activation, p73 phosphorylation, and nuclear cytoplasmic distribution were found between untreated and treated cells (Figure 6C). Empty vector cells showed elevated nuclear distribution of p73 after treatment (Figure 6D).

### Aurora-A Phosphorylation Inactivates Mitotic SAC Function of p73

SAC is impaired without p73; thus, we investigated whether Aurora-A phosphorylation of p73 affects SAC response. We ectopically expressed mCherry fusion construct of p73 phosphor mutants in HeLa cells in which the chromatin was labeled with stably expressing GFP-tagged histone H2B protein. Time-lapse microscopy revealed that the duration from nuclear envelope breakdown to anaphase was shorter in S235D mutant cells than in controls and S235A mutant cells. S235A mutant

(D) WCE prepared as in (Figure 3A) were incubated with (+) or without (-) 0.01% glutaraldehyde for 15 min, and the products were resolved in SDS-PAGE, followed by immunoblotting with anti-GFP antibody.

(E) Cos-1 cells were transfected with GFP-empty vector or with GFP-Aurora-A WT. Twenty-four hours later, cells were grown for an additional 6 hr with or without MLN8054 and immunostained with anti-p73 antibody (red). DNA was counterstained with DAPI (blue). Arrow indicates GFP-positive cells. Scale bar corresponds to 20  $\mu$ m.

(F) Subcellular distribution of p73 in GFP-positive cells in (Figure 3E) was analyzed and quantified for nuclear and cytoplasmic localization. Mean values  $\pm$  SD are from two independent experiments (n = 100).

(G) Distribution of the proteins in cellular fractions from samples prepared as in (Figure 3E), analyzed by immunoblotting with the indicated antibodies.

(H) MCF-7 and Panc-1 cells were incubated with or without MLN8054 for 6 hr and subjected to immunostaining as described in (E). Scale bar corresponds to 20  $\mu$ m.

(I) Protein distribution in cellular fractions from samples prepared in (Figure 3H), analyzed by immunoblotting with the indicated antibodies.

See also Figure S2.

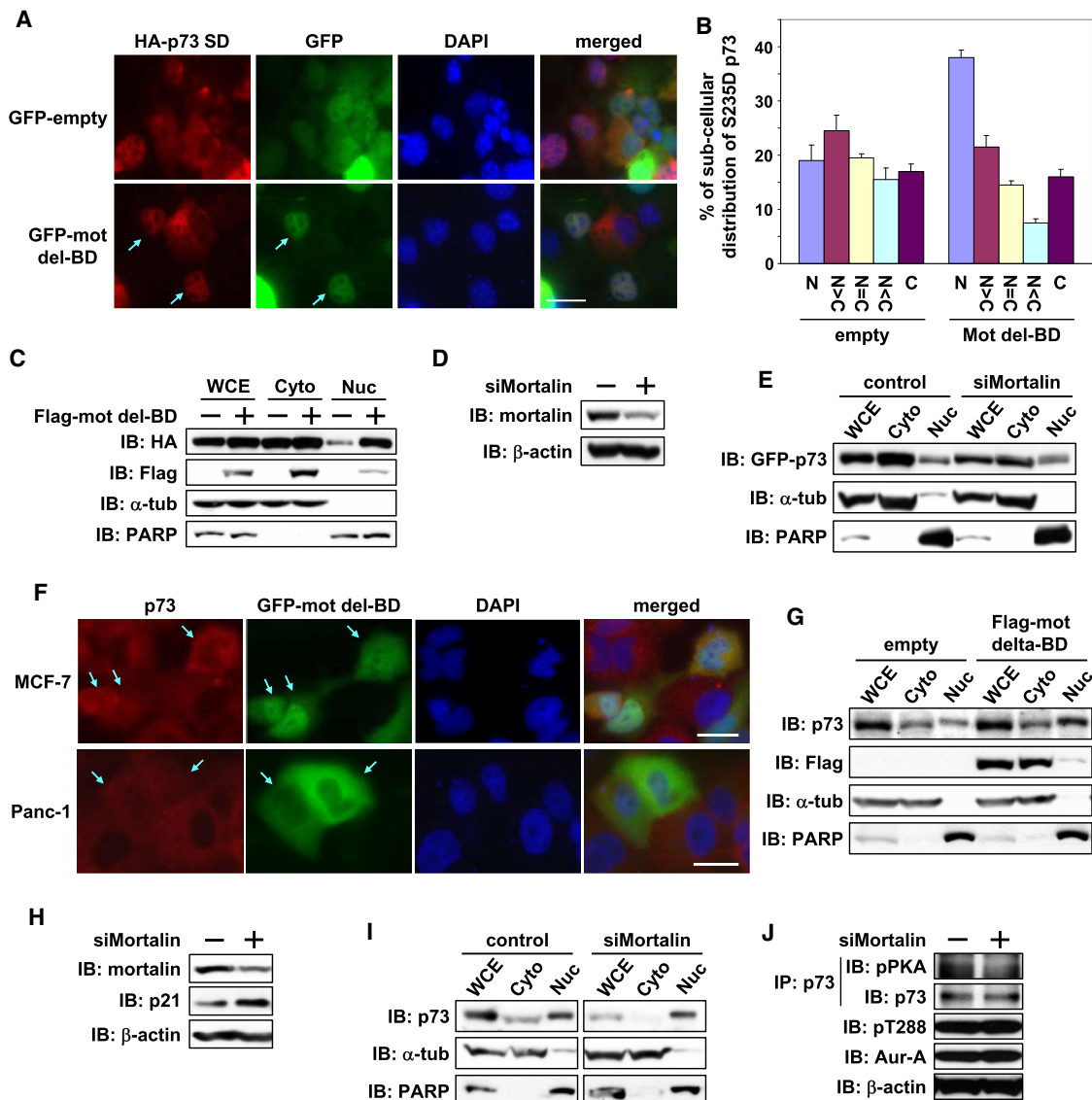


**Figure 5. Mortalin Interaction Regulates Cytoplasmic Distribution of p73**

(A) HA-p73 $\alpha$ -SD was cotransfected with GFP-empty vector or GFP-mortalin-del-BD into Cos-1 cells. Twenty-four hours later, cells were immunostained with anti-HA antibody (red) and counterstained for DNA with DAPI (blue). Arrow shows GFP-positive cells with nuclear staining of HA-p73 $\alpha$ -SD. Scale bar corresponds to 20  $\mu$ m.

(B) Subcellular distribution of HA-p73 $\alpha$ -SD in GFP-positive Cos-1 cells prepared as in (Figure 5A) was analyzed and quantified. Mean values  $\pm$  SD are from three independent experiments ( $n = 100$ ).

(C) Cos-1 cells prepared as in (Figure 5A) were fractionated into cytosolic (Cyto) and nuclear (Nuc) fractions and analyzed by immunoblotting with anti-HA and anti-Flag antibodies. The purity of Cyto and Nuc fractions was confirmed by immunoblotting for anti- $\alpha$ -tubulin and anti-PARP antibodies, respectively.

(D) Cos-1 cells were transfected with control siRNA (–) or mortalin siRNA (+) for 48 hr and subjected to immunoblotting with anti-mortalin (top) and anti- $\beta$ -actin (bottom) antibodies, respectively.

(E) Cos-1 cells transfected with control or mortalin siRNA for 24 hr were transfected with GFP-p73 $\alpha$ -SD. Twenty-four hours later, cells were subjected to fractionations, followed by immunoblotting, as in (Figure 5C).

(F) MCF-7 and Panc-1 cells were transfected with GFP-mortalin-del-BD for 24 hr, immunostained with anti-p73 antibody (red), and counterstained for DNA with DAPI (blue). Arrow indicates GFP-positive cells. Scale bar corresponds to 20  $\mu$ m.

(G) Panc-1 cells were transfected with Flag-empty vector or Flag-mortalin-del-BD. Twenty-four hours later, cells were subjected to fractionation, followed by immunoblotting as in (Figure 5C).

(H) Panc-1 cells were transfected with control siRNA (–) or mortalin siRNA (+) for 48 hr and subjected to immunoblotting with anti-mortalin (top) and anti- $\beta$ -actin (bottom) antibodies, respectively.

(I) Panc-1 cells prepared in (Figure 5H) were subjected to fractionations, followed by immunoblotting as in (Figure 5C).

(J) WCE prepared in (Figure 5H) were immunoprecipitated with anti-p73 antibody, followed by immunoblotting with the indicated antibodies (top and second). WCE were directly immunoblotted with the indicated antibodies also (third and bottom).

See also Figure S4.

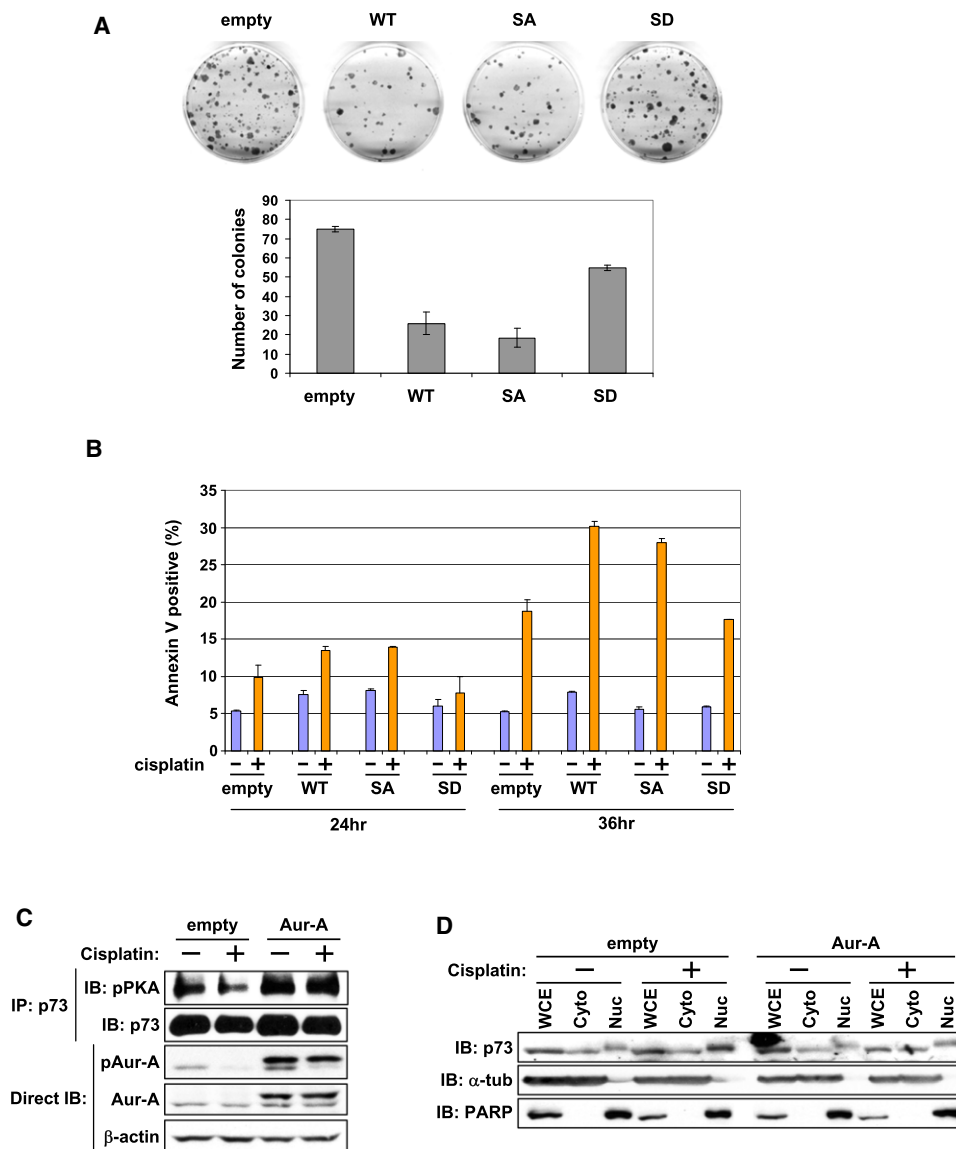


**Figure 6. Role of Phospho-p73 Mutant in Cell Growth and Response to DNA Damage-Induced Cell Death**

(A) Colony formation assay in SAOS-2 cells grown for 3 weeks under G418 selection after transfection with the indicated p73 expression constructs. Representative photos of culture plates from one experiment are shown (top). Mean colony numbers  $\pm$  SD from three independent experiments are shown in the graphs (bottom).

(B) H1299 cells were transfected with the indicated expression constructs. Twenty-four hours later, untreated cells (–) and cells treated with cisplatin (+) for 24 or 36 hr were subjected to annexin-V assay. The graph represents the mean annexin-V-positive apoptotic cells  $\pm$  SD from two independent experiments.

(C) Flag-empty vector or Flag-Aurora-A cells, transfected for 24 hr, were treated with cisplatin (50  $\mu$ M) for 6 hr. Cells were subjected to immunoprecipitation with anti-p73 antibody, followed by immunoblotting with the indicated antibodies (top and second). WCE were directly immunoblotted with antibodies, as shown.

(D) Cells prepared as in (C) were subjected to fractionations, followed by immunoblotting with the indicated antibodies.

cells took the longer to transition into anaphase (Figure 7A). S235D mutant cells had no abnormal chromosome alignment but had frequent chromosome bridges in anaphase-telophase cells, reflecting defects in the chromosome segregation process. To determine whether this resulted from aberrant SAC function, we grew cells expressing p73 phosphor mutants, with or without nocodazole, and quantified them in terms of mono- and multinucleation, presence in mitosis, or apoptosis induction (Figure 7B). Nocodazole treatment of empty vector and S235A mutant cells

had similar effects, with  $48.8 \pm 1.9\%$  and  $46.2 \pm 0.4\%$ , respectively, in mitosis and  $14 \pm 2.4\%$  and  $19.4 \pm 1.4\%$ , respectively, displaying multinucleation. In contrast, nocodazole treatment resulted in fewer S235D mutant cells in mitosis ( $31.3 \pm 1.3\%$ ) and more multinucleation ( $41 \pm 2.2\%$ ). Increased multinucleation was also seen in untreated S235D mutant cells, compared with untreated empty vector and S235A mutant cells (Figure 7B), indicating that Aurora-A phosphorylation of p73 has a role in inactivating the SAC response. Furthermore, p73 phosphor cells were

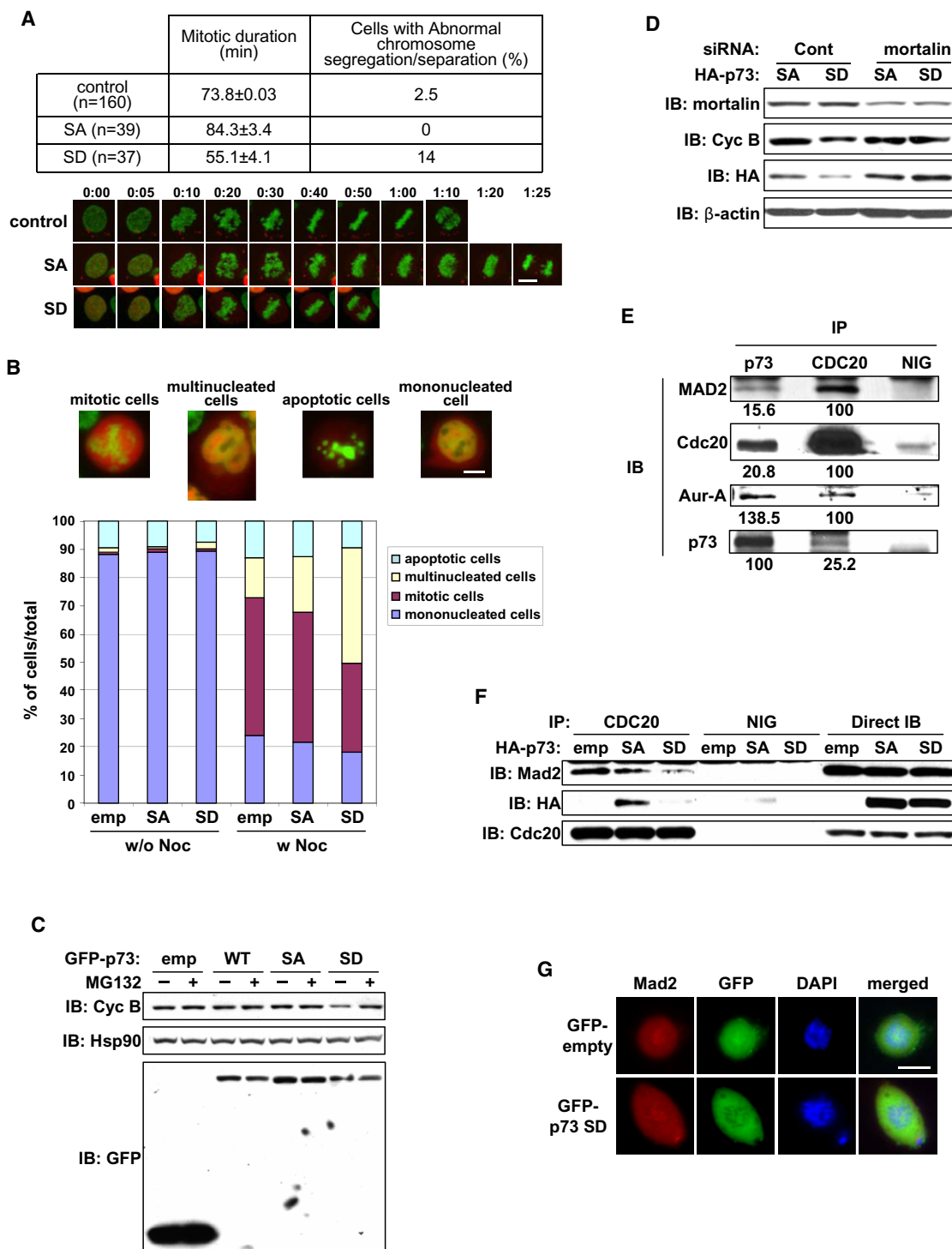


**Figure 7. Effects of Aurora-A Phosphorylated p73 on Mitosis and SAC Complex**

(A) HeLa/GFP-H2B cells were transfected with mCherry-p73α-SA or -SD mutant. Twenty-four hours later, cells were monitored by time-lapse microscopy using a low level of light intensity to determine the duration from nuclear envelope breakdown to anaphase. Mock-transfected cells were used as the control. The table represents mean mitotic durations ± SD and percentages of cells with defects in chromosome segregation or separation (top). Selected still frames from time-lapse microscopy of transfected cells at time intervals of minutes and seconds are shown (bottom). Scale bar corresponds to 10 μm.

(B) HeLa/GFP-H2B cells transfected with mCherry-empty vector, p73α-SA, or -SD mutant for 24 hr were cultured with (w Noc) or without (w/o Noc) nocodazole. Eighteen hours later, cells were fixed, and the fate of mCherry-positive cells was analyzed by fluorescence microscopy and quantified. The percentage values of cells in mitosis, with the indicated nuclear phenotypes from three independent experiments (n = 200), are shown. Scale bar corresponds to 10 μm.

treated with nocodazole, with or without MG132, a proteasome inhibitor that blocks E3 ubiquitin ligase anaphase-promoting complex/cyclosome (APC/C) involved in cyclin B1 degradation. Cyclin B1 levels in S235D mutant cells were lower than in empty vector and S235A mutant cells without MG132 but with MG132, cyclin B1 levels were similar in these cells, demonstrating that S235D mutant expression impairs nocodazole-induced mitotic arrest (Figure 7C). Nocodazole-treated p73-knockdown cells, however, had reduced cyclin B1 levels, compared with levels in control cells (Figure S5A).

We next investigated whether Aurora-A phosphorylation of p73 is a normal physiological event in cells with basal Aurora-A expression or an unnatural event in Aurora-A-overexpressing tumor cells. For the purpose, Aurora-A phosphorylation of p73 was evaluated in synchronized MCF-10A and Cos-1 at prophase; metaphase and anaphase stages. Western blotting of immunoprecipitated p73 with anti-phospho-PKA substrate antibody revealed that p73 phosphorylation progressively peaked at metaphase but was barely detectable in anaphase, when both amount and activity of Aurora-A were significantly reduced (Figure S5B). These findings indicate that Aurora-A phosphorylation of p73 has a role in regulating SAC during normal mitosis in cells with basal Aurora-A expression. It is conceivable that elevated Aurora-A expression weakens the SAC due to precocious phosphorylation of p73 in tumor cells. Interestingly, co-transfection of S235D mutant with mortalin siRNA failed to override mitotic arrest, as evident from the similar expression levels of cyclin B1 in control and mortalin siRNA transfected cells (Figure 7D), suggesting that silencing of mortalin can rescue phosphor-p73-mediated SAC inactivation.

Coimmunoprecipitation with anti-p73 and anti-CDC20 antibodies revealed complex formation of p73 with Mad2, CDC20, and Aurora-A (Figure 7E). Thus, we determined the effect of p73-S235D mutant expression on these protein-protein interactions in cells treated with nocodazole and MG132. Coimmunoprecipitation experiments with anti-CDC20 antibody revealed a marked reduction in the interaction of both S235D mutant and MAD2 with CDC20, compared with that in empty vector and S235A mutant cells, whereas BubR1's interaction with CDC20 was not affected in S235D mutant cells (Figure 7F; data not shown). Immunoprecipitation with BubR1 and MAD2 antibodies did not reveal the two proteins in the same complex from nocodazole-treated cell extracts (data not shown), indicating that the two checkpoint proteins form independent complexes with CDC20, as reported earlier (Fang, 2002). Immunofluorescence microscopy revealed that kinetochore-localized Mad2 is not affected by ectopic expression of S235D mutant

(Figure 7G). These results demonstrate that p73 is involved in the formation of a cytoplasmic ternary complex with MAD2 and CDC20. Aurora-A phosphorylation of p73 in this complex releases p73 and the inhibitory complex between MAD2 and CDC20, with the released CDC20 expected to facilitate activation of APC/C, leading to mitotic exit.

### Aurora-A Overexpressing Primary Pancreatic Cancer Shows High Cytoplasmic p73 Distribution

To determine whether cytoplasmic sequestration of p73, consequent to Aurora-A phosphorylation, is reflected in cytoplasmic p73 distribution in Aurora-A-overexpressing tumors, we performed immunohistochemical analyses of p73 and Aurora-A in two sets of primary human pancreatic cancer tissues—114 pancreatic ductal adenocarcinoma (PDAC) samples from M.D. Anderson and 20 from the University of Alabama at Birmingham (UAB). p53 localization was also determined because Aurora-A phosphor-mimetic p53-S215D mutant demonstrated cytoplasmic localization and preferential interaction with mortalin (Figures S2A and S3B). Fifty-one (44.7%) PDAC samples showed high Aurora-A expression. Cytoplasmic p73 staining was clearly detected, but positive cytoplasmic p53 staining was almost undetectable. Among 51 tumors, 37 (72.5%) had high cytoplasmic staining of p73 and 22 (43%) had nuclear staining of p53. Among the remaining 63 Aurora-A low tumors, only 18 (28.6%) had strong cytoplasmic p73 staining and 40 (63%) had nuclear p53 staining (Figure 8). These results reveal a relationship between Aurora-A expression and cytoplasmic p73 localization and between Aurora-A expression and nuclear p53 localization in primary PDAC tissue. A similar trend between Aurora-A expression and p73 distribution was also found in the UABCC tissue set (data not shown). Nuclear localized mutant p53 is reported in 50%–75% of PDAC; thus, the predominant p53 nuclear distribution was not unexpected. The relationship between high Aurora-A expression and low p53 nuclear staining suggests that Aurora-A overexpression is correlated with p53 gene mutations in PDAC, whereas p53-WT remains undetectable in the cytoplasm, possibly because of enhanced protein degradation after Aurora-A phosphorylation, as previously described (Katayama et al., 2004; Morton et al., 2010).

### DISCUSSION

Aurora-A overexpression is detected in various tumor types and confers resistance to chemotherapeutic drugs and irradiation (Zhou et al., 1998; Marumoto et al., 2002; Yang et al., 2006). We present evidence that the p73 tumor suppressor protein is a direct downstream target of Aurora-A, which influences cell

(C) 293T cells transfected for 24 hr with GFP-empty vector, p73 $\alpha$ -WT, -SA, or -SD mutant were cultured with nocodazole. Sixteen hours later, cells were grown with (+) or without (–) MG132 for 4 hr and subjected to immunoblotting with the indicated antibodies.

(D) HeLa/GFP-H2B cells transfected with control or mortalin siRNA for 24 hr were subsequently transfected with HA-p73 $\alpha$ -SA or -SD mutant expression constructs. Twelve hours later, cells were cultured with nocodazole for 18 hr and subjected to immunoblotting with the indicated antibodies.

(E) WCE from nocodazole-treated 293T cells were immunoprecipitated with normal IgG (NIG) or with anti-p73 or anti-CDC20 antibody. Immunoprecipitates were subjected to immunoblotting with the indicated antibodies.

(F) 293T cells transfected with the indicated expression constructs for 24 hr were incubated with nocodazole for 20 hr and then MG132 for 4 hr. Cells were subjected to immunoprecipitation with normal IgG (NIG) or anti-CDC20 antibody, followed by immunoblotting with the indicated antibodies.

(G) Saos-2 cells were transfected with the GFP-empty vector or GFP-p73 $\alpha$ -SD mutant construct. Twenty-four hours later, cells were immunostained with anti-Mad2 antibody (red) and counterstained for DNA with DAPI (blue). Scale bar corresponds to 10  $\mu$ m.

See also Figure S5.

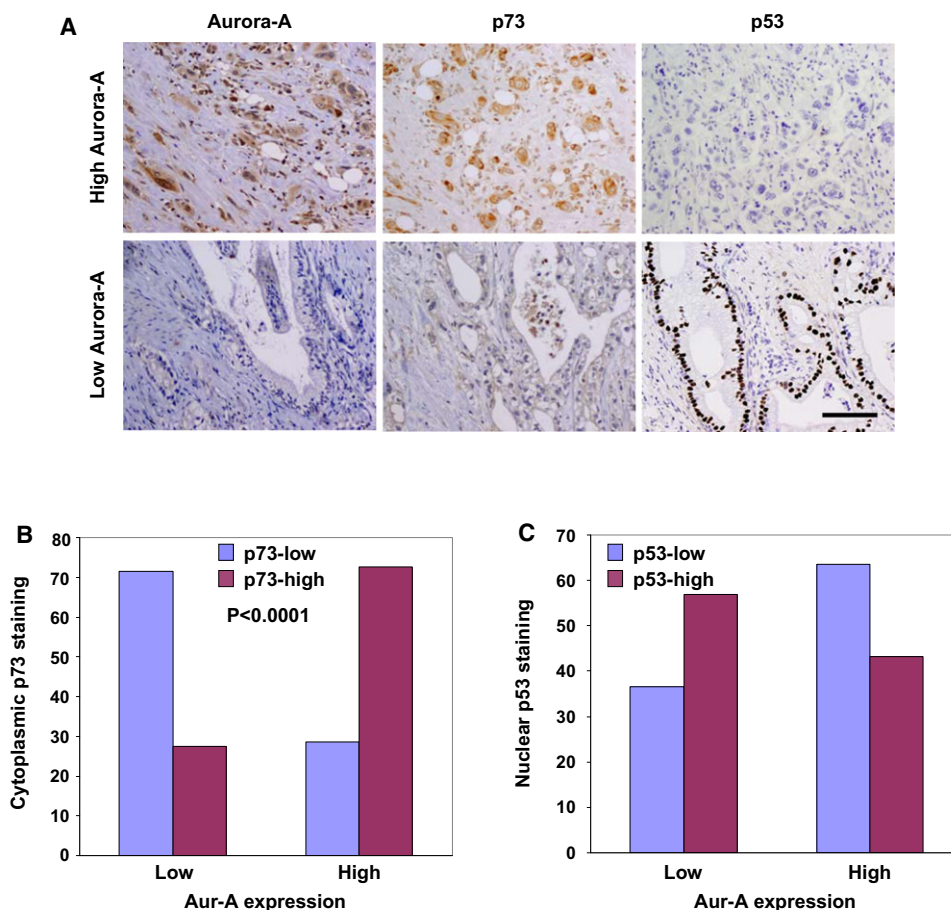


**Figure 8. Correlation of Aurora-A Expression Levels with p73 and p53 Localization in Human PDAC**

(A) Representative micrographs of PDAC tissues with varying levels of Aurora-A, p73, and p53 expression. Scale bar corresponds to 50  $\mu$ m.

(B and C) Bar graph representation of relative cytoplasmic p73 expression and nuclear p53 expression in relation to high or low Aurora-A expression in the tissue microarray containing 114 PDAC tissue samples. Aurora-A expression was correlated significantly with cytoplasmic p73 expression ( $p < 0.0001$ ). Nuclear p53 staining showed a trend towards being inversely correlated with the levels of Aurora-A expression in these PDAC tissue samples.

fate after chemotherapeutic drug-induced DNA and spindle damage in tumor cells. Aurora-A phosphorylation of p73 at serine 235 is critical in Aurora-A overexpression-mediated abrogation of apoptotic response and mitotic checkpoint override.

#### **Aurora-A Inhibits p73 and p53 Transactivation Functions through a Common Molecular Mechanism**

We, as well as others, have reported that Aurora-A phosphorylation of p53 compromises its apoptosis response function induced after cisplatin and irradiation treatment, whereas Aurora-A knockdown sensitizes cells to DNA damage-induced p53-dependent apoptosis (Katayama et al., 2004; Liu et al., 2004). The current findings reveal that Aurora-A phosphorylations abrogate DNA damage response functions of both p53 and p73 consequent to their interactions with mortalin and cytoplasmic sequestration. It also appears that, with progressively increasing Aurora-A kinase activity during mitosis, p53 and p73 remain localized in the cytoplasm coincidentally with nuclear envelope breakdown. Phosphorylation-mediated binding to mortalin, promoting nuclear exclusion of p53 and p73, may be common in tumor cells (Walker et al., 2006; Walker and Böttger,

2008) and consistent with the earlier observations that p53-binding domain on mortalin (Kaul et al., 2001) negatively regulates transcriptional activity, inhibits nuclear translocation of p53, and abolishes p53-dependent suppression of centrosome duplication (Wadhwa et al., 1998; Walker et al., 2006; Ma et al., 2006). Because the mortalin-binding domain of p53 at its C terminus (Kaul et al., 2001; Wadhwa et al., 2002) is not conserved in p73, it is worth investigating whether Aurora-A phosphorylation of p53 and p73 creates a mortalin-binding site or recruits a mortalin interaction factor in a phosphorylation-dependent manner. Complex formation between mortalin and p53 has been detected in the mitochondria during p53-induced apoptosis, with and without DNA damage (Marchenko et al., 2000), implicating involvement of mortalin-p53 complex in the transactivation-independent apoptotic signaling pathway. However, the molecular mechanisms regulating activation of this pathway remains to be elucidated. WWOX, a putative tumor suppressor protein, interacts with p53 and p73, regulating their subcellular distribution and apoptosis response functions elicited in mitochondria (Chang et al., 2003; Chang et al., 2005; Aqeilan et al., 2004). On the basis of the current findings, it

may be suggested that Aurora-A phosphorylation-induced mortalin binding influences interactions of p53 and p73 with WWOX and/or proapoptotic mitochondria proteins. Further investigation is needed to understand these pathways.

### Molecular Mechanism of Aurora-A-Mediated Inactivation of Mitotic SAC Function of p73

Aurora-A overexpression has been shown to override mitotic SAC and induce aberrant chromosome segregation, resulting in aneuploidy (Anand et al., 2003). However, the underlying molecular mechanism of this effect has remained unclear. We found that p73 was involved in the inhibitory mitotic checkpoint complex of Mad2 and CDC20, preventing activation of the E3 ubiquitin ligase APC/C, and that Aurora-A phosphorylation of p73 caused dissociation of the Mad2-CDC20 complex, facilitating mitotic exit. Because p73 is detected in large macromolecular complexes including mortalin, further studies are needed to determine their functional significance in the regulation of the Mad2-CDC20 containing SAC complex.

We observed no specific localization of WT or phosphor-mimetic p73 mutants at the mitotic apparatuses or an effect of phosphor-mimetic mutant on Mad2 mislocalizations at the kinetochore. However, immunostaining with anti-p73 antibody revealed cytoplasmic and mitotic spindle p73 localization. Mitotic SAC generates a diffusible wait signal at microtubule-unattached kinetochores that inhibits CDC20-mediated APC activation. MAD2 and BubR1 are the two most critical proteins of this signal (Shah et al., 2004; Peters, 2006), which form separate inactive complexes with CDC20 (Fang, 2002). Although evidence suggests that the soluble MAD2-CDC20 complex acts as a transient precursor to the BubR1-CDC20 inhibitory complex (Kulukian et al., 2009), the exact mechanism is still not well understood. Failure of BubR1 to rescue SAC dysfunction in cells expressing a mutant CDC20 allele that does not bind MAD2 (Li et al., 2009) clearly illustrates a critical, nonredundant role of Mad2 in SAC activation. Aurora-A phosphorylation of p73 dissociated the MAD2-CDC20 complex, providing evidence that Aurora-A negatively regulates a critical step in the SAC activation pathway. Unlike its effect on Mad2-CDC20 interaction, phosphor-mimetic mutant p73 did not affect the interaction of BubR1 with CDC20. Progressively increasing Aurora-A phosphorylation of p73 from prophase through metaphase, followed by a sharp decline at anaphase and telophase in synchronized nontumorigenic MCF-10A cells, with basal Aurora-A expression, suggests that this phosphorylation has a role in inactivating SAC during the metaphase–anaphase transition of normal mitosis. Constitutively phosphorylated p73-expressing cells underwent an early transition to anaphase and overrode the mitotic checkpoint, indicating that Aurora-A-overexpressing cells are predisposed to abrogate the checkpoint response because of precocious p73 phosphorylation. Our findings do not reveal how this phosphorylation is temporally regulated to coincide with SAC inactivation after chromosome biorientation in normal mitosis. Structural studies have revealed that an open conformation of MAD2 prevents association with MAD1 or CDC20 (Musacchio and Hardwick, 2002). Thus, it will be interesting to determine whether Mad2-bound p73 phosphorylation induces open conformation changes in the latter, leading to its dissociation from CDC20. Our findings indicate that p73 is a critical regulator of the cytoplasmic

MAD2-CDC20 checkpoint protein complex. Additional studies are required to unravel the details of these molecular interactions.

p73-deficient mice have a high incidence of spontaneous tumors (Tomasini et al., 2008) and loss of function is correlated with induction of chromosomal instability (Talos et al., 2007). Evidence supports a role for p73 in mitosis (Fulco et al., 2003; Merlo et al., 2005), including SAC regulation (Tomasini et al., 2009). Thus, p73 plays an important role in faithful chromosome segregation and maintenance of genomic stability. p73 is up-regulated during the transformation process in response to aberrant Rb pathway expression, and a genetic alteration with a dominant negative effect is required to block tumor suppressor function of p73. Published data indicate that overexpression of the dominant negative p73 protein  $\Delta$ Np73 compromises tumor suppressor function of p73 in premalignant stages (Oswald and Stiewe, 2008).  $\Delta$ Np73 overexpression may disrupt the stochastic balance of Aurora-A-mediated p73 SAC function because the two isoforms, despite forming a heterotetramer, do not share the predominant site of Aurora-A phosphorylation in p73.

Our findings demonstrate that elevated Aurora-A expression, a common oncogenic event in human cancers, has the dominant negative effect of inactivating p73 function through increased phosphorylation of the protein sequestered in the cytoplasm. The positive correlation between Aurora-A overexpression and cytoplasmic p73 localization in human pancreatic cancer tissue corroborate the experimental findings and indicates that these tumors have weakened or inactivated DNA and spindle damage-induced apoptosis and SAC pathways, making them refractory to conventional radiation and chemotherapeutic regimens. Detailed analyses of p73 phosphorylation profiles of these tumors together with chemosensitivities and radiosensitivities would help resolve the issue and future design of appropriately targeted therapies.

In conclusion, we uncovered a signaling pathway of Aurora-A–p73 axis in which Aurora-A phosphorylation inactivates p73 function in both DNA damage-induced cell death and mitotic SAC pathways. Further in-depth studies of Aurora-A involvement in both signaling pathways will improve our understanding of oncogenic function of Aurora-A in cancer biology and help us develop more effective strategies for cancer prevention and treatment.

### EXPERIMENTAL PROCEDURES

All cell lines were obtained from ATCC. Immunohistochemical staining for Aurora-A, p73, and p53 was performed on 4- $\mu$ m unstained sections from tissue microarray blocks consisting of 114 PDAC and 20 pancreatic tumor tissues from patients who had undergone pancreaticoduodenectomy at M.D. Anderson and UAB, respectively. The studies were approved by both institutional review boards.

Detailed experimental procedures are available in the [Supplemental Experimental Procedures](#).

### Transfection, Luciferase Assay, and siRNA

For transfection, Fugene 6 transfection reagent (Roche), oligofectamine, and lipofectamine 2000 (Invitrogen) were used according to manufacturer's instructions. For luciferase assays, H1299 or Saos-2 cells were cotransfected with the same amount of WT or mutant pEGFPp73 $\alpha$  (100–200 ng), luciferase reporter construct (100 ng), and internal control Renilla luciferase expression plasmid (10 ng), with or without increasing amounts of Flag-Aurora-A WT or KD expression plasmids. The total amount of plasmid DNA was kept

constant (1  $\mu$ g) at pcDNA3. We measured luciferase activities 24 hr after transfection using a dual-luciferase reporter assay kit (Promega). The siRNA sequences were as follows: p73, 5'-CGGAUUCAGCAUGGACGdTdT-3' (Basu et al., 2003); mortalin, 5'-CCGUCUCUGUGGGCGCCGAdTdT-3' (Ma et al., 2006). Additional siRNAs for both genes from Santa-Cruz Biotechnology (Catalog Nos. sc-35520 for mortalin and sc-36167 for p73) were also used.

#### Cell Fractionation, Cross-Linking Assay, In Vitro Kinase Assay, Semiquantitative RT-PCR, Immunoprecipitation, Western Blotting, and Immunofluorescence Microscopy

Biochemical protein fractionation of cells was performed according to the manufacturer's protocol (Pierce). Whole cell extracts were prepared in RIPA buffer. All other experimental procedures, conditions, and primer sequences for semiquantitative RT-PCR have been described (Kawai et al., 2007; Katayama et al., 2007, 2008; Li et al., 2007).

#### EMSA

p73 proteins, produced by an in vitro transcription and translation kit (Promega), were incubated with <sup>32</sup>P-labeled p21 probe containing the p53 DNA-binding site (5'-TACAGAACATGTCTAAGCATGCTGGGG-3') in the binding buffer (20 mM HEPES, pH 7.9, 1 mM MgCl<sub>2</sub>, 10  $\mu$ M ZnCl<sub>2</sub>, 1 mM DTT, 5% glycerol, 670 ng/ $\mu$ l BSA, and 0.5  $\mu$ g/ $\mu$ l poly(dI-dC) at room temperature for 20 min. For the competition assay, 1  $\mu$ g of unlabeled probe was added to the reaction. The protein-DNA complexes were resolved by electrophoresis through 4.5% polyacrylamide gel at 4°C.

#### $\lambda$ PPase Treatment

Whole cell extracts were incubated with 20 units of  $\lambda$ PPase (New England Biolabs) or glycerol (solvent) in the supplemented buffer for 30 min at 30°C. The reaction was terminated by adding SDS sample buffer and subjected to SDS-PAGE.

#### Gel Filtration Column Chromatography

Gel filtration column chromatography was carried out as described previously (Samanta et al., 2010). In brief, 3 mg of whole cell extracts prepared in column elution buffer (30 mM HEPES, pH 7.4, containing 150 mM NaCl and 10% glycerol, and 0.5% NP-40, 1  $\mu$ M microcystin LR, protease inhibitor cocktail [Roche]) were loaded on the column packed with Superose 6 prep grade gel (GE Healthcare), and 500  $\mu$ l of elution was collected in each fraction. Equal volumes of eluted fractions were subjected to immunoblotting. The mixture of protein markers containing keyhole limpet hemocyanin (KLH; MW 8.5 million Da), blue dextran (MW 2 million Da),  $\beta$ -amylase (MW 200 kDa), BSA (MW 66 kDa), and cytochrome C (MW 12.4 kDa) was used as the MW standard.

#### Time-Lapse Microscopy

We performed time-lapse microscopy using a Perkin Elmer UltraVIEW ERS spinning disc confocal microscope equipped with an environmental control chamber that maintained the cells at 37°C in a humidified stream of 5% CO<sub>2</sub>. Individually tagged image format files were imported into Photoshop (Adobe) for analysis.

#### Colony Formation Assay and Drug Treatment

Saos-2 cells (transfected with pEGFP-empty vector, WT, and mutants of pEGFP-p73 $\alpha$ ) were cultured in media containing 200  $\mu$ g/ml of G418 for 3 weeks and stained with crystal violet. Colonies of 1 mm diameter were counted. H1299 cells transfected for 24 hr were treated with cisplatin at 50  $\mu$ M for 24 hr and 36 hr. Annexin V-FITC assay was performed according to the manufacturer's protocol (BD Pharmingen). Nocodazole was used at 50 ng/ml for GFP-H2B HeLa, 350 ng/ml for 293T, 500 ng/ml for MCF-7 and Panc-1, and 1  $\mu$ g/ml for Cos-1 cells. Aurora-A inhibitor MLN8054 was used at 0.5  $\mu$ M with or without 20  $\mu$ M of MG132 for 4–6 hr.

#### SUPPLEMENTAL INFORMATION

Supplemental Information includes five figures and Supplemental Experimental Procedures and can be found with this article online at doi:10.1016/j.ccr.2011.12.025.

#### ACKNOWLEDGMENTS

The authors thank Dr. Zhi-Min Yuan for the GFP-tagged p73 expression construct and luciferase reporter constructs, Dr. Elsa Flores for the HA-tagged p73 expression constructs, Dr. Kenji Fukasawa for the mortalin expression constructs, Dr. Richard Behringer for the mCherry vector, and Dr. Mei Leng for the GFP-H2B-expressing HeLa cells. We acknowledge the technical assistance of Ms. Yvette Gonzales and Ms. Aimee LeBlanc. Editorial help of Ms Amy Sutton from the Department of Scientific Publications is acknowledged. This study was supported by grants awarded to S.S. from the National Institutes of Health (R01CA089716 and NCI/EDRN UO1CA111302), the University Cancer Foundation, and the M.D. Anderson Cancer Center. The DNA analysis facility used in the study is supported by Cancer Center Support Grant CA16672. UAB Pancreatic SPORE (5P50CA0101955) supported W.E.G. and J.A.M.

Received: March 11, 2010

Revised: September 21, 2011

Accepted: December 23, 2011

Published: February 13, 2012

#### REFERENCES

- Anand, S., Penrhyn-Lowe, S., and Venkitaraman, A.R. (2003). AURORA-A amplification overrides the mitotic spindle assembly checkpoint, inducing resistance to Taxol. *Cancer Cell* 3, 51–62.
- Aqeilan, R.I., Pekarsky, Y., Herrero, J.J., Palamarchuk, A., Letofsky, J., Druck, T., Trapasso, F., Han, S.Y., Melino, G., Huebner, K., and Croce, C.M. (2004). Functional association between Wwox tumor suppressor protein and p73, a p53 homolog. *Proc. Natl. Acad. Sci. USA* 101, 4401–4406.
- Basu, S., Totty, N.F., Irwin, M.S., Sudol, M., and Downward, J. (2003). Akt phosphorylates the Yes-associated protein, YAP, to induce interaction with 14-3-3 and attenuation of p73-mediated apoptosis. *Mol. Cell* 11, 11–23.
- Chang, N.S., Doherty, J., Ensign, A., Lewis, J., Heath, J., Schultz, L., Chen, S.T., and Oppermann, U. (2003). Molecular mechanisms underlying WOX1 activation during apoptotic and stress responses. *Biochem. Pharmacol.* 66, 1347–1354.
- Chang, N.S., Doherty, J., Ensign, A., Schultz, L., Hsu, L.J., and Hong, Q. (2005). WOX1 is essential for tumor necrosis factor-, UV light-, staurosporine-, and p53-mediated cell death, and its tyrosine 33-phosphorylated form binds and stabilizes serine 46-phosphorylated p53. *J. Biol. Chem.* 280, 43100–43108.
- Dar, A.A., Belkhir, A., Ecsedy, J., Zaika, A., and El-Rifai, W. (2008). Aurora kinase A inhibition leads to p73-dependent apoptosis in p53-deficient cancer cells. *Cancer Res.* 68, 8998–9004.
- Deocaris, C.C., Widodo, N., Ishii, T., Kaul, S.C., and Wadhwa, R. (2007). Functional significance of minor structural and expression changes in stress chaperone mortalin. *Ann. N Y Acad. Sci.* 1119, 165–175.
- Ewart-Toland, A., Briassoulis, P., de Koning, J.P., Mao, J.H., Yuan, J., Chan, F., MacCarthy-Morrogh, L., Ponder, B.A., Nagase, H., Burn, J., et al. (2003). Identification of Stk6/STK15 as a candidate low-penetrance tumor-susceptibility gene in mouse and human. *Nat. Genet.* 34, 403–412.
- Fang, G. (2002). Checkpoint protein BubR1 acts synergistically with Mad2 to inhibit anaphase-promoting complex. *Mol. Biol. Cell* 13, 755–766.
- Fulco, M., Costanzo, A., Merlo, P., Mangiacasale, R., Strano, S., Blandino, G., Balsano, C., Lavia, P., and Levrero, M. (2003). p73 is regulated by phosphorylation at the G2/M transition. *J. Biol. Chem.* 278, 49196–49202.
- Katayama, H., Sasai, K., Kawai, H., Yuan, Z.M., Bondaruk, J., Suzuki, F., Fujii, S., Arlinghaus, R.B., Czerniak, B.A., and Sen, S. (2004). Phosphorylation by aurora kinase A induces Mdm2-mediated destabilization and inhibition of p53. *Nat. Genet.* 36, 55–62.
- Katayama, H., Sasai, K., Czerniak, B.A., Carter, J.L., and Sen, S. (2007). Aurora-A kinase phosphorylation of Aurora-A kinase interacting protein (AIP) and stabilization of the enzyme-substrate complex. *J. Cell. Biochem.* 102, 1318–1331.

- Katayama, H., Sasai, K., Kloc, M., Brinkley, B.R., and Sen, S. (2008). Aurora kinase-A regulates kinetochore/chromatin associated microtubule assembly in human cells. *Cell Cycle* 7, 2691–2704.
- Kaul, S.C., Reddel, R.R., Mitsui, Y., and Wadhwa, R. (2001). An N-terminal region of mot-2 binds to p53 in vitro. *Neoplasia* 3, 110–114.
- Kawai, H., Lopez-Pajares, V., Kim, M.M., Wiederschain, D., and Yuan, Z.M. (2007). RING domain-mediated interaction is a requirement for MDM2's E3 ligase activity. *Cancer Res.* 67, 6026–6030.
- Kulukian, A., Han, J.S., and Cleveland, D.W. (2009). Unattached kinetochores catalyze production of an anaphase inhibitor that requires a Mad2 template to prime Cdc20 for BubR1 binding. *Dev. Cell* 16, 105–117.
- Li, D., Zhu, J., Firozi, P.F., Abbruzzese, J.L., Evans, D.B., Cleary, K., Friess, H., and Sen, S. (2003). Overexpression of oncogenic STK15/BTAK/Aurora A kinase in human pancreatic cancer. *Clin. Cancer Res.* 9, 991–997.
- Li, M., Fang, X., Wei, Z., York, J.P., and Zhang, P. (2009). Loss of spindle assembly checkpoint-mediated inhibition of Cdc20 promotes tumorigenesis in mice. *J. Cell Biol.* 185, 983–994.
- Li, X., Lee, Y.K., Jeng, J.C., Yen, Y., Schultz, D.C., Shih, H.M., and Ann, D.K. (2007). Role for KAP1 serine 824 phosphorylation and sumoylation/desumoylation switch in regulating KAP1-mediated transcriptional repression. *J. Biol. Chem.* 282, 36177–36189.
- Liu, Q., Kaneko, S., Yang, L., Feldman, R.I., Nicosia, S.V., Chen, J., and Cheng, J.Q. (2004). Aurora-A abrogation of p53 DNA binding and transactivation activity by phosphorylation of serine 215. *J. Biol. Chem.* 279, 52175–52182.
- Ma, Z., Izumi, H., Kanai, M., Kabuyama, Y., Ahn, N.G., and Fukasawa, K. (2006). Mortalin controls centrosome duplication via modulating centrosomal localization of p53. *Oncogene* 25, 5377–5390.
- Macûrek, L., Lindqvist, A., Lim, D., Lampson, M.A., Klompmaker, R., Freire, R., Clouin, C., Taylor, S.S., Yaffe, M.B., and Medema, R.H. (2008). Polo-like kinase-1 is activated by aurora A to promote checkpoint recovery. *Nature* 455, 119–123.
- Marchenko, N.D., Zaika, A., and Moll, U.M. (2000). Death signal-induced localization of p53 protein to mitochondria. A potential role in apoptotic signaling. *J. Biol. Chem.* 275, 16202–16212.
- Marumoto, T., Hirota, T., Morisaki, T., Kunitoku, N., Zhang, D., Ichikawa, Y., Sasayama, T., Kuninaka, S., Mimori, T., Tamaki, N., et al. (2002). Roles of aurora-A kinase in mitotic entry and G2 checkpoint in mammalian cells. *Genes Cells* 7, 1173–1182.
- Marumoto, T., Zhang, D., and Saya, H. (2005). Aurora-A - a guardian of poles. *Nat. Rev. Cancer* 5, 42–50.
- Merlo, P., Fulco, M., Costanzo, A., Mangiacasale, R., Strano, S., Blandino, G., Taya, Y., Lavia, P., and Levrero, M. (2005). A role of p73 in mitotic exit. *J. Biol. Chem.* 280, 30354–30360.
- Morton, J.P., Timpson, P., Karim, S.A., Ridgway, R.A., Athineos, D., Doyle, B., Jamieson, N.B., Oien, K.A., Lowy, A.M., Brunton, V.G., et al. (2010). Mutant p53 drives metastasis and overcomes growth arrest/senescence in pancreatic cancer. *Proc. Natl. Acad. Sci. USA* 107, 246–251.
- Musacchio, A., and Hardwick, K.G. (2002). The spindle checkpoint: structural insights into dynamic signalling. *Nat. Rev. Mol. Cell Biol.* 3, 731–741.
- Oswald, C., and Stiewe, T. (2008). In good times and bad: p73 in cancer. *Cell Cycle* 7, 1726–1731.
- Ouchi, M., Fujiuchi, N., Sasai, K., Katayama, H., Minamishima, Y.A., Ongusaha, P.P., Deng, C., Sen, S., Lee, S.W., and Ouchi, T. (2004). BRCA1 phosphorylation by Aurora-A in the regulation of G2 to M transition. *J. Biol. Chem.* 279, 19643–19648.
- Peters, J.M. (2006). The anaphase promoting complex/cyclosome: a machine designed to destroy. *Nat. Rev. Mol. Cell Biol.* 7, 644–656.
- Plotnikova, O.V., Pugacheva, E.N., and Golemis, E.A. (2011). Aurora A kinase activity influences calcium signaling in kidney cells. *J. Cell Biol.* 193, 1021–1032.
- Samanta, A.K., Chakraborty, S.N., Wang, Y., Schlette, E., Reddy, E.P., and Arlinghaus, R.B. (2010). Destabilization of Bcr-Abl/Jak2 Network by a Jak2/Abl Kinase Inhibitor ON044580 Overcomes Drug Resistance in Blast Crisis Chronic Myelogenous Leukemia (CML). *Genes Cancer* 1, 346–359.
- Seki, A., Coppinger, J.A., Jang, C.Y., Yates, J.R., and Fang, G. (2008). Bora and the kinase Aurora a cooperatively activate the kinase Plk1 and control mitotic entry. *Science* 320, 1655–1658.
- Sen, S., Zhou, H., and White, R.A. (1997). A putative serine/threonine kinase encoding gene BTAK on chromosome 20q13 is amplified and overexpressed in human breast cancer cell lines. *Oncogene* 14, 2195–2200.
- Shah, J.V., Botvinick, E., Bonday, Z., Furnari, F., Berns, M., and Cleveland, D.W. (2004). Dynamics of centromere and kinetochore proteins; implications for checkpoint signaling and silencing. *Curr. Biol.* 14, 942–952.
- Talos, F., Nemajero, A., Flores, E.R., Petrenko, O., and Moll, U.M. (2007). p73 suppresses polyploidy and aneuploidy in the absence of functional p53. *Mol. Cell* 27, 647–659.
- Tomasini, R., Tsuchihara, K., Wilhelm, M., Fujitani, M., Rufini, A., Cheung, C.C., Khan, F., Itie-Youten, A., Wakeham, A., Tsao, M.S., et al. (2008). TAp73 knockout shows genomic instability with infertility and tumor suppressor functions. *Genes Dev.* 22, 2677–2691.
- Tomasini, R., Tsuchihara, K., Tsuda, C., Lau, S.K., Wilhelm, M., Ruffini, A., Tsao, M.S., Iovanna, J.L., Jurisicova, A., Melino, G., and Mak, T.W. (2009). TAp73 regulates the spindle assembly checkpoint by modulating BubR1 activity. *Proc. Natl. Acad. Sci. USA* 106, 797–802.
- Vernole, P., Neale, M.H., Barcaroli, D., Munarriz, E., Knight, R.A., Tomasini, R., Mak, T.W., Melino, G., and De Laurenzi, V. (2009). TAp73alpha binds the kinetochore proteins Bub1 and Bub3 resulting in polyploidy. *Cell Cycle* 8, 421–429.
- Wadhwa, R., Takano, S., Robert, M., Yoshida, A., Nomura, H., Reddel, R.R., Mitsui, Y., and Kaul, S.C. (1998). Inactivation of tumor suppressor p53 by mot-2, a hsp70 family member. *J. Biol. Chem.* 273, 29586–29591.
- Wadhwa, R., Yaguchi, T., Hasan, M.K., Mitsui, Y., Reddel, R.R., and Kaul, S.C. (2002). Hsp70 family member, mot-2/mthsp70/GRP75, binds to the cytoplasmic sequestration domain of the p53 protein. *Exp. Cell Res.* 274, 246–253.
- Walker, C., Böttger, S., and Low, B. (2006). Mortalin-based cytoplasmic sequestration of p53 in a nonmammalian cancer model. *Am. J. Pathol.* 168, 1526–1530.
- Walker, C.W., and Böttger, S.A. (2008). A naturally occurring cancer with molecular connectivity to human diseases. *Cell Cycle* 7, 2286–2289.
- Yang, H., He, L., Kruk, P., Nicosia, S.V., and Cheng, J.Q. (2006). Aurora-A induces cell survival and chemoresistance by activation of Akt through a p53-dependent manner in ovarian cancer cells. *Int. J. Cancer* 119, 2304–2312.
- Zhou, H., Kuang, J., Zhong, L., Kuo, W.L., Gray, J.W., Sahin, A., Brinkley, B.R., and Sen, S. (1998). Tumour amplified kinase STK15/BTAK induces centrosome amplification, aneuploidy and transformation. *Nat. Genet.* 20, 189–193.

# TEM8/ANTXR1 Blockade Inhibits Pathological Angiogenesis and Potentiates Tumoricidal Responses against Multiple Cancer Types

Amit Chaudhary,<sup>1</sup> Mary Beth Hilton,<sup>1,2</sup> Steven Seaman,<sup>1</sup> Diana C. Haines,<sup>3</sup> Susan Stevenson,<sup>4</sup> Peter K. Lemotte,<sup>4</sup> William R. Tschantz,<sup>4</sup> Xiaoyan M. Zhang,<sup>4,5</sup> Saurabh Saha,<sup>4,5</sup> Tony Fleming,<sup>4</sup> and Brad St. Croix<sup>1,\*</sup>

<sup>1</sup>Tumor Angiogenesis Section, Mouse Cancer Genetics Program, National Cancer Institute (NCI), National Institutes of Health (NIH), Frederick, MD 21702, USA

<sup>2</sup>Basic Research Program

<sup>3</sup>Veterinary Pathology Section, Pathology/Histotechnology Laboratory  
Science Applications International Corporation (SAIC), NCI, NIH, Frederick, MD 21702, USA

<sup>4</sup>Novartis Institutes for BioMedical Research, Cambridge, MA 02139, USA

<sup>5</sup>Present address: BioMed Valley Discoveries, Kansas City, MO 64111, USA

\*Correspondence: [stcroix@ncifcrf.gov](mailto:stcroix@ncifcrf.gov)

DOI 10.1016/j.ccr.2012.01.004

## SUMMARY

Current antiangiogenic agents used to treat cancer only partially inhibit neovascularization and cause normal tissue toxicities, fueling the need to identify therapeutic agents that are more selective for pathological angiogenesis. Tumor endothelial marker 8 (TEM8), also known as anthrax toxin receptor 1 (ANTXR1), is a highly conserved cell-surface protein overexpressed on tumor-infiltrating vasculature. Here we show that genetic disruption of *Tem8* results in impaired growth of human tumor xenografts of diverse origin including melanoma, breast, colon, and lung cancer. Furthermore, antibodies developed against the TEM8 extracellular domain blocked anthrax intoxication, inhibited tumor-induced angiogenesis, displayed broad antitumor activity, and augmented the activity of clinically approved anticancer agents without added toxicity. Thus, TEM8 targeting may allow selective inhibition of pathological angiogenesis.

## INTRODUCTION

Solid tumors have an insidious ability to nourish their own expansive growth by evoking the sprouting of new blood vessels, or angiogenesis, from nearby vessels of neighboring nonmalignant tissues. Upon vascularization, tumor blood vessels supply tumor cells with vital oxygen and nutrients needed to support their continued growth, and provide a key escape route for metastasis. Due to their critical role in promoting tumor growth and metastasis, tumor blood vessels have become a major target of current anticancer therapy (Kerbel, 2008). Vascular endothelial growth factor (VEGF) and its receptor, VEGFR2, represent the most advanced targets of current antiangiogenic therapy,

and agents that target the VEGF/VEGFR2 axis have been clinically approved to treat patients with colon, lung, brain, and kidney cancer (Brastianos and Batchelor, 2010; Kerbel, 2008). Although therapies targeting VEGF/VEGFR2 have improved the efficacy of current anticancer treatment strategies, angiogenesis is seldom completely halted, and both angiogenesis and tumor growth inevitably progress in the face of continued therapy. Furthermore, in addition to its well-known role in physiological angiogenesis of the adult, for example, during menstruation, ovulation, and wound healing, VEGF is also widely expressed in nonangiogenic normal adult tissues, where it plays critical roles in normal adult physiology (Maharaj and D'Amore, 2007). For example, it is required for normal kidney filtration (Eremina

## Significance

Inhibiting angiogenesis has become an important adjunct to traditional anticancer therapy, but current antiangiogenic agents, including VEGF/VEGFR2 pathway inhibitors, disrupt normal physiological processes and are associated with an increasing number of adverse side effects. TEM8 is an appealing target for selective inhibition of tumor angiogenesis because it is functionally required for optimal tumor angiogenesis and growth but dispensable for normal development and physiological angiogenesis. Function-blocking antibodies specific to the extracellular domain of TEM8 blocked pathological angiogenesis and tumor growth and augmented the activity of various classes of anticancer agents, including VEGFR inhibitors. Thus, targeting TEM8 on tumor vasculature may provide opportunities for the selective blockade of cancer and other diseases dependent on pathological angiogenesis.

et al., 2006), preventing neural degeneration (Oosthuysen et al., 2001), and maintaining functional hematopoietic, endocrine, and skeletal systems (Sung et al., 2010). Given the pleiotropic activities of the VEGF pathway, it is not surprising that anti-VEGF/VEGFR2 therapies are associated with a number of toxicities, such as hypertension, proteinuria, hypothyroidism, diarrhea, deep vein thromboses, fatigue, and surgical wound healing complications (Verheul and Pinedo, 2007). VEGF-blocking agents have also been associated with some rare, more serious, side effects including life-threatening thromboembolic events and severe bleeding complications (Chen and Cleck, 2009; Verheul and Pinedo, 2007). Antiangiogenic therapies need to be administered for months to years and may eventually prove useful in long-term adjuvant therapy for the prevention of recurrent disease, raising further concerns about long-term toxicities. Thus, drugs that can selectively target pathological host vasculature with minimal side effects are urgently needed.

Tumor endothelial marker 8 (TEM8) is a highly conserved single-pass cell-surface glycoprotein that was originally identified based on its overexpression in the endothelial cells (ECs) that line the tumor vasculature of human colorectal cancer (St. Croix et al., 2000). Although our understanding of its physiological function is limited, TEM8 has been found to bind to collagens and promote migration of ECs in vitro (Nanda et al., 2004; Werner et al., 2006). TEM8 was also identified as an anthrax toxin receptor (ANTXR1) (Bradley et al., 2001), and it shares 58% amino acid identity with CMG2, a second receptor for anthrax toxin protein (ANTXR2) (Scobie et al., 2003). TEM8 is upregulated on tumor vessels of various tumor types in both mice and humans (Carson-Walter et al., 2001; Fernando and Fletcher, 2009; Nanda et al., 2004), and in some tumors is also expressed by the tumor cells themselves (Carson-Walter et al., 2001; Jinnin et al., 2008; Yang et al., 2011b). TEM8 was unique among the original TEMs identified in that it could not be detected in the angiogenic corpus luteum of human ovaries (Nanda et al., 2004; St. Croix et al., 2000), and developmental angiogenesis and wound healing are unperturbed in *Tem8* knockout (KO) mice (Cullen et al., 2009). Indeed, aside from misaligned incisors, adult *Tem8* KO mice are overtly normal in appearance. However, murine B16 melanoma tumor growth was impaired in *Tem8* KO versus wild-type mice, demonstrating that host-derived TEM8 can promote tumor growth on an immunocompetent background (Cullen et al., 2009). Furthermore, previous studies have shown that a soluble TEM8-Fc trap, TEM8 vaccines, or sublethal doses of anthrax toxin can inhibit angiogenesis, slow tumor growth, and prolong survival (Duan et al., 2007; Felicetti et al., 2007; Liu et al., 2008; Rouleau et al., 2008; Ruan et al., 2009; Yang et al., 2010). Taken together, these studies suggest that TEM8 may be required for tumor angiogenesis but not physiological angiogenesis. Here we sought to develop anti-TEM8 antibodies that can block TEM8 function in an effort to selectively block pathological angiogenesis.

## RESULTS

### TEM8 Functions in Pathological but Not Physiological Angiogenesis

To obtain further evidence that TEM8 is selectively associated with pathological angiogenesis, we compared the *Tem8* expres-

sion pattern between tumor ECs and adult regenerating liver ECs. Following 70% partial hepatectomy, the remaining liver grows rapidly in a highly regulated angiogenesis-dependent process (Drixler et al., 2002; Seaman et al., 2007). In this model, quiescent ECs enter the cell cycle synchronously at around 24 hr postsurgery and cease proliferation about 72 hr later. To examine gene expression, we performed quantitative RT-PCR (QPCR) on ECs purified from tumor xenografts derived from DLD1, HCT116, or LS174T cells, or ECs isolated from quiescent resting liver (0 hr) or regenerating liver taken at various postsurgical time points (6, 18, 48, 72, or 96 hr). Although markers of proliferation, such as *Ki67*, protein regulator of cytokinesis 1 (*Prc1*), and thymidine kinase (*TK*) were highly induced in liver ECs by 48 hr postpartial hepatectomy, *Tem8* expression levels remained baseline in regenerating liver ECs. In contrast, *Tem8* was expressed 32- to 55-fold higher in each of the tumor EC fractions compared to resting liver ECs (Figure 1A). The peak expression levels of the cell-cycle genes in regenerating liver ECs were higher than that in tumor ECs, presumably because of the synchronous nature of the proliferating liver EC population.

To investigate whether *Tem8* is expressed by tumor-associated inflammatory cells, such as CD11b<sup>+</sup> myeloid cells or other bone marrow-derived cells that have been shown to promote tumor angiogenesis and may be involved in the refractoriness of tumors to VEGF inhibition (Du et al., 2008; Shojaei et al., 2007), we examined its expression in CD45<sup>+</sup> (pan hematopoietic), CD11b<sup>+</sup> (myeloid), and CD105<sup>+</sup> (endothelial) cells isolated from tumors. *Tem8* was highly expressed only in the endothelial fraction (Figure S1A available online). To determine potential tumor microenvironmental factors that induce TEM8 expression on tumor vasculature, we examined cultured human microvascular endothelial cells (HMECs) in response to several conditions. Neither coculture with tumor cells nor exposure to hypoxia induced TEM8 (Figures S1B and S1C). However, upon serum starvation, TEM8 levels steadily increased in these cells, which normally express low endogenous TEM8 levels, resulting in a 4-fold increase in *TEM8* mRNA (Figure 1B) and a 5-fold increase in TEM8 protein (Figure 1C) by day 10. In contrast, TEM8 levels remained low in cells maintained in complete medium, and the slight increase in TEM8 expression noted at later time points (Figures 1B and 1C) may have been due to rapid growth factor depletion caused by increasing cell numbers (Figure 1D, top). The increase in TEM8 expression upon growth factor starvation was not influenced by the amount of cell-cell contact, based on comparisons of sparse versus confluent cells wherein the cell numbers were held constant but the surface area was altered (data not shown). Importantly, TEM8 elevation in growth factor-starved cells could be inhibited by fibroblast growth factor (FGF), VEGF, or serum treatment, and the combination of all three resulted in the lowest TEM8 levels (Figures 1E and 1F; Figure S1D). Thus, TEM8 may be part of a compensatory angiogenic or survival pathway that is activated, at least in part, by insufficient local angiogenic growth factors.

### Host-Derived TEM8 Promotes the Growth of Human Tumor Xenografts

To determine whether TEM8 could promote the growth of human tumor xenografts, we generated *Tem8* KO mice on an

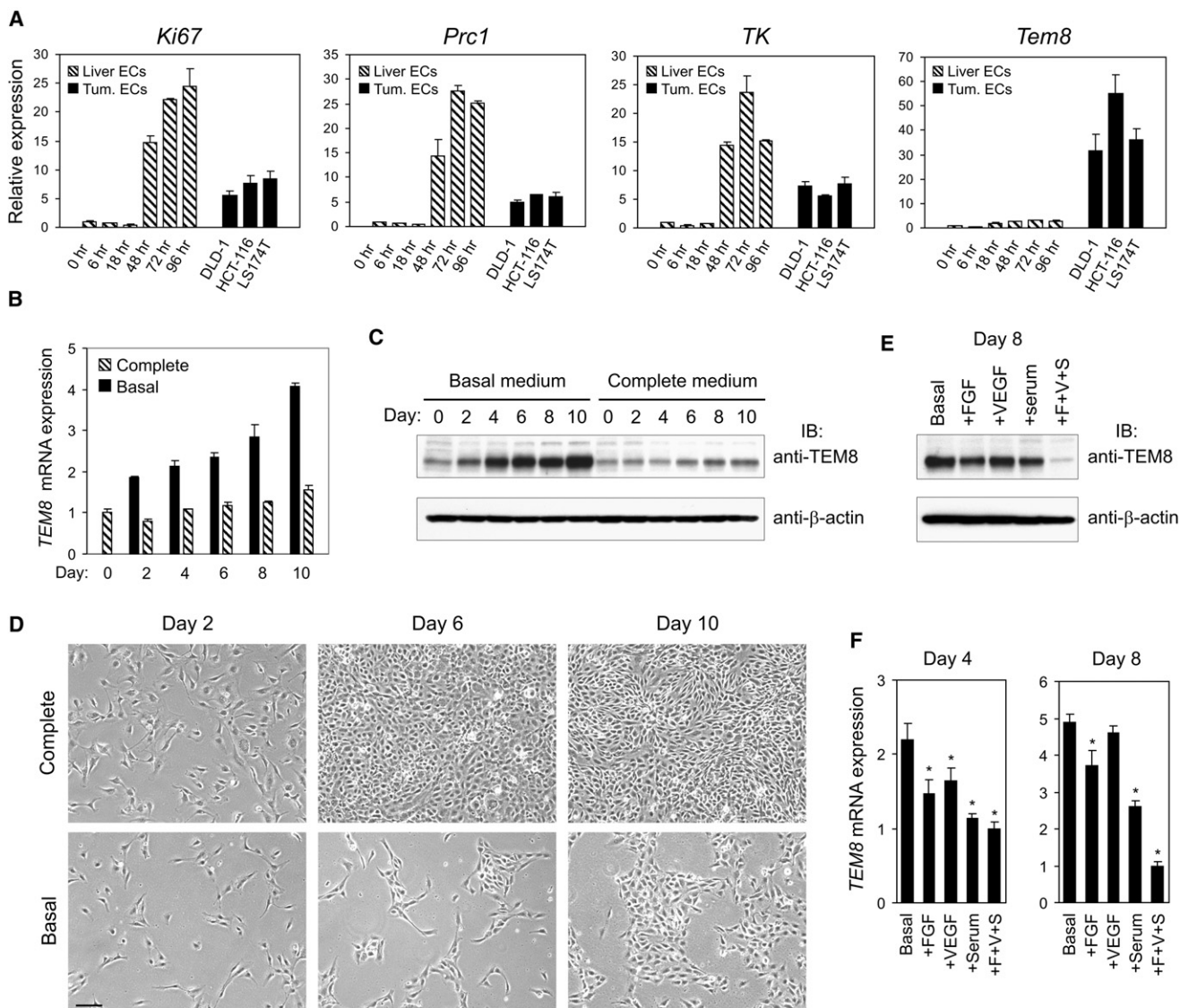


**Figure 1. TEM8 Is Selectively Upregulated on Tumor Vasculature and Is Elevated in Cultured HMECs in Response to Growth Factor Deprivation**

(A) QPCR was used to evaluate the expression of the indicated genes in ECs isolated from resting adult liver (0 hr), regenerating liver taken 6, 18, 48, 72, or 96 hr following 70% partial hepatectomy, or DLD1, HCT116, or LS174T colon cancer xenografts.

(B) TEM8 mRNA levels over the course of 10 days in HMECs grown in endothelial basal medium (EBM-2) or in complete medium (EBM-2 supplemented with FGF [F], VEGF [V], and 5% fetal bovine serum [S]).

(C) TEM8 protein levels over the course of 10 days in HMECs grown in basal medium or in complete medium. The media are the same as in (B).

(D) The appearance of the cells used in (B) and (C) is shown. Note that HMECs became confluent by day 6 in complete medium but formed only small colonies by day 10 in basal medium. The media are the same as in (B). The scale bar represents 100  $\mu$ m.

(E and F) Effect of supplementation of basal growth medium with FGF, VEGF, or serum alone or all three together on the expression of TEM8 protein (E) and mRNA (F) (\* $p < 0.05$ ). Values in (A), (B), and (F) represent mean  $\pm$  SD.

See also Figure S1.

immunocompromised athymic nude background. Tumor growth was inhibited in the *Tem8* KO mice compared to WT littermate controls when challenged with various tumor types including melanoma (UACC and LOX), breast (MDA-MB-231), lung (NCI-H460), and colon cancer (SW620, HCT116, and DLD1) (Figure 2). The MDA-MB-231 breast tumors were grown orthotopically in the mammary fat pad, whereas the melanoma and other tumor

types were grown subcutaneously. Tumor growth was consistently slower in *Tem8* KO versus WT mice, and SW620 tumors required over 100 days to reach an average size of 800 mm<sup>3</sup>, compared to only 35 days for WT littermates (Figure 2G). Thus, host-derived TEM8 functions to promote the subcutaneous and orthotopic growth of human tumor xenografts of diverse origin.

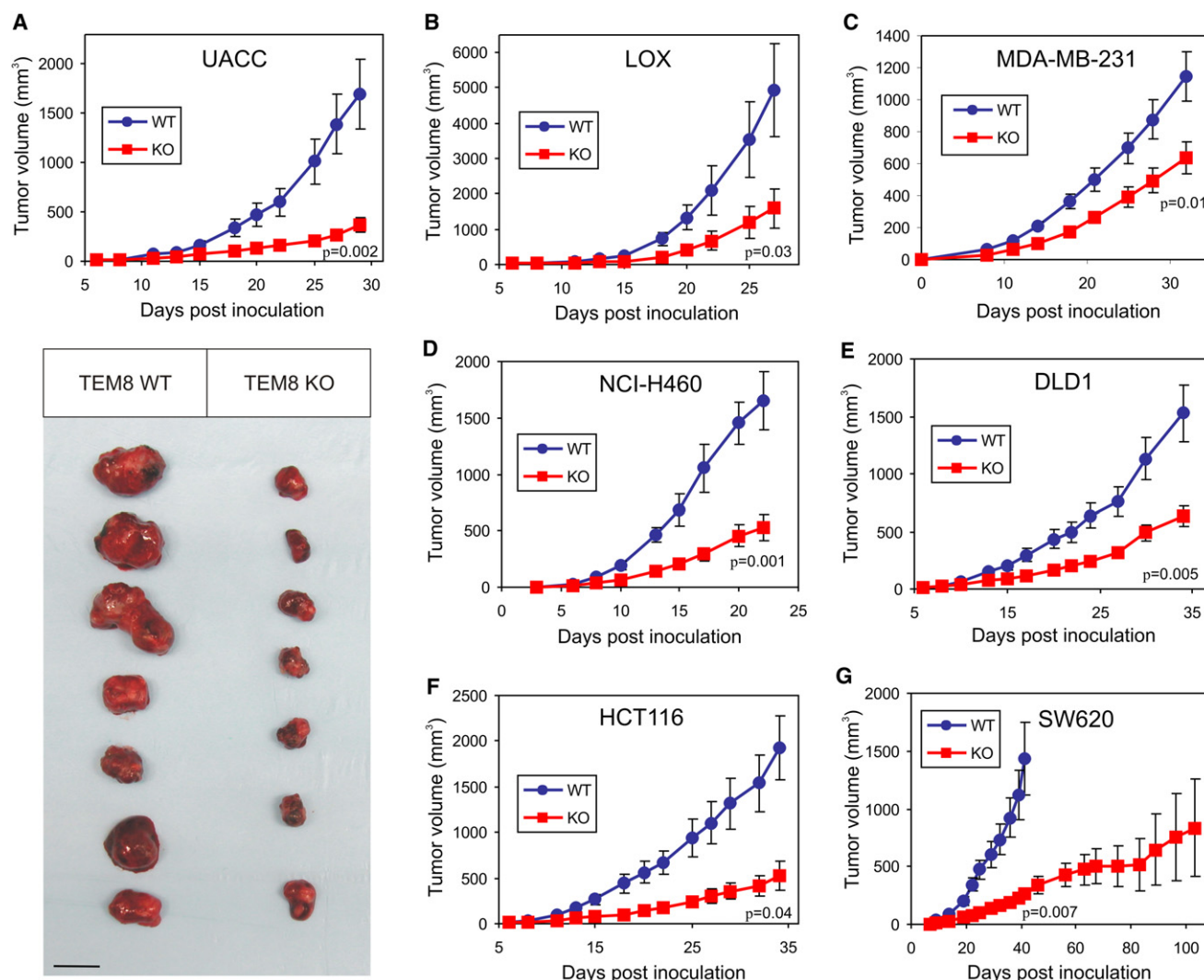


**Figure 2. The Growth of Human Tumor Xenografts Is Impaired in *Tem8* KO Mice**

Melanoma (A and B), breast (C), lung (D), and colon (E–G) cancer cell lines were injected into *Tem8* wild-type (blue) or knockout (red) mice and tumor volume was monitored over time. The physical appearance of the resected UACC tumors is shown in (A). p values were calculated from the final tumor measurement (A–F) or at day 41 (G), when the WT group reached its maximum size and had to be euthanized (Student's t test). n = 7–15 mice/group. Values represent mean  $\pm$  SE. The scale bar represents 10 mm.

### Development of Anti-TEM8 IgGs

Based on the functional importance of TEM8 in tumor growth promotion, we sought to develop therapeutic anti-TEM8 antibodies that could block TEM8 function in vivo. We had previously generated the SB series of anti-TEM8 antibodies (Nanda et al., 2004). However, these antibodies were murine derived and none of these could bind the predominant native form of TEM8 on the cell surface (Nanda et al., 2004; Yang et al., 2011b). To overcome these obstacles and circumvent potential difficulties associated with breaking tolerance, we developed another panel of fully human anti-TEM8 antibodies in vitro using antibody phage display. The selection strategy, which involved panning of Fab libraries on *Tem8*-transfected mammalian cells and purified recombinant mammalian-derived TEM8-ED (extracellular domain), resulted in the identification of five indepen-

dent Fabs, L1, L2, L3, L5, and ID2. Each of the Fabs was found to react with both mouse and human TEM8 in an ELISA and on the surface of live TEM8-positive cells by immunofluorescence and flow cytometry (Figures S2A–S2C). Although the physiologic ligand(s) of TEM8 in vivo is unclear, the TEM8 extracellular region contains a single structural motif, that is, a von Willebrand factor type A (vWA) domain, where physiologic TEM8 ligand(s) is most likely to bind. vWA domains are found in many extracellular eukaryotic proteins including integrins, and are known to mediate adhesion to other proteins via metal-ion-dependent adhesion sites. We reasoned that the protective antigen (PA) subunit of anthrax toxin, which binds the exposed vWA domain of TEM8 in a metal-ion-dependent manner, may usurp the physiologic binding site of a natural ligand. Thus, we screened the Fabs for the ability to block FITC-labeled

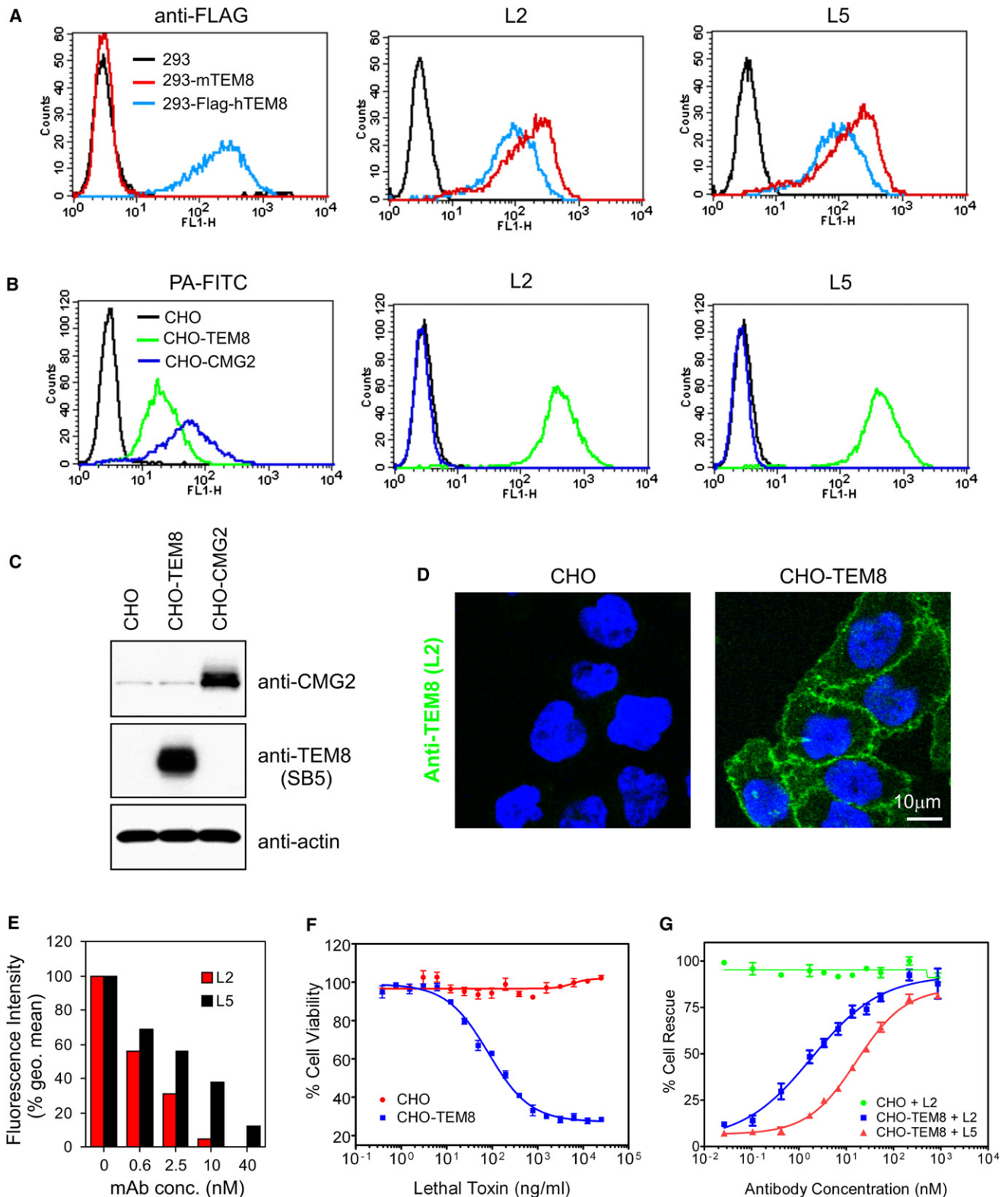


**Figure 3. L2 and L5 IgGs React Selectively with TEM8 and Block Binding and Toxicity of Anthrax Toxin Proteins**

(A) L2 and L5 antibodies were used for flow cytometry staining of 293 cells stably transfected with mouse *Tem8* (293-mTEM8) or a FLAG-tagged human *TEM8* (293-Flag-hTEM8).

(B) L2 and L5 were used for flow cytometry staining of CHO/PR230 (CHO) cells (an anthrax toxin receptor-deficient cell line) that had been stably transfected with human *TEM8* (CHO-TEM8) or human *CMG2* (CHO-CMG2). FITC-labeled protective antigen (PA-FITC), which binds both TEM8 and CMG2, was used as a positive control.

anthrax toxin PA binding to the surface of cells expressing TEM8. Each of the Fabs blocked FITC-PA binding in a dose-dependent manner (Figure S2D). Thus, we identified five human anti-TEM8 Fabs that were positive in all screens and that contained a unique variable domain.

Fabs have a relatively short half-life in vivo (several hours) compared to full IgGs (several days). To enhance their stability in vivo, two of the Fabs, L2 and L5, were selected for reformatting to full IgG. For preclinical testing in mice, the constant domains of mouse IgG2a (C<sub>H</sub>1, C<sub>H</sub>2, C<sub>H</sub>3, and C<sub>L</sub>) were fused to the human variable domains (V<sub>H</sub> and V<sub>L</sub>) in order to minimize immunogenicity, resulting in human-mouse chimeric antibodies. After reformatting, both L2 and L5 IgGs maintained their activity against TEM8 in the same screens used to test the Fabs, and were specific because they failed to react with mouse or human CMG2, the closest homolog of TEM8 (Figures 3A–3D and data not shown). Upon titration and comparison at nonsaturating concentrations, L2 bound TEM8-expressing cells with 7-fold higher affinity than L5 (EC<sub>50</sub> 0.4 and 2.8 nM, respectively; see Figure S2E). Similarly, L2 was ~4-fold more potent at blocking the binding of FITC-labeled protective antigen and ~9-fold more potent at preventing cytotoxicity caused by anthrax lethal toxin (Figures 3E–3G).

#### Anti-TEM8 IgGs Inhibit Tumor Growth but Do Not Delay Wound Healing

We tested the L2 and L5 antibodies for their activity against UACC, HCT116, and DLD1 colon tumor xenografts in athymic nude mice. In these studies, mice were treated with L2 or L5 once tumors reached an average size of 50 mm<sup>3</sup>. For each tumor type analyzed, a marked tumor growth inhibition was observed in each of the treated groups compared to vehicle (PBS) alone (Figures 4A–4E). The antitumor activity was comparable to that of anti-VEGFR2 antibodies (Figure 4C). When L2 and L5 were compared in a dose-escalation study to determine the amount of antibody required for optimal tumor growth inhibition, L2 showed superior activity. A partial growth inhibition was observed when mice were given 2 mg/kg of L2, whereas maximum growth inhibition was observed with 15 mg/kg (Figure 4E). L5, on the other hand, only showed partial growth inhibition at 15 mg/kg, similar to that observed in the 2 mg/kg L2 treatment group, and in each tumor study required 30–40 mg/kg to achieve its optimal biologic dose (OBD). Although L5 required a higher dose than L2 to achieve maximum efficacy, at their OBDs the two antibodies showed similar antitumor activity. Taken together, these studies demonstrate a marked in vivo anti-tumor activity of two independent anti-TEM8 antibodies. Because the full IgG of L2 appeared more potent than L5 both in vitro and in vivo, we focused on L2 for the remainder of our studies.

The aforementioned studies were conducted in immunocompromised mice. To determine whether L2 could suppress tumor

growth in the presence of an intact immune system, we injected murine B16 melanoma cells into syngeneic C57BL/6 mice and began treating mice with L2 at a tumor size of 50 mm<sup>3</sup>. The L2-treated group had a 60% reduction in tumor growth by the end of the study (Figure 4F). Midway through the therapeutic course, we also inflicted 6-mm-diameter wounds into each of the tumor-bearing mice to determine whether L2 treatment would interfere with wound healing. Wound closure rates were not significantly altered by L2 (Figure 4G), despite its clear antitumor activity in the same mice. Immunofluorescence staining for CD31 showed no alteration in the amount of vasculature present within the healing wound granulation tissue (Figure 4H). Matrigel-induced vascularization was also unaffected by L2 treatment (Figure 4I). Thus, L2 antibodies inhibited chronic pathological tumor growth while not interfering with normal healing processes dependent on physiological angiogenesis.

#### L2 Has No Detectable Toxicity

Two types of toxicology studies were conducted to determine how well the L2 anti-TEM8 antibody was tolerated. The first study involved dose escalation, wherein mice were administered 20, 50, or 100 mg/kg of L2 every other day for a total of three treatments and then analyzed 24 hr later. All serum chemistry and blood cell counts in the group treated with 100 mg/kg L2 were similar to that of the control group, and no dose-dependent alterations were observed (Table 1; data not shown). Treated mice consumed food and socialized similarly to control animals, and both body and organ weights were unchanged (Figures S3A and S3B). A comprehensive histopathologic analysis of 44 organs or tissues derived from 6 mice/group failed to reveal any abnormalities (data not shown). The second toxicology study involved treatment of mice with 20 mg/kg of L2 three times per week for up to 6 weeks, followed by an analysis of the same toxicology parameters. Again, no abnormalities were noted (Figure S3C; data not shown).

#### L2 Targets Tumor Vasculature In Vivo

To determine the specificity of L2 for TEM8 in vivo, we decided to treat tumor-bearing *Tem8* WT and KO mice with L2, reasoning that L2 should only have activity against tumors in *Tem8* WT mice if the tumor cells employed do not themselves express endogenous TEM8. TEM8 expression varied among cultured tumor cell lines, among which DLD1 tumor cells expressed undetectable TEM8 both in cell culture and following purification from established tumors in vivo (Figures S4A and S4B). Therefore, to test the specificity of the L2 antibody in vivo, *Tem8* WT and KO mice were challenged with DLD1 cells and treated with L2 or control IgG (Figure 5A). As expected, tumors grew more slowly in *Tem8* KO compared to *Tem8* WT mice treated with

(C) Western blot analysis was used to evaluate the expression of TEM8 and CMG2 in stably transfected CHO-TEM8 and CHO-CMG2 cells.

(D) L2 antibodies were used for cell-surface immunofluorescence labeling of CHO and CHO-TEM8 cells.

(E) The ability of L2 and L5 antibodies to block binding of PA-FITC to CHO-TEM8 cells was measured by flow cytometry.

(F) The viability of CHO and CHO-TEM8 cells was evaluated 48 hr posttreatment with lethal toxin.

(G) The ability of L2 and L5 antibodies to protect cells from toxicity following treatment with 1 μg of lethal toxin was evaluated. In this assay, the EC<sub>50</sub> for L2 and L5 was 1.9 and 16.6 nM, respectively. Values in (F) and (G) represent mean ± SE.

See also Figure S2.

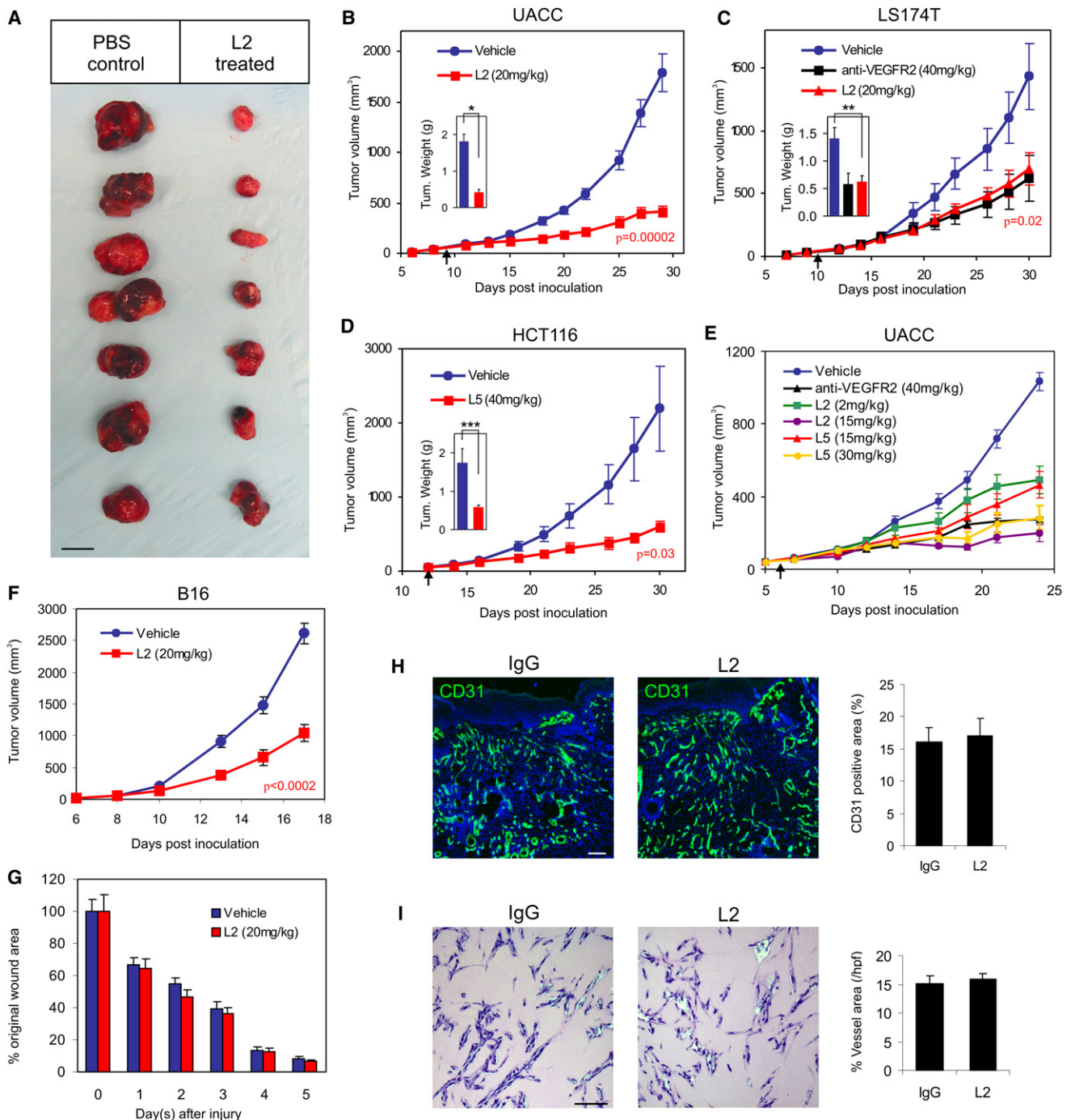


**Figure 4. Anti-TEM8 Antibodies Inhibit Tumor Growth but Do Not Delay Wound Healing**

(A–F) Melanoma (A, B, and E: UACC; F: B16) or colon cancer (C: LS174T; D: HCT116) tumor cells were inoculated subcutaneously into athymic nude (UACC, LS174T, HCT116) or C57BL/6 (B16) mice and tumor growth was monitored. Treatments with PBS (vehicle), anti-VEGFR2 antibodies, or anti-TEM8 antibodies (L2 or L5) were administered three times per week and were initiated when tumors reached a size of 50 mm<sup>3</sup> (arrows). A Student's *t* test was used to calculate *p* values between the vehicle and L2 treatment groups at the final tumor measurement. Tumors were excised at the end of the study to calculate final tumor weights (insets in B–D). \**p* = 0.00005, \*\**p* = 0.002, \*\*\**p* = 0.02.

(A) The physical appearance of the UACC melanoma tumors at the end of the study following surgical excision. The scale bar represents 10 mm.

(B) L2 inhibition of UACC melanoma tumor growth.

(C) L2 and DC101 (anti-VEGFR2) inhibition of LS174T tumor growth.

(D) L5 inhibition of HCT116 tumor growth.

(E) L2 and L5 dose-dependent inhibition of UACC tumor growth.

(F) L2 inhibition of B16 melanoma tumor growth.

control IgG. When the L2 antibody was administered to *Tem8* WT mice, tumor growth was inhibited relative to the IgG control group but was indistinguishable from that in the *Tem8* KO group. Importantly, L2 treatment of *Tem8* KO tumor-bearing mice did not result in any further tumor growth inhibition. Taken together, these results indicate that TEM8 is the sole target of L2 in vivo, and supports the hypothesis that L2 is a function-blocking monoclonal antibody.

The previously described expression of TEM8 in tumor endothelium (Fernando and Fletcher, 2009; Nanda et al., 2004; St. Croix et al., 2000) suggests that the target tissue of L2 in vivo may be the tumor-associated vasculature. To assess this, we performed CD31 vessel staining of the human DLD1 colon cancer xenografts and found a reduced number of vessels in tumors derived from *Tem8* KO or L2-treated mice (Figure 5B). Quantification of the number of CD31-positive ECs in tumors using flow cytometry revealed significantly lower EC numbers following both pharmacologic and genetic ablation of TEM8 (Figure 5C). We reasoned that TEM8 may promote proliferation of tumor ECs, based on previous studies that showed a role for CMG2 in promoting endothelial proliferation (Reeves et al., 2010). However, endothelial proliferation in DLD1 tumors was not altered in response to L2 treatment (Figure S4C), although the number of apoptotic ECs was significantly increased ( $p < 0.02$ ; Figure S4D).

To further assess the specificity of L2 in vivo, L2 was labeled with FITC and then intravenously injected into DLD1 tumor-bearing mice. Immunofluorescence analysis revealed localization of TEM8 selectively in tumor-associated vasculature but not in any of the normal control tissues analyzed including brain, heart, intestine, liver, muscle, spleen, and stomach (Figure 5D). Some tumor-associated perivascular stromal cells, including pericytes based on their adjacent proximity to endothelium, were also positive. However, stromal cell staining was confined to the tumor region in *Tem8* WT mice and was absent from the tumors in *Tem8* KO mice, confirming the specificity of antibody staining (Figure 5E).

### L2 Can Elicit NK-Mediated and Complement-Mediated Cytotoxicity

We reasoned that the antitumor activity of L2 in vivo may involve multiple mechanisms, and that antibody-dependent cellular cytotoxicity (ADCC) and/or complement-dependent cytotoxicity (CDC) could contribute to this activity. To determine whether TEM8 could potentially function as a target of ADCC, we mixed effector natural killer cells with TEM8-expressing 293 target cells at various ratios and found that L2, but not control IgG, was able to elicit cytotoxicity that was dependent on both the antibody and effector cell concentration (Figures 5F and 5G). Similarly, L2 elicited CDC in both an antibody- and complement-dependent manner (Figures 5H and 5I). Although these in vitro studies support a role for ADCC and CDC, further work is required to

**Table 1. Selected Toxicological Results and Organ Weights**

	Control	100 mg/kg L2 Anti-TEM8
Selected Parameters		
White blood cells (K/ $\mu$ l)	5.9 $\pm$ 2.5	6.3 $\pm$ 2.4
Red blood cells (M/ $\mu$ l)	9.5 $\pm$ 0.4	9.6 $\pm$ 0.4
Albumin (g/dl)	4.0 $\pm$ 0.4	3.9 $\pm$ 0.1
Alanine aminotransferase (U/l)	52.7 $\pm$ 10.1	51.9 $\pm$ 27.4
Total bilirubin (mg/dl)	$\leq 0.2$	$\leq 0.2$
Creatine (mg/dl)	$\leq 0.2$	$\leq 0.2$
Hemoglobin (g/dl)	13.9 $\pm$ 0.6	13.9 $\pm$ 0.4
Total protein (g/dl)	5.6 $\pm$ 0.2	5.7 $\pm$ 0.4
Blood urea nitrogen (mg/dl)	19.7 $\pm$ 2.0	17.5 $\pm$ 3.4
Selected Organ Weights (mg)		
Brain	462 $\pm$ 19	465 $\pm$ 15
Heart	137 $\pm$ 15	155 $\pm$ 21
Kidney	312 $\pm$ 58	308 $\pm$ 63
Liver	1,173 $\pm$ 180	1,152 $\pm$ 271
Lung	153 $\pm$ 20	168 $\pm$ 34
Spleen	80 $\pm$ 13	83 $\pm$ 15

Represented toxicological data and organ weights from mice ( $n = 6$ /group) dosed i.p. every second day with saline (control) or 100 mg/kg anti-TEM8 mAb. Values are mean  $\pm$  SD.

See also Figure S3.

determine whether these mechanisms contribute to the anti-tumor activity of L2 in vivo.

### L2 Potentiates Tumoricidal Responses

The delayed tumor growth in *Tem8* KO mice and the encouraging antitumor activity of L2 against relatively small established 50 mm<sup>3</sup> tumors prompted us to explore the activity of L2 against larger tumors. Importantly, even tumors that were 200 mm<sup>3</sup> in size prior to L2 treatment showed a significant response to the antibody such that when the control tumors reached an average size of 2,000 mm<sup>3</sup>, treated tumors had an average size of 1,288 mm<sup>3</sup> (Figure 6A). However, because the L2-mediated growth inhibition was less effective against relatively large (200 mm<sup>3</sup>) preestablished tumors compared to small (50 mm<sup>3</sup>) tumors (compare L2-treated group in Figure 6A with that in Figure 4B), we determined whether the combination of L2 with other types of anticancer agents would result in enhanced antitumor efficacy. When L2 treatment was combined with the anti-VEGFR2 antibody DC101, which prevents VEGF from binding VEGFR2, L2 significantly enhanced the activity of DC101 against UACC melanoma ( $p < 0.05$ ; Figure 6A). Furthermore, the combination of L2 with DMXAA (ASA404), a vascular targeting agent that has shown promising activity in early clinical trials against lung cancer (Baguley and McKeage, 2010), proved highly

(G) Wound closure rates following treatment with L2 or vehicle (PBS) alone. In this experiment, wounds were generated in the same tumor-bearing mice as shown in (F).

(H) CD31 immunofluorescence staining of granulation tissue vasculature in control and L2-treated groups. Control mice received nonspecific IgG in this experiment ( $n = 6$  wounds/group).

(I) Matrigel plug vascularization was assessed following treatment with nonspecific IgG or L2 anti-TEM8 antibodies. Vessel areas were calculated from six plugs per group. Values in (B)–(I) represent mean  $\pm$  SE. The scale bars (H and I) represent 100  $\mu$ m.

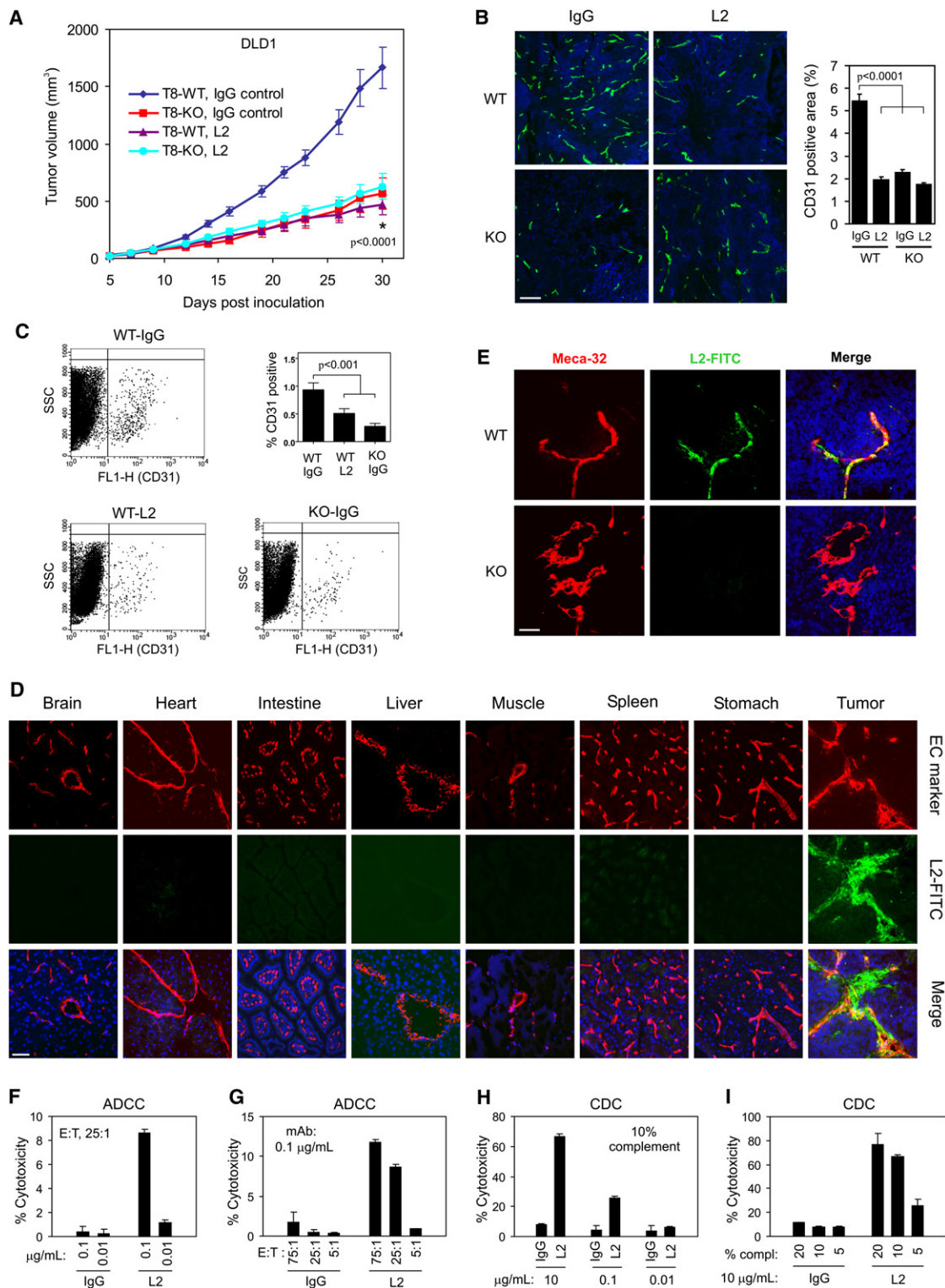


**Figure 5. L2 Targets Tumor Vasculature In Vivo and Engages ADCC and CDC In Vitro**

(A) Nonspecific antibodies (IgG control) or L2 anti-TEM8 antibodies were administered to *Tem8* wild-type (T8-WT) or *Tem8* knockout (T8-KO) mice at 20 mg/kg mice three times per week beginning 1 day post-subcutaneous inoculation of TEM8-negative DLD1 tumor cells. At day 30 (asterisk), the tumors in the T8-WT + IgG control group were significantly larger than those in each of the other three groups ( $p < 0.0001$ ), but there was no difference in tumor size between the T8-KO + IgG, T8-WT + L2, and T8-KO + L2 groups (one-way ANOVA with Bonferroni posttest) ( $n = 12$  mice/group).

(B) Immunofluorescence vessel staining of *Tem8* WT and KO mice following treatment with L2 or IgG. Right: quantification of CD31-positive vessel area.  $p < 0.0001$  between each of the groups and the IgG WT control group (one-way ANOVA). The scale bar represents 200  $\mu\text{m}$ .

effective against NCI-H460 lung cancer xenografts (Figure 6B). Both L2 and DMXAA significantly delayed tumor growth, but the combination was even more efficacious than either treatment alone ( $p < 0.001$ ; DMXAA + L2 versus DMXAA alone). Finally, when L2 was combined with 5-fluorouracil (5FU) and irinotecan (IRT), chemotherapeutic agents that are currently used to treat patients with colorectal cancer, L2 significantly enhanced their efficacy against HCT116 tumors ( $p < 0.0001$ , 5FU + L2 versus 5FU;  $p < 0.02$ , IRT + L2 versus IRT; Figures 6C and 6D). L2 also enhanced the efficacy of irinotecan against SW620 ( $p < 0.02$ , IRT + L2 versus IRT; Figure 6E), another colon cancer tumor model, demonstrating the generality of this response. Combination of L2 with IRT was highly efficacious, such that tumors in 5 of 11 mice in the HCT116 study and 4 of 11 mice in the SW620 study had completely regressed by 100 days postinoculation, and these mice remained tumor free for the duration of the study, an additional 7 months (Figures 6D and 6E). No complete tumor responses were observed in any of the monotherapy treatment arms. To further assess the inhibitory activity of L2 + IRT following long-term therapy, treatment was discontinued after 100 days, which resulted in rapid expansion of the remaining tumors that had not completely regressed. Analysis of body weights, food consumption, serum chemistry, and hematological profiles in these combination drug trials failed to reveal a change in toxicity caused by the addition of L2 to the chemotherapeutic agent (Figure 6F; Table S1). Taken together, these studies demonstrate that L2 treatment can enhance the anti-tumor responses of a wide variety of anticancer agents without added toxicity.

### L2 Binds Human Tumor Vasculature

To examine the specificity of L2 binding in human tumors, in situ immunofluorescence staining with L2 was performed on colorectal tumors or adjacent normal colonic mucosa derived from six cases of late-stage colorectal cancer, four of which were patient matched. Although staining was undetectable in all cases of normal colonic mucosa, in each of the tumor samples L2-FITC strongly labeled the tumor stroma, including von Willebrand factor (vWF)-positive ECs as well as some perivascular stromal cells that, based on morphology, appeared to include pericytes and possibly fibroblasts (Figure 7). Although the intensity of stromal staining was variable in different regions of the tumor, the staining was considered specific because it was completely blocked by the addition of unlabeled L2 but not isotype-matched

control IgG. Thus, in tumors derived from both patients and mouse xenografts, TEM8 is found in tumor-associated vasculature and tumor-associated perivascular stromal cells.

### DISCUSSION

These studies demonstrate that TEM8 is critical for promoting pathological angiogenesis evoked by a variety of tumor types, and that antibody-mediated targeting of TEM8 provides a rational strategy for combating cancer. Most angiogenesis regulators that have been discovered to date cannot distinguish physiological and pathological angiogenesis. In immunocompetent mice, L2 inhibited tumor growth but had no effect on wound healing in the same mice, consistent with earlier studies demonstrating no difference in wound healing between *Tem8* WT and KO mice (Cullen et al., 2009). TEM8 was also dispensable for developmental angiogenesis and normal physiological angiogenesis of the corpus luteum (Cullen et al., 2009; Nanda et al., 2004; St. Croix et al., 2000). A function for TEM8 in these normal physiological processes could potentially be masked through compensation by another molecule. However, CMG2 is the only other protein that shares significant amino acid identity with TEM8 and, aside from misaligned incisors, *Cmg2/Tem8* double-mutant mice, like *Tem8* KO mice, appear to develop normally (Liu et al., 2009). These results support the conclusion that physiological and pathological angiogenesis are distinct and that antibody-mediated targeting of TEM8 can selectively inhibit pathological tumor growth while sparing normal healing processes that also require vascularization.

Based on our results, we propose that TEM8 overexpression in tumor vasculature may be caused, at least in part, by local decreases in the availability of stromal growth factors, such as VEGF and FGF. At first, this might seem counterintuitive, given the overall proangiogenic nature of tumors. However, blood flow through the tortuous vessels in tumors is known to be slow, erratic, and often static, which could contribute to the rapid local depletion of angiogenic growth factors. Tumor ECs may also have to compete for growth factors with tumor cells that often express VEGF and/or FGF receptors themselves and can sometimes utilize angiogenic growth factors for their own growth (Dallas et al., 2007; Masood et al., 2001). Finally, hypoxia, a well-known inducer of VEGF gene transcription, may also lead to overexpression of the high-affinity VEGFR1

(C) Flow cytometry staining of dispersed tumor tissues was used to determine the percentage of CD31-positive cells in L2-treated tumors from *Tem8* WT mice (WT-L2), IgG-treated tumors from *Tem8* KO mice (KO-IgG), and IgG-treated tumors from *Tem8* wild-type mice (WT-IgG). The dot plots show representative data for each of the groups, and the bar graph displays the average percentage of CD31-positive cells ( $n = 6/\text{group}$ ). Both the WT-L2 and KO-IgG groups had significantly fewer cells than the WT-IgG group, as determined by a one-way ANOVA.

(D) L2 localization in vivo was assessed by immunofluorescence staining of various tissues following i.v. injection of FITC-labeled L2 into DLD1 tumor-bearing mice. An overlay of the L2 image (green) with the endothelial marker image (Meca-32 or CD31, red) was used to assess colocalization with vasculature (yellow, merge). The scale bar represents 50  $\mu\text{m}$ .

(E) The specificity of L2-FITC for TEM8 in vivo was assessed by comparing the staining of tumor stroma from *Tem8* wild-type and *Tem8* knockout mice. The scale bar represents 50  $\mu\text{m}$ .

(F) NK-mediated toxicity against TEM8-expressing target cells was measured in the presence of L2 or control IgG. The effector:target (E:T) cell ratio in this experiment was 25:1.

(G) The impact of increasing E:T cell ratios on L2-mediated ADCC was evaluated.

(H) Complement-dependent cytotoxicity was assessed with varying amounts of L2 or control IgG.

(I) To evaluate complement dependency, variable amounts of complement were added to the CDC assay. Values in (A)–(C) and (F)–(I) represent mean  $\pm$  SE.

See also Figure S4.

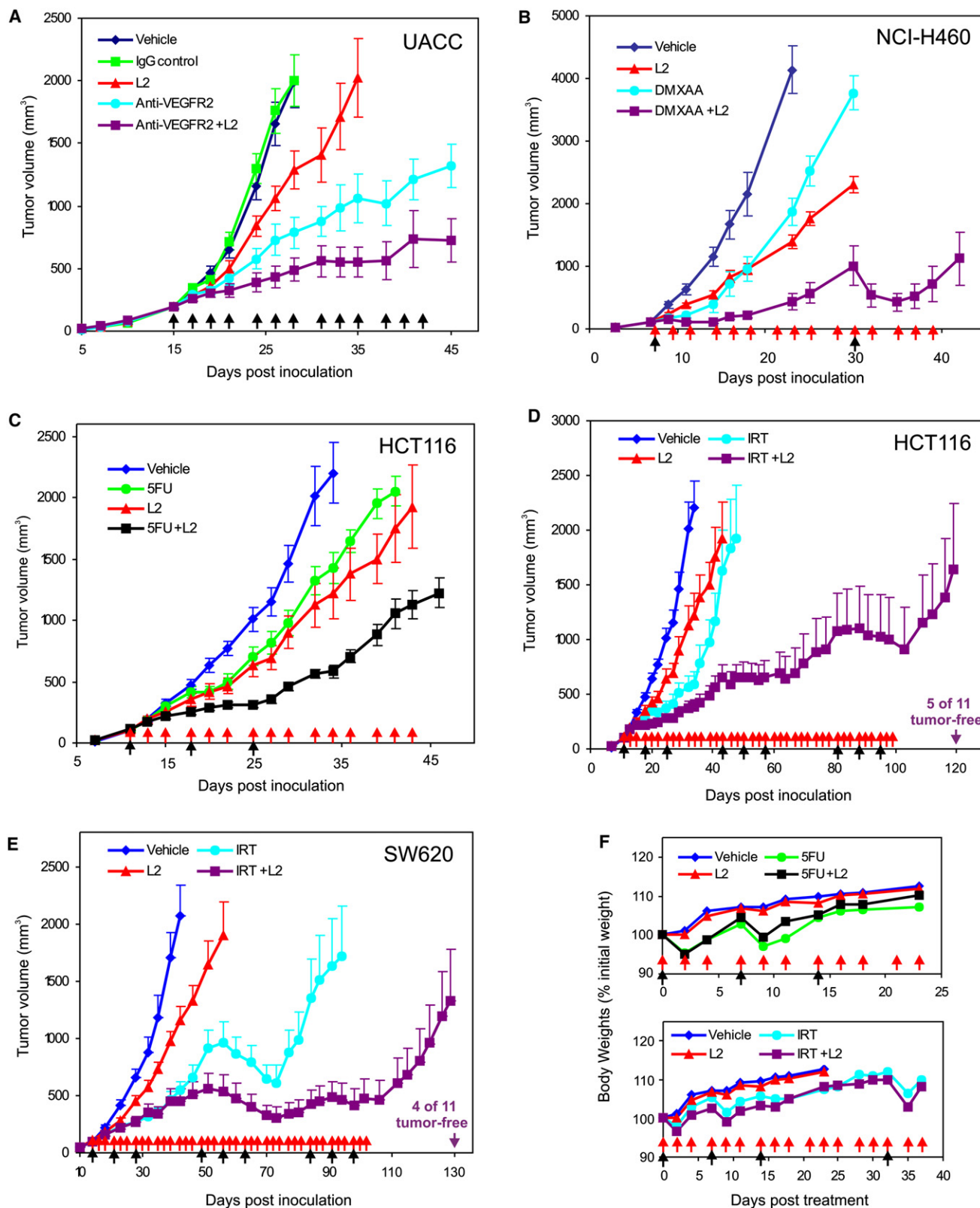


**Figure 6. L2 Anti-TEM8 Antibodies Augment the Efficacy of Various Classes of Anticancer Agents**

(A) UACC tumor growth was compared following treatment with vehicle (PBS), nonspecific mouse IgG (20 mg/kg), L2 anti-TEM8 (20 mg/kg), anti-VEGFR2 (40 mg/kg), or a combination of L2 (20 mg/kg) and anti-VEGFR2 (40 mg/kg). Treatments were administered three times per week (arrows) beginning 15 days post-tumor cell inoculation when tumors reached a size of 200 mm<sup>3</sup>.

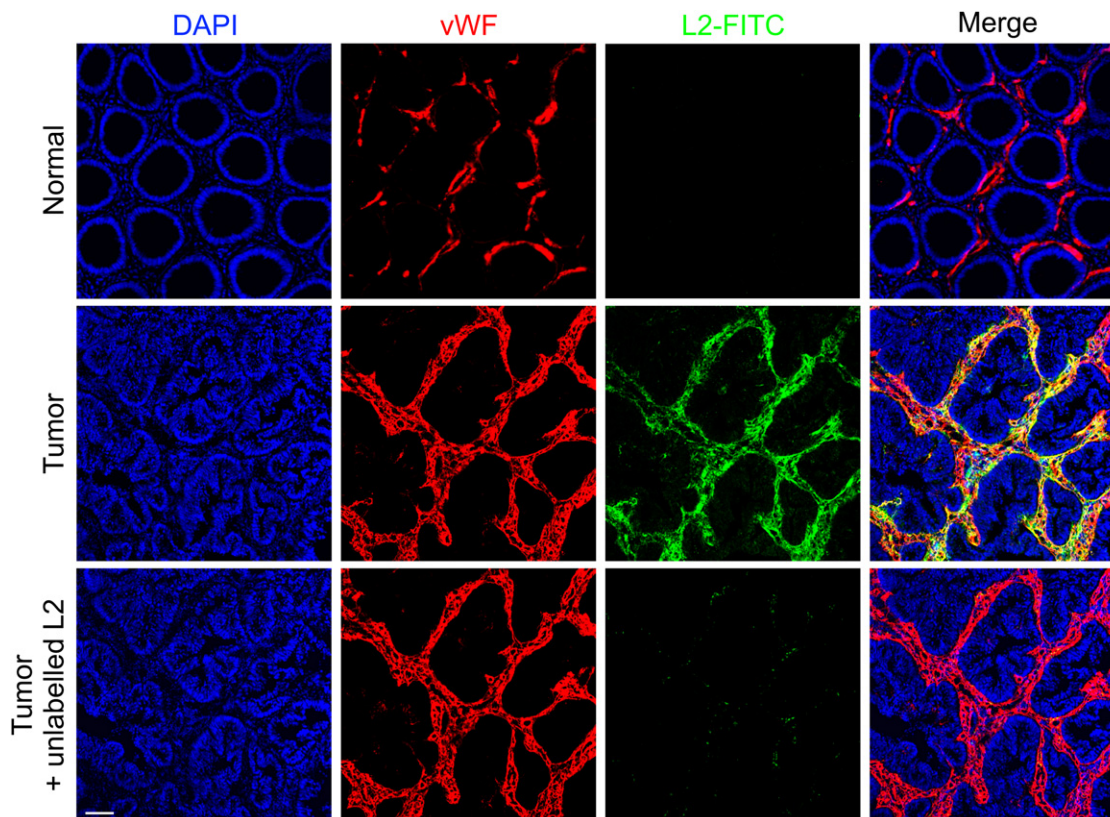


**Figure 7. L2 Anti-TEM8 Antibodies Bind to the Vasculature of Human Colorectal Cancer**

FITC-conjugated L2 (green) was used for immunofluorescence labeling of human colorectal tumors and normal colonic mucosa. The vasculature was costained with antibodies against von Willebrand factor (red), a pan endothelial marker, and overlapping immunofluorescence is shown in the merged image (yellow). The normal and tumor samples shown were patient-matched and processed in parallel. To prevent nonspecific binding, immunofluorescence staining was performed in the presence of a 50-fold excess of isotype-matched (human-mouse chimeric) control IgG that was generated against a foreign antigen (cyclosporine A). The staining was abolished by blocking the samples with unlabeled L2 (bottom) prior to adding L2-FITC. The middle and bottom panels were taken from serial sections. The scale bar represents 100  $\mu\text{m}$ .

(Gerber et al., 1997) or its soluble splice variant sVEGFR1 that can act as decoy receptors, limiting VEGF bioavailability (Lamszus et al., 2003; Yamaguchi et al., 2007; Yang et al., 2011a).

Elevated TEM8 expression in tumor ECs in response to growth factor deprivation and possibly other unidentified microenvironmental stressors may be part of a survival pathway that helps

(B) NCI-H460 tumor growth was compared following treatment with vehicle, L2 anti-TEM8, DMXAA, or a combination of L2 and DMXAA beginning 15 days post-tumor inoculation when tumors reached an average size of 100  $\text{mm}^3$ . In this experiment, L2 (20 mg/kg) was administered three times per week (red arrows) for the duration of the study, whereas DMXAA was administered at a high dose of 25 mg/kg (black arrows), followed by 5 mg/kg/day the following 2 days.

(C) HCT116 tumor growth was compared following treatment with vehicle, L2 anti-TEM8 (20 mg/kg), 5-fluorouracil (100 mg/kg), or a combination of L2 and 5FU beginning 11 days post-tumor inoculation when tumors reached an average size of 100  $\text{mm}^3$ . In this experiment, L2 was administered three times per week (red arrows), whereas 5FU was administered once a week for 3 weeks (black arrows).

(D) HCT116 tumor growth was compared following treatment with vehicle, L2 anti-TEM8 (20 mg/kg), irinotecan (80 mg/kg), or a combination of L2 and irinotecan beginning 11 days post-tumor inoculation when tumors reached a size of 100  $\text{mm}^3$ . In this experiment, L2 was administered three times per week (red arrows) until 100 days postinoculation. To maximize efficacy without excessive toxicity and mimic the clinical situation, IRT was administered in three cycles (where 1 cycle = 1 treatment per week for 3 weeks; black arrows) that were separated by a 2 week rest period to allow recovery. The HCT116 tumor studies in (C) and (D) were conducted simultaneously and contain the same vehicle and L2 groups, which were duplicated for ease of comparison.

(E) SW620 tumor growth was compared following treatment with vehicle, L2 anti-TEM8 (20 mg/kg), irinotecan (80 mg/kg), or a combination of L2 and irinotecan beginning 14 days post-tumor inoculation when tumors reached a size of 100  $\text{mm}^3$ . The treatments in this study were the same as those described for HCT116 above. IRT caused tumor regression in many of the treated mice. A decrease in tumor size caused by IRT is readily observed in both IRT arms (IRT and IRT + L2) during the second cycle of IRT treatment. During the subsequent 2 week rest period the tumors rapidly rebounded. Following the last cycle of IRT, many of the tumors in the combination group (IRT + L2) regressed again, whereas the larger tumors in the control group did not respond. For ease of comparison, only half of the error bars are shown in (D) and (E).

(F) Body weights in HCT116 tumor-bearing mice from the 5FU study (upper, corresponding to C) or the irinotecan study (lower, corresponding to D) were monitored from the start of therapy until the tumors in the control groups reached their maximum allowable size and mice had to be euthanized. Data represent mean values. The SD ranged from 2% to 8% and error bars are omitted for clarity. The apparent reduction in mean body weight observed following 5-fluorouracil and irinotecan treatments (black arrows) were nonsignificant and were not altered by L2 treatment (red arrows). Values in (A)–(E) represent mean  $\pm$  SE. See also Figure S5.

ECs cope during suboptimal growth conditions. *Tem8* KO mice provide a valuable tool for assessing the role of TEM8 in pathological angiogenesis. For most pharmacological angiogenesis inhibitors, it is difficult to find animal models completely lacking the drug target because the target proteins are usually required for developmental angiogenesis, and temporally induced deletion of a conditional “floxed” target gene in adult mice using cre-lox technology is often incomplete. Importantly, by treating *Tem8* WT or KO mice with L2 anti-TEM8 antibody, we could verify that TEM8 is the target of this antibody in vivo, and that L2 treatment inhibits tumor growth to a level similar to complete genetic ablation. Further evidence for antibody specificity was obtained using FITC-labeled L2 that selectively reacted with the tumor vessels in *Tem8* WT but not KO mice.

Multiple mechanisms could potentially contribute to the anti-tumor activity of L2 in vivo, but so far the evidence suggests that the antibodies work primarily by blocking TEM8 function and that ADCC and CDC may play a more limited role. The extent of tumor growth delay observed in *Tem8* KO mice was found to vary depending on the tumor type employed, but the same tumor-type-dependent responses were observed following L2 blockade. For example, UACC tumors consistently displayed the most pronounced growth delay in *Tem8* KO versus WT mice, and were also the most responsive to L2. Indeed, the tumor growth patterns observed in *Tem8* KO mice were found to be indistinguishable from those observed in the L2-treated *Tem8* WT mice, provided that L2 treatment began immediately following tumor cell inoculation (for example, see Figure 5A). It is currently unclear why some tumor types rely more on host-derived TEM8 than others, but the degree of TEM8 dependence does not appear to correlate with the tumor cells' ability to evoke TEM8 expression in nearby tumor-associated ECs. For example, in *Tem8* WT mice, tumor ECs isolated from LLC tumors expressed four times more TEM8 than those isolated from B16 tumors, yet comparisons of tumor growth in *Tem8* WT and KO mice revealed that B16 tumors are more dependent on host-derived TEM8 than LLC cells (Cullen et al., 2009). We expect that if ADCC and CDC were the major mechanisms governing tumor responses in vivo, then tumor responsiveness would have correlated with TEM8 expression levels in tumor ECs, because ADCC and CDC both depend on target antigen expression levels. Therefore, further studies are required to establish whether ADCC and CDC contribute significantly to L2's activity in vivo. Nevertheless, affinity maturation of the variable domain and modifications to the Fc domain that enhance ADCC and CDC activity (Natsume et al., 2009) could lead to further enhancement of antitumor efficacy.

Although anti-TEM8 antibodies inhibited tumor growth as a monotherapy, based on our results we predict that TEM8 antibodies may be most useful in combination with other agents. TEM8 antibodies were completely nontoxic and displayed efficacy when combined with various classes of anticancer agents. That anti-TEM8 antibodies augment the activity of VEGFR2-neutralizing antibodies suggests that signaling pathways involving TEM8 may be responsible, at least in part, for angiogenesis that persists following VEGF/VEGFR2 inhibition. Although human-mouse chimeric antibodies were employed in the preclinical studies described here, reengineering of the Fc

domain can be used to make the IgG fully human for future clinical development.

In summary, we report the development of anti-TEM8 antibodies that retard tumor growth by inhibiting tumor angiogenesis. Anti-TEM8 antibodies were nontoxic and maintained efficacy in combination with various classes of anticancer agents. Thus, anti-TEM8 antibodies provide a rationally designed tool for selectively inhibiting pathological angiogenesis with important ramifications for the management of angiogenesis-dependent diseases.

## EXPERIMENTAL PROCEDURES

### Antibody Production and Purification

In vitro selection of the Morphosys HuCAL Gold phage library involved two rounds of sequential panning on biotinylated, purified recombinant TEM8(ED)-Fc fusion proteins, prepared as described in Supplemental Experimental Procedures, and one round of panning on HEK293 cells transfected with human TEM8 (293/Flag-hTEM8). DNA inserts for the Fab heavy and light chains were subcloned and expressed, and bivalent Fabs were evaluated for TEM8 binding by ELISA (see Supplemental Experimental Procedures). Two of the TEM8-binding clones (L2 and L5) were reformatted to generate mouse-human chimeric full IgGs. Anti-TEM8 antibodies were collected from HEK293T culture supernatants and purified by protein A and size exclusion chromatography.

### Western Blotting

Western blotting was performed using antibodies against TEM8 (clone SB5; Nanda et al., 2004), CMG2 (a kind gift from Stephen Leppa), actin (Chemicon), or HIF-1 $\alpha$  (Novus Biologicals) as previously described (Cullen et al., 2011).

### Animal and Tumor Studies

To derive *Tem8* KO mice on an immunodeficient background, *Tem8* KO mice on a C57BL/6 background (Cullen et al., 2009) were crossed with athymic NCr-nu/nu mice, and only *Tem8* WT and KO littermates derived from *Tem8* heterozygous intercrosses were used for comparison. Tumors were measured with a caliper, and tumor volumes were calculated using the formula length  $\times$  width<sup>2</sup>  $\times$  0.5 and presented as the mean  $\pm$  SE. All animal studies were carried out in accordance with protocols approved by the NCI Animal Care and Use Committee.

### Immunofluorescence

For in vivo target identification, FITC-labeled L2 was coinjected with nonspecific mouse IgG intraperitoneally into DLD1 tumor-bearing *Tem8* WT and KO mice. Frozen sections were labeled with rat anti-PV-1 (Meca-32) or rat anti-CD31 (BD Pharmingen) antibodies. For immunofluorescence staining of human normal colonic mucosa or colorectal cancer, frozen tissue sections were blocked with nonspecific mouse-human chimeric IgG antibodies (mouse Fc/human Fab) generated against cyclosporine A and detected with L2-labeled FITC. The anonymized human colon tissue samples were obtained from the Cooperative Human Tissue Network with approval from the NIH Office of Human Subject Research. Further details regarding the immunofluorescence staining can be found in Supplemental Experimental Procedures.

### Statistical Analysis

A Student's t test was used to calculate differences in tumor volumes or weights between two groups (for example, *Tem8* WT and KO mice) at the time when the WT (or control) group reached its maximum size and had to be euthanized. For comparisons between multiple tumor groups, a one-way ANOVA was used with a Bonferroni posttest. A one-way ANOVA was used for comparisons of microvascular densities and the fraction of CD31-positive cells by flow cytometry. p values < 0.05 were considered significant.

## SUPPLEMENTAL INFORMATION

Supplemental Information includes four figures, one table, and Supplemental Experimental Procedures and can be found with this article online at doi:10.1016/j.ccr.2012.01.004.

## ACKNOWLEDGMENTS

We thank Drs. Bert Vogelstein, Terry Van Dyke, Lino Tessarollo, and Isaiah J. Fidler for helpful suggestions. We thank Rou-Fun Kwong for help with the initial selection and characterization of anti-TEM8 antibodies. We thank Dr. Stephen H. Leppla, National Institute of Allergy and Infectious Diseases, NIH, for the CHO, CHO/TEM8, and CHO/CMG2 cells, recombinant PA, and lethal factor, and Dr. Arthur E. Frankel for the AF334 hybridoma. This work was supported in part by a Cooperative Research and Development Agreement between the Novartis Institutes for BioMedical Research and the intramural research program of the NCI, NIH, Department of Health and Social Services (DHSS), and with federal funds from the NCI under contract no. HHSN261200800001E. The content of this publication does not necessarily reflect the views or policies of the DHSS nor does mention of trade names, commercial products, or organizations imply endorsement by the U.S. government.

Received: May 12, 2011

Revised: September 19, 2011

Accepted: January 5, 2012

Published: February 13, 2012

## REFERENCES

- Baguley, B.C., and McKeage, M.J. (2010). ASA404: a tumor vascular-disrupting agent with broad potential for cancer therapy. *Future Oncol.* 6, 1537–1543.
- Bradley, K.A., Mogridge, J., Mourez, M., Collier, R.J., and Young, J.A. (2001). Identification of the cellular receptor for anthrax toxin. *Nature* 414, 225–229.
- Brastianos, P.K., and Batchelor, T.T. (2010). Vascular endothelial growth factor inhibitors in malignant gliomas. *Target. Oncol.* 5, 167–174.
- Carson-Walter, E.B., Watkins, D.N., Nanda, A., Vogelstein, B., Kinzler, K.W., and St. Croix, B. (2001). Cell surface tumor endothelial markers are conserved in mice and humans. *Cancer Res.* 61, 6649–6655.
- Chen, H.X., and Cleck, J.N. (2009). Adverse effects of anticancer agents that target the VEGF pathway. *Nat. Rev. Clin. Oncol.* 6, 465–477.
- Cullen, M., Seaman, S., Chaudhary, A., Yang, M.Y., Hilton, M.B., Logsdon, D., Haines, D.C., Tessarollo, L., and St. Croix, B. (2009). Host-derived tumor endothelial marker 8 promotes the growth of melanoma. *Cancer Res.* 69, 6021–6026.
- Cullen, M., Elzarrad, M.K., Seaman, S., Zudaire, E., Stevens, J., Yang, M.Y., Li, X., Chaudhary, A., Xu, L., Hilton, M.B., et al. (2011). GPR124, an orphan G protein-coupled receptor, is required for CNS-specific vascularization and establishment of the blood-brain barrier. *Proc. Natl. Acad. Sci. USA* 108, 5759–5764.
- Dallas, N.A., Fan, F., Gray, M.J., Van Buren, G., II, Lim, S.J., Xia, L., and Ellis, L.M. (2007). Functional significance of vascular endothelial growth factor receptors on gastrointestinal cancer cells. *Cancer Metastasis Rev.* 26, 433–441.
- Drixler, T.A., Vogten, M.J., Ritchie, E.D., van Vroonhoven, T.J., Gebbink, M.F., Voest, E.E., and Borel Rinkes, I.H. (2002). Liver regeneration is an angiogenesis-associated phenomenon. *Ann. Surg.* 236, 703–711, discussion 711–712.
- Du, R., Lu, K.V., Petritsch, C., Liu, P., Ganss, R., Passequé, E., Song, H., Vandenberg, S., Johnson, R.S., Werb, Z., and Bergers, G. (2008). HIF1 $\alpha$  induces the recruitment of bone marrow-derived vascular modulatory cells to regulate tumor angiogenesis and invasion. *Cancer Cell* 13, 206–220.
- Duan, H.F., Hu, X.W., Chen, J.L., Gao, L.H., Xi, Y.Y., Lu, Y., Li, J.F., Zhao, S.R., Xu, J.J., Chen, H.P., et al. (2007). Antitumor activities of TEM8-Fc: an engineered antibody-like molecule targeting tumor endothelial marker 8. *J. Natl. Cancer Inst.* 99, 1551–1555.
- Eremina, V., Cui, S., Gerber, H., Ferrara, N., Haigh, J., Nagy, A., Ema, M., Rossant, J., Jothy, S., Miner, J.H., and Quaggin, S.E. (2006). Vascular endothelial growth factor A signaling in the podocyte-endothelial compartment is required for mesangial cell migration and survival. *J. Am. Soc. Nephrol.* 17, 724–735.
- Felicetti, P., Mennecozzi, M., Barucca, A., Montgomery, S., Orlandi, F., Manova, K., Houghton, A.N., Gregor, P.D., Concetti, A., and Venanzi, F.M. (2007). Tumor endothelial marker 8 enhances tumor immunity in conjunction with immunization against differentiation Ag. *Cytotherapy* 9, 23–34.
- Fernando, S., and Fletcher, B.S. (2009). Targeting tumor endothelial marker 8 in the tumor vasculature of colorectal carcinomas in mice. *Cancer Res.* 69, 5126–5132.
- Gerber, H.P., Condorelli, F., Park, J., and Ferrara, N. (1997). Differential transcriptional regulation of the two vascular endothelial growth factor receptor genes. Flt-1, but not Flk-1/KDR, is up-regulated by hypoxia. *J. Biol. Chem.* 272, 23659–23667.
- Jinnin, M., Medici, D., Park, L., Limaye, N., Liu, Y., Boscolo, E., Bischoff, J., Vikkula, M., Boye, E., and Olsen, B.R. (2008). Suppressed NFAT-dependent VEGFR1 expression and constitutive VEGFR2 signaling in infantile hemangioma. *Nat. Med.* 14, 1236–1246.
- Kerbel, R.S. (2008). Tumor angiogenesis. *N. Engl. J. Med.* 358, 2039–2049.
- Lamszus, K., Ulbricht, U., Matschke, J., Brockmann, M.A., Fillbrandt, R., and Westphal, M. (2003). Levels of soluble vascular endothelial growth factor (VEGF) receptor 1 in astrocytic tumors and its relation to malignancy, vascularity, and VEGF-A. *Clin. Cancer Res.* 9, 1399–1405.
- Liu, S., Wang, H., Currie, B.M., Molinolo, A., Leung, H.J., Moayeri, M., Basile, J.R., Alfano, R.W., Gutkind, J.S., Frankel, A.E., et al. (2008). Matrix metalloproteinase-activated anthrax lethal toxin demonstrates high potency in targeting tumor vasculature. *J. Biol. Chem.* 283, 529–540.
- Liu, S., Crown, D., Miller-Randolph, S., Moayeri, M., Wang, H., Hu, H., Morley, T., and Leppla, S.H. (2009). Capillary morphogenesis protein-2 is the major receptor mediating lethality of anthrax toxin in vivo. *Proc. Natl. Acad. Sci. USA* 106, 12424–12429.
- Maharaj, A.S., and D'Amore, P.A. (2007). Roles for VEGF in the adult. *Microvasc. Res.* 74, 100–113.
- Masood, R., Cai, J., Zheng, T., Smith, D.L., Hinton, D.R., and Gill, P.S. (2001). Vascular endothelial growth factor (VEGF) is an autocrine growth factor for VEGF receptor-positive human tumors. *Blood* 98, 1904–1913.
- Nanda, A., Carson-Walter, E.B., Seaman, S., Barber, T.D., Stampfl, J., Singh, S., Vogelstein, B., Kinzler, K.W., and St. Croix, B. (2004). TEM8 interacts with the cleaved C5 domain of collagen  $\alpha$ 3(VI). *Cancer Res.* 64, 817–820.
- Natsume, A., Niwa, R., and Satoh, M. (2009). Improving effector functions of antibodies for cancer treatment: enhancing ADCC and CDC. *Drug Des. Devel. Ther.* 3, 7–16.
- Oosthuysen, B., Moons, L., Storkebaum, E., Beck, H., Nuyens, D., Brusselmans, K., Van Dorpe, J., Hellings, P., Gorselink, M., Heymans, S., et al. (2001). Deletion of the hypoxia-response element in the vascular endothelial growth factor promoter causes motor neuron degeneration. *Nat. Genet.* 28, 131–138.
- Reeves, C.V., Dufraigne, J., Young, J.A., and Kitajewski, J. (2010). Anthrax toxin receptor 2 is expressed in murine and tumor vasculature and functions in endothelial proliferation and morphogenesis. *Oncogene* 29, 789–801.
- Rouleau, C., Menon, K., Boutin, P., Guyre, C., Yoshida, H., Kataoka, S., Perricone, M., Shankara, S., Frankel, A.E., Duesbery, N.S., et al. (2008). The systemic administration of lethal toxin achieves a growth delay of human melanoma and neuroblastoma xenografts: assessment of receptor contribution. *Int. J. Oncol.* 32, 739–748.
- Ruan, Z., Yang, Z., Wang, Y., Wang, H., Chen, Y., Shang, X., Yang, C., Guo, S., Han, J., Liang, H., and Wu, Y. (2009). DNA vaccine against tumor endothelial marker 8 inhibits tumor angiogenesis and growth. *J. Immunother.* 32, 486–491.
- Scobie, H.M., Rainey, G.J., Bradley, K.A., and Young, J.A. (2003). Human capillary morphogenesis protein 2 functions as an anthrax toxin receptor. *Proc. Natl. Acad. Sci. USA* 100, 5170–5174.
- Seaman, S., Stevens, J., Yang, M.Y., Logsdon, D., Graff-Cherry, C., and St. Croix, B. (2007). Genes that distinguish physiological and pathological angiogenesis. *Cancer Cell* 11, 539–554.
- Shojaei, F., Wu, X., Malik, A.K., Zhong, C., Baldwin, M.E., Schanz, S., Fuh, G., Gerber, H.P., and Ferrara, N. (2007). Tumor refractoriness to anti-VEGF treatment is mediated by CD11b<sup>+</sup>Gr1<sup>+</sup> myeloid cells. *Nat. Biotechnol.* 25, 911–920.
- St. Croix, B., Rago, C., Velculescu, V., Traverso, G., Romans, K.E., Montgomery, E., Lal, A., Riggins, G.J., Lengauer, C., Vogelstein, B., and

- Kinzler, K.W. (2000). Genes expressed in human tumor endothelium. *Science* 289, 1197–1202.
- Sung, H.K., Michael, I.P., and Nagy, A. (2010). Multifaceted role of vascular endothelial growth factor signaling in adult tissue physiology: an emerging concept with clinical implications. *Curr. Opin. Hematol.* 17, 206–212.
- Verheul, H.M., and Pinedo, H.M. (2007). Possible molecular mechanisms involved in the toxicity of angiogenesis inhibition. *Nat. Rev. Cancer* 7, 475–485.
- Werner, E., Kowalczyk, A.P., and Faundez, V. (2006). Anthrax toxin receptor 1/tumor endothelium marker 8 mediates cell spreading by coupling extracellular ligands to the actin cytoskeleton. *J. Biol. Chem.* 281, 23227–23236.
- Yamaguchi, T., Bando, H., Mori, T., Takahashi, K., Matsumoto, H., Yasutome, M., Weich, H., and Toi, M. (2007). Overexpression of soluble vascular endothelial growth factor receptor 1 in colorectal cancer: association with progression and prognosis. *Cancer Sci.* 98, 405–410.
- Yang, F., Jin, C., Jiang, Y.J., Li, J., Di, Y., and Fu, D.L. (2011a). Potential role of soluble VEGFR-1 in antiangiogenesis therapy for cancer. *Expert Rev. Anticancer Ther.* 11, 541–549.
- Yang, M.Y., Chaudhary, A., Seaman, S., Dunty, J., Stevens, J., Elzarrad, M.K., Frankel, A.E., and St. Croix, B. (2011b). The cell surface structure of tumor endothelial marker 8 (TEM8) is regulated by the actin cytoskeleton. *Biochim. Biophys. Acta* 1813, 39–49.
- Yang, X., Zhu, H., and Hu, Z. (2010). Dendritic cells transduced with TEM8 recombinant adenovirus prevents hepatocellular carcinoma angiogenesis and inhibits cells growth. *Vaccine* 28, 7130–7135.

# Inhibition of PI3K/mTOR Leads to Adaptive Resistance in Matrix-Attached Cancer Cells

Taru Muranen,<sup>1</sup> Laura M. Selfors,<sup>1,3</sup> Devin T. Worster,<sup>1,3</sup> Marcin P. Iwanicki,<sup>1</sup> Loling Song,<sup>1</sup> Fabiana C. Morales,<sup>2</sup> Sizhen Gao,<sup>1</sup> Gordon B. Mills,<sup>2</sup> and Joan S. Brugge<sup>1,\*</sup>

<sup>1</sup>Department of Cell Biology, Harvard Medical School, 240 Longwood Avenue, Boston, MA 02115, USA

<sup>2</sup>Department of Systems Biology, M.D. Anderson Cancer Center, Houston, TX 77030, USA

<sup>3</sup>These authors contributed equally to this work

\*Correspondence: joan\_brugge@hms.harvard.edu

DOI 10.1016/j.ccr.2011.12.024

## SUMMARY

The PI3K/mTOR-pathway is the most commonly dysregulated pathway in epithelial cancers and represents an important target for cancer therapeutics. Here, we show that dual inhibition of PI3K/mTOR in ovarian cancer-spheroids leads to death of inner matrix-deprived cells, whereas matrix-attached cells are resistant. This matrix-associated resistance is mediated by drug-induced upregulation of cellular survival programs that involve both FOXO-regulated transcription and cap-independent translation. Inhibition of any one of several upregulated proteins, including Bcl-2, EGFR, or IGF1R, abrogates resistance to PI3K/mTOR inhibition. These results demonstrate that acute adaptive responses to PI3K/mTOR inhibition in matrix-attached cells resemble well-conserved stress responses to nutrient and growth factor deprivation. Bypass of this resistance mechanism through rational design of drug combinations could significantly enhance PI3K-targeted drug efficacy.

## INTRODUCTION

The most prevalent forms of cancer are of epithelial origin. Normal epithelial cells form well-organized polarized cell layers under the influence of extracellular matrix (ECM), and attachment to ECM is required for the control of normal epithelial cell proliferation, differentiation, and survival (Debnath and Brugge, 2005). However, during cancer progression, the normal epithelial organization is disrupted and malignant cells proliferate and survive outside their normal niches (Chiarugi and Giannoni, 2008). This process is not well recapitulated in two-dimensional (2D) cell cultures and may explain, in part, the failure of many therapeutic approaches in clinical trials. Thus, there is a need and opportunity to explore mechanisms of drug response and resistance under culture conditions that more closely mimic the in vivo environment.

Three-dimensional (3D) cell culture models have been widely utilized in epithelial cancer research to probe mechanisms involved in tumor initiation and progression (Debnath and Brugge, 2005; Weigelt and Bissell, 2008; Yamada and Cukierman, 2007). Nontransformed epithelial cells cultured in reconstituted basement membrane form hollow, growth-arrested, polarized 3D structures that recapitulate many features of epithelial cells in vivo. Survival of 3D spheroid structures is dependent on attachment to ECM; inner cells, lacking ECM attachment, undergo apoptosis, generating a hollow lumen (Chiarugi and Giannoni, 2008; Debnath and Brugge, 2005). However, cells that harbor alterations that inhibit apoptosis are still compromised in their survival because of metabolic impairment caused by ECM deprivation leading to decreased growth factor signaling, mostly due to loss of nutrient uptake (Schafer et al., 2009). These findings suggest that survival of tumor cells

## Significance

To fulfill the promise of PI3K/mTOR-pathway inhibition in cancer, it is critical to identify mechanisms of resistance and develop therapies to overcome it. Here, we show that resistance of matrix-attached cells to PI3K/mTOR-inhibitors is associated with upregulation of an evolutionarily well-conserved program that resembles nutrient deprivation, leading to translation of IRES-containing mRNAs previously associated with cellular stress responses. This adaptive response leads to upregulation of prosurvival proteins, and inhibition of this program abrogates resistance to PI3K/mTOR-inhibition in breast and ovarian cancer cells and ovarian cancer xenografts. These studies provide a platform for rational development of effective drug combinations through the use of three-dimensional (3D) model systems together with high-throughput proteomics approaches and identify drug combinations for further analysis as cancer therapeutics.

outside their natural matrix niches may require alterations that allow them to escape both apoptosis and metabolic impairment. Introduction of oncogenes into nontumorigenic cells in 3D can result in the formation of solid, filled structures that resemble tumor cells grown in 3D as well as the filled alveoli characteristic of ductal carcinoma in situ, a noninvasive form of breast cancer (Debnath and Brugge, 2005). Oncogenic alterations in the phosphatidylinositol 3-kinase (PI3K) pathway have been shown to rescue matrix-deprived cells from apoptosis and metabolic impairment and to cause filling of the luminal space in 3D cultures (Debnath et al., 2003b; Isakoff et al., 2005).

In epithelial cancers, the signaling pathway most frequently activated by genetic alterations is the PI3K pathway (Engelman, 2009; Samuels and Velculescu, 2004; Yuan and Cantley, 2008) and can be activated by multiple mechanisms, including altered DNA copy number and mutations of several of the components of this pathway (Carpten et al., 2007; Gewinner et al., 2009; Li et al., 1997; Samuels et al., 2004). Thus, this pathway presents an attractive candidate for targeted therapeutics. In recent years, many small molecule inhibitors targeting PI3K, AKT, and the downstream effector mTOR, have been developed; several are in clinical trials, and some (specifically, rapamycin analogs targeting mTOR) have been approved for therapy (Baselga, 2011; Courtney et al., 2010). Most initial in vitro studies of these inhibitors were performed in 2D monolayer cell cultures where it is not feasible to examine the effects of the targeted therapeutics on tumor-specific phenotypes such as loss of polarity and survival without ECM attachment. However, in studies using 3D cultures, the effects of PI3K inhibition on tumor growth in vivo correlated with effects on cell proliferation in 3D cultures more accurately than in 2D cultures, suggesting that 3D cultures better reflect drug sensitivity in vivo (Howes et al., 2007; Polo et al., 2010). In addition, other studies have shown that signaling pathway activation and drug responses in 3D cultures differ substantially from 2D cultures (Kenny et al., 2007; Liu et al., 2004; Weigelt et al., 2010), emphasizing the potential use of 3D culture to ascertain underlying mechanisms of sensitivity and resistance to targeted therapeutics as well as to predict effective drug combinations.

Inhibition of PI3K/AKT can lead to upregulation and activation of receptor tyrosine kinases (RTKs) through engagement of several homeostatic feedback loops aimed at maintaining the PI3K pathway in equilibrium. This includes a FOXO-dependent pathway (Chandarlapaty et al., 2011; Garrett et al., 2011), as well as compensatory activation of the MAPK pathway (Carrao et al., 2008; Engelman et al., 2008; Serra et al., 2011). Inhibition of upstream components of the PI3K pathway has been shown to lead to compensatory activation of HER3 (Sergina et al., 2007). In addition, inhibition of mTORC1 by allosteric inhibitors (e.g., rapamycin family) relieves a negative feedback loop from S6K to IRS1, among others, leading to activation of IGF1R, PI3K, and AKT (Cloughesy et al., 2008; Harrington et al., 2004; O'Reilly et al., 2006). Activation of compensatory pathways in response to PI3K/mTOR inhibition may limit the efficacy of drugs targeting this pathway, leading to paradoxical responses and possibly contributing to emergence of drug-resistant clones.

In this report, we examined the response of ovarian and breast tumor cells in 3D spheroid cultures to PI3K and mTOR inhibitors

in order to monitor drug-induced phenotypic changes that could not be assayed in standard 2D cultures.

## RESULTS

### Dichotomous Response to PI3K Pathway Inhibition in Tumor Spheroids

To examine how ovarian cancer cells cultured as 3D spheroids in reconstituted basement membrane (Matrigel) respond to inhibition of the PI3K/mTOR pathway, we treated several ovarian cancer cell lines with BEZ235, a dual-specificity PI3K/mTOR inhibitor (Maira et al., 2008). In 3D culture, OV2008, SKOV3, and OVCA432 cell lines form spheroid structures with a constitutive low level of proliferation (marked by Ki67 staining) localized predominantly in the outer matrix-attached cell layer (Figure 1A). A small number of apoptotic cells, marked by cleaved caspase-3 staining, were detected almost exclusively in the middle of the structures. Treatment of 6-day-old spheroids with BEZ235 induced a striking dichotomy in the induction of apoptosis between outer and inner cells, with apoptosis being exclusively localized in the inner region of the spheroids (Figure 1B; Figure S1A available online). MCAS cells, which form structures with hollow lumens, were largely resistant to apoptosis. Although apoptosis was restricted to inner cells, BEZ235 treatment suppressed proliferation throughout the structures (data not shown). OV2008 cells were treated with a wider selection of PI3K or mTOR inhibitors (Rapamycin, LY294002, GDC0941, and PIK-90) to determine the generality of this response. All inhibitors induced a similar dichotomy in apoptosis between the drug-resistant matrix-attached outer cells and the inner matrix-deprived cells (Figure S1B).

### Multiple Signaling Pathways Are Upregulated by PI3K/mTOR Inhibition

Outer 3D tumor spheroid cells could be intrinsically drug resistant, or drug treatment could induce resistance. To examine these possibilities, we performed reverse phase protein array (RPPA) analysis of ~120 proteins and phosphoproteins representing many major signaling pathways (Figure 2A). As expected, BEZ235 treatment decreased phosphorylation of proteins downstream of PI3K and mTOR (p-FOXO3a, p-4E-BP1) and reduced cell proliferation markers (PCNA, cyclinB1, cyclinE1) (Figure 2A). However, BEZ235 also induced upregulation and/or activation of multiple prosurvival proteins (Figure 2A), including several RTKs (EGFR, HER2, c-Kit, and IGF1R), cytoplasmic kinases (p-p90RSK, p-SrcY), antiapoptotic proteins (Bcl-2, XIAP1), and transcription factors (p-STAT3, p-STAT6, p-c-Jun, p-SMAD3). This response was not unique to 3D cell cultures, as 2D cultures treated with BEZ235 displayed similar responses, with multiple survival pathways being activated by BEZ235 (Figure 2A). A comparable response was also observed in BEZ235-treated MCAS spheroids and monolayer cultures (Figures S2A and S2B), with upregulation of Bcl-2, IGF1R $\beta$ , p-STAT3, p-STAT6, p-c-Jun, p-SMAD3, p-p90RSK, EGFR, and p-HER2; however, Bcl-xL and p-Erk were also upregulated in MCAS cells.

RPPA results were validated by western blot for Bcl-2, p-IGF1R $\beta$ , c-Jun, p-p90RSK, p-EGFR, p-S6, and p-4E-BP1 (Figures 2B; Figure S2B). While detectable changes in total

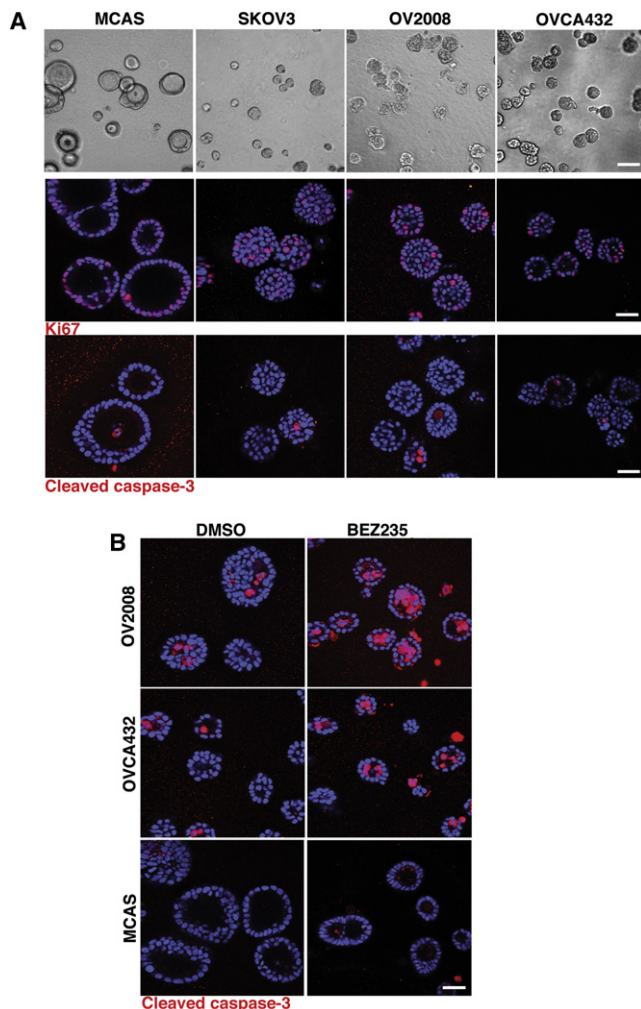


**Figure 1. Ovarian Cancer Cell Lines Form Acinlike Structures in Reconstituted Basement Membrane and Matrix-Attached Cells Show Resistance to BEZ235-Induced Apoptosis**

(A) Ovarian cancer cell lines (*PIK3CA* mutations indicated in parentheses) MCAS (H1047R), SKOV3 (H1047R), OVCA432 (unknown) and OV2008 (E545K) were cultured in Matrigel for 6 days and stained for Ki67 (red) or cleaved caspase-3 (red) and counterstained with DAPI (blue). (Mutation information was provided by S. Jones and V. Velculescu, personal communication.) One representative phase or confocal section is shown.

(B) OV2008, MCAS, and OVCA432 cells were cultured in Matrigel for 4 days and 1  $\mu$ M BEZ235 was added for 48 hr before the cells were fixed, stained for cleaved caspase-3 (red) and DAPI (blue) and imaged by confocal microscopy. Confocal scale bar, 50  $\mu$ m; phase contrast scale bar, 200  $\mu$ m. See also Figure S1.

IGF1R $\beta$  and p-AKT<sup>S473</sup> were modest by RPPA, we reproducibly detected up- or downregulation, respectively, upon BEZ235 treatment by western blotting. Total protein levels of 4E-BP1 inversely correlated with those of p-4E-BP1 as previously reported (Yamaguchi et al., 2008). Furthermore, we confirmed that p-Erk was unaffected by BEZ235 treatment (Figure 2B).

To examine whether the proteins induced by BEZ235 were specifically induced in matrix-attached outer cells, we performed immunofluorescence analysis of Bcl-2 and Bcl-xL in

BEZ235-treated OV2008 and MCAS cells. Indeed, upregulation of Bcl-2 and Bcl-xL was strongly enriched in outer, ECM-attached cells (Figure S2C). As ECM contact activates integrins, we addressed whether blocking integrin signaling could inhibit the adaptive response of the matrix-attached outer cells. Downregulation of  $\beta$ 1-integrin,  $\beta$ 4-integrin, FAK, or ILK alone did not abrogate Bcl-2 or IGF1R upregulation; however, inhibition of several integrin-pathway components in parallel, prevented upregulation of these proteins (Figure S2H). These results suggest that multiple integrins may contribute to the adaptive program; this possibility was supported by the evidence that additional integrins are induced at the transcriptional level by BEZ235 treatment (Figure S2I).

#### **Inhibition of Bcl-2, IGF1R, or EGFR in Combination with BEZ235 Abrogates Matrix Protection**

As BEZ235 treatment induced upregulation of several cell survival pathways, we assessed whether these pathways are critical for the resistance of matrix-attached cells. Given the critical role of Bcl-2 family members in regulation of cell survival (Walensky, 2006), we first examined the effects of inhibiting Bcl-2 family proteins in combination with BEZ235. Treatment with the Bcl-2 family inhibitor ABT-737, which targets Bcl-2, Bcl-xL, and Bcl-w (Oltersdorf et al., 2005), induced apoptosis of inner spheroid cells but did not affect survival of outer cells (Figure 2C). However, combined treatment with ABT-737 and BEZ235 induced massive disintegration of the spheroids. Immunostaining for cleaved caspase-3 confirmed extensive apoptosis throughout the entire spheroid structure (Figure 2C). Similar effects were observed using the structurally distinct Bcl-2 inhibitor, HA-14.1 (Figure S2D). Analysis of four additional ovarian cancer cell lines revealed similar synthetic lethality of ABT-737 and BEZ235 (Figure S2E).

We also examined whether the BEZ235-induced RTKs EGFR and IGF1R are essential for survival of BEZ235-treated cells. BEZ235 treatment together with EGFR inhibitors PD168393 or Gefitinib caused marked cell death (Figure S2F). In addition, downregulation of IGF1R with shRNAs caused death of ECM-attached cells treated with BEZ235 (Figure S2G). To address whether inhibition of other antiapoptotic signaling proteins that were not induced in the ECM-attached cells by BEZ235 would synergize with BEZ235, we incubated BEZ235-treated cells with inhibitors of MEK, PKC, PKA, Jak, or IKK. Inhibition of these proteins in combination with BEZ235 did not enhance death of outer, ECM-attached cells (Figure S2D; data not shown). These results imply that BEZ235-treatment selectively induces expression of several prosurvival proteins in ECM-attached cells and indicate that some of these induced proteins, such as Bcl-2, EGFR, and IGF-1R, are required for cancer cell survival. Our studies also validate RPPA as an efficient tool in identifying drug resistance proteins and pathways.

#### **Many Induced Proteins Are Upregulated at the mRNA Level through FOXO-Dependent Transcription**

To address whether BEZ235-induced protein upregulation reflects changes in mRNA expression, we performed mRNA microarray analyses on drug-treated OV2008 and MCAS cells cultured in 3D. Several genes, such as *IGF1R*, *EGFR*, *BCL2*, *IRS1*, and *SMAD3*, displayed increased mRNA expression,

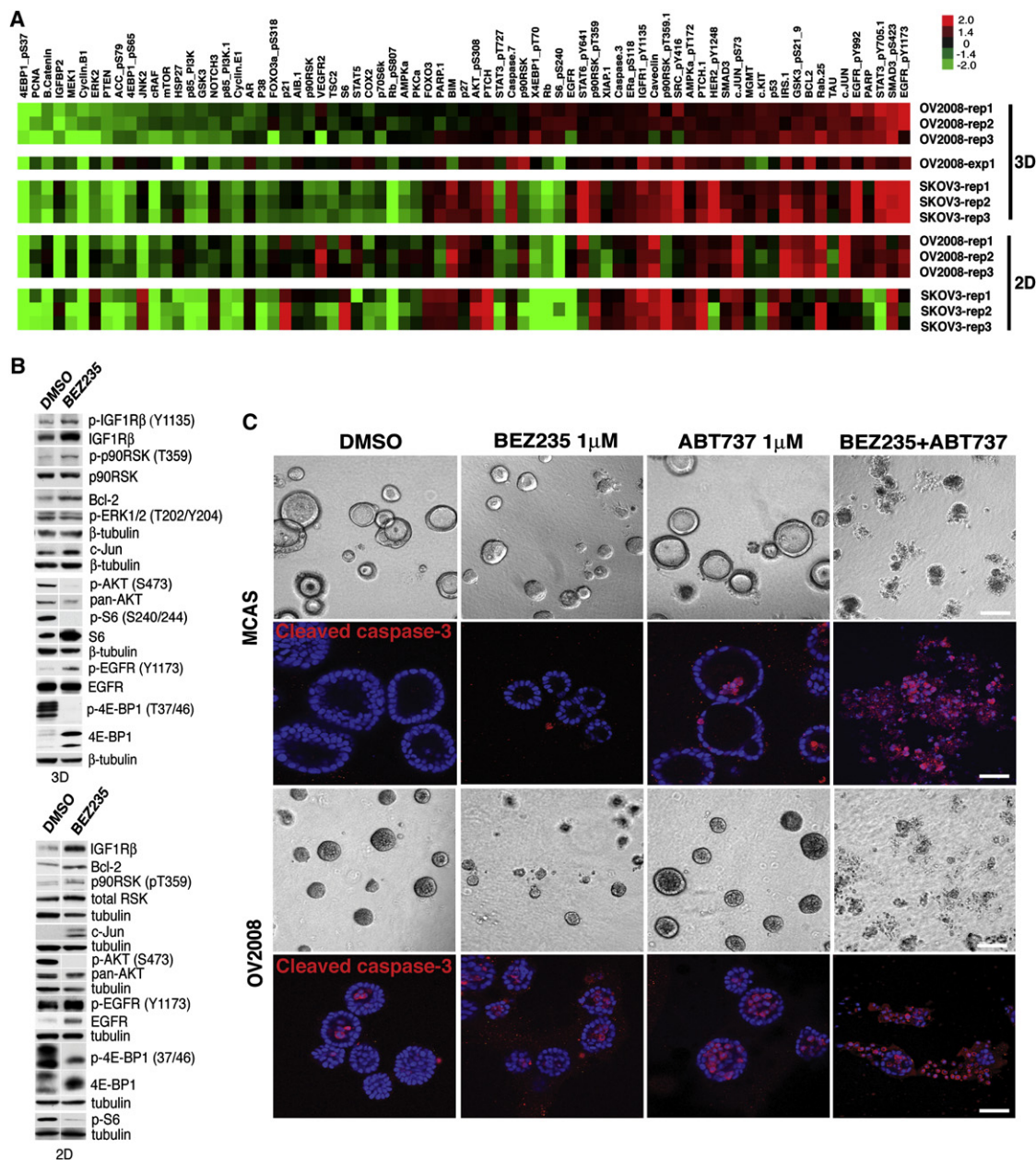


### Figure 2. RPPA Reveals Multiple Proteins Upregulated in BEZ235-Treated Cells

(A) OV2008 and SKOV3 cells were cultured in Matrigel (3D) or monolayer (2D) and treated with BEZ235 or DMSO, and the protein lysates were analyzed by RPPA (red, increased signal; and green, decreased signal, upon BEZ235 treatment). Samples are normalized against DMSO-treated controls. Proteins with significant differences ( $p < 0.05$ , Student's  $t$  test) between BEZ235- and DMSO-treated OV2008 cells in an experiment performed in triplicate are shown for all experiments. (B) Several of the up- and downregulated proteins from OV2008 RPPA were validated by western blot analysis.

(C) Bcl-2 inhibition abrogates outer cell resistance to PI3K/mTOR inhibition. MCAS and OV2008 cell lines were cultured in 3D and treated with DMSO, BEZ235, or ABT737 alone or in combination for 48 hr. Cells were imaged by phase contrast, fixed, stained for cleaved caspase-3 (red), and imaged by phase contrast or confocal microscopy. Confocal scale bar, 50  $\mu$ m; phase contrast scale bar, 200  $\mu$ m. See also [Figure S2](#).

indicating that a subset of the RPPA results reflect, at least in part, changes in mRNA levels (Figure 3A).

Inhibition of PI3K prevents activation of AKT1/2/3, which phosphorylates FOXO family transcription factors, preventing their nuclear translocation (Brunet et al., 1999; Kops et al., 1999). Because FOXO family members were recently demon-

strated to induce transcription of several RTKs upon AKT inhibition (Chandarlapaty et al., 2011), we analyzed the mRNA expression array for FOXO targets. A significant enrichment of known FOXO target genes were upregulated after BEZ235 treatment ( $p = 0.00335$ , hypergeometric probability distribution), including *CDKN1B* (p27Kip1), *TSC1*, *IRS2*, and *FOXO1/3* (Figure 3B).

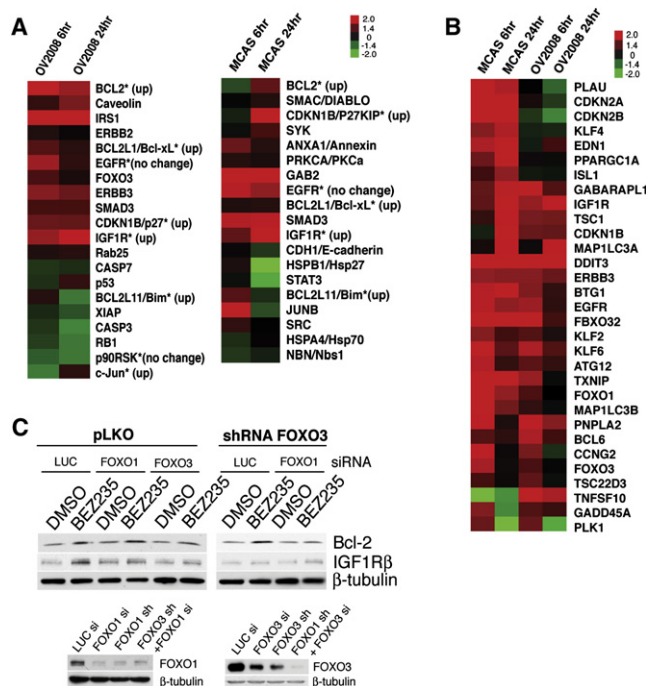


**Figure 3. Many of the Induced Proteins Are Upregulated at the mRNA Level through FOXO-Dependent Transcription**

(A) Heatmaps showing relative levels of mRNA of proteins that were upregulated in the RPPA in OV2008 and MCAS cells; additional RTKs not present in RPPA were also selected for analysis. mRNA values were normalized relative to DMSO-treated cells. Red, upregulation in response to BEZ235 treatment; and green, downregulation. Approximately 60% (12/20 for OV2008 and 11/19 for MCAS) of the proteins that are detectably upregulated in response to BEZ235 in RPPAs and detected in the mRNA expression array show elevated mRNA at either time point ( $p = 0.000385$  for OV2008 and  $p = 0.041$  for MCAS, hypergeometric probability distribution). Proteins validated by western blots are marked by an asterisk, and the direction of change is indicated in parentheses.

(B) Heatmap showing relative levels of mRNAs previously reported as FOXO targets; of 117 reported FOXO targets, 31 are upregulated in at least two conditions ( $p < .01$ ), showing a significant enrichment ( $p = 0.00335$ , hypergeometric probability distribution).

(C) FOXO1 and FOXO3 were downregulated in OV2008 cells by siRNAs targeting FOXO1 or FOXO3 (left) or transduction of a lentiviral vector encoding shRNA for FOXO3, together with FOXO1 siRNAs (right). Lysates were probed with antibodies to Bcl-2 and IGF1Rβ to monitor upregulation upon 18-hr BEZ235 treatment. The efficacy of the knockdowns was verified by western blotting of FOXO1 and FOXO3.

Several FOXO-regulated RTKs (*ERBB3*, *EGFR*, and *IGF1R*) were upregulated in BEZ235-treated cells (Figure 3B), suggesting that FOXO could mediate transcription of some of the upregulated proteins. Knockdown of either FOXO1 or FOXO3 reduced IGF1Rβ upregulation by BEZ235, whereas FOXO3 knockdown reduced Bcl-2 as well; knockdown of both FOXO1 and FOXO3 inhibited upregulation of both Bcl-2 and IGF1Rβ (Figure 3C).

#### Inhibition of the mTORC1 Target 4E-BP1 Correlates with Upregulation of Bcl-2 and IGF1Rβ

BEZ235 is a dual inhibitor of both PI3K and mTORC1/2. To assess whether inhibition of either PI3K or TORC1/2 is necessary

and/or sufficient to induce Bcl-2 and synergize with ABT-737, we examined several additional inhibitors of PI3K or mTOR: GDC0941 (PI3K inhibitor at 250nM, PI3K, and mTOR at 1 μM), rapamycin (allosteric mTOR inhibitor selective for mTORC1), and Torin1 (mTORC1/2 catalytic inhibitor). The most cell death was induced with ABT-737 in combination with either BEZ235, Torin1, or GDC0941 at a concentration that also inhibits mTOR (Figures 4A and 4B). Neither the PI3K-selective (250 nM GDC0941) nor the mTORC1-specific (rapamycin) inhibitors induced spheroid disintegration with ABT-737 (Figures 4A and 4B). Western blots demonstrated decreased p-4E-BP1 correlated with Bcl-2 upregulation (Figure 4C). 4E-BP1 phosphorylation is relatively insensitive to rapamycin, and long-term suppression of 4E-BP1 requires inhibition of mTOR catalytic activity (Choo et al., 2008; Feldman et al., 2009; Thoreen et al., 2009). We also noticed that inhibition of PI3K enhanced Bcl-2 upregulation, as 250 nM Torin1 significantly inhibited p-4E-BP1, but did not induce Bcl-2 as efficiently as 1 μM Torin or 1 μM GDC0941, which inhibit both 4E-BP1 and AKT phosphorylation (Figure 4C). These findings demonstrate that reduced 4E-BP1 phosphorylation correlates with upregulation of Bcl-2, but PI3K inhibition enhances this effect, likely through other mechanisms such as FOXO activation.

#### Increased Cap-Independent Translation in Response to mTOR Inhibition

mTORC1 activates cap-dependent translation by phosphorylating and inhibiting 4E-BP1. However, cell stress can suppress cap-dependent translation through inhibition of mTOR. Under these conditions, essential cell survival proteins (i.e., regulators of cell cycle, development, apoptosis, and stress response) are translated through a cap-independent mechanism (Holcik and Sonenberg, 2005; Silvera et al., 2010). A switch to cap-independent translation can also be achieved by direct inhibition of mTORC1 or perturbation of 4E-BP1 (Braunstein et al., 2007; Choo et al., 2008; Feldman et al., 2009; Hsieh et al., 2010; Moerke et al., 2007; She et al., 2010; Thoreen et al., 2009). mRNAs translated under these conditions have a highly structured 5'-untranslated region (5'-UTR), which often harbors an IRES sequence and several upstream AUGs. It is interesting that multiple proteins upregulated by BEZ235—including Bcl-2, Bcl-xL, IGF1R, XIAP, c-Jun, and p53—can all be translated in a cap-independent manner under cellular stress. To address whether cap-independent translation increases in response to PI3K/mTOR inhibition, we used a bicistronic luciferase reporter where Renilla luciferase is cap dependent and firefly luciferase is regulated by the cap-independent cricket paralysis virus IRES. Indeed, OV2008 and MCAS cells treated with BEZ235 or Torin1 (Figure 5A), but not rapamycin or 250 nM GDC0941 (Figures S3A and S3B), upregulated cap-independent translation, suggesting that an IRES translation is induced by mTOR inhibitors.

We also utilized a BCL-2 IRES reporter that contains the BCL-2 5'-UTR upstream of firefly luciferase and is only translated by cap-independent translation (Suo et al., 2010). A short unstructured 5'-UTR reporter was used to monitor cap-dependent translation. BEZ235 treatment caused an ~38% increase in Bcl-2 IRES translation with a concomitant 60% decrease in cap-dependent reporter translation (Figure 5B). These results provide evidence

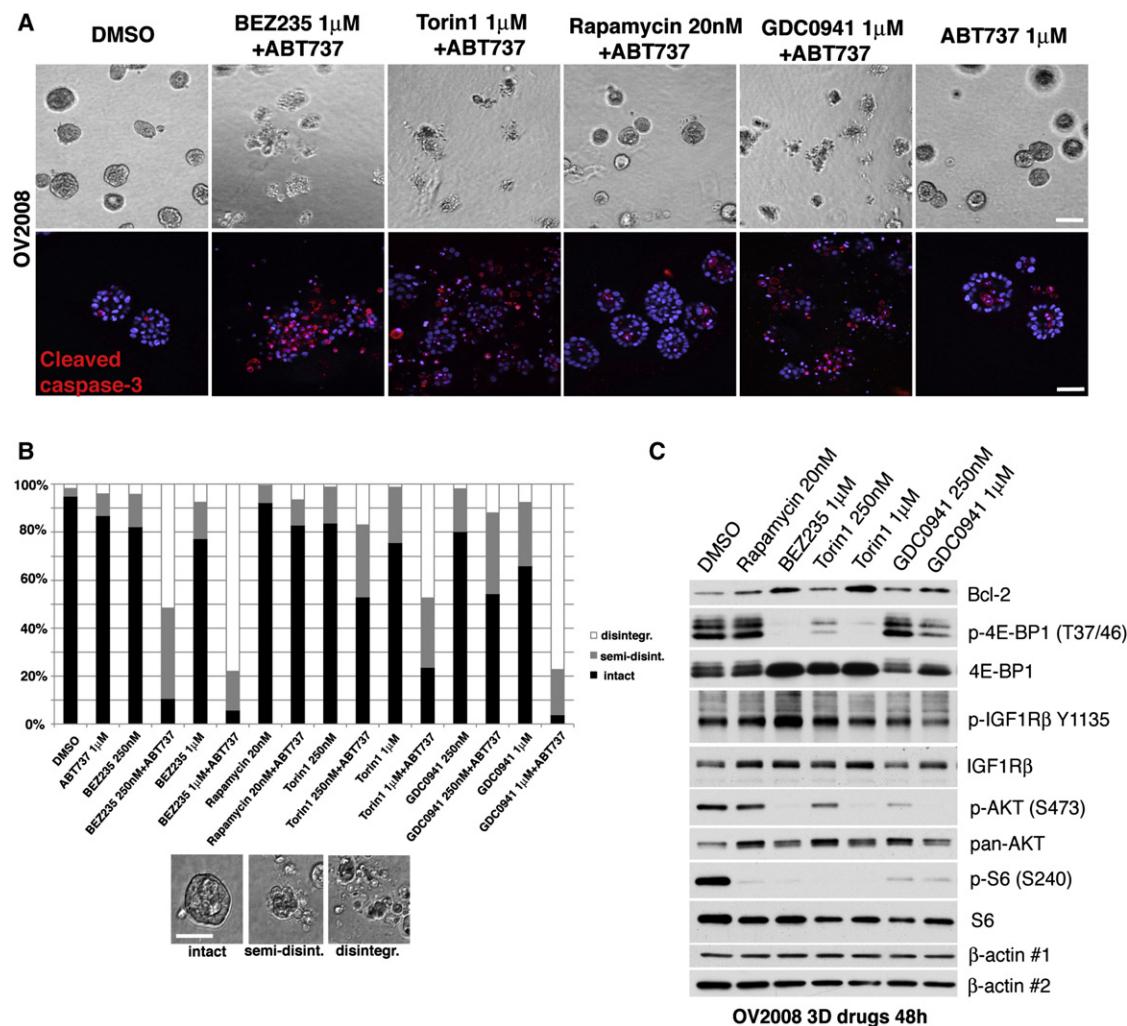


**Figure 4. Inhibition of 4E-BP1 Phosphorylation Correlates with the Upregulation of Bcl-2 and IGF1R and Disintegration of 3D Spheroids**

(A) OV2008 cells were grown in 3D cultures for 4 days and treated with indicated inhibitors targeting PI3K and/or mTOR in combination with ABT-737 for 48 hr. The cells were fixed, stained for cleaved caspase-3 (red) and DAPI (blue), and imaged with phase and confocal microscopy. Confocal scale bar, 50  $\mu$ m; phase contrast scale bar, 200  $\mu$ m.

(B) OV2008 cells were grown in 3D culture and treated with indicated drugs and quantitated for structural integrity after a 48-hr drug treatment as described in [Experimental Procedures](#). Representative images of scored structures (intact, semidisintegrated, and disintegrated) are shown in the lower panel; scale bar, 100  $\mu$ m.

(C) Lysates were harvested from structures cultured in 3D and analyzed for Bcl-2 and IGF1R $\beta$ , p-4E-BP1<sup>T37/46</sup>, p-S6<sup>S240</sup>, and p-AKT<sup>S473</sup> expression after the indicated 48-hr drug treatments.

that BEZ235 treatment increases cap-independent Bcl-2 translation while cap-dependent translation is inhibited.

Phosphorylation of the eukaryotic translation initiation factor 2 alpha (eIF2 $\alpha$ ), a component of the ternary translation initiation complex, selectively suppresses cap-dependent translation in response to cellular stress ([Holcik and Sonenberg, 2005](#); [Raven and Koromilas, 2008](#); [Silvera et al., 2010](#); [Wek et al., 2006](#)). BEZ235 treatment increased eIF2 $\alpha$  phosphorylation over time, reaching a plateau at 24 hr in OV2008 and 48 hr in MCAS cells ([Figure 5C](#)). Additionally, of 23 significantly upregulated proteins after BEZ235 treatment identified by RPPA, 10 have putative or validated IRES motifs. This represents a significant enrichment ( $p = 0.0083$ ), as only 3%–5% of all mRNAs have potential IRES sequences ([Johannes et al., 1999](#)).

### Breast Tumor Cell Lines Also Display the Adaptive Response to BEZ235 and Are Sensitive to Combined PI3K/mTOR and Bcl-2 Inhibition

To test whether the BEZ235 response is induced in other epithelial tumors, we performed RPPA on BEZ235-treated breast cancer cell lines harboring mutations in *PIK3CA* or deletions in *PTEN*. While there were variations in individual proteins that were affected by treatment, the adaptive response was strikingly similar, with PI3K/mTOR inhibition causing an induction of RTKs (HER3, IGF1R $\beta$ , HER2, and EGFR), as well as Bcl-2 and Bcl-xL ([Figure 6A](#)). We also detected an adaptive response to BEZ235 in nontransformed MCF10A cells, although the most strongly upregulated proteins varied relative to the breast tumor cell lines. This likely reflects the dominance of the EGFR-ERK signaling

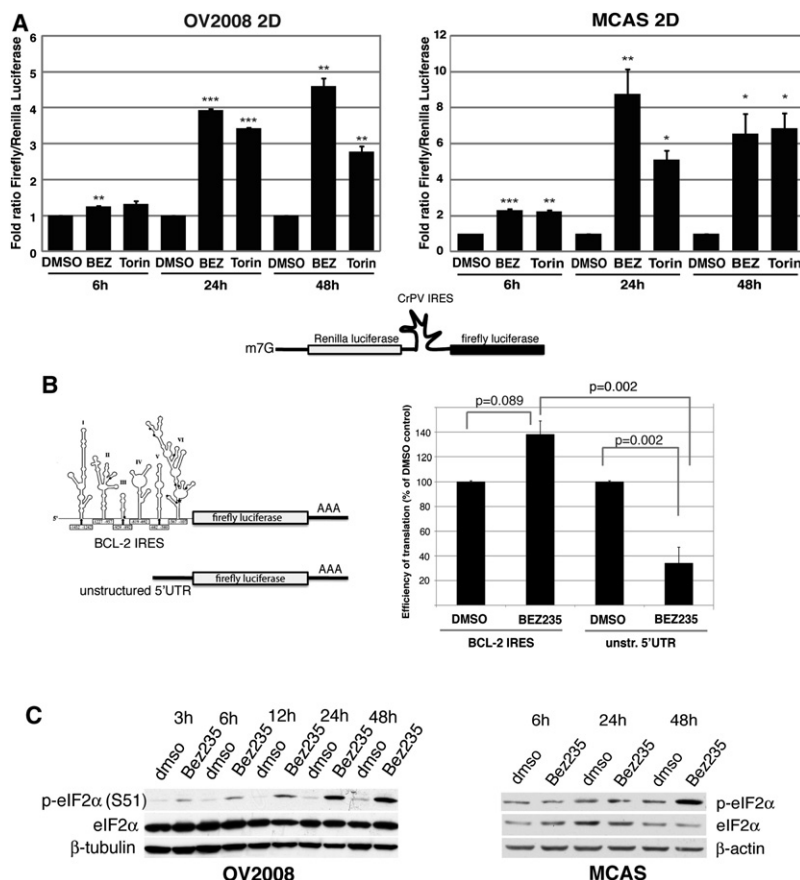


**Figure 5. Cap-Independent Translation Increases in Response to BEZ235 Treatment**

(A) A dual luciferase reporter (Renilla luciferase expression mediated by cap-dependent translation and firefly luciferase expression by CrPV IRES) was used to monitor cap-independent translation in OV2008 and MCAS cells in response to BEZ235 or Torin1 treatment. The fold increase in the ratio of the firefly/Renilla luciferase levels was calculated as described in [Experimental Procedures](#). \*p < 0.05; \*\*p < 0.01; \*\*\*p < 0.001.

(B) BCL-2 IRES translational activity was monitored by a reporter containing the BCL2 IRES sequence upstream of firefly luciferase. Cap-dependent translation was monitored with a reporter containing a short unstructured 5'UTR fused to firefly luciferase. Luciferase expression from both reporters was normalized to luciferase mRNA expression and shown as fold change compared to DMSO control. Cartoon modified from [Suo et al., 2010](#).

(C) Upregulation of eIF2α phosphorylation was monitored in response to BEZ235 treatment over time in OV2008 and MCAS cells. Error bars shown as ± SEM. See also [Figure S3](#).

subcutaneous injection of MCAS and OV2008 cells. Tumors were treated with the PI3K/mTOR inhibitor GNE493 ([Sutherland et al., 2010](#)) and ABT-737 either alone or in combination every 24 hr for 7–9 days. Vehicle and ABT-737-treated MCAS tumors showed similar growth rates, whereas GNE493 significantly decreased tumor growth. Remarkably, combined treatment caused marked inhibition of tumor cell growth relative to GNE493 alone ([Figure 7A](#)). Similar results were obtained with OV2008 xenograft tumors ([Figure 7A](#)). Furthermore, hematoxylin and eosin (H&E) staining of tumor sections revealed that combination treatment induced increased cell death relative to single agents ([Figure 7B](#)). Combination treatment caused weight loss during the 7-day treatment (5% on average), and one mouse (of 23) showed more significant weight loss (~20%) and died on Day 7 of treatment, indicating that the combination may have some toxicity.

Lysates from GNE493-treated MCAS tumors showed the expected decrease in AKT, 4EBP1, and S6 phosphorylation, and it is important to note that Bcl-2, Bcl-xL, and IGF1Rβ were upregulated in response to treatment ([Figure 7C](#)). These results provide evidence that PI3K/mTOR inhibition *in vivo* induces a similar adaptive response as in 3D spheroids and monolayer culture *in vitro* and that Bcl-2 family inhibition can significantly enhance the efficacy PI3K/mTOR inhibition *in vivo*.

To address whether primary patient samples are sensitive to combination treatment, we isolated cancer cells from pleural and peritoneal fluid exudates from two breast cancer patients and two ovarian cancer patients. These samples were cultured in reconstituted basement membrane for 8 days followed by treatment with BEZ235, ABT-263 (BCL2 inhibitor similar to ABT-737; [Ackler et al., 2008](#)), PD168393, and combinations for 48 hr. Single-agent inhibition did not show significant efficacy in any of the treated patient samples ([Figure 7D](#)). The response to dual inhibition of PI3K/mTOR and EGFR was heterogeneous, only reaching significance in ovarian sample F44 ([Figure 7D](#)).

pathway in these cells (note upregulated p-EGFR, p-ERK, p-BAD<sup>S112</sup>, and downregulated Bim) ([Figures 6A and 6D](#)).

We also examined whether the breast tumor cell lines would display enhanced cell death with combined inhibition of PI3K/mTOR and Bcl-2 in 3D cultures. In contrast to the well-organized ovarian cell lines, the breast cancer lines were less organized, precluding detection of a clear dichotomy between the outer and inner cell layers. However, as seen with ovarian lines, inhibition of PI3K/mTOR or Bcl-2 family members alone did not induce dramatic cell death, but combined treatment caused significant structural disintegration and cell death in MDA-MB-468 and HCC-1569 cells and, to a lesser extent, in T-47D cells ([Figure 6B](#)). In contrast, the overall integrity of non-transformed MCF-10A cell structures treated with both BEZ235 and ABT-737 was not significantly affected, as cells in contact with reconstituted matrix were resistant to apoptotic effects of the combination ([Figure 6C](#)). Nontransformed, nonimmortalized human mammary epithelial cells (HMECs) also showed no sensitivity to the dual treatment ([Figure S4](#)), indicating that cancer cells are more sensitive to this treatment than normal epithelial cells.

#### Mouse Xenografts and Primary Ovarian and Breast Cancer Patient Samples Show Sensitivity to Dual Inhibition of PI3K/mTOR and Bcl-2

To test the effectiveness of inhibiting PI3K/mTOR and/or the Bcl-2 family *in vivo*, we performed xenograft studies with

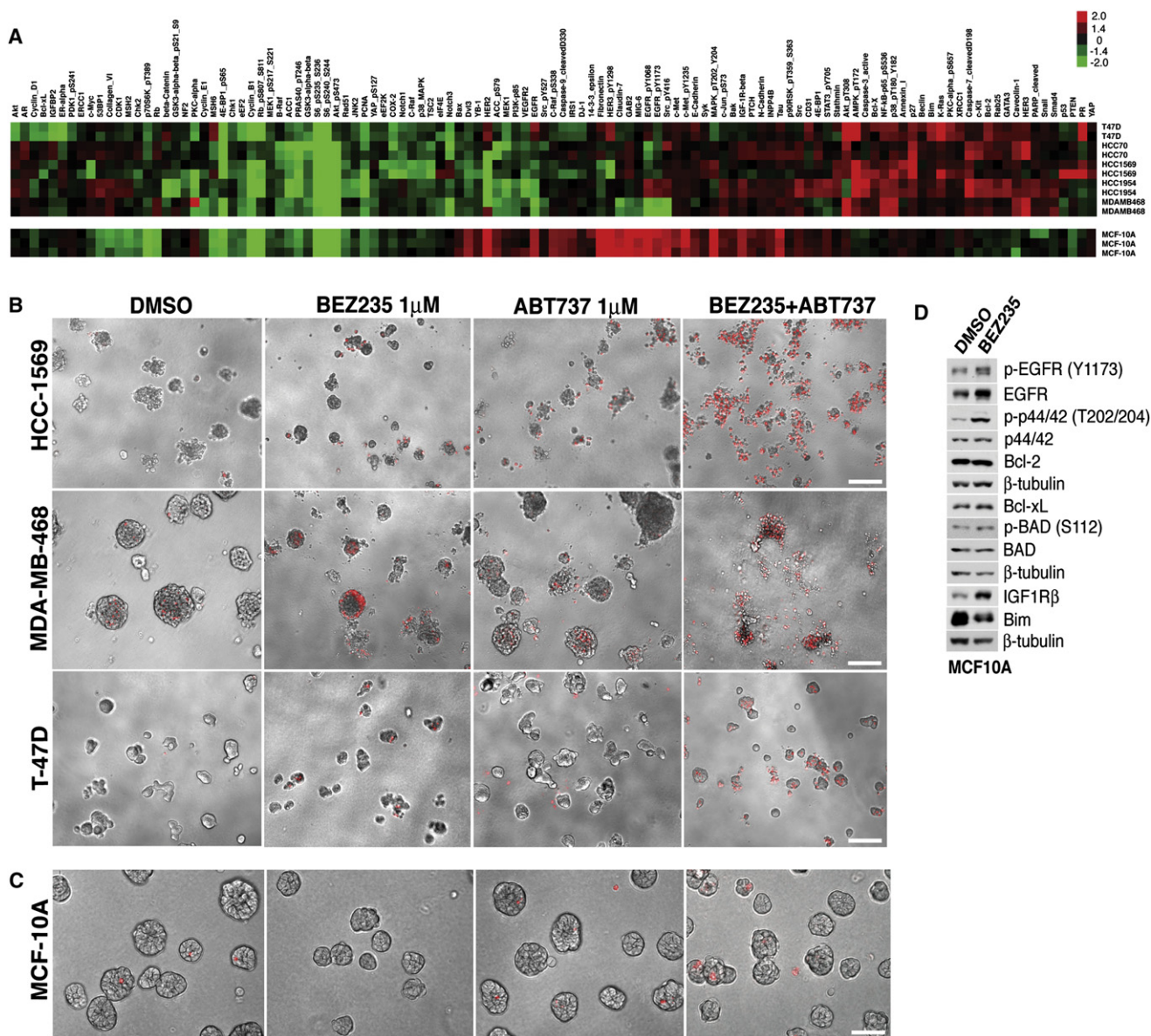


**Figure 6. Analysis of BEZ235-Treated Normal Breast Epithelial Cells and Breast Tumor Cell Lines**

(A) RPPA analysis of breast cancer cell line spheroids and MCF10A cell monolayers treated with BEZ235 for 48 hr (red, increased signal upon BEZ235 treatment; green, decreased signal upon BEZ235 treatment). Samples are normalized against DMSO-treated controls.

(B and C) T-47D, MDA-MB-468, and HCC-1569 breast cancer cell lines (in 6B) and nontransformed immortalized MCF10A breast epithelial cells (in 6C) were cultured in Matrigel and treated with DMSO, BEZ235, or ABT737 alone or in combination for 48 hr. Cells were imaged by phase contrast, fixed, stained with EtBr (red) to mark dead cells, and imaged by wide-field phase contrast microscopy. Scale bar, 200  $\mu$ m.

(D) Immunoblots of MCF-10A cells treated with DMSO or BEZ235 for 48 hr. See also Figure S4.

However, all four samples showed significant response to dual treatment of BEZ235 and ABT-263 (Figure 7D). Together, these preliminary results suggest that further evaluation of this drug combination in more in vivo models and primary human tumor samples is warranted.

## DISCUSSION

Here, using 3D spheroid cell cultures, we show that matrix-attached tumor cells are specifically resistant to dual PI3K/

mTOR inhibition by inducing an adaptive response involving up-regulation of multiple prosurvival proteins. Induction of the adaptive response involves increased cap-independent translation and FOXO mediated transcription. It is interesting that this response resembles the highly conserved stress response induced in organisms deprived of nutrients and growth factors (Gilbert et al., 2007; Jefferson and Kimball, 2003; Marr et al., 2007; Puig and Tjian, 2005; Villa-Cuesta et al., 2010). In addition, this work establishes the 3D-based model system, particularly in combination with a high throughput proteomics approach, as

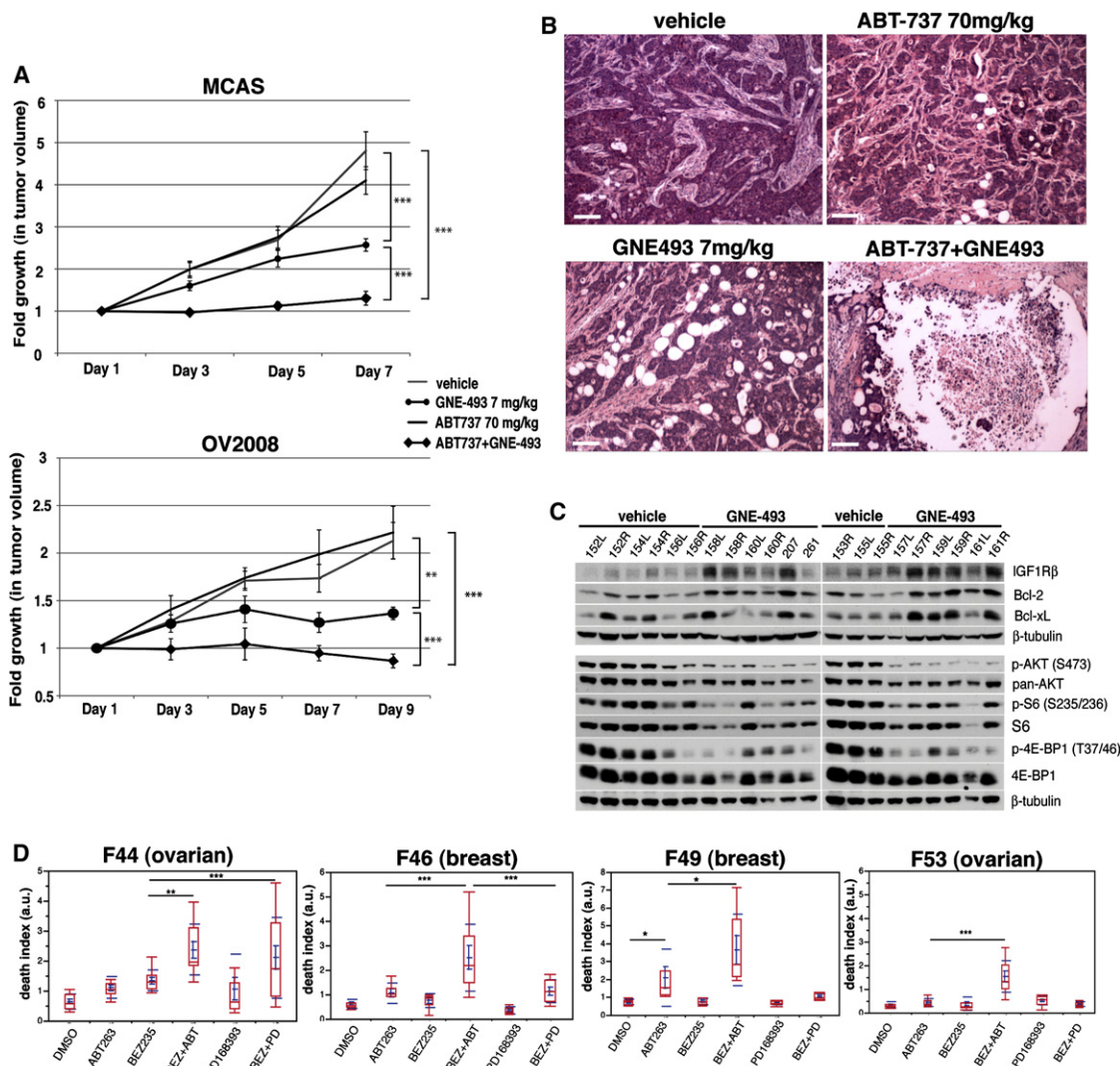


**Figure 7. Dual Inhibition of Bcl-2 and PI3K/mTOR in an In Vivo Xenograft Model and in Primary Patient Samples Causes Decreased Tumor Growth and Enhanced Cell Death**

(A) MCAS and OV2008 cells were injected subcutaneously into female nod/scid mice and, after tumors were palpable, mice were treated every 24 hr with vehicle, GNE493 (mTOR inhibitor, 7mg/kg), ABT-737 (70 mg/kg), or a combination of both. Tumors were measured on indicated days, and the data are reported as the fold change relative to size of the same tumor on Day 1. The data, represented as the average  $\pm$  SEM, were derived from experiments in which 72 tumors were monitored in 43 mice for MCAS and 40 tumors were monitored in 20 mice for OV2008. \*\*\* $p < 0.001$ ; \*\* $p < 0.005$ .

(B) Tumor sections from MCAS xenografts were stained with H&E and imaged at 4 $\times$ . Representative images of tumors of similar size ( $\sim 300\text{mm}^3$ ) for each treatment are shown. Scale bar, 100  $\mu\text{m}$ .

(C) Western blot analysis of vehicle- and GNE493-treated MCAS tumors. Tumors were harvested 4 hr after the last dosing on Day 7 and probed with the indicated antibodies. Numbers above each lane indicate tumor numbers.

(D) Tumor cells isolated from peritoneal or pleural fluid exudates were cultured in Matrigel for 8 days and treated with the indicated inhibitors (ABT-263, an identical Bcl-2 inhibitor to ABT-737). Cell death was quantified by analysis of dead cells (as marked by EtBr) over total cell number (as analyzed by Hoechst stain). \* $p < 0.05$ ; \*\* $p < 0.01$ ; \*\*\* $p < 0.005$ . Red boxes indicate average data distribution, and highest and lowest value are indicated with connected red caps. Single blue caps indicate SD and connected blue caps indicate  $\pm$  SEM.

a valuable approach for rational prediction of effective drug combinations.

Although treatment of cancer cells in monolayer cultures with PI3K/mTOR inhibitors suppresses cell proliferation, apoptosis is not commonly observed. In contrast, these inhibitors are potent inducers of apoptosis of inner cells within 3D spheroid cultures that are not attached to matrix, whereas cells in 2D cultures and the outer cells of tumor spheroids induce a strong survival

program and provide an explanation for the lack of toxicity of PI3K/mTOR inhibitors in traditional 2D cultures. The enhanced sensitivity of the inner cells of 3D spheroids to apoptosis infers that PI3K activity is specifically required for survival of this population of tumor cells. The inner cells in 3D spheroids lack exposure to ECM components and likely rely on sustained PI3K activity for anchorage-independent survival. Indeed, oncogenic mutant variants of PI3K have been shown to rescue cells

from apoptosis caused by loss of matrix signaling (Isakoff et al., 2005; Martin et al., 2006; Schafer et al., 2009). These studies, together with our studies of spheroid cultures, highlight the critical role of the PI3K pathway in the survival of matrix-deprived cells and raise the question whether human epithelial tumor cells may display differential sensitivity to PI3K inhibitors depending on their differential association with ECM components.

The matrix-attached tumor cells initiate a transcriptional and translational program in response to PI3K/mTOR inhibition involving expression of signaling proteins that regulate survival. Whether the induction of this program by PI3K/mTOR inhibitors is exclusively due to ECM attachment or is dependent on other features of the outer cells (e.g., cell-cell adhesion or polarity) remains to be established. Weaver and coworkers have shown that  $\alpha 6/\beta 4$ -integrin-dependent cell polarity controls responses to apoptotic stimuli via NF $\kappa$ B activation in normal epithelial cells (Friedland et al., 2007; Weaver et al., 2002); however, polarity of the outer cells was not required for protection in this study, and inhibition of NF $\kappa$ B signaling by expression of the NF $\kappa$ B super-repressor did not induce cell death in OV2008 BEZ235-treated cells. It has also been shown that  $\beta 4$ -integrin signaling can enhance RTK signaling, invasion, and metastasis through c-Jun and STAT3 (Guo et al., 2006); however, expression of dominant-negative c-Jun or downregulation of STAT3 did not prevent the adaptive response to PI3K/mTOR inhibition in our system (T.M., unpublished results). While integrins are likely critical for the induction of the adaptive response, we were unable to identify a specific integrin or downstream component that plays a dominant role in the response, suggesting that this adaptive response is robust and likely includes several components of the integrin-signaling pathway.

Inhibition of PI3K pathway has been shown to relieve negative feedback inhibition of upstream pathways. Recently, two reports (Chandralapaty et al., 2011; Garrett et al., 2011) described induction of expression of RTKs by FOXO transcription factors after inhibition of HER2 or AKT. We also observed significant enrichment in FOXO transcriptional targets after BEZ235 treatment, suggesting a role for FOXO transcription factors in the induction of the adaptive response at the mRNA level. However, our studies involving a more comprehensive proteomic approach revealed a much broader BEZ235-induced program involving significant translational regulation. Several lines of evidence support a role for cap-independent translation in the adaptive response. First, decreased p-4E-BP1 correlated with upregulation of Bcl-2 and IGF1R $\beta$ . Because 4E-BP1 is a potent inhibitor of cap-dependent translation (Choo et al., 2008; Hsieh et al., 2010; Thoreen et al., 2009), this evidence, together with the presence of predicted or validated IRES sequences in many of the upregulated proteins, raised the possibility that cap-independent translation contributes to this program. In addition, using two reporters, we found that BEZ235 (but not rapamycin, which does not inhibit 4E-BP1 significantly, or a selective PI3K inhibitor) caused an increase in IRES-mediated translation and a significant decrease in cap-dependent translation, supporting the utilization of cap-independent translation in the context of mTOR inhibition.

Cells downregulate global translation under stress and rely on the less efficient cap-independent translation for production of proteins critical for cell survival (Holcik and Sonenberg,

2005; Silvera et al., 2010). Our results suggest that cancer cells may use a similar program to mediate survival under the stress of PI3K/mTOR inhibition. PI3K pathway inhibition not only reduces growth factor signaling but also inhibits nutrient uptake, mimicking nutrient starvation. It is not surprising that the adaptive response to PI3K/mTOR inhibition resembles the highly conserved stress responses observed in lower eukaryotes in response to nutrient deprivation as well as endoplasmic reticulum, irradiation, or oxidative stress (Fels and Koumenis, 2006; Sengupta et al., 2010; Wek et al., 2006). In *Drosophila melanogaster*, nutrient deprivation leads to repression of cap-dependent translation and dFoxO-mediated induction of insulin receptor expression. Both dFoxO and insulin receptor can be translated via IRES-mediated mechanisms and are required for survival (Marr et al., 2007; Villa-Cuesta et al., 2010). A similar response to dietary restriction is also observed in *Caenorhabditis elegans* (Syntichaki et al., 2007). The adaptive response to nutrient or amino acid starvation also requires eIF2 $\alpha$  phosphorylation, which decreases translation initiation generally; however, some IRES-containing mRNAs are preferentially translated (Allam and Ali, 2010; Fernandez et al., 2002; Gerlitz et al., 2002; Terenin et al., 2008). It is interesting that eIF2 $\alpha$  phosphorylation also contributes to cell survival upon glucose deficiency and is associated with increased XIAP and Bcl-xL translation, both of which have been shown to harbor IRES sequences (Muaddi et al., 2010). Given that PI3K pathway inhibition suppresses glucose and amino acid transport and that mTOR inhibition suppresses cap-dependent translation (Choo et al., 2008; Hsieh et al., 2010; Thoreen et al., 2009), the evidence that combined PI3K/mTOR inhibitors elicit responses similar to those induced by nutrient starvation is not surprising. However, it has not been appreciated that targeted therapies would elicit these types of responses and that these would be amenable to rational therapeutic targeting.

Among the PI3K/mTOR inhibitor upregulated proteins, RTKs and antiapoptotic Bcl-2 family members were the most attractive targets for combination therapies, given their known role in cell survival. It is of interest that tamoxifen- or HER2/EGFR-resistant tumors display upregulation of several of the same targets, such as IGF1R, EGFR, and HER2 (Creighton et al., 2008; Massarweh et al., 2008; Plati et al., 2011; Riggins et al., 2007), and chemoresistance in ovarian carcinomas is associated with upregulation of Bcl-2 and Bcl-xL (Giménez-Bonafé et al., 2009; Jain and Meyer-Hermann, 2011; Plati et al., 2011; Walensky, 2006). In addition, irradiation (Holcik et al., 1999; Holcik et al., 2000) and hypoxia can both induce the switch to cap-independent translation (Braunstein et al., 2007), suggesting that upregulation of the pathways that we observed in this study could represent a mechanistic explanation of resistance to multiple types of cancer therapy.

Although further studies are required, our initial in vivo xenograft studies and analysis of breast and ovarian cancer patient samples suggest that inhibition of both Bcl-2 and PI3K/mTOR may be more effective than either alone. Furthermore, the effects of inhibition of Bcl-2 family members and PI3K/mTOR may be more general than the combination of PI3K/mTOR and EGFR if different RTKs are activated in tumor samples. It is interesting that nontransformed epithelial cells were highly resistant to combined treatment with BEZ235 and ABT737. We speculate

that one contributing factor might be the proapoptotic protein Bim, which is upregulated in the BEZ235-treated tumor cell lines but not in MCF-10A cells.

The results presented here demonstrate that inhibition of PI3K/mTOR in matrix-attached cancer cells initiates an evolutionarily conserved cellular stress response, mediated by FOXO transcription factors and preferential translation of IRES-containing mRNAs. This response leads to upregulation of signaling pathways required for cancer cell survival but only in populations of tumor cells within a specific niche (i.e., matrix-attached cells). It is possible that this stress response could contribute to relapse after treatment and possibly to the development of resistant tumor cells within matrix-associated niches in human tumors exposed to PI3K/mTOR inhibitors.

### EXPERIMENTAL PROCEDURES

Additional experimental procedures are described in detail in the [Supplemental Experimental Procedures](#).

#### Antibodies and Reagents, Cell Culture, Cell Lines, and Virus Production

These are described in the [Supplemental Experimental Procedures](#).

#### In Vivo Xenograft Experiments

One million cells (MCAS and OV2008) were injected per flank, subcutaneously, into 10- to 12-week-old female Nod/Scid mice in a 1:1 mix of PBS and Matrigel. Once tumors became palpable (~250 mm<sup>3</sup>), generally Day 8 postinjection for MCAS and Day 28 for OV2008, drugs were administered daily intraperitoneally. GNE493 (70mg/kg) was dissolved in 0.5% methylcellulose/0.2% Tween 80, and ABT-737 was dissolved in 30% propylene glycol/5% Tween 80/65% D5W (5% dextrose in water). All animal studies were performed according to protocols approved by the Institutional Animal Care and Use Committee, the Standing Committee on Animals at Harvard University.

#### Primary Patient Samples

Primary cells were obtained from patients at Brigham and Women's Hospital (BWH) who underwent paracentesis for malignant ascites. The protocol was approved by the BWH Institutional Review Board (IRB), the Harvard Medical School Office for Research Subject Protection, and the Partners Human Research Committee. Consent from patients was obtained as per IRB guidelines. The fluid exudate samples were briefly centrifuged, and the cell pellet was washed with PBS. Red blood cells were lysed with Hybri-Max red blood cell lysis buffer (Sigma No. 7757), and the tumor cells were washed in PBS and media and allowed to grow one passage in 2D culture before they were used for the 3D assays. Media for the primary samples was same as for the ovarian cell lines.

#### 3D Acinar Morphogenesis Assay and Scoring of 3D Structures

Our previously reported MCF-10A 3D cell culture protocol ([Debnath et al., 2003a](#)) (<https://brugge.med.harvard.edu/>) was modified in the following way for 3D culture of ovarian cancer cell lines: Cells were grown in MCB105:199 media (described in Supplemental Experimental Procedures) supplemented with 2% inactivated calf serum that was replaced every 4 days. For protein and mRNA, cells were grown on poly-HEMA-coated plates with 2% matrigel. The 3D structures were scored according to 3D structure integrity based on the resemblance to images shown in [Figure 3B](#). Over 200 structures were scored for each condition.

#### RPPA Assay

RPPA experiments were performed as previously described ([Hennessy et al., 2010](#)).

### ACCESSION NUMBERS

The data from the microarrays have been deposited in the GEO database with accession number GSE28992.

### SUPPLEMENTAL INFORMATION

Supplemental Information includes four figures and Supplemental Experimental Procedures and can be found with this article online at [doi:10.1016/j.ccr.2011.12.024](https://doi.org/10.1016/j.ccr.2011.12.024).

### ACKNOWLEDGMENTS

We thank Joel Levenson and Steve Elmore from Abbott Laboratories and Deepak Sampath from Genentech for ABT737 and GNE493 and for providing helpful advice on the in vivo study design. We thank Ed Cibas for fluid exudates; Nathanael Grey (Dana-Farber Cancer Institute) for Torin1; Dennis Slamon and Gottfried Konecny (University of California, Los Angeles) for the breast and ovarian cell lines; Yiling Lu (M.D. Anderson Cancer Center) for help with RPPA; Jennifer Waters and the Nikon Imaging Center at Harvard Medical School for microscopy; Gerhard Wagner (Harvard Medical School) for the CrPV-IRES plasmid; Richard Lloyd (Baylor College of Medicine) for the Bcl-2 IRES reporter; and Victor Velculescu for sharing *PIK3CA* mutation status on the ovarian cancer cell lines before publication. We also thank David Sabatini, Shomit Sengupta, Cheuk Leong, Alexandra Grassian, and Jonathan Coloff for their critical review of the manuscript and helpful discussions. These studies were supported by the Emil Aaltonen Foundation (T.M.), the Academy of Finland (T.M.), Stand Up to Cancer (SU2C) (J.B., G.M.), Ovarian SPORE Grant P50CA083639 (G.M.), the Dr. Miriam and Sheldon G. Adelson Medical Research Foundation (J.B.), and National Cancer Institute Grant CA105134 (J.B.).

Received: April 29, 2011

Revised: October 7, 2011

Accepted: December 20, 2011

Published: February 13, 2012

### REFERENCES

- Ackler, S., Xiao, Y., Mitten, M.J., Foster, K., Oleksijew, A., Refici, M., Schllessinger, S., Wang, B., Chemburkar, S.R., Bauch, J., et al. (2008). ABT-263 and rapamycin act cooperatively to kill lymphoma cells in vitro and in vivo. *Mol. Cancer Ther.* 7, 3265–3274.
- Allam, H., and Ali, N. (2010). Initiation factor eIF2-independent mode of c-Src mRNA translation occurs via an internal ribosome entry site. *J. Biol. Chem.* 285, 5713–5725.
- Baselga, J. (2011). Targeting the phosphoinositide-3 (PI3) kinase pathway in breast cancer. *Oncologist* 16 (Suppl. 1), 12–19.
- Braunstein, S., Karpisheva, K., Pola, C., Goldberg, J., Hochman, T., Yee, H., Cangiarella, J., Arju, R., Formenti, S.C., and Schneider, R.J. (2007). A hypoxia-controlled cap-dependent to cap-independent translation switch in breast cancer. *Mol. Cell* 28, 501–512.
- Brunet, A., Bonni, A., Zigmond, M.J., Lin, M.Z., Juo, P., Hu, L.S., Anderson, M.J., Arden, K.C., Blenis, J., and Greenberg, M.E. (1999). Akt promotes cell survival by phosphorylating and inhibiting a Forkhead transcription factor. *Cell* 96, 857–868.
- Carpten, J.D., Faber, A.L., Horn, C., Donoho, G.P., Briggs, S.L., Robbins, C.M., Hostetter, G., Boguslawski, S., Moses, T.Y., Savage, S., et al. (2007). A transforming mutation in the pleckstrin homology domain of AKT1 in cancer. *Nature* 448, 439–444.
- Carracedo, A., Ma, L., Teruya-Feldstein, J., Rojo, F., Salmena, L., Alimonti, A., Egia, A., Sasaki, A.T., Thomas, G., Kozma, S.C., et al. (2008). Inhibition of mTORC1 leads to MAPK pathway activation through a PI3K-dependent feedback loop in human cancer. *J. Clin. Invest.* 118, 3065–3074.
- Chandrapatya, S., Sawai, A., Scaltriti, M., Rodrik-Outmezguine, V., Grbovic-Huezo, O., Serra, V., Majumder, P.K., Baselga, J., and Rosen, N. (2011).

- AKT inhibition relieves feedback suppression of receptor tyrosine kinase expression and activity. *Cancer Cell* 19, 58–71.
- Chiarugi, P., and Giannoni, E. (2008). Anoikis: a necessary death program for anchorage-dependent cells. *Biochem. Pharmacol.* 76, 1352–1364.
- Choo, A.Y., Yoon, S.-O., Kim, S.G., Roux, P.P., and Blenis, J. (2008). Rapamycin differentially inhibits S6Ks and 4E-BP1 to mediate cell-type-specific repression of mRNA translation. *Proc. Natl. Acad. Sci. USA* 105, 17414–17419.
- Cloughesy, T.F., Yoshimoto, K., Nghiemphu, P., Brown, K., Dang, J., Zhu, S., Hsueh, T., Chen, Y., Wang, W., Youngkin, D., et al. (2008). Antitumor activity of rapamycin in a Phase I trial for patients with recurrent PTEN-deficient glioblastoma. *PLoS Med.* 5, e8.
- Courtney, K.D., Corcoran, R.B., and Engelman, J.A. (2010). The PI3K pathway as drug target in human cancer. *J. Clin. Oncol.* 28, 1075–1083.
- Creighton, C.J., Massarweh, S., Huang, S., Tsimelzon, A., Hilsenbeck, S.G., Osborne, C.K., Shou, J., Malorni, L., and Schiff, R. (2008). Development of resistance to targeted therapies transforms the clinically associated molecular profile subtype of breast tumor xenografts. *Cancer Res.* 68, 7493–7501.
- Debnath, J., and Brugge, J.S. (2005). Modelling glandular epithelial cancers in three-dimensional cultures. *Nat. Rev. Cancer* 5, 675–688.
- Debnath, J., Muthuswamy, S.K., and Brugge, J.S. (2003a). Morphogenesis and oncogenesis of MCF-10A mammary epithelial acini grown in three-dimensional basement membrane cultures. *Methods* 30, 256–268.
- Debnath, J., Walker, S.J., and Brugge, J.S. (2003b). Akt activation disrupts mammary acinar architecture and enhances proliferation in an mTOR-dependent manner. *J. Cell Biol.* 163, 315–326.
- Engelman, J.A. (2009). Targeting PI3K signalling in cancer: opportunities, challenges and limitations. *Nat. Rev. Cancer* 9, 550–562.
- Engelman, J.A., Chen, L., Tan, X., Crosby, K., Guimaraes, A.R., Upadhyay, R., Maira, M., McNamara, K., Perera, S.A., Song, Y., et al. (2008). Effective use of PI3K and MEK inhibitors to treat mutant Kras G12D and PIK3CA H1047R murine lung cancers. *Nat. Med.* 14, 1351–1356.
- Feldman, M.E., Apsel, B., Uotila, A., Loewith, R., Knight, Z.A., Ruggero, D., and Shokat, K.M. (2009). Active-site inhibitors of mTOR target rapamycin-resistant outputs of mTORC1 and mTORC2. *PLoS Biol.* 7, e38.
- Fels, D.R., and Koumenis, C. (2006). The PERK/eIF2 $\alpha$ /ATF4 module of the UPR in hypoxia resistance and tumor growth. *Cancer Biol. Ther.* 5, 723–728.
- Fernandez, J., Yaman, I., Sarnow, P., Snider, M.D., and Hatzoglou, M. (2002). Regulation of internal ribosomal entry site-mediated translation by phosphorylation of the translation initiation factor eIF2 $\alpha$ . *J. Biol. Chem.* 277, 19198–19205.
- Friedland, J.C., Lakins, J.N., Kazanietz, M.G., Chernoff, J., Boettiger, D., and Weaver, V.M. (2007).  $\alpha$ 6 $\beta$ 4 integrin activates Rac-dependent p21-activated kinase 1 to drive NF- $\kappa$ B-dependent resistance to apoptosis in 3D mammary acini. *J. Cell Sci.* 120, 3700–3712.
- Garrett, J.T., Olivares, M.G., Rinehart, C., Granja-Ingram, N.D., Sánchez, V., Chakrabarty, A., Dave, B., Cook, R.S., Pao, W., McKinley, E., et al. (2011). Transcriptional and posttranslational up-regulation of HER3 (ErbB3) compensates for inhibition of the HER2 tyrosine kinase. *Proc. Natl. Acad. Sci. USA* 108, 5021–5026.
- Gerlitz, G., Jagus, R., and Elroy-Stein, O. (2002). Phosphorylation of initiation factor-2  $\alpha$  is required for activation of internal translation initiation during cell differentiation. *Eur. J. Biochem.* 269, 2810–2819.
- Gewinner, C., Wang, Z.C., Richardson, A., Teruya-Feldstein, J., Etemadmoghadam, D., Bowtell, D., Barretina, J., Lin, W.M., Rameh, L., Salmena, L., et al. (2009). Evidence that inositol polyphosphate 4-phosphatase type II is a tumor suppressor that inhibits PI3K signaling. *Cancer Cell* 16, 115–125.
- Gilbert, W.V., Zhou, K., Butler, T.K., and Doudna, J.A. (2007). Cap-independent translation is required for starvation-induced differentiation in yeast. *Science* 317, 1224–1227.
- Giménez-Bonafé, P., Tortosa, A., and Pérez-Tomás, R. (2009). Overcoming drug resistance by enhancing apoptosis of tumor cells. *Curr. Cancer Drug Targets* 9, 320–340.
- Guo, W., Pylayeva, Y., Pepe, A., Yoshioka, T., Muller, W.J., Inghirami, G., and Giancotti, F.G. (2006). Beta 4 integrin amplifies ErbB2 signaling to promote mammary tumorigenesis. *Cell* 126, 489–502.
- Harrington, L.S., Findlay, G.M., Gray, A., Tolkacheva, T., Wigfield, S., Rebholz, H., Barnett, J., Leslie, N.R., Cheng, S., Shepherd, P.R., et al. (2004). The TSC1-2 tumor suppressor controls insulin-PI3K signaling via regulation of IRS proteins. *J. Cell Biol.* 166, 213–223.
- Hennessy, B., Lu, Y., Gonzalez-Angulo, A.M., Myhre, S., Carey, M., Ju, Z., Coombes, K., Liu, W., Meric-Bernstam, F., Bedrosian, I., et al. (2010). A technical assessment of the utility of reverse phase protein arrays for the study of the functional proteome in non-microdissected human breast cancer. *Clin. Proteomics* 6, 129–151.
- Holcik, M., and Sonenberg, N. (2005). Translational control in stress and apoptosis. *Nat. Rev. Mol. Cell Biol.* 6, 318–327.
- Holcik, M., Lefebvre, C., Yeh, C., Chow, T., and Korneluk, R.G. (1999). A new internal-ribosome-entry-site motif potentiates XIAP-mediated cytoprotection. *Nat. Cell Biol.* 1, 190–192.
- Holcik, M., Yeh, C., Korneluk, R.G., and Chow, T. (2000). Translational upregulation of X-linked inhibitor of apoptosis (XIAP) increases resistance to radiation induced cell death. *Oncogene* 19, 4174–4177.
- Howes, A.L., Chiang, G.G., Lang, E.S., Ho, C.B., Powis, G., Vuori, K., and Abraham, R.T. (2007). The phosphatidylinositol 3-kinase inhibitor, PX-866, is a potent inhibitor of cancer cell motility and growth in three-dimensional cultures. *Mol. Cancer Ther.* 6, 2505–2514.
- Hsieh, A.C., Costa, M., Zollo, O., Davis, C., Feldman, M.E., Testa, J.R., Meyhuas, O., Shokat, K.M., and Ruggero, D. (2010). Genetic dissection of the oncogenic mTOR pathway reveals druggable addiction to translational control via 4EBP-eIF4E. *Cancer Cell* 17, 249–261.
- Isakoff, S.J., Engelman, J.A., Irie, H.Y., Luo, J., Brachmann, S.M., Pearlman, R.V., Cantley, L.C., and Brugge, J.S. (2005). Breast cancer-associated PIK3CA mutations are oncogenic in mammary epithelial cells. *Cancer Res.* 65, 10992–11000.
- Jain, H.V., and Meyer-Hermann, M. (2011). The molecular basis of synergism between carboplatin and ABT-737 therapy targeting ovarian carcinomas. *Cancer Res.* 71, 705–715.
- Jefferson, L.S., and Kimball, S.R. (2003). Amino acids as regulators of gene expression at the level of mRNA translation. *J. Nutr.* 133 (6, Suppl 1), 2046S–2051S.
- Johannes, G., Carter, M.S., Eisen, M.B., Brown, P.O., and Sarnow, P. (1999). Identification of eukaryotic mRNAs that are translated at reduced cap binding complex eIF4F concentrations using a cDNA microarray. *Proc. Natl. Acad. Sci. USA* 96, 13118–13123.
- Kenny, P.A., Lee, G.Y., Myers, C.A., Neve, R.M., Semeiks, J.R., Spellman, P.T., Lorenz, K., Lee, E.H., Barcellos-Hoff, M.H., Petersen, O.W., et al. (2007). The morphologies of breast cancer cell lines in three-dimensional assays correlate with their profiles of gene expression. *Mol. Oncol.* 1, 84–96.
- Kops, G.J., de Ruiter, N.D., De Vries-Smits, A.M., Powell, D.R., Bos, J.L., and Burgering, B.M. (1999). Direct control of the Forkhead transcription factor AFX by protein kinase B. *Nature* 398, 630–634.
- Li, J., Yen, C., Liaw, D., Podsypanina, K., Bose, S., Wang, S.I., Puc, J., Miliareis, C., Rodgers, L., McCombie, R., et al. (1997). PTEN, a putative protein tyrosine phosphatase gene mutated in human brain, breast, and prostate cancer. *Science* 275, 1943–1947.
- Liu, H., Radisky, D.C., Wang, F., and Bissell, M.J. (2004). Polarity and proliferation are controlled by distinct signaling pathways downstream of PI3-kinase in breast epithelial tumor cells. *J. Cell Biol.* 164, 603–612.
- Maira, S.M., Stauffer, F., Brueggen, J., Furet, P., Schnell, C., Fritsch, C., Brachmann, S., Chène, P., De Pover, A., Schoemaker, K., et al. (2008). Identification and characterization of NVP-BEZ235, a new orally available dual phosphatidylinositol 3-kinase/mammalian target of rapamycin inhibitor with potent in vivo antitumor activity. *Mol. Cancer Ther.* 7, 1851–1863.
- Marr, M.T., 2nd, D'Alessio, J.A., Puig, O., and Tjian, R. (2007). IRES-mediated functional coupling of transcription and translation amplifies insulin receptor feedback. *Genes Dev.* 21, 175–183.

- Martin, M.J., Melnyk, N., Pollard, M., Bowden, M., Leong, H., Podor, T.J., Gleave, M., and Sorensen, P.H. (2006). The insulin-like growth factor I receptor is required for Akt activation and suppression of anoikis in cells transformed by the ETV6-NTRK3 chimeric tyrosine kinase. *Mol. Cell. Biol.* 26, 1754–1769.
- Massarweh, S., Osborne, C.K., Creighton, C.J., Qin, L., Tsimelzon, A., Huang, S., Weiss, H., Rimawi, M., and Schiff, R. (2008). Tamoxifen resistance in breast tumors is driven by growth factor receptor signaling with repression of classic estrogen receptor genomic function. *Cancer Res.* 68, 826–833.
- Moerke, N.J., Aktas, H., Chen, H., Cantel, S., Reibarkh, M.Y., Fahmy, A., Gross, J.D., Degterev, A., Yuan, J., Chorev, M., et al. (2007). Small-molecule inhibition of the interaction between the translation initiation factors eIF4E and eIF4G. *Cell* 128, 257–267.
- Muaddi, H., Majumder, M., Peidis, P., Papadakis, A.I., Holcik, M., Scheuner, D., Kaufman, R.J., Hatzoglou, M., and Koromilas, A.E. (2010). Phosphorylation of eIF2 $\alpha$  at serine 51 is an important determinant of cell survival and adaptation to glucose deficiency. *Mol. Biol. Cell* 21, 3220–3231.
- O'Reilly, K.E., Rojo, F., She, Q.-B., Solit, D., Mills, G.B., Smith, D., Lane, H., Hofmann, F., Hicklin, D.J., Ludwig, D.L., et al. (2006). mTOR inhibition induces upstream receptor tyrosine kinase signaling and activates Akt. *Cancer Res.* 66, 1500–1508.
- Oltersdorf, T., Elmore, S.W., Shoemaker, A.R., Armstrong, R.C., Augeri, D.J., Belli, B.A., Brunccko, M., Deckwerth, T.L., Dinges, J., Hajduk, P.J., et al. (2005). An inhibitor of Bcl-2 family proteins induces regression of solid tumours. *Nature* 435, 677–681.
- Plati, J., Bucur, O., and Khosravi-Far, R. (2011). Apoptotic cell signaling in cancer progression and therapy. *Integr. Biol. (Camb.)* 3, 279–296.
- Polo, M.L., Arnoni, M.V., Riggio, M., Wargon, V., Lanari, C., and Novaro, V. (2010). Responsiveness to PI3K and MEK inhibitors in breast cancer. Use of a 3D culture system to study pathways related to hormone independence in mice. *PLoS ONE* 5, e10786.
- Puig, O., and Tjian, R. (2005). Transcriptional feedback control of insulin receptor by dFOXO/FOXO1. *Genes Dev.* 19, 2435–2446.
- Raven, J.F., and Koromilas, A.E. (2008). PERK and PKR: old kinases learn new tricks. *Cell Cycle* 7, 1146–1150.
- Riggins, R.B., Schrecengost, R.S., Guerrero, M.S., and Bouton, A.H. (2007). Pathways to tamoxifen resistance. *Cancer Lett.* 256, 1–24.
- Samuels, Y., and Velculescu, V.E. (2004). Oncogenic mutations of PIK3CA in human cancers. *Cell Cycle* 3, 1221–1224.
- Samuels, Y., Wang, Z., Bardelli, A., Silliman, N., Ptak, J., Szabo, S., Yan, H., Gazdar, A., Powell, S.M., Riggins, G.J., et al. (2004). High frequency of mutations of the PIK3CA gene in human cancers. *Science* 304, 554.
- Schafer, Z.T., Grassian, A.R., Song, L., Jiang, Z., Gerhart-Hines, Z., Irie, H.Y., Gao, S., Puigserver, P., and Brugge, J.S. (2009). Antioxidant and oncogene rescue of metabolic defects caused by loss of matrix attachment. *Nature* 461, 109–113.
- Sengupta, S., Peterson, T.R., and Sabatini, D.M. (2010). Regulation of the mTOR complex 1 pathway by nutrients, growth factors, and stress. *Mol. Cell* 40, 310–322.
- Sergina, N.V., Rausch, M., Wang, D., Blair, J., Hann, B., Shokat, K.M., and Moasser, M.M. (2007). Escape from HER-family tyrosine kinase inhibitor therapy by the kinase-inactive HER3. *Nature* 445, 437–441.
- Serra, V., Scaltriti, M., Prudkin, L., Eichhorn, P.J.A., Ibrahim, Y.H., Chandarlapaty, S., Markman, B., Rodriguez, O., Guzman, M., Rodriguez, S., et al. (2011). PI3K inhibition results in enhanced HER signaling and acquired ERK dependency in HER2-overexpressing breast cancer. *Oncogene* 30, 2547–2557.
- She, Q.-B., Halilovic, E., Ye, Q., Zhen, W., Shirasawa, S., Sasazuki, T., Solit, D.B., and Rosen, N. (2010). 4E-BP1 is a key effector of the oncogenic activation of the AKT and ERK signaling pathways that integrates their function in tumors. *Cancer Cell* 18, 39–51.
- Silvera, D., Formenti, S.C., and Schneider, R.J. (2010). Translational control in cancer. *Nat. Rev. Cancer* 10, 254–266.
- Suo, J., Snider, S.J., Mills, G.B., Creighton, C.J., Chen, A.C., Schiff, R., Lloyd, R.E., and Chang, E.C. (2010). Int6 regulates both proteasomal degradation and translation initiation and is critical for proper formation of acini by human mammary epithelium. *Oncogene* 30, 724–736.
- Sutherland, D.P., Sampath, D., Berry, M., Castaneda, G., Chang, Z., Chuckowree, I., Dotson, J., Folkes, A., Friedman, L., Goldsmith, R., et al. (2010). Discovery of (thienopyrimidin-2-yl)aminopyrimidines as potent, selective, and orally available pan-PI3-kinase and dual pan-PI3-kinase/mTOR inhibitors for the treatment of cancer. *J. Med. Chem.* 53, 1086–1097.
- Syntichaki, P., Troulinaki, K., and Tavernarakis, N. (2007). eIF4E function in somatic cells modulates ageing in *Caenorhabditis elegans*. *Nature* 445, 922–926.
- Terenin, I.M., Dmitriev, S.E., Andreev, D.E., and Shatsky, I.N. (2008). Eukaryotic translation initiation machinery can operate in a bacterial-like mode without eIF2. *Nat. Struct. Mol. Biol.* 15, 836–841.
- Thoreen, C.C., Kang, S.A., Chang, J.W., Liu, Q., Zhang, J., Gao, Y., Reichling, L.J., Sim, T., Sabatini, D.M., and Gray, N.S. (2009). An ATP-competitive mammalian target of rapamycin inhibitor reveals rapamycin-resistant functions of mTORC1. *J. Biol. Chem.* 284, 8023–8032.
- Villa-Cuesta, E., Sage, B.T., and Tatar, M. (2010). A role for *Drosophila* dFoxO and dFoxO 5'UTR internal ribosomal entry sites during fasting. *PLoS ONE* 5, e11521.
- Walensky, L.D. (2006). BCL-2 in the crosshairs: tipping the balance of life and death. *Cell Death Differ.* 13, 1339–1350.
- Weaver, V.M., Lelièvre, S., Lakins, J.N., Chrenek, M.A., Jones, J.C.R., Giaccotti, F., Werb, Z., and Bissell, M.J. (2002). beta4 integrin-dependent formation of polarized three-dimensional architecture confers resistance to apoptosis in normal and malignant mammary epithelium. *Cancer Cell* 2, 205–216.
- Weigelt, B., and Bissell, M.J. (2008). Unraveling the microenvironmental influences on the normal mammary gland and breast cancer. *Semin. Cancer Biol.* 18, 311–321.
- Weigelt, B., Lo, A.T., Park, C.C., Gray, J.W., and Bissell, M.J. (2010). HER2 signaling pathway activation and response of breast cancer cells to HER2-targeting agents is dependent strongly on the 3D microenvironment. *Breast Cancer Res. Treat.* 122, 35–43.
- Wek, R.C., Jiang, H.-Y., and Anthony, T.G. (2006). Coping with stress: eIF2 kinases and translational control. *Biochem. Soc. Trans.* 34, 7–11.
- Yamada, K.M., and Cukierman, E. (2007). Modeling tissue morphogenesis and cancer in 3D. *Cell* 130, 601–610.
- Yamaguchi, S., Ishihara, H., Yamada, T., Tamura, A., Usui, M., Tominaga, R., Munakata, Y., Satake, C., Katagiri, H., Tashiro, F., et al. (2008). ATF4-mediated induction of 4E-BP1 contributes to pancreatic beta cell survival under endoplasmic reticulum stress. *Cell Metab.* 7, 269–276.
- Yuan, T.L., and Cantley, L.C. (2008). PI3K pathway alterations in cancer: variations on a theme. *Oncogene* 27, 5497–5510.

# Tumorigenic Cells Are Common in Mouse MPNSTs but Their Frequency Depends upon Tumor Genotype and Assay Conditions

Johanna Buchstaller,<sup>1</sup> Paul E. McKeever,<sup>2</sup> and Sean J. Morrison<sup>1,3,\*</sup>

<sup>1</sup>Department of Internal Medicine, Life Sciences Institute, and Center for Stem Cell Biology

<sup>2</sup>Department of Pathology

University of Michigan, Ann Arbor, MI 48109-2216, USA

<sup>3</sup>Howard Hughes Medical Institute, Children's Research Institute, Department of Pediatrics, University of Texas Southwestern Medical Center, Dallas, TX 75390, USA

\*Correspondence: [sean.morrison@utsouthwestern.edu](mailto:sean.morrison@utsouthwestern.edu)

DOI 10.1016/j.ccr.2011.12.027

## SUMMARY

Tumor-initiating cells have been suggested to be rare in many cancers. We tested this in mouse malignant peripheral nerve sheath tumors (MPNSTs) and found that 18% of primary and 49% of passaged MPNST cells from *Nf1*<sup>+/-</sup>; *Ink4a/Arf*<sup>-/-</sup> mice formed tumors upon transplantation, whereas only 1.8% to 2.6% of MPNST cells from *Nf1*<sup>+/-</sup>; *p53*<sup>+/-</sup> mice did. MPNST cells of both genotypes require laminin binding to  $\beta$ 1-integrin for clonogenic growth. Most MPNST cells from *Nf1*<sup>+/-</sup>; *Ink4a/Arf*<sup>-/-</sup> mice expressed laminin, whereas most MPNST cells from *Nf1*<sup>+/-</sup>; *p53*<sup>+/-</sup> mice did not. Exogenous laminin increased the percentage of MPNST cells from *Nf1*<sup>+/-</sup>; *p53*<sup>+/-</sup> but not *Nf1*<sup>+/-</sup>; *Ink4a/Arf*<sup>-/-</sup> mice that formed tumorigenic colonies. Tumor-forming potential is common among MPNST cells, but the assay conditions required to detect it vary with tumor genotype.

## INTRODUCTION

The question of which cells contribute to cancer growth and progression has fundamental implications for therapy. If tumor growth and metastasis are driven primarily by rare, or at least infrequent, cancer stem cells then cancer might be more effectively treated by specifically targeting the cancer stem cells (Reya et al., 2001; Pardal et al., 2003; Dick, 2008). On the other hand, if many cancer cells are capable of driving tumor growth and metastasis it will be necessary to eliminate most or all cancer cells.

Evidence suggests that small populations of cancer stem cells drive the growth and progression of a number of cancers, including some germ lineage cancers (Kleinsmith and Pierce, 1964; Illmensee and Mintz, 1976), myeloid leukemias (Lapidot et al., 1994; Bonnet and Dick, 1997; Yilmaz et al., 2006; Oravec-Wilson et al., 2009), breast cancers (Al-Hajj et al., 2003), gliomas (Singh et al., 2004), and colon cancers (Dalerba

et al., 2007; O'Brien et al., 2007; Ricci-Vitiani et al., 2007; Merlos-Suárez et al., 2011). In each case, transplantation of cancer cells into highly immunocompromised mice revealed a small, phenotypically distinct subpopulation of cells that was uniquely capable of transferring disease and forming phenotypically diverse nontumorigenic progeny. This suggests that some cancers are hierarchically organized, with small numbers of cancer stem cells that sustain tumor growth by forming large numbers of cancer cells with limited proliferative potential (Reya et al., 2001; Pardal et al., 2003; Dick, 2008).

In contrast to this model, human melanomas (Quintana et al., 2008, 2010), mouse melanomas (Held et al., 2010), and some mouse leukemias (Kelly et al., 2007; Williams et al., 2007) have many cells with tumorigenic potential. For example, 30% of single cells obtained directly from melanomas in patients and over 50% of cells obtained from primary mouse melanomas can form tumors in highly immunocompromised mice (Quintana

### Significance

Our results demonstrate that mouse MPNSTs contain high frequencies of tumorigenic cells, which were similar upon transplantation into immunocompetent or immunocompromised mice. However, tumor genotype influenced the laminin expression pattern, and therefore the dependence of MPNST cells on exogenous laminin and the frequency of tumorigenic cells that could be detected in some assays. Although laminin binding to  $\beta$ 1-integrin was important for clonogenic growth, the laminin could either be intrinsic or extrinsic to MPNST cells. Tumors of different genotypes, even with the same malignant phenotype, can therefore require different assay conditions to detect the full range of cells with tumorigenic potential.

et al., 2008; Held et al., 2010; Quintana et al., 2010). These results raise three critical questions.

- (1) Is melanoma unique among solid cancers in having common tumorigenic cells?
- (2) Can high frequencies of tumorigenic cells be detected in immunocompetent recipients for some cancers or does the immune system play such a central role in the control of tumor-initiating cells that common tumorigenic cells can only be detected in immunocompromised recipients? To address this question it is necessary to examine mouse models of cancer, which can be transplanted into syngeneic recipients without a confounding xenogeneic immune barrier that rejects human cells by mechanisms that are very different from the autologous immune responses that can occur within patients.
- (3) Finally, what other factors influence the frequency of cancer cells that can form tumors?

Malignant peripheral nerve sheath tumors (MPNSTs) are aggressive soft tissue sarcomas that arise within peripheral nerves. Most MPNSTs arise in the context of Neurofibromatosis type 1, a hereditary tumor syndrome caused by mutations in *NF1* that encodes Neurofibromin, a GTPase-activating protein that negatively regulates Ras signaling (Rubin and Gutmann, 2005). About 30% of NF1 patients develop benign plexiform neurofibromas, which can transform into MPNSTs. Plexiform neurofibromas and MPNSTs arise from Schwann cells in peripheral nerves (Zhu et al., 2002; Joseph et al., 2008; Zheng et al., 2008). Beyond the loss of NF1 function, *CDKN2A* (*p16<sup>Ink4a</sup>*), *CDKN2D* (*p14<sup>Arf</sup>*, the human ortholog of mouse *p19<sup>Arf</sup>*), and *TP53* are often inactivated in MPNSTs by deletion or promoter hypermethylation (Menon et al., 1990; Perrone et al., 2003; Agensen et al., 2005). Mutations of these genes in mice also lead to the development of MPNSTs. Thus, mice that are heterozygous for a deletion of both *Nf1* and *p53* (*Nf1<sup>+/-</sup>; p53<sup>+/-</sup>*; Cichowski et al., 1999; Vogel et al., 1999) and mice heterozygous for *Nf1* and deficient for *Ink4a/Arf* (*Nf1<sup>+/-</sup>; Ink4a/Arf<sup>-/-</sup>*; Joseph et al., 2008) develop MPNSTs.

We developed in vitro and in vivo assays to determine the frequency of MPNST cells with tumorigenic potential in these mouse models of MPNST.

## RESULTS

### More Tumorigenic Cells Were Detected among Primary MPNST Cells from *Nf1<sup>+/-</sup>; Ink4a/Arf<sup>-/-</sup>* Mice

*Nf1<sup>+/-</sup>; Ink4a/Arf<sup>-/-</sup>* and *Nf1<sup>+/-</sup>; p53<sup>+/-</sup>* mice were backcrossed onto a C57BL/Ka background (at least six generations) and then aged to monitor the development of MPNSTs. Approximately 25% to 50% of *Nf1<sup>+/-</sup>; Ink4a/Arf<sup>-/-</sup>* mice and *Nf1<sup>+/-</sup>; p53<sup>+/-</sup>* mice developed MPNSTs on the legs and abdomens, typically between 4 and 7 months of age, as previously reported (Cichowski et al., 1999; Joseph et al., 2008). Tumors of both genotypes grew rapidly and at comparable rates (data not shown). Three of four primary and four of four secondary MPNSTs from *Nf1<sup>+/-</sup>; p53<sup>+/-</sup>* mice exhibited *p16<sup>Ink4a</sup>* and *p19<sup>Arf</sup>* expression, whereas *p16<sup>Ink4a</sup>* and *p19<sup>Arf</sup>* were not detected in MPNSTs from *Nf1<sup>+/-</sup>; Ink4a/Arf<sup>-/-</sup>* mice, as expected

(Figure S1 available online). *p53* was not detected in most MPNSTs from *Nf1<sup>+/-</sup>; p53<sup>+/-</sup>* mice, as expected (Vogel et al., 1999), but was detected in most MPNSTs from *Nf1<sup>+/-</sup>; Ink4a/Arf<sup>-/-</sup>* mice (data not shown).

We sacrificed *Nf1<sup>+/-</sup>; Ink4a/Arf<sup>-/-</sup>* and *Nf1<sup>+/-</sup>; p53<sup>+/-</sup>* mice at  $6.1 \pm 0.9$  or  $5.3 \pm 1.4$  (mean  $\pm$  SD) months of age, respectively, for analysis. Tumors of both genotypes contained tightly packed spindle cells with tapered nuclei arranged in a fascicular pattern (Figures 1A–1F). Of 25 tumors analyzed, 24 were focally positive for the Schwann cell marker S100 $\beta$  (Figures 1A and 1D). In tumors of both genotypes, we observed frequent mitotic figures (an average of  $1.1 \pm 0.7$  in *Nf1<sup>+/-</sup>; Ink4a/Arf<sup>-/-</sup>* MPNSTs and  $1.6 \pm 0.6$  in *Nf1<sup>+/-</sup>; p53<sup>+/-</sup>* MPNSTs per high power field, objective  $\times$  ocular magnification =  $400\times$ ) and a high frequency of Ki-67 positive cells ( $39 \pm 16\%$  for *Nf1<sup>+/-</sup>; Ink4a/Arf<sup>-/-</sup>* and  $52 \pm 9\%$  for *Nf1<sup>+/-</sup>; p53<sup>+/-</sup>* MPNSTs; Figures 1C, 1F, and 1G).

We also administered bromo-deoxyuridine (BrdU) to tumor-bearing mice. After 6 hr of administration, 10% and 14% of cells were BrdU+ in primary MPNSTs from *Nf1<sup>+/-</sup>; Ink4a/Arf<sup>-/-</sup>* and *Nf1<sup>+/-</sup>; p53<sup>+/-</sup>* mice, respectively. Similar results were obtained when secondary MPNSTs were analyzed: 9% and  $10 \pm 6\%$  of cells from MPNSTs obtained from *Nf1<sup>+/-</sup>; Ink4a/Arf<sup>-/-</sup>* and *Nf1<sup>+/-</sup>; p53<sup>+/-</sup>* mice incorporated BrdU, respectively. After 5 or 10 days of administration, over 80% of cells were BrdU+ in MPNSTs of both genotypes (Figure 1H). MPNSTs from both *Nf1<sup>+/-</sup>; Ink4a/Arf<sup>-/-</sup>* and *Nf1<sup>+/-</sup>; p53<sup>+/-</sup>* mice therefore contained similarly high frequencies of rapidly dividing cells.

To obtain MPNST cells for experiments, primary tumors of comparable size from mice of both genotypes were enzymatically dissociated and stained with antibodies. Only tumors that were confirmed to be MPNSTs by histopathology were included in our analysis. The cells were sorted by flow cytometry to exclude debris (based on light scatter), dead cells (4',6-diamidino-2-phenylindole+ (DAPI+)), hematopoietic cells (Ter119+ or CD45+), and endothelial cells (CD31+; Figure 1I). Viable cells that were negative for hematopoietic/endothelial markers were used in all experiments. These cells comprised an average of  $48 \pm 17\%$  and  $44 \pm 14\%$  (mean  $\pm$  SD) of nucleated cells in MPNSTs from *Nf1<sup>+/-</sup>; Ink4a/Arf<sup>-/-</sup>* and *Nf1<sup>+/-</sup>; p53<sup>+/-</sup>* mice, respectively.

We injected MPNST cells subcutaneously, into sciatic nerves, or under the kidney capsules of wild-type C57BL/Ka mice. The kidney capsule is a common site for heterologous cell grafting, where many cell types are able to efficiently engraft. We rarely observed the formation of tumors after subcutaneous injection, even when we injected large numbers of cells, but transplanted cells readily formed tumors in sciatic nerve and under the kidney capsule at higher cell doses (Table S1). At lower cell doses the cells engrafted more efficiently under the kidney capsule, where the cells were retained after injection (Table S1). Injection of cells into the endoneurial space increased pressure within nerves and led to the ejection of the injected material through the needle track, rendering the assay nonquantitative in peripheral nerve. For this reason, subsequent experiments to quantify the frequency of cells with tumorigenic potential were conducted by transplanting cells under the kidney capsule.

We transplanted aliquots of 100 cells, ten cells, or single cells from ten primary MPNSTs obtained from *Nf1<sup>+/-</sup>; Ink4a/Arf<sup>-/-</sup>* mice and eight primary MPNSTs from *Nf1<sup>+/-</sup>; p53<sup>+/-</sup>* mice under

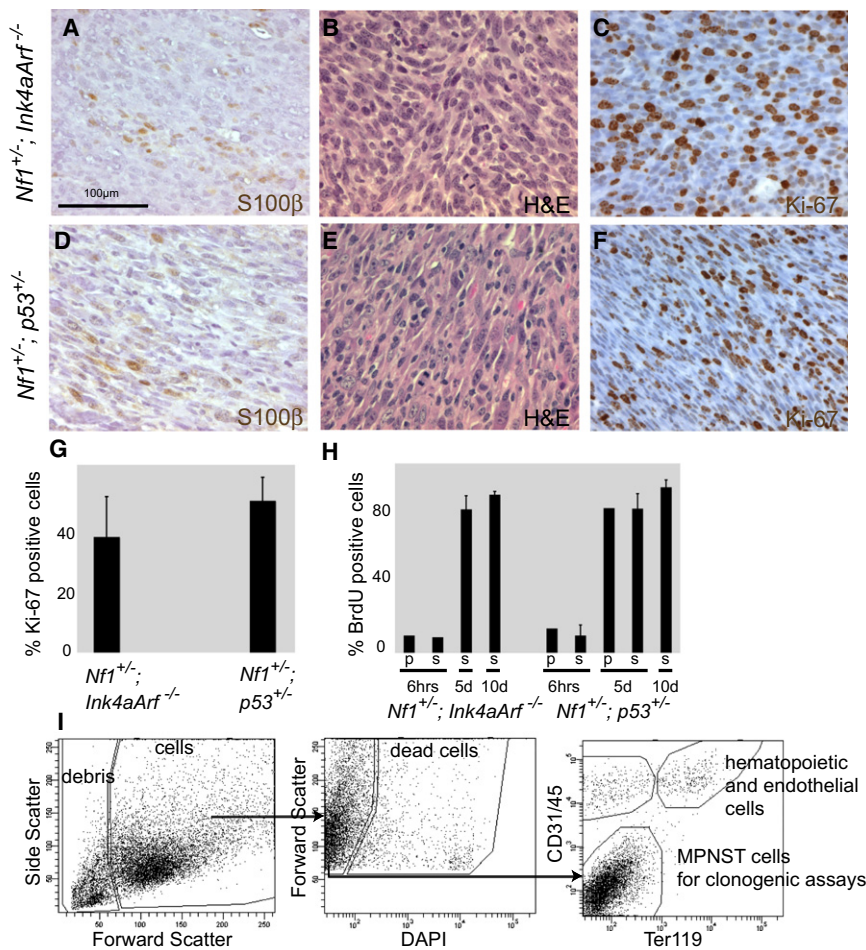


**Figure 1. *Nf1*<sup>+/-</sup>; *Ink4a/Arf*<sup>-/-</sup> and *Nf1*<sup>+/-</sup>; *p53*<sup>+/-</sup> Mice Develop MPNSTs that Contain a High Frequency of Proliferating Cells**

(A–F) Paraffin sections of *Nf1*<sup>+/-</sup>; *Ink4a/Arf*<sup>-/-</sup> and *Nf1*<sup>+/-</sup>; *p53*<sup>+/-</sup> MPNSTs were stained with antibodies against S100β (A and D), hematoxylin and eosin (B and E), and antibodies against Ki-67 (C and F). Sections were counterstained with hematoxylin (blue) in (A), (D), (C), and (F). Each panel reflects a different section.

(G) The percentage of MPNST cells that were Ki-67-positive was determined for four tumors of each genotype on at least 20 high-power fields (400× magnification, ocular x objective) for each tumor.

(H) The percentage of MPNST cells (that stained negatively for blood or endothelial markers) in mice bearing primary (p) or secondary (transplanted into wild-type mice; s) MPNSTs treated with BrdU for either 6 hr or 5 or 10 days that were BrdU-positive. The data reflect one primary and eight secondary tumors from *Nf1*<sup>+/-</sup>; *Ink4a/Arf*<sup>-/-</sup> mice and three primary and nine secondary tumors from *Nf1*<sup>+/-</sup>; *p53*<sup>+/-</sup> mice. All statistics represent mean ± SD.

(I) Isolation of MPNST cells from primary tumors using flow cytometry.

See also Figure S1 and Tables S1 and S2.

the kidney capsule of C57BL/Ka mice. We monitored the mice for at least 15 weeks after transplantation. When tumors became evident by palpation or at the end of the experiment, the mice were sacrificed for gross and histological examination. Sorted events from the debris fraction (Figure 1I) did not form tumors upon transplantation and cells from the fractions that stained positively for hematopoietic or endothelial markers rarely formed tumors (Table S2). When viable MPNST cells from the nonhematopoietic/nonendothelial fraction of *Nf1*<sup>+/-</sup>; *Ink4a/Arf*<sup>-/-</sup> mice were injected, 28 of 29 mice (97%) injected with 100 cells, 28 of 39 mice (72%) injected with 10 cells, and 16 of 76 mice (21%) injected with single cells formed MPNSTs (Table 1). Almost all of these tumors were observed within ten weeks after transplantation and appeared histologically similar to the primary tumors from which they derived (Figure S2A). Limit dilution analysis indicated that 18 ± 14% (mean ± SD; range = 6% to 53%) of cells from primary MPNST formed tumors after transplantation. Tumorigenic cells were therefore common within primary MPNSTs obtained from *Nf1*<sup>+/-</sup>; *Ink4a/Arf*<sup>-/-</sup> mice.

When nonhematopoietic/nonendothelial cells from primary tumors obtained from 8 *Nf1*<sup>+/-</sup>; *p53*<sup>+/-</sup> mice were injected, 24 of 37 mice (65%) injected with 100 cells, 6 of 43 mice (14%) injected with 10 cells, and 2 of 38 mice (5%) injected with single cells formed MPNSTs (Table 1). All of these tumors were observed within ten weeks after transplantation and appeared

histologically similar to the primary tumors from which they derived (Figure S2B). Limit dilution analysis indicated that an average of 1.8 ± 1.6% (mean ± SD; range = 0.6% to 5.0%) of cells from these MPNSTs formed tumors after

transplantation. The frequency of tumorigenic cells in MPNSTs from *Nf1*<sup>+/-</sup>; *p53*<sup>+/-</sup> mice was therefore significantly lower (10-fold, *p* = 0.008) in this assay than in MPNSTs from *Nf1*<sup>+/-</sup>; *Ink4a/Arf*<sup>-/-</sup> mice. This demonstrates that MPNST genetic background can affect tumorigenic cell frequency.

### MPNSTs from *Nf1*<sup>+/-</sup>; *Ink4a/Arf*<sup>-/-</sup> Mice Retain Higher Frequencies of Tumorigenic Cells upon Secondary Transplantation

We wondered whether the reduced frequency of tumorigenic cells within primary MPNSTs from *Nf1*<sup>+/-</sup>; *p53*<sup>+/-</sup> mice reflected increased infiltration of normal cells into these tumors as compared to MPNSTs from *Nf1*<sup>+/-</sup>; *Ink4a/Arf*<sup>-/-</sup> mice. To test this, we performed secondary transplants of dissociated cells from tumors that arose under the kidney capsule of primary recipient mice. Transplanted MPNST cells form focal masses that are distinct from normal kidney tissue. We reasoned that only cancer cells would proliferate extensively in primary recipient mice, reducing or eliminating normal cells from the passaged tumors. Therefore, if normal cells within primary MPNSTs from *Nf1*<sup>+/-</sup>; *p53*<sup>+/-</sup> mice diluted the cancer cells, then secondary transplantation of these MPNSTs should eliminate the difference in tumorigenic cell frequency among MPNSTs of different genotypes. When MPNST cells from eleven first-generation grafts from five different primary MPNSTs from

**Table 1. Tumor Formation by Primary MPNST Cells**

Tumor	Injected Cell Dose (No. of Tumors/ No. of Injections)			Cells that Formed Tumors (%)	95% CI (%)
	100 Cells	10 Cells	1 Cell		
<i>Nf1<sup>+/-</sup>; Ink4a/Arf<sup>-/-</sup></i> mice					
10	3/3	nd	1/8	13	1.9–95
11	1/2	1/2	2/6	16	4.3–61
12	5/5	4/6	6/8	27	11–65
14	3/3	4/4	0/8	18	6.6–48
15	3/3	3/6	0/7	6.0	2.1–18
16	4/4	6/6	4/10	53	22–100
17	4/4	4/5	1/9	15	5.9–37
23	nd	nd	1/10	10	nd
29	nd	2/5	1/10	6.2	1.9-20
35	5/5	4/5	nd	16	5.4–48
Total	28/29 (97%)	28/39 (72%)	16/76 (21%)	18	6.8–55
<i>Nf1<sup>+/-</sup>; p53<sup>+/-</sup></i> mice					
1	1/3	0/4	1/10	0.7	0.1–3.0
3	4/5	0/5	nd	1.3	0.5–3.6
4	4/5	2/5	1/10	2.6	1.0–6.8
5	4/5	1/5	0/10	1.7	0.6–4.3
6	2/4	0/5	0/8	0.6	0.1–2.2
7	5/5	3/8	nd	5.0	1.8–13
8	4/6	0/5	nd	1.0	0.3–2.6
9	0/4	0/6	nd	nd	nd
Total	24/37 (65%)	6/43 (14%)	2/38 (5%)	1.8**	0.5–4.0

Tumorigenic cell frequency significantly differed in this assay between MPNSTs from *Nf1<sup>+/-</sup>; Ink4a/Arf<sup>-/-</sup>* and *Nf1<sup>+/-</sup>; p53<sup>+/-</sup>* mice (\*\**p* = 0.008). nd, not determined; CI, confidence interval.

For tumor histology, see Figure S2.

*Nf1<sup>+/-</sup>; Ink4a/Arf<sup>-/-</sup>* mice were injected into secondary recipients, 14 of 15 (93%) ten-cell injections and 44 of 99 (44%) single-cell injections gave rise to tumors (Table 2). Virtually all tumors became palpable within ten weeks of transplantation. Limit dilution analysis indicated that  $49 \pm 8.6\%$  (mean  $\pm$  SD; range = 40% to 58%) of cells from each of these serially transplanted MPNST formed tumors after transplantation. Thus, approximately half of the cells within MPNSTs are capable of forming tumors by the time the MPNSTs have been passaged once.

When MPNST cells from six first-generation grafts from four primary MPNSTs from *Nf1<sup>+/-</sup>; p53<sup>+/-</sup>* mice were injected into secondary recipients, 6 of 32 (19%) injections of 10 cells and 3 of 30 (10%) injections of single cells gave rise to tumors (Table 2). All tumors became palpable within ten weeks of transplantation. Limit dilution analysis indicated that an average of  $2.6 \pm 2.3\%$  (mean  $\pm$  SD; range = 0.3% to 5.7%) of cells from each of these serially transplanted MPNSTs formed tumors after transplantation. Thus, MPNSTs from *Nf1<sup>+/-</sup>; Ink4a/Arf<sup>-/-</sup>* mice retained a significantly (19-fold; *p* =  $2 \times 10^{-5}$ ) higher frequency of tumorigenic cells than MPNSTs from *Nf1<sup>+/-</sup>; p53<sup>+/-</sup>* mice,

**Table 2. Tumor Formation after Secondary Transplantation of MPNST Cells**

	Injected Cell Dose			Cells that	
Tumor	100 Cells	10 Cells	1 Cell	Formed Tumors (%)	95% CI (%)
<i>Nf1<sup>+/-</sup>; Ink4a/Arf<sup>-/-</sup></i> mice					
9 (N = 1)	nd	nd	4/8	50	nd
10 (N = 1)	nd	nd	5/9	56	nd
11 (N = 3)	nd	3/3	8/25	40	21–76
12 (N = 4)	nd	11/12	15/38	40	24–65
17 (N = 2)	nd	nd	12/19	58	nd
Total	nd	14/15 (93%)	44/99 (44%)	49	22–71
<i>Nf1<sup>+/-</sup>; p53<sup>+/-</sup></i> mice					
3 (N = 2)	7/9	2/11	1/10	1.8	0.9–3.6
4 (N = 2)	3/10	0/10	0/10	0.3	0.1–1.0
5 (N = 1)	4/4	1/5	2/10	5.7	1.9–17
8 (N = 1)	3/4	3/6	nd	2.5	0.9–7.1
Total	17/27 (63%)	6/32 (19%)	3/30 (10%)	2.6**	0.9–7.3

Tumorigenic cell frequency significantly differed in this assay between MPNSTs from *Nf1<sup>+/-</sup>; Ink4a/Arf<sup>-/-</sup>* and *Nf1<sup>+/-</sup>; p53<sup>+/-</sup>* mice (\*\*, *p* =  $2 \times 10^{-5}$ ).

nd, not determined; CI, confidence interval.

even upon secondary transplantation. This suggests that the reduced frequency of tumorigenic cells within primary MPNSTs from *Nf1<sup>+/-</sup>; p53<sup>+/-</sup>* mice did not reflect the presence of normal cells in these tumors.

#### MPNSTs from *Nf1<sup>+/-</sup>; Ink4a/Arf<sup>-/-</sup>* Mice Retain Higher Frequencies of Tumorigenic Cells upon Transplantation into NOD/SCID ILR2<sup>γ</sup>null Mice

To test whether MPNST cells from *Nf1<sup>+/-</sup>; p53<sup>+/-</sup>* mice were more immunogenic than MPNST cells from *Nf1<sup>+/-</sup>; Ink4a/Arf<sup>-/-</sup>* mice we transplanted dissociated cells from primary MPNSTs into immunocompetent C57BL/Ka recipients or into highly immunocompromised NOD/SCID ILR2<sup>γ</sup>null mice, which lack B, T, and natural killer cells (Shultz et al., 2005). We found that 16%–20% of cells from two primary MPNSTs from *Nf1<sup>+/-</sup>; Ink4a/Arf<sup>-/-</sup>* mice formed tumors irrespective of whether they were transplanted into C57BL/Ka or NOD/SCID ILR2<sup>γ</sup>null mice. Similarly, 1%–5% of MPNST cells from *Nf1<sup>+/-</sup>; p53<sup>+/-</sup>* mice formed tumors in C57BL/Ka recipients and 0.6%–2.5% formed tumors in NOD/SCID ILR2<sup>γ</sup>null recipients (Table 3). These results indicate that the recipient immune system has little effect on the frequency of MPNST cells that form tumors after transplantation, irrespective of genotype, and the reduced frequency of tumorigenic MPNST cells from *Nf1<sup>+/-</sup>; p53<sup>+/-</sup>* mice cannot be explained by increased immunogenicity.

#### Higher Percentage of MPNST Cells from *Nf1<sup>+/-</sup>; Ink4a/Arf<sup>-/-</sup>* Mice Formed Colonies in Nonadherent Culture as Compared to *Nf1<sup>+/-</sup>; p53<sup>+/-</sup>* Mice

We cultured primary mouse MPNST cells, 1 cell/well in 96 well plates for 10–14 days in nonadherent conditions (Molofsky et al., 2003). We found that  $35 \pm 20\%$  (mean  $\pm$  SD) of MPNST

**Table 3. Tumor Formation by Primary MPNST Cells in Immunocompetent C57BL/Ka Mice and Immunocompromised NOD/SCID ILR2 $\gamma$ <sup>null</sup> Mice**

Tumor	Recipient Mice	Injected Cell Dose			Tumorigenic Cells (%)	95% CI
		100 Cells	10 Cells	5 Cells		
Nf1 <sup>+/-</sup> ; Ink4a/Arf <sup>-/-</sup> (35)	C57BL/Ka	5/5	4/5		16	5.4–48
Nf1 <sup>+/-</sup> ; Ink4a/Arf <sup>-/-</sup> (35)	NOD/SCID ILR2 $\gamma$ <sup>null</sup>	5/5	4/5		16	5.4–48
Nf1 <sup>+/-</sup> ; Ink4a/Arf <sup>-/-</sup> (40)	C57BL/Ka			4/7	17	6.2–46
Nf1 <sup>+/-</sup> ; Ink4a/Arf <sup>-/-</sup> (40)	NOD/SCID ILR2 $\gamma$ <sup>null</sup>			5/8	20	7.9–49
Nf1 <sup>+/-</sup> ; p53 <sup>+/-</sup> (7)	C57BL/Ka	5/5	3/8		5.0	1.8–13
Nf1 <sup>+/-</sup> ; p53 <sup>+/-</sup> (7)	NOD/SCID ILR2 $\gamma$ <sup>null</sup>	4/5	3/7		2.5	1.0–6.5
Nf1 <sup>+/-</sup> ; p53 <sup>+/-</sup> (28)	C57BL/Ka	3/5	1/8		1.0	0.4–2.8
Nf1 <sup>+/-</sup> ; p53 <sup>+/-</sup> (28)	NOD/SCID ILR2 $\gamma$ <sup>null</sup>	2/5	1/8		0.6	0.2–2.1

The frequency of tumorigenic cells and the 95% confidence interval (CI) around this frequency were determined by extreme limiting dilution (ELDA) software (see [Experimental Procedures](#) for software URL).

cells from 12 different Nf1<sup>+/-</sup>; Ink4a/Arf<sup>-/-</sup> mice formed colonies, and 62% of these colonies (62 of 100) formed tumors after transplantation under the kidney capsule of C57BL/Ka mice. In contrast, only 4.1 ± 3.4% of MPNST cells from 12 Nf1<sup>+/-</sup>; p53<sup>+/-</sup> mice formed colonies, and 32% of these colonies (13 of 40) formed tumors after transplantation into C57BL/Ka mice (Table 4). Averaging across tumors, 23 ± 21% of single MPNST cells from Nf1<sup>+/-</sup>; Ink4a/Arf<sup>-/-</sup> mice and 2.0 ± 2.9% of MPNST cells from Nf1<sup>+/-</sup>; p53<sup>+/-</sup> mice formed tumorigenic colonies. This indicates that tumorigenic cells were also significantly less common (11-fold,  $p = 0.02$ ) in MPNSTs from Nf1<sup>+/-</sup>; p53<sup>+/-</sup> mice as compared to Nf1<sup>+/-</sup>; Ink4a/Arf<sup>-/-</sup> mice, even when these cells were initially propagated in culture instead of transplanting uncultured cells directly in vivo (as in Tables 1, 2, 3).

The reduced colony formation by MPNST cells from Nf1<sup>+/-</sup>; p53<sup>+/-</sup> mice was largely attributable to increased cell death as compared to MPNST cells from Nf1<sup>+/-</sup>; Ink4a/Arf<sup>-/-</sup> mice. Ten to 14 days after adding MPNST cells to culture, we carefully examined the wells. We found that 43 ± 2.4% of wells in which we had plated single MPNST cells from Nf1<sup>+/-</sup>; Ink4a/Arf<sup>-/-</sup> mice did not contain any cells, indicating that these cells must have undergone cell death. In contrast, 69 ± 13% of wells in which we had plated single MPNST cells from Nf1<sup>+/-</sup>; p53<sup>+/-</sup> mice did not contain any cells. This suggests that a significantly ( $p = 0.02$ ) higher percentage of single MPNST cells from Nf1<sup>+/-</sup>; p53<sup>+/-</sup> mice underwent cell death after being added to culture. The remaining wells that did not contain colonies but were not empty contained small numbers of cells (<10), indicating that these cells underwent a limited number of divisions.

We examined the number of apoptotic cells in MPNSTs in vivo and in MPNST cells cultured under nonadherent conditions (Figure S3). MPNST tumors in Nf1<sup>+/-</sup>; Ink4a/Arf<sup>-/-</sup> and Nf1<sup>+/-</sup>; p53<sup>+/-</sup> mice in vivo contained similar frequencies of cleaved caspase-3 positive cells. In culture, we found that a significantly higher percentage of cells from Nf1<sup>+/-</sup>; p53<sup>+/-</sup> mice compared to Nf1<sup>+/-</sup>; Ink4a/Arf<sup>-/-</sup> mice expressed cleaved caspase-3 after 12 days of culture (5.8 ± 3.4% versus 2.2 ± 2.4%; mean ± SD;  $p = 0.03$ ). MPNST cells from Nf1<sup>+/-</sup>; Ink4a/Arf<sup>-/-</sup> mice are therefore more likely to survive nonadherent culture than MPNST cells from Nf1<sup>+/-</sup>; p53<sup>+/-</sup> mice, even though no difference in the frequency of apoptotic cells was observed in tumors in vivo. This suggests that differences in the rate of cell death between

MPNSTs from different genetic backgrounds are context-dependent. We therefore decided to explore whether changes in assay conditions could increase the frequency of clonogenic MPNST cells.

#### Laminin Is Expressed by More MPNST Cells in Nf1<sup>+/-</sup>; Ink4a/Arf<sup>-/-</sup> Mice than in Nf1<sup>+/-</sup>; p53<sup>+/-</sup> Mice

One common way of improving the growth and survival of cells in culture is by growing cells adherently on extracellular matrix, rather than nonadherently, as described above. Adherent culture on laminin, in particular, enhances the growth and survival of neural stem/progenitor cells and glioma cells (Sun et al., 2008; Pollard et al., 2009; Lathia et al., 2010). Because MPNST cells from Nf1<sup>+/-</sup>; p53<sup>+/-</sup> mice did not exhibit increased cell death in vivo, in contrast to what was observed in culture, we wondered whether MPNST cells were exposed to laminin in the tumor environment in vivo. We examined the expression of laminin-111/-211 (laminin  $\alpha$ 1/ $\beta$ 1/ $\gamma$ 1 and  $\alpha$ 2/ $\beta$ 1/ $\gamma$ 1) on sections through MPNSTs from Nf1<sup>+/-</sup>; Ink4a/Arf<sup>-/-</sup> and Nf1<sup>+/-</sup>; p53<sup>+/-</sup> mice (Figures 2A–2D). In MPNSTs from Nf1<sup>+/-</sup>; Ink4a/Arf<sup>-/-</sup> mice laminin-111/-211 was widely expressed by most tumor cells, including cancer cells and vascular/perivascular stromal cells (Figures 2B and 2D). In contrast, in MPNSTs from Nf1<sup>+/-</sup>; p53<sup>+/-</sup> mice laminin appeared to be expressed by many fewer cells and to be mainly vascular/perivascular (Figures 2A and 2C).

We found that dissociated MPNST cells from Nf1<sup>+/-</sup>; Ink4a/Arf<sup>-/-</sup> mice exhibited much stronger laminin-111/211 staining than MPNST cells from Nf1<sup>+/-</sup>; p53<sup>+/-</sup> mice (Figure 2E). Indeed, 70 ± 11% of MPNST cells from Nf1<sup>+/-</sup>; Ink4a/Arf<sup>-/-</sup> mice and 28 ± 22% of MPNST cells from Nf1<sup>+/-</sup>; p53<sup>+/-</sup> mice stained with laminin by flow cytometry. This demonstrates that most MPNST cells from Nf1<sup>+/-</sup>; Ink4a/Arf<sup>-/-</sup> mice carry laminin with them after dissociation, whereas only a minority of MPNST cells from Nf1<sup>+/-</sup>; p53<sup>+/-</sup> mice do so. If laminin promotes the survival or proliferation of MPNST cells, then MPNST cells from Nf1<sup>+/-</sup>; p53<sup>+/-</sup> mice would be expected to depend more upon exogenous laminin, as compared to MPNST cells from Nf1<sup>+/-</sup>; Ink4a/Arf<sup>-/-</sup> mice.

We administered a 6 hr pulse of BrdU to mice and then stained sections through their MPNSTs with antibodies against BrdU and laminin-111/211 to assess the localization of dividing cells relative to laminin-expressing cells. BrdU+ cells tended to

**Table 4. Colony Formation by Single Primary MPNST Cells Cultured under Nonadherent Conditions and Tumor Formation by These Colonies after Transplantation In Vivo**

Tumor	Single Cells that Formed Colonies (%)	Tumors/ Colonies Injected (%)	Single Cells that Formed Tumorigenic Colonies (%)
<i>Nf1<sup>+/-</sup>; Ink4a/Arf<sup>-/-</sup></i> mice			
6	26	2/9 (22)	5.8
7	47	4/5 (80)	38
8	39	2/7 (29)	11
9	14	5/11 (45)	6.2
10	22	5/10 (50)	11
11	34	8/13 (62)	21
12	66	12/13 (92)	60
14	11	4/5 (80)	8.7
15	7.6	2/7 (29)	2.2
16	38	9/11 (82)	31
17	66	9/10 (90)	59
23	55	nd	nd
Mean ± SD	35 ± 20	62/100 (62)	23 ± 21
<i>Nf1<sup>+/-</sup>; p53<sup>+/-</sup></i> mice			
1	10	nd	nd
2	3.1	nd	nd
3	6.1	0/10 (0)	0.0
4	2.4	1/5 (20)	0.5
5	0.5	nd	nd
6	8.3	4/4 (100)	8.3
7	0.5	nd	nd
8	5.6	4/10 (40)	2.2
9	1.6	nd	nd
12	0.5	1/1 (100)	0.5
13	8.1	1/6 (17)	1.4
14	2.9	2/4 (50)	1.5
Mean ± SD	4.1 ± 3.4**	13/40 (32)	2.0 ± 2.9*

For each tumor, we determined the percentage of cells that formed colonies in culture and the percentage of these colonies that formed tumors upon transplantation into C57BL/Ka mice. The last column represents the product of these statistics, that is, the percentage of MPNST cells that formed tumorigenic colonies.

\*\*p = 3 × 10<sup>-5</sup>; \*p = 0.02. All statistics represent mean ± SD.

nd, not determined.

For data on cell death in culture, see Figure S3.

localize adjacent to laminin-expressing cells and regions of the tumor that lacked laminin staining also had fewer dividing cells. MPNSTs from *Nf1<sup>+/-</sup>; Ink4a/Arf<sup>-/-</sup>* and *Nf1<sup>+/-</sup>; p53<sup>+/-</sup>* mice included 9 ± 5 and 8 ± 2% (mean ± SD) BrdU+ cells, respectively (Figures 2F–2H). In MPNSTs from *Nf1<sup>+/-</sup>; Ink4a/Arf<sup>-/-</sup>* mice, laminin was widely expressed such that almost all cells (88 ± 18%), including nearly all BrdU+ cells (97 ± 1%), were adjacent to laminin-stained cells (Figures 2F and 2H). However, in MPNSTs from *Nf1<sup>+/-</sup>; p53<sup>+/-</sup>* mice, laminin was more restricted in its expression such that only 39 ± 6% of MPNST cells were adjacent to laminin-stained cells. Yet, most BrdU+ cells (83 ± 7%) remained adjacent to laminin-stained cells in these tumors (Figures 2G and

2H). Therefore, BrdU+ cells were more than twice as likely as all MPNST cells to localize adjacent to laminin-expressing cells in MPNSTs from *Nf1<sup>+/-</sup>; p53<sup>+/-</sup>* mice. This is consistent with the possibility that laminin may promote the proliferation of MPNST cells, though laminin staining may also be associated with vasculature that promotes proliferation through other mechanisms.

#### MPNSTs from *Nf1<sup>+/-</sup>; p53<sup>+/-</sup>* but Not *Nf1<sup>+/-</sup>; Ink4a/Arf<sup>-/-</sup>* Mice Form More Colonies on Laminin

If laminin promotes clonogenic growth by MPNST cells and MPNST cells from *Nf1<sup>+/-</sup>; p53<sup>+/-</sup>* mice are less likely to carry laminin after dissociation (Figure 2E), then exogenous laminin might stimulate clonogenic growth by MPNST cells from *Nf1<sup>+/-</sup>; p53<sup>+/-</sup>* mice to a greater extent than MPNST cells from *Nf1<sup>+/-</sup>; Ink4a/Arf<sup>-/-</sup>* mice. To test this, we compared colony formation by single MPNST cells from both genetic backgrounds in nonadherent cultures and in adherent cultures on laminin-111 (Figure 3A). Adherent culture on laminin did not affect the percentage of MPNST cells from *Nf1<sup>+/-</sup>; Ink4a/Arf<sup>-/-</sup>* mice that formed colonies compared to nonadherent cultures (Figure 3A); however, it significantly increased the percentage of MPNST cells from *Nf1<sup>+/-</sup>; p53<sup>+/-</sup>* mice that formed colonies from 6.7 ± 9.8% to 25 ± 18% (p = 0.003; Figure 3A). Although the percentage of cells that formed colonies varied between tumors, the rate of colony formation on laminin was always at least as high as in nonadherent cultures, and the effect was statistically significant in a paired t test (p = 0.003). Adherent culture on fibronectin or collagen may have enhanced the rate of tumor formation to some extent, but the effects were variable among tumors and not statistically significant (Table S3). Exposure to laminin thus increased colony-formation by MPNST cells from *Nf1<sup>+/-</sup>; p53<sup>+/-</sup>* mice but not *Nf1<sup>+/-</sup>; Ink4a/Arf<sup>-/-</sup>* mice, consistent with the difference in endogenous laminin expression between these genetic backgrounds.

Adherent colonies grown on laminin by MPNST cells from *Nf1<sup>+/-</sup>; p53<sup>+/-</sup>* mice, but not *Nf1<sup>+/-</sup>; Ink4a/Arf<sup>-/-</sup>* mice, also tended to be larger than those that grew in nonadherent cultures (data not shown). Consistent with this, a significantly higher frequency of cells within colonies from *Nf1<sup>+/-</sup>; p53<sup>+/-</sup>* mice incorporated a pulse of BrdU when cultured on laminin-111 compared to nonadherent culture conditions, whereas adherent culture on laminin did not significantly affect the rate of BrdU incorporation into colonies cultured from *Nf1<sup>+/-</sup>; Ink4a/Arf<sup>-/-</sup>* mice (Figure 3B).

To assess the proliferative potential of MPNST cells that formed colonies on laminin, we dissociated the colonies that arose from single cells and replated them into secondary cultures. Twenty-three of 24 (96%) colonies from three primary MPNSTs obtained from *Nf1<sup>+/-</sup>; p53<sup>+/-</sup>* mice gave rise to secondary colonies, yielding an average of 2573 ± 626 secondary colonies per primary colony. An average of 30 ± 10% of cells within the primary colonies formed secondary colonies upon replating. These results suggest that many MPNST cells from *Nf1<sup>+/-</sup>; p53<sup>+/-</sup>* mice have the potential to proliferate extensively if assayed under permissive conditions.

To assess whether colony-forming MPNST cells from *Nf1<sup>+/-</sup>; p53<sup>+/-</sup>* mice had the potential to form tumors in vivo, we dissociated individual colonies and injected the cells under the kidney capsule of C57BL/Ka mice. In these experiments,

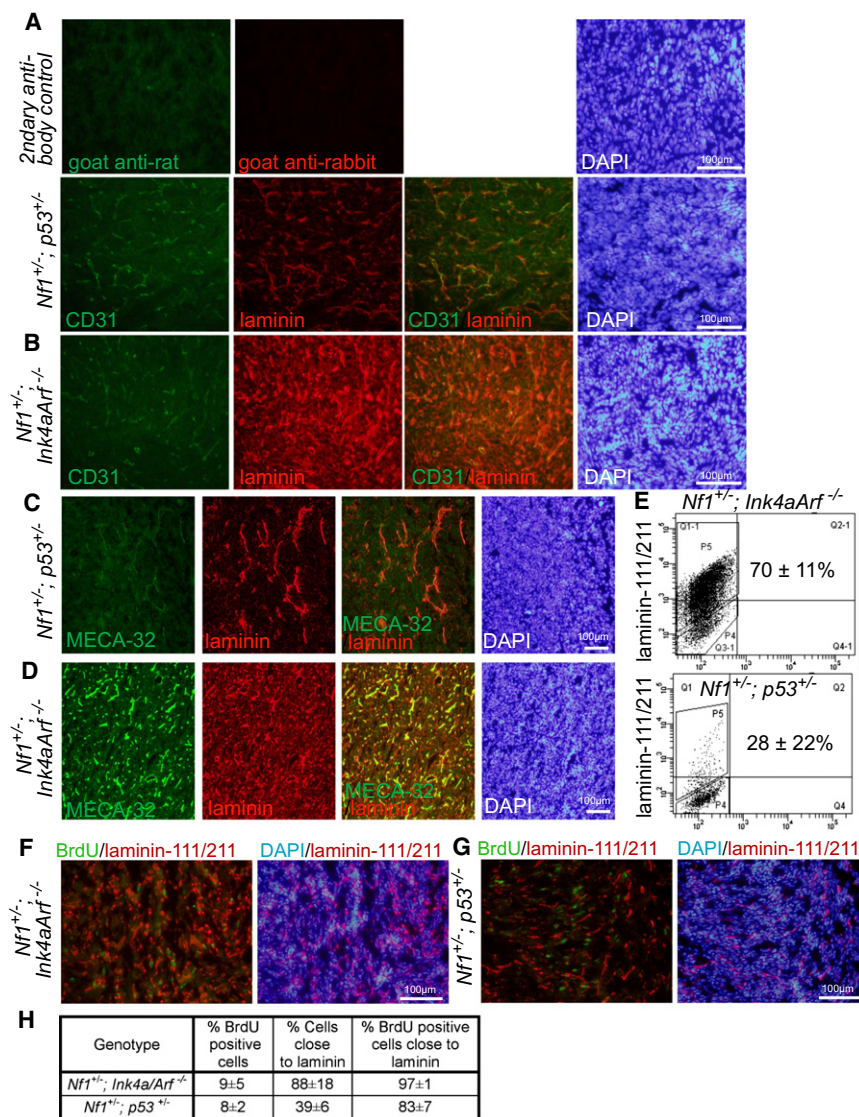


**Figure 2. Laminin Is Expressed by Most MPNST Cells from *Nf1*<sup>+/-</sup>; *Ink4a/Arf*<sup>-/-</sup> Mice but Only by a Subset of MPNST Cells from *Nf1*<sup>+/-</sup>; *p53*<sup>+/-</sup> Mice**

(A–D) MPNSTs from *Nf1*<sup>+/-</sup>; *p53*<sup>+/-</sup> (A and C) and *Nf1*<sup>+/-</sup>; *Ink4a/Arf*<sup>-/-</sup> (B and D) mice were stained with antibodies against laminin-111/211, CD31, and MECA-32 (to label endothelial cells), as well as DAPI to identify nuclei.

(E) Dissociated MPNST cells, after exclusion of blood and endothelial cells, were stained with antibodies against laminin-111/211 and analyzed by flow cytometry. Numbers reflect the percentage of cells that stained more strongly than isotype control (3–5 MPNSTs/genotype,  $p = 0.02$  between the two genotypes).

(F–H) Mice bearing MPNSTs were treated with BrdU for 6 hr and cryosections were stained with DAPI, as well as antibodies against laminin-111/211 and BrdU. In MPNSTs from *Nf1*<sup>+/-</sup>; *p53*<sup>+/-</sup> mice, BrdU+ cells were 2.1-fold more likely ( $p = 0.04$ ) than the average MPNST cell to localize adjacent to laminin (the data reflect three tumors/genotype and 2,200–3,200 cells/tumor). All statistics are mean ± SD.

MPNST cells varies with tumor genotype and assay conditions and that many primary MPNST cells are capable of forming tumors in immunocompetent mice.

To test whether endogenous laminin expression distinguishes intrinsically tumorigenic from intrinsically nontumorigenic subpopulations of MPNST cells, we sorted laminin-positive and laminin-negative MPNST cells from both genetic backgrounds and transplanted them under the kidney capsule of C57BL/Ka mice. Both laminin-positive and laminin-

negative MPNST cells formed tumors, though the rate of tumor formation by the laminin-positive cells was significantly higher in both genetic backgrounds (2.2-fold difference,  $p = 0.02$  for cells from *Nf1*<sup>+/-</sup>; *Ink4a/Arf*<sup>-/-</sup> mice; 2.5-fold difference,  $p = 0.049$  for *Nf1*<sup>+/-</sup>; *p53*<sup>+/-</sup> mice; Figures 3F and 3G). Because 6.6% and 1.3% of laminin negative MPNST cells from *Nf1*<sup>+/-</sup>; *Ink4a/Arf*<sup>-/-</sup> mice and *Nf1*<sup>+/-</sup>; *p53*<sup>+/-</sup> mice, respectively, formed tumors in vivo, our data do not support the idea that laminin negative cells intrinsically lack tumor-forming capacity. Rather, the data suggest that laminin increases the clonogenic potential of MPNST cells but that it does not matter whether the laminin is intrinsic or extrinsic to the cells. It remains possible there is a hierarchy of tumorigenic and nontumorigenic MPNST cells that can be identified with other markers. Thus, our data demonstrate that many MPNST cells are capable of forming tumors, depending on assay conditions and genetic background, but the formal question of whether MPNSTs exhibit a hierarchical organization consistent with the cancer stem cell model is not addressed by our study.

25 ± 18% of the MPNST cells formed adherent colonies on laminin-111 and 36 of 54 colonies formed tumors in vivo (Figure 3C). Thus, 19 ± 13% of single MPNST cells from *Nf1*<sup>+/-</sup>; *p53*<sup>+/-</sup> mice formed tumorigenic colonies in the presence of laminin-111. The histological appearance of the tumors that arose from transplanted colonies was similar to primary MPNSTs (Figure S4).

Given the increased colony formation by MPNST cells on laminin, we tested whether the tumorigenicity of uncultured primary MPNST cells in vivo was increased by mixing the cells with Matrigel (of which laminin is the main component; Kleinman and Martin, 2005). Suspension of primary MPNST cells in Matrigel prior to injection approximately doubled the frequency MPNST cells from both genetic backgrounds that formed tumors (Figures 3D and 3E). Limit dilution analysis indicated that 4.7% of primary MPNST cells from *Nf1*<sup>+/-</sup>; *p53*<sup>+/-</sup> mice and 30% of primary MPNST cells from *Nf1*<sup>+/-</sup>; *Ink4a/Arf*<sup>-/-</sup> mice formed tumors when injected under the kidney capsule with Matrigel. These results further emphasize that the frequency of tumorigenic

negative MPNST cells formed tumors, though the rate of tumor formation by the laminin-positive cells was significantly higher in both genetic backgrounds (2.2-fold difference,  $p = 0.02$  for cells from *Nf1*<sup>+/-</sup>; *Ink4a/Arf*<sup>-/-</sup> mice; 2.5-fold difference,  $p = 0.049$  for *Nf1*<sup>+/-</sup>; *p53*<sup>+/-</sup> mice; Figures 3F and 3G). Because 6.6% and 1.3% of laminin negative MPNST cells from *Nf1*<sup>+/-</sup>; *Ink4a/Arf*<sup>-/-</sup> mice and *Nf1*<sup>+/-</sup>; *p53*<sup>+/-</sup> mice, respectively, formed tumors in vivo, our data do not support the idea that laminin negative cells intrinsically lack tumor-forming capacity. Rather, the data suggest that laminin increases the clonogenic potential of MPNST cells but that it does not matter whether the laminin is intrinsic or extrinsic to the cells. It remains possible there is a hierarchy of tumorigenic and nontumorigenic MPNST cells that can be identified with other markers. Thus, our data demonstrate that many MPNST cells are capable of forming tumors, depending on assay conditions and genetic background, but the formal question of whether MPNSTs exhibit a hierarchical organization consistent with the cancer stem cell model is not addressed by our study.

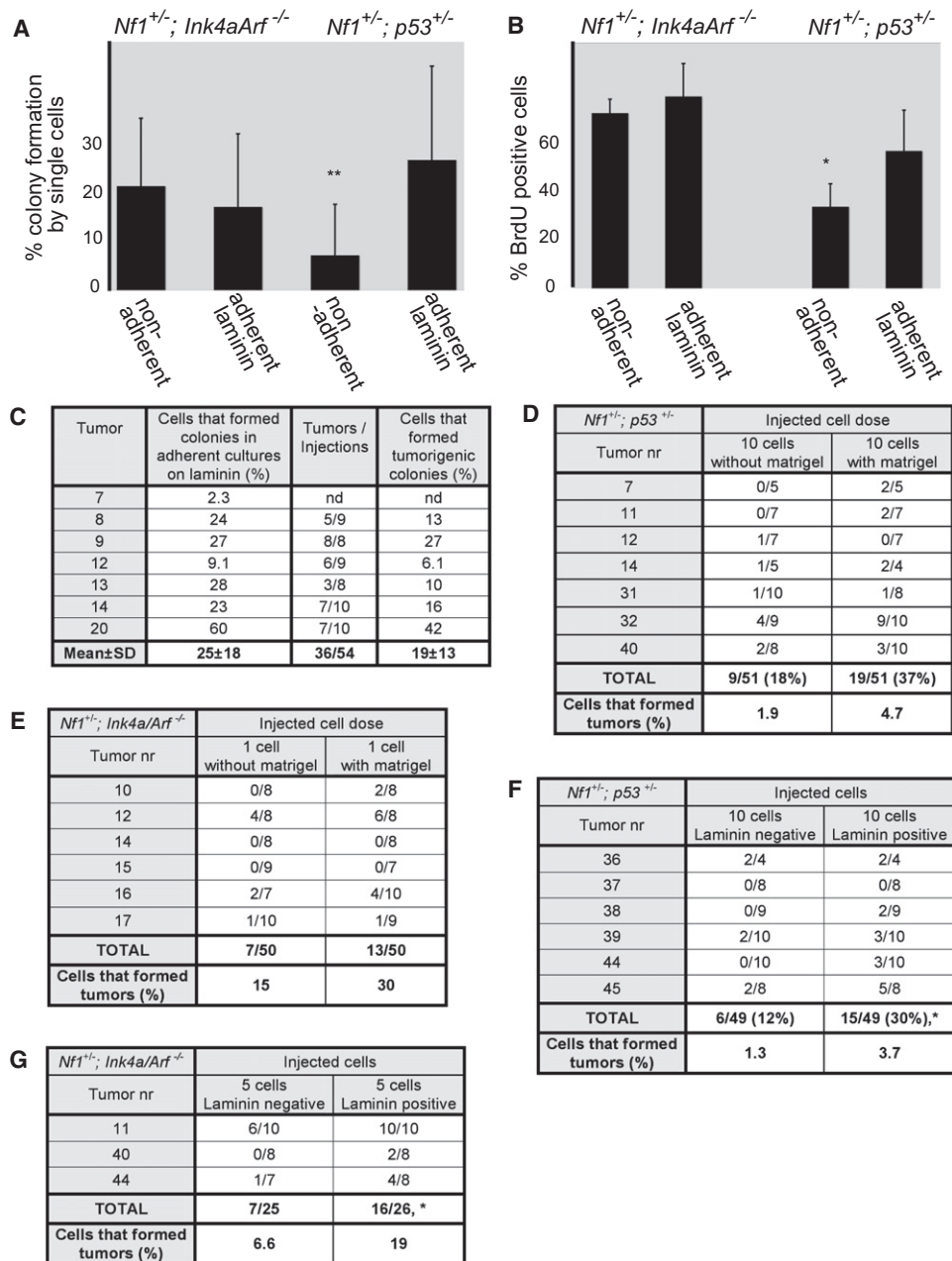


**Figure 3. MPNST Cells from *Nf1*<sup>+/-</sup>; *p53*<sup>+/-</sup> Mice Formed More Colonies When Plated Adherently on Laminin**

(A) Single MPNST cells from *Nf1*<sup>+/-</sup>; *Ink4a/Arf*<sup>-/-</sup> (N = 6) and *Nf1*<sup>+/-</sup>; *p53*<sup>+/-</sup> mice (N = 7) were sorted into individual wells of 96-well plates and cultured either nonadherently or adherently on laminin-111. \*\*, p = 0.003 by paired t test between adherent and nonadherent cultures of cells from *Nf1*<sup>+/-</sup>; *p53*<sup>+/-</sup> mice. (B) 10,000 MPNST cells from *Nf1*<sup>+/-</sup>; *Ink4a/Arf*<sup>-/-</sup> or *Nf1*<sup>+/-</sup>; *p53*<sup>+/-</sup> mice (three tumors each) were cultured nonadherently or adherently on laminin-111 for 1–3 days. Then a 3 hr pulse of BrdU was administered (\*p < 0.05). Error bars in (A) and (B) represent SD. (C) Adherent colonies from single MPNST cells from *Nf1*<sup>+/-</sup>; *p53*<sup>+/-</sup> mice grown on laminin-111 were trypsinized, injected under the kidney capsules of C57BL/Ka mice, and then monitored for the ability to form tumors for 15 weeks. The last column represents the percentage of MPNST cells that formed adherent colonies and that went on to form tumors upon transplantation of the colonies in vivo (the product of columns 1 and 2). nd, not determined. (D and E) Freshly isolated MPNST cells from *Nf1*<sup>+/-</sup>; *p53*<sup>+/-</sup> (D) or *Nf1*<sup>+/-</sup>; *Ink4a/Arf*<sup>-/-</sup> (E) mice were transplanted under the kidney capsule of C57BL/Ka mice, with or without Matrigel, and then monitored for tumor formation for at least 15 weeks. (F and G) Freshly dissociated laminin-positive or laminin-negative MPNST cells from *Nf1*<sup>+/-</sup>; *p53*<sup>+/-</sup> (F) or *Nf1*<sup>+/-</sup>; *Ink4a/Arf*<sup>-/-</sup> (G) mice were transplanted under the kidney capsule of C57BL/Ka mice. Cells that stained positively for laminin were more likely to form tumors in both genetic backgrounds (p = 0.02 for *Nf1*<sup>+/-</sup>; *Ink4a/Arf*<sup>-/-</sup> mice and p = 0.049 for *Nf1*<sup>+/-</sup>; *p53*<sup>+/-</sup> mice, paired t test).

See also Table S3 and Figure S4.

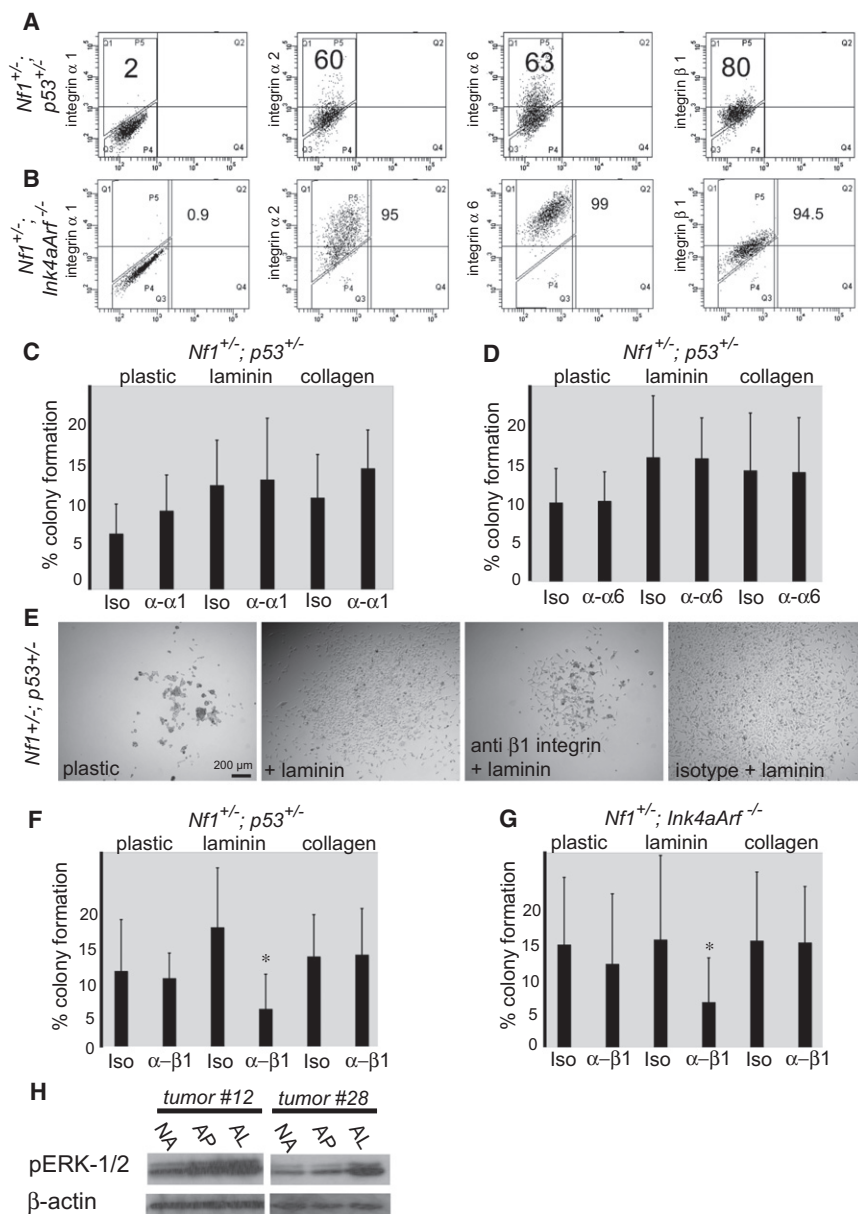


**Figure 4. MPNST Cells Expressed Laminin Receptors and Blocking Antibodies against  $\beta 1$  Integrin Decreased Colony Formation on Laminin**

(A and B) Expression of indicated integrins by MPNST cells from *Nf1*<sup>+/-</sup>; *p53*<sup>+/-</sup> (A) and *Nf1*<sup>+/-</sup>; *Ink4a/Arf*<sup>-/-</sup> (B) mice. Numbers reflect the percentages of cells that stained more strongly than isotype control.

(C and D) Colony formation by MPNST cells from *Nf1*<sup>+/-</sup>; *p53*<sup>+/-</sup> mice on the indicated substrate treated with function-blocking antibodies against  $\alpha 1$  (C) or  $\alpha 6$  (D) integrin. (Iso means isotype control antibody.)

(E) Representative pictures of colonies formed by MPNST cells from *Nf1*<sup>+/-</sup>; *p53*<sup>+/-</sup> mice in the presence of function blocking antibodies against  $\beta 1$  integrin or isotype control.

(F and G) The effect of blocking antibody against  $\beta 1$  integrin on the percentage of cells that formed colonies. \*,  $p = 0.02$  for *Nf1*<sup>+/-</sup>; *p53*<sup>+/-</sup> mice (F) and  $p = 0.05$  for *Nf1*<sup>+/-</sup>; *Ink4a/Arf*<sup>-/-</sup> (G) on laminin. No significant difference on plastic or collagen.

(H) Western blots of extracts from MPNSTs cells obtained from *Nf1*<sup>+/-</sup>; *p53*<sup>+/-</sup> mice using antibodies against phospho-ERK1/2. Cells were cultured for three days under nonadherent conditions (NA), adherently on plastic (AP), or adherently on laminin-111 (AL). Error bars represent SD.

See also Figure S5.

### Laminin Promotes the Survival and Proliferation of MPNST Cells via $\beta 1$ Integrin

$\alpha 1\beta 1$ ,  $\alpha 2\beta 1$ ,  $\alpha 3\beta 1$ ,  $\alpha 6\beta 1$ ,  $\alpha 7\beta 1$ , and  $\alpha 6\beta 4$  integrins are laminin receptors (Miner and Yurchenco, 2004). By flow cytometry, we found that integrins  $\alpha 2$ ,  $\alpha 6$ , and  $\beta 1$  were widely expressed on the surface of MPNST cells from *Nf1*<sup>+/-</sup>; *Ink4a/Arf*<sup>-/-</sup> and *Nf1*<sup>+/-</sup>; *p53*<sup>+/-</sup> mice (Figure 4A). Integrins  $\alpha 1$  (Figure 4A) and  $\beta 4$  (data not shown) were rarely expressed at detectable levels. Thus, MPNST cells appear to express multiple laminin receptors, including  $\alpha 2\beta 1$  and  $\alpha 6\beta 1$ . Laminin-111/211 is also strongly expressed by basement membranes under the kidney capsule (Figure S5), just as in MPNSTs (Figure 2), potentially explaining why the kidney capsule creates a permissive environment for tumor formation by MPNST cells.

We examined whether antibodies that block the binding of laminin-111 to integrin receptors would impede colony forma-

tion. We were unable to find a preservative-free antibody against  $\alpha 2$ -integrin suitable for use in these experiments. Addition of blocking antibodies against  $\alpha 1$ -integrin (Figure 4C) or  $\alpha 6$ -integrin (Figure 4D) to culture did not affect the percentage of MPNST cells from *Nf1*<sup>+/-</sup>; *p53*<sup>+/-</sup> mice that formed colonies or the size of colonies. In contrast, addition of blocking antibodies against  $\beta 1$ -integrin (Milner and Campbell, 2002) but not isotype control antibody significantly decreased the percentage of MPNST cells from *Nf1*<sup>+/-</sup>; *p53*<sup>+/-</sup> mice (Figure 4F)

and *Nf1*<sup>+/-</sup>; *Ink4a/Arf*<sup>-/-</sup> mice (Figure 4G) that formed colonies on laminin-111, as well as the size of these colonies (Figure 4E), but did not affect the percentage of cells that formed adherent colonies on uncoated plastic or collagen 1 (Figures 4F and 4G). These data demonstrate that laminin binding to  $\beta 1$ -integrin-containing receptors increases the clonogenicity of MPNST cells from both genetic backgrounds.

Laminin promotes the survival of Schwann cells (Yu et al., 2005), and MPNSTs arise from Schwann cells (Zhu et al., 2002; Joseph et al., 2008; Zheng et al., 2008). Integrin receptors signal through the ERK pathway (Guo and Giancotti, 2004), and ERK provides a survival and proliferation signal to Schwann lineage cells (Newbern et al., 2011) and MPNST cells (Ambrosini et al., 2008). We found that adherent culture on laminin-111 increased the levels of phosphorylated ERK1/2 in MPNST cells from some *Nf1*<sup>+/-</sup>; *p53*<sup>+/-</sup> mice compared to nonadherent culture or

adherent culture on plastic (Figure 4H). Laminin binding to  $\beta 1$ -integrin may therefore promote the survival and proliferation of MPNST cells by increasing ERK signaling.

## DISCUSSION

Our data demonstrate that cells with tumorigenic potential are common in MPNSTs of both genotypes but that tumors with different genotypes sometimes require different assay conditions to read-out the full spectrum of cells with tumorigenic potential. If tumor genotype commonly influences the assay conditions that must be used to detect tumorigenic cells then assay conditions that detect the full spectrum of tumorigenic cells in one cancer patient may not detect the full spectrum of tumorigenic cells in other patients with the same cancer type. Studies of mouse lung cancers (Curtis et al., 2010), mouse mammary cancers (Vaillant et al., 2008), and mouse myeloid leukemias (Somerville and Cleary, 2006; Kennedy et al., 2007) have shown that cancers from different genetic backgrounds have different frequencies of tumorigenic cells, differences in the extent to which they follow a cancer stem cell model, or tumorigenic cells that express different markers. Human acute lymphoblastic leukemia samples that differ with respect to *CDKN2A/B* genotype also display differences in leukemogenic cell frequencies in immunocompromised mice (Notta et al., 2011). We demonstrate here that tumors of different genotypes can have similarly high frequencies of cells with tumorigenic potential but can require different assay conditions to detect these tumorigenic cells. Furthermore, we show that sarcomas sometimes contain common tumorigenic cells.

Our data suggest that the binding of laminin to  $\beta 1$ -integrin-containing receptors promotes the survival and proliferation of MPNST cells. MPNST cells from *Nf1*<sup>+/-</sup>; *p53*<sup>+/-</sup> and *Nf1*<sup>+/-</sup>; *Ink4a/Arf*<sup>-/-</sup> mice depended upon the binding of laminin to  $\beta 1$ -integrin for proliferation and survival (Figure 4), but MPNST cells from *Nf1*<sup>+/-</sup>; *Ink4a/Arf*<sup>-/-</sup> mice did not require the addition of exogenous laminin to culture (Figures 3A and 3B), presumably because these cells were much more likely to carry endogenous laminin as compared to MPNST cells from *Nf1*<sup>+/-</sup>; *p53*<sup>+/-</sup> mice. Suspension of MPNST cells from either genetic background in Matrigel doubled the frequency of cells that formed tumors in vivo (Figures 3D and 3E), and dividing cells in primary MPNSTs in vivo almost always had contact with laminin-expressing cells (Figures 2F–2H). Thus, laminin appears to be one important determinant of clonogenicity in MPNST cells, but it does not appear to matter whether the laminin is intrinsic or extrinsic to the MPNST cells.

Our results raise the possibility that the failure to restore critical extracellular matrix cues after tumor dissociation may lead to underestimates of the frequency of tumor-initiating cells. The common use of sphere-formation assays in nonadherent cultures to identify tumor-initiating cells may exacerbate this problem by depriving dissociated cancer cells of extracellular matrix.

Our data demonstrate that melanoma is not unique among solid tumors in containing common cells with tumorigenic potential. We have demonstrated that at least 30% of human melanoma cells obtained directly from patients have the potential to form tumors upon transplantation into NOD/SCID IL2 $\gamma$ <sup>null</sup>

mice (Quintana et al., 2008, 2010). An even higher percentage of single cells obtained from primary mouse melanomas can form tumors upon transplantation (Held et al., 2010). Whereas some cancers are likely to have only rare cells with the potential to proliferate extensively, other cancers are likely to contain common tumorigenic cells, and it remains uncertain what fraction of cancers fall in each category. Some mouse leukemias contain common leukemogenic cells (Somerville and Cleary, 2006; Kelly et al., 2007; Williams et al., 2007). However, other hematopoietic malignancies contain only rare leukemogenic cells (Lapidot et al., 1994; Kennedy et al., 2007), even when mouse leukemias are transplanted into histocompatible mice (Yilmaz et al., 2006; Oravec-Wilson et al., 2009). A recent study discovered that human hematopoietic stem cells engraft more efficiently in female as compared to male mice (Notta et al., 2010), a variable that has rarely been taken into account in xenotransplantation experiments. Thus, whereas many solid cancers have appeared to contain only rare tumorigenic cells (Ishizawa et al., 2010), an open question concerns the extent to which existing assays underestimate the frequency of cells with tumorigenic potential.

Our observation that approximately 20% of MPNST cells from *Nf1*<sup>+/-</sup>; *p53*<sup>+/-</sup> and *Nf1*<sup>+/-</sup>; *Ink4a/Arf*<sup>-/-</sup> mice have the potential to form tumors is likely an underestimate, because there are likely to be important features of the tumor environment that are not adequately modeled in the tumorigenesis assays we used. For example, it is possible that tumor-associated fibroblasts or tumor-infiltrating inflammatory cells promote the survival or proliferation of MPNST cells (Le et al., 2009; Staser et al., 2010) in a way that is not initially replicated when we place small numbers of dissociated MPNST cells in culture or under the kidney capsule in vivo. More sophisticated models of this tumor microenvironment could reveal even higher frequencies of MPNST cells that have the potential to form tumors.

Although we found that cells with tumorigenic potential were common in mouse MPNSTs, a separate question concerns the spectrum of cells that are actually fated to contribute to disease progression in vivo. Our data demonstrating that many cells divide rapidly within MPNSTs (Figure 1H) suggests that many cells contribute to tumor growth. However, it is also possible that many of these cells divide only a limited number of times and that only a small fraction of the cells with the potential to proliferate extensively actually does so in vivo. Fate-mapping studies will be required to assess whether many or few MPNST cells actually contribute extensively to tumor growth or disease progression in vivo.

The question of whether MPNSTs follow a cancer stem cell model, in which cancer cells are hierarchically organized into intrinsically different subpopulations of tumorigenic and nontumorigenic cells, also remains an open question. One possibility is that MPNSTs contain common tumorigenic cells with no hierarchical organization. Another possibility is that MPNSTs contain a shallow hierarchy in which common tumorigenic cells differentiate into nontumorigenic MPNST cells. Even if the latter is the case, MPNST would be quite different from other cancers suggested to follow the cancer stem cell model.

Our data demonstrate that cells with tumorigenic potential are common in MPNSTs and that tumors from different genetic backgrounds can require different assay conditions to read-out

the full spectrum of cells with tumorigenic potential. This suggests that efforts to quantify the frequency of tumorigenic cells in human cancers may be complicated by confounding effects of tumor genotype on assay conditions. As assays improve it is likely that estimates of tumorigenic cell frequencies will continue to increase in many cancers. It remains to be determined what fraction of cancers have only rare tumorigenic cells and what fraction of cancers have common tumorigenic cells. Determining which cancers fall in each category has fundamental implications for therapy as attempts to target small subpopulations of cancer cells are not likely to improve the treatment of cancers in which many cells can drive disease progression.

## EXPERIMENTAL PROCEDURES

### Mice

*Nf1*<sup>+/-</sup> (Jacks et al., 1994) mice were bred with *Ink4aArf*<sup>-/-</sup> mice (Serrano et al., 1996) to yield compound mutant *Nf1*<sup>+/-</sup>; *Ink4a/Arf*<sup>-/-</sup> mice (Joseph et al., 2008). *Nf1*<sup>+/-</sup>; *Ink4a/Arf*<sup>-/-</sup> mice and *Nf1*<sup>+/-</sup>; *p53*<sup>+/-</sup> mice (Cichowski et al., 1999) were backcrossed on a C57BL/Ka background for at least six generations. Genotyping was performed as described by Joseph et al. (2008). All animal experiments were performed in accordance with protocols approved by the University of Michigan's Committee on the Use and Care of Animals.

### Dissociation of MPNSTs and Flow Cytometry

Tumors were harvested from mice and minced using a scalpel. Minced tissue was washed in Ca<sup>2+</sup> and Mg<sup>2+</sup>-free Hank's buffered salt solution (HBSS; Invitrogen, Grand Island, NY, USA), centrifuged, and treated for 20 min at 37°C with a mixture of 25% Ca<sup>2+</sup> and Mg<sup>2+</sup>-free HBSS, 25% Collagenase IV (Worthington [Lakewood, NJ, USA]; resuspended to 2,000 U/ml in HBSS containing Ca<sup>2+</sup> and Mg<sup>2+</sup>, Invitrogen), and 50% Trypsin-EDTA solution (0.05%, Invitrogen) with constant agitation. The reaction was quenched with staining medium consisting of L15 medium (Invitrogen), 1 mg/ml BSA (Sigma-Aldrich, St. Louis, MO, USA), 10 mM HEPES (BioWhittaker # 17-738E), 1% penicillin/streptomycin (Invitrogen), supplemented with DNase 1 (100 U/ml; Sigma), and filtered through 70 µm nylon filter (Fisher Scientific, Ottawa, Ontario). The cells were centrifuged, resuspended in staining medium, and then counted on a hemocytometer. Cells were stained with antibodies against CD31 (BioLegend, San Diego, CA, USA), CD45 (eBioscience, San Diego, CA, USA), and Ter119 (BioLegend) in 200 µl of staining medium for 20 min at 4°C. The cells were then washed and resuspended in staining medium supplemented with DAPI (10 µg/ml; Sigma). To evaluate the expression of laminin receptors, cells were stained with antibodies against integrin  $\alpha$ 1 (BD Biosciences, San Diego, CA, USA),  $\alpha$ 2 (BD Biosciences),  $\alpha$ 6 (eBioscience), and integrin  $\beta$ 1 (BD Biosciences), as well as appropriate secondary antibodies prior to staining with blood lineage markers. Flow cytometry was performed with a FACSVantage SE-dual laser, three-line flow cytometer, or with a FACSAria II (Becton Dickinson, Franklin Lakes, NJ, USA).

### Cell Culture

Cells were typically cultured in 96-well tissue culture plates (Corning, Lowell, MA, USA) at a density of 1 cell/well. For nonadherent cultures, ultra-low binding plates (Corning) were used. For adherent cultures, plates were coated with fibronectin (Biomedical Technologies, Stoughton, MA, USA), laminin-111 (Invitrogen), or collagen-1 (BD Bioscience), all at 50 µg/ml. The culture medium for both adherent and nonadherent cultures was based on a 5:3 mixture of Dulbecco's modified eagle medium-low:Neurobasal medium (Invitrogen). The medium was supplemented with 15% chick embryo extract (prepared as described; Stemple and Anderson, 1992), 20 ng/ml recombinant human bFGF (R&D Systems, Minneapolis, MN), 20 ng/ml IGF1 (R&D Systems), 1% N2 supplement (Invitrogen), 2% B27 supplement (Invitrogen), 50 mM 2-mercaptoethanol (Acros Organics), 35 ng/ml retinoic acid (Sigma), and 1% penicillin/streptomycin (Invitrogen). In some cases, the medium was supplemented with laminin-111 or fibronectin, both at 50 µg/ml. All cultures were maintained at 37°C in 6% CO<sub>2</sub>/balance air. For experiments using blocking antibodies,

cells were cultured at a density of 50–100 cells/well on 24-well plates on plastic or laminin-111 (50 µg/ml) in the presence or absence of antibodies against integrin  $\alpha$ 1 (BD Bioscience),  $\alpha$ 6 (clone GoH3; R&D Systems), or  $\beta$ 1 (BD Bioscience) or corresponding isotype controls (all at 10 µg/ml). Colony formation was assessed after 5–8 days.

### Kidney Capsule Injections

MPNST cells were resuspended in 30 µl of sterile staining medium. Mice were anesthetized by intraperitoneal injection of ketamine/xylazine. After shaving the skin and prepping with betadine (Fisher Scientific), a 1 cm longitudinal incision was made in the skin of the abdomen and in the body wall above the kidney. Cell suspensions were injected under the capsule of the exposed kidney using an insulin syringe with a 31G needle (BD Bioscience). In some cases, 50% Matrigel (BD Bioscience) was added to the cell suspension. The incisions were closed using absorbable suture (Tevdek, Genzyme Surgical #7-734). Animals were given antibiotic water (1.1 g/l neomycin sulfate and 10<sup>6</sup> U/l polymixin B sulfate) and monitored closely. Tumor formation was assessed by weekly palpation of the abdomen or by magnetic resonance imaging for at least 15 weeks. The frequency of tumorigenic cells and the 95% confidence interval were calculated using extreme limiting dilution software (<http://bioinf.wehi.edu.au/software/elda/index.html>).

## SUPPLEMENTAL INFORMATION

Supplemental Information includes five figures, three tables, and Supplemental Experimental Procedures and can be found with this article online at doi:10.1016/j.ccr.2011.12.027.

## ACKNOWLEDGMENTS

This work was supported by the National Institute of Neurological Disorder and Stroke (grant NS-040750), the Howard Hughes Medical Institute, and the Liddy Shriver Sarcoma Initiative. J.B. was supported by postdoctoral fellowships from the Swiss National Foundation of Science and the Children's Tumor Foundation. Thanks to Kristina Harter for technical assistance. Thanks to David Adams and Martin White for assistance with flow cytometry, which was partially supported by the University of Michigan (UM) Comprehensive Cancer Center (National Institutes of Health grant CA46592). Thanks to Maria Ripberger, Alan Burgess, and Nancy McAnsh for paraffin embedding, sectioning, and immunohistochemistry. Thanks to Amanda Welton in the UM Center for Molecular Imaging for magnetic resonance imaging. Thanks to Tyler Jacks for providing *Nf1* germline knockout mice, Tyler Jacks and Karlyne Reilly for providing *Nf1*<sup>+/-</sup>; *p53*<sup>+/-</sup> mice, and Ron DePinho for providing *Ink4a/Arf* mutant mice.

Received: December 7, 2010

Revised: October 12, 2011

Accepted: December 26, 2011

Published: February 13, 2012

## REFERENCES

- Agese, T.H., Florenes, V.A., Molenaar, W.M., Lind, G.E., Berner, J.M., Plaats, B.E., Komdeur, R., Myklebost, O., van den Berg, E., and Lothe, R.A. (2005). Expression patterns of cell cycle components in sporadic and neurofibromatosis type 1-related malignant peripheral nerve sheath tumors. *J. Neuropathol. Exp. Neurol.* 64, 74–81.
- Al-Hajj, M., Wicha, M.S., Benito-Hernandez, A., Morrison, S.J., and Clarke, M.F. (2003). Prospective identification of tumorigenic breast cancer cells. *Proc. Natl. Acad. Sci. USA* 100, 3983–3988.
- Ambrosini, G., Cheema, H.S., Seelman, S., Teed, A., Sambol, E.B., Singer, S., and Schwartz, G.K. (2008). Sorafenib inhibits growth and mitogen-activated protein kinase signaling in malignant peripheral nerve sheath cells. *Mol. Cancer Ther.* 7, 890–896.
- Bonnet, D., and Dick, J.E. (1997). Human acute myeloid leukemia is organized as a hierarchy that originates from a primitive hematopoietic cell. *Nat. Med.* 3, 730–737.

- Cichowski, K., Shih, T.S., Schmitt, E., Santiago, S., Reilly, K., McLaughlin, M.E., Bronson, R.T., and Jacks, T. (1999). Mouse models of tumor development in neurofibromatosis type 1. *Science* 286, 2172–2176.
- Curtis, S.J., Sinkevicius, K.W., Li, D., Lau, A.N., Roach, R.R., Zamponi, R., Woolfenden, A.E., Kirsch, D.G., Wong, K.K., and Kim, C.F. (2010). Primary tumor genotype is an important determinant in identification of lung cancer propagating cells. *Cell Stem Cell* 7, 127–133.
- Dalerba, P., Dylla, S.J., Park, I.K., Liu, R., Wang, X., Cho, R.W., Hoey, T., Gurney, A., Huang, E.H., Simeone, D.M., et al. (2007). Phenotypic characterization of human colorectal cancer stem cells. *Proc. Natl. Acad. Sci. USA* 104, 10158–10163.
- Dick, J.E. (2008). Stem cell concepts renew cancer research. *Blood* 112, 4793–4807.
- Guo, W., and Giancotti, F.G. (2004). Integrin signalling during tumour progression. *Nat. Rev. Mol. Cell Biol.* 5, 816–826.
- Held, M.A., Curley, D.P., Dankort, D., McMahon, M., Muthusamy, V., and Bosenberg, M.W. (2010). Characterization of melanoma cells capable of propagating tumors from a single cell. *Cancer Res.* 70, 388–397.
- Illmensee, K., and Mintz, B. (1976). Totipotency and normal differentiation of single teratocarcinoma cells cloned by injection into blastocysts. *Proc. Natl. Acad. Sci. USA* 73, 549–553.
- Ishizawa, K., Rasheed, Z.A., Karisch, R., Wang, Q., Kowalski, J., Susky, E., Pereira, K., Karamboulas, C., Moghal, N., Rajeshkumar, N.V., et al. (2010). Tumor-initiating cells are rare in many human tumors. *Cell Stem Cell* 7, 279–282.
- Jacks, T., Shih, T.S., Schmitt, E.M., Bronson, R.T., Bernards, A., and Weinberg, R.A. (1994). Tumour predisposition in mice heterozygous for a targeted mutation in Nf1. *Nat. Genet.* 7, 353–361.
- Joseph, N.M., Mosher, J.T., Buchstaller, J., Snider, P., McKeever, P.E., Lim, M., Conway, S.J., Parada, L.F., Zhu, Y., and Morrison, S.J. (2008). The loss of Nf1 transiently promotes self-renewal but not tumorigenesis by neural crest stem cells. *Cancer Cell* 13, 129–140.
- Kelly, P.N., Dakic, A., Adams, J.M., Nutt, S.L., and Strasser, A. (2007). Tumor growth need not be driven by rare cancer stem cells. *Science* 317, 337.
- Kennedy, J.A., Barabe, F., Poepl, A.G., Wang, J.C., and Dick, J.E. (2007). Comment on “Tumor growth need not be driven by rare cancer stem cells.” *Science* 318, 1722.
- Kleinman, H.K., and Martin, G.R. (2005). Matrigel: basement membrane matrix with biological activity. *Semin. Cancer Biol.* 15, 378–386.
- Kleinsmith, L.J., and Pierce, G.B., Jr. (1964). Multipotentiality of single embryonal carcinoma cells. *Cancer Res.* 24, 1544–1551.
- Lapidot, T., Sirard, C., Vormoor, J., Murdoch, B., Hoang, T., Caceres-Cortes, J., Minden, M., Paterson, B., Caligiuri, M.A., and Dick, J.E. (1994). A cell initiating human acute myeloid leukemia after transplantation into SCID mice. *Nature* 367, 645–648.
- Lathia, J.D., Gallagher, J., Heddleston, J.M., Wang, J., Eyler, C.E., Macsworlds, J., Wu, Q., Vasanji, A., McLendon, R.E., Hjelmeland, A.B., and Rich, J.N. (2010). Integrin  $\alpha 6$  regulates glioblastoma stem cells. *Cell Stem Cell* 6, 421–432.
- Le, L.Q., Shipman, T., Burns, D.K., and Parada, L.F. (2009). Cell of origin and microenvironment contribution for NF1-associated dermal neurofibromas. *Cell Stem Cell* 4, 453–463.
- Menon, A.G., Anderson, K.M., Riccardi, V.M., Chung, R.Y., Whaley, J.M., Yandell, D.W., Farmer, G.E., Freiman, R.N., Lee, J.K., Li, F.P., et al. (1990). Chromosome 17p deletions and p53 gene mutations associated with the formation of malignant neurofibrosarcomas in von Recklinghausen neurofibromatosis. *Proc. Natl. Acad. Sci. USA* 87, 5435–5439.
- Merlos-Suárez, A., Barriga, F.M., Jung, P., Iglesias, M., Céspedes, M.V., Rossell, D., Sevillano, M., Hernando-Momblona, X., da Silva-Diz, V., Muñoz, P., et al. (2011). The intestinal stem cell signature identifies colorectal cancer stem cells and predicts disease relapse. *Cell Stem Cell* 8, 511–524.
- Milner, R., and Campbell, I.L. (2002). Cytokines regulate microglial adhesion to laminin and astrocyte extracellular matrix via protein kinase C-dependent activation of the  $\alpha 6 \beta 1$  integrin. *J. Neurosci.* 22, 1562–1572.
- Miner, J.H., and Yurchenco, P.D. (2004). Laminin functions in tissue morphogenesis. *Annu. Rev. Cell Dev. Biol.* 20, 255–284.
- Molofsky, A.V., Pardal, R., Iwashita, T., Park, I.K., Clarke, M.F., and Morrison, S.J. (2003). Bmi-1 dependence distinguishes neural stem cell self-renewal from progenitor proliferation. *Nature* 425, 962–967.
- Newbern, J.M., Li, X., Shoemaker, S.E., Zhou, J., Zhong, J., Wu, Y., Bonder, D., Hollenback, S., Coppola, G., Geschwind, D.H., et al. (2011). Specific functions for ERK/MAPK signaling during PNS development. *Neuron* 69, 91–105.
- Notta, F., Doulatov, S., and Dick, J.E. (2010). Engraftment of human hematopoietic stem cells is more efficient in female NOD/SCID/IL-2R $\gamma$  null recipients. *Blood* 115, 3704–3707.
- Notta, F., Mullighan, C.G., Wang, J.C., Poepl, A., Doulatov, S., Phillips, L.A., Ma, J., Minden, M.D., Downing, J.R., and Dick, J.E. (2011). Evolution of human BCR-ABL1 lymphoblastic leukaemia-initiating cells. *Nature* 469, 362–367.
- O’Brien, C.A., Pollett, A., Gallinger, S., and Dick, J.E. (2007). A human colon cancer cell capable of initiating tumour growth in immunodeficient mice. *Nature* 445, 106–110.
- Oravec-Wilson, K.I., Philips, S.T., Yilmaz, O.H., Ames, H.M., Li, L., Crawford, B.D., Gauvin, A.M., Lucas, P.C., Sitwala, K., Downing, J.R., et al. (2009). Persistence of leukemia-initiating cells in a conditional knockin model of an imatinib-responsive myeloproliferative disorder. *Cancer Cell* 16, 137–148.
- Pardal, R., Clarke, M.F., and Morrison, S.J. (2003). Applying the principles of stem-cell biology to cancer. *Nat. Rev. Cancer* 3, 895–902.
- Perrone, F., Tabano, S., Colombo, F., Dagrada, G., Birindelli, S., Gronchi, A., Colecchia, M., Pierotti, M.A., and Pilotti, S. (2003). p15INK4b, p14ARF, and p16INK4a inactivation in sporadic and neurofibromatosis type 1-related malignant peripheral nerve sheath tumors. *Clin. Cancer Res.* 9, 4132–4138.
- Pollard, S.M., Yoshikawa, K., Clarke, I.D., Danovi, D., Stricker, S., Russell, R., Bayani, J., Head, R., Lee, M., Bernstein, M., et al. (2009). Glioma stem cell lines expanded in adherent culture have tumor-specific phenotypes and are suitable for chemical and genetic screens. *Cell Stem Cell* 4, 568–580.
- Quintana, E., Shackleton, M., Sabel, M.S., Fullen, D.R., Johnson, T.M., and Morrison, S.J. (2008). Efficient tumour formation by single human melanoma cells. *Nature* 456, 593–598.
- Quintana, E., Shackleton, M., Foster, H.R., Fullen, D.R., Sabel, M.S., Johnson, T.M., and Morrison, S.J. (2010). Phenotypic heterogeneity among tumorigenic melanoma cells from patients that is reversible and not hierarchically organized. *Cancer Cell* 18, 510–523.
- Reya, T., Morrison, S.J., Clarke, M.F., and Weissman, I.L. (2001). Stem cells, cancer, and cancer stem cells. *Nature* 414, 105–111.
- Ricci-Vitiani, L., Lombardi, D.G., Pilozzi, E., Biffoni, M., Todaro, M., Peschle, C., and De Maria, R. (2007). Identification and expansion of human colon-cancer-initiating cells. *Nature* 445, 111–115.
- Rubin, J.B., and Gutmann, D.H. (2005). Neurofibromatosis type 1 - a model for nervous system tumour formation? *Nat. Rev. Cancer* 5, 557–564.
- Serrano, M., Lee, H., Chin, L., Cordon-Cardo, C., Beach, D., and DePinho, R.A. (1996). Role of the INK4a locus in tumor suppression and cell mortality. *Cell* 85, 27–37.
- Shultz, L.D., Lyons, B.L., Burzenski, L.M., Gott, B., Chen, X., Chaleff, S., Kotb, M., Gillies, S.D., King, M., Mangada, J., et al. (2005). Human lymphoid and myeloid cell development in NOD/LtSz-scid IL2R gamma null mice engrafted with mobilized human hemopoietic stem cells. *J. Immunol.* 174, 6477–6489.
- Singh, S.K., Hawkins, C., Clarke, I.D., Squire, J.A., Bayani, J., Hide, T., Henkelman, R.M., Cusimano, M.D., and Dirks, P.B. (2004). Identification of human brain tumour initiating cells. *Nature* 429, 396–401.
- Somervaille, T.C., and Cleary, M.L. (2006). Identification and characterization of leukemia stem cells in murine MLL-AF9 acute myeloid leukemia. *Cancer Cell* 10, 257–268.
- Staser, K., Yang, F.C., and Clapp, D.W. (2010). Mast cells and the neurofibroma microenvironment. *Blood* 116, 157–164.
- Stemple, D.L., and Anderson, D.J. (1992). Isolation of a stem cell for neurons and glia from the mammalian neural crest. *Cell* 71, 973–985.

- Sun, Y., Pollard, S., Conti, L., Toselli, M., Biella, G., Parkin, G., Willatt, L., Falk, A., Cattaneo, E., and Smith, A. (2008). Long-term tripotent differentiation capacity of human neural stem (NS) cells in adherent culture. *Mol. Cell. Neurosci.* 38, 245–258.
- Vaillant, F., Asselin-Labat, M.L., Shackleton, M., Forrest, N.C., Lindeman, G.J., and Visvader, J.E. (2008). The mammary progenitor marker CD61/beta3 integrin identifies cancer stem cells in mouse models of mammary tumorigenesis. *Cancer Res.* 68, 7711–7717.
- Vogel, K.S., Klesse, L.J., Velasco-Miguel, S., Meyers, K., Rushing, E.J., and Parada, L.F. (1999). Mouse tumor model for neurofibromatosis type 1. *Science* 286, 2176–2179.
- Williams, R.T., den Besten, W., and Sherr, C.J. (2007). Cytokine-dependent imatinib resistance in mouse BCR-ABL+, Arf-null lymphoblastic leukemia. *Genes Dev.* 21, 2283–2287.
- Yilmaz, O.H., Valdez, R., Theisen, B.K., Guo, W., Ferguson, D.O., Wu, H., and Morrison, S.J. (2006). Pten dependence distinguishes haematopoietic stem cells from leukaemia-initiating cells. *Nature* 441, 475–482.
- Yu, W.M., Feltri, M.L., Wrabetz, L., Strickland, S., and Chen, Z.L. (2005). Schwann cell-specific ablation of laminin gamma1 causes apoptosis and prevents proliferation. *J. Neurosci.* 25, 4463–4472.
- Zheng, H., Chang, L., Patel, N., Yang, J., Lowe, L., Burns, D.K., and Zhu, Y. (2008). Induction of abnormal proliferation by nonmyelinating schwann cells triggers neurofibroma formation. *Cancer Cell* 13, 117–128.
- Zhu, Y., Ghosh, P., Charnay, P., Burns, D.K., and Parada, L.F. (2002). Neurofibromas in NF1: Schwann cell origin and role of tumor environment. *Science* 296, 920–922.

# Adult Murine Prostate Basal and Luminal Cells Are Self-Sustained Lineages that Can Both Serve as Targets for Prostate Cancer Initiation

Nahyun Choi,<sup>1,4</sup> Boyu Zhang,<sup>1,4</sup> Li Zhang,<sup>1</sup> Michael Ittmann,<sup>2,3</sup> and Li Xin<sup>1,2,3,\*</sup>

<sup>1</sup>Department of Molecular and Cellular Biology

<sup>2</sup>Department of Pathology and Immunology

<sup>3</sup>Dan L. Duncan Cancer Center

Baylor College of Medicine, One Baylor Plaza, Houston, TX 77030, USA

<sup>4</sup>These authors contributed equally to this work

\*Correspondence: [xin@bcm.edu](mailto:xin@bcm.edu)

DOI 10.1016/j.ccr.2012.01.005

## SUMMARY

The prostate epithelial lineage hierarchy and the cellular origin for prostate cancer remain inadequately defined. Using a lineage-tracing approach, we show that adult rodent prostate basal and luminal cells are independently self-sustained *in vivo*. Disrupting the tumor suppressor *Pten* in either lineage led to prostate cancer initiation. However, the cellular composition and onset dynamics of the resulting tumors are distinctive. Prostate luminal cells are more responsive to *Pten* null-induced mitogenic signaling. In contrast, basal cells are resistant to direct transformation. Instead, loss of *Pten* activity induces the capability of basal cells to differentiate into transformation-competent luminal cells. Our study suggests that deregulation of epithelial differentiation is a critical step for the initiation of prostate cancers of basal cell origin.

## INTRODUCTION

Defining the cells of origin for cancer is of great value for accurate tumor prognosis and efficient prevention and therapeutics (Visvader, 2011). Previously, the identities of the cells of origin for cancer were assumed based on histological characterization of cancers. However, recent transcriptome studies have revealed that molecular signatures of cancer cells do not always match their histological appearance (Lim et al., 2009). Therefore, it can be misleading to determine cells of origin in the absence of functional lineage-tracing studies (Molyneux et al., 2010).

Though prostate cancer is the second leading cause of cancer-related death in males in the United States, it is still mainly described by qualitative clinical measurements, including the TNM system and the Gleason grading system (Iczkowski and Lucia, 2011). The identity of the cellular origin for prostate

cancer remains unclear, partly because the prostate epithelial lineage hierarchy per se has not been clearly characterized. Prostate epithelia are composed of three types of epithelial cells, luminal cells, basal cells, and neuroendocrine cells, of which the latter are extremely rare (Abate-Shen and Shen, 2000). When prostate epithelial cells are cultured *in vitro*, a population of transit-amplifying cells is frequently observed (Litvinov et al., 2006; Peehl, 2005). These transit-amplifying cells express antigenic markers for both basal and luminal cells. Transit-amplifying cells are abundant at the developmental stage but are not detectable *in vivo* in adults under physiological conditions (Wang et al., 2001).

Using a functional prostate regeneration assay, several independent groups, including ours, have demonstrated that some basal cells in human and murine prostates can generate all three prostate epithelial cell lineages (Burger et al., 2005; Goldstein et al., 2010; Lawson et al., 2007; Leong et al.,

## Significance

Understanding the cellular origin for cancer can help improve disease prevention and therapeutics. Our genetic studies directly demonstrate that prostate cancer can initiate from both the basal and luminal cell lineages. However, prostate basal cells are less susceptible than luminal cells to direct transformation. Instead, disease initiation from prostate basal cells requires oncogenic-signaling-induced differentiation of adult prostate basal cells into luminal cells, which is absent under physiological conditions. These studies suggest that deregulation of the normal-prostate epithelial differentiation program is a critical step for initiation of human prostate cancer with a basal cell origin. Furthermore, suppressing signaling pathways that induce basal-luminal differentiation may provide an efficient approach to prevent prostate cancer initiation.

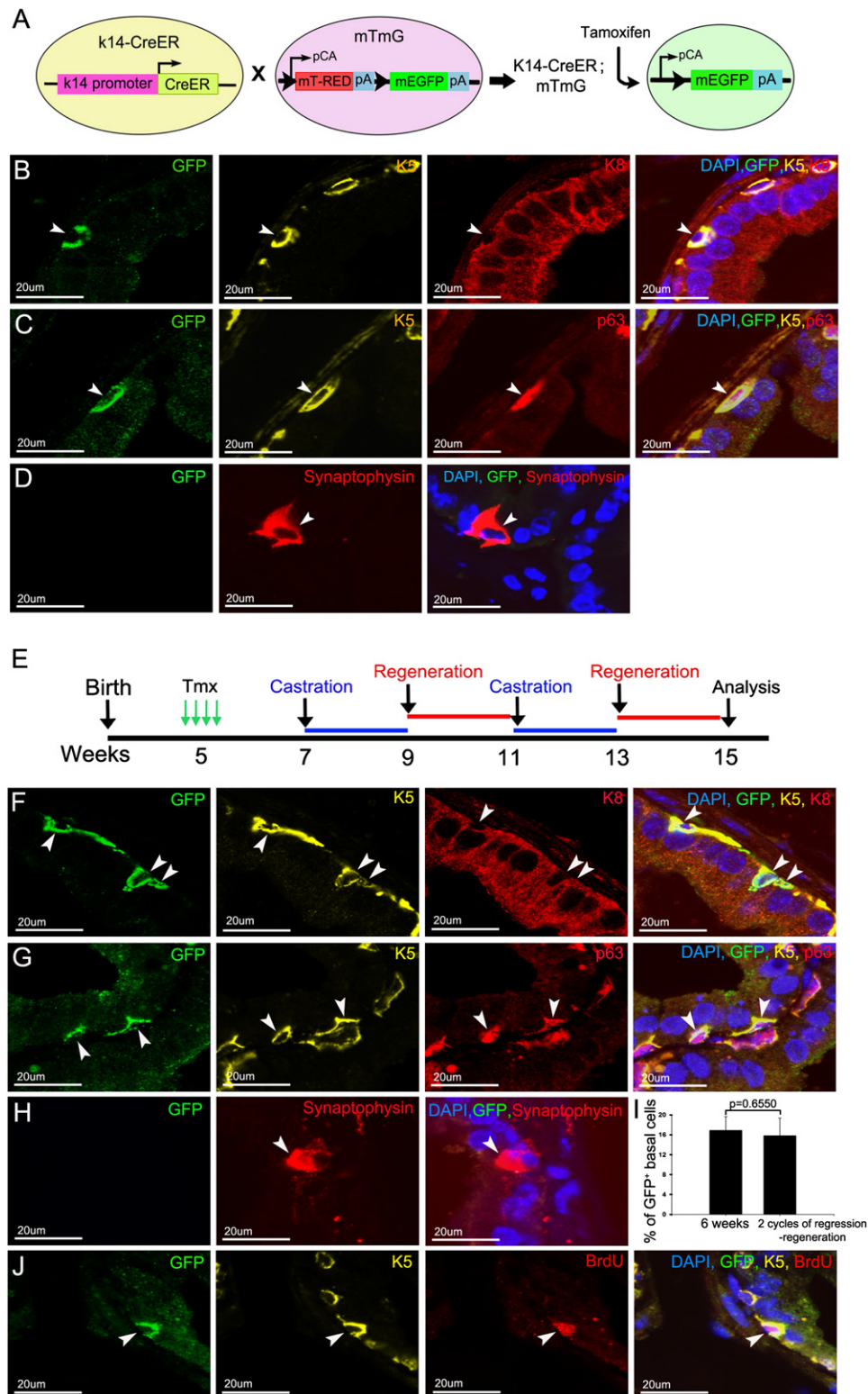


**Figure 1. Lineage Tracing Shows that Prostate Basal Cells Only Generate Basal Cells In Vivo**

(A) Schematic illustration of the lineage-tracing strategy.

(B–D) Costaining of GFP with K5 and K8 (B), K5 and P63 (C), and synaptophysin (D) in tamoxifen-treated K14-mTmG mice. Arrowheads in (B) and (C) indicate GFP-labeled basal cells. Arrowhead in (D) points to a neuroendocrine cell.

(E) Timeline for androgen deprivation and replacement experiments.

2008; Xin et al., 2005, 2007; Zhang et al., 2011). In addition, Wang et al. discovered that a rare castration-resistant luminal prostate cell population also possesses multipotent stem cell activity (Wang et al., 2009). Of note, the conclusions of those studies are based on experimental conditions involving cell transplantation that do not reflect physiological conditions. Therefore, it remains an open question whether the activities measured in those assays reflect the obligate or facultative function of prostate stem cells. Pertaining to this caveat, Liu et al. recently showed by lineage tracing that prostate luminal cells are derived from pre-existing luminal cells (Liu et al., 2011). In addition, a very recent comprehensive lineage-tracing study on the mammary gland epithelial lineage hierarchy showed that in the postnatal mammary gland, distinct stem cells contribute to the maintenance of the myoepithelial and luminal cell lineages (Van Keymeulen et al., 2011). A similar comprehensive study on prostate lineage hierarchy is required to address these controversies.

Previously, prostate luminal cells, transit-amplifying cells, and basal cells have all been implicated as the cells of origin for prostate cancer (Lawson and Witte, 2007). Two distinct functional approaches have been used recently to directly investigate the identity of the cellular origin for prostate cancer. One approach is to employ genetically engineered mouse models (Ellwood-Yen et al., 2003; Foster et al., 1997; Iwata et al., 2010; Majumder et al., 2003; Wang et al., 2003, 2009) to introduce oncogenic signaling in different prostate cell lineages. Most of these studies utilized two prostate-specific promoters (*Probasin* and *Nkx3.1*). However, recently it has been shown that these promoters are active in both luminal cells and some basal cells (Mulholland et al., 2009; Wu et al., 2007; Zhang et al., 2011). Therefore, one cannot determine definitively the identities of the cells of origin for cancer using this approach. Wang et al. recently demonstrated that some very rare NKX3.1-positive luminal cells in castrated mice can serve as targets for transformation (Wang et al., 2009), but it remains undetermined whether other luminal cells also can serve as the cells of origin for cancer. A prostate-specific antigen-CreER<sup>T2</sup> model has recently been demonstrated to mediate luminal-cell-specific gene expression, but to date this model has not been extensively utilized (Liu et al., 2011; Ratnacaram et al., 2008).

The other approach is to genetically modify different prospectively isolated prostate epithelial cell lineages and investigate their tumorigenic potential by in vivo transplantation assays. Using this approach, we and others have demonstrated that murine and human prostate basal cells, but not luminal cells, can efficiently initiate prostate carcinogenesis in various oncogenic contexts (Goldstein et al., 2010; Lawson et al., 2010; Xin et al., 2005). However, a caveat for this approach is that luminal cells by nature do not proliferate and regenerate prostate tissues in the in vivo transplantation assay; hence, these studies cannot exclude that luminal cells also serve as the cells of origin for

cancer in vivo. In summary, due to a lack of mouse models that enable strict lineage targeting in the prostate, it has not been comprehensively determined previously whether individual cell lineages can serve as targets for transformation orthotopically in the prostate. This study aims to reveal how prostate basal and luminal cell lineages are maintained and the roles of these two lineages in prostate cancer initiation.

## RESULTS

### Lineage Tracing Shows that Prostate Basal Cells Only Generate Basal Cells In Vivo

We employed a lineage-tracing approach to determine in vivo whether adult murine prostate basal epithelial cells would generate all three prostate epithelial cell lineages. A K14-CreER transgenic mouse line was generated previously (Vasioukhin et al., 1999) in which *CreER* is driven by the promoter of Keratin 14, a prostate basal cell marker. *CreER* encodes a Cre recombinase fused to a mutant estrogen ligand-binding domain so that its activity is induced only in the presence of tamoxifen. To investigate whether *CreER* is specifically expressed in prostate basal cells, K14-CreER transgenic mice were bred with *mTmG* reporter mice to generate K14-CreER<sup>Tg/Tg</sup>; *mTmG*<sup>Tg/Tg</sup> mice (hereafter referred to as the K14-mTmG mice). The *mTmG* mouse line is a double fluorescent reporter line that replaces the expression of a membrane-targeted Tomato-Red (mT) protein with a membrane-targeted enhanced green fluorescence protein (mG) upon Cre-LoxP-mediated homologous recombination (Muzumdar et al., 2007) (Figure 1A).

Tamoxifen was injected intraperitoneally (i.p.) into male K14-mTmG bigenic mice. In contrast to the highly efficient Cre-mediated recombination observed in the skin (Figure S1A available online), the recombination efficiency in the prostate was lower and varied among different prostate lobes. On average, 17% of basal cells in lateral lobes were pulse-labeled with GFP (Table S1). In contrast, rare and heterogeneously distributed GFP-positive basal cells were observed in other lobes, and these cells were hard to quantify. The recombination frequencies among lobes did not correlate with the K14 promoter activity (Figure S1B). All GFP-positive cells expressed the basal cell marker keratin 5 (K5) (Figure 1B, Table S1; n = 2095 cells from five mice). All of the observed cell nuclei of these GFP-positive cells were positively stained with another nuclear-localized basal cell marker, P63 (Figure 1C; n = 1952 cells). In contrast, none of the examined GFP-positive cells expressed the luminal cell marker keratin 8 (K8), or the neuroendocrine cell marker synaptophysin (Figures 1B and 1D). These data demonstrate that the *CreER* expression is restricted to prostate basal cells in the K14-CreER model.

Adult murine prostate epithelia turn over extremely slowly under physiological conditions. To determine the fate of prostate basal cells, we induced extensive epithelial turnover by a classic

(F–H) Costaining of GFP with K5 and K8 (F), K5 and P63 (G), and synaptophysin (H) in tamoxifen-treated K14-mTmG mice after induced epithelial turnover. Arrowheads in (F) and (G) indicate GFP-labeled basal cells. Arrowhead in (H) points to a neuroendocrine cell.

(I) Bar graph shows the percentage of GFP-labeled basal cells in lateral prostate lobes of K14-mTmG mice 5 days after tamoxifen induction (6 weeks) and after 2 cycles of epithelial regression-regeneration. Data represent the mean  $\pm$  SD. Also see Table S1.

(J) GFP-labeled basal cells (arrowhead) incorporated BrdU.

See also Figure S1 and Table S1.

prostate regression-regeneration model, as schematically illustrated in Figure 1E. In this model, prostate tissues atrophy and regenerate repeatedly in response to fluctuating serum testosterone levels. Substantial epithelial cell turnover was induced after two cycles of prostate regression-regeneration. Immunohistochemistry (IHC) analyses showed that all GFP-positive cells remained basal cells because they expressed K5 but not K8 or synaptophysin ( $n = 1295$  cells from four mice, Figures 1F and 1H). In addition, the percentage of GFP-labeled basal cells in lateral prostates did not change after induced epithelial turnover (Figure 1I; Table S1), suggesting that either all basal cells possess equal regenerative capacity or the unipotent basal stem cells and differentiated basal cells are labeled at equal frequency. The GFP-labeled basal cells have proliferated because they incorporated BrdU (Figure 1J). Collectively, these data demonstrate that during prostate regeneration, the GFP-labeled basal cells proliferated but only gave rise to prostate basal cells and did not differentiate or undergo lineage conversion to generate other cell lineages.

#### Prostate Luminal Cell Lineage Is Self-Sustained In Vivo

We generated a K8-CreER<sup>T2</sup> mouse model via bacterial artificial chromosome transgenesis (Zhang et al., 2012), in which CreER<sup>T2</sup> is driven by the promoter of the prostate luminal cell marker keratin 8. The same lineage-tracing approach was employed using K8-CreERT2<sup>Wt/Tg</sup>;mTmG<sup>Wt/Tg</sup> (hereafter referred to as K8-mTmG) mice to determine how prostate luminal epithelial cells are sustained. GFP was undetectable in vehicle-treated K8-mTmG mouse prostates (data not shown), but was expressed abundantly in tamoxifen-treated mouse prostates (Figure S2A). All GFP-positive cells expressed K8, but not K5 or synaptophysin [ $n = 31,319$  from seven mice (Figures 2A and 2B)], demonstrating that CreER<sup>T2</sup> is only expressed by prostate luminal epithelial cells in this model. The recombination efficiency varied among different prostate lobes, with that in lateral lobes the highest (Figures 2E and S2A; Tables S2 and S4). The recombination frequencies did not correlate with the K8 promoter activity (CreER expression level) among lobes (Figure S2B). Therefore, the variation in recombination efficiency may be due to differential local tamoxifen concentrations and CreER activation status as a result of distinct blood vessel densities among these different lobes.

To determine how the prostate luminal cell lineage is maintained, we aged tamoxifen-treated K8-mTmG mice for 4 months. As shown in Figure 2E and Tables S2–S4, the percentage of GFP-positive luminal cells in individual lobes did not change after aging. Since prostate tissues gain weight significantly from 6 weeks to 24 weeks (Figure S2C), it is unlikely that the invariant percentage of GFP-positive luminal cells after aging is due to rare cellular turnover. Instead, this result suggests that the luminal cell lineage may be self-sustained. To further interrogate this possibility, tamoxifen-treated K8-mTmG mice were subjected to two cycles of prostate regression-regeneration to induce extensive epithelial turnover, as illustrated in Figure 1E. IHC analyses showed that the percentages of GFP-positive luminal cells were not statistically different before and after induction of epithelial turnover (Figure 2E; Tables S2–S4). In addition, all GFP-positive cells still expressed K8, but not K5 or synaptophysin (Figures 2C and 2D), demonstrating that GFP-

labeled luminal cells only generate other luminal cells. Overall these results imply that prostate luminal cells are not replenished by stem/progenitor cells from other cell lineages during prostate regeneration.

In addition, the approach illustrated in Figure 2F was employed to directly investigate the origin of newly formed prostate luminal cells. Tamoxifen-treated K8-mTmG mice were subjected to one cycle of prostate regression-regeneration to induce extensive epithelial turnover. BrdU was administered to label dividing cells during the period of regeneration. As shown in Figures 2G and 2H and Tables S2–S4, the GFP<sup>+</sup> new luminal cells (BrdU<sup>+</sup>K8<sup>+</sup>) in individual prostate lobes were generated at a frequency equal to that of the initial pulse-labeling (i.e., the percentage of GFP<sup>+</sup> luminal cells). These data suggest that if the labeling efficiency of luminal cells is 100%, all new K8<sup>+</sup> luminal cells will be GFP<sup>+</sup>, which means that they would all come from cells in the luminal lineage existing at the time of castration and androgen replacement. In summary, these data directly demonstrate that the luminal cell lineage is self-sustained.

#### Prostate Cancer Initiated from Basal-Cell-Specific Loss of Function of PTEN

To determine the susceptibility of the prostate basal cell lineage to transformation induced by the loss of function of the tumor suppressor Pten, we generated K14-CreER<sup>Tg</sup>;Pten<sup>fl/fl</sup> (K14-Pten) bigenic mice. Tamoxifen was administered to 5-week-old K14-Pten mice so that Pten was specifically disrupted in prostate basal cells. An ARR2PB-Cre;Pten<sup>fl/fl</sup> mouse model for prostate cancer was used as a control, in which Pten is disrupted in both basal and luminal cells (Wang et al., 2006; Zhang et al., 2011).

The disease progression status observed in all experimental mice is summarized in Table 1. Tamoxifen-treated K14-Pten mice displayed a shaggy fur phenotype (Figure S3A) with complete penetrance, as reported previously (Backman et al., 2004; Yao et al., 2006). Disrupting PTEN activity leads to phosphorylation of AKT that accumulates at the plasma membrane, which serves as a reliable marker for PTEN loss. AKT phosphorylation was uniformly detected in the epidermis (Figures S3B and S3C), demonstrating an efficient Pten knockout in the skin. As we showed previously, the activation of the CreER activity in K14-Pten mouse prostate basal cells was less efficient (Figure 1), but Pten was disrupted only in prostate basal cells, as demonstrated by costaining pAKT with P63 (Figures 3A–3A'). Pten deletion in prostate basal cells was further confirmed by PCR genotyping in *in vitro* cultured prostate spheres derived from basal cells in tamoxifen-treated K14-Pten mice (Mulholland et al., 2009) (Figure S3D). Surprisingly, no abnormal epithelial growth was noted in all the mice examined 1 month post tamoxifen treatment (Table 1). However, by 3 months post tamoxifen treatment, focal hyperplastic growth (Figure 3B) was observed in 4 out of 11 mice. Those prostatic intraepithelial neoplasia (PIN) lesions were graded from PIN1 to PIN4 using the nomenclature and criteria developed by Park et al. (2002). The PIN lesions, but not the adjacent normal tissues, expressed pAKT (Figure 3C). They contained both K5 positive basal cells and K8 positive luminal cells (Figures 3D and 3E). Luminal cells expanded in the PIN lesions as measured by the ratio of basal

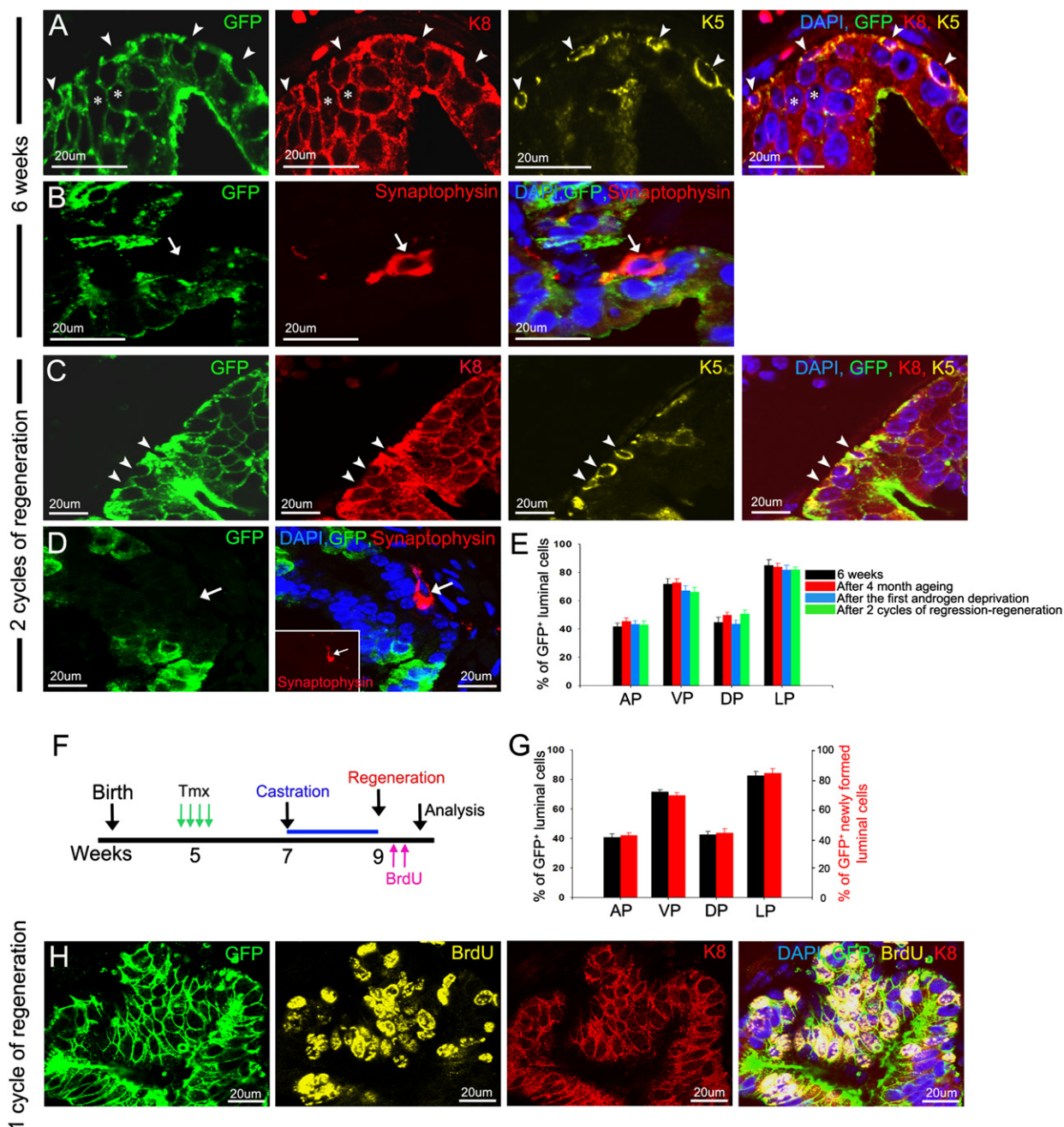


**Figure 2. The Prostate Luminal Cell Lineage Is Self-Sustained In Vivo**

(A and B) Costaining of GFP with K5 and K8 (A) and synaptophysin (B) in tamoxifen-treated K8-mTmG mice. Arrowheads and asterisks in (A) denote basal cells that are not GFP-labeled and GFP-labeled luminal cells, respectively. Arrow in (B) points to a neuroendocrine cell.

(C and D) Costaining of GFP with K5 and K8 (C) and synaptophysin (D) in tamoxifen-treated K8-mTmG mice after induced epithelial turnover. Arrowheads indicate that all basal cells are GFP negative. Arrow points to a neuroendocrine cell.

(E) Bar graph shows the percentage of GFP-labeled luminal cells 5 days after tamoxifen induction (6 weeks, black bars), after 4-month aging (red bars), after the first androgen deprivation (blue bars), and after two cycles of androgen deprivation-replacement experiments (green bars) in anterior (AP), ventral (VP), dorsal (DP), and lateral (LP) prostate lobes. Data represent the mean  $\pm$  SD. See Tables S2–S4 for more details.

(F) Timeline for investigating the origin of newly formed luminal cells by BrdU labeling.

(G) Bar graph shows that the frequency of newly formed GFP-positive luminal (GFP<sup>+</sup>K8<sup>+</sup>BrdU<sup>+</sup>/K8<sup>+</sup>BrdU<sup>+</sup>) cells reflects that of GFP-labeled luminal (GFP<sup>+</sup>K8<sup>+</sup>/K8<sup>+</sup>) cells in all four prostate lobes. Data represent the mean  $\pm$  SD. Also see Tables S2–S4.

(H) A representative image showing BrdU incorporated into luminal cells during prostate regeneration.

See also Figure S2 and Tables S2–S4.

**Table 1. Summary of Disease Progression in K14-Pten and K8-Pten Mice**

Month(s) Post Tmx Treatment	Tumor Incidence	Disease Stage/ Numbers of Mice	Mouse ID
K14-PTEN			
1	0/5	Normal/5	321,322,323,324,411
3	4/11	Normal/6	293,504,505,509,544
		PIN1/1	295
		PIN2/1	294
		PIN3/1	55
4		Normal/1	92
		PIN4/1	91
6	29/31	Normal/2	711,713
		PIN2/2	58,59
		PIN3/2	52,712
		PIN4/4	51,53,56,112
		Early cancer/2	57,111
7		PIN3/1	50
		PIN4/9	47,48,49,93,94, 95,98,456,460
8		PIN2/1	105
		PIN3/2	100,102
		PIN4/5	99,103,104,106,865
		Early cancer/1	101
K8-PTEN			
1	3/3	PIN1/1	89
		PIN2/1	69
		PIN3/1	146
2	9/9	Early cancer/2	159,924
3		PIN4/3	86,87,773
		Early cancer/3	89,772,774
4		Early cancer/1	307
6	15/15	PIN4/1	374
		Early cancer/12	226,229,237,375, 451,454,455,498, 499,503,876,898
		Adenocarcinoma/2	456,903

Disease stage is defined by the most advanced foci observed in tissues, most of which are within dorsolateral lobes.

versus luminal cells in epithelia (Figure 3F). Figures 3G and 3H show clearly that pAKT was also expressed in some basal cells, further corroborating that *Pten* deletion has taken place in those basal cells.

Six to eight months post tamoxifen induction, 29 out of 31 mice developed neoplastic foci at various stages (Table 1). Figures 4A and 4A' shows images of K14-Pten mouse prostate glands 8 months after tamoxifen or vehicle treatment. The prostate lobes appeared less transparent in tamoxifen-treated mice. H&E staining revealed multifocal lesions that developed in all four lobes in this mouse (Figures 4B–4E). A majority of mice developed focal PIN4 and a few mice developed early prostate cancer, most frequently in the dorsolateral prostate (DLP). In most cases, the lumen of a few DLP lobes in individual mice

was filled with epithelial cells with nuclear pleomorphism and hyperchromasia displaying tufting and cribriform patterns. The K14-Pten cancers were mainly composed of cells that were either positive for K5 or K8 (Figures 4F and 4H), with a small percentage of cells dual positive for K5 and K8. These double-positive cells express pAKT, suggesting they were also derived from *Pten* null basal cells (Figures S4A–S4C). In contrast, there were many K5<sup>+</sup>K8<sup>+</sup> cells within the ARR2PB-Pten tumors (Figures 4G and 4H). Most of the K5 positive cells in K14-Pten mice were also positive for P63 (Figures 4I and 4J). Cells within the cancerous foci of K14-Pten mice express the androgen receptor and display secretory function, as demonstrated by the immunostaining of the secretory proteins of murine dorsolateral lobes (mDLP) (Donjacour et al., 1990) (Figures S4D–S4G). Finally, very few cells in K14-Pten tumors expressed the neuroendocrine cell marker synaptophysin (Figure 4K).

Sporadic basal cells that express pAKT were observed in glandular structures displaying normal histology (Figure 4L), suggesting that ablating *Pten* in basal cells is not sufficient to initiate prostate cancer. In contrast, cancer only initiated upon the emergence of pAKT-expressing luminal cells, thus suggesting that transition of basal cells into luminal cells may be both essential and a limiting step for cancer initiation in this model. We found that disease progression dynamics among experimental mice varied, with some developing into PIN4 to early cancer; while others remained as PIN2/3 even 6–8 months post tamoxifen induction (Figure 4M–4O). This is probably because the transition from basal cells to luminal cells occurred with different kinetics in those mice. Overall, our study suggests that loss of function of PTEN induces differentiation of prostate basal cells into luminal cells, which is an essential step for disease initiation in this model.

To investigate whether K14-Pten tumor cells have functional repopulating activity, we enzymatically dissociated primary tumors into single cells, mixed them with embryonic urogenital sinus mesenchymal cells, and transplanted them subcutaneously into immunodeficient host mice for 2 months, as done previously using the PB-Pten mouse model (Mulholland et al., 2009). Figure 4Q showed that K14-Pten tumor cells were capable of regenerating hyperplastic prostate glandular structures. Those glands were composed of basal cells and luminal cells that both expressed activated pAKT (Figures 4P–4S), further confirming that they were *Pten* null.

### Prostate Cancer Derived from Luminal-Cell-Specific Loss of Function of PTEN

K8-CreERT2<sup>Tg/wt</sup>; *Pten*<sup>fl/fl</sup> (K8-Pten) mice were generated to determine whether prostate cancer initiates as a result of luminal-cell-specific loss of function of *Pten* (Table 1). K8-Pten mice developed low-grade PIN lesions in all lobes at full penetrance 1 month post tamoxifen treatment (Figures 5A–5A'). There were fewer pAKT-expressing cells in the anterior prostate (AP) (data not shown), suggesting that the homologous recombination is less efficient in the AP. We showed that even when *Pten* disruption was induced in very few luminal cells using a lower dosage of tamoxifen, hyperplastic foci still formed 1 month post tamoxifen induction (Figures S5A–S5G). This suggests that the more rapid disease progression in the K8-Pten model, compared with the K14-Pten model, is due to the intrinsic differential response of these two cell lineages to *Pten* ablation, but is

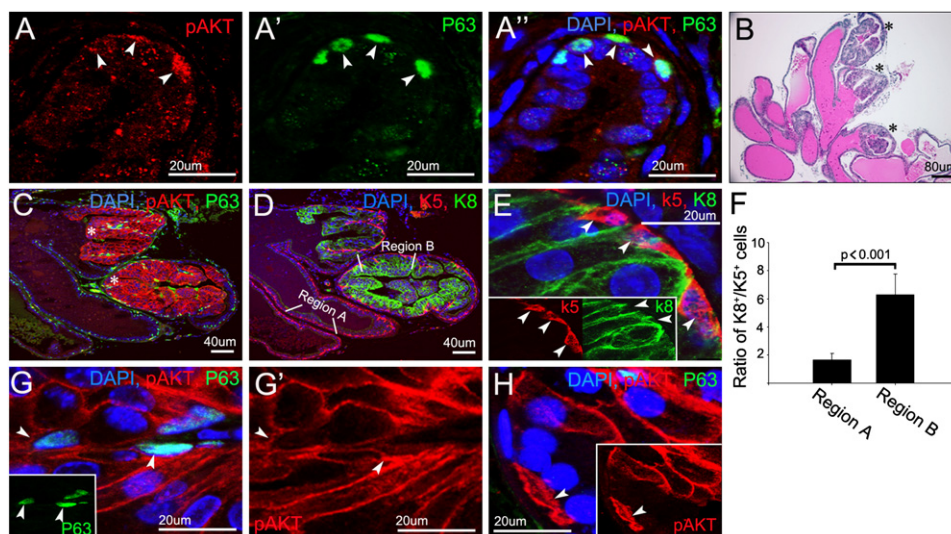


**Figure 3. Prostate Cancer Initiated from Basal Cell-Specific Loss of Function of PTEN**

(A-A'') Costaining of basal cell marker P63 (A', A'') with pAKT (A, A'') in K14-Pten mice 1 month post tamoxifen induction. Arrowheads point to pAKT<sup>+</sup>P63<sup>+</sup> cells. (B) H&E staining of a K14-Pten prostate 3 months post tamoxifen induction reveals the formation of PIN lesions (asterisks).

(C) PIN lesions (asterisks), but not adjacent normal glands, express pAKT.

(D and E) PIN lesions contain both K5-expressing basal cells and K8-expressing luminal cells. Arrowheads indicate K5-expressing basal cells that encapsulate glands.

(F) Quantification of the expansion of luminal cells in PIN lesions (region B) as compared in normal glands (region A). Data represent the mean  $\pm$  SD.

(G and H) Pten is disrupted in some basal cells. Arrowheads in (G) and (G') denote a P63-expressing basal cell that expresses pAKT. Arrowhead in (H) points to an anatomically typical basal cell that expresses pAKT.

See also Figure S3.

not likely because that Pten deletion was induced in more cells in the K8-Pten model. The prostate hyperplasia progressed to PIN4 or early cancers 2–4 months post treatment (Figures 5B–5B''). Mitotic figures and large atypical cells with enlarged nuclei, prominent nucleoli, and hyperchromasia were observed. Early cancer or even frank adenocarcinoma formed unanimously 6 months post tamoxifen induction (Figures 5C–5C''). More than 95% of the glands in DLP and ventral prostate (VP) displayed a tufting and cribriform growth pattern, while the APs were more histologically heterogeneous, consisting of both normal and cancerous glands. This is probably due to the relatively lower frequency of homologous recombination in AP, as mentioned above.

The PIN lesions in ventral prostates were composed predominantly of K8 positive luminal cells, while K5- or P63-positive basal cells were almost completely lost (Figure 5D). In comparison, in the AP and DLP, there was a dramatic expansion of the cells that were dual positive for K5 and K8 (Figures 5E and 5F), similar to the double-positive cells observed in the ARR2PB-Pten model (Figure 4G). The K5 staining in these dual-positive cells was cytoplasmic, in sharp contrast to the typical K5 staining in basal cells that highlights cellular contour. Since these double positive cells expressed activated AKT, they should have been derived from K8-positive luminal cells, presumably becoming putative transit-amplifying cells through dedifferentiation (Figures 5H and 5I) (Litvinov et al., 2006). They did not express P63 (Figures 5G–5I). In contrast, P63 was only expressed by the K5-positive basal cells residing at the basement membrane and did not express activated AKT (Figures 5J–5L), suggesting that these

P63-expressing cells were bona fide basal cells that did not undergo homologous recombination. The differential phenotypes among lobes were observed consistently during the 6 months post tamoxifen treatment. Cancer cells in all lobes express the androgen receptor and mDLP, while synaptophysin-expressing neuroendocrine cells were very rare in all lobes (Figures S5H–S5N). The same observations were made when both Pten and P53 were knocked out in luminal cells using K8-CreERT2<sup>Tg/Wt</sup>; Pten<sup>fl/fl</sup>;P53<sup>fl/fl</sup> (K8-Pten;P53) mice (data not shown).

Transplantation assays again were performed to determine whether K8-Pten tumor cells were capable of functional repopulation. H&E staining shows that the outgrowth tissues contained both normal glandular structures and cancerous lesions (Figures 5M–5O). The normal prostate glandular structures were composed of a single layer of epithelial cells encircling lumen filled with eosinophilic secretions. Both prostate basal and luminal cells were detected in those glands (Figure 5P). They did not express pAKT (data not shown). We previously showed that only prostate basal cells are capable of forming such prostate glandular structures upon transplantation (Lawson et al., 2007; Xin et al., 2005). These results suggest that those normal glands were derived from prostate basal cells and further corroborate that Pten was not disrupted in prostate basal cells in the K8-Pten model. In contrast, the focal cancerous lesions were composed of cells that were double-positive for K5 and K8 and expressed pAKT (Figures 5Q and 5R). They did not express P63 (data not shown). This phenotype recapitulates that of the original tumors in the AP and DLP, suggesting that those lesions were derived from Pten-null luminal cells. Collectively, these

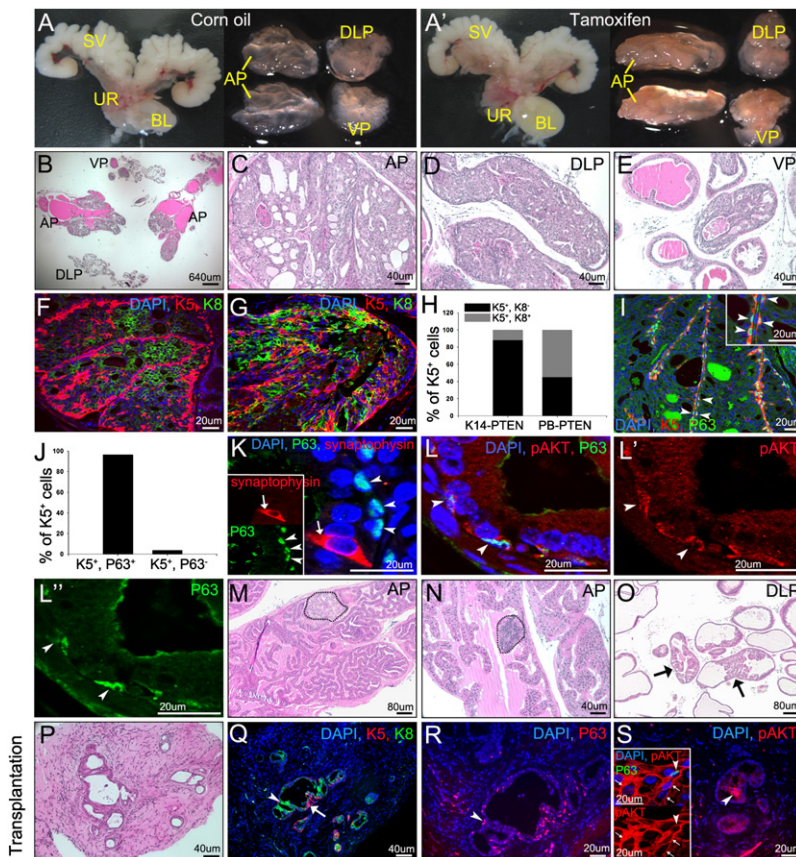


**Figure 4. Progression of Prostate Cancer in the K14-Pten Model**

(A and A') Representative images of urogenital organs and dissected prostate lobes from K14-Pten mice 8 months after induction with vehicle (A') or tamoxifen (A).

(B–E) Representative images of H&E staining of total prostate (B), AP (C), DLP (D), and VP (E) lobes of a K14-Pten mouse 8 months after tamoxifen treatment.

(F–H) Immunostaining of K5 and K8 of a K14-Pten mouse 3 months after tamoxifen treatment (F) and a 4-month old ARR2PB-Pten mouse (G). (H) Quantification of the percentage of K5<sup>+</sup>K8<sup>+</sup> and K5<sup>+</sup>K8<sup>−</sup> cells in the two models.

(I and J) Immunostaining of K5 and P63 in K14-Pten mice (I) and quantification of the percentage of K5<sup>+</sup>P63<sup>+</sup> and K5<sup>+</sup>P63<sup>−</sup> cells (J).

(K) Synaptophysin-expressing neuroendocrine cells (arrow) are rare in K14-Pten prostate tumor. Arrowheads point to P63-expressing basal cells.

(L–L'') Prostate basal cells in normal glands in tamoxifen-treated K14-Pten mice express pAKT. Arrowheads point to P63-expressing basal cells that express pAKT.

(M–O) Representative images of H&E staining show that only mild focal PIN lesions (dot-circled and arrow-pointed regions) are developed in many K14-Pten mice 6–8 months post tamoxifen treatment.

(P–S) Dissociated prostate cells from K14-Pten tumors are capable of regenerating abnormal glandular structures. (P) H&E staining of the outgrown tissues. (Q–S) Immuno-

staining of K5 (Q, arrow) and K8 (Q, arrowhead), P63 (R, arrowhead), and pAKT (S, arrowhead). Insets in (S) indicate that both basal (arrowhead) and luminal (arrow) cells express pAKT.

See also Figure S4.

data further support that disruption of *Pten* in prostate luminal cells causes prostate cancer.

### Castration-Resistant Prostate Cancer Cells Exist in K8-Pten Prostate Tumors

To investigate the response of K8-Pten tumors to androgen deprivation, we castrated K8-Pten mice 4 months after tamoxifen induction. Seminal vesicles and prostate tumors shrunk significantly after androgen ablation (Figure 6A and 6A'), which demonstrated successful androgen ablation and corroborated that many cancer cells were dependent on androgen for their survival. Histological analysis confirmed substantial cell death in the prostate 10 days and 2 months postcastration, as evidenced by significant apoptotic bodies inside tumor masses and cellular debris inside prostate lumen (Figures 6B–6D). IHC analysis showed that two months postcastration the remaining VP tumors were composed predominantly of luminal cells (Figure 6E). The K5 and K8 double-positive cells decreased significantly but still persisted in the AP and DLP tumors (Figures 6F and 6G). These data demonstrate that these luminal cells survive androgen deprivation and suggest that they may serve as the cellular origin for castration-resistant prostate cancer.

### Prostate Basal Cells Are Resistant to Direct Oncogenic Transformation

The above studies showed that prostate basal cells were less sensitive than luminal cells to mitogenic signals mediated by

*Pten* deletion. We wondered whether this was due to the insufficient oncogenic potency conferred by *Pten* loss or to the indolent nature of basal cells to transformation. P53-dependent PTEN-deletion-induced cellular senescence has been shown to impede the rapid progression of fully developed prostate adenocarcinoma in the *Pten*-null prostate cancer model (Alimonti et al., 2010; Chen et al., 2005). We generated K14-CreER<sup>Tg/Tg</sup>; *Pten*<sup>fl/fl</sup>; *P53*<sup>fl/fl</sup> (K14-Pten;P53) mice and sought to determine whether prostate basal cells can be directly transformed upon simultaneous deletion of *Pten* and *P53*. Two months post tamoxifen induction, experimental mice developed severe hyperplastic growth in facial skin, showed signs of morbidity such as loss of weight and hunched postures, and had to be euthanized (Figures S6A–S6D). Seminal vesicles and prostates from tamoxifen-treated K14-Pten;P53 mice were much smaller compared to the control mice, probably due to morbidity (Figure S6E). H&E staining showed that prostate epithelial cells packed tightly due to reduced cytoplasmic volumes. There were no signs of hyperproliferation (Figures 7A and 7B; N = 9 mice), which was corroborated by a lack of Ki67-expressing cells (data not shown). The glandular structures were mostly composed of K5-positive basal cells that encapsulated K8-positive luminal cells (Figure 7C). Occasionally, basal cells were reduced in number in some glands (Figure 7D). IHC analyses showed clearly that pAKT was activated only in P63-expressing basal cells, demonstrating that *Pten* was only disrupted in basal cells (Figure 7E). PCR analysis confirmed that

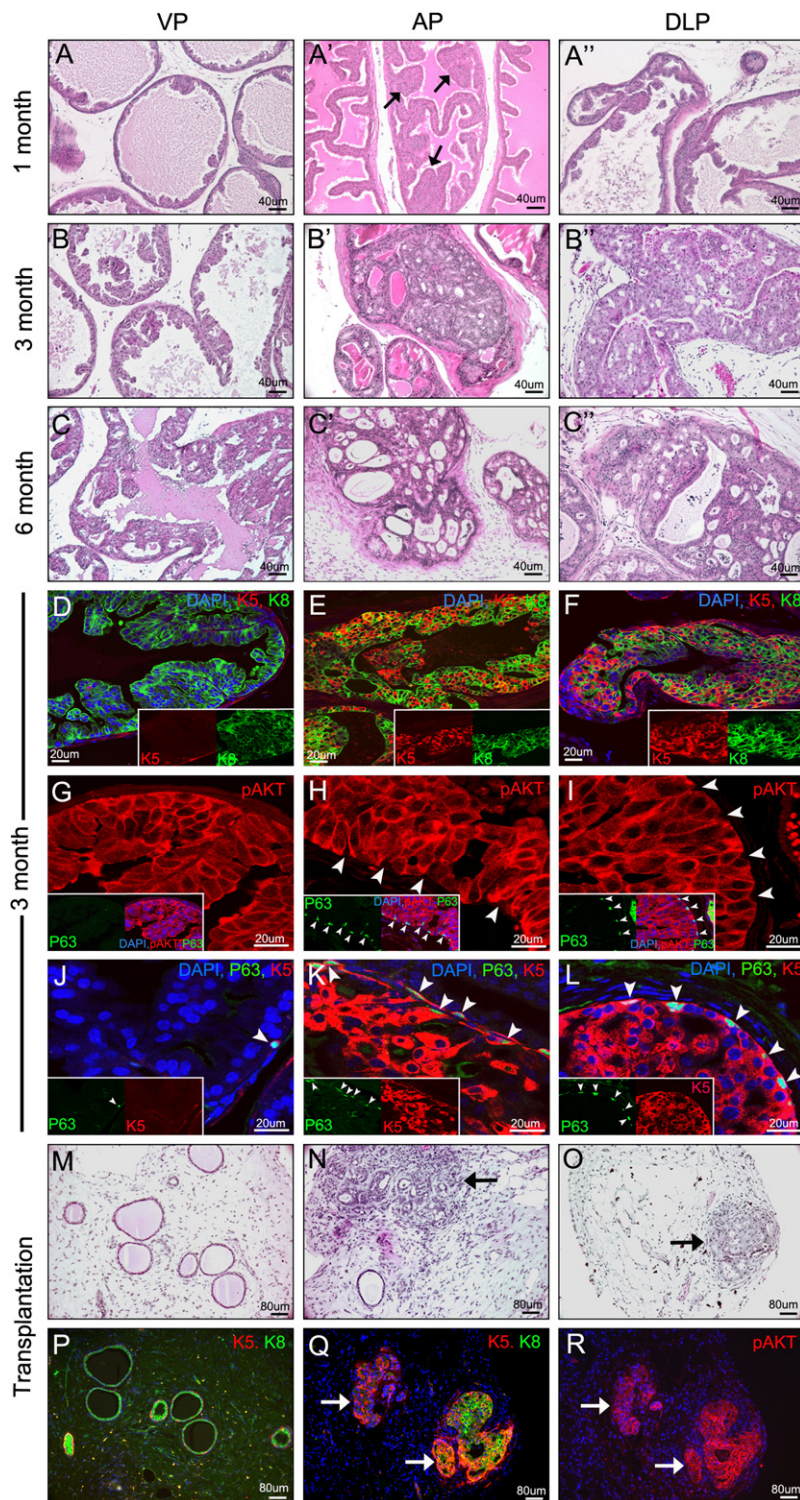


**Figure 5. Prostate Cancer Derived from Luminal-Cell-Specific Disruption of PTEN**

(A–C) H&E staining of AP (A', B', C'), VP (A, B, C), and DLP (A'', B'', C'') lobes of K8-Pten mice at 1, 3, and 6 months post tamoxifen induction. Arrows point to focal hyperplasia in AP.

(D–F) Immunostaining of K5 and K8 reveals a distinct lineage composition among VP (D), AP (E), and DLP (F). (G–I) P63-expressing basal cells (arrowheads) do not express pAKT in VP (G), AP (H), and DLP (I).

(J–L) Only K5-expressing basal cells residing at the basement membrane express P63 (arrowheads) in VP (J), AP (K), and DLP (L).

(M–R) K8-Pten prostate tumor can repopulate. Representative images of H&E staining of outgrown tissues from dissociated K8-Pten tumor tissues (M–O). Immunostaining of K5 and K8 (P and Q), and pAKT (R) of outgrown tissues. Arrows indicate cancerous foci.

See also Figure S5.

only or both K5 and K8 (Figure 7G). Some P63-expressing basal cells expressed pAKT, suggesting that *Pten* was disrupted in those cells (Figure 7H). To exclude that the morbidity of experimental mice interferes with disease progression in the prostate, we collected intact prostate lobes from K14-Pten;P53 mice 2 months post tamoxifen treatment and transplanted them under the kidney capsules of immunodeficient male hosts. Only a few PIN1 lesions were noted in 7-week transplants (Figures 7I–7K). In contrast, massive lesions at the PIN4 or early cancer stages were observed in 15-week transplants (Figures 7L–7N). Within those cancerous regions, some P63-expressing basal cells express pAKT while other do not, suggesting that *Pten* was disrupted in only a fraction of basal cells (Figures 7O–7P). Collectively, these results imply that basal cells in situ are by nature relatively resistant to direct transformation by oncogenic stimuli, which partly explains why prostate basal cell carcinoma is so rare (Ali and Epstein, 2007).

## DISCUSSION

### Obligate versus Facultative Stem Cell Capacity of the Prostate Basal Cells

Our study demonstrates that adult murine prostate basal and luminal cell lineages are independently sustained. We and others also showed previously, using a transplantation-based prostate regeneration assay, that some prostate basal cells in both humans and rodents are

successful ablation of *P53* (Figure S6F). We were able to keep four K14-Pten;P53 mice for 3 months after tamoxifen treatment and observed one PIN4 lesion in one mouse (Figure 7F, arrow), which demonstrates that cancer can initiate from basal cells with *Pten* and *P53* deletion. The PIN4 lesion is mainly composed of luminal cells expressing K8, with some cells expressing K5

capable of generating all three prostate epithelial cell lineages (Burger et al., 2005; Goldstein et al., 2010; Lawson et al., 2007; Leong et al., 2008; Xin et al., 2005; Zhang et al., 2011). These two observations are not mutually contradictory since they may illustrate the obligate versus facultative activities of stem cells in the prostate basal cell lineage. In the prostate

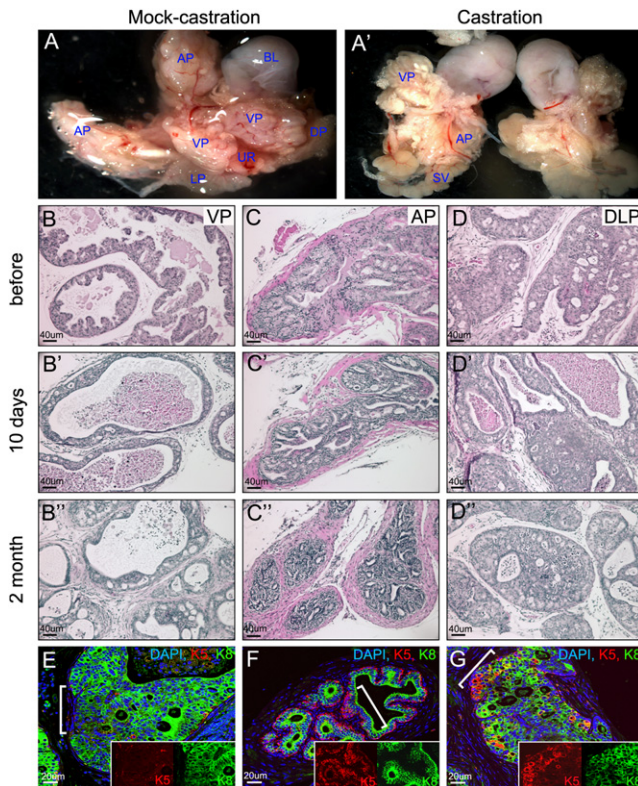


**Figure 6. Castration-Resistant Prostate Cancer Cells Exist in K8-Pten Prostate Tumors**

(A and A') Representative images of urogenital organs excluding seminal vesicles from K8-Pten mice 2 months after a mock surgery (A) and castration (A'). BL, bladder; UR, Urethra; AP, anterior prostate; VP, ventral prostate; DP, dorsal prostate; LP, lateral prostate.

(B–G) H&E staining (B–D) and immunostaining of K5 and K8 (E–G) of VP (B and E), AP (C and F), and DLP (D and G) of K8-Pten mice before castration (B–D), and 10 days (B'–D') and 2 months (B''–D'') after castration. Insets in (E)–(G) show staining of K5 and K8 at bracketed regions in respective images.

regeneration assay, basal cells are dissociated into single cells, removed from their natural environmental cues, and cocultured with embryonic urogenital sinus mesenchyme (UGSM) cells (Xin et al., 2003). It has been shown that embryonic stromal cells provide inductive signals that are absent in adult murine stromal cells, which affects epithelial cell differentiation or even changes their lineage status (Neubauer et al., 1983; Taylor et al., 2006). On the other hand, stromal-epithelial and epithelial-epithelial interactions in adult mouse prostate may mediate signaling that prevents basal cells from differentiating into other lineages. Our observations from the K14-mTmG and K14-Pten models demonstrate that oncogenic signals like *Pten* loss can alter the differentiation program of basal cells. In conclusion, we demonstrated that at least some prostate basal cells possess unipotent stem cell activity to maintain this lineage during prostate homeostasis and regeneration. In contrast, the results obtained using the prostate regeneration assay revealed the plasticity of the basal cell lineage in response to changes in environmental cues.

Of note, since only up to 21% of prostate basal cells were labeled with GFP in the K14-mTmG model, we cannot exclude the possibility that some of unlabeled basal cells can generate

luminal cells and neuroendocrine cells. However, our complementary lineage tracing experiment using the K8-mTmG model suggests that the luminal cell lineage is mainly self-sustained. Therefore, even if these additional multipotent basal cells exist, differentiation of basal cells into luminal cells most likely would be rare during prostate regeneration. Recently, similar conclusions have been made in the mammary gland (Van Keymeulen et al., 2011). Though the mammary gland myoepithelial cells are capable of regenerating the mammary gland in vivo in transplantation assays, genetic lineage-tracing experiments demonstrated that the myoepithelial and luminal cell lineages are independently maintained in adults.

### Maintenance of the Luminal Cell Lineage

Previously, a population of castration-resistant NKX3.1-expressing (CARN) luminal cells was shown to be able to generate all three prostate epithelial lineages (Wang et al., 2009). However, we did not observe in the K8-mTmG mice any descendant of GFP-positive luminal cells that expressed K5 or synaptophysin, suggesting that GFP-labeled luminal cells do not differentiate or convert into the other two epithelial cell lineages, at least in this mouse model. Since not all prostate luminal cells were labeled with GFP in the K8-mTmG model, we cannot exclude the possibility that CARN cells were preferentially not labeled under our experimental conditions.

Several lines of evidence imply the existence of a lineage hierarchy within the luminal cell lineage. Luminal cells are heterogeneous with regard to their capacity to retain BrdU labeling (Tsujimura et al., 2002). The androgen receptor expression level and activation status are heterogeneous among adult murine luminal cells (L.X., unpublished data). In addition, some luminal cells can survive androgen deprivation for an extended period (Tsujimura et al., 2002). It has been suspected that those androgen-independent luminal cells represent the committed progenitor cells in the luminal lineage. Our results showed that the percentage of GFP-positive luminal cells in castrated mice was approximately the same as that in intact mice (Figure 2E), which suggests that differentiated androgen-dependent luminal cells and androgen-independent luminal progenitor cells were GFP-labeled at a similar frequency. To date, the identity of the putative “luminal progenitor cells” remains undefined.

Alternatively, the androgen-independent survival of prostate luminal cells may be accounted for by a stochastic model in which any luminal cells could be conferred with the capacity for castration resistance when they happen to reside in a specific niche, such as a specialized anatomical location or a direct contact with a certain subtype of basal cells. In this scenario, the luminal cell lineage may be sustained simply by cell duplication, like the  $\beta$  cells in the pancreas (Dor et al., 2004). Future effort should be made to distinguish the two models.

### Prostate Basal Cells as the Cellular Origin for Prostate Cancer

Our studies demonstrated that although both prostate basal and luminal cells can serve as the cellular origin for prostate cancer, prostate luminal cells are more sensitive to mitogenic signaling, while basal cells are relatively resistant to transformation. This is consistent with the fact that luminal cells

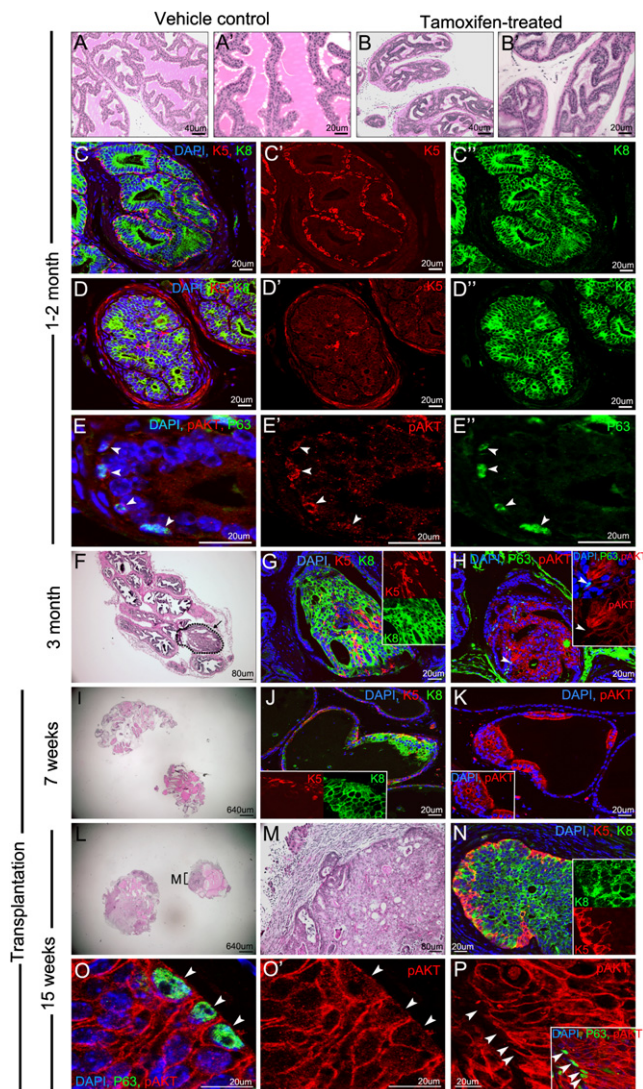


**Figure 7. Prostate Basal Cells Are Resistant to Direct Oncogenic Transformation**

(A and B) H&E staining of K14-Pten;P53 mouse prostates 2 months after vehicle (A) or tamoxifen (B) induction. A' and B' show images of higher magnification.

(C and D) Representative images of immunostaining of K5 and K8 of prostates from K14-Pten;P53 mice 2 months post tamoxifen induction.

(E) Pten is disrupted only in basal cells in K14-Pten;P53 mice, as demonstrated by costaining of pAKT (E and E') and P63 (E and E'). Arrowheads indicate pAKT-expressing cells that also express P63.

(F–H) H&E (F) and immunostaining of K5/K8 (G) and pAKT/P63 (H) of K14-Pten;P53 mouse prostates 3 months after tamoxifen induction. Arrow in F points to a dot-circled PIN4 lesion. Arrowhead in H points to a basal cell expressing pAKT.

(I–P) Two months after tamoxifen treatment, K14-Pten;P53 prostate glands were transplanted under renal capsules of immunodeficient male hosts. H&E staining (I, L, and M) and immunostaining of K5/K8 (J and N) and pAKT/P63 (K, O, and P) of 7-week (I–K) and 15-week (L–P) transplants. Arrowheads in O and P denote P63-expressing cells that express and do not express pAKT, respectively.

See also Figure S6.

possess low levels of H2A.X and hence are more vulnerable to oncogenic stress (Jäämaa et al., 2010). The distinctive responses of these two cell lineages to oncogenic insults explain why treatment-naïve prostate cancers are mostly composed of luminal cells, while prostate basal cell carcinoma is very rare.

Intuitively, prostate basal cells would seem to be the preferred cellular origin for cancer because they are more prone to accumulating genetic alterations than luminal cells. They are less well differentiated and proliferate more frequently (Bonkhoff et al., 1994). Additionally, they are proposed to act as a natural barrier to protect the luminal cell lineage from various insults. Thus, they are exposed to a more “hostile” environment than are luminal cells. For example, the basal cells are in closer contact with various cancer-promoting cytokines generated by the surrounding reactive stroma as a result of chronic inflammation (Tuxhorn et al., 2001). However, since most prostate cancers display a luminal cell phenotype, differentiation of basal cells into luminal cells becomes an essential and probably a rate-limiting step for cancer initiation and progression, if the cellular origin for cancer is of the basal cell lineage. This is supported by our result from the K14-Pten model. Prostate cancer was initiated in the K14-Pten model with an increased latency. Though Pten was disrupted specifically only in the prostate basal cells, the initiation of cancer did not start until the emergence of pAKT-expressing luminal cells. Since direct differentiation of basal cells to luminal cells is absent under physiological conditions based on our lineage-tracing experiments, these results suggest that deregulation of the normal prostate epithelial differentiation program is a critical step for initiation of human prostate cancer with a basal cell origin.

It should be noted that the most ideal way to investigate the cells of origin for cancer is to perform lineage tracing in the cancer models. However, we were not able to perform our study in this way for two reasons. First, activation of CreER<sup>T2</sup> by tamoxifen is transient. Therefore, homologous recombination may not be achieved in all the cells that express CreER<sup>T2</sup>, as we have shown in the K14-mTmG and K8-mTmG lineage-tracing experiments (Figures 1 and 2). Second, the recombination efficiencies at different genomic loci are not identical. As shown in Figures S5O and S5P, GFP expression does not guarantee Pten deletion in tamoxifen-treated K8-Pten<sup>fl/fl</sup>-mTmG triple transgenic mice. Nevertheless, we found that the specificities of the K14 and K8 promoters are not affected by the genetic background of the experimental mice (Figures S5Q and S5R). In addition, we confirmed lineage specific Pten deletion by costaining pAKT with lineage markers in the K14-Pten and K8-Pten models. Therefore, we can conclude that neoplasia and tumors in the K14-Pten and K8-Pten models are derived from basal and luminal cells, respectively.

A unique feature of prostate cancer is that the disease is strictly age-dependent. Men under 35 seldom develop prostate cancer. Our data showed that it takes at least 3 months for K14-Pten mouse prostate basal cells to differentiate into luminal cells, which is almost equivalent to 10 years of human life, suggesting that this is still an extremely lengthy and inefficient biological process under certain genetic contexts. This may provide an additional explanation for the strict age-dependent nature of human prostate cancer.

### Prostate Luminal Cells as the Cellular Origin for Primary and Castration-Resistant Prostate Cancer

Our genetic model also supports that luminal cells can be the cellular origin for prostate cancer. An intriguing observation from our K8-Pten model is that the same genetic change causes tumors with lobe-specific phenotypes with regard to their cellular composition. The phenotype in VP resembles that of the human disease because markers of basal cells are absent in prostate carcinoma, which has served as a diagnostic criterion for prostate cancer. In comparison, tumors in the AP and DLP are composed of cells that express both K5 and K8, and basal cells remain largely unaffected. A previous study has revealed a compartmentalization of gene expression between prostate lobes and identified dozens of differentially expressed genes between prostate lobes (Abbott et al., 2003). It is possible that the cellular context, i.e., the intrinsic differences in gene expression between prostate lobes, leads to the differential responses of the lobes to the oncogenic insult. It will be interesting to investigate whether human prostate luminal cells share more similarity with murine VP luminal cells in terms of gene expression profiles. The mechanism by which basal cells are depleted in the VP is also unknown. We recently reported that dissociation of basal cells leads to cellular apoptosis induced by activation of the RhoA/ROCK kinases (Zhang et al., 2011). One potential mechanism, therefore, could be that the basal cell layer in ventral prostate is less resilient to cellular perturbations, so that when prostate glands are enlarged and distorted due to excessive proliferation of prostate luminal cells, the cellular contact between ventral prostate basal cells is attenuated, which alters the signaling that regulates basal cell survival, such as the RhoA/ROCK-mediated signaling.

Our study also demonstrates that castration-resistant cells in prostate cancers may originate from luminal cells. This result excludes the possibility that prostate basal cells are the only cellular origin for castration-resistant disease. Since there is no evidence that CARN cells (Wang et al., 2009) were genetically manipulated by tamoxifen induction in the K8-CreER<sup>T2</sup> model (Figure 2), our study also suggests that CARN cells are not the only cells of origin for prostate cancer in the luminal cell lineage, and that castration resistance is not a unique feature of CARN cells. This observation further highlights the need to identify the androgen-independent prostate luminal progenitor cells and to determine the essential signaling that confers the capacity for androgen-independent survival to luminal cells.

### EXPERIMENTAL PROCEDURES

#### Mouse Procedures

The sources of experimental mice and the genotyping strategies are described in *Supplemental Experimental Procedures*. Castration, androgen replacement, dissociation of primary prostate tumors, and tumor cell transplantation were performed using standard techniques described in *Supplemental Experimental Procedures*. Tamoxifen (Sigma-Aldrich, St. Louis, MO) was dissolved into corn oil and was administered i.p. into experimental mice at the age of 5 weeks once a day for four consecutive days. The dosages used for K14-CreER and K8-CreER<sup>T2</sup> mice were 9 mg/40 g and 2 mg/40 g, respectively. All animal work were approved by and performed under the regulation of the Institutional Animal Care Committee of the Baylor College of Medicine.

#### Histology, Immunohistochemical, and Immunofluorescent Analysis

The procedures for histological and IHC analyses and the information about primary antibodies were described in *Supplemental Experimental Procedures*.

Paraffin-embedded sections were stained and counterstained with 4,6-diamidino-2-phenylindole (DAPI) (Sigma-Aldrich, St. Louis, MO). Secondary antibodies were labeled with Alexa Fluor 488, 594, 633 (Invitrogen, Carlsbad, CA). Immunofluorescence staining was imaged using an Olympus BX60 fluorescence microscope or a Leica EL6000 confocal microscope. Cell counting was performed either manually or via ImagePro Software.

#### Statistics

All experiments were performed using 4–10 mice in independent experiments. Data are presented as mean  $\pm$  SD. Student's *t* test was used to determine significance between groups. For all statistical tests, the 0.05 level of confidence was accepted for statistical significance.

### SUPPLEMENTAL INFORMATION

Supplemental Information includes six figures, four tables, and Supplemental Experimental Procedures and can be found with this article online at doi:10.1016/j.ccr.2012.01.005.

### ACKNOWLEDGMENTS

We thank Dr. Larry Donhower for the P53 conditional mice, Dr. Hong Wu for the Pten conditional mice, Dr. Gerald Cunha for antiserum against mDLP, Dr. Jeffrey Rosen for critical comments, Dr. Michael Lewis for sharing the NOD/SCID mouse colony. This work is supported by NIH R00CA125937, R01DK092202, and U01CA141497.

Received: October 28, 2011

Revised: January 2, 2012

Accepted: January 6, 2012

Published: February 13, 2012

### REFERENCES

- Abate-Shen, C., and Shen, M.M. (2000). Molecular genetics of prostate cancer. *Genes Dev.* 14, 2410–2434.
- Abbott, D.E., Pritchard, C., Clegg, N.J., Ferguson, C., Dumpit, R., Sikes, R.A., and Nelson, P.S. (2003). Expressed sequence tag profiling identifies developmental and anatomic partitioning of gene expression in the mouse prostate. *Genome Biol.* 4, R79.
- Ali, T.Z., and Epstein, J.I. (2007). Basal cell carcinoma of the prostate: a clinicopathologic study of 29 cases. *Am. J. Surg. Pathol.* 31, 697–705.
- Alimonti, A., Nardella, C., Chen, Z., Clohessy, J.G., Carracedo, A., Trotman, L.C., Cheng, K., Varmeh, S., Kozma, S.C., Thomas, G., et al. (2010). A novel type of cellular senescence that can be enhanced in mouse models and human tumor xenografts to suppress prostate tumorigenesis. *J. Clin. Invest.* 120, 681–693.
- Backman, S.A., Ghazarian, D., So, K., Sanchez, O., Wagner, K.U., Hennighausen, L., Suzuki, A., Tsao, M.S., Chapman, W.B., Stambolic, V., and Mak, T.W. (2004). Early onset of neoplasia in the prostate and skin of mice with tissue-specific deletion of Pten. *Proc. Natl. Acad. Sci. USA* 101, 1725–1730.
- Bonkhoff, H., Stein, U., and Remberger, K. (1994). The proliferative function of basal cells in the normal and hyperplastic human prostate. *Prostate* 24, 114–118.
- Burger, P.E., Xiong, X., Coetzee, S., Salm, S.N., Moscatelli, D., Goto, K., and Wilson, E.L. (2005). Sca-1 expression identifies stem cells in the proximal region of prostatic ducts with high capacity to reconstitute prostatic tissue. *Proc. Natl. Acad. Sci. USA* 102, 7180–7185.
- Chen, Z., Trotman, L.C., Shaffer, D., Lin, H.K., Dotan, Z.A., Niki, M., Koutcher, J.A., Scher, H.I., Ludwig, T., Gerald, W., et al. (2005). Crucial role of p53-dependent cellular senescence in suppression of Pten-deficient tumorigenesis. *Nature* 436, 725–730.
- Donjacour, A.A., Rosales, A., Higgins, S.J., and Cunha, G.R. (1990). Characterization of antibodies to androgen-dependent secretory proteins of the mouse dorsolateral prostate. *Endocrinology* 126, 1343–1354.

- Dor, Y., Brown, J., Martinez, O.I., and Melton, D.A. (2004). Adult pancreatic beta-cells are formed by self-duplication rather than stem-cell differentiation. *Nature* 429, 41–46.
- Ellwood-Yen, K., Graeber, T.G., Wongvipat, J., Iruela-Arispe, M.L., Zhang, J., Matusik, R., Thomas, G.V., and Sawyers, C.L. (2003). Myc-driven murine prostate cancer shares molecular features with human prostate tumors. *Cancer Cell* 4, 223–238.
- Foster, B.A., Gingrich, J.R., Kwon, E.D., Madias, C., and Greenberg, N.M. (1997). Characterization of prostatic epithelial cell lines derived from transgenic adenocarcinoma of the mouse prostate (TRAMP) model. *Cancer Res.* 57, 3325–3330.
- Goldstein, A.S., Huang, J., Guo, C., Garraway, I.P., and Witte, O.N. (2010). Identification of a cell of origin for human prostate cancer. *Science* 329, 568–571.
- Iczkowski, K.A., and Lucia, M.S. (2011). Current perspectives on Gleason grading of prostate cancer. *Curr. Urol. Rep.* 12, 216–222.
- Iwata, T., Schultz, D., Hicks, J., Hubbard, G.K., Mutton, L.N., Lotan, T.L., Bethel, C., Lotz, M.T., Yegnashubramanian, S., Nelson, W.G., et al. (2010). MYC overexpression induces prostatic intraepithelial neoplasia and loss of Nkx3.1 in mouse luminal epithelial cells. *PLoS ONE* 5, e9427.
- Jäämaa, S., Af Hällström, T.M., Sankila, A., Rantanen, V., Koistinen, H., Stenman, U.H., Zhang, Z., Yang, Z., De Marzo, A.M., Taari, K., et al. (2010). DNA damage recognition via activated ATM and p53 pathway in nonproliferating human prostate tissue. *Cancer Res.* 70, 8630–8641.
- Lawson, D.A., and Witte, O.N. (2007). Stem cells in prostate cancer initiation and progression. *J. Clin. Invest.* 117, 2044–2050.
- Lawson, D.A., Xin, L., Lukacs, R.U., Cheng, D., and Witte, O.N. (2007). Isolation and functional characterization of murine prostate stem cells. *Proc. Natl. Acad. Sci. USA* 104, 181–186.
- Lawson, D.A., Zong, Y., Memarzadeh, S., Xin, L., Huang, J., and Witte, O.N. (2010). Basal epithelial stem cells are efficient targets for prostate cancer initiation. *Proc. Natl. Acad. Sci. USA* 107, 2610–2615.
- Leong, K.G., Wang, B.E., Johnson, L., and Gao, W.Q. (2008). Generation of a prostate from a single adult stem cell. *Nature* 456, 804–808.
- Lim, E., Vaillant, F., Wu, D., Forrest, N.C., Pal, B., Hart, A.H., Asselin-Labat, M.L., Gyorki, D.E., Ward, T., Partanen, A., et al. (2009). Aberrant luminal progenitors as the candidate target population for basal tumor development in BRCA1 mutation carriers. *Nat. Med.* 15, 907–913.
- Litvinov, I.V., Vander Griend, D.J., Xu, Y., Antony, L., Dalrymple, S.L., and Isaacs, J.T. (2006). Low-calcium serum-free defined medium selects for growth of normal prostatic epithelial stem cells. *Cancer Res.* 66, 8598–8607.
- Liu, J., Pascal, L.E., Isharwal, S., Metzger, D., Ramos Garcia, R., Pilch, J., Kasper, S., Williams, K., Basse, P.H., Nelson, J.B., et al. (2011). Regenerated luminal epithelial cells are derived from preexisting luminal epithelial cells in adult mouse prostate. *Mol. Endocrinol.* 25, 1849–1857.
- Majumder, P.K., Yeh, J.J., George, D.J., Febbo, P.G., Kum, J., Xue, Q., Bikoff, R., Ma, H., Kantoff, P.W., Golub, T.R., et al. (2003). Prostate intraepithelial neoplasia induced by prostate restricted Akt activation: the MPAKT model. *Proc. Natl. Acad. Sci. USA* 100, 7841–7846.
- Molyneux, G., Geyer, F.C., Magnay, F.A., McCarthy, A., Kendrick, H., Natrajan, R., Mackay, A., Grigoriadis, A., Tutt, A., Ashworth, A., et al. (2010). BRCA1 basal-like breast cancers originate from luminal epithelial progenitors and not from basal stem cells. *Cell Stem Cell* 7, 403–417.
- Mulholland, D.J., Xin, L., Morim, A., Lawson, D., Witte, O., and Wu, H. (2009). Lin-Sca-1+CD49f<sup>high</sup> stem/progenitors are tumor-initiating cells in the Pten-null prostate cancer model. *Cancer Res.* 69, 8555–8562.
- Muzumdar, M.D., Tasic, B., Miyamichi, K., Li, L., and Luo, L. (2007). A global double-fluorescent Cre reporter mouse. *Genesis* 45, 593–605.
- Neubauer, B.L., Chung, L.W., McCormick, K.A., Taguchi, O., Thompson, T.C., and Cunha, G.R. (1983). Epithelial-mesenchymal interactions in prostatic development. II. Biochemical observations of prostatic induction by urogenital sinus mesenchyme in epithelium of the adult rodent urinary bladder. *J. Cell Biol.* 96, 1671–1676.
- Park, J.H., Walls, J.E., Galvez, J.J., Kim, M., Abate-Shen, C., Shen, M.M., and Cardiff, R.D. (2002). Prostatic intraepithelial neoplasia in genetically engineered mice. *Am. J. Pathol.* 161, 727–735.
- Peehl, D.M. (2005). Primary cell cultures as models of prostate cancer development. *Endocr. Relat. Cancer* 12, 19–47.
- Ratnacaram, C.K., Teletin, M., Jiang, M., Meng, X., Chambon, P., and Metzger, D. (2008). Temporally controlled ablation of PTEN in adult mouse prostate epithelium generates a model of invasive prostatic adenocarcinoma. *Proc. Natl. Acad. Sci. USA* 105, 2521–2526.
- Taylor, R.A., Cowin, P.A., Cunha, G.R., Pera, M., Trounson, A.O., Pedersen, J., and Risbridger, G.P. (2006). Formation of human prostate tissue from embryonic stem cells. *Nat. Methods* 3, 179–181.
- Tsujimura, A., Koikawa, Y., Salm, S., Takao, T., Coetzee, S., Moscatelli, D., Shapiro, E., Lepor, H., Sun, T.T., and Wilson, E.L. (2002). Proximal location of mouse prostate epithelial stem cells: a model of prostatic homeostasis. *J. Cell Biol.* 157, 1257–1265.
- Tuxhorn, J.A., Ayala, G.E., and Rowley, D.R. (2001). Reactive stroma in prostate cancer progression. *J. Urol.* 166, 2472–2483.
- Van Keymeulen, A., Rocha, A.S., Ousset, M., Beck, B., Bouvencourt, G., Rock, J., Sharma, N., Dekoninck, S., and Blanpain, C. (2011). Distinct stem cells contribute to mammary gland development and maintenance. *Nature* 479, 189–193.
- Vasioukhin, V., Degenstein, L., Wise, B., and Fuchs, E. (1999). The magical touch: genome targeting in epidermal stem cells induced by tamoxifen application to mouse skin. *Proc. Natl. Acad. Sci. USA* 96, 8551–8556.
- Visvader, J.E. (2011). Cells of origin in cancer. *Nature* 469, 314–322.
- Wang, S., Gao, J., Lei, Q., Rozengurt, N., Pritchard, C., Jiao, J., Thomas, G.V., Li, G., Roy-Burman, P., Nelson, P.S., et al. (2003). Prostate-specific deletion of the murine Pten tumor suppressor gene leads to metastatic prostate cancer. *Cancer Cell* 4, 209–221.
- Wang, S., Garcia, A.J., Wu, M., Lawson, D.A., Witte, O.N., and Wu, H. (2006). Pten deletion leads to the expansion of a prostatic stem/progenitor cell subpopulation and tumor initiation. *Proc. Natl. Acad. Sci. USA* 103, 1480–1485.
- Wang, X., Kruithof-de Julio, M., Economides, K.D., Walker, D., Yu, H., Halli, M.V., Hu, Y.P., Price, S.M., Abate-Shen, C., and Shen, M.M. (2009). A luminal epithelial stem cell that is a cell of origin for prostate cancer. *Nature* 461, 495–500.
- Wang, Y., Hayward, S., Cao, M., Thayer, K., and Cunha, G. (2001). Cell differentiation lineage in the prostate. *Differentiation* 68, 270–279.
- Wu, C.T., Altuwaijri, S., Ricke, W.A., Huang, S.P., Yeh, S., Zhang, C., Niu, Y., Tsai, M.Y., and Chang, C. (2007). Increased prostate cell proliferation and loss of cell differentiation in mice lacking prostate epithelial androgen receptor. *Proc. Natl. Acad. Sci. USA* 104, 12679–12684.
- Xin, L., Ide, H., Kim, Y., Dubey, P., and Witte, O.N. (2003). In vivo regeneration of murine prostate from dissociated cell populations of postnatal epithelia and urogenital sinus mesenchyme. *Proc. Natl. Acad. Sci. USA* 100 (Suppl 1), 11896–11903.
- Xin, L., Lawson, D.A., and Witte, O.N. (2005). The Sca-1 cell surface marker enriches for a prostate-regenerating cell subpopulation that can initiate prostate tumorigenesis. *Proc. Natl. Acad. Sci. USA* 102, 6942–6947.
- Xin, L., Lukacs, R.U., Lawson, D.A., Cheng, D., and Witte, O.N. (2007). Self-renewal and multilineage differentiation in vitro from murine prostate stem cells. *Stem Cells* 25, 2760–2769.
- Yao, D., Alexander, C.L., Quinn, J.A., Porter, M.J., Wu, H., and Greenhalgh, D.A. (2006). PTEN loss promotes rasHa-mediated papillomatogenesis via dual up-regulation of AKT activity and cell cycle deregulation but malignant conversion proceeds via PTEN-associated pathways. *Cancer Res.* 66, 1302–1312.
- Zhang, L., Valdez, J.M., Zhang, B., Wei, L., Chang, J., and Xin, L. (2011). ROCK inhibitor Y-27632 suppresses dissociation-induced apoptosis of murine prostate stem/progenitor cells and increases their cloning efficiency. *PLoS ONE* 6, e18271.
- Zhang, L., Zhang, B., Han, S.J., Shore, A.M., Rosen, J.M., DeMayo, F.J., and Xin, L. (2012). Targeting CreERT2 expression to Keratin 8-expressing murine simple epithelia using bacterial artificial chromosome transgenesis. *Transgenic Research*, in press.

# Activation of p53 by SIRT1 Inhibition Enhances Elimination of CML Leukemia Stem Cells in Combination with Imatinib

Ling Li,<sup>1</sup> Lisheng Wang,<sup>1</sup> Liang Li,<sup>1</sup> Zhiqiang Wang,<sup>2</sup> Yinwei Ho,<sup>1</sup> Tinisha McDonald,<sup>1</sup> Tessa L. Holyoake,<sup>3</sup> WenYong Chen,<sup>2,4,\*</sup> and Ravi Bhatia<sup>1,4,\*</sup>

<sup>1</sup>Division of Hematopoietic Stem Cell and Leukemia Research

<sup>2</sup>Department of Cancer Biology

City of Hope National Medical Center, Duarte, CA 91010, USA

<sup>3</sup>Section of Experimental Haematology, Institute of Cancer Sciences, University of Glasgow, Glasgow, G12 8QQ Scotland, UK

<sup>4</sup>These authors contributed equally to this work

\*Correspondence: [wechen@coh.org](mailto:wechen@coh.org) (W.C.), [rbhatia@coh.org](mailto:rbhatia@coh.org) (R.B.)

DOI 10.1016/j.ccr.2011.12.020

## SUMMARY

BCR-ABL tyrosine kinase inhibitors (TKI) fail to eliminate quiescent leukemia stem cells (LSC) in chronic myelogenous leukemia (CML). Thus, strategies targeting LSC are required to achieve cure. We show that the NAD<sup>+</sup>-dependent deacetylase SIRT1 is overexpressed in human CML LSC. Pharmacological inhibition of SIRT1 or SIRT1 knockdown increased apoptosis in LSC of chronic phase and blast crisis CML and reduced their growth in vitro and in vivo. SIRT1 effects were enhanced in combination with the BCR-ABL TKI imatinib. SIRT1 inhibition increased p53 acetylation and transcriptional activity in CML progenitors, and the inhibitory effects of SIRT1 targeting on CML cells depended on p53 expression and acetylation. Activation of p53 via SIRT1 inhibition represents a potential approach to target CML LSC.

## INTRODUCTION

Chronic myelogenous leukemia (CML) results from malignant transformation of a hematopoietic stem cell (HSC) by the BCR-ABL oncogene. CML usually presents in a chronic phase (CP) but progresses to an accelerated phase (AP) and a terminal blast crisis (BC) (Sawyers, 1999). The BCR-ABL tyrosine kinase inhibitors (TKI) imatinib (IM), nilotinib, and dasatinib are effective in inducing remissions and prolonging survival of CP CML patients but is less effective against advanced phase CML (Eiring et al., 2011). However, even in CP CML, primitive leukemia stem cells (LSC) are retained in patients achieving remission with TKI treatment (Chu et al., 2011). Primitive, quiescent CML LSC are resistant to apoptosis following TKI treatment despite effective inhibition of BCR-ABL kinase activity (Holtz et al., 2005; Corbin et al., 2011), the mechanisms for which are not well understood.

Disease recurrence is usually seen following cessation of drug treatment, even in patients with undetectable BCR-ABL expression by q-PCR (Mahon et al., 2010). These observations suggest that “cure” may be elusive for most CML patients with TKI alone. CML patients currently need to take TKI treatment indefinitely, with risks of toxicity, lack of compliance, drug resistance, relapse, and associated expense.

Recent studies from our group have shown that pan-histone deacetylase (HDAC) inhibitors in combination with IM significantly increase apoptosis in quiescent CML stem cells (Zhang et al., 2010). However, toxicity of this approach to normal stem cells remains a potential concern. Sirtuins are NAD-dependent histone deacetylases that have been linked to longevity in lower organisms and to mammalian metabolism (Bordone and Guarente, 2005; Liu et al., 2009a). Sirtuin 1 (SIRT1) is a member of the sirtuin family that regulates numerous processes, including

## Significance

BCR-ABL kinase inhibitors (TKI) are effective in the treatment of CML but do not eliminate leukemia stem cells (LSC), which remain a potential source of recurrence. The NAD-dependent deacetylase SIRT1 is reported to protect stem cells against stress and functions as a tumor suppressor or tumor promoter depending on cellular context. Our studies show that SIRT1 is overexpressed in CML LSC and that SIRT1 inhibition selectively reduces CML LSC survival and growth through acetylation and activation of the p53 tumor suppressor. These results are important because they show that SIRT1-mediated p53 deacetylation contributes to CML LSC survival and resistance to TKI treatment. SIRT1 inhibition is an attractive approach to selectively target LSC that resist elimination by current treatments.

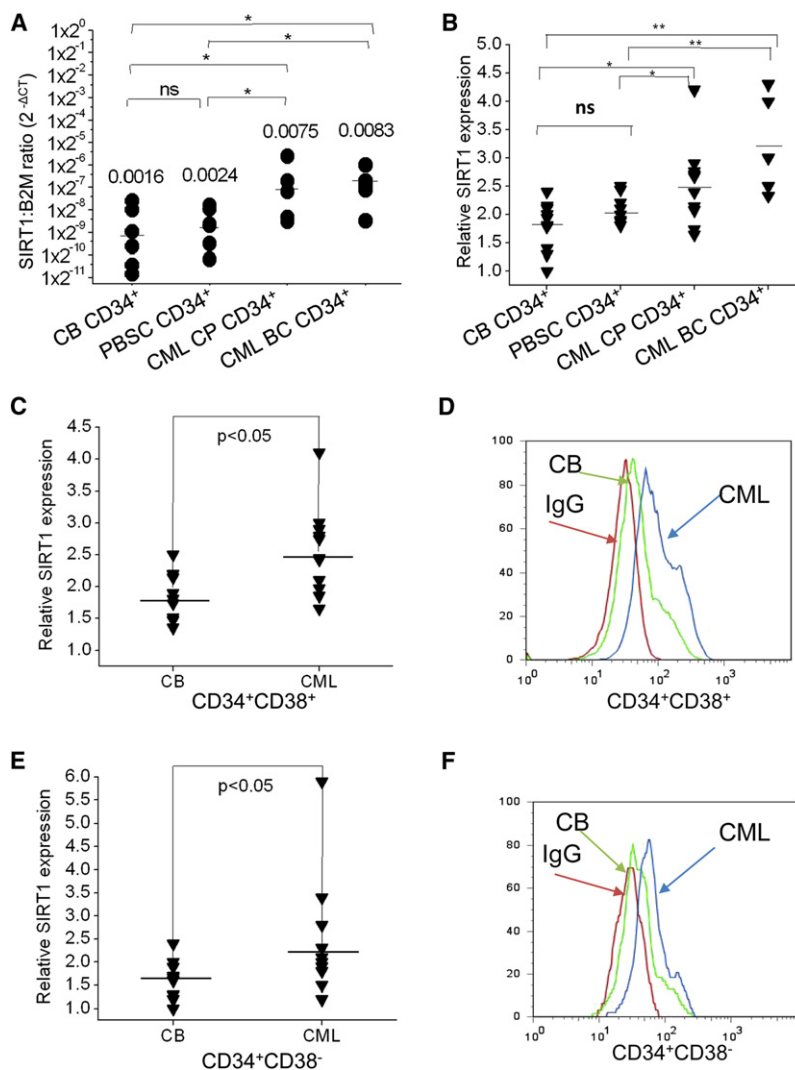


**Figure 1. Increased SIRT1 Expression in CML Patients Compared with Normal Stem/Progenitor Cells**

(A) Expression of *SIRT1* mRNA in CP CML (n = 5), BC CML (n = 5), cord blood (CB) (n = 6), and PBSC (n = 6) CD34<sup>+</sup> cells analyzed by Q-PCR. (B) Expression of SIRT1 protein in CP CML (n = 11) and BC CML (n = 5) compared with CB CD34<sup>+</sup> cells (n = 10) and PBSC CD34<sup>+</sup> cells (n = 8) analyzed by intracellular labeling with anti-SIRT1 antibody. Median fluorescence intensity (MFI) of SIRT1 was expressed relative to IgG control. (C) Expression of SIRT1 in CML (n = 11) and CB (n = 10) CD34<sup>+</sup>CD38<sup>+</sup> committed progenitors (right panel). Representative results are shown in panel (D): CML (blue), CB (green), IgG (red). (E) Expression of SIRT1 in CML (n = 11) and CB (n = 10) CD34<sup>+</sup>CD38<sup>-</sup> stem cells/primitive progenitors. Representative results are shown in panel (F): CML (blue), CB (green), IgG (red). Significance: \*p < 0.05, \*\*p < 0.01 for the indicated comparisons. See also Figure S1 and Table S1.

the specific cell or tumor type and the presence or absence of p53 (Brooks and Gu, 2009).

Previous studies have shown that SIRT1 expression is increased in CML blast crisis (BC) cell lines (Chen et al., 2005). Here we investigated the contribution of SIRT1 to the survival and growth of CP and BC CML LSC and progenitor cells and in LSC resistance to TKI treatment. We also investigated the role of p53 in mediating the effects of SIRT1 inhibition on CML progenitors.

## RESULTS

### SIRT1 Is Overexpressed in CML CD34<sup>+</sup> Cells

*SIRT1* mRNA levels were significantly elevated in CP and BC CML CD34<sup>+</sup> cells (Table S1 available online) compared to CD34<sup>+</sup> cells from cord blood (CB) or normal peripheral blood stem cell collections (PBSC) (Figure 1A).

SIRT1 protein levels in CML and normal CD34<sup>+</sup>CD38<sup>+</sup> committed progenitors and CD34<sup>+</sup>CD38<sup>-</sup> primitive progenitors were measured by intracellular labeling with anti-SIRT1 antibody and flow cytometry (Figure S1A). The ability of intracellular labeling to reliably measure SIRT1 expression was confirmed by western blotting (Figure S1B). SIRT1 protein levels were significantly elevated in CML CP and BC CD34<sup>+</sup> cells (Figure 1B), CML CP CD34<sup>+</sup>CD38<sup>+</sup> (Figures 1C and 1D), and CD34<sup>+</sup>CD38<sup>-</sup> cells (Figures 1E and 1F) compared to their normal counterparts.

### SIRT1 Inhibition Using shRNA Reduces CML Progenitor Proliferation, Survival, and Colony Growth

To investigate the functional role of SIRT1 in CML and normal progenitors, CML and normal CD34<sup>+</sup> cells were transduced with lentivirus vectors coexpressing SIRT1 or control shRNAs together with RFP. CD34<sup>+</sup>RFP<sup>+</sup> cells were selected using flow cytometry. Western blotting confirmed effective inhibition of SIRT1 expression, whereas the expression of the related SIRT2 was not affected (Figures 2A and 2B).

aging, DNA repair, cell cycle, metabolism, and cell survival under stress conditions (Bordone and Guarente, 2005; Liu et al., 2009a). In contrast to Class I, II, and IV HDACs, SIRT1 activity is not inhibited by pan-HDAC inhibitors (Liu et al., 2009a). SIRT1 plays an important role in maintaining self-renewal and differentiation of murine embryonic stem cells (ESC) and HSC, especially under conditions of stress (Han et al., 2008; Narala et al., 2008; Ou et al., 2011). Importantly, SIRT1 may have a pathogenetic role in solid tumors and leukemias (Brooks and Gu, 2009; Liu et al., 2009a). SIRT1 can potentially regulate the acetylation of several transcription factors, including p53 (Luo et al., 2001), Ku70, and FoxOs (Brooks and Gu, 2009). Despite the clear inhibitory effect of increased SIRT1 expression on tumor suppressors like p53 and FoxOs, other studies suggest that SIRT1 may also have tumor-suppressive functions. In the *Apc*<sup>+/-</sup> mouse model of colon cancer, increased SIRT1 expression resulted in reduced cell proliferation and tumor formation (Firestein et al., 2008). Activation of SIRT1 by resveratrol can limit cell growth and reduce tumor formation in BRCA1-deficient tumor cells and in *Trp53*<sup>+/-</sup>; *Sirt1*<sup>+/-</sup> mice (Wang et al., 2008a, 2008b). The precise role of SIRT1 in cancer may depend on

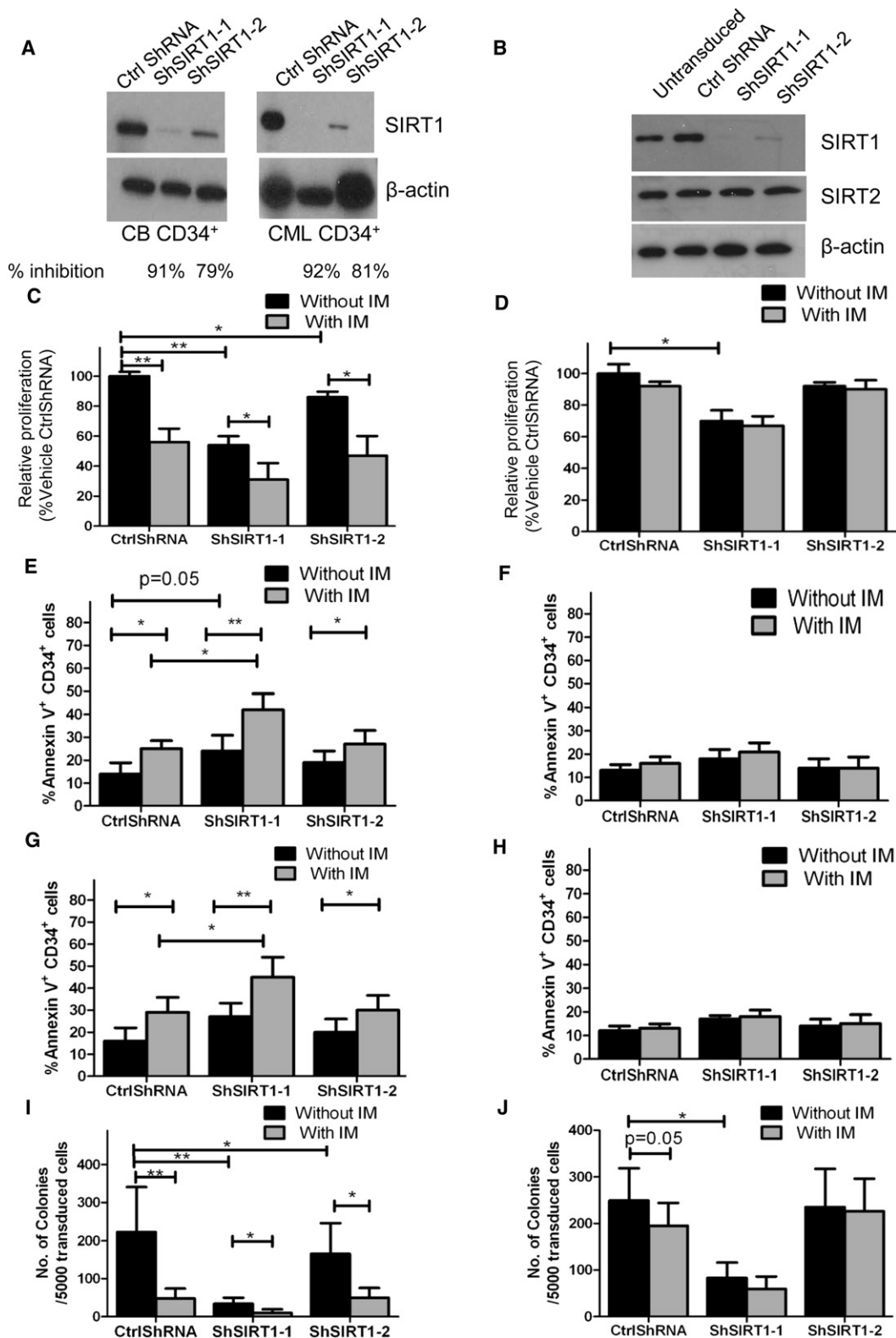


**Figure 2. SIRT1 Knockdown Using Specific Anti-SIRT1 shRNA Increases Apoptosis and Inhibits Proliferation of CML Progenitors**

(A) Western blotting of SIRT1 and  $\beta$ -actin in CB CD34<sup>+</sup> and CML CD34<sup>+</sup> cells transduced with SIRT1 shRNAs (ShSIRT1-1 and ShSIRT1-2) or with Ctrl shRNA. (B) Western blotting for SIRT1, SIRT2, and  $\beta$ -actin in ShSIRT1-1, ShSIRT1-2, or CtrlShRNA transduced TF-1 cells. Results are representative of 3 independent experiments.

CD34<sup>+</sup> cells were labeled with carboxyfluorescein diacetate succinimidyl ester (CFSE) followed by culture for 72 hr in low growth factor concentrations. SIRT1 knockdown inhibited CML progenitor proliferation as measured by reduction in CFSE fluorescence. Treatment with IM resulted in further reduction of proliferation (Figure 2C). SIRT1 knockdown inhibited proliferation of CB CD34<sup>+</sup> cells to a lesser extent than CML CD34<sup>+</sup> cells (Figure 2D). Expression of ShSIRT1-1, which results in near complete inhibition of SIRT1 expression, resulted in reduced survival of CML CD34<sup>+</sup> cells (Figure 2E). IM treatment significantly increased apoptosis of SIRT1 knockdown cells, indicating that SIRT1 inhibition enhanced sensitivity of CML progenitors to IM-induced apoptosis (Figure 2E). Enhanced apoptosis of CML CD34<sup>+</sup> cells following SIRT1 knockdown, and further increase in apoptosis with IM treatment, was confirmed by Wright-Giemsa staining (Figure S2A), trypan blue staining (Figure S2B), and activated caspase-3 labeling (Figure S2C). Interestingly, SIRT1 knockdown did not affect survival of normal progenitors, with or without IM treatment (Figure 2F). Primitive, quiescent CML CD34<sup>+</sup> cells are especially resistant to IM-induced apoptosis (Holtz et al., 2005). Importantly, the combination of SIRT1 inhibition and IM enhanced apoptosis of quiescent CML progenitors identified on the basis of high CFSE fluorescence (Figure 2G). In contrast, SIRT1 inhibition did not affect survival of quiescent normal progenitors (Figure 2H). Expression of both ShSIRT1-1 and ShSIRT1-2 significantly reduced CML colony forming cell (CFC) frequency in methylcellulose progenitor assays, which was enhanced by IM (Figure 2I). Inhibition of normal CFC growth was also seen, but was significantly less than for CML progenitors (Figure 2J).

The increased effects of ShSIRT1-1, compared to ShSIRT1-2, suggest that partial inhibition of SIRT1 expression is sufficient to inhibit CML progenitor proliferation, but that near complete knockdown is required to inhibit survival. To exclude the possibility that these results were related to off-target effects, we designed a SIRT1 construct resistant to ShSIRT1-1 (SIRT1-R) (Figure S2D). Lentivirus-mediated expression of wild-type (WT) or SIRT1-R resulted in enhanced SIRT1 protein levels in TF-1/BCR-ABL cells transduced with ShSIRT1-1 (Figure S2E) and abrogated the ability of ShSIRT1-1 to induce apoptosis and inhibit growth (Figures S2F and S2G). These results indicate that ShSIRT1-1 shRNA effects are related to SIRT1 knockdown, rather than off-target effects, and confirm that near complete SIRT1 suppression is required to induce apoptosis in CML cells.

### Pharmacological Inhibition of SIRT1 Induces Apoptosis and Inhibits Proliferation of CML Stem/Primitive Progenitor Cells

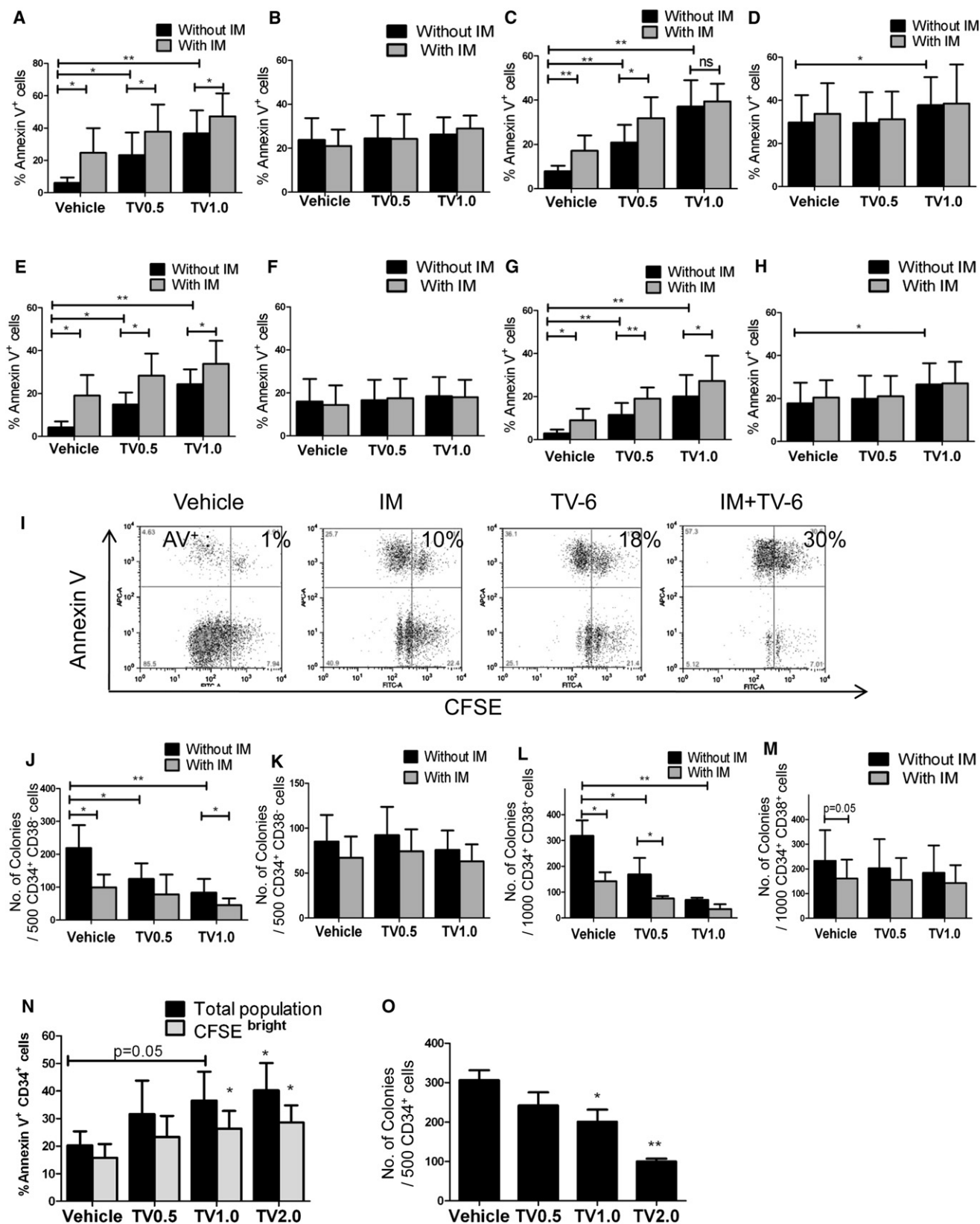
We tested the effects of tenovin-6 (TV-6), a small-molecule inhibitor of SIRT1, on CML and normal stem/progenitor cells (Lain et al., 2008). CFSE-labeled CML and normal CD34<sup>+</sup>CD38<sup>−</sup> and

CD34<sup>+</sup>CD38<sup>+</sup> cells were cultured for 72 hr with TV-6, IM, or the combination. TV-6 significantly increased apoptosis of CML CD34<sup>+</sup>CD38<sup>−</sup> cells and CD34<sup>+</sup>CD38<sup>+</sup> cells, but not normal cells (Figures 3A–3D). A small increase in apoptosis of normal CD34<sup>+</sup>CD38<sup>+</sup> cells was seen with higher doses of TV-6 (Figure 3D). Normal progenitor apoptosis was significantly less than for CML progenitors ( $p < 0.05$ ). The combination of IM and TV-6 increased apoptosis in CML progenitors compared to either agent alone, and to a significantly greater extent than normal progenitors (Figures 3A–3D). Importantly, TV-6 also resulted in increased apoptosis of CFSE<sup>high</sup> undivided CML CD34<sup>+</sup>CD38<sup>−</sup> and CD34<sup>+</sup>CD38<sup>+</sup> cells, but did not increase apoptosis of undivided normal cells (Figures 3E–3I). A small increase in apoptosis of undivided normal cells was seen with higher doses of TV-6 (Figure 3H), but was significantly less than for CML cells ( $p < 0.05$ ). Pretreatment with TV-6 for 72 hr inhibited CFC production from CML CD34<sup>+</sup>CD38<sup>−</sup> and CD34<sup>+</sup>CD38<sup>+</sup> cells but not normal CD34<sup>+</sup>CD38<sup>−</sup> and CD34<sup>+</sup>CD38<sup>+</sup> cells (Figures 3J–3M). The combination of TV-6 with IM enhanced inhibition of CML CFC growth compared to either agent alone, but did not enhance inhibition of normal CFC. Similar results were seen for cells exposed to TV-6 in methylcellulose for the 14-day duration of the CFC assay (Figures S3A and S3B). Exposure to IM for 14 days markedly inhibited CML and normal CFC growth ( $p < 0.01$ ) compared to 14 days of exposure to TV-6 (Figures S3A and S3B). TV-6 also increased apoptosis in total and undivided CD34<sup>+</sup> cells from CML BC patients for whom IM treatment failed, and inhibited growth of CD34<sup>+</sup> cells in CFC assays (Figures 3N and 3O). In addition, TV-6 inhibited BaF3 cells expressing the IM-resistant T315I BCR-ABL mutant (BaF3/T315I) to a similar extent as BaF3 cells expressing wild-type BCR-ABL (BaF3/BA) (Figure S3C).

The effects of SIRT1 deletion on BM progenitors from young mice are apparent only when cells are grown at low O<sub>2</sub> tensions (Ou et al., 2011). We investigated whether selective effects of SIRT1 inhibition on CML compared to normal cells were maintained at low O<sub>2</sub> tensions. TV-6-induced (2  $\mu$ M) apoptosis of total (Figures S3D–S3K) or undivided normal CD34<sup>+</sup>CD38<sup>+</sup> cells was increased in hypoxic compared to normoxic conditions (Figures S3G and S3K). Inhibition of normal CD34<sup>+</sup>CD38<sup>+</sup> cell proliferation and CFC formation was also increased in hypoxic conditions (Figures S3O and S3S). On the other hand, the effects of TV-6 on survival, proliferation, and colony formation of normal CD34<sup>+</sup>CD38<sup>−</sup> cells (Figures S3E, S3I, S3M, and S3Q) or CML CD34<sup>+</sup>CD38<sup>−</sup> cells (Figures S3D, S3H, S3L, and S3P) and CD34<sup>+</sup>CD38<sup>+</sup> cells were not significantly different in hypoxic versus normoxic conditions (Figures S3F, S3J, S3N, and S3R).

TV-6 did not result in additional inhibition of proliferation of SIRT1 knockdown TF-1/BCR-ABL cells (Figure S3T). In addition, MEF from SIRT1 knockout mice (SIRT1-KO) cells were resistant to TV-6 (data not shown). Finally, ectopic expression of SIRT1

(C–J) CML ( $n = 5$ ) and normal CB ( $n = 5$ ) CD34<sup>+</sup> cells transduced with Ctrl ShRNA, ShSIRT1-1, or ShSIRT1-2 vectors were cultured with or without IM (2.5  $\mu$ M) for 72 hr. Division of CML (C) and normal CD34<sup>+</sup> (D) cells was analyzed according to reduction in CFSE intensity, and a proliferation index was determined using ModFit software. Relative proliferation was calculated normalized to untreated controls. Apoptosis of CML (E) and normal (F) CD34<sup>+</sup>RFP<sup>+</sup> cells was analyzed by Annexin V-Cy5 labeling. Apoptosis of undivided (CFSE<sup>high</sup>) CML (G) and CB CD34<sup>+</sup> (H) cells was analyzed by Annexin V-Cy5 labeling. CFC assays were performed on CML (I) and normal CD34<sup>+</sup> (J) RFP<sup>+</sup> cells after culture with or without IM (2.5  $\mu$ M) for 72 hr. Erythroid and granulocytic colonies were enumerated after 14 days. Results represent mean  $\pm$  SEM of separate experiments. Significance: \* $p < 0.05$ , \*\* $p < 0.01$ , \*\*\* $p < 0.001$ , compared with untreated cells. See also Figure S2.



decreased the sensitivity of TF-1/BCR-ABL cells to TV-6 ( $IC_{50}$  2  $\mu$ M in parental TF-1/BCR-ABL and 4.3  $\mu$ M in ectopic SIRT1 expressing TF-1/BCR-ABL cells). These results suggest that TV-6 effects are indeed SIRT1 mediated.

### SIRT1 Inhibition Impairs CML LSC Engraftment in Immunodeficient Mice

We evaluated the effect of ex vivo treatment with TV-6 on CML and normal CD34<sup>+</sup> stem cells capable of engraftment in NOD/SCID interleukin-2 receptor- $\gamma$  chain-deficient (NSG) mice (Shultz et al., 2005) (Figure 4A). We observed reduced engraftment of CML CD34<sup>+</sup> cells treated with TV-6 (1  $\mu$ M) for 72 hr at 4 weeks (short-term engraftment) ( $p < 0.05$ ) (Figure S4A) and 12 weeks posttransplantation (longer term engraftment) (Figures S4C and S4D). Engraftment of CD33<sup>+</sup> and CD14<sup>+</sup> myeloid cells was decreased (Figures S4E and S4F). Q-PCR analysis confirmed that engrafted human cells expressed BCR-ABL (Figure S4G), and FISH analysis showed that 90% of engrafted human cells were BCR-ABL<sup>+</sup>. These results show that SIRT1 inhibition by TV-6 selectively targets primitive human CML cells with in vivo engraftment capacity. We also compared the effect of IM (2.5  $\mu$ M), TV-6 (1  $\mu$ M), or the combination on CML CD34<sup>+</sup> cell engraftment in NSG mice (Figures 4B–4G). CML cells treated with IM alone ( $p = 0.06$ ) and TV-6 alone ( $p < 0.05$ ) demonstrated reduced engraftment in BM at 12 weeks posttransplant compared to untreated controls (Figure 4B). The combination of IM and TV-6 resulted in further inhibition of CML CD34<sup>+</sup> cell engraftment compared to IM or TV-6 alone (Figures 4B–4D), including reduced engraftment of myeloid cells (Figures 4E and 4F). Q-PCR analysis confirmed that engrafted cells expressed BCR-ABL, and that BCR-ABL expression was reduced in cells treated with IM and IM plus TV-6 (Figure 4G). Interestingly, engraftment of CB CD34<sup>+</sup> cells at both 4 weeks (Figure S4B) and 12 weeks (Figures 4H–4K) was not reduced after treatment with TV-6.

### SIRT1 Inhibitor Treatment Reduces CML Stem and Progenitor Cell Growth In Vivo

The low levels of longer term engraftment of CML CP cells in NSG mice limits the use of this model to evaluate the effects of treatments administered in vivo. An inducible BCR-ABL transgenic mouse model of CML provides a representative model of CP CML that can be used for in vivo therapeutic studies (Zhang et al., 2010). These BCR-ABL mice were crossed with GFP transgenic mice, and BM cells were obtained 4 weeks after BCR-ABL induction. GFP-expressing cells selected using flow cytometry

were transplanted into wild-type FVB/N mice irradiated at 900 cGy. Following engraftment, mice were treated for 3 weeks with IM (200 mg/kg/day by gavage), TV-6 (50 mg/kg/day intraperitoneally), the combination of TV-6 and IM, or vehicle (controls) (Figure 5A). TV-6 treated mice demonstrated loss of weight (data not shown) compared to control or IM-treated mice. Leukemic GFP<sup>+</sup> WBC and BM myeloid cells were reduced in TV-6 or IM treated mice, with further reduction with combination treatment (Figures 5B and 5C and Figure S5A). Flow cytometry analysis (Figure 5D) showed that combined TV-6 and IM treatment inhibited primitive GFP<sup>+</sup>Lin<sup>−</sup>Sca-1<sup>+</sup>Kit<sup>+</sup> cells (LSK cells) (Figure S5B), LTHSC (LSK Flt3<sup>−</sup>CD150<sup>+</sup>CD48<sup>−</sup> cells) (Figures 5E and 5F), common myeloid progenitors (CMP) and granulocytic-macrophage progenitors (GMP) in the BM of CML mice to a greater extent than IM or TV-6 alone (Figure 5G and Figure S5C). Similar results were observed for splenic cells (Figure 5H, Figure S5D, and data not shown). In vivo administration of IM and TV-6 resulted in inhibition of LSK cell proliferation measured by EdU and DAPI labeling (Figure 5I) and enhanced LSK cells apoptosis (Figure 5J). Mice treated with the combination demonstrated significantly improved survival and maintained normal WBC counts with only small number of residual GFP<sup>+</sup> WBCs after discontinuation of treatment, compared to control, IM and TV-6 treated mice (Figures 5K–5M).

Consistent with previous reports, BC CML cells demonstrate robust engraftment in NSG mice with primitive CD34<sup>+</sup> cells (Figure S5E–S5I), allowing evaluation of in vivo treatment with TV-6. NSG mice engrafted with cells from an IM-resistant CML BC patient were treated with TV-6 (50 mg/kg/day intraperitoneally) or vehicle control for 3 weeks. TV-6 significantly reduced total human cells ( $p < 0.01$ ) (Figures S5F and S5G) and human CD34<sup>+</sup> cells and myeloid cells in the BM, spleen, and peripheral blood (Figures S5H–S5K). TV-6 treatment also enhanced survival of mice transplanted with BaF3/T3151 cells that are resistant to treatment with IM (Figure S5L), further demonstrating its in vivo activity against IM-resistant cells.

### SIRT1 Inhibition Enhances p53 Acetylation in CML Progenitors

SIRT1 activity can be assessed by examining acetylation of p53 at K382, a known SIRT1 deacetylation site. SIRT1 knockdown using shRNA resulted in an increase in acetylated p53 protein levels in CP CML CD34<sup>+</sup> cells (Figure 6A and Figure S6A). Although increased p53 acetylation was detectable in SIRT1 knockdown cells in the absence of TSA (Figure S6A), it was more clearly seen in cells in which classic HDAC activity was

### Figure 3. Pharmacological Inhibition of SIRT1 Induces Apoptosis and Inhibits Proliferation of CML Stem/Primitive Progenitor Cells

(A–D) CML CD34<sup>+</sup>CD38<sup>−</sup> (n = 6) (A), normal CD34<sup>+</sup>CD38<sup>−</sup> (n = 4, 2 CB and 2 PBSC) (B), CML CD34<sup>+</sup>CD38<sup>+</sup> (n = 6) (C), and normal CD34<sup>+</sup>CD38<sup>+</sup> cells (n = 4, 2 CB and 2 PBSC) cells (D) were exposed to TV-6 (0.5  $\mu$ M [TV0.5] or 1  $\mu$ M [TV1.0]), IM (2.5  $\mu$ M), or the combination for 72 hr. Apoptosis was analyzed by Annexin V-Cy5 labeling.

(E–H) Apoptosis of undivided CML CD34<sup>+</sup>CD38<sup>−</sup>CFSE<sup>high</sup> (E), normal CD34<sup>+</sup>CD38<sup>−</sup>CFSE<sup>high</sup> (F), CML CD34<sup>+</sup>CD38<sup>+</sup>CFSE<sup>high</sup> (G), and normal CD34<sup>+</sup>CD38<sup>+</sup>CFSE<sup>high</sup> cells (H) analyzed by Annexin V labeling.

(I) Representative flow cytometry plots showing Annexin V<sup>+</sup> versus CFSE expression.

(J–M) CML (J) or normal (K) CD34<sup>+</sup>CD38<sup>−</sup> cells, and CML (L) or normal (M) CD34<sup>+</sup>CD38<sup>−</sup> cells were cultured with TV-6 (0.5 or 1  $\mu$ M), IM (2.5  $\mu$ M), or the combination for 72 hr, then were plated in methylcellulose progenitor culture, and colonies were enumerated after 14 days.

(N) Apoptosis of total or undivided CFSE<sup>high</sup> CML BC (n = 4) CD34<sup>+</sup> cells exposed to TV-6 (0.5, 1, or 2  $\mu$ M) for 72 hr analyzed by Annexin V-Cy5 labeling.

(O) CML BC (n = 4) CD34<sup>+</sup> cells exposed to TV-6 (0.5, 1, or 2  $\mu$ M) were plated in methylcellulose progenitor culture and erythroid, and granulocytic colonies were enumerated after 14 days. Results represent the mean  $\pm$  SEM of separate experiments. Significance: \* $p < 0.05$ , \*\* $p < 0.01$ , \*\*\* $p < 0.001$ , compared with untreated controls. See also Figure S3.

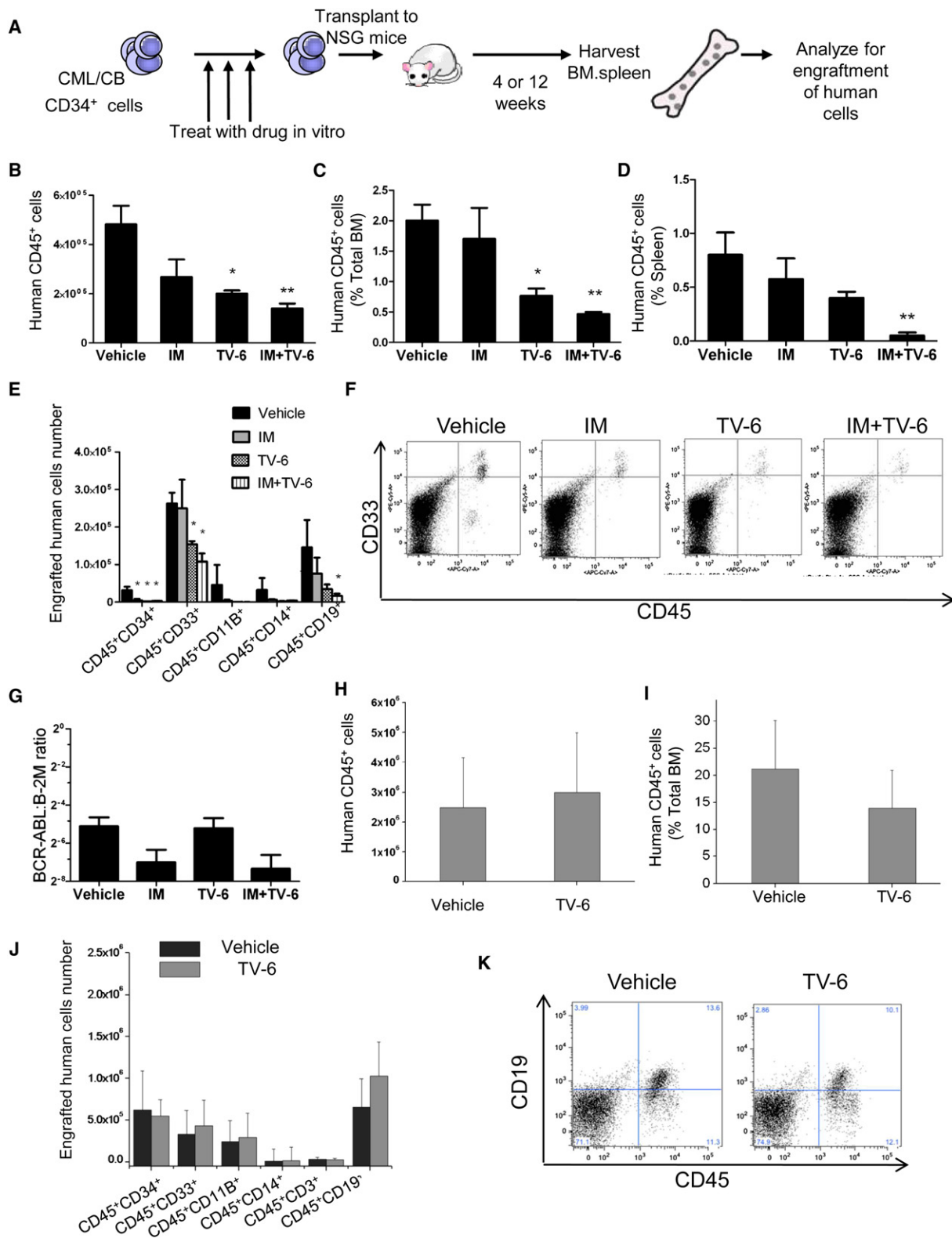


**Figure 4. SIRT1 Inhibition Reduces Longer Term Engraftment of CML Stem Cells in Immunodeficient Mice**

(A) CML or normal CD34<sup>+</sup> cells were treated with TV-6, IM, or combination in vitro and were injected into sublethally irradiated (300 cGy) NSG mice. After 4 or 12 weeks, human cell engraftment was analyzed by flow cytometric assessment of human CD45<sup>+</sup> cells.

(B and C) The number (B) and the percentage (C) of human CD45<sup>+</sup> cells engrafted in the BM 12 weeks after transplantation of CML CD34<sup>+</sup> cells ( $1 \times 10^6$  cells/mouse).

inhibited by TSA treatment (Luo et al., 2001; Cheng et al., 2003). Exposure of CML CP or BC CD34<sup>+</sup> cells to TV-6 also significantly enhanced acetylated p53 levels in both hypoxic and normoxic conditions (Figures 6B and 6C and Figures S6B and S6C). TV-6 treatment also increased total p53 levels, possibly by reducing degradation (Lain et al., 2008). Cells pretreated with the MDM2 antagonist Nutlin-3 to stabilize p53 levels (Vassilev et al., 2004) before the addition of TV-6 showed a rapid and marked increase in p53 acetylation without a change in total p53 levels (Figure 6B). In contrast, TV-6 did not increase acetylated p53 or total p53 levels in normal CD34<sup>+</sup> cells (Figure S6D). Acetylated p53 signals were increased and showed a nuclear distribution in SIRT1 knockdown cells (Figure 6D). A modest increase in acetylation of the SIRT2 substrate  $\alpha$ -tubulin (Lain et al., 2008) was also seen after 48 hr, suggesting that prolonged TV-6 exposure may also modestly inhibit SIRT2 activity (Figure S6E). However, the more rapid and pronounced effect on p53 acetylation indicates more efficient inhibition of SIRT1 compared to SIRT2 activity. Ectopic expression of BCR-ABL in CB CD34<sup>+</sup> cells also resulted in increased expression of SIRT1, which was associated with reduced levels of acetylated p53 despite increased levels of total p53 (Figure S6F).

Treatment with classic HDACs can reduce BCR-ABL expression in cell lines and BC CML cells (Fiskus et al., 2006). BCR-ABL protein levels were not reduced in CP or BC CML CD34<sup>+</sup> cells after SIRT1 inhibition using either shRNA or TV-6 (Figures 6B, 6C, and 6E and Figures S6B and S6C). Treatment with IM reduced tyrosine phosphorylation of the BCR-ABL substrate CrkL in CML CD34<sup>+</sup> cells, confirming inhibition of BCR-ABL kinase activity (Figure 6A and Figure S6B). In contrast, SIRT1 inhibition did not reduce phosphorylation in CML CD34<sup>+</sup> cells (Figures 6A and 6C and Figures S6B and S6C). Therefore, the effects of SIRT1 inhibition on CML CD34<sup>+</sup> cells cannot be explained by inhibition of BCR-ABL expression or activity. Treatment with IM resulted in modest reduction in SIRT1 levels and in total p53 but not acetylated p53 levels (Figure 6A and Figure S6B).

### SIRT1 Inhibition Increases p53 Transcriptional Activity

Irradiation of CML CD34<sup>+</sup> progenitors resulted in increased p53 levels (Figure 7A) and increased expression of p53 target genes, including *p21*, *Necdin* (*Ndn*), *Puma*, and *Bax* (Figure 7B). Knockdown of p53 in CML CD34<sup>+</sup> cells using lentivirus vectors expressing anti-p53 shRNA (Figure 7C) resulted in reduced expression of *p21* and *Ndn* (Figure 7D). These results indicate that p53 signaling remains subject to activation in CP CML CD34<sup>+</sup> cells. To examine the effect of SIRT1 knockdown on p53 transcriptional activity in BCR-ABL expressing cells, we

cotransfected a p53 expression vector and the BP-100 p53 reporter plasmid (MDM2 promoter cloned upstream of the luciferase gene) (Dai et al., 2004) into the p53 null CML cell line K562 (Bi et al., 1992). SIRT1 knockdown resulted in increased p53 activity ( $p < 0.05$ ) compared with controls (Figure 7E). SIRT1 knockdown also increased the activity of endogenous p53 in 293 cells (Figure S7A). Importantly, SIRT1 knockdown increased expression of p53 target genes in CML CD34<sup>+</sup> cells on Q-PCR analysis, including *Gfi-1*, *Ndn*, and *Bax* ( $p < 0.05$ ) (Figure 7F). Although *p21* is also a p53-regulated gene in CML CD34<sup>+</sup> cells, it was not further induced by SIRT1 knockdown.

Treatment with IM resulted in a modest reduction in p53 levels in CML CD34<sup>+</sup> progenitors (Figures 6A and 7G) but did not significantly affect p53 acetylation or expression of p53 target genes (Figure S7B). Knockdown of p53 in CML CD34<sup>+</sup> cells using anti-p53 shRNA did not affect the ability of IM to induce apoptosis (Figure S7C) or inhibit proliferation (Figure S7D), indicating that IM-mediated inhibition of CML progenitors is independent of p53 expression. The combination of IM and Nutlin-3 induced significantly more apoptosis than either agent did alone (data not shown), indicating that p53 signaling can be activated in IM-treated CML CD34<sup>+</sup> cells. SIRT1 inhibition in IM-treated CML CD34<sup>+</sup> progenitors by anti-SIRT1 shRNA expression resulted in increased expression of acetylated p53 (Figure 6A). Upregulation of p53 target genes was also seen following SIRT1 knockdown in IM-treated cells (Figure 7H). These observations indicate that SIRT1 knockdown can activate p53 signaling in IM-treated CML cells.

### Inhibition of CML Progenitor Survival by SIRT1 Knockdown Requires p53 Expression and Acetylation

To determine the role of p53 in mediating the effects of SIRT1 inhibition on CML progenitors, we evaluated whether shRNA-mediated p53 knockdown could mitigate the effects of SIRT1 inhibition on CML progenitors. CML CD34<sup>+</sup> cells were cotransduced with a lentivirus vector coexpressing SIRT1 shRNA and RFP and a second vector coexpressing p53 shRNA and GFP, followed by selection of cells expressing both RFP and GFP (Figure 8A). Inhibition of p53 expression significantly reduced apoptosis (Figures 8A and 8B) and enhanced growth (Figure 8C) of SIRT1-knockdown CML CD34<sup>+</sup> cells. In addition, p53 knockdown CML progenitors exposed to TV-6 showed reduced apoptosis compared with control cells exposed to TV-6 (Figure 8D). These results confirm an important role for p53 in SIRT1-mediated signaling in CML progenitors.

To determine the role of p53 acetylation in mediating SIRT1 effects, we expressed an acetylation-defective p53 mutant (p53-8KR, with all eight potential acetylation sites mutated) in

(D) The percentage of human CD45<sup>+</sup> cells engrafted in the spleen at 12 weeks. Cells from two patients were injected. The figure shows representative results from one patient ( $n = 3$  for untreated control and TV-6 treated cells,  $n = 4$  for IM and combination treatment).

(E) Engraftment of human CD34, CD33, CD11b, CD14, and CD19 subsets (no CD3-positive cells were seen).

(F) Representative results for CD45 and CD33 expression.

(G) *BCR-ABL* mRNA levels in CD45<sup>+</sup> cells engrafted in BM at 12 weeks were measured by Q-PCR.

(H and I) The total number (H) and percentage (I) of human CD45<sup>+</sup> cells engrafted in the BM of NSG mice receiving CB CD34<sup>+</sup> cells at 12 weeks ( $1 \times 10^5$  cells injected/mouse;  $n = 4$  for untreated control;  $n = 7$  for TV-6 treated cells).

(J) Engraftment of human CD34, CD33, CD11b, CD14, CD3, and CD19 cell subsets.

(K) Representative results for CD45 and CD19 expression. Results represent the mean  $\pm$  SEM of separate experiments. Significance: \* $p < 0.05$ , \*\* $p < 0.01$  compared with untreated cells. See also Figure S4.

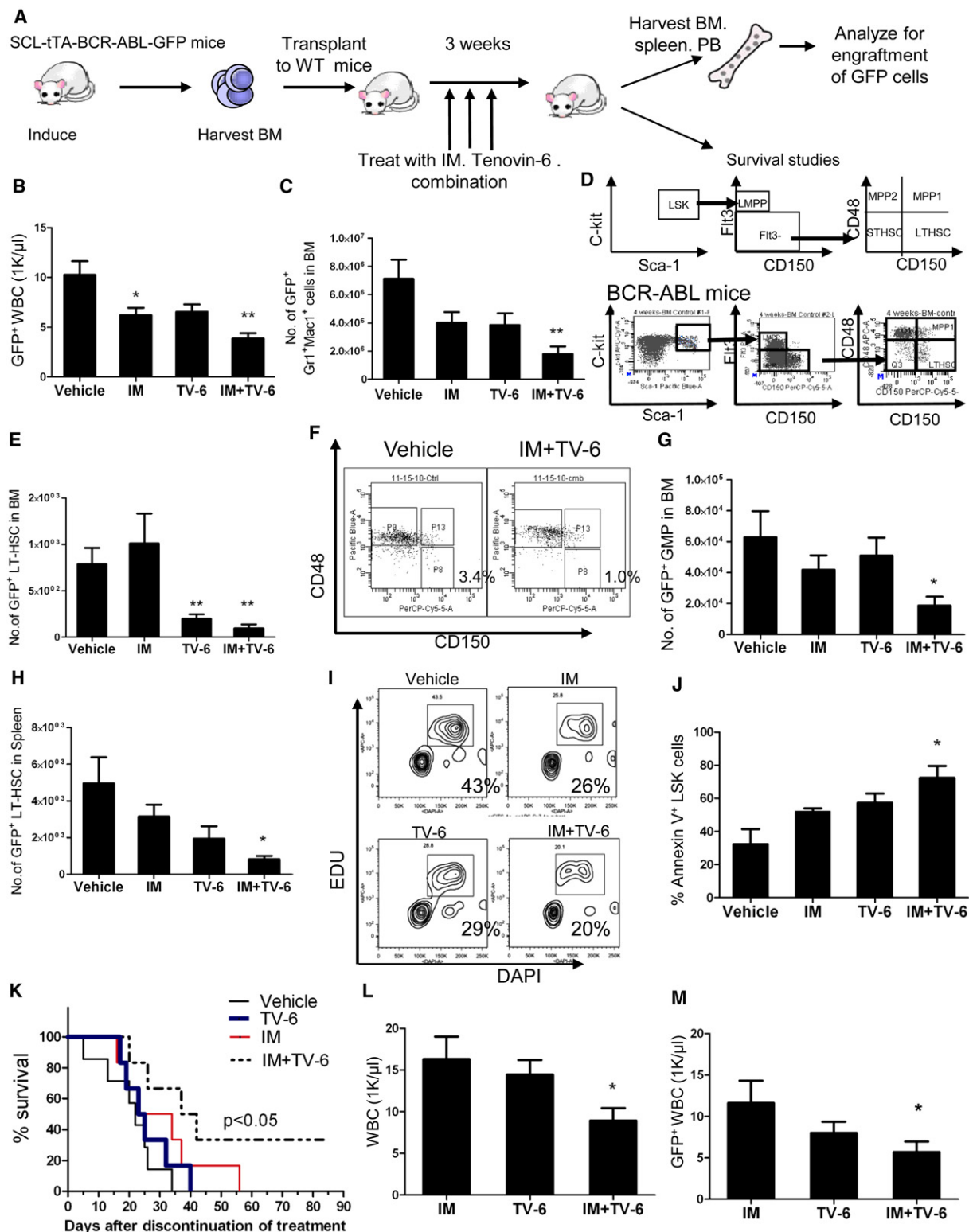


**Figure 5. SIRT1 Inhibition Reduces In Vivo Growth of CML Stem Cells**

(A) BCR-ABL mice were crossed with GFP transgenic mice and BM cells obtained 4 weeks after induction of BCR-ABL expression. GFP<sup>+</sup> cells selected by flow cytometry were transplanted into wild-type FVB/N mice irradiated at 900 cGy. Following engraftment, mice were treated for 3 weeks with IM (200 mg/kg/day by gavage), TV-6 (50 mg/kg/day intraperitoneally), the combination of TV-6 and IM, or vehicle (controls) (n = 6 mice each).

(B) GFP<sup>+</sup> WBC counts 3 weeks after start of treatment.

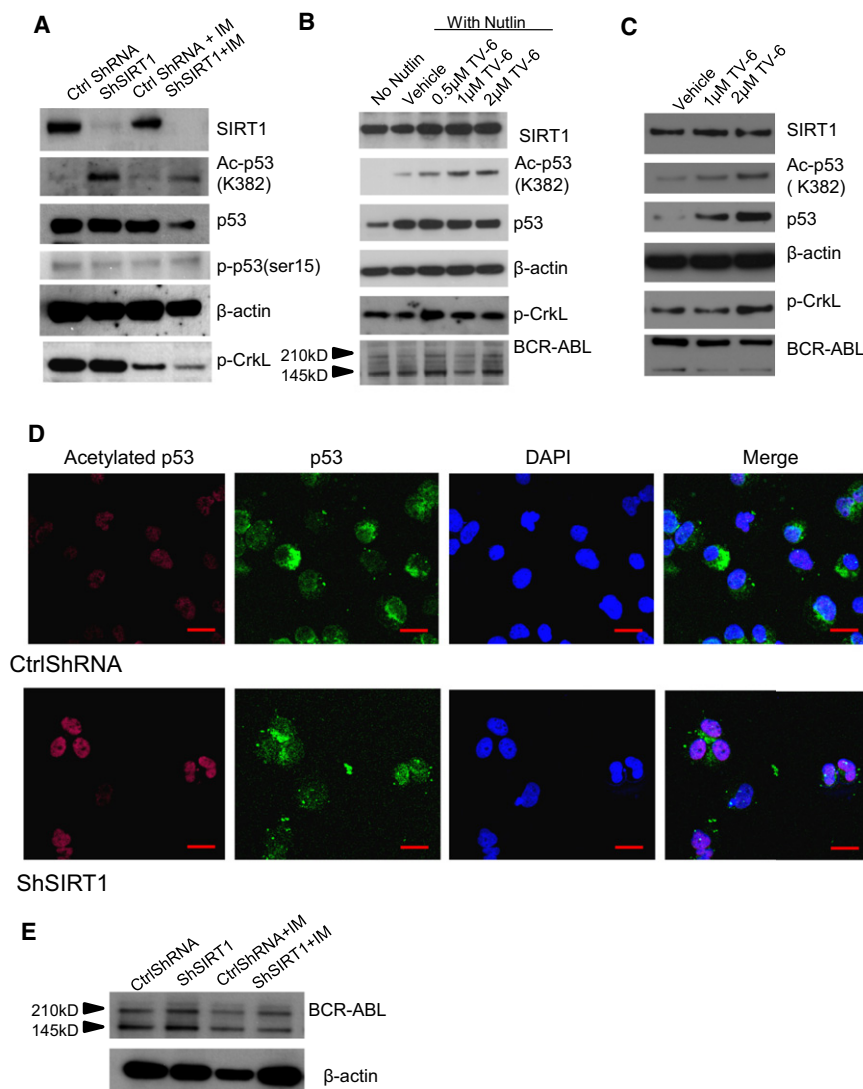


**Figure 6. Increased p53 Acetylation and Nuclear Localization in SIRT1-Inhibited CML CD34<sup>+</sup> Cells**

(A) Western blotting for acetylated p53 (K382), total p53, p-p53 (ser 15), β-actin, SIRT1, and p-CrkL in SIRT1 knockdown in CML CD34<sup>+</sup> cells cultured with TSA (0.1 μM) for 2 hr and exposed to IM (2.5 μM) for 8 hr.

(B) Western blotting for acetylated p53 (K382), total p53, β-actin, SIRT1, p-CrkL, and BCR-ABL in CML CD34<sup>+</sup> cells cultured with Nutlin-3 (10 μM) for 2 hr and exposed to TV-6 for 6 hr.

(C) Western blotting for acetylated p53 (K382), total p53, β-actin, SIRT1, p-CrkL, and BCR-ABL in CML BC CD34<sup>+</sup> cells cultured with TV-6 (1 or 2 μM) for 16 hr.

(D) Immunofluorescence analysis of Ac-p53 and p53 in CD34<sup>+</sup> cells. All scale bars represent a size of 10 μm. Results are representative of 3 independent experiments.

(E) Western blotting for BCR-ABL and β-actin in SIRT1 knockdown CML CD34<sup>+</sup> cells exposed to IM 2.5 μM for 24 hr. See also Figure S6.

expressed p53-8KR was not acetylated following SIRT1 knockdown (Figure 8H), and K562 cells transfected with p53-8KR did not show significant growth inhibition or apoptosis following SIRT1 knockdown (Figures 8I and 8J). These results indicate that p53 acetylation is required for growth inhibition and apoptosis following SIRT1 inhibition in BCR-ABL-expressing cells.

## DISCUSSION

Our results show that inhibition of SIRT1 deacetylase enhances targeting of LSC from CML patients by TKI treatment via activation of p53 signaling, indicating an

p53 null K562 cells. Inhibition of SIRT1 using shRNA or TV-6 did not inhibit growth or induce apoptosis in parental K562 cells ( $p > 0.05$ ) (Figure S8). However, SIRT1 knockdown in K562 cells that ectopically expressed WT p53 protein led to increased p53 acetylation (Figure 8E) and significant growth inhibition and apoptosis ( $p < 0.05$ ) (Figures 8F and 8G). In contrast, ectopically

important role for SIRT1 in maintaining LSC growth and survival. Both BCR-ABL kinase-dependent and kinase-independent mechanisms contribute to increased SIRT1 activity in CML cells, with the latter potentially including epigenetic silencing of HIC1, a negative regulator of SIRT1, through methylation (Chen et al., 2005), or altered miRNA regulation of SIRT1 expression (Strum

(C) GFP<sup>+</sup> myeloid cells (Gr-1<sup>+</sup>Mac-1<sup>+</sup>) cells in the BM.

(D) Schema for analysis of LTHSC (E) GFP<sup>+</sup> LTHSC in BM.

(F) Representative plot for BM LTHSC for vehicle control and combination.

(G) GFP<sup>+</sup> GMP in BM.

(H) GFP<sup>+</sup> LTHSC in spleen. Apoptosis and cell cycling in BM LSK cells was evaluated after 5 days of treatment.

(I) Mice were injected intraperitoneally with EdU and were euthanized 2 hr later. The percentage of stem cells in S-phase was determined according to EdU incorporation in BM LSK cells. Representative results from one of two experiments are shown.

(J) Apoptosis was evaluated by Annexin-V and DAPI labeling ( $n = 3$  mice per group). Significance: \* $p < 0.05$ , \*\* $p < 0.01$ , compared with vehicle control.

(K) Mice were followed for survival for 85 days after discontinuation of treatment ( $n = 6$  per group). Survival of mice receiving combination treatment was significantly longer than that of mice receiving IM or TV-6 alone or vehicle-treated cohorts ( $p < 0.05$ , Wilcoxon test). Two mice receiving combination treatment remained alive until day 85, when the experiment was terminated.

(L and M) The total WBC count (L) and GFP<sup>+</sup> WBC count (M) in PB of mice 4 weeks after discontinuation of treatment. Significance: \* $p < 0.05$ , \*\* $p < 0.01$ , compared with IM. Results represent the mean  $\pm$  SEM of separate experiments. See also Figure S5.

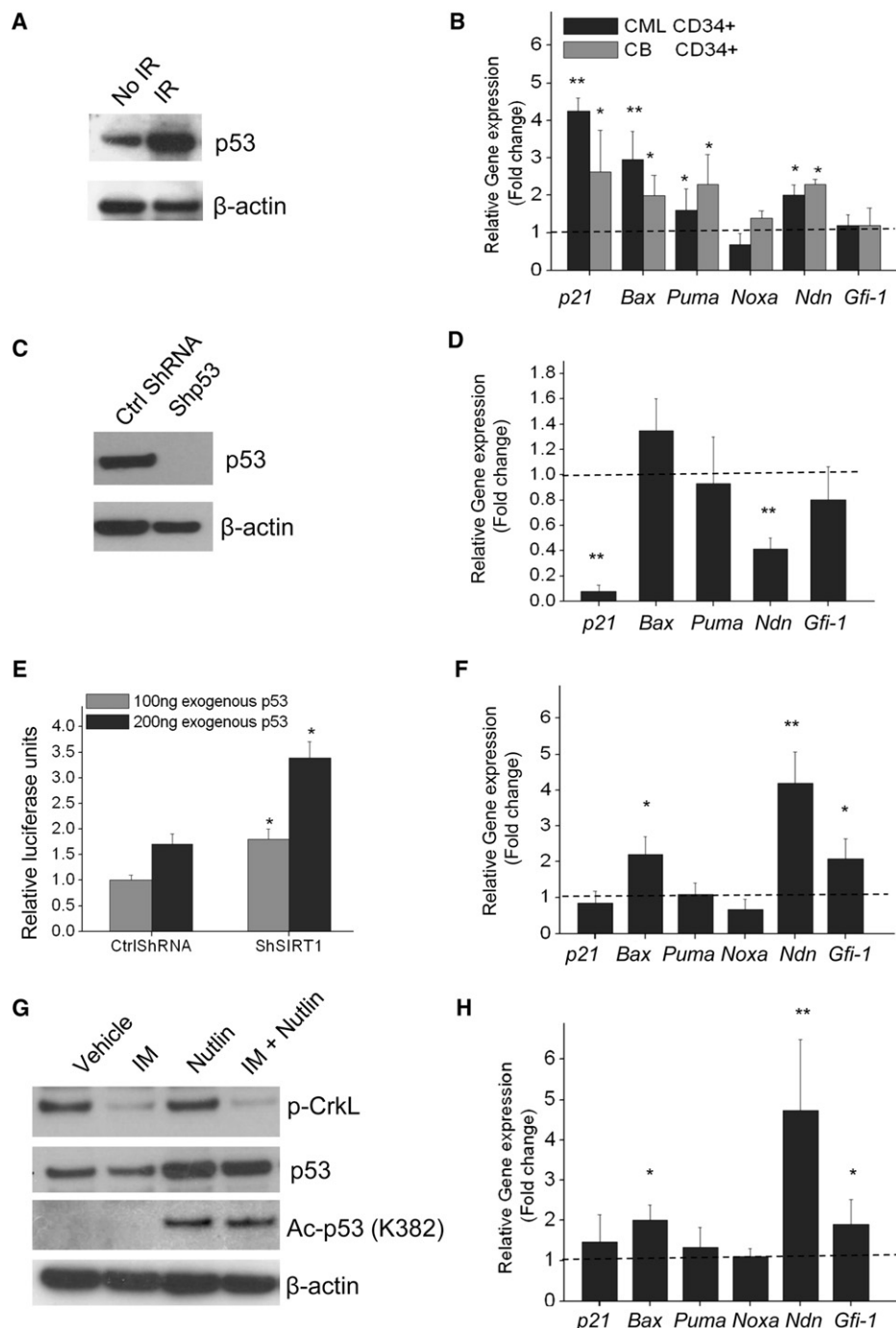


**Figure 7. Signaling through p53 Is Intact in CML Progenitors, Is Enhanced by SIRT1 Knockdown, and Is Not Affected by IM**

(A) Western blotting for p53 in CML CD34<sup>+</sup> cells 6 hr after exposure to irradiation (3 Gy). Results are representative of 3 independent experiments.

(B) Q-PCR analysis of p53 target genes in CP CML and normal CD34<sup>+</sup> cells 6 hr after irradiation (3 Gy) compared with nonirradiated control cells.  $\beta$ -2M was used as an internal control.

(C) Western blotting for p53 expression in CML CD34<sup>+</sup> cells transduced with an anti-p53 shRNA vector. Results are representative of 3 independent experiments.

(D) Q-PCR analysis of p53 target genes in p53 knockdown and control cells.

(E) SIRT1 knockdown or control K562 cells (n = 3) were cotransfected with plasmids expressing p53, a luciferase reporter for p53 transcription (BP100) and  $\beta$ -galactosidase. Relative luciferase units are normalized to  $\beta$ -gal expression.

(F) Q-PCR analysis of p53 target genes in shSIRT1 compared with ctrl shRNA expressing CML CD34<sup>+</sup> cells (n = 3).

(G) Western blotting for acetylated p53 (K382), total p53, p-Crkl, and  $\beta$ -actin in CML CD34<sup>+</sup> cells treated with IM (2.5  $\mu$ M), Nutlin-3, or the combination for 8 hr.

(H) Q-PCR analysis for p53 target genes in shSIRT1 compared with control shRNA-transduced CML CD34<sup>+</sup> cells treated with IM (2.5  $\mu$ M) for 24 hr (n = 4).

Significance: \*p < 0.05, \*\*p < 0.01, compared with controls. Results shown represent the mean  $\pm$  SEM of separate experiments. See also Figure S7.

et al., 2009). The selectivity of SIRT1 inhibition toward CML stem/progenitor cells is maintained in hypoxic conditions, where SIRT1 plays an important role in supporting normal hematopoiesis (Ou et al., 2011).

SIRT1 can deacetylate several lysine residues in the tumor suppressor p53 (Luo et al., 2001; Brooks and Gu, 2009). A variety of posttranslational modifications that can regulate p53 activity, including phosphorylation, acetylation, methylation, and sumoylation, have been described (Vousden and Lane, 2007). Acetylation is reported to play an important role in stabilization, nuclear localization, and transcriptional activation of p53 (Prives and Manley, 2001) and can lead to p53 activation independently of phosphorylation status (Tang et al., 2008). Although p53 mutations may occur on progression to BC CML, they are rare in CP CML (Prokocimer and Rotter, 1994). Our results indicate that p53 remains responsive to stress-induced activation in CML progenitors. SIRT1 inhibition increased p53 acetylation and expression of several p53 target genes, including *Bax*, *Necdin*, and *Gfi-1*, in CML CD34<sup>+</sup> cells. *Bax* is an important proapoptotic gene, and *Necdin* and *Gfi-1* may be important for p53-regulated quiescence of HSC (Liu et al., 2009b). Additional p53 target genes besides those identified here may also contribute to the effects of SIRT1 inhibition. Although *p21* expression was reduced in CML progenitors after p53 knockdown, SIRT1 knockdown did not increase expression of *p21* in CML progenitors, suggesting that other SIRT1-regulated pathways may counteract the effects of p53 acetylation on *p21* induction (Cheng et al., 2003). BC CML cells also demonstrated increased p53 acetylation following SIRT1 inhibition, consistent with recent reports that p53 can be activated in CML BC cells (Peterson et al., 2011). Of note, the CML BC samples studied here did not have p53 mutations (Table S1).

Although previous studies indicated that the p53 inactivation by SIRT1 promotes cell survival during stress (Luo et al., 2001), other studies have suggested that small-molecule SIRT1 inhibitors do not affect cell survival (Solomon et al., 2006) and that developmental defects in a SIRT1 knockout mouse strain are not rescued by crossing to p53 null mice (Kamel et al., 2006). The importance of p53 in mediating SIRT1 effects may depend on the cellular context. SIRT1 deacetylates several other proteins that regulate cell growth and survival besides p53. The importance of individual SIRT1 targets may depend on the cell process and cell type studied. Recent studies within our group indicate an important role for SIRT1 regulation of Ku70 in DNA repair and mutagenicity of CML cells (unpublished data). The role of other SIRT1 targets such as the FoxOs and E2F1 transcription factors in regulating quiescence and survival of CML stem and progenitor cells requires further evaluation.

There is considerable interest in restoring p53 function in cancer cells as a means of inhibiting their proliferation, or inducing senescence or apoptosis. Deacetylation of p53 via SIRT1 may play an important role in preventing p53 activation in TKI-treated CML progenitors. BCR-ABL kinase activity could also modulate p53 in CML cells by upregulation of ARF (Williams et al., 2006), phosphorylation and inactivation of MDM2 and MDMX (Zuckerman et al., 2009), or increased translation of MDM2 (Trotta et al., 2003). Despite the complex regulation of p53 in CML cells, our studies show that enhanced p53 acetylation following SIRT1 inhibition is sufficient to increase p53

transcriptional activity in CML progenitor cells and that p53 deacetylation is an important protective mechanism for CML LSC following TKI treatment. Therefore, p53 activation is a potential strategy to enhance targeting of CML LSC, especially in combination with TKI.

SIRT1 inhibitors are being investigated as potential anticancer treatments. We observed weight loss in mice during the course of three-week TV-6 treatment, but it is unclear whether this was related to SIRT1 inhibition or an off-target effect of this agent. Although TV-6 itself may not be a candidate for drug development, our observations support further investigation of SIRT1 inhibition as an approach for targeting of CML stem/progenitor cells in combination with TKI treatment. The potential tumor suppressive effects of SIRT1 need to be kept in mind when considering SIRT1 inhibitors for cancer treatment. Improved understanding of mechanisms underlying the anticancer versus tumor-promoting effects of SIRT1 inhibition in specific cell types will aid the development of more selective, nontoxic approaches for targeting LSCs in future. The results of the current studies have broader implication to other leukemias, such as AML, where SIRT1 overexpression is also observed and p53 mutations are rare (Kojima et al., 2005).

## EXPERIMENTAL PROCEDURES

### Samples and Materials

CB samples were provided by StemCyte (Arcadia, CA). CP CML samples were obtained from previously untreated patients at the City of Hope (COH) and the University of Glasgow. CML BC samples were obtained from patients at COH (Table S1). CD34<sup>+</sup> cell isolation and CD3<sup>+</sup> cell depletion were performed using magnetic beads (StemCell Technologies, Vancouver, BC, Canada). Leukopheresis samples were processed for CD34<sup>+</sup> cell selection with CliniMACS (Miltenyi Biotech, Germany). CD34<sup>+</sup>CD38<sup>−</sup> and CD34<sup>+</sup>CD38<sup>+</sup> cells were obtained by flow cytometry sorting. All subjects signed an informed consent form. Sample acquisition was approved by the Institutional Review Boards at the City of Hope, in accordance with an assurance filed with and approved by the Department of Health and Human Services, and the North Glasgow University Hospital Division of NHS Greater Glasgow and Clyde, and met all requirements of the Declaration of Helsinki. Details of cell lines, drugs, and DNA constructs are provided in the [Supplemental Experimental Procedures](#).

### Cell Transduction and Transfection

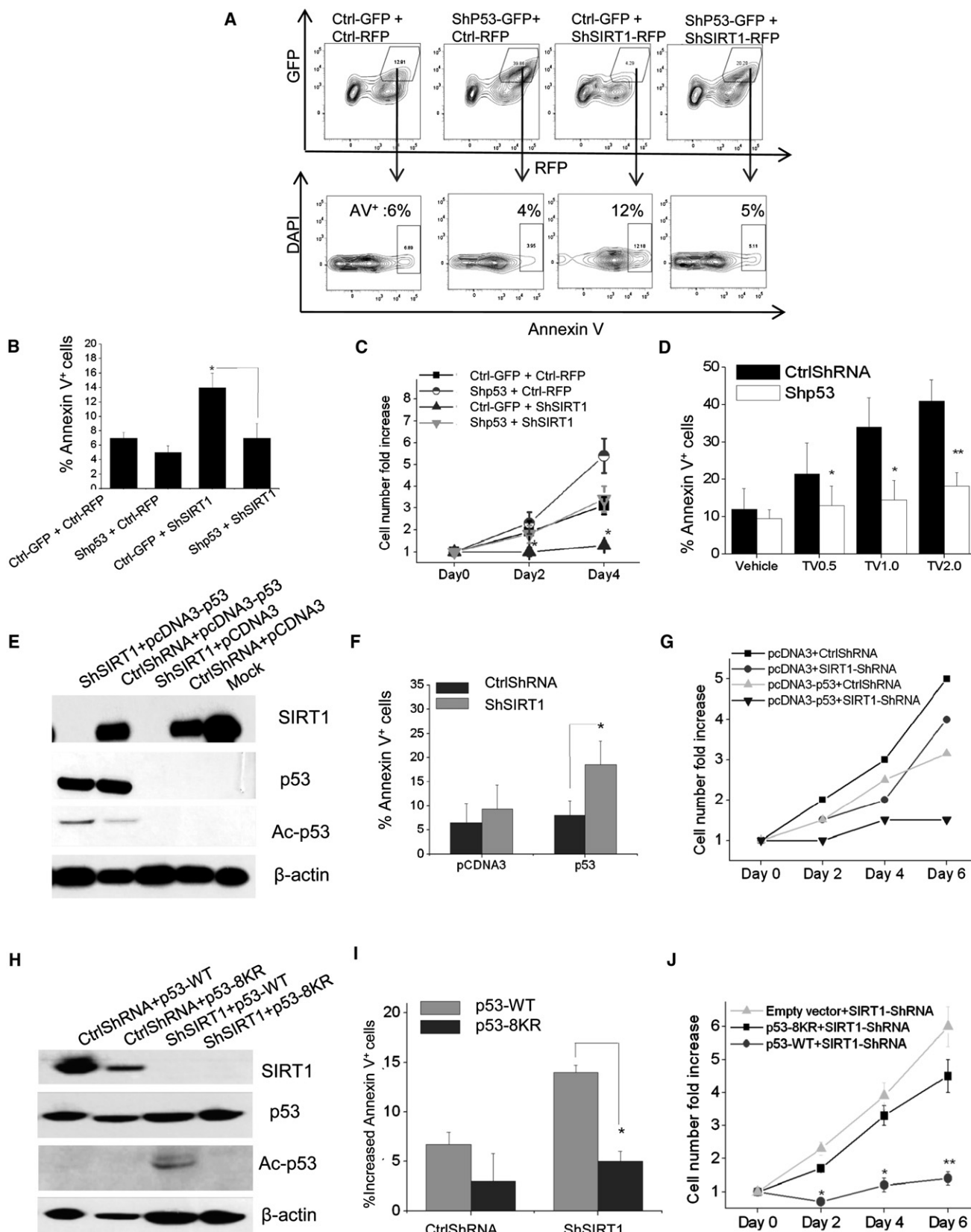
CD34<sup>+</sup> cells were transduced with lentivirus vectors expressing SIRT1 shRNA or p53 shRNA. TF-1/BCR-ABL (TF-1/BA) cells were transduced with PITA-SIRT1-R, PITA-SIRT1-WT, and vector controls (PITA). Details of the transduction procedure are provided in the [Supplemental Experimental Procedures](#).

### Intracellular Staining for SIRT1

CD34<sup>+</sup> cells were labeled with antibodies to CD34-PeCy7, Lin-APC-Cy7 (including CD2, CD7, CD10, CD11B, CD19, CD33, and CD235a), and CD38-APC (e-Bioscience), followed by fixation and permeabilization (Cytotfix/Cytoperm Kit, Beckman Coulter, Fullerton, CA). Cells were then labeled with rabbit anti-human SIRT1 (Epitomics) followed by Alexa 488-conjugated goat anti-rabbit antibodies (Molecular Probes) and were analyzed by flow cytometry. Data were analyzed using FlowJo software (version 8.5.2; TreeStar, Ashland, OR). For immunofluorescence analysis, cells were labeled with anti-p53-FITC (DO-7, BD) and antiacetylated p53-K382-Alex647 (BD), as described in the [Supplemental Experimental Procedures](#).

### Analysis of Proliferation, Apoptosis, and Colony Growth

CD34<sup>+</sup> cells were labeled with CFSE (Molecular Probes, Eugene, OR), labeled with CD34-PE-Cy7 and CD38-APC, and CD34<sup>+</sup>CD38<sup>−</sup> and CD34<sup>+</sup>CD38<sup>+</sup> cells with uniform CFSE labeling were selected by flow cytometry (MoFlo; Cytomation, Fort Collins, CO). Cells were cultured with low



concentrations of growth factors at 37°C for up to 72 hr in normoxic conditions (21% O<sub>2</sub>). For specific experiments, cells were cultured hypoxic conditions (5% O<sub>2</sub>) as specifically indicated in the [Results](#). Cells were analyzed by flow cytometry for apoptosis by Annexin V labeling and for proliferation by reduction in CFSE labeling. Committed progenitors or colony forming cells (CFC) were evaluated in methylcellulose progenitor assays as previously described. Details are provided in [Supplemental Experimental Procedures](#).

#### Engraftment of Human Cells in Immunodeficient Mice

CML CD34<sup>+</sup> cells (1 × 10<sup>6</sup> cells/mouse) or CB CD34<sup>+</sup> cells (1 × 10<sup>5</sup> cells/mouse) were cultured for 72 hr with TV-6 (1 μM), IM (2.5 μM), or the combination or without drug (control) and were transplanted via tail vein injection into sublethally irradiated (300 cGy) 8-week-old NOD.Cg-Prkdcscid IL2rgtm1Wjl/SzJ mice (NSG mice, Jackson Laboratory, Bar Harbor, ME). Mice were euthanized after 4 or 12 weeks, and marrow contents of femurs, spleen cells, and blood cells were obtained. For CML BC samples, MNC depleted of CD3<sup>+</sup> cells were transplanted via tail vein injection (5 × 10<sup>6</sup> cells/mouse). Blood samples were obtained 4 weeks after transplantation to confirm human CD45<sup>+</sup> cells engraftment. Mice were treated with TV-6 (50 mg/kg intraperitoneally daily for 21 days) ([Lain et al., 2008](#)) or vehicle (control) for 3 weeks and were euthanized, and marrow and spleen cells were obtained and analyzed as described in [Supplemental Experimental Procedures](#). Mouse care and experimental procedures were performed in accordance with established institutional guidance and approved protocols from the Institutional Animal Care and Use Committee at COHNMC.

#### In Vivo Treatment of Transgenic BCR-ABL Mice

These experiments were performed using inducible, transgenic GFP-Scl-tTa-BCR-ABL mice in the FVB/N background crossed with transgenic GFP-expressing mice (FVB.Cg-Tg [ACTB-EGFP] B5Nagy/J, Jackson Laboratories) ([Zhang et al., 2010](#)). Mice were treated with IM (200 mg/kg daily by gavage for 21 days), TV-6 (50 mg/kg body weight intraperitoneally daily for 21 days), the combination, or vehicle alone (control). After 3 weeks of treatment, animals were euthanized, and marrow and spleen cells were obtained. The number of total nucleated cells, GFP-expressing cells, and GFP<sup>+</sup> myeloid, progenitor, and stem cell populations were measured by flow cytometry. The effect of drug administration on apoptosis and cycling of stem cells in vivo was evaluated. Another subset of mice was followed after discontinuation of treatment, and survival was monitored for 85 days, PB counts were monitored for 28 days. Details are provided in the [Supplemental Experimental Procedures](#). Mouse care and experimental procedures were performed in accordance with established institutional guidance and approved protocols from the Institutional Animal Care and Use Committee at COHNMC.

#### Luciferase Reporter Assays

K562 or 293 cells were transfected with reporter and internal control (β-gal or Renilla-CMV) plasmids. Luciferase assays were performed after 48 hr in triplicate using the luciferase reporter assay system (Promega).

#### Real-Time Q-PCR Analysis

Q-PCR analysis performed with primers and probes for *p21*, *Bax*, *Puma*, *Noxa*, *Necdin*, *Gfi-1*, and *Sirt1*, and *BCR-ABL* (B3A2) transcripts were measured using a real-time TaqMan assay as previously described ([Chu et al., 2011](#)). Details are provided in the [Supplemental Experimental Procedures](#).

#### Western Blotting

Western blotting was performed for p53, acetylated p53, phospho-p53, SIRT1, CrkL, phospho-CrkL, Bax, ABL, tubulin, and actin. Details are provided in the [Supplemental Experimental Procedures](#).

#### Statistics

Data from independent experiments were reported as the mean ± SEM. Student's *t* test analysis was performed to determine statistical significance.

#### SUPPLEMENTAL INFORMATION

Supplemental Information includes one table, eight figures, Supplemental Experimental Procedures and can be found with this article online at doi:10.1016/j.ccr.2011.12.020.

#### ACKNOWLEDGMENTS

This work was supported by the National Institutes of Health (grants R01 HL77847 and R01 CA95684), a research grant from the Samuel Waxman Cancer Research Foundation, a Translational Research grant from the Leukemia and Lymphoma Society (to R.B.), and a V Foundation translational grant (to W.Y.C. and R.B.). W.Y.C. is supported by National Institutes of Health grant R01 CA143421. T.L.H. is supported by Cancer Research UK Programme grant C11074/A11008. We acknowledge the excellent technical support of the COHNMC Analytical Cytometry, Synthetic Chemistry, and Cytogenetics cores, and the Animal Resources Center. We thank StemCyte for their generous gift of CB samples, and Allen Lin for collection of patient samples. This study was supported by the Glasgow Experimental Cancer Medicine Centre (ECMC), which is funded by Cancer Research UK and by the Chief Scientist's Office (Scotland). We thank Dr. M.S. Dai (Oregon Health and Sciences University) for the generous gift of the pcDNA3-p53 and mdm2-luc (BP100) plasmids, and Dr. Wei Gu (Columbia University) for the generous gift of the PTRE2-hyg-p53 and pTRE2-hyg-p53-8KR plasmids. Ling Li designed and performed research, analyzed and interpreted data, and wrote the manuscript. L.W. designed and performed experiments and reviewed the

#### Figure 8. Effect of SIRT1 Inhibition in CML Progenitors Is Dependent on p53 Expression and Acetylation

(A–C) CML CD34<sup>+</sup> cells were cotransduced with PLKO-GFP vectors expressing anti-p53 or control shRNA and PHIV7-RFP vectors expressing anti-SIRT1 or control shRNA.

(A) CD34<sup>+</sup>GFP<sup>+</sup>RFP<sup>+</sup> cells were analyzed for apoptosis by Annexin V labeling. A representative plot is shown.

(B) Cumulative results for apoptosis (n = 3).

(C) The total number of CD34<sup>+</sup>GFP<sup>+</sup>RFP<sup>+</sup> cells normalized to ctrl ShRNA expressing cells (n = 3).

(D) p53 knockdown or control CML progenitors were exposed to TV-6 for 48 hr, and apoptosis was analyzed by Annexin V labeling (n = 3). Significance values: \*p < 0.05, \*\*p < 0.01, \*\*\*p < 0.001, compared with untreated cells.

(E–G) K562 cells transduced with HIV7-RFP vectors expressing anti-SIRT1 or control shRNA were transfected with p53 expressing plasmids.

(E) Western blotting for acetylated p53 (K382), total p53, SIRT1, and β-actin.

(F) Apoptosis was assessed after 48 hr by Annexin V labeling.

(G) The fold change in cell numbers was calculated at day 2, day 4, and day 6 relative to day 0.

(H–J) K562 cells expressing a *tet* transactivator gene (K562-TTA) were generated and transduced with HIV7-RFP vectors expressing ShSIRT1 or Ctrl ShRNA. RFP<sup>+</sup> cells were selected and transfected with acetylation-defective (p53-8KR) and wild-type p53 constructs (n = 3). Similar transfection efficiency was confirmed by cotransfection with a β-gal plasmid.

(H) Western blotting for acetylated p53 (K382), total p53, SIRT1, and β-actin.

(I) Apoptosis was evaluated after 48 hrs by Annexin V labeling. Results are normalized to K562-RFP cells transfected with empty vector.

(J) The fold change in cell numbers at day 2, day 4, and day 6 was calculated relative to day 0. Results represent mean ± SEM for separate experiments. Significance: \*p < 0.05, \*\*p < 0.01, compared with controls. See also [Figure S8](#).

manuscript. Liang Li designed and performed experiments and reviewed the manuscript. Z.W. designed and performed experiments and reviewed the manuscript. Y.H. performed experiments and reviewed the manuscript. T.M. performed experiments and reviewed the manuscript. T.H. provided material, interpreted data, and reviewed the manuscript. W.Y.C. designed the study, analyzed and interpreted data, and wrote the manuscript. R.B. designed the study, analyzed and interpreted data, and wrote the manuscript.

Received: April 29, 2011

Revised: November 1, 2011

Accepted: December 20, 2011

Published: February 13, 2012

## REFERENCES

- Bi, S., Hughes, T., Bungey, J., Chase, A., de Fabritiis, P., and Goldman, J.M. (1992). p53 in chronic myeloid leukemia cell lines. *Leukemia* 6, 839–842.
- Bordone, L., and Guarente, L. (2005). Calorie restriction, SIRT1 and metabolism: understanding longevity. *Nat. Rev. Mol. Cell Biol.* 6, 298–305.
- Brooks, C.L., and Gu, W. (2009). How does SIRT1 affect metabolism, senescence and cancer? *Nat. Rev. Cancer* 9, 123–128.
- Chen, W.Y., Wang, D.H., Yen, R.C., Luo, J., Gu, W., and Baylin, S.B. (2005). Tumor suppressor HIC1 directly regulates SIRT1 to modulate p53-dependent DNA-damage responses. *Cell* 123, 437–448.
- Cheng, H.L., Mostoslavsky, R., Saito, S., Manis, J.P., Gu, Y., Patel, P., Bronson, R., Appella, E., Alt, F.W., and Chua, K.F. (2003). Developmental defects and p53 hyperacetylation in Sir2 homolog (SIRT1)-deficient mice. *Proc. Natl. Acad. Sci. USA* 100, 10794–10799.
- Chu, S., McDonald, T., Lin, A., Chakraborty, S., Huang, Q., Snyder, D.S., and Bhatia, R. (2011). Persistence of leukemia stem cells in chronic myelogenous leukemia patients in prolonged remission with imatinib treatment. *Blood* 118, 5565–5572.
- Corbin, A.S., Agarwal, A., Loriaux, M., Cortes, J., Deininger, M.W., and Druker, B.J. (2011). Human chronic myeloid leukemia stem cells are insensitive to imatinib despite inhibition of BCR-ABL activity. *J. Clin. Invest.* 121, 396–409.
- Dai, M.S., Zeng, S.X., Jin, Y., Sun, X.X., David, L., and Lu, H. (2004). Ribosomal protein L23 activates p53 by inhibiting MDM2 function in response to ribosomal perturbation but not to translation inhibition. *Mol. Cell. Biol.* 24, 7654–7668.
- Eiring, A.M., Khorashad, J.S., Morley, K., and Deininger, M.W. (2011). Advances in the treatment of chronic myeloid leukemia. *BMC Med.* 9, 99.
- Fiskus, W., Pranpat, M., Balasis, M., Bali, P., Estrella, V., Kumaraswamy, S., Rao, R., Rocha, K., Herger, B., Lee, F., et al. (2006). Cotreatment with vorinostat (suberoylanilide hydroxamic acid) enhances activity of dasatinib (BMS-354825) against imatinib mesylate-sensitive or imatinib mesylate-resistant chronic myelogenous leukemia cells. *Clin. Cancer Res.* 12, 5869–5878.
- Firestein, R., Blander, G., Michan, S., Oberdoerffer, P., Ogino, S., Campbell, J., Bhimavarapu, A., Luikenhuis, S., de Cabo, R., Fuchs, C., et al. (2008). The SIRT1 deacetylase suppresses intestinal tumorigenesis and colon cancer growth. *PLoS ONE* 3, e2020.
- Han, M.K., Song, E.K., Guo, Y., Ou, X., Mantel, C., and Broxmeyer, H.E. (2008). SIRT1 regulates apoptosis and Nanog expression in mouse embryonic stem cells by controlling p53 subcellular localization. *Cell Stem Cell* 2, 241–251.
- Holtz, M.S., Forman, S.J., and Bhatia, R. (2005). Nonproliferating CML CD34+ progenitors are resistant to apoptosis induced by a wide range of proapoptotic stimuli. *Leukemia* 19, 1034–1041.
- Kamel, C., Abrol, M., Jardine, K., He, X., and McBurney, M.W. (2006). SirT1 fails to affect p53-mediated biological functions. *Aging Cell* 5, 81–88.
- Kojima, K., Konopleva, M., Samudio, I.J., Shikami, M., Cabreira-Hansen, M., McQueen, T., Ruvalo, V., Tsao, T., Zeng, Z., Vassilev, L.T., and Andreeff, M. (2005). MDM2 antagonists induce p53-dependent apoptosis in AML: implications for leukemia therapy. *Blood* 106, 3150–3159.
- Lain, S., Hollick, J.J., Campbell, J., Staples, O.D., Higgins, M., Aoubala, M., McCarthy, A., Appleyard, V., Murray, K.E., Baker, L., et al. (2008). Discovery, in vivo activity, and mechanism of action of a small-molecule p53 activator. *Cancer Cell* 13, 454–463.
- Liu, T., Liu, P.Y., and Marshall, G.M. (2009a). The critical role of the class III histone deacetylase SIRT1 in cancer. *Cancer Res.* 69, 1702–1705.
- Liu, Y., Elf, S.E., Miyata, Y., Sashida, G., Liu, Y., Huang, G., Di Giandomenico, S., Lee, J.M., Deblasio, A., Menendez, S., et al. (2009b). p53 regulates hematopoietic stem cell quiescence. *Cell Stem Cell* 4, 37–48.
- Luo, J., Nikolaev, A.Y., Imai, S., Chen, D., Su, F., Shiloh, A., Guarente, L., and Gu, W. (2001). Negative control of p53 by Sir2alpha promotes cell survival under stress. *Cell* 107, 137–148.
- Mahon, F.X., Réa, D., Guilhot, J., Guilhot, F., Huguet, F., Nicolini, F., Legros, L., Charbonnier, A., Guerci, A., Varet, B., et al; Intergroupe Français des Leucémies Myéloïdes Chroniques. (2010). Discontinuation of imatinib in patients with chronic myeloid leukaemia who have maintained complete molecular remission for at least 2 years: the prospective, multicentre Stop Imatinib (STIM) trial. *Lancet Oncol.* 11, 1029–1035.
- Narala, S.R., Allsopp, R.C., Wells, T.B., Zhang, G., Prasad, P., Coussens, M.J., Rossi, D.J., Weissman, I.L., and Vaziri, H. (2008). SIRT1 acts as a nutrient-sensitive growth suppressor and its loss is associated with increased AMPK and telomerase activity. *Mol. Biol. Cell* 19, 1210–1219.
- Ou, X., Chae, H.D., Wang, R.H., Shelley, W.C., Cooper, S., Taylor, T., Kim, Y.J., Deng, C.X., Yoder, M.C., and Broxmeyer, H.E. (2011). SIRT1 deficiency compromises mouse embryonic stem cell hematopoietic differentiation, and embryonic and adult hematopoiesis in the mouse. *Blood* 117, 440–450.
- Peterson, L.F., Mitrikeska, E., Giannola, D., Lui, Y., Sun, H., Bixby, D., Malek, S.N., Donato, N.J., Wang, S., and Talpaz, M. (2011). p53 stabilization induces apoptosis in chronic myeloid leukemia blast crisis cells. *Leukemia* 25, 761–769.
- Prives, C., and Manley, J.L. (2001). Why is p53 acetylated? *Cell* 107, 815–818.
- Prokocimer, M., and Rotter, V. (1994). Structure and function of p53 in normal cells and their aberrations in cancer cells: projection on the hematologic cell lineages. *Blood* 84, 2391–2411.
- Sawyers, C.L. (1999). Chronic myeloid leukemia. *N. Engl. J. Med.* 340, 1330–1340.
- Shultz, L.D., Lyons, B.L., Burzenski, L.M., Gott, B., Chen, X., Chaleff, S., Kotb, M., Gillies, S.D., King, M., Mangada, J., et al. (2005). Human lymphoid and myeloid cell development in NOD/LtSz-scid IL2R gamma null mice engrafted with mobilized human hemopoietic stem cells. *J. Immunol.* 174, 6477–6489.
- Solomon, J.M., Pasupuleti, R., Xu, L., McDonagh, T., Curtis, R., DiStefano, P.S., and Huber, L.J. (2006). Inhibition of SIRT1 catalytic activity increases p53 acetylation but does not alter cell survival following DNA damage. *Mol. Cell. Biol.* 26, 28–38.
- Strum, J.C., Johnson, J.H., Ward, J., Xie, H., Feild, J., Hester, A., Alford, A., and Waters, K.M. (2009). MicroRNA 132 regulates nutritional stress-induced chemokine production through repression of SirT1. *Mol. Endocrinol.* 23, 1876–1884.
- Tang, Y., Zhao, W., Chen, Y., Zhao, Y., and Gu, W. (2008). Acetylation is indispensable for p53 activation. *Cell* 133, 612–626.
- Trotta, R., Vignudelli, T., Candini, O., Intine, R.V., Pecorari, L., Guerzoni, C., Santilli, G., Byrom, M.W., Goldoni, S., Ford, L.P., et al. (2003). BCR/ABL activates mdm2 mRNA translation via the La antigen. *Cancer Cell* 3, 145–160.
- Vassilev, L.T., Vu, B.T., Graves, B., Carvajal, D., Podlaski, F., Filipovic, Z., Kong, N., Kammlott, U., Lukacs, C., Klein, C., et al. (2004). In vivo activation of the p53 pathway by small-molecule antagonists of MDM2. *Science* 303, 844–848.
- Vousden, K.H., and Lane, D.P. (2007). p53 in health and disease. *Nat. Rev. Mol. Cell Biol.* 8, 275–283.
- Wang, R.H., Sengupta, K., Li, C., Kim, H.S., Cao, L., Xiao, C., Kim, S., Xu, X., Zheng, Y., Chilton, B., et al. (2008a). Impaired DNA damage response, genome instability, and tumorigenesis in SIRT1 mutant mice. *Cancer Cell* 14, 312–323.
- Wang, R.H., Zheng, Y., Kim, H.S., Xu, X., Cao, L., Luhasen, T., Lee, M.H., Xiao, C., Vassilopoulos, A., Chen, W., et al. (2008b). Interplay among BRCA1, SIRT1, and Survivin during BRCA1-associated tumorigenesis. *Mol. Cell* 32, 11–20.

Williams, R.T., Roussel, M.F., and Sherr, C.J. (2006). Arf gene loss enhances oncogenicity and limits imatinib response in mouse models of Bcr-Abl-induced acute lymphoblastic leukemia. *Proc. Natl. Acad. Sci. USA* **103**, 6688–6693.

Zhang, B., Strauss, A.C., Chu, S., Li, M., Ho, Y., Shiang, K.D., Snyder, D.S., Huettnr, C.S., Shultz, L., Holyoake, T., and Bhatia, R. (2010). Effective targeting of quiescent chronic myelogenous leukemia stem cells by histone deace-

tylase inhibitors in combination with imatinib mesylate. *Cancer Cell* **17**, 427–442.

Zuckerman, V., Lenos, K., Popowicz, G.M., Silberman, I., Grossman, T., Marine, J.C., Holak, T.A., Jochemsen, A.G., and Haupt, Y. (2009). c-Abl phosphorylates Hdmx and regulates its interaction with p53. *J. Biol. Chem.* **284**, 4031–4039.